# Applications and Industry

January 1960

## Transactions Papers


| | | |
|---|---|---|
| 59-813 | Transistor Amplistat-Regulated Sectional Drive.....Vickery, Shaad | 369 |
| 59-682 | Multisampled-Loop Systems.....Lendaris, Jury | 375 |
| | Analysis of Nonlinear Sampled-Data Control Systems.....Kinnen, Tou | |
| 59-828 | Part I | 386 |
| 59-829 | Part II | 390 |
| 59-821 | Cathodic Protection Applications at the Hanford Works.....Bucholz | 394 |
| 59-848 | Solid Rotor A-C Generator for High-Temperature Systems....Bateman | 400 |
| 59-840 | Dual-Mode Relay Servos.....Buland, Furumoto | 405 |
| 59-810 | Constant-Frequency Power Using Variable Speed Gen...Jessee, Spaven | 411 |
| 59-879 | Ripple in Aircraft Electric Power Systems.....Markowitz | 418 |
| 59-873 | Nuclear Radiation and Electronic Equipment.....Crittenden | 423 |
| 59-888 | Reliability Analysis for Aircraft Generators.....Duane, Yeager | 426 |
| 59-907 | Computer Evaluation of Aircraft A-C System Designs..Sollecito, Swann | 434 |
| 59-867 | Elementary Design Discussion of Thermoelectric Generation..Bollmeier | 445 |
| 59-883 | New Materials for Transformer-Rectifier in Aircraft....Hoop, McIlvaine | 450 |
| 59-820 | Cathodic Protection of Underground Structures.....Landry, Howell | 456 |
| 59-913 | Temperature Predicition in Thermal-Lag Equipment.....Richards | 462 |
| 58-89 | Transistors and Reactors in High-Performance Servo..Cox, Johannessen | 466 |
| 56-837 | Rapid Transit Is Expanding in Chicago.....Forsythe | 474 |
| 59-1157 | Analysis of A-C Servomotors.....Lind, Schmitz | 476 |
| 59-1153 | Suppressed-Carrier Signal Generator for Servosystem.....Pollard | 481 |
| 59-1156 | Control by Stochastic Adjustment.....Bertram | 485 |
| 59-1162 | Flash-Welded Aluminum-Copper Joints.....Dixon, Nelson | 491 |
| 59-1151 | Response and Stabilization of Feedback Amplifiers.....Mulligan | 495 |
| 59-1112 | Practices for Motor Controllers for Rubber and Plastics.....Watkins | 504 |
| 59-1158 | Math. Error Criterion in Design of Adaptive Control Systems..Merriam | 506 |
| 59-1183 | Analysis of Linear Periodic Feedback Systems.....Gilbert | 512 |
| 59-1181 | Executive-Controlled Adaptive Systems.....Staffin | 523 |
| | Erratum | 530 |
| | Index | 531 |
| | Conference Papers Open for Discussion | See 3rd Cover |




NUMBER 46

*Published Bimonthly by*

AMERICAN INSTITUTE OF ELECTRICAL ENGINEERS

# Communication and Electronics—January 1960


| | | | |
|---|---|---|---|
| 59-511 | Use of D-C Overpotential Testing as Maintenance Tool | Weddendorf | 729 |
| 59-793 | Polyethylene-Insulated Multipair Telephone Cable | Windeler | 736 |
| 59-790 | Magnetic Amplifier Circuits | McMurtrie | 739 |
| 59-824 | Impedance Matching Circuit for Conference Repeater | Grandstaff | 751 |
| 59-788 | Theory of Ferroresonance | Salihi | 755 |
| 59-826 | High-Speed Transistor and Ferrite-Core Memory System | Shafer, Jr., Toy, Priebe, Jr. | 763 |
| 58-1182 | Status of Sampled-Data Systems | Jury | 769 |
| 59-182 | Electronic Telephone Switching System | Brightman, Tubinis | 777 |
| 59-917 | Mixed Transcendental and Polynomial Transformers | Smith | 786 |
| 59-890 | Simulation of Data-Switching Systems on a Digital Computer | Gross | 796 |
| 59-889 | Microwave Systems on Pacific Great Eastern Railway | Doble, Raftis | 800 |
| 59-925 | An Approach to the Study of Automatic Target Tracking | Pode | 806 |
| 59-920 | Global Public Telephone Service—1958 | Donald, Chandler | 811 |
| 59-909 | Thermoelectric Generators Utilizing Lead Telluride | Fritts | 817 |
| 59-943 | Flagstaff-Phoenix TJ Radio System | Hidy | 821 |
| 59-944 | Transistorized Pulse Code Repeater | Partridge | 826 |
| 59-919 | Recurrence Relations in the Solution of Nonlinear Systems | Wolf | 830 |
| 59-1054 | Magnetic-Amplifier–Silicon-Transistor Power Suppl | Mokrytzki, Stuart | 835 |
| 59-1051 | D-C Charged Magnetic Pulse Modulator | Manteuffel, Cooper | 843 |
| 59-1046 | Magnetic Amplifiers Using a Resistive Reactor Model | Frankenthal | 850 |
| 59-1053 | Elimination of Coupling Problems in Multistage Magnetic Amplifiers | McMurray | 858 |
| 59-1042 | Miniature Amplifiers for Magnetic Memory Sensing | Briggs, Hu | 863 |
| 59-1058 | Mathematical Model for Magnetic-Amplifier Reactor Core | Woodson | 872 |
| 59-1060 | Theory of 3-Phase Bridge Magnetic Amplifier—I | Storm, Flairty | 878 |
| 59-1050 | Two-Step Switching of Saturable Reactors | Lovell | 895 |
| 59-1061 | Methods of Obtaining Time of Response | Van Allen, Covert, Wilson | 900 |
| 59-1059 | Self-Regulation in Magnetic Transistor-Amplifiers | Hardies, Van Allen | 905 |
| 59-1044 | Magnetic Amplifier Binary-to-Analog Conversion | Danylchuk, Katz | 909 |
| 59-1086 | A-C Resistance of Solid Magnetic Wires | Gohar | 912 |
| 59-1106 | Error-Detection System for 5-Unit-Code Teletypewriter | Barry, Whitman | 916 |
| 59-1091 | SSB and ISB Systems for Long-Distance Radiotelegraph | Lyons | 921 |
| 59-1090 | Tests for Realizability of the Inductance Matrix | Tokad, Reed | 924 |
| 59-1111 | New Frequency Shift Carrier Telegraph System | Stephens | 927 |
| 59-1085 | Circular-Polarization Duplexer for Millimeter Waves | Fellers | 934 |
| 59-1102 | Conducting Sphere in Alternating Magnetic Fields | Poritsky | 937 |
| 59-1145 | Effects of Nonlinearity on Propagation in Ionized Media | Cohn | 942 |
| 59-210 | Electronic Switchboard Employing Time-Division Multiplexing | Perkins, Jr. | 949 |
| 59-1128 | Computing Correlation and Spectral Functions by Orthogonal Filtering | Gilbert | 954 |
| 59-1105 | Small Automatic Teletypewriter Switching System | Shimmin, Vanderlippe, Whitman | 959 |
| 59-1132 | Designs for Large Organic Reactor Power Plants | Bosworth, Parkins | 964 |
| 59-1148 | The Challenge of Universal Mobile Communications | Culbertson | 973 |
| 59-1120 | Relation Between Magnet Configuration and Performance | Cioffi | 979 |
| 59-1125 | Use of Computers to Study Switching Networks | Chang, George | 982 |
| 59-1175 | Transistorized Multifrequency Ringing Generator | Kostelich, Howald | 987 |
| 59-1180 | General Form of Some Common Network Theorems | Adamson, El-Sobki | 991 |
| 59-1193 | Ripple-Type Time-Delay Networks Using Elliptic Functions | Kiseda, Ford | 996 |
| 59-1186 | Subarea Determination of Capacitance of Cocentric Annular-Plate Capacitors | Reitan, Higgins | 1002 |
| 59-1147 | Detection of Errors in 5-Level Punched Tape | Steeneck, Caley | 1005 |
| 59-1107 | Application of a New Carrier Telegraph System | Collins, Jr., Pitts | 1009 |
| 59-1144 | Network Response to Transient Frequency Modulation Inputs | Bucher | 1017 |
| 59-1179 | Two-Oscillator Scan Stability | Joseph | 1022 |
| 59-1136 | Synthesis of Linear Algebraic Matrix Equations | Horn, Honnell | 1028 |
| 59-1117 | Effects of Temperature on Magnetic Properties of Core Materials | Pasnak, Lundsten | 1033 |
| 59-1160 | Comparison of Sequential and Iterative Circuits | McCluskey | 1039 |
| 59-1104 | K24A Syncroplex Telephone Carrier System | Coetsee, Curtis, Halina | 1044 |
| 59-1146 | Asynchronous Multiplexing | Taylor | 1054 |
| 59-1203 | Ultrasonic Frequency Power Generator Using Transistors | Wei | 1062 |
| 59-1184 | DN Detection of Reactor Fuel Element Failures | Dewes, Childs | 1065 |
| 59-1204 | Effect of Flux Distribution on Iron Losses | Schindler | 1069 |
| 59-204 | Matrix Algebra of Sequential Logic | Schubert | 1074 |
| 59-1192 | Simultaneous Logical Equations | Schubert | 1080 |
| 59-205 | Symmetric Switching Functions | Schubert | 1083 |
| 59-1187 | Some Multihorned Dilemmas in the Magnetic Field | Avčin | 1087 |
| 59-1099 | Microwaves and Their Use in Power Systems | Bartlett | 1095 |
| 59-1293 | Functional Life Tests as Compared with Insulation Life Tests | Manning | 1107 |
| | Index | | 1112 |


*(See inside back cover)*

---

*Note to Librarians.* The six bimonthly issues of "Applications and Industry," March 1959–January 1960, will also be available in a single volume (no. 78) entitled "AIEE Transactions—Part II. Applications and Industry," which includes all technical papers on that subject presented during 1959. Bibliographic references to Applications and Industry and to Part II of the Transactions are therefore equivalent.

*Applications and Industry.* Published bimonthly by the American Institute of Electrical Engineers, from 20th and Northampton Streets, Easton, Pa. AIEE Headquarters: 33 West 39th Street, New York 18, N. Y. Address changes must be received at AIEE Headquarters by the first of the month to be effective with the succeeding issue. Copies undelivered because of incorrect address cannot be replaced without charge. Editorial and Advertising offices: 33 West 39th Street, New York 18, N. Y. Nonmember subscription $8.00 per year (plus 75 cents extra for foreign postage payable in advance in New York exchange). Member subscriptions: one subscription at $5.00 per year to any one of three divisional publications: Communication and Electronics, Applications and Industry, or Power Apparatus and Systems: additional annual subscriptions $8.00 each. Single copies when available $1.50 each. Second-class mail privileges authorized at Easton, Pa. This publication is authorized to be mailed at the special rates of postage prescribed by Section 132.122.



Printed in United States of America

Number of copies of this issue 5,500

# ransistor Amplistat-Regulated Sectional Drive at Southland Paper Mills

A. E. VICKERY
MEMBER AIEE

G. E. SHAAD
MEMBER AIEE

HE HISTORY of the paper industry and the history of paper machine ves is a story of continued progress; gress in improved performance, in- ased reliability, and operator con- ience.

his progress has not been the result a whim or a slogan. It has come as er necessity since the economic founda- n of today's paper machines, large or ll, is based on the ability continuously produce a high-quality product. The gressive outlook of the paper industry l a desire for new and better systems provided the co-operation required ween manufacturer and user to make h advances possible.

he progress in machine drives did take place overnight. It began in 1920's and has continued to advance ough the past two decades.

he early drives of the 1920's were ut as crude as can be imagined in the t of today's sophisticated engineering cepts. It must be remembered, how- r, that the electric sectional drive of se days was only required to provide al or better performance than the exist- mechanical drives that were difficult to intain, dangerous to personnel, and ited in capacity. Typical of the elec- drive of those days was the original ve system installed in Crown Willa- tte Paper Company, West Lynn, Oreg., 1920; see Fig. 1. Synchronous motors re connected to the d-c motor shafts ough cone pulleys and belts, providing synchronizing means, while the large w-speed d-c motors provided the bulk the driving power.

n the 1920's, this powerful synchronous tor tie was superseded by the mechan- l commutator-type rheostat position- ulating systems such as that shown in . 2. The next decade saw the intro- ction of a position-regulating system utilizing a master selsyn transmitter, belt-driven selsyns on each section, and differential selsyns operating carbon pile resistors in the motor field circuits. By a specialized cam arrangement, the sensitivity of this selsyn system could be maintained essentially constant over a fairly wide range of machine speeds. (The previous systems had reduced sensitivity at reduced speeds.) This selsyn-regulating system furnished throughout the 1930's by the General Electric Company, is shown in Fig. 3.

These various modifications provided considerable improvement in over-all drive performance but by the late 1930's and early 1940's, these regulating systems were reaching the limit of their performance capabilities. It then became necessary to find a system providing faster response with essentially the same regulating accuracy.

To meet this demand for improved performance, several trial installations of high-accuracy speed-regulating systems were made in 1940 and 1941. The performance of these initial installations made it apparent that high-gain speed-regulated systems would provide greatly improved transient performance with more-than-adequate steady-state performance. Fig. 4 shows the electronic amplidyne speed-regulating system furnished by the General Electric Company for the past 10 years. This regulating system consists of a high-accuracy reference system, a d-c tachometer-generator feedback system, an electronic preamplifier, and an amplidyne generator operating in either the motor or the generator field circuits. This high-response speed-regulating system, combined with individual generator power supplies for the various sections, provided excellent performance with great flexibility. From 1946 to 1958, over 100 such machine drives were installed representing more than 1,000 individual regulated sections.

These speed-regulated electronic-amplidyne multiple-generator drives provided very satisfactory performance. The steady-state performance was good and the transient performance shown in Fig. 5 was amply satisfactory for paper-making. From an operator's standpoint, it was convenient, easy to use, fast in response, and generally a quite satisfactory system. In terms of equipment availability and machine lost time attributable to drive performance, the modern drives (installed in the early- and middle-1950's) are averaging well under 2 minutes per day.

Such an operating record would appear to be quite satisfactory but there are always possibilities for improvement. In 1954, the General Electric Company initiated a study program aimed at further reduction of the drive maintenance. Consideration was given to all types of speed-sensing systems, amplifiers, power amplifiers, and generating equipment with due regard for the economics that must always be considered. As a result of this study, a development was initiated to design, test, and evaluate a high-accuracy transistor amplistat speed-regulating system with performance equal to the electronic amplidyne system.

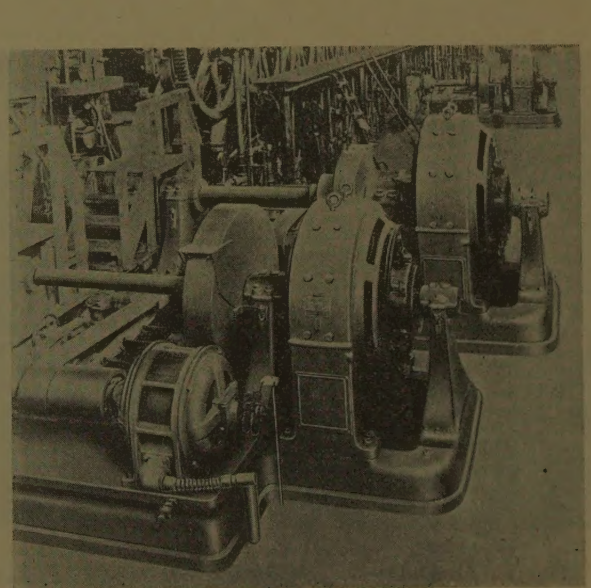

Fig. 1. Sectional drive installed in 1920

er 59-813, recommended by the AIEE General ustry Applications Committee and approved by AIEE Technical Operations Department for entation at the AIEE Summer and Pacific eral Meeting and Air Transportation Confer- e, Seattle, Wash., June 21–26, 1959. Manu- pt submitted March 23, 1959; made available printing April 16, 1959.

E. VICKERY is with Southland Paper Mills, kin, Tex., and G. E. SHAAD is with the General ctric Company, Schenectady, N. Y.

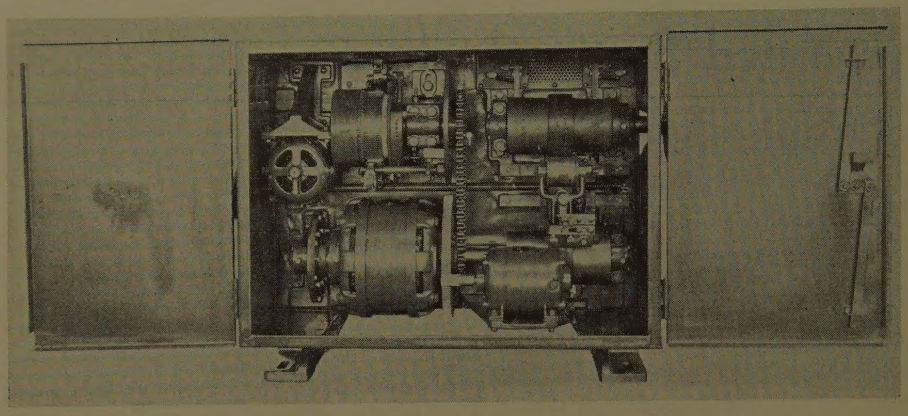

Fig. 2. Rheostat-type position regulator

The attainment of the objective of maintenance without sacrifice of drive performance involved three major points of consideration: (1) circuit design, (2) regulator mechanical design, and (3) over-all control-panel design and system design.

The first consideration represented the major portion of the design and development work. It was necessary to have minimum system drift (due to temperature or other causes), adequate system loop gain for system response and regulation, and high-impedance input circuitry (essentially to impose zero-loading on the high-accuracy d-c tachometer speed-sensing element). Of the many possible methods of approach, the final circuit arrangement was selected on the basis of over-all simplicity and a minimum of components that might require maintenance or replacement. This design is shown in block fashion in Fig. 6. The reference power supply provides an accurately regulated set of bus voltages for the individual section preamplifiers and the master speed control. The master speed reference supply provides a stiff reference voltage (common to all sections) adjustable over the full range from zero to 100% machine speed. Built into this transistorized speed reference system is a linear timing circuit which provides controlled rates of acceleration and deceleration when changing the over-all machine speed.

In each section, the master reference voltage is compared with the section speed in a conventional bridge circuit which permits the use of a simple series rheostat for vernier adjustment (draw) of individual section speeds. This input circuit represents a load on the speed-sensing tachometer generator of about 1 megohm. Any error voltage is amplified and through the power amplistat changes the section generator excitation as required to maintain the section speed.

The drift-free amplification of such low-level high-source impedance signals represented a major design problem. Temperature-controlled ovens' drift could have been controlled by temperature or compensation circuits but the added complications were not desirable. The final design uses a-c amplification of the input signal to convert the initial low-level high impedance signal into a higher-level lower impedance signal that no longer represents a problem from a temperature-drift standpoint. A conventional 60-cycle vibrator-chopper is used to convert the d-c input to a-c and demodulate the output of the a-c amplifier to a d-c power output. Similar choppers are used throughout the paper industry in the process instrumentation systems and their record of operational life is exceptionally high.

The remainder of the amplifier system is conventional transistor d-c amplification up to a sufficiently high power level to drive the 400-cycle amplistat power amplifier. It is necessary, of course, to provide a very flexible lead-lag notch network system in the amplifier so that the over-all system performance can readily be matched to the inertia and characteristics of the driven section. In addition, a rate circuit in each section preamplifier provides a controlled rate of acceleration when the section is started.

The basic design was first tested in our own factory in bread-board construction and following these tests a full-sized panel suitable for field testing was constructed. Through the co-operation of a major mill this trial panel was operated for several months on both high-inertia and low-inertia sections of a high-speed paper machine. From observations of the system performance under conditions of load, temperature, voltage, frequency, etc., a final design was evolved that would meet the operating performance requirements of today's machines and provide the industry with reduced maintenance and freedom from lost time (that can be expected from elements having essentially unlimited life).

The design of the circuit is important but the best of circuits can be inadequate

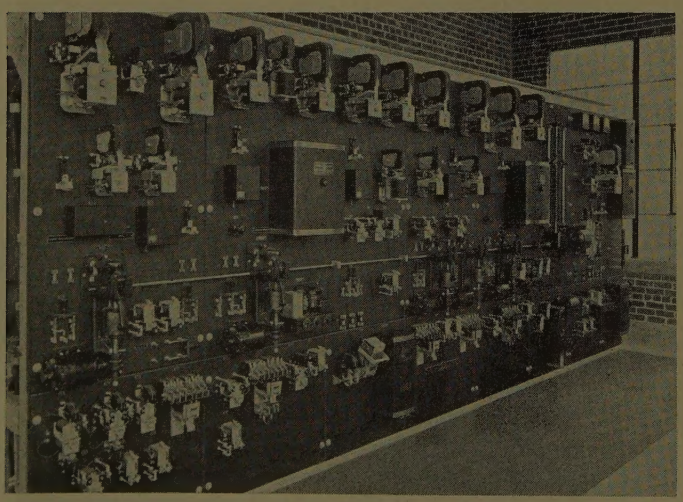

Fig. 3. Block diagram of electronic amplidyne sectional drive

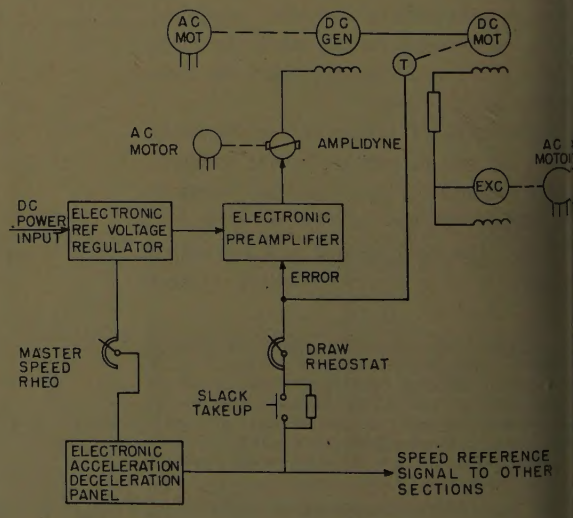


Fig. 4. Carbon pile position-regulator control panel

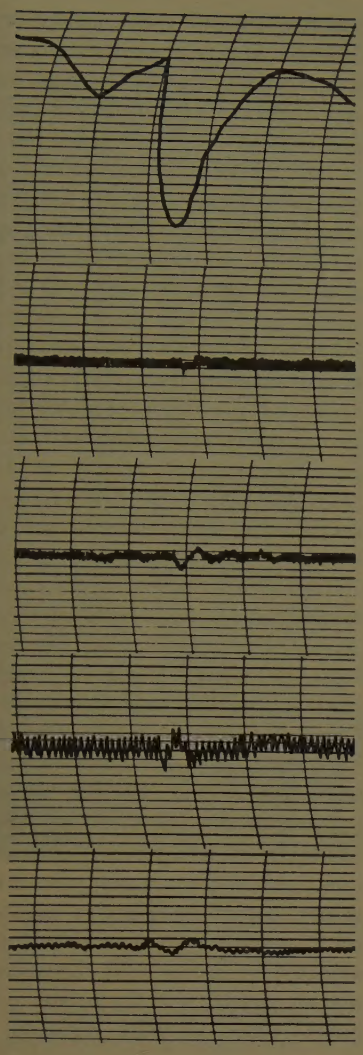

**Fig 5 (left).. Speed records resulting from frequency disturbance in an electronic amplidyne regulator**

A—Power system frequency
B—Couch to dual press
C—Dual press to smooth press
D—First dryer to first calender
E—First calender to bottom coater

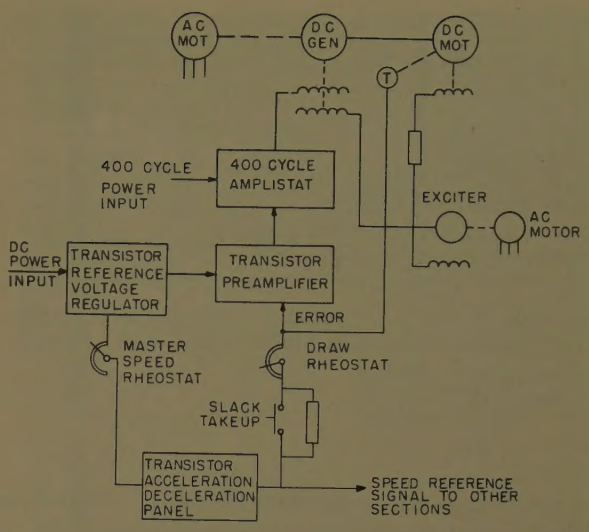


**Fig. 6 (right). Block diagram transistor-amplistat sectional drive**

he mechanical design and components not suitable for the conditions and vice involved.

Because corrosion conditions represent major problem in paper mill design, it s desirable to isolate all small com- nts from the mill atmosphere. It s also desirable to have the potted sub- tions of such size as to be reasonable in replacement costs. With this in mind, the preamplifier circuit was divided into modules, each a complete subsystem, which were then potted for component protection. Interconnections between modules use high-pressure line contact connectors which have a proved history of maintaining good contact under corrosive conditions.

The complete preamplifier shown in Fig. 7 shows the over-all preamplifier construction.

The amplistat power amplifier is a 400-cycle unit supplied from a separate motor-driven 400-cycle alternator. The selection of 400 cycles was based upon the space and weight of the section amplistats rather than upon the slight increase in speed of response. The mill power supply at 60 cycles is not used for it is desirable completely to isolate the regulating system and the drive performance from the multitude of transient voltage inherent in all mill power systems.

From the regulator to the hermetically sealed control relays and heavy-duty armature components the entire control was designed for the continuous service requirements of the paper industry.

The Southland Paper Mill was conceived and built by its president, Ernest L. Kurth, Sr. It was the first commercial newsprint mill ever built to make newsprint from southern pine. It has grown from one 1,500 fpm (feet per minute) newsprint machine to four newsprint machines totalling 7,800 fpm in a period of 20 years.

The no. 4 paper machine shown in Fig. 8 is a 270-inch Fourdrinier machine of Pusey and Jones manufacture. The drive (motors, gear units, generators, and control) is designed for a speed range of 1,000 to 2,700 fpm on 32-pound basis weight newsprint. The speed is continuously adjustable from a dead stop through 2,700 fpm from the operator's control console at the tending side of the machine.

Considerable over-all planning was

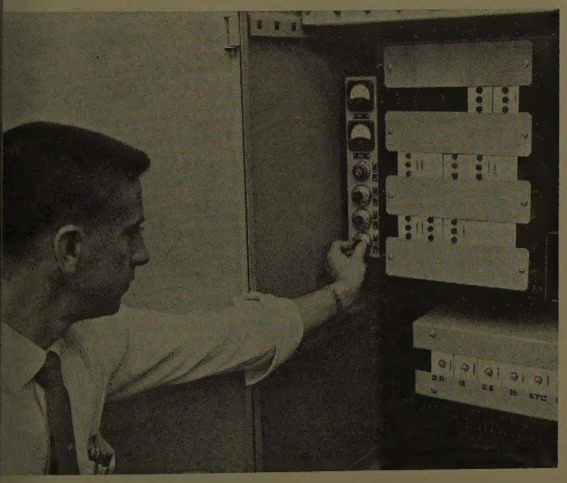

**Fig. 7. Transistorized preamplifier panel**

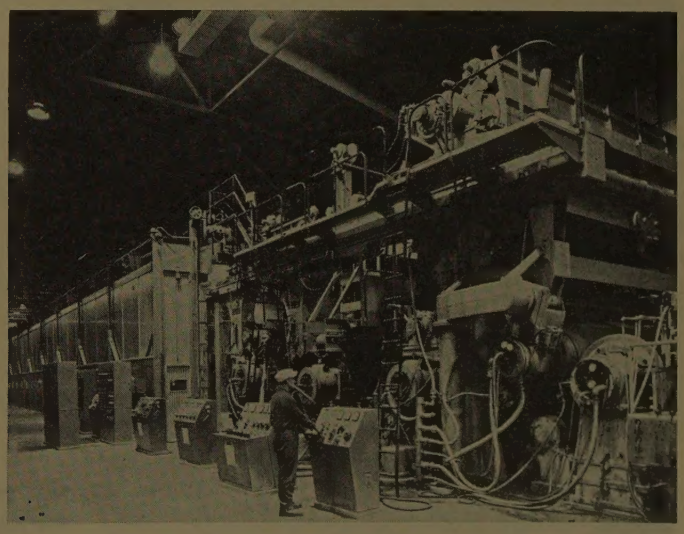

**Fig. 8. Southland Paper Mills no. 4 machine**

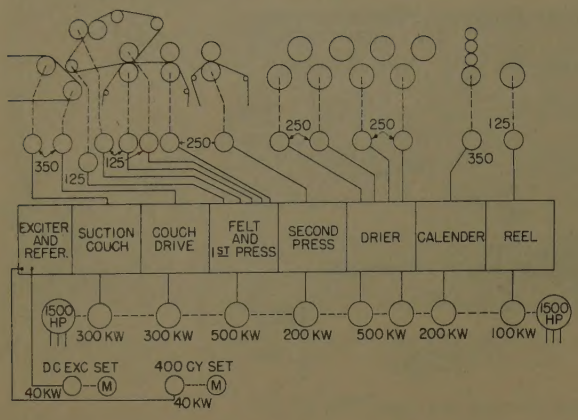


**Fig. 9. Southland Paper Mills no. 4 machine drive**

given to each item of the drive including the selection of paper-mill-type brushes for the drive motors and generators. Flexibility, reduced maintenance, and reduced down time attributable to electrical repairs and adjustments were important factors in the selection and installation of this drive. Although the drive was only a comparatively small portion of the overall installation, it could not be overlooked as an important item in reducing maintenance and production down time.

A sectional drive meeting these requirements was the objective in the selection of this drive with transistorized preamplifiers and amplistat (self-saturating magnetic amplifier) power amplifiers. As many moving parts as possible within the regulating loop were eliminated as were other potential sources of trouble such as vacuum tubes and thyratrons. All the conventional and proved regulating systems were considered and finally eliminated in favor of this all-static amplifier.

The amplifier's general physical arrangement is shown in Fig. 9. Its generators were divided into two motor-generator sets, each driven by 1,500-hp (horsepower) synchronous motors. The generators were selected in a minimum number of ratings (three 500 kw, three 300 kw, one 200 kw, and one 100 kw) making for greater flexibility in maintenance and provision for spares. Generator positions on the lineshaft of the motor-generator set are in the same sequence as their respective paper machine sections. The second press generator is mounted on the dry-end motor-generator set t balance the loads on the two sets wit a provision for mounting and driving spare generator from the wet-end moto generator set.

The sectional drive motors, like th generators, were kept to a minimum three basic sizes. There are three 35 hp motors, six 250-hp motors, and fo 125-hp motors in the drive. The motor shown in Fig. 10, are of conventiona splashproof forced ventilated construc tion with air entering at the back end each motor and being discharged int the room at the commutator end. *BC4* permanent-magnet-excited tachometer generators provide the speed signal for th regulating system and the speed and dra indicators on the machine.

The over-all drive control has six speed regulated sections: couch drive roll, firs press, second press, drier, calender, an reel. In addition to the speed-regulate sections, the suction couch drive is re ulated to follow the couch drive roll wit the amount of load on the suction couc drive determined by the amount vacuum in the couch roll. The suctio pickup roll, wringer roll, top transfe press, and bottom transfer press drives ar helper motors operating in parallel wit the first press with their operating loa adjusted by motor field rheostats. Th section panels, and the master referenc panel (which provides regulated powe

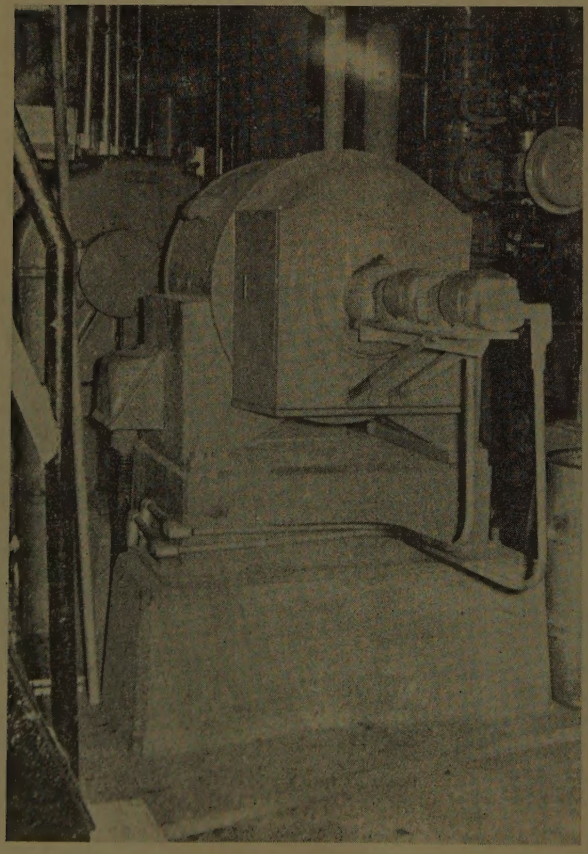

**Fig. 10 (left). Section drive motor**

**Fig. 11 (right). Machine drive control panel**

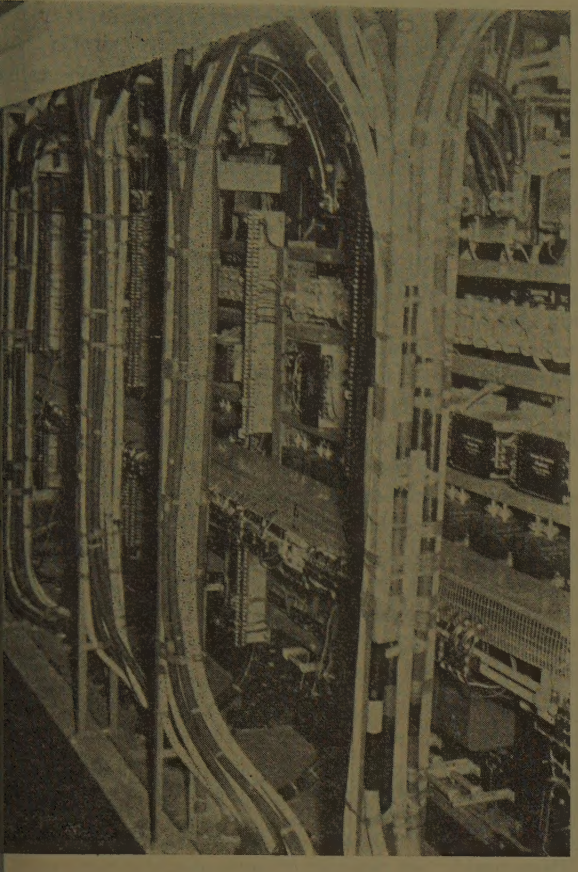

Fig. 12 (left). Back view of drive control panel

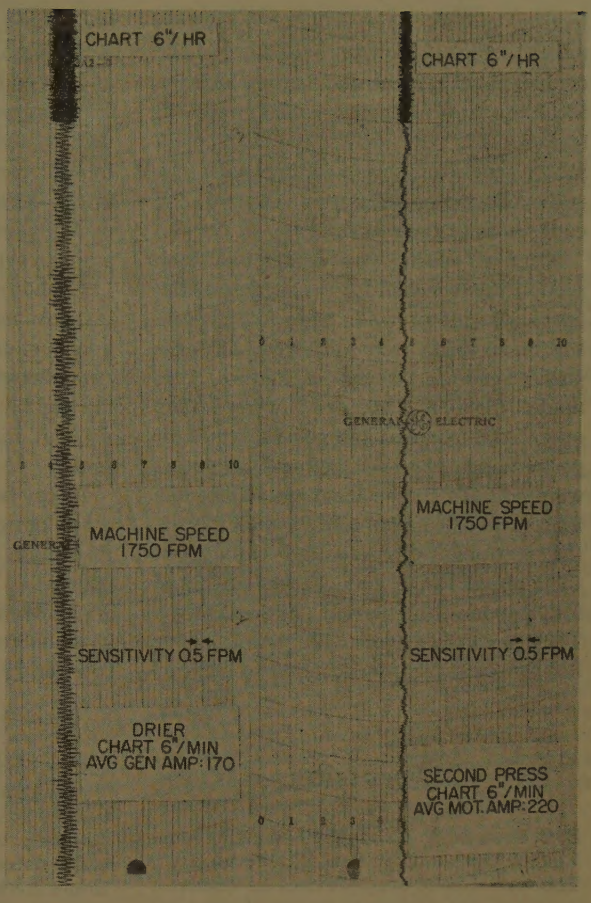


Fig. 14 (right). Speed charts of no. 4 machine

r the preamplifiers, and regulated 400-cle power for the power amplifiers) are own in Fig. 11.

A rate amplifier, mounted on the refer-ce panel, provides a definite rate of ac-leration and deceleration when the entire eed of the machine is changed. The celeration and deceleration rates are dependently adjustable. The regulated rect current from the reference panel pplies the master speed-adjusting heli-t located on the drier operator's console hich provides a master reference signal hich in turn is fed to the rate amplifier. he rate amplifier output is the reference r all the section speed regulators. This mmon reference is fed to each of the eed regulators (except the drier regula-r) through individual helipots for draw djustment. (Drier reference is directly om the rate amplifier output.) Slack

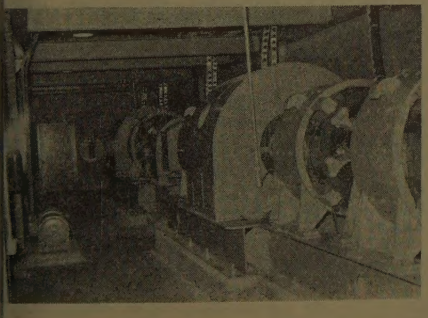

g. 13. Main motor-generator sets and 400-cycle units

takeup, where desired, is provided by means of a pushbutton short-circuiting out a resistor in series with the reference circuit.

The control room in which these panels are installed has a closed air system with air conditioning. The corrosion conditions that had been encountered in other areas of the mill made this construction desirable even though the small regulating components and relays had been sealed to protect them against corrosion and contamination.

The regulator panels mounted on the front of each section panel have no moving parts except for the sealed Stevens-Arnold 6-volt 60-cycle chopper used in the first stage of the regulator. These regulator panels are identical for each section. The units are completely interchangeable with the only adjustment necessary being the setting of the three adjusting rheostats to the same settings as were previously used.

Each section panel is also arranged with essentially identical circuitry permitting maintenance personnel to become readily familiar with the relay sequencing and basic adjustments. The slide-wire resistors for adjustment of crawl speed, regenerative braking current limit, etc., are conveniently mounted on the front of the panel while the larger resistors for motor field adjustments are rack mounted at the top of the panel.

Two modes of operation (at very low or crawl speed) were provided for each section. One uses the transistorized speed regulator and the other uses the amplistat as a voltage regulator. The speed is not adjustable by the operator in either mode but is readily set at the required value by maintenance personnel. To change from transistor speed regulation to amplistat voltage regulation requires the change of one jumper by the electrician. This option applies to slow or crawl speed only. Regulation at operating speeds is always under the control of the transistor amplifier. This amplistat crawl option is intended for maintenance purposes only wherein it may be desired to remove one of the transistor amplifier panels for testing during a wire change or other scheduled shutdown. A spare amplifier panel is on hand and can be installed and adjusted in a matter of 20 to 30 minutes and the drive returned to operation. This will allow checking of the removed panel on the bench in a methodical manner without penalizing the machine for excessive electrical down time.

Armored power and control cables were used in making the connections between the section generators, section panels,

section motors, and section operator's panels. Fig. 12 shows a back view of the control panel and the manner in which the incoming and outgoing cables were installed. Fig. 13 shows the two main motor-generator sets together with the 400-cycle motor-generator set and the cable runs to these units.

After all wiring was completed, each section was checked for proper sequential operation, motor fields were set, generator buck fields were adjusted, and the static settings of the regulators were made. Section motors were then operated uncoupled and general regulator performance observed before the motors were coupled to the machine. Once the motors were coupled to their final inertia, the sections were operated throughout their speed range and checked in detail for response, regulation, and stability. These tests were made with high-accuracy fast-response recorders capable of measuring minute errors in the regulating system performance. Fig. 14 showing the drier and second press sections in operation at 1,750 fpm provides a picture of recorder performance. As the chart shows, a minute gear eccentricity exists in the drier section and the 2-cycle-per-second cyclic operation is clearly defined. Full scale on the chart shown in 25 fpm.

A photoelectric recorder (for accurate fast-response recording of section speed) and a standard cathode-ray oscilloscope (for checking the regulator performance) are the basic instruments used in setting up and maintaining the regulating system.

As can be expected in the installation of a new design regulating system, the initial inspection and adjustment involved some changes. These were primarily concerned with added filtering in the regulator panel to eliminate stray voltage pickup that was interfering with regulator performance.

The machine was placed in operation with stock on the wire in October 1958 with no operating problems insofar as the drive was concerned. After several weeks of operation, a 50-ampere silicon rectifier in one of the power amplistats failed and had to be replaced. This failure was located and corrected by the electricians in a minimum of time. After about a month of operation, erratic performance on several sections with a resultant lost time of about 4 hours was traced to loose connections. A subsequent, complete recheck of the panel by the electricians located and tightened many additional loose connections that could cause trouble in future operations.

The experience in these initial months of operation has been very satisfactory. It appears likely that the transistor amplistat regulator will establish a pattern of maintenance and production that will be most satisfactory.

## Discussion

**E. C. Fox** and **S. J. Campbell** (Westinghouse Electric Corporation, East Pittsburgh, Pa.): The use of solid-state devices as regulator amplifiers has proved to be one of the most important steps in recent years to improve reliability and reduce maintenance on paper machine drives. The use of 400-cycle magnetic amplifiers on sectional drives is, of course, not a new development. The Westinghouse Electric Corporation has a total of 12 sectional drives in operation using 400-cycle magnetic amplifiers, the first of which dates back to early 1956. These machines cover a range of products from newsprint to 300-pound board, with operating speeds from 180 to 2,500 fpm.

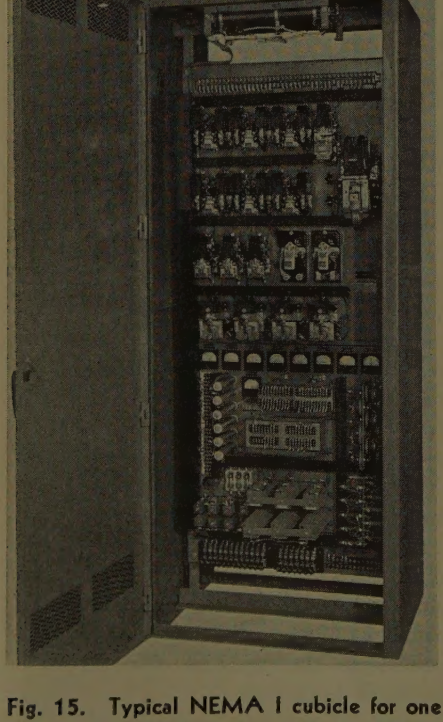

**Fig. 15. Typical NEMA I cubicle for one section of a multiple generator sectional drive; 400-cycle magnetic amplifier located below magnetic panel**

The paper mentions that the selection of 400 cycles for the magnetic amplifier was based primarily on weight and space considerations. It has been our experience that the trend to higher machine speeds makes necessary more rapid transient response and higher steady-state accuracies. These requirements are more easily met with 400-cycle regulator power supplies as compared to those of 60 cycles. These drives include selenium rectifiers in the regulator circuits, as shown in Fig. 15. Experience has shown that these rectifiers are very reliable. Rectifier aging has had no appreciable effect on regulator operation. Future drives will see an increased use of silicon rectifiers, primarily because of their associated reduction in space requirements. More care must be taken in applying silicon rectifiers than selenium rectifiers because voltage surges are more apt to damage the former.

We should appreciate the authors' comments on three items:

1. Published figures on down time for sectional drives indicate that approximately 32% of electrical down time is chargeable to regulator components and regulator readjustments. Certainly the use of static amplifiers will reduce this figure. However, d-c pilot generators and draw rheostats operating into high-impedance input circuits are still used. We wonder whether any immediate developments are underway to change the nature of the speed cue and draw-adjusting devices to reduce down time chargeable to these devices.

2. The speed charts of Fig. 14 indicate that section speed is being held within 1 fpm at 1,700 fpm. This represents a steady-state accuracy of approximately ±0.03%. Previous papers on tachometer feedback regulators state that the drift of this type of tachometer is guaranteed to be less than 0.03%, and that accuracies as high as 0.04% are required on some machine sections. It is difficult to see how a steady-state accuracy of ±0.3% can be obtained on a prolonged basis when the tachometer drift is of the same order of magnitude. We note that the 60-cycle vibrator chopper and d-c pilot generator have been used in other paper industry applications as elements of integrating amplifiers to offset amplifier drift and to increase the speed regulating accuracy. Is the chopper described in the paper also being used as part of an integrating circuit, as it has on these other applications?

3. The magnetic control and regulators are supplied as open panels, located in a control room with closed air conditioning. This is an excellent example of what appears to be a recent industry trend. We should appreciate the authors' comments on the relative installed cost and operating merits of this system as compared to NEMA (National Electrical Manufacturers Association) I cubicles in a control room supplied with filtered air only.


### References

1. Magnetic Amplifier Regulated Drives in the Paper Industry, M. H. Fisher. *TAPPI* Technical Association of the Pulp and Paper Industry, Easton, Pa., vol. 38, Sept. 1955, pp. 513–22.

2. Integrating Amplifiers Broaden Fields for Application of Electric Drives, C. D. Beck. *Electrical Engineering*, vol. 74, no. 10, Oct. 1955, pp. 901–04.

3. Discussion by C. D. Beck, of Control of Speed and Cut in Continuous Processing, E. G. Anger, D. L. Pettit. *AIEE Transactions*, pt. II (*Applications and Industry*), vol. 73, 1954 (Jan. 1955 section), pp. 491–92.


**A. E. Vickery** and **G. E. Shaad**: The Fox-Campbell discussion covers several points of

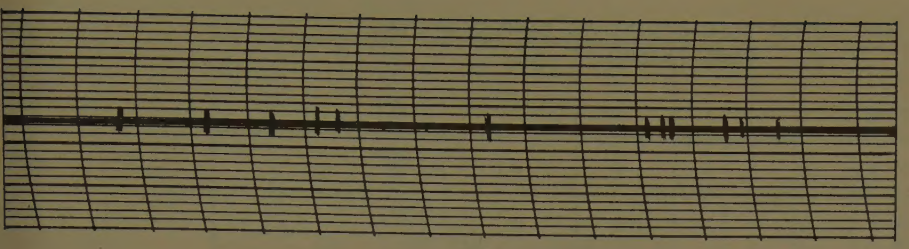

**Fig. 16. Tachometer generator accuracy: chart sensitivity 0.01% per small division; chart speed 3 inches per hour**

interest that are subject to considerable misunderstanding. They are therefore well worth some additional comment.

The selection of 400-cycle magnetic amplifiers was based upon space and weight, as stated in the paper. A speed-regulated system having adequate preamplifier gain, proper degeneration around the system time constants, and adequate stabilizing components will show little difference between 60-cycle and 400-cycle magnetic amplifiers. Other factors such as roll unbalance, gear backlash, inertia time constants, etc., are limiting on the system response long before the time constants of the magnetic amplifier become a significant factor.

Experience over the past decade has proved beyond any question the reliability of the *BC46* Alnico excited d-c tachometer generators. Care in installation and reasonable preventive maintenance make these units a source of negligible lost time. Improperly installed or maintained, they or any other component can and will cause lost production.

Draw rheostats do not have the 100% reliability record that we should like to obtain. Even so, given proper protection from water and stock, their operating record is quite good. The simplicity of the system has such advantages from a maintenance standpoint that possible rheostat failures become a secondary item.

The d-c tachometer generator has a guaranteed 8-hour drift of 0.03%. This is based upon a 1-megohm, or higher, resistance load in a constant ambient of 20 to 50 degrees centigrade. Actual charts of tachometer performance, given in the 2-hour test chart, show drift to be considerably less than this figure; see Fig. 16. Mill-operating experience has shown that under constant load conditions, the drift and wander (including tachometer generator drift), of a well-designed system will be well within ±0.02%. Many dry end sections require drift and wander performance of this level for satisfactory operation.

The a-c chopper amplifier portion of the preamplifier is not used as an integrating system but merely as a means of providing a-c amplification of the very low level input signal. By the use of a-c amplification at this point the problems associated with temperature drift of transistorized d-c amplifiers are largely eliminated.

The use of open panels with an air-conditioned control room was the result of several factors: It was possible to locate the control room so as to keep unauthorized personnel out of the room. This established, the open panels are convenient to install and to maintain, and they require a minimum control room area. Air conditioning with a closed system was desired from a corrosion standpoint for NEMA I enclosures and normal filtering does not remove the gas contaminants that have caused operating problems in so many mills. There are, of course, methods of removing such gases from the incoming air but in this case air conditioning was the preferred solution.

# Input-Output Relationships for Multisampled-Loop Systems

GEORGE G. LENDARIS
ASSOCIATE MEMBER AIEE

ELIAHU I. JURY
MEMBER AIEE

**Synopsis:** A general gain expression for a multisampled-loop sampled-data system is proposed, and an extended table of systems (Table I) to which this gain expression has been applied is presented.

THE FIRST requisite to the study of sampled-data systems is that an expression for the output as a function of the input and the system variables be found. This is not an easy matter for sampled-data systems of any degree of complexity. The methods that have generally appeared in the literature to date all require a somewhat hit-or-miss type of procedure. The equations for the output are set up, and, in general, equations containing both sampled and unsampled forms of the same variable result. The trick is then to perform analytical sampling (or starring) of one such equation, solve for the sampled variable, and finally search for the right equations in which to substitute. Unfortunately no optimum way of carrying out this procedure has yet been formulated. It would be desirable then to devise a systematic procedure for formulating the output of a sampled-data system in terms of the input and the system variables, as Mason[1,2] has done with continuous systems.

Salzer[3] has presented the technique of replacing the sampler in a sampled-data system by a signal source and defining what he calls the "cut transfer function." He applies his method to single-sampled-loop systems only; this paper will undertake to extend this technique to multiple sampled-loop systems.

This concept of replacing the sampler with a signal source enables one to liken sampled-data systems to multi-input continuous-data systems, and consequently set up the system equations in operational matrix form. Hence a systematic procedure is available for obtaining the output of sampled-data systems.

In general, however, this procedure requires the inversion of matrices, and hence involves a fair amount of computations. Therefore, instead of using this brute force algebraic method, it would be worthwhile to obtain a general expression for the gain of a multisampled-loop system using the kind of topological techniques developed by Mason for continuous systems.

A gain expression is proposed in this paper, and it is shown to work in a large number of systems. The authors have not found any counter examples to the proposed gain expression, and therefore feel that it may be general.

This paper begins by introducing Mason's theorem and proceeds to introduce Salzer's technique of replacing the sampler with a signal source. The ideas of the two methods are considered together and extended to the multisampled-

Paper 59-682, recommended by the AIEE Feedback Control Systems Committee and approved by the AIEE Technical Operations Department for presentation at the AIEE Summer and Pacific General Meeting and Air Transportation Conference, Seattle, Wash., June 21–26, 1959. Manuscript submitted October 30, 1958; made available for printing March 30, 1959.

GEORGE G. LENDARIS and ELIAHU I. JURY are with the University of California, Berkeley, Calif.

This research was supported by the U. S. Air Force through the Air Force Office of Scientific Research of the Air Research and Development Command, under contract no. *AF 18(600)-1521.*

TABLE I INPUT-OUTPUT RELATIONSHIPS FOR SAMPLED SYSTEMS

| | SYSTEM | $G'_{io}$ | $G'_{is}$ | $G'_{so}$ | $G^*_{ss}$ | C |
|---|---|---|---|---|---|---|
| 1 | 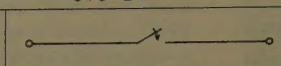 | 0 | 1 | 1 | 0 | $R^*$ |
| 2 | 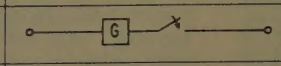 | 0 | $G$ | 1 | 0 | $\overline{RG}^*$ |
| 3 | 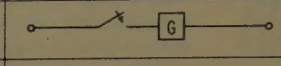 | 0 | 1 | $G$ | 0 | $R^*G$ |
| 4 | 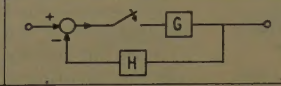 | 0 | 1 | $G$ | $-\overline{GH}^*$ | $\frac{R^*G}{1+\overline{GH}^*}$ |
| 5 | 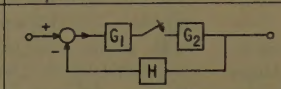 | 0 | $G_1$ | $G_2$ | $-\overline{G_2HG_1}^*$ | $\frac{\overline{RG_1}^*G_2}{1+\overline{G_1G_2H}^*}$ |
| 6 | 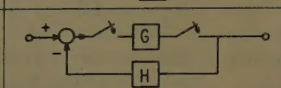 | 0 | 1 | $G^*$ | $-G^*H^*$ | $\frac{R^*G^*}{1+G^*H^*}$ |
| 7 | 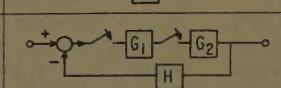 | 0 | 1 | $G_1^*G_2$ | $-G_1^*\overline{G_2H}^*$ | $\frac{R^*G_1^*G_2}{1+G_1^*\overline{G_2H}^*}$ |

| | SYSTEM | $G'_{io}$ | $G'_{is}$ | $G'_{so}$ | $G^*_{ss}$ | C |
|---|---|---|---|---|---|---|
| 8 | 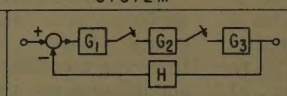 | 0 | $G_1$ | $G_2^*G_3$ | $-G_2^*\overline{G_3HG_1}^*$ | $\frac{\overline{RG_1}^*G_2^*G_3}{1+G_2^*\overline{G_1G_3H}^*}$ |
| 9 | 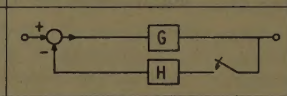 | $G$ | $G$ | $-GH$ | $-\overline{GH}^*$ | $RG-\frac{\overline{RG}^*GH}{1+\overline{GH}^*}$ |
| 10 | 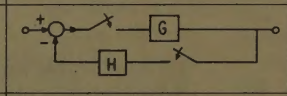 | 0 | 1 | $G$ | $-G^*H^*$ | $\frac{R^*G}{1+G^*H^*}$ |
| 11 | 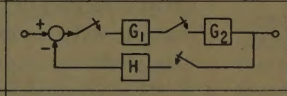 | 0 | 1 | $G_1^*G_2$ | $-G_1^*G_2^*H^*$ | $\frac{R^*G_1^*G_2}{1+G_1^*G_2^*H^*}$ |
| 12 | 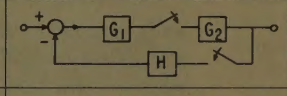 | 0 | $G_1$ | $G_2$ | $-G_2^*\overline{HG_1}^*$ | $\frac{\overline{RG_1}^*G_2}{1+G_2^*\overline{HG_1}^*}$ |
| 13 | 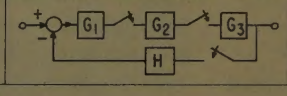 | 0 | $G_1$ | $G_2^*G_3$ | $-G_2^*G_3^*\overline{HG_1}^*$ | $\frac{\overline{RG_1}^*G_2^*G_3}{1+G_2^*G_3^*\overline{HG_1}^*}$ |

| | SYSTEM | $G'_{io}$ | $G'_{is}$ | $G'_{so}$ | $G^*_{ss}$ | C |
|---|---|---|---|---|---|---|
| 14 | 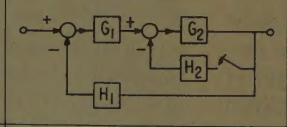 | $G_1A$<br>$A=\frac{G_2}{1+H_1G_1G_2}$ | $G_1A$ | $-H_2A$ | $-\overline{H_2A}^*$ | $RG_1A-\frac{\overline{RG_1A}^*H_2A}{1+\overline{H_2A}^*}$ |
| 15 | 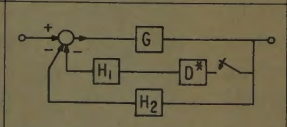 | $\frac{G}{1+GH_2}=B$ | $B$ | $-D^*H_1B$ | $-D^*\overline{H_1B}^*$ | $RB-\frac{\overline{RB}^*D^*H_1B}{1+D^*\overline{H_1B}^*}$ |
| 16 | 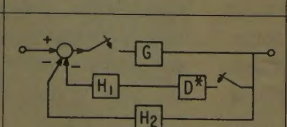 | 0 | 1 | $G$ | $-G^*D^*H_1^*-\overline{GH_2}^*$ | $\frac{R^*G}{1+\overline{GH_2}^*+G^*D^*H_1^*}$ |
| 17 | 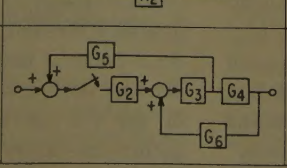 | 0 | 1 | $G_4E$<br>$E=\frac{G_2G_3}{1-G_3G_4G_6}$ | $\overline{G_5E}^*$ | $\frac{R^*G_4E}{1-\overline{G_5E}^*}$ |

Table I (cont.)

| | SYSTEM | $G'_{i0}$ | $G'_{is}$ | $G'_{s0}$ | $G^*_{ss}$ | C |
|---|---|---|---|---|---|---|
| 18 | 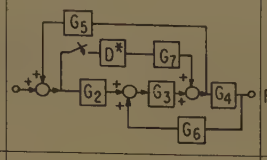 | $G_2G_3G_4F$ <br> $F=\frac{1}{1-G_2G_3G_5G_3G_4G_6}$ | $(1-G_3G_4G_6)F$ | $D^*G_7G_4F$ | $D^*\overline{G_7G_5F}^*$ | $RG_2G_3G_4F+\frac{\overline{R(1-G_3G_4G_6)F}^*D^*G_7G_4F}{1-D^*\overline{G_7G_5F}^*}$ |
| 19 | 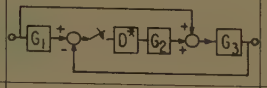 | $G_3$ | $(G_1-G_3)$ | $D^*G_2G_3$ | $-D^*\overline{G_2G_3}^*$ | $RG_3+\frac{\overline{R(G_1-G_3)}^*D^*G_2G_3}{1+D^*\overline{G_2G_3}^*}$ |
| 20 | 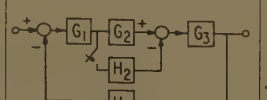 | $G_1G_2G_3J$ <br> $J=\frac{1}{1+H_1G_1G_2G_3}$ | $G_1J$ | $-H_2G_3J$ | $+\overline{H_2G_3H_1G_1J}^*$ | $RG_1G_2G_3J-\frac{\overline{RJG_1}^*H_2G_3J}{1-\overline{H_1H_2G_1G_3J}^*}$ |
| 21 | 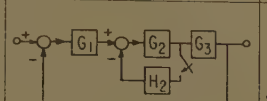 | $G_1G_2G_3J$ <br> $J=\frac{1}{1+H_1G_1G_2G_3}$ | $G_1G_2J$ | $-H_2G_2G_3J$ | $-\overline{H_2G_2J}^*$ | $RG_1G_2G_3J-\frac{\overline{RG_1G_2J}^*H_2G_2G_3J}{1+\overline{H_2G_2J}^*}$ |

| | SYSTEM | $G'_{i0}$ | $G'_{is_1}$ | $G'_{s_1 0}$ | $G^*_{s_1 s_1}$ | $G'_{is_2}$ | $G'_{s_2 0}$ | $G^*_{s_2 s_2}$ | $G^*_{s_1 s_2}$ | $G^*_{s_2 s_1}$ | C |
|---|---|---|---|---|---|---|---|---|---|---|---|
| 22 | 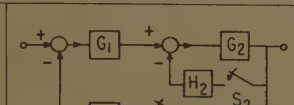 | $G_1G_2$ | $G_1G_2$ | $-H_1G_1G_2$ | $-\overline{H_1G_1G_2}^*$ | $G_1G_2$ | $-H_2G_2$ | $-\overline{H_2G_2}^*$ | $-\overline{H_1G_1G_2}^*$ | $-\overline{H_2G_2}^*$ | $RG_1G_2-\frac{\overline{RG_1G_2}^*H_1G_1G_2+\overline{RG_1G_2}^*H_2G_2}{1+\overline{G_1G_2H_1}^*+\overline{G_2H_2}^*}$ |
| 23 | 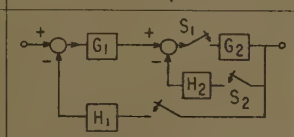 | 0 | $G_1$ | $G_2$ | $-G_2^*\overline{H_1G_1}^*$ | 0 | $H_2^*G_2$ | $-H_2^*G_2^*$ | $G_2^*$ | $H_2^*G_2^*\overline{H_1G_1}^*$ | $\frac{\overline{RG_1}^*G_2}{1+G_2^*\overline{G_1H_1}^*+G_2^*H_2^*}$ |
| 24 | 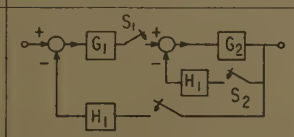 | 0 | $G_1$ | $G_2$ | $-G_2^*\overline{H_1G_1}^*$ | 0 | $-H_2G_2$ | $-\overline{H_2G_2}^*$ | $G_2^*$ | $\overline{H_2G_2}^*\overline{H_1G_1}^*$ | $\frac{\overline{RG_1}^*(G_2+\overline{H_2G_2}^*G_2-G_2^*H_2G_2)}{1+G_2^*\overline{G_1H_1}^*+\overline{G_2H_2}^*}$ |
| 25 | 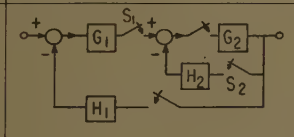 | 0 | $G_1$ | $G_2$ | $-G_2^*\overline{H_1G_1}^*$ | 0 | $H_2^*G_2$ | $-G_2^*H_2^*$ | $G_2^*$ | $H_2^*G_2^*\overline{H_1G_1}^*$ | $\frac{\overline{RG_1}^*G_2}{1+G_2^*\overline{G_1H_1}^*+G_2^*H_2^*}$ |

| | SYSTEM | $G'_{i0}$ | $G'_{is_1}$ | $G'_{s_1 0}$ | $G^*_{s_1 s_1}$ | $G'_{is_2}$ | $G'_{s_2 0}$ | $G^*_{s_2 s_2}$ | $G^*_{s_1 s_2}$ | $G^*_{s_2 s_1}$ | C |
|---|---|---|---|---|---|---|---|---|---|---|---|
| 26 | 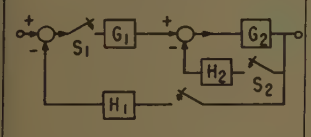 | 0 | 1 | $G_1G_2$ | $-\overline{G_1G_2}^*H_1^*$ | 0 | $-H_2G_2$ | $-\overline{H_2G_2}^*$ | $\overline{G_1G_2}^*$ | $\overline{H_2G_2}^*H_1^*$ | $\frac{\overline{R}^*(G_1G_2+\overline{H_2G_2}^*G_1G_2-\overline{G_1G_2}^*H_2G_2)}{1+\overline{G_1G_2}^*H_1^*+\overline{G_2H_2}^*}$ |
| 27 | 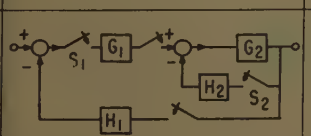 | 0 | 1 | $G_1^*G_2$ | $-G_1^*G_2^*H_1^*$ | 0 | $-H_2G_2$ | $-\overline{H_2G_2}^*$ | $G_1^*G_2^*$ | $\overline{H_2G_2}^*H_1^*$ | $\frac{R^*G_1^*(G_2+\overline{H_2G_2}^*G_2-G_2^*H_2G_2)}{1+G_1^*G_2^*H_1^*+\overline{G_2H_2}^*}$ |
| 28 | 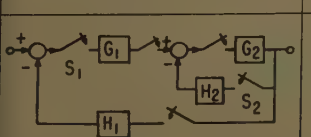 | 0 | 1 | $G_1^*G_2$ | $-G_1^*G_2^*H_1^*$ | 0 | $H_2^*G_2$ | $-H_2^*G_2^*$ | $G_1^*G_2^*$ | $H_2^*G_2^*H_1^*$ | $\frac{R^*G_1^*G_2}{1+G_1^*G_2^*H_1^*+G_2^*H_2^*}$ |
| 29 | 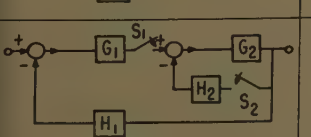 | 0 | $G_1$ | $G_2$ | $-\overline{G_2H_1G_1}^*$ | 0 | $-H_2G_2$ | $-\overline{H_2G_2}^*$ | $G_2^*$ | $\overline{H_2G_2H_1G_1}^*$ | $\frac{\overline{RG_1}^*(G_2+\overline{H_2G_2}^*G_2-G_2^*H_2G_2)}{1+\overline{G_1G_2H_1}^*+\overline{G_2H_2}^*+\overline{H_2G_2}^*\overline{G_2H_1G_1}^*-G_2^*H_2G_2H_1G_1^*}$ |

Table I (cont.)

| | SYSTEM | $G'_{i0}$ | $G'_{is_1}$ | $G'_{s_1 0}$ | $G^*_{s_1 s_1}$ | $G'_{is_2}$ | $G'_{s_2 0}$ | $G^*_{s_2 s_2}$ | $G^*_{s_1 s_2}$ | $G^*_{s_2 s_1}$ | C |
|---|---|---|---|---|---|---|---|---|---|---|---|
| 30 | 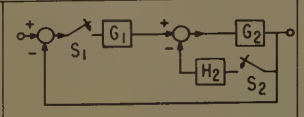 | 0 | 1 | $G_1G_2$ | $-\overline{G_1G_2}^*$ | 0 | $-H_2G_2$ | $-\overline{H_2G_2}^*$ | $\overline{G_1G_2}^*$ | $\overline{H_2G_2}^*$ | $\dfrac{R^*(G_1G_2+\overline{H_2G_2}^*G_1G_2-\overline{G_1G_2}^*H_2G_2)}{1+\overline{G_1G_2}^*+\overline{G_2H_2}^*}$ |
| 31 | 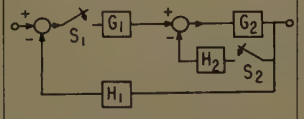 | 0 | 1 | $G_1G_2$ | $-\overline{G_1G_2H_1}^*$ | 0 | $-H_2G_2$ | $-\overline{H_2G_2}^*$ | $\overline{G_1G_2}^*$ | $\overline{H_2G_2H_1}^*$ | $\dfrac{R^*(G_1G_2+\overline{H_2G_2}^*G_1G_2-\overline{G_1G_2}^*H_2G_2)}{1+\overline{G_1G_2H_1}^*+\overline{G_2H_2}^*+\overline{G_1G_2H_1}^*\,\overline{H_2G_2}^*-\overline{G_1G_2}^*\overline{H_2G_2H_1}^*}$ |
| 32 | 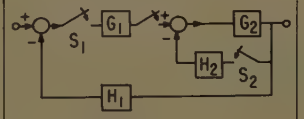 | 0 | 1 | $G_1^*G_2$ | $-G_1^*\overline{G_2H_1}^*$ | 0 | $-H_2G_2$ | $-\overline{H_2G_2}^*$ | $G_1^*G_2^*$ | $\overline{H_2G_2H_1}^*$ | $\dfrac{R^*G_1^*(G_2+\overline{H_2G_2}^*G_2-G_2^*H_2G_2)}{1+G_1^*\overline{G_2H_1}^*+\overline{H_2G_2}^*+G_1^*\overline{G_2H_1}^*\;\overline{H_2G_2}^*-G_1^*G_2^*\overline{H_2G_2H_1}^*}$ |
| 33 | 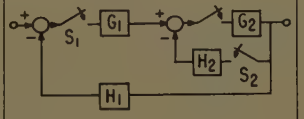 | 0 | 1 | $G_1^*G_2$ | $-G_1^*\overline{G_2H_1}^*$ | 0 | $H_2^*G_2$ | $-H_2^*G_2^*$ | $G_1^*G_2^*$ | $H_2^*\overline{G_2H_1}^*$ | $\dfrac{R^*G_1^*G_2}{1+G_1^*\overline{G_2H_1}^*+G_2^*H_2^*}$ |

| | SYSTEM | $G'_{i0}$ | $G'_{is_1}$ | $G'_{s_1 0}$ | $G^*_{s_1 s_1}$ | $G'_{is_2}$ | $G'_{s_2 0}$ | $G^*_{s_2 s_2}$ | $G^*_{s_1 s_2}$ | $G^*_{s_2 s_1}$ | C |
|---|---|---|---|---|---|---|---|---|---|---|---|
| 34 | 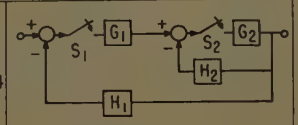 | 0 | 1 | $G_1^*G_2$ | $-G_1^*\overline{G_2H_1}^*$ | 0 | $G_2$ | $-\overline{G_2H_2}^*$ | $G_1^*\overline{G_2H_1}^*$ | $\overline{G_2H_1}^*$ | $\dfrac{R^*G_1^*G_2}{1+G_1^*\overline{G_2H_1}^*+\overline{G_2H_2}^*}$ |
| 35 | 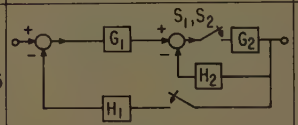 | 0 | $G_1$ | $G_2$ | $G_2^*\overline{G_1H_1}^*$ | 0 | $G_2$ | $\overline{G_2H_2}^*$ | $\overline{G_2H_2}^*$ | $G_2^*\overline{H_1G_1}^*$ | $\dfrac{\overline{RG_1^*}G_2}{1+\overline{G_2H_2}^*+G_2^*\overline{H_1G_1}^*}$ |
| 36 | 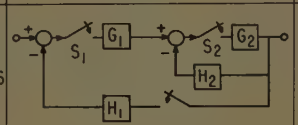 | 0 | 1 | $G_1^*G_2$ | $-G_1^*G_2^*H_1^*$ | 0 | $G_2$ | $-\overline{G_2H_2}^*$ | $G_1^*\overline{G_2H_2}^*$ | $G_2^*H_1^*$ | $\dfrac{R^*G_1^*G_2}{1+G_1^*G_2^*H_1^*+\overline{G_2H_2}^*}$ |

| | SYSTEM | $G'_{i0}$ | $G'_{is_1}$ | $G'_{s_1 0}$ | $G^*_{s_1 s_1}$ | $G'_{is_2}$ | $G'_{s_2 0}$ | $G^*_{s_2 s_2}$ | $G^*_{s_1 s_2}$ | $G^*_{s_2 s_1}$ | C |
|---|---|---|---|---|---|---|---|---|---|---|---|
| 37 | 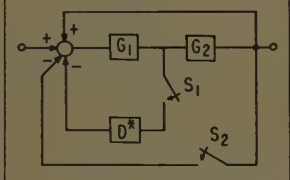 | $G_2L$<br>$L=\dfrac{G_1}{1+G_1G_2}$ | L | $-D^*G_2L$ | $-D^*L^*$ | $G_2L$ | $-G_2L$ | $-\overline{G_2L}^*$ | $-D^*\overline{G_2L}^*$ | $-L^*$ | $RG_2L-\dfrac{\overline{RL}^*D^*G_2L+\overline{RG_2L}^*G_2L}{1+D^*L^*+\overline{G_2L}^*}$ |
| 38 | 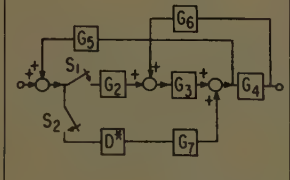 | 0 | 1 | $G_2G_3G_4M$<br>$M=\dfrac{1}{1-G_3G_4G_6}$ | $\overline{G_2G_3G_5M}^*$ | 1 | $D^*G_7G_4M$ | $D^*\overline{G_7G_5M}^*$ | $\overline{G_2G_3G_5M}^*$ | $D^*\overline{G_7G_5M}^*$ | $\dfrac{R^*G_2G_3G_4M+R^*D^*G_7G_4M}{1-\overline{G_2G_3G_5M}^*-D^*\overline{G_7G_5M}^*}$ |

loop case. From these later considerations the proposed general expression is derived. A list of rules for applying the gain expression and a table of systems to which the expression has been applied are then given.

## Single-Sampled-Loop Systems

An important background to the derivation of the desired gain expression is the method of one-step reductions of continuous-data linear systems as established by Mason. Mason has shown, for continuous systems, that the transfer gain between two nodes can be determined by inspection for any multiple-loop system from its signal-flow graph. This property is expressed in the following theorem: The

Table I (cont.)

| | SYSTEM | $G'_{i0}$ | $G'_{is_1}$ | $G'_{s_1 0}$ | $G^*_{s_1 s_1}$ | $G'_{is_2}$ | $G'_{s_2 0}$ | $G^*_{s_2 s_2}$ | $G'_{is_3}$ | $G'_{s_3 0}$ | $G^*_{s_3 s_3}$ | $G^*_{s_1 s_2}$ | $G^*_{s_2 s_3}$ | $G^*_{s_3 s_1}$ | C |
|---|---|---|---|---|---|---|---|---|---|---|---|---|---|---|---|
| 39 | 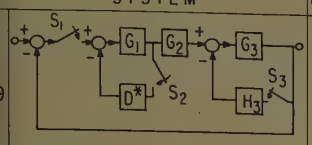 | 0 | 1 | $G_1G_2G_3$ | $-\overline{G_1G_2G_3}^*$ | 0 | $-D^*G_1G_2G_3$ | $-D^*\overline{G_1}^*$ | 0 | $-H_3G_3$ | $-\overline{H_3G_3}^*$ | $\overline{G_1}^*$ | $D^*\overline{G_1G_2G_3}^*$ | $\overline{H_3G_3}^*$ | $\dfrac{R^*G_1G_2G_3(1+\overline{H_3G_3}^*)-R^*\overline{G_1G_2G_3}^*H_3G_3}{1+\overline{G_1G_2G_3}^*+G_1^*D^*+\overline{G_3H_3}^*+D^*G_1^*\overline{H_3G_3}^*}$ |
| 40 | 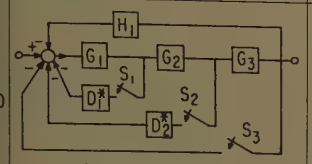 $L_1=\dfrac{G_1}{1+G_1G_2G_3H_1}$ $L_2=\dfrac{G_1G_2}{1+G_1G_2G_3H_1}$ $L_3=\dfrac{G_1G_2G_3}{1+G_1G_2G_3H_1}$ | $L_3$ | $L_1$ | $-D_1^*L_3$ | $-D_1^*L_1^*$ | $L_2$ | $-D_2^*L_3$ | $-D_2^*L_2^*$ | $L_3$ | $-L_3$ | $-L_3^*$ | $-D_1^*L_2^*$ | $-D_2^*L_3^*$ | $-L_1^*$ | $RL_3-\dfrac{\overline{RL_1}^*D_1^*L_3+\overline{RL_2}^*D_2^*L_3+\overline{RL_3}^*L_3}{1+L_1^*D_1^*+L_2^*D_2^*+L_3^*}$ |

41

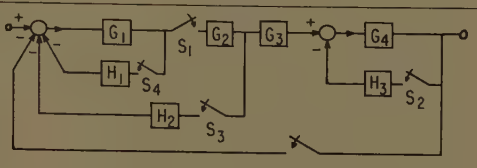

$G'_{i0}=0$ $\quad G^*_{s_1s_2}=\overline{G_2G_3G_4}^*$ $\quad G^*_{s_2s_3}=\overline{H_3G_4}^*G_1^*G_2^*$ $\quad G^*_{s_3s_4}=-\overline{H_2G_1}^*$ $\quad G^*_{s_4s_1}=-\overline{H_1G_1}^*$

$G'_{is_1}=G_1$ $\quad G'_{is_2}=0$ $\quad G'_{is_3}=0$ $\quad G'_{is_4}=G_1$

$G'_{s_10}=G_2G_3G_4$ $\quad G'_{s_20}=-H_3G_4$ $\quad G'_{s_30}=0$ $\quad G'_{s_40}=0$

$G^*_{s_1s_1}=\overline{G_2G_3G_4}^*G_1^*$ $\quad G^*_{s_2s_2}=-\overline{H_3G_4}^*$ $\quad G^*_{s_3s_3}=-\overline{H_2G_1}^*G_2^*$ $\quad G^*_{s_4s_4}=-\overline{H_1G_1}^*$

$$C=\frac{\overline{RG_1}^*G_2G_3G_4(1+\overline{H_3G_4}^*)-\overline{RG_1}^*\,\overline{G_2G_3G_4}^*H_3G_4}{1+G_1^*\overline{G_2G_3G_4}^*+\overline{H_3G_4}^*+G_2^*\overline{H_2G_1}^*+\overline{H_1G_1}^*+\overline{H_3G_4}^*\overline{H_2G_1}^*G_2^*+\overline{H_3G_4}^*\,\overline{H_1G_1}^*}$$

NOTE: The corrections indicated by Dr. Salzer in his discussion have been incorporated in the table.

ransfer gain between any two nodes of a ystem is equal to a quotient whose enominator is equal to: one minus the um of the loop gains taken one at a time, lus the sum of the products of the loop ains taken two at a time for all loops that o not touch (have common branch or ode), minus the sum of the products of he loop gains taken three at a time r all loops that do not touch, and so n. The numerator of the quotient is ual to the sum of the forward path gains here each of these terms is multiplied by factor made up of the number *1* and all gned loop gains and products of loop ains that appear in the denominator and o not touch any node or branch found in he forward path.

In this theorem, a feedback loop is a ntinuous succession of branches, tra- rsed in the indicated branch direction, hich forms a closed cycle along which ch node is encountered once per cycle. he loop gain of a feedback loop is equal the product of the gains of the branches rming the loop. A forward path is a ntinuous succession of branches, tra- rsed in the indicated branch direction from the input node to the output node, along which no node is encountered more than once. The forward path gain is equal to the product of the branch gains along the forward path.

The theorem will be illustrated by calculating the gain of the multiple-loop system shown in Fig. 1. The system has three feedback loops with gains *bc*, *fg*, and *fibj* respectively, and four forward paths with gains *abd*, *efh*, *abjfh*, and *efibd* respectively. Two of the feedback loops (*bc* and *fg*) do not touch. By direct application of the theorem the gain (transfer function) is equal to:

$$C=\frac{abd(1-fg)+efh(1-bc)+abjfh+efibd}{1-bc-fg-fibj+bcfg} \qquad (1)$$

It is thus apparent that the direct reduction of even the most complex systems is possible by Mason's method. If this were a sampled-data system in which the signal in each branch were sampled, then all the transfer functions would be sampled-data transfer functions (discrete filters), and all node variables would be sampled functions. The identical procedure just described would constitute a valid one-step reduction, except the notation could be changed by putting an asterisk after every letter in equation 1 and by showing a sampler at the end of each branch in Fig. 1.

The situation is quite different when the system contains both sampled data and continuous data, as would be the case if a sampler were inserted at the beginning of branch *a*, for example. It turns out that the reduction process as discussed could not be directly represented by a transfer function. The problem being that in passing through the sampler in branch *a* the operation is not a multiplication in the frequency domain; rather a summation.

For this reason, one is led toward searching for a technique to handle the sampler. It is at this point that Salzer introduced an artificial signal source in place of the sampler as an aid to analyzing these systems.

To introduce the use of the artificial source, consider the system of Fig. 2. (In this paper it will suffice to show that this artifice works. For a more complete

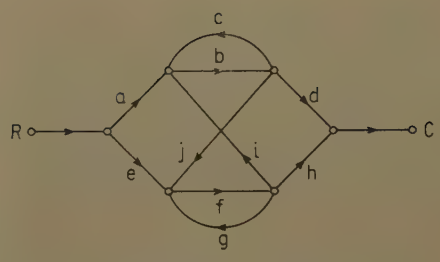


Fig. 1. Flow graph of a multiloop continuous-feedback system

discussion, see reference 3.) If the sampler is opened and a source inserted, call it $S^*$, and if the transfer functions from input to output, input to sampler, and sampler to output with the sampler open are denoted with a primed notation, then the system output will be given by:

$$C=RG_{io}'+S^*G_{so}' \tag{2}$$

where $G_{io}'$ is the transfer function from the input to the output with the sampler open, and $G_{so}'$ is the transfer function from the sampler to the output with the sampler open. If the system had more loops with samplers, then the output would be given by:

$$C=RG_{io}'+S_1^*G_{s_1o}'+S_2^*G_{s_2o}'+\ldots+S_n^*G_{s_no}' \tag{3}$$

where the prime means that all the samplers are open (except as noted later) when obtaining the given cut-transfer function.

The source $S^*$ is restricted to be equal to the sampled form of the signal entering the sampler.

The signal appearing at the input to the sampler is:

$$S=RG_{is}'+S^*G_{ss}^* \tag{4}$$

where $G^*_{ss}$ is the transfer function from the output side of the sampler around the loop to the input side of the sampler with the sampler open (and if there were other samplers in the system, they would also be open, except as noted later).

Starring equation 4 the following is obtained:

$$S^*=\overline{RG_{is}'^*}+S^*G_{ss}^* \tag{5}$$

$$S^*=\frac{\overline{RG_{is}'^*}}{1-G_{ss}^*} \tag{6}$$

Substituting equation 6 into equation 2:

$$C=RG_{io}'+\frac{(RG_{is}')^*}{1-G_{ss}^*}G_{so}' \tag{7}$$

Thus a general expression for the output of a one-sampler sampled-data system has been derived. (The discussion to this point has followed closely that of Salzer in reference 3.)

We have at this point managed to 1. bypass the problem presented by the sampler, and 2. find a means by which

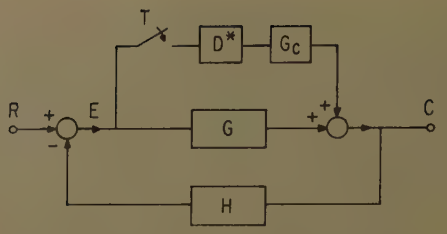


Fig. 2. Single-sampled-loop sampled-data feedback system. D indicates discrete filter (input and output sampled); asterisk replaces sampler that would ordinarily follow box

Mason's methods can be used to find input-output relationships for sampled-data systems.

As an example of this, consider more precisely the system of Fig. 2.

An expression for the output in terms of the input and the system parameters is desired.

First, apply the formula derived for a one-sampler system. One can write the terms of the formula by inspection via Mason's theorem cited earlier:

$$G_{io}'=\frac{G}{1+GH};\quad G_{is}'=\frac{1}{1+GH};\quad G_{so}'=\frac{D^*G_c}{1+GH}$$

$$G_{ss}^*=-D^*\left(\frac{G_cH}{1+GH}\right)^* \tag{8}$$

Then substituting these terms into equation 7:

$$C=\frac{RC}{1+GH}+\frac{\left(\frac{R}{1+GH}\right)^*}{1+D^*\left(\frac{G_cH}{1+GH}\right)^*}D^*\frac{G_c}{1+GH} \tag{9}$$

Now, for comparison purposes, try to find the output of this system by ordinary algebraic manipulations. The mathematics proceeds as follows:

$$C=EG+E^*D^*G_c \tag{10}$$

$$E=R-CH \tag{11}$$

$$C=RG-CHG+E^*D^*G_c \tag{12}$$

$$C(1+GH)=RG+E^*D^*G_c \tag{13}$$

$$C=\frac{RG}{1+GH}+E^*\frac{D^*G_c}{1+GH} \tag{14}$$

$$E=R-EGH-E^*D^*G_cH \tag{15}$$

$$E(1+GH)=R-E^*D^*G_cH \tag{16}$$

$$E=\frac{R}{1+GH}-E^*D^*\frac{G_cH}{1+GH} \tag{17}$$

$$E^*=\left(\frac{R}{1+GH}\right)^*-E^*D^*\left(\frac{G_cH}{1+GH}\right)^* \tag{18}$$

$$E^*=\frac{\left(\frac{R}{1+GH}\right)^*}{1+D^*\left(\frac{G_cH}{1+GH}\right)^*} \tag{19}$$

And finally, from equation 14 the output is obtained:

$$C=\frac{RG}{1+GH}+\frac{\left(\frac{R}{1+GH}\right)^*}{1+D^*\left(\frac{G_cH}{1+GH}\right)^*}D^*\frac{G_c}{1+GH} \tag{20}$$

It is thus quite apparent that even for this simple system the technique using the formula gives a much more direct answer than does the technique using the algebraic equations. In addition, due to its systematic nature, the formula method is considerably less susceptible to errors.

It will suffice now to say that the method works, and that the answers are obtained in a very straightforward systematic manner. The desired end now is to generalize this method to systems with many sampled loops.

## Multisampled-Loop Systems

The extension of this method to multi-sampled-loop sampled-data systems will be derived along heuristic lines. Following this, some rules will be given, then some examples will be demonstrated. (For a more complete presentation of this subject see the authors' closure.)

In comparing the derivation of the general equations given by Mason for continuous systems, and the derivation of equation 7, it is noted that much similarity exists. By logical inference then, one could investigate the nature of these similarities and make some appropriate extensions.

It has been mentioned before that the output of a system with samplers in $n$ loops is given by the following expression (equation 3):

$$C=RG_{io}'+S_1^*G_{s_1o}'+S_2^*G_{s_2o}'+\ldots+S_n^*G_{s_no}' \tag{3}$$

The only terms of this expression that have not been defined are the terms $S_n^*$. This is the quantity that represents the

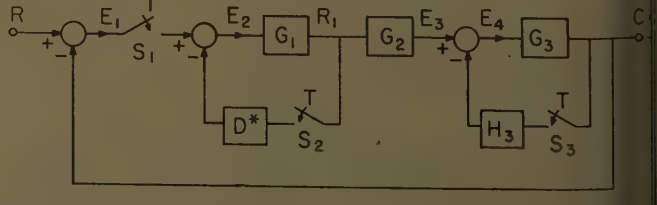


Fig. 3. Multisampled-loop sampled-data feedback system

ave source. This source is obviously ependent upon the input ($R$) to the sys-m; therefore, it is expected that an ex-ression defining $S_n^*$ would contain a rm relating the input and the trans-rence from the input to the switch, nce a term $RG'_{is_n}$. The next question how is this term further modified? At is point compare the derivation of equa-on 6 with those of Mason, and by ex-nsion it can be said that the new equa-on should contain a denominator which ould be made up of: one minus the sum the gains of the sampled loops in the stem, plus the sum of the product of all e gains of the sampled loops, taken two a time, that do not touch each other, c.

Now all that is left is to define the rm sampled-loop gain; this is taken care very nicely by the term already de-ned as $G^*_{s_ns_n}$. In addition to the rms derived by analogy via Mason's uation, it turns out that for these sys-ms another term is required in the nominator: the product of the self-rms less the product of the cross-terms. hat is, the product of the $G^*_{s_ns_n}$ terms, ss the product $G^*_{s_1s_2}G^*_{s_2s_3}G^*_{s_3s_4}\ldots G^*_{s_ns_1}$. Hence, a general expression for the out-ut of a multisampled-loop sampled-data stem with $n$ sampled loops may be

$$=RG_{io}'+S_1^*G_{s_1o}'+S_2^*G_{s_2o}'+\ldots+S_n^*G_{s_no}' \quad (21)$$

here

$$^*=\frac{\overline{RG_{is_n}^*}}{1-\sum_{k=1}^{n}G_{s_ks_k}^*+\sum P_2-\sum P_3+\ldots+\prod_{k=1}^{n}G_{s_ks_k}^*-G_{s_1s_2}^*G_{s_2s_3}^*\ldots G_{s_ns_1}^*}$$

here

$\sum P_2$ = product of loop gains taken two at a time that do not touch each other

$\sum P_3$ = product of loop gains taken three at a time that do not touch each other

This equation then should give the out-ut of any sampled-data system in terms the input and the system parameters. pply this equation to a multisampled-op system and again compare the two chniques for finding the output.

Consider Fig. 3. Again the component rms of the formula can be obtained by spection. Note that the system con-ins three sampled loops, two of which o not touch. Therefore, the equation r the slave source will contain an extra oduct term in the denominator. The rms are as follows:

$$G_{io}'=0 \quad G_{s_1s_2}^*=G_1^* \quad G_{s_2s_3}^*=-D^*\overline{G_1G_2G_3^*} \quad G_{s_3s_1}^*=\overline{H_3G_3^*}$$

$$G_{is_1}'=1 \quad G_{is_2}'=0 \quad G_{is_3}'=0$$

$$G_{s_1o}'=G_1G_2G_3 \quad G_{s_2o}'=-D^*G_1G_2G_3 \quad G_{s_3o}'=-H_3G_3$$

$$G_{s_1s_1}^*=-\overline{G_1G_2G_3^*} \quad G_{s_2s_2}^*=-D^*G_1^* \quad G_{s_3s_3}^*=-\overline{H_3G_3^*} \quad (22)$$

The equation for the output follows directly as:

$$C=\frac{R^*G_1G_2G_3(1+\overline{H_3G_3^*})+R^*\overline{G_1G_2G_3^*}H_3G_3}{1+\overline{G_1G_2G_3^*}+G_1^*D^*+\overline{G_3H_3^*}+D^*G_1^*\overline{H_3G_3^*}} \quad (23)$$

and

$$C^*=\frac{R^*\overline{G_1G_2G_3^*}}{1+\overline{G_1G_2G_3^*}+G_1^*D^*+\overline{G_3H_3^*}+D^*G_1^*\overline{H_3G_3^*}} \quad (24)$$

Now find the same relationship using standard algebraic techniques. The calculations proceed as follows:

$$C=E_3G_3-C^*H_3G_3 \quad (25)$$

$$=R_1G_2G_3-C^*H_3G_3 \quad (26)$$

$$=E_2G_1G_2G_3-C^*H_3G_3 \quad (27)$$

$$R_1=E_1^*G_1-R_1^*D^*G_1 \quad (28)$$

$$R_1^*=E_1^*G_1^*-R_1^*D^*G_1^* \quad (29)$$

$$R_1^*=\frac{E_1^*G_1^*}{1+D^*G_1^*} \quad (30)$$

$$C=E_1^*G_1G_2G_3-R_1^*D^*G_1G_2G_3-C^*H_3G_3 \quad (31)$$

Let

$$A\triangleq G_1G_2G_3,\ B^*\triangleq G_1^*D^* \quad (32)$$

then

$$C=E_1^*A-\frac{E_1^*B^*}{1+B^*}A-C^*H_3G_3 \quad (33)$$

since

$$E_1^*=R^*-C^* \quad (34)$$

$$C=R^*A-C^*A-R^*A\frac{B^*}{1+B^*}+C^*\frac{B^*}{1+B_*}-C^*H_3G_3 \quad (35)$$

$$C^*=\frac{R^*\left(A^*-A^*\frac{B^*}{1+B^*}\right)}{1+A^*-A^*\frac{B^*}{1+B^*}+\overline{H_3G_3^*}}=\frac{R^*\left(\frac{A^*}{1+B^*}\right)}{1+\frac{A^*}{1+B^*}+\overline{H_3G_3^*}} \quad (36)$$

$$C^*=\frac{R^*A^*}{1+B^*+A^*+\overline{H_3G_3^*}+\overline{BH_3G_3^*}} \quad (37)$$

and finally,

$$C^*=\frac{R^*\overline{G_1G_2G_3^*}}{1+G_1^*D^*+\overline{G_1G_2G_3^*}+\overline{H_3G_3^*}+G_1^*D^*\overline{H_3G_3^*}} \quad (38)$$

The expression for $C$ is obtained by substituting equation 38 into equation 35. The computations are lengthy and will not be included, but the answer is the same as in equation 23.

It is again apparent that the formula gives a much more direct, straightforward solution to the problem The use of the formula minimizes (in general) the time required to find a solution of this type; however, and more important, due to its systematic nature, it minimizes the chance of error involved in finding the solution.

A few rules will now be given for applying this formula to sampled-data systems.

1. $n$ is equal to the number of separate loops with samplers in them.

2. If a sampler immediately follows a summing junction other than the first, always move it back through the summer before numbering samplers and evaluating the system gains.

3. When evaluating a particular loop gain (primed or starred functions) if the loop has more than one sampler in it, replace the box(es) between each set of samplers with a starred function, and delete the latter sampler(s).

4. When evaluating the cut transfer functions (primed functions) and the $G_{s_ns_n}^*$ terms, consider all the samplers not in the loop as being open, and use Mason's rule and rule *3* for finding the transmission of the rest of the system.

5. When numbering the samplers, the following must be observed: (*a*). count only the first sampler in each loop; and (*b*). the order of numbering must be such that when evaluating the expression $G_{s_1s_2}^*G_{s_2s_3}^*\ldots G_{s_ns_1}^*$ there are the same number of starred terms as appear in the expression $\prod_{k=1}^{n}G_{s_ks_k}^*$. (Usually, if a cyclic order of numbering is observed, starting from the major loop around to all the minor loops, this condition is fulfilled.)

Table I showing sampled-data systems analyzed by this method is given for ready reference of the input-output relationships of the given systems and to assist in using this formulation.

The last column in the table is described only by $C$. The user can do any of three things with this expression: 1. he can consider both sides of the equation as functions of $s$ and thus will have the Laplace transform of the output; 2. he can take the $z$-transform of both sides of the equation and thus have the output of the system at sampling instants only; and 3.

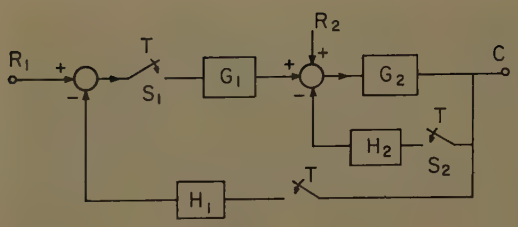


Fig. 4 (left). Multi-input multisampled-loop sampled-data feedback system

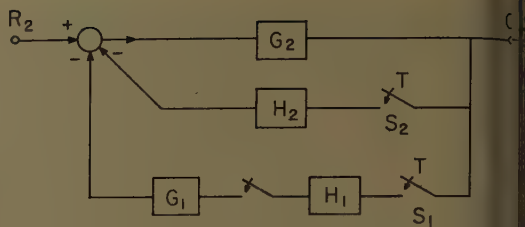


Fig. 5 (right). Fig. 4 considered for $R_2$ input only

take the modified $z$-transform of both sides of the equation, and have the continuous output of the system in terms of the $z$-transform.

All the samplers in the tabled systems are assumed to be in synchronism.

## Multiple-Input Systems

This method can easily be extended to multiple-input multiple-sampled-loop sampled-data systems. Since the sampled-data system can be considered as linear (at sampling instants), multiple inputs can be considered as in the continuous case; that is, each input can be considered independently, and by superposition the output can be obtained by adding the components due to each input. For multiple-input multiple-sampled-loop sampled-data systems, one has only; to find the output for each input as described earlier and then add the components to find the total output.

Consider for example, the system of Fig. 4.

The output of this system is desired. By superposition, the output $C$ is the sum of the responses to the two inputs, $R_1$ and $R_2$. Considering the system for just $R_1$, it is noted that the system is the same as no. *26* in Table I. Therefore

$$C_1=\frac{R_1^*(G_1G_2+\overline{H_2G_2}^*G_1G_2-\overline{G_1G_2}^*H_2G_2)}{1+\overline{G_1G_2}^*H_1^*+\overline{G_2H_2}^*} \tag{39}$$

Considering the output due to $R_2$, the system becomes as shown in Fig. 5.

This system is readily solved by comparing it to system *16* in the table. The only term that changes is $G_{ss}^*$, and it becomes instead $G^*D^*H_1^*-G^*H^*_{20}$. With the proper substitutions the output is given by:

$$C_2=\frac{R_2^*G_2}{1+G_2^*H_2^*+G_2^*G_1^*H_1^*} \tag{40}$$

Then the total solution becomes:

$$C=C_1+C_2$$
$$=\frac{R_1^*(G_2G_2+\overline{H_2G_2}^*G_1G_2-\overline{G_1G_2}^*H_2G_2)}{1+\overline{G_1G_2}^*H_1^*+\overline{G_2H_2}^*}+\frac{R_2^*G_2}{1+G_1^*G_2^*H_1^*+G_2^*H_2^*} \tag{41}$$

Again it is noted that a quick solution is available using the method herein introduced.

## Conclusions

In this paper, an expression giving the output of a multisampled-loop sampled-data system has been heuristically derived. The equation works for all systems of the nature introduced in this paper, and the authors feel that there may not be any difficulties in applying the equation to any linear sampled-data system with all the samplers in synchronism. However, the authors would like to suggest as an area of study that a formal derivation of this expression be found, or at least the derivatiou of an explicit definition of the class of systems for which this formulation will work if it is not absolutely general.

## References


1. Feedback Theory—Some Properties o Signal Flow Graphs, S. J. Mason. *Proceeding* Institute of Radio Engineers, New York, N. Y vol. 41, Sept. 1953, pp. 1144–56.

2. Feedback Theory—Further Properties o Signal Flow Graphs, S. J. Mason. *Ibid.*, vo 44, July 1956, pp. 920–26.

3. Signal Flow Reductions in Sampled-Dat Systems, J. M. Salzer. *Wescon Conventio Record*, Institute of Radio Engineers, pt. 4, 195 pp. 166–70.

4. Extension of Conventional Techniques i the Design of Sampled-Data Systems, W. R Linvill, R. W. Sittler. *Convention Record*, Institut of Radio Engineers, pt. I, 1953, pp. 99–104.

5. Design of Sampled-Data Systems B Extension of Conventional Techniques, W K. Linvill, R. W. Sittler. *Report no. R-22.* Massachusetts Institute of Technology, Cambridg Mass., July 1957.

6. Extension of Continuous-Data Syste Design Techniques to Sampled-Data Contro Systems, G. W. Johnson, D. P. Lindorff, C. G. Nordling. *AIEE Transactions*, pt. II (*Applicatio and Industry*), vol. 74, Sept. 1955, pp. 252–63.

7. Sampled-Data Control Systems (book), E I. Jury. John Wiley & Sons, Inc., New Yor N. Y., 1958, chaps. 1–4.

8. Additions to the Modified z-Transfor Method, E. I. Jury. *Wescon Convention Reco* Institute of Radio Engineers, pt. 4, 1957, p 136–56.

9. The Geometry of the Zeros of a Pol nomial in a Complex Variable, M. Marde American Mathematical Society, New York, N. Y 1949, p. 152.

10. Theory of Servomechanisms (book), H M. James, N. B. Nichols, P. S. Phillips. McGra Hill Book Company, Inc., New York, N. Y., 194

11. The Analysis of Sampled-Data Systems J. R. Ragazzini, L. A. Zadeh. *AIEE Transaction* pt. II (*Applications and Industry*), vol. 71, No 1952, p. 225–34.

12. General Synthesis Procedure for Com puter Control of Single and Multi-Loo Linear Systems, R. E. Kalman, J. E. Bertram *Technical Report T-201B*, Columbia Universit New York, N. Y., 1957.

13. Conditional Feedback Systems Applie to Stabilizing a Missile in Pitch Attitude D. R. Katt. *Wescon Convention Record*, Institut of Radio Engineers, 1957, pp. 171–75.


# Discussion

**John M. Salzer** (Thompson Ramo Wooldridge Inc., Los Angeles, Calif.): The authors have made a notable stab at solving a rather nasty problem of finding the input-output relationship of systems which have several samplers and any number of loops.

The authors reached an intuitive formulation of this solution. Admittedly they do not prove this formulation; they claim, however, that it gives the answer for all the system solutions they attempted.

I would like to emphasize that the solution of such multiloop and multisampled systems is complex, treacherous, and full of pitfalls. Moreover, offering a general solution without proof leaves one full of doubt and uneasiness. The work originally done by the authors probably got close to a solution, but the method and result presented were incorrect and so were many of the specific examples.

Of the specific examples cited (Table I of the paper), the discusser considers the following solutions correct: 1 through 21, 23, 25, 33, 34, 35, 37, 38, and 40. The following solutions were incorrect but contain only what appeared to be slight typographical errors: 22, 28, and 36. The following solutions were conceptually and basically incorrect: 24, 26, 27, 29, 30, 31, 32, 39, and 41.

It might seem peculiar that I claim that the method presented was wrong and ye so many of the solutions turn out to b correct. This is due purely to the fac that in the simpler system configuration many of the terms of a general solutio are zero so that their erroneous absenc in the general formula does not influenc the answer. As the system configuration become a little more complex, as in the cas which this paper was written to solve, th method presented starts producing in correct answers. It is noted, however that except for misprints, the author find the correct denominators in the solutio of all examples. This suggests, but doe not prove, that the denominator in th authors' generalized equation 21 is correct Another point to note is that the sample

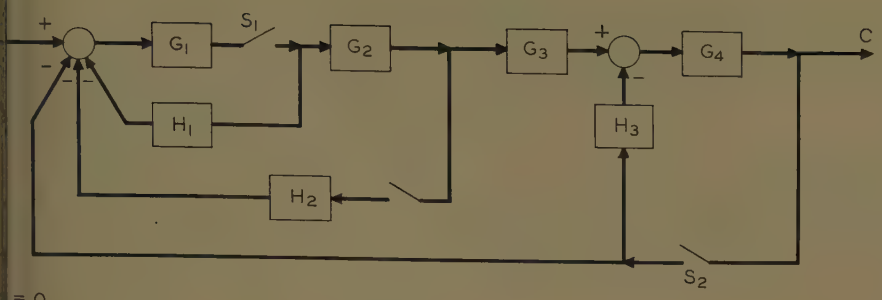


$= 0$

$= G_1$

$s_1 = -\overline{H_1G_1}^* - G_2\,\overline{H_2G_1}^*$

$s_2 = \overline{G_2G_3G_4}^*$

$o = G_2G_3G_4$

$G_{is_2} = 0$

$G^*_{s_2s_2} = -\overline{H_3G_4}^*$

$G^*_{s_2s_1} = -G_1^*$

$G_{s_20} = -G_1^*G_2G_3G_4$

$$\frac{\overline{RG_1}^*\,(1+\overline{H_3G_4}^*)\,G_2G_3G_4 - \overline{RG_1}^*\,\overline{G_2G_3G_4}^*\,H_3G_4}{1+\overline{H_1G_1}^* + G_2^*\,\overline{H_2G_1}^* + \overline{H_3G_4}^* + G_1^*\,\overline{G_2G_3G_4}^* + \overline{H_1G_1}^*\,\overline{H_3G_4}^* + G_2^*\,\overline{H_2G_1}^*\,\overline{H_3G_4}^*}$$

**Fig. 6. Simplified solution of example 41**

n of the system output is correctly
en in all examples after the continuous-
a part of the numerator is sampled.
t is interesting that the block diagrams
ll the examples can be rearranged in a
nner requiring only two sampled-data
nts to interrupt all self-loops. This
mits then the solution of all problems
e presented by a method adequate for
two-sampled-loop case. For example,
last block diagram 41 is shown to
tain five samplers, but it can be re-
anged to contain only two sampled-
a loops as shown in Fig. 6. The two
plers $S_1$ and $S_2$ are adequate to inter-
t all loops.

n the process of studying the subject
er, the discusser has arrived at the
eral equation for a two-sampled-loop
em. Using the notation of the article,
equation reads as follows:

$$RG_{10}'+$$

$$G_{4s_1}^*(1-G_{s_2s_2}^*)G_{s_10}'+\overline{RG_{4s_1}}^*G_{s_1s_2}^*G_{s_20}'+$$

$$2G_{4s_2}^*(1-G_{s_1s_1}^*)G_{s_20}'+\overline{RG_{4s_2}}^*G_{s_2s_1}^*G_{s_10}'$$

$$-G_{s_1s_1}^*-G_{s_2s_2}^*-G_{s_1s_2}^*G_{s_2s_1}^*+G_{s_1s_1}^*G_{s_2s_2}^*$$

(42)

e derivation of equation 42 will be
ussed in a forthcoming article. For
mple 41 of Table I, after rearrangement
shown in Fig. 6, the various quantities
listed and the final formula derived as
t of Fig. 6. It is readily visualized
t the answer for this example as was
en in the article is not correct because it
ntuitively clear that $H_2$ must have an
ct on the continuous output of the
em. It is one of the interpolating
tinuous-data transfer functions con-
ting $S_2$ to the output.
Equation 42 can be utilized to solve all
other examples.

**B. Ash, W. H. Kim,** and **G. M. Kranc** (Columbia University, New York, N. Y.): The authors have made an interesting contribution to the theory of sampled-data systems. Their paper extends the topological ideas of Mason to multiloop sampled-data systems. However, the authors' general gain formula, as presented in the paper, does not appear to be valid. First of all, the authors imply in their rule *5* that the application of the formula depends upon a certain technique to be observed in numbering the sampled loops. The authors unfortunately do not reveal this technique. Second, the general expression for $S_n^*$, equation 21, is open to question. According to equation 22 the function $S_3^*$ is zero. Since the input to sampler $S_3$, however, is the system output, $S_3^* = C^*$, which is certainly not zero.

Equation 21 implies that all one has to do is to place a sampling switch in series with the input in order to make the sampled output identically zero.

Most of the examples which appear in Table I are incorrect. For instance, the output of system 30, as computed algebraically, is

$$C = \frac{R^*G_1G_2 + R^*G_1G_2(G_2H_2)^* - R^*(G_1G_2)^*(G_2H_2)}{1+(G_1G_2)^*+(G_2H_2)^*}$$

Only the first term in the numerator is present in the paper. However, the sampled output:

$$C^* = \frac{R^*(G_1G_2)^*}{1+(G_1G_2)^*+(G_2H_2)^*}$$

agrees with the authors' result.

In almost every example considered by the authors, the actual output contains terms of the form $AB^*-A^*B$ which do not appear in the paper. If the sampled output is taken, these terms drop out, since $(AB^*-A^*B)^*=0$. Thus the sampled output as computed by the authors is invariably correct.

The discussers are preparing a paper on the signal-flow-graph approach to sampled-data systems. A general gain formula, somewhat similar in appearance to that of the authors', will be presented with proof.

**George G. Lendaris** and **Eliahu I. Jury:** The authors wish to thank Dr. Salzer for taking the time and effort to study the paper in as much detail as he did and for pointing out that there exists a limitation to equation 21 for the output of an $n$-sampled-loop system. Also the authors would like to thank Dr. Salzer for indicating the typographical and gross errors that appeared in Table I. These corrections have been incorporated so that the present form of the table should be correct in its entirety.

It may be noted at this point that it was quite fortuitous that the last three entries in the table turned out being $n \not\geq 2$ systems, for this was not the original intention of the authors. Note also that even though these systems appeared to have more than two loops, the formulation gave the right denominator for the output.

The authors would also like to thank Mr. Ash, Mr. Kim, and Mr. Kranc for their discussion and for their efforts in pointing out the inaccuracies that appear in the paper.

Both discussions indicate that equation 21 is not valid for the general case of the continuous output, but that it may be valid for the general case of the sampled form of the output (at least for $n=2$). Subsequent work by Mr. Lendaris indicates that this latter fact is not correct either. The numerator is not completely general, even for the sampled case.

In his discussion, Dr. Salzer presented a general equation for the continuous output of the $n=2$ system. This equation is correct, for it is a special case of the general solution of the problem which was recently derived.

Messrs. Ash, Kim, and Kranc made a statement in their first paragraph concerning the value of $S_3^*$. Their comment implies that they do not fully appreciate the concept of the fictitious signal source as is borne out again by their comment in the succeeding paragraph regarding equation 21.

The authors could continue point by point to discuss the items mentioned by the discussers, however it is much more useful to present instead the subsequent work done in this area by Mr. Lendaris with the purpose of clearing up all the inaccuracies and misconceptions pointed out and perhaps those not yet noted. (who wishes to express thanks to Professor C. A. Desoer for his inspiration and guidance in formulating this material).

For context purposes one might consider the following to be inserted in the paper in place of the section entitled "Multi-sampled-Loop Systems."

### Algebraic Method

For extending this approach to the multisampler system, consider Fig. 7 as a

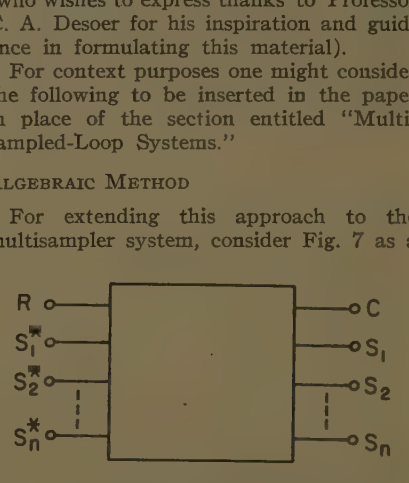


**Fig. 7. Multi-input multi-output model of n-sampler sampled-data system**

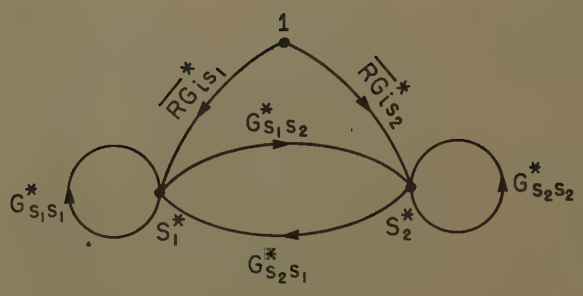


**Fig. 8 (left). Signal-flow-graph representation of equations 49 and 50**

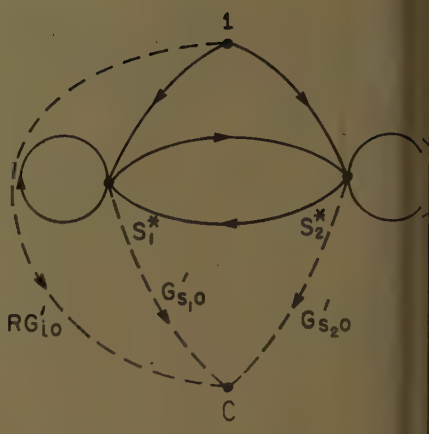


**Fig. 9 (right). Information from equation 48 added to signal-flow graph of Fig. 8**

model of a sampled-data system. In this model the system has been rearranged such that the input node, the output node, and all of the samplers are outside the box, and the rest of the system is inside the box. The nodes on the right, which will be called output nodes, represent the output terminal of the system, $C$, and the input terminal of each of the samplers, $S_1$, $S_2$, ..., $S_n$. The nodes on the left, input nodes, represent the system input terminal, $R$, and the output terminal of each of the samplers, $S_1^*$, $S_2$, ..., $S_n^*$. The latter represent the fictitious signal sources introduced earlier in the paper.

The resulting multi-input multi-output system inside the box is a linear time-invariant (because it has no samplers) system, hence there exists a continuous transfer function from each of the input nodes to each of the output nodes. These transfer functions will be denoted by $G'$ with the appropriate subscripts; the first one referring to the input node, the second to the output node.

Keeping these definitions in mind, the following set of equations describe the input-output relationships of the system located inside the box:

$$S_1 = RG_{1s_1}' + S_1^* G_{s_1s_1}' + \ldots + S_n^* G_{s_ns_1}' \qquad [43(1)]$$

$$\vdots$$

$$S_n = RG_{1s_n}' + S_1^* G_{s_1s_n}' + \ldots + S_n^* G_{s_ns_n}' \qquad [43(n)]$$

$$C = RG_{1o}' + S_1^* G_{s_1o}' + \ldots + S_n^* G_{s_no}' \qquad [43(n+1)]$$

Since the sampled signal sources ($S_k^*$, $k=1, 2, \ldots, n$) are by definition the sampled form of the input to the samplers ($S_k$, $k=1, 2, \ldots, n$), equations [43(1)] to [43($n$)] can be starred and rearranged, yielding:

$$\overline{RG_{1s_1}}^* = S_1^*(1-G_{s_1s_1}^*) - S_2^* G_{s_2s_1}^* - \ldots - S_n^* G_{s_ns_1}^* \qquad [44(1)]$$

$$\vdots$$

$$\overline{RG_{1s_n}}^* = -S_1^* G_{s_1s_n}^* - S_2^* G_{s_2s_n}^* - \ldots + S_n^*(1-G_{s_ns_n}^*) \qquad [44(n)]$$

or rewriting in matrix form:

$$\begin{bmatrix} (G_{s_1s_1}^*-1) & G_{s_2s_1}^* & G_{s_3s_1}^* \ldots G_{s_ns_1}^* \\ G_{s_1s_2}^* & (G_{s_2s_2}^*-1) & G_{s_3s_2}^* \ldots G_{s_ns_2}^* \\ \vdots & & \\ G_{s_1s_n}^* & G_{s_2s_n}^* & G_{s_3s_n}^* \ldots (G_{s_ns_n}^*-1) \end{bmatrix} \begin{bmatrix} S_1^* \\ S_2^* \\ \vdots \\ S_n^* \end{bmatrix} = - \begin{bmatrix} \overline{RG_{1s_1}'^*} \\ \overline{RG_{1s_2}'^*} \\ \vdots \\ \overline{RG_{1s_n}'^*} \end{bmatrix} \qquad (45)$$

This set of $n$ equations can be solved for $S_1^*$, $S_2^*$, ..., $S_n^*$ using standard algebraic techniques. When this is done, the resulting equations can be substituted into equation [43($n$+1)] to obtain an expression for $C$ in terms of the input $R$ and the system parameters.

As an example of this method, consider the case where $n=2$. The equations for this system can be written as:

$$S_1 = RG_{1s_1}' + S_1^* G_{s_1s_1}' + S_2^* G_{s_2s_1}' \qquad (46)$$

$$S_2 = RG_{1s_2}' + S_1^* G_{s_1s_2}' + S_2^* G_{s_2s_2}' \qquad (47)$$

$$C = RG_{1o}' + S_1^* G_{s_1o}' + S_2^* G_{s_2o}' \qquad (48)$$

Starring and rearranging, equations 46 and 47 become:

$$\overline{RG_{1s_1}}^* = S_1^*(1-G_{s_1s_1}^*) - S_2^* G_{s_2s_1}^* \qquad (49)$$

$$\overline{RG_{1s_2}}^* = -S_1^* G_{s_1s_2}^* + S_2^*(1-G_{s_2s_2}^*) \qquad (50)$$

Solving equations 49 and 50 for $S_1^*$ and $S_2^*$, and substituting these into equation 48, there results:

$$C = RG_{1o}' + \frac{RG_{1s_1}^*[G_{s_1o}'(1-G_{s_2s_2}^*)+G_{s_1s_2}^* G_{s_2o}'] + RG_{1s_2}^*[G_{s_2o}'(1-G_{s_1s_1}^*)+G_{s_2s_1}^* G_{s_1o}']}{1-G_{s_1s_1}^*-G_{s_2s_2}^*-G_{s_1s_2}^* G_{s_2s_1}^*+G_{s_1s_1}^* G_{s_2s_2}^*} \qquad (51)$$

Equation 51 is the general equation for the output of any sampled-data system containing two samplers (which are in synchronism). This equation is identical to Dr. Salzers' equation 42, and this represents a formal derivation of it.

One could continue in this manner and, using this algebraic method, derive a general expression for the output of an $n$-sampler system for each $n$. It is obvious, however, that these general formulas become very lengthy and unwieldy for $n \geq 3$. For this reason, recourse is made to topological methods of finding the output of an $n$-sampler sampled-data system in terms of the input $R$ and the system parameters.

### Topological Method

Consider again the set of equation 45. Instead of solving this set algebraically, one can associate to it a signal-flow gra and then apply Mason's theorem to fi signal-flow graph for obtaining the desir relationships.

(The signal-flow-graph techniques Mason are given in references 1 and 2 the paper. It should be pointed out th more recent work has been done in th area by Coates.[1] The method he presen is guaranteed to give a minimal ter expression for the gain, and for this reas is in many cases superior to Mason method. His method will not be given i the present discussion, however, so as n to confuse the issue at hand.)

To illustrate this process, consider aga the case where $n=2$. From equations and 50 one can readily construct the signa flow graph shown in Fig. 8. (The inp node in this signal-flow graph is label with a *1* and the branches leading fro it with an $RG_{1o}'$ or $RG_{1s_k}'^*$ term becau Mason's theorem gives the transfer ga from one node to the other, and by maki the input node variable *1*, an expression f the output is obtained directly.) Th adding the information contained in equ tion 48 the signal-flow graph becomes shown in Fig. 9. Applying Mason theorem to find the gain between the nod labeled *1* and $C$, one obtains equation This expression, which was construct directly from the signal-flow graph, aga represents the general equation for t output of any sampled-data system co taining two samplers (which are in sy chronism).

The topological method will not be use however, to derive the general formul for the $n$-sampler sampled-data syste the reason being, as noted earlier, th these general formulas are too lengthy be practical. Instead, the topological tec nique will be applied directly to ea individual system under consideratio This approach is advantageous because a simplifications arising out of a particul system configuration are borne out in t

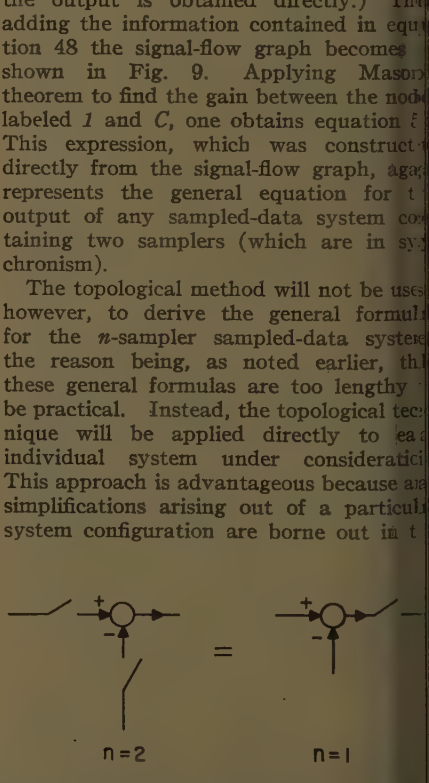


**Fig. 10. Example of reducing number samplers in block diagram**

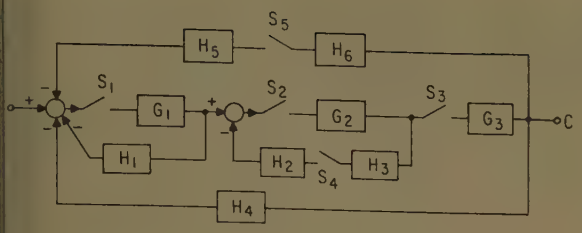


**Fig. 11 (left). An n = 5 sampled-data system**

**Fig. 12 (below). Signal-flow graph of system in Fig. 11**

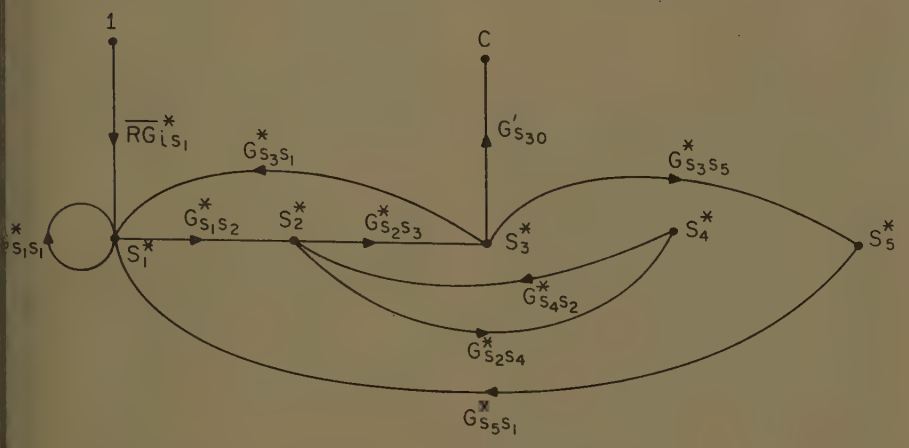


gnal-flow graph before the calculations re made.

Now that the procedure of constructing signal-flow graph of the type indicated Fig. 9 has been justified, one can bypass ne process of using the model and the quations used before. Instead, one can o directly from the usual block-diagram orm of the sampled system to the signal-ow-graph form. The important thing o notice about the signal-flow-graph epresentation of the system is that all the ode variables are sampled functions, and ll the transfer functions are starred ransfer functions, hence, as mentioned in ne paper, one can apply Mason's theorem o find the desired output. (These comments do not, and need not, apply to the utput node nor the branches leading to it.)

To apply the results of the foregoing, se the following procedure:

. Eliminate all redundant samplers in ne original block diagram. See Fig. 10 or an example. This step is not necessary or correct results, but it simplifies the esulting flow graph.

. Number all samplers in any fashion esired.

. On a separate sheet of paper draw a node for each sampler indicated in step *2* and label these $S_1^*$, $S_2^*$, ..., $S_n^*$.

4. Open all samplers in the block diagram.

5. Start from sampler *1* and traverse all possible continuous paths from the output of sampler *1* to the input of all samplers. Where these exist, draw in a branch on the signal-flow graph from node $S_1^*$ to the respective node $S_k^*$ with the direction indicated and the appropriate sampled transfer function. Then start at sampler *2* and repeat the procedure until all samplers are covered.

6. Now add two other nodes: one labeled with a *1* (the input), and one labeled with a *C* (the output). From the input node draw a branch to each of the nodes which has a corresponding continuous path in the block diagram, and label with the appropriate gain ($RG_{i0}'$ to the output, and $\overline{RG_{is_k}}^*$ to the other nodes). Then draw a branch from each of the nodes $S_k^*$ which has a corresponding continuous path in the block diagram to the output node *C* and label appropriately ($G_{sk0}'$).

7. Apply Mason's theorem between the input node and the output node of the resulting configuration to find the desired output.

As an example of this procedure, consider the system in Fig. 11. The samplers are numbered from *1* to *5*. The signal-flow graph given in Fig. 12 was constructed directly using these rules. Using Mason's theorem on Fig. 12, the output is given by:

$$C=\frac{\overline{RG_{is_1}}^*G_{s_1s_2}^*G_{s_2s_3}^*G_{s_30}}{1-G_{s_1s_1}^*-G_{s_2s_4}^*G_{s_4s_2}^*-G_{s_1s_2}^*G_{s_2s_3}^*G_{s_3s_5}^*G_{s_5s_1}^*-G_{s_1s_2}^*G_{s_2s_3}^*G_{s_3s_1}^*+G_{s_1s_1}^*G_{s_2s_4}^*G_{s_4s_2}^*} \tag{52}$$

where

$$G_{is_1}'=1 \qquad G_{s_1s_1}^*=-\overline{G_1H_1}^* \quad G_{s_3s_1}^*=-\overline{G_3H_1}^*$$

$$G_{s_1s_2}^*=G_1^*G_{s_2s_4}^*=\overline{G_2H_3}^* \qquad G_{s_4s_2}^*=-H_2^*$$

$$G_{s_3s_3}^*=G_2^*G_{s_3s_5}^*=\overline{G_3H_6}^*$$

$$G_{s_50}'=G_3 \qquad G_{s_5s_1}^*=-H_5^*$$

This result was obtained with a minimum amount of calculations. If the algebraic method had been used, this whole page would not have sufficed to carry the general formula for the $n=5$ system.

There are several techniques for minimizing the number of nodes, and hence the computations, in the signal-flow graph, such as, perhaps eliminating nodes $S_4^*$ and $S_5^*$ in Fig. 12 by inspection. This would be done by replacing the appropriate transfer function(s) by a starred transfer function. But due to space limitations these techniques will not be presented in this discussion.

The method presented is completely general, and Mr. Lendaris foresees no difficulties in its application to any *n*-sampler systems no matter how complicated so long as all its samplers are in synchronism.

This concludes the closure to the discussions. We would again like to thank the discussers for indicating the errors that appeared in the paper and for stimulating me to do further work in this area. It is hoped that the short presentation of this material will suffice to clear up any difficulties arising out of the paper, and help to clean up this general topic of signal-flow-graph applications to sampled-data systems.

## Reference

1. Flow Graph Solutions of Linear Algebraic Equations, C. L. Coates. *Report no. 58-RL-1997*, General Electric Company, Schenectady, N. Y.; also *Transactions*, Professional Group on Circuit Theory, Institute of Radio Engineers, New York, N. Y., vol. PGCT-6, no. 2, June 1959, pp. 170–87.

# Analysis of Nonlinear Sampled-Data Control Systems—I

E. KINNEN
ASSOCIATE MEMBER AIEE

J. TOU
MEMBER AIEE

AN INTERESTING SIMILARITY exists between the mechanical sampling and zero-order hold function of sampled-data systems, and the mathematical "sampling" which is characteristic of numerical methods of analysis. This paper describes an investigation into this similarity. The results are numerical methods of analysis principally adapted to the transient solution of nonlinear sampled-data control systems. While numerical methods generally provide approximate solutions to nonlinear continuous systems, numerical methods applied to many nonlinear sampled-data systems provide exact solutions. Approximate solutions exist when exact solutions are not possible, i.e., for the more complex system configurations.

The methods developed are useful for the solution of transient problems which arise in systems containing any one of a wide variety of nonlinearities. The procedures are not applicable, however, to problems containing stochastic relationships. The $z$-transformation is used extensively to provide notational simplicity and to take advantage of existing transform techniques and tables.

In this paper specific systems which can be effectively reduced to the block diagram form appearing in Fig. 1 are considered. The block containing $N$ represents a nonlinear relationship between its input and output terminals, and the block containing $G_1$ indicates a linear transfer function. Systems containing a nonlinearity between two frequency-sensitive elements are considered in Part II of this report.[1] While the block diagram used in this paper certainly cannot represent all sampled-data control systems, it is sufficiently general to represent, mathematically, many systems presently undergoing analysis. Furthermore, only those systems are considered which have a constant sampling period and a zero-order hold in the error channel before the continuous portion of the system. The nonlinear relationships have the one restriction that a unique output be determined for every specified input.

An expression is developed which, by repetitive application, permits the sampled error values of a nonlinear sampled-data system to be found in response to any specified input disturbance. The step, impulse, and ramp input functions, however, have simplifying advantages. Although the results are easily adapted to machine programming, the specific intent of this development is to provide a practical procedure not dependent on a machine solution.

Known techniques for analyzing nonlinear sampled-data control systems are limited essentially to three: the describing function method, the phase-plane method, and numerical methods. The describing function method, when applied to a system containing a nonlinearity and a sampler, is generally inadequate.[2] Basically, the sampling phenomenon is replaced by a dead time, a procedure which becomes less descriptive as the sampling period approaches the speed of response of the linear portion of the system. Methods using the phase plane have more pertinent application but are limited, practically, to systems with a second-order transfer function. The methods of phase-plane analysis, where possible and sufficiently complete to predict transient phenomena, may also require relatively complex techniques which vary with the type of nonlinearity considered, etc.[2-4]

The principle of numerical methods of analysis has been adapted to continuous nonlinear control systems,[5-7] and more recently to discontinuous nonlinear control systems.[8] Reference 8 develops a special transform table to estimate a time-domain convolution combined with a relatively fast mathematical sampling rate. The solution involves a polynomial long division with the nonlinear coefficients of the system equation changing at each step of the division. This method is not easily applied to systems with higher-order transfer functions or with relatively complex nonlinearities.

## Method of Analysis

The method of analysis described in this paper provides an exact solution to the transient problem and is applicable to the system block diagram configuration shown in Fig. 1. For simplicity, initially assume that:

1. $G_1(s)$ is the transfer function of the linear frequency sensitive elements of the system and contains no dead time (transport delay).

2. $N$ is a uniquely defined time-independent functional relationship

$$E_{cn}(t) = N[E_c(t)] \tag{1}$$

i.e., any given input condition determines a unique output, dependent only on the instantaneous input magnitude.

3. The sampler function is adequately and unambiguously described as

$$E_c(t) = \sum_{k=-\infty}^{\infty} (E(kT)\{U(t-kT) - U\{t-(k+1)T\}\}) \tag{2}$$

where $T$ is the sampling period, and $U(t-kT)$ is a positive unit step function occurring at $t=kT$. The lower limit on the summation would be zero if this equation were applied to a system solution which neglects negative time effects or memory.

The effects of system dead time, and storage states in the nonlinearity, are considered separately in the following sections.

From Fig. 1 the Laplace transform of the error can be written as

$$E(s) = R(s) - G_1(s)E_{cn}(s) \tag{3}$$

The Laplace transform of equation 2 is

$$E_c(s) = \sum_{k=-\infty}^{\infty} \left\{ E(kT)\epsilon^{-kTs}\left(\frac{1-\epsilon^{-Ts}}{s}\right)\right\} \tag{4}$$

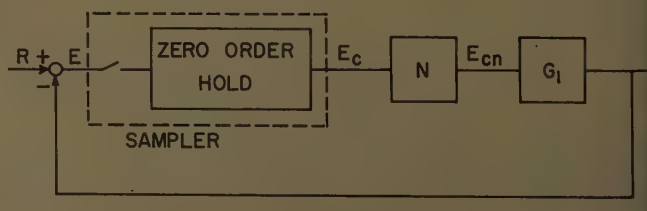


Fig. 1. System configuration for an exact solution

Paper 59-828, recommended by the AIEE Feedback Control Systems Committee and approved by the AIEE Technical Operations Department for presentation at the AIEE Summer and Pacific General Meeting and Air Transportation Conference, Seattle, Wash., June 21–26, 1959. Manuscript submitted October 3, 1958; made available for printing May 5, 1959.

E. KINNEN is with the University of Minnesota, Minneapolis, Minn., and J. TOU is with Purdue University, Lafayette, Ind.

The research reported here was supported by the Westinghouse Electric Corporation through a fellowship grant. The authors wish to express their appreciation to Prof. E. M. Sabbagh of Purdue University for suggestions and encouragement.

quations 2 and 4 represent a series of lses, each $T$ seconds in duration, spaced seconds apart and with amplitudes $kT$). Equation 1 states the $E_{cn}$ differs om $E_c$ only by the nonlinear relation $N$, dependent of time. Therefore

$$n(s)=\sum_{k=-\infty}^{\infty}\{N[E(kT)]\epsilon^{-kTs}\}\left(\frac{1-\epsilon^{-Ts}}{s}\right) \tag{5}$$

ere $N[E(kT)]=N[E_k]$ is defined as e output amplitude of the nonlinearity as a result of an input amplitude $kT$).

From equations 3 and 5, it follows at

$$s)-E(s)=G(s)\sum_{k=-\infty}^{\infty}N[E(kT)]\epsilon^{-kTs} \tag{6}$$

ere

$$s)=G_1(s)\left(\frac{1-\epsilon^{-Ts}}{s}\right) \tag{7}$$

Applying the $z$-transform, equation 6 n be written as

$$z)-E(z)=G(z)\sum_{k=-\infty}^{\infty}N[E(kT)]z^{-k} \tag{8}$$

As the information in the $z$-transm of a time function is contained at mple instants only, equation 8 contains unknown value of the error function $t=kT$.

Using a definition of the $z$-transformaon and assuming that $G_1(s)$ is realizable, $z)$ can be expanded into a power ies of $z$.

$$)=g_0+g_1z^{-1}+g_2z^{-2}+\ldots g_kz^{-k}\ldots \tag{9}$$

ere $g_k$ is the value of the impulse reonse of $G(s)$, $g(t)$, at $t=kT$. An input ction, zero for negative time values, n also be expanded in a power series of

$$)=R_0+R_1z^{-1}+R_2z^{-2}+\ldots \tag{10}$$

Equating the unknown error function a similar power series

$$)=E_0+E_1z^{-1}+E_2z^{-2}+\ldots \tag{11}$$

becomes the value of the unknown or function at $t=kT$. Equation 11 umes for convenience that the error ction is zero for negative time. Subting equations 9 through 11 into equan 8, it follows that

$$\begin{aligned}&_0-E_0)+(R_1-E_1)z^{-1}+\\&\quad(R_2-E_2)z^{-2}+\ldots\}\\&\quad=(g_0+g_1z^{-1}+g_2z^{-2}+\ldots)(N[E_0]+\\&\quad N[E_1]z^{-1}+N[E_2]z^{-2}+\ldots)\end{aligned} \tag{12}$$

satisfy this equation the coefficients of corresponding powers of $z$ must be equal, or

$$\begin{aligned}&E_0=R_0-g_0N[E_0]\\&E_1=R_1-g_0N[E_1]-g_1N[E_0]\\&\vdots\\&E_k=R_k-\sum_{n=0}^{k}g_nN[E_{k-n}]\\&\qquad=R_k-\sum_{n=0}^{k}g_{k-n}N[E_n]\end{aligned} \tag{13}$$

Each equation in equation 13 has one unknown. The solution of each unknown is used in the solution of subsequent equations, a characteristic of many numerical methods.

The application of equation 13 is greatly simplified if $g_0=0$, a condition often found in practice. The implication of $g_0=0$ is that sufficient delay exists in $G(s)$ to limit its impulse response, $g(t)$, to zero at $t=0$. Noting equation 7, a minimum of a single time constant delay in $G_1(s)$ will insure this condition. If $g_0=0$, equation 13 reduces to

$$\begin{aligned}&E_1=R_1-g_1N[E_0]\\&E_2=R_2-g_1N[E_1]-g_2N[E_0]\\&\vdots\\&E_k=R_k-\sum_{n=0}^{k}g_nN[E_{k-n}],\ g_0=0\end{aligned} \tag{14}$$

where $E_0$ is equal to the magnitude of the step disturbance. For each $E_k$ value equation 13 may require the solution of an algebraic equation of the order of the analytic description of $N$, or a solution by trial and error if $N$ is known graphically. However, if equation 14 is applicable, each $E_k$ is found by determining $N[E_{k-1}]$ and summing a sequence of numerical products. Generally a graphical form of $N$ is best adapted for use with either equation 13 or 14.

Equation 13 can be rearranged and written in matrix form:

$$\|R-E\|=\|G\|\|N[E]\| \tag{15}$$

It is interesting to note that $\|G\|$ in equation 15 is defined as a transmission matrix by Friedland[9] in a discussion of a numerical technique for the analysis of time-varying sampled-data systems.

Another form of equation 14 can be developed by subtracting two consecutive error values, $E_k$ and $E_{k-1}$. Then, after rearrangement

$$\begin{aligned}&R_1=E_0-a_0N[E_0]\\&E_2=E_1+R_1-R_0-a_0N[E_1]-a_1N[E_0]\\&\vdots\\&E_{k+1}=E_k+R_{k+1}-R_k-a_0N[E_k]-\\&\qquad a_1N[E_{k-1}]-a_2N[E_{k-2}]-\ldots\\&\qquad=E_k+R_{k+1}-R_k-\sum_{n=0}^{k}a_nN[E_{k-n}]\end{aligned} \tag{16}$$

where

$$\begin{aligned}&a_0=g_1\\&a_1=g_2-g_1\\&\vdots\\&a_k=g_{k+1}-g_k\end{aligned} \tag{17}$$

The expression of equation 16 has an important advantage over equation 14, as the series $a_k$ often converges rapidly toward zero, whereas the series $g_k$ may converge toward a constant. Consequently the number of terms in equation 16 for an $E_k$, as $k$ increases, approaches a limit, while those in equation 14 continually increases.

## Intersample Analysis

Quite often the information obtained about the system error at sampling instants permits adequate interpolation of the error between sampling instants. When this is not possible or desirable, intersample values may be found at the expense of additional calculations.

Barker[10] (Section 3.4) describes the use of the modified $z$-transform to obtain intersample information for linear unity feedback systems. A similar method can be used here. Referring again to Fig. 1, a specific error value at any sample time is found by considering a function of all previous error samples $N[E_k]$, and the impulse response of $G(s)$. Specific error values between sample instants consider all previous sampled errors $N[E_k]$, and the delayed impulse response of $G(s)$, the delay limited to a maximum of one sampling period. The modified $z$-transform, $G(z,m)$ is defined as

$$G(z,m)=z^{-1}\sum_{k=0}^{\infty}g(kT+mT)z^{-k} \tag{18}$$

$0\leq m<1$

The lower limit on the sum is zero, assuming $g(t)$ to be the impulse response of a realizable transfer function.[11] Let $g_{mk}$ be the coefficient of the $z^{-k}$ term in

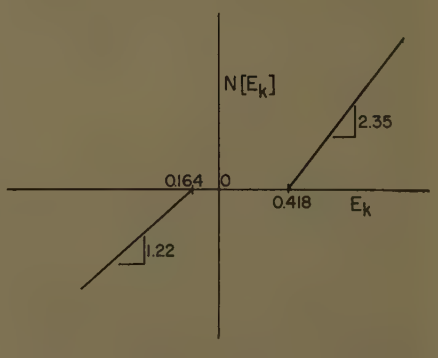


**Fig. 2. Simple nonlinearity for Fig. 1**

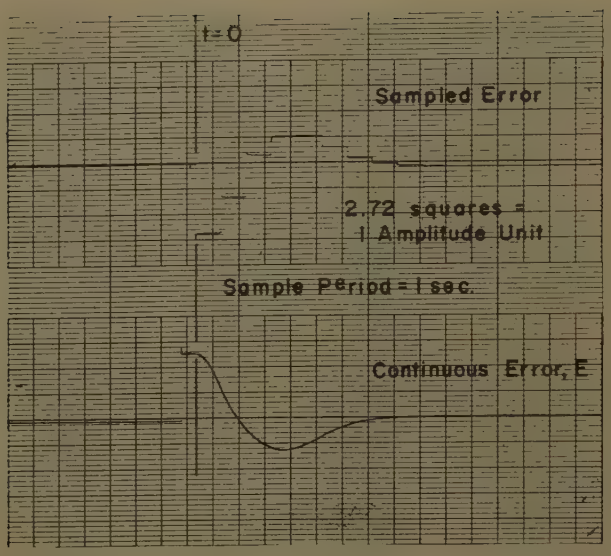


Fig. 3. Error response for a system with a simple nonlinearity

the series expansion of $G(z,m)$, similar to the notation used in equation 9. If the input is expanded as in equation 10, it is readily shown that

$$E_{m0}=0$$

$$E_{mk}=R_k-\sum_{n=1}^{\infty} g_{mn}N[E_{k-n}],\ k>0 \qquad (19)$$

Notice that $E_{mk}$ is not a function of past delayed sampled error values but a function of past sampled error values.

## Systems with Simple Nonlinearity, Example I

To illustrate the method of analysis just described, a solution is derived for the system appearing in Fig. 1 with a $G(s)$

$$G(s)=\left(\frac{1-\epsilon^{-s}}{s}\right)\left(\frac{1}{s(s+1)}\right) \qquad (20)$$

and the asymmetrical simple nonlinearity shown in Fig. 2. A simple nonlinearity is defined as a nonlinear output-input relation dependent only on the instantaneous input magnitude, and independent of any past input values or storage state. Assume a unit positive step function input and all initial error conditions zero. Then, from a standard $z$-transform table,[12] and with $T$, the sample period, equal to one second

$$G(z)=\frac{0.368z+0.264}{z^2-1.368z+0.368} \qquad (21)$$

This can be expanded by division

$$G(z)=0.368z^{-1}+0.768z^{-2}+0.914z^{-3}+0.967z^{-4}+0.987z^{-5}+0.994z^{-6}+0.997z^{-7}+0.998z^{-8}+\ldots \qquad (22)$$

As $g_0=0$, and $g_k$ approaches a constant as $k$ approaches infinity, equation 16 is easier to apply than equation 14. From equation 17 it follows that

$$\begin{aligned}
a_0&=0.368\\
a_1&=0.768-0.368=0.400\\
a_2&=0.146\\
a_3&=0.053\\
a_4&=0.019\\
a_5&=0.007\\
a_6&=0.003\\
a_7&=0.001\\
&\vdots
\end{aligned} \qquad (23)$$

$R(z)$, the step function input, is also expanded:

$$R(z)=\frac{z}{z-1}=1+z^{-1}+z^{-2}+\ldots$$

Substituting this and the coefficients of equation 23 into equation 16 yields

$$\begin{aligned}
E_0&=1\\
E_1&=1-0.368N[1]=1-0.368(1.37)=0.497\\
E_2&=0.497-0.368N[0.497]-0.400N[1]\\
&=0.497-0.368(0.186)-0.400(1.37)\\
&=-0.118\\
E_3&=-0.392\\
E_4&=-0.390\\
E_5&=-0.213\\
E_6&=-0.054\\
E_7&=-0.020\\
&\vdots
\end{aligned}$$

The result of an analog computer simulation of this solution for comparison with these calculated values is shown in Fig. 3.

Although a 10-inch slide rule was used for all calculations, the cumulative errors for the calculated values of $E_k$ are within a nominal $\pm 0.03$ experimental reading error for the corresponding values of $E_k$, through the seventh sampled value.

## Systems with Single-Storage Nonlinearity

A single-storage nonlinearity is defined as a nonlinear output-input relation dependent on the instantaneous input magnitude and a storage state created by the one previous input magnitude. If the system in the last example contained a single-storage nonlinearity, such as hysteresis loop or mechanical backlash, the method of solution would differ only in the evaluation of $N[E_k]$ in the application of equations 13, 14, or 16. $N[E_k]$ would depend on the value of $E_{k-1}$ as well as $E_k$ to establish the input-output uniqueness. For a single-storage nonlinearity the nonlinear function might be written $N[E_k, E_{k-1}]$.

Consider the idealized saturation curve in Fig. 4. Assume that the system is at rest for negative time, $E_{-k}=0$ and $N[E_{-k}]=0$ for $k>0$, and that the initial error, $E_0$, is established by a step input occurring at $t=0$. Then, the corresponding nonlinear output must be on the curve *abdoeij* in Fig. 4. Let $E_0$ be equal to the abscissa value of the point $g$; $N[E_0]$ the ordinate value of point $g$. Then the point $g$ establishes a curve from which the next nonlinear function value $N[E_k]$ is determined, i.e., *abfgij*. Continuing this procedure for other $N[E_k]$ values, it is apparent that the $E_k$ sequence is just traced along the single-storage nonlinearity according to the basic definition or interpretation of the nonlinearity.

An extension of this modification will permit the inclusion of a multistorage nonlinearity into the system of Fig. 1 which is of the form

$$N[E_k]=N[E_k, E_{k-1}, E_{k-2}, \ldots E_{k-n}] \qquad (24)$$

as long as a unique output is determined for each input condition, ($E_k$, $E_{k-1}$, $E_{k-n}$).

To illustrate a problem with a single-storage nonlinearity, consider the $G(s)$ given by equation 20 and the single-storage nonlinearity shown in Fig. 5. Again assume a unit step function input; however, assume an initial constant error value of $-0.08$ with $N[-0.08]=$ (This is due to the open-loop drift of the test equipment used to check the solution.)

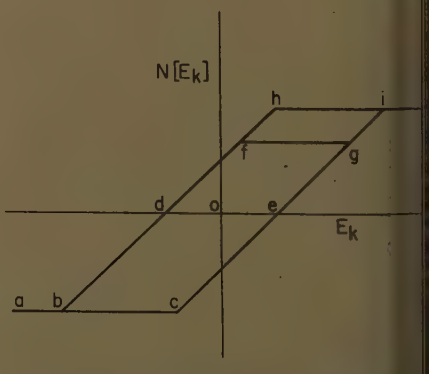


Fig. 4. Single-storage nonlinearity

Combining the coefficients of equation 23 with equation 16 and the nonlinearity given in Fig. 4 yields

$$E_{-1} = -0.08)$$
$$= -0.08 + 1.00 = 0.92$$
$$= 0.92 - 0.368N[0.92] = 0.92 - 0.368(0.644) = 0.683$$
$$= 0.683 - 0.368N[0.683] = 0.400(0.644) = 0.118$$
$$= -0.401$$
$$= -0.823$$
$$= -0.826$$
$$= -0.500$$
$$= -0.056$$

The evaluation of a single-storage nonlinear function can be made easier if the last computed value is placed on a graphical representation of the nonlinearity. Fig. 5 illustrates the $E_k$ values that were plotted for this example calculation.

Fig. 6 shows an analog computer response for this example, easily verifying these computed values. In the method of calculation and the accuracy of the result this example corresponds to the previous illustrative example.

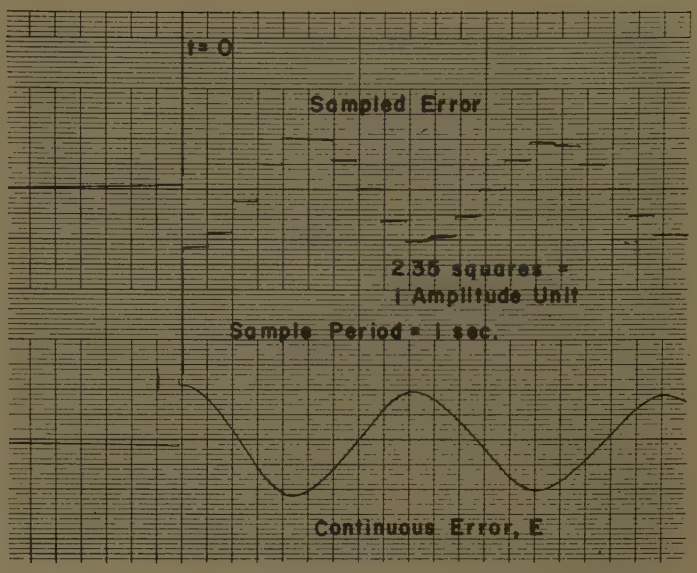


**Fig. 6. Error response for a system with a single-storage nonlinearity**

## Systems Containing a Transport Delay

The linear portion of the system may include a transport delay which is an even multiple $p$, of $T$. Then $G(s)$ has the same form as the right side of equation 7 but multiplied by a term $\epsilon^{-pTs}$; $G(z)$ has the same form as the right side of equation 8 but multiplied by $z^{-p}$. The equation corresponding to equation 12 is

$$(R_0 - E_0) + (R_1 - E_1)z^{-1} + (R_2 - E_2)z^{-2} + \ldots\} = (g_0 z^{-p} + g_1 z^{-p-1} + g_2 z^{-p-2} + \ldots) \times (N[E_0] + N[E_1]z^{-1} + \ldots)$$

where $g_k$ is determined from that part of $G(s)$ which does not include the transport delay.

Equating coefficients of like powers of $z$, and rearranging, leads to the development of the following equations:

$$E_0 = R_0$$
$$E_1 = R_1$$
$$\vdots$$
$$E_p = R_p - g_0 N[E_0],$$
$$\vdots$$
$$E_k = R_k - \sum_{n=0}^{k-p} g_n N[E_{k-p-n}], \quad k > p \qquad (25)$$

The first $p$ values of the error, all equal to the magnitude of the disturbing function, indicate no system error correction until the initial nonzero error has traversed the transport lag.

The effect of a transport lag which is not an even multiple of $T$ can be investigated by applying the techniques described in the literature.[13,14] Let $\lambda T$ be the transport delay, where $\lambda$ is a positive number but not an integer. Also let $G_d(s)$ be that portion of $G(s)$ excluding the effect of the transport delay. Define $\lambda = p - \Delta$, where $p$ is a positive integer and $0 \leqslant \Delta < 1$.

$$G(s) = G_d(s)\epsilon^{-\lambda Ts} = G_d(s)\epsilon^{-pTs}\epsilon^{\Delta Ts}$$

As

$$\mathcal{L}^{-1}[G_d(s)\epsilon^{\Delta Ts}] = g_d(t + \Delta T)$$

it is possible to define $G_d(z)$ as

$$G_d(z) = \sum_{n=0}^{\infty} g_d(nT + \Delta T)z^{-n}$$

Then, it is possible to write

$$G(z) = G_d(z)z^{-p} \qquad (26)$$

Table II in reference 13, or any modified $z$-transform table, can be used for the evaluation of $G_d(z)$. If $G_d(z)$ is expanded in a $z^{-1}$ power series, the $k$th coefficient $g_k$ may be found and substituted into equation 25.

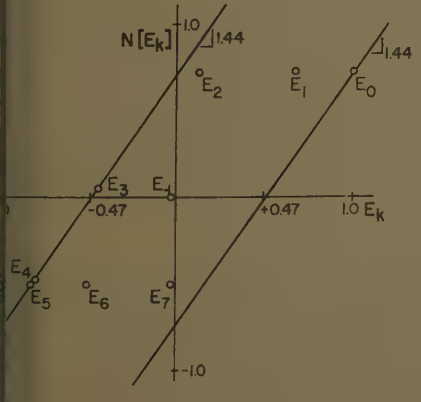


**5. Single-storage nonlinearity for Fig. 1**

## Modifications and Extensions

In the examples discussed a simple $G_1(s)$ transfer was used. A more complex $G_1(s)$ only increases the work needed to derive equation 22, the $G(z)$ series expansion. The complexity of subsequent work remains unchanged.

It is apparent from the examples that any form of intricate description of $N$ adds no significant increase in the solution time. Furthermore, as equation 24 may be the effective form of a digital computer command, a generalization of equation 24 will be a nonlinear functional relation not only of all past sampled error values, but also all functions of any past sampled values, etc. Then the computation of any value of the sampled error sequence $E_k$ will depend on the evaluation of the particular numerical program that created the $N$ designated in the block diagram. Although the application to systems containing involved digital programs does not appear attractive, application to dual mode system operation, for example, is straightforward and only as involved as the dual mode switching criterion.

Nonstep input functions are easily considered. If, for example, the input is a unit ramp function, beginning at a sample instant, and $g_0 = 0$, the equation corresponding to equation 14 is

$$E_{k+1} = E_k + T - \sum_{n=0}^{k} a_n N[E_{k-n}] \qquad (27)$$

Equation 17 defines $a_k$. Other nonconstant inputs, such as a sine function, can be included by obtaining the corresponding $R(z)$ in a power series expansion and combining this with equations 8, 9, and 11. Usually, however, it is not possible to write the $k$th term in as concise a form as is done in equations 14 or 27.

The methods discussed are not particularly suited to the manipulation of (slowly) time-varying parameters. However, the procedure used by Boxer and Thaler,[7] and Kukel,[8] may be modified for use with these methods. Thus, if a system parameter is not constant but a slowly varying function of time, an approximate solution can be developed as described in this paper but with a readjustment of the magnitude of the time-varying parameters at each increment or sample of the time solution. This would be laborious if the varying parameter changed many terms in the $g_k$ or $a_k$ series.

## Conclusions

A significant application of numerical techniques to the analysis of nonlinear sampled-data control systems has been described. The methods developed are relatively easily and quickly applied, requiring only algebraic operations and a $z$-transform table. The latter is a convenient aid in the initial expansion of the linear portion of the system.

The applications of these methods do not become appreciably more complicated with higher-order system transfer functions or involved nonlinear functional descriptions. This is in direct contrast to conventional methods applied to nonlinear analysis. An exact solution results if the nonlinearity precedes the system frequency-sensitive transfer functions. A second paper considers this problem with the nonlinearity effectively located between two transfer functions.[1]

These methods are well adapted to systems with sample periods approximately equal to the predominant time constants of the system, i.e., for transients significantly controlled by sampler action. They may also quickly provide limited information of limit cycles, following specific initial conditions. This information is generally very difficult to obtain by analytical methods.

## References


1. Analysis of Nonlinear Sampled-Data Control Systems—II, E. Kinnen, J. Tou. *AIEE Transactions*, see pp. 390–94 of this issue.

2. Nonlinear Aspects of Sampled-Data Control Systems, R. E. Kalman. *Proceedings*, Symposium on Nonlinear Circuit Analysis, Polytechnic Institute of Brooklyn, Interscience Publishers, Inc., New York, N. Y., vol. 6, 1957, pp. 273–83.

3. Contactor Servomechanisms Employing Sampled Data, C. K. Chow. *AIEE Transactions*, pt. II (*Applications and Industry*), vol. 73, Mar. 1954, pp. 51–64.

4. Analysis and Design of Relay Type Servomechanisms with Dead Time and Sampli... L. E. Weaver. *Ph.D. Thesis*, Purdue Universi... Lafayette, Ind., 1958.

5. Sampled-Data Representation of No... linear Systems, R. K. Cheng. *Ph.D.Thesis*, P... due University, Lafayette, Ind., 1957.

6. A Step-by-Step Method for Transie... Analysis of Feedback Systems with One No... linear Element, T. M. Stout. *AIEE Tra... actions*, pt. II (*Applications and Industry*), vol. ... 1956 (Jan. 1957 section), pp. 378–90.

7. A Simplified Method of Solving Line... and Nonlinear Systems, R. Boxer, S. Thal... *Proceedings*, Institute of Radio Engineers, N... York, N. Y., vol. 44, Jan. 1956, pp. 89–100.

8. Sampling in Linear and Nonlinear Fee... back Control Systems, J. Kukel. *Conventi... Record*, Institute of Radio Engineers, vol. 5, ... 4, 1957, pp. 43–56.

9. A Technique for the Analysis of Tim... Varying Sampled-Data Systems, B. Friedlan... *AIEE Transactions*, pt. II (*Applications a... Industry*), vol. 75, 1956 (Jan. 1957 section), p... 407–14.

10. The Pulse Transfer Function and I... Application to Sampling Servosystems (book... R. H. Barker. "Frequency Response", R. Oldel... burger, editor. The MacMillan Company, Ne... York, N. Y., 1956, pp. 325–37.

11. Additions to the Modified Z-Transfor... Method, E. I. Jury. *Convention Record*, Institut... of Radio Engineers, vol. 1, pt. 4, 1957, pp. 136–5...

12. Analysis and Synthesis of Sampled-Da... Control Systems, E. I. Jury. *AIEE Transactio...* pt. II (*Applications and Industry*), vol. 73, Se... 1954, pp. 332–46.

13. Sampled-Data Processing Techniques f... Feedback Control Systems, A. R. Bergen, J. Ragazzini. *Ibid.*, 1954, pp. 236–47.

14. Digital and Sampled-data Control Sys... tems (book), J. Tou. McGraw-Hill Book Co... pany, Inc., New York, N. Y., 1959, pp. 285–8... 588–92.


# Analysis of Nonlinear Sampled-Data Control Systems—II


E. KINNEN
ASSOCIATE MEMBER AIEE

J. TOU
MEMBER AIEE


GENERAL METHODS of numerical analysis are developed in a previous paper[1] for nonlinear sampled-data control systems in which the nonlinearity effectively occurs before the linear frequency-sensitive elements in the sampled error channel. These methods are inadequate if the system nonlinearity effectively occurs between two linear frequency-sensitive elements, as shown in Fig. 1. This paper extends the application of numerical analysis to this more complex problem. The resulting methods no longer lead to an exact solution.

If a nonlinearity exists between two frequency-sensitive functions, it is possible to approximate the input to the nonlinearity with a sequence of pulses and then to apply a numerical procedure of analysis. This is done in the following sections. Modified $z$-transforms an... multirate sampler notation are used fo... brevity in the thoeretical developmen... but only standard $z$-transform tables ar... needed in the ultimate applications. Th... methods are readily adapted to mechan... ical programming but do not necessaril... require a machine solution.

A statement of the general method... which are developed is involved. Th... application of these methods, however, i... not complex because of simplifying ap... proximations that can be made. A... the expense of computational labor, th... solution can be obtained to any degree o... accuracy. The methods have direct ap... plication to the solution of nonlinear sys... tem transient problems, and indirec... application to limit cycle descriptions an... system design. The input function an... type of nonlinearity that may be con... sidered are relatively general but do no...


Paper 59-829, recommended by the AIEE Feedback Control Systems Committee and approved by the AIEE Technical Operations Department for presentation at the AIEE Summer and Pacific General Meeting and Air Transportation Conference, Seattle, Wash., June 21–26, 1959. Manuscript submitted October 3, 1958; made available for printing May 5, 1959.



E. Kinnen is with the University of Minnesota, Minneapolis, Minn., and J. Tou is with Purdue University, Lafayette, Ind.



The research reported in this paper was supported by the Westinghouse Electric Corporation through a fellowship grant. The authors wish to express their appreciation to Prof. E. M. Sabbagh, Purdue University, for suggestions and encouragement.


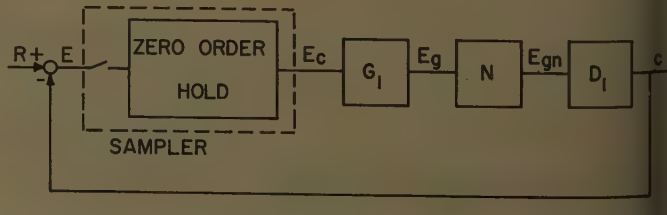


Fig. 1. System configuration for an approximate solution

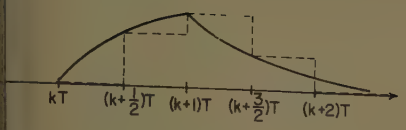


2. Pulse response with a straight-line approximation

ıde those which are controlled by hastic processes.

## Problem

onsider the block diagram configura- in Fig. 1; $G_1$ and $D_1$ are linear uency-sensitive transfer functions, e $N$ represents a nonlinear re- nship between two signal terminals. ally assume that: $G_1(s)$ and $D_1(s)$ ain no dead-time delay; $N$ is a uely defined time-independent func- al relationship of one input; and the pler function is adequately and un- iguously described as

$$)=\sum_{k=-\infty}^{\infty}\{E(kT)(U(t-kT)-U(t-(k+1)T))\} \quad (1)$$

re $T$ is the sampling period, and $U(t-$ is a positive unit step function oc- ing at $t=kT$. Modifications of these litions are discussed following the c development.

With the use of the notation suggested ig. 1, the nonlinear relation is written

$$t)=N[E_g(t)] \quad (2)$$

nique output amplitude at a given e, $E_{gn}(t)$, is dependent on a nonlinear tion of a unique input amplitude at same time, $E_g(t)$, and possible past it magnitudes or storage state. It is possible to write

$$)=E_c(t)*g_1(t) \quad (3)$$

re $g_1(t)$ is the impulse response of ). It is convenient to combine equa- s 1 and 3 and insert the result into the tional notation of equation 2.

$$(t)=\sum_{k=-\infty}^{\infty} N[E_k\{g_1^{-1}(t-kT)-g_1^{-1}(t-(k+1)T)\}] \quad (4)$$

re

$$^1(a)-g_1^{-1}(b))=\int_b^a g_1\,dt, \text{ and } E(kT)=E_k$$

he nonlinear function $N$ cannot be bined with $D_1$ and $E_g$ with linear volution or superposition techniques. s, of course, is the basic quandary in analysis of continuous nonlinear sys- s. A technique is suggested to ap-

Fig. 3. Multirate sampler approximation to the system in Fig. 1

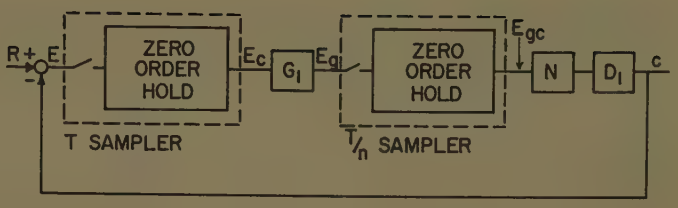


proximate the summation term of equation 4 by a sequence of zero-slope straight line segments (staircase approximation).

For example, let

$$G(s)=\frac{K_1}{1+\tau s}$$

Then the time function $E_g(t)$ can be shown[2] to have the shape of the smooth curve illustrated in Fig. 2. To make maximum use of the $z$-transform techniques, a square pulse approximation is made of the time response. These pulses are sketched in Fig. 2 with the use of arbitrarily, three approximating nonzero pulses.

The straight-line or pulse approximation shown in Fig. 2 is simply an effective mathematical sampling operation between $G_1$ and $N$. Therefore a second sampler is added to the block diagram, as illustrated in Fig. 3. $T$ is the mechanical sampler period, $T/n$ the mathematical sampler period $n>1$. As a consequence of the added sampler, an approximate solution can be found by modifying the methods of multirate sampled-data system analysis.

## Method of Analysis

Following the methods of reference 3, a new block diagram is first constructed (Fig. 4) which is equivalent to the block diagram in Fig. 3. This diagram considers the high-rate sampler as a series of synchronized base-rate samplers, each with a period $T$, and each placed between a mathematical lead and lag time translation of a multiple of the high-speed sampler period.

When equations 1 and 3 are transformed and combined, $E_g(s)$ becomes

$$E_g(s)=\sum_{k=-\infty}^{\infty}(E(kT)^{-kTs})G(s)(1-\epsilon^{-kTs}) \quad (5)$$

where

$$G(s)=\frac{G_1(s)}{s}$$

Referring to Fig. 4, consider only the contribution, $C_p(s)$, of the $p$th channel to the output $C(s)$. It follows that

$$C_p(s)=N\left[\sum_{k=-\infty}^{\infty}E_a(kT)\epsilon^{-kTs}\right]D(s)\times(\epsilon^{-pTs/n}-\epsilon^{-(p+1)Ts/n}) \quad (6)$$

where

$$D(s)=\frac{D_1(s)}{s} \text{ and } E_a(s)=E_g(s)\epsilon^{pTs/n}$$

The $N$ with the bracketed term in this equation, and in those which follow, has the same meaning as the corresponding notation in equation 2, i.e., $N[\ ]$ signifies a unique quantity related in a nonlinear manner to a unique condition represented by the function inside the brackets. Thus, in equation 6

$$N\left[\sum_{k=-\infty}^{\infty}E_a(kT)\epsilon^{-kTs}\right]=\sum_{k=-\infty}^{\infty}N[E_a(kT)]\epsilon^{-kTs}$$

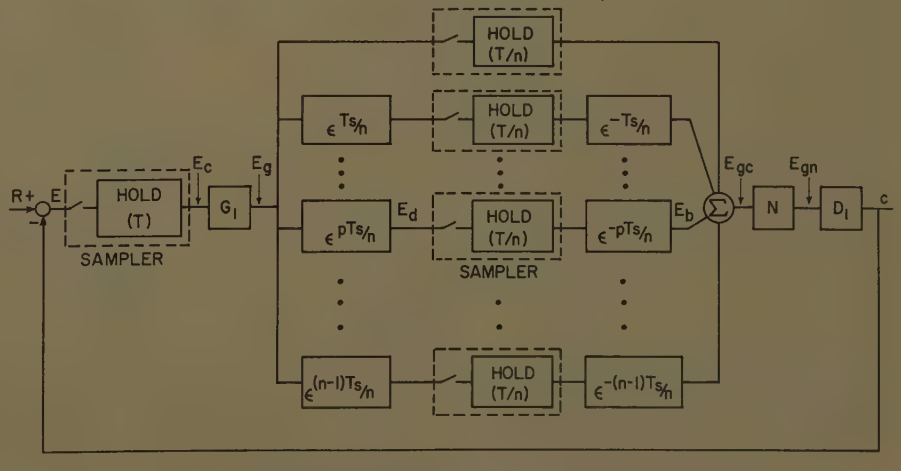


Fig. 4. Multirate sampler approximation to the system in Fig. 1

Equation 6 can be $z$-transformed and combined with the equation $[R(s)-E(s)=C(s)]$, and a summation made on $p$, the parallel branches in Fig. 4. Using the modified $z$-transformation, it can be shown that[2]

$$R(z)-E(z)=\sum_{p=0}^{n-1}\left\{N[E(z)G(z,p/n)(z-1)]\times\left(D(z,1-p/n)-D\left(z,1-\frac{p+1}{n}\right)\right)\right\} \quad (7)$$

Equation 7 can be reduced to a more convenient form:

$$R(z)-E(z)=\sum_{p=0}^{n-1}\left(N\left[E(z)\sum_{u=-\infty}^{\infty}\bar{g}_{nu+p}\,z^{-u}\right]\times\sum_{v=0}^{\infty}\bar{d}_{nv-p}\,z^{-v}\right) \quad (8)$$

where $\bar{g}_{nu+p}$ is the $z_n^{-(nu+p)}$ coefficient in the series expansion of the $z$-transformation

$$Z\left(\frac{G_1(s)}{s}(1-\epsilon^{-Ts})\right)\Big|_{z_n=\epsilon^{Ts/n}}$$

and $\bar{d}_{nv-p}$ is the $z_n^{-(nv-p)}$ coefficient in the series expansion of

$$Z\left(\frac{D_1(s}{s}(1-\epsilon^{-Ts/n})\right)\Big|_{zn=\epsilon^{Ts/n}}$$

The summation on $p$ in the last two equations is a time summation of a sequence of noncoincident pulses, one from each $p$th channel, cycling consecutively every $T$ seconds. Equations 7 and 8 contain the assumption that the order of $D_1(s)$ is at least $s^{-1}$ as $s\to\infty$, a condition often realized in practice. If this assumption is not valid, the summation in equations 7 and 8 must be from $p=1$ to $p=n-1$ with an added term for the $p=0$ channel.

$R(z)$ and $E(z)$ can be expanded in a power series of known and unknown coefficients respectively, and substituted into equations 7 and 8. The resulting unknown $E(kT)$ values can then be found by an expansion, and equating the coefficients of like powers of $z^{-k}$, similar to the methods described in reference 1.

In both equations 7 and 8 the basic sample period of the error solution is $T$ seconds; each $z$ in these equations is defined as $\epsilon^{sT}$. If the sampled error solution is desired at $T/n=T'$ second intervals, equation 8 is easily adapted. To do this:

1. Consider $R(z)$ and $E(z)$ on the left of the equation expanded in terms of $\epsilon^{sT'}$.

2. Consider $z^{-u}$ and $z^{-v}$ to be equal to $\epsilon^{-uT's}$ and $\epsilon^{-uT's}$ respectively.

3. Develop $\bar{g}_{nu+p}$ from

$$Z\left(\frac{D_1(s)}{s}(1-\epsilon^{-nT's})\right)\Big|_{z=\epsilon^{T's}}$$

and

$$\bar{d}_{nv-p}\text{ from }Z\left(\frac{D_1(s)}{s}(1-\epsilon^{-T's})\right)\Big|_{z=\epsilon^{T's}}$$

4. In connection with the foregoing, insure that $E(z)$, within the nonlinear brackets, has coefficients of a series expansion which change only to the values of every $n$th coefficient of the new $E(z)$ solution. Symbolically[3,4]

$$R(z)_n-E(z)_n=\sum_{p=0}^{n-1}\left\{N\left[E(z)\sum_{n=0}^{\infty}\bar{g}_{nu+p}\,z_n^{-u}\right]\times\left(\sum_{v=0}^{\infty}\bar{d}_{nv-p}\,z_n^{-v}\right)\right\} \quad (9)$$

In equation 9 the subscript $n$ refers to a $z$-transformation with $z=\epsilon^{Ts/n}$.

The term $\bar{g}_{nu+p}$ can be shown[2] to be the magnitude of the $nu+p$th approximating pulse of the $G_1(s)$ pulse response. In Fig. 2, for example, $\bar{g}_1$, $\bar{g}_2$, and $\bar{g}_3$ are the only nonzero approximating pulses.

Equations 7, through 9 appear to be formidable expressions, but it must be remembered that they are general results. the $n$ represents the number of approximations made for $E_0(t)$ during one base period $T$. This would be kept to a minimum in practice, say two or three, if possible. The term $u$ is an index on the series expansion of the $z$-transform of

$$G_1(s)\left(\frac{1-\epsilon^{-Ts}}{s}\right)$$

If a sketch, such as Fig. 2, is made, the series $\bar{g}_{nu+p}\,z^{-(nu+p)}$ may be terminated after the coefficients become less than some value, or after a given number of terms. Also, by means of this sketch the computed values of $\bar{g}_{nu+p}$ could be replaced by any other approximating values.

## Simplification of the General Problem

Consider the effects on equation 8 from three reasonable simplifications to the general analysis problem presented by the system in Fig. 1:

1. The mathematical sampler operates at twice the mechanical or base sampler frequency.

2. Four straight-line approximations to the pulse response of $G_1(s)$ are adequate.

3. The terms $g_1(t)$ and $d_1(t)$ do not contain an impulse at $t=0$, i.e., $\bar{g}_0=0$ and $\bar{d}_0=0$.

The approximation in Fig. 2 satisfies these simplifications.

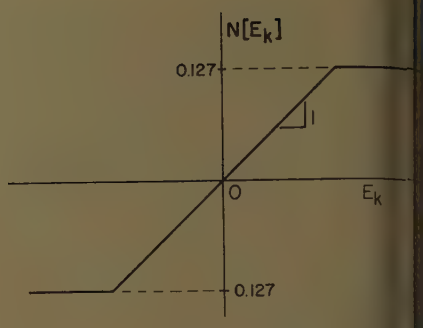


**Fig. 5. Simple nonlinearity for illustratic**

Assume a unit positive step input fu tion. Noting that $n=2$ and $u_{max}=$ a result of the first two simplificatio equation 8 can be reduced to

$$[(1-E_0)+(1-E_1)z^{-1}+(1-E_2)z^{-2}+\ldots]=\left\{N[E(z)(\bar{g}_1+\bar{g}_3z^{-1})]\sum_{v=1}^{\infty}\bar{d}_{nv-1}\,z^{-v}\right\}\left\{N[E(z)(\bar{g}_2z^{-1})]\sum_{v=1}^{\infty}\bar{d}_{nv}\,z^{-v}\right\}$$

The terms $\bar{g}_1$, $\bar{g}_2$, and $\bar{g}_3$ are the ma tudes of the three nonzero straight-l approximations to the pulse respo of $G_1(s)(1-\epsilon^{-Ts})/s$. Solving for coefficients of the unknown error se the following equations result:

$$E_0=1$$
$$E_1=E(T)=1-\bar{d}_1N[E_0\bar{g}_1]$$
$$E_2=E(2T)=1-\bar{d}_1\{N[E_1\bar{g}_1]+N[E_0\bar{g}_3]\}-\bar{d}_2N[E_0\bar{g}_2]-\bar{d}_3N[E$$
$$E_3=E(3T)=1-\bar{d}_1\{N[E_1\bar{g}_3]+N[E_2\bar{g}_1]\}-\bar{d}_2N[E_1\bar{g}_2]-\bar{d}_3\{N[E_0\bar{g}_3]+N[E_1\bar{g}_1]\}-\bar{d}_4N[E_0\bar{g}_2]-\bar{d}_5N[E$$
$$\vdots$$

or

$$E_k=E_{k-1}-\sum_{x=1}^{k}(\bar{d}_{2x-1}-\bar{d}_{2x-3})\times(N[E_{k-x}\,\bar{g}_1]+N[E_{k-x-1}\,\bar{g}_3])-\sum_{y=1}^{y=1}(\bar{d}_{2y}-\bar{d}_{2y-2})(N[E_{k-y-1}\,\bar{g}_2])$$

In the equation for a general $E_k$, terms $(\bar{d}_{2x-1}-\bar{d}_{2x-3})$, and $(\bar{d}_{2y}-\bar{d}_{2y-2})$ u ally approach zero rapidly. $\bar{g}$ and $\bar{d}$ defined with equation 8.

## Illustrative Example

For an example, consider the syst in Fig. 1 with

$$G_1(s)=\frac{0.405}{(s+1)},\quad D(s)=\frac{2}{s(s+2)}$$

$T=1$ second, $R(s)=1/s$, and the sim $N$ shown in Fig. 5. Let $n=2$, the mat matical sampler operating at twice mechanical sampler frequency.

The two expansions which determ

and $\bar{d}_k$, using the expressions with ation 8, are

$$\left.\frac{0.405}{s(s+1)}(1-\epsilon^{-s})\right)\Big|_{z=e^{0.8s}}$$

$$=\frac{0.1597}{z}\left(\frac{z+1}{z-0.606}\right)=\bar{g}(z)$$

$$=0.1597z^{-1}+0.2565z^{-2}+0.1552z^{-3}+$$
$$0.0941z^{-4}+0.0572z^{-5}+\ldots \quad (12)$$

$$\left.\frac{2}{s(s+2)}(1-\epsilon^{-0.58})\right)\Big|_{z=e^{0.5s}}$$

$$=\frac{0.184z+0.132}{z^2-1.368z+0.368}=\bar{d}(z)$$

$$=0.184z^{-1}+0.384z^{-2}+0.457z^{-3}+$$
$$484z^{-4}+0.494z^{-5}+0.497z^{-6}+\ldots \quad (13)$$

onsider only the first three terms of ation 12 ($u_{max}=4$, but $g_0=0$). Then, three simplifications mentioned in the section are satisfied and equation 11 pplicable. Note the convergent se- nce:

0.184
0.384
$\bar{d}_1=0.273$
$\bar{d}_2=0.100$
$\bar{d}_3=0.037$
$\bar{d}_4=0.013$

n, it follows that

$$E_0=1$$
$$E_1=E_0-\bar{d}_1N[E_0\bar{g}_1]=1-0.184N[0.1597]$$
$$=1-0.184(0.127)=0.977$$
$$E_2=E_1-\bar{d}_1(N[E_1\bar{g}_1]+N[E_0\bar{g}_3])-$$
$$(\bar{d}_3-\bar{d}_1)N[E_0\bar{g}_1]-\bar{d}_2N[E_0\bar{g}_2]=0.977-$$
$$0.184(0.127+0.127)-0.273(0.127)-$$
$$0.284(0.127)=0.847$$
$$\vdots$$

The results are given in Table I. For comparison and checking, this example was placed on an analog computer with two samplers, the first operating at 1 cycle per second as stated in the problem, and the second operating at 2 cycles per second, simulating $n=2$ in Fig. 4. The computer solution, however, does not limit $u_{max}$ to four, but considers all terms in the $g(z)$ series. The computer results are shown in Fig. 6 with the sampled error values also listed in Table I. To check the approximation caused by including a second sampler and by letting $n=2$, the computer results for the problem without the second sampler are given in Fig. 7. The sampler error values in Table I from the solution show very close correspondence to those from the approximate solutions. The computed results, including the seemingly severe roundoff effects of equation 11, the accuracy of the measured quantities, and the 10-inch slide rule calculations, are within 10% of the maximum error through the seventh sampled value.

**Table I. Calculated and Experimental Sampled Error Values for the Numerical Example**

| Sampled Error | Approximation: Calculated n=2, u=4 | Approximation: Experimental n=2, u=∞ | Experimental |
|---|---|---|---|
| $E_0$ | 1.000 | 1.00 | 1.00 |
| $E_1$ | 0.977 | 0.97 | 0.94 |
| $E_2$ | 0.847 | 0.82 | 0.77 |
| $E_3$ | 0.665 | 0.65 | 0.60 |
| $E_4$ | 0.480 | 0.47 | 0.48 |
| $E_5$ | 0.311 | 0.28 | 0.24 |
| $E_6$ | 0.169 | 0.10 | 0.08 |
| $E_7$ | 0.053 | −0.05 | −0.06 |
| | | ±0.03 | ±0.03 |

A comparison of the two experimental results suggests that the slowness of the calculated response is due to the samll value of $u_{max}$. However, the accuracy of the approximation resulting from the use of the second sampler with one half the base period, is within the instrumentation tolerance.

The signal out of $G_1$ and the derivative of the signal out of $D_1$ are included in both Figs. 6 and 7. The filtering which is apparent on these signals is basically responsible for the close check of the approximate solution (with $n=2$) and the exact solution.

The accuracy of these approximating results for the low $n$ and $u_{max}$ values in

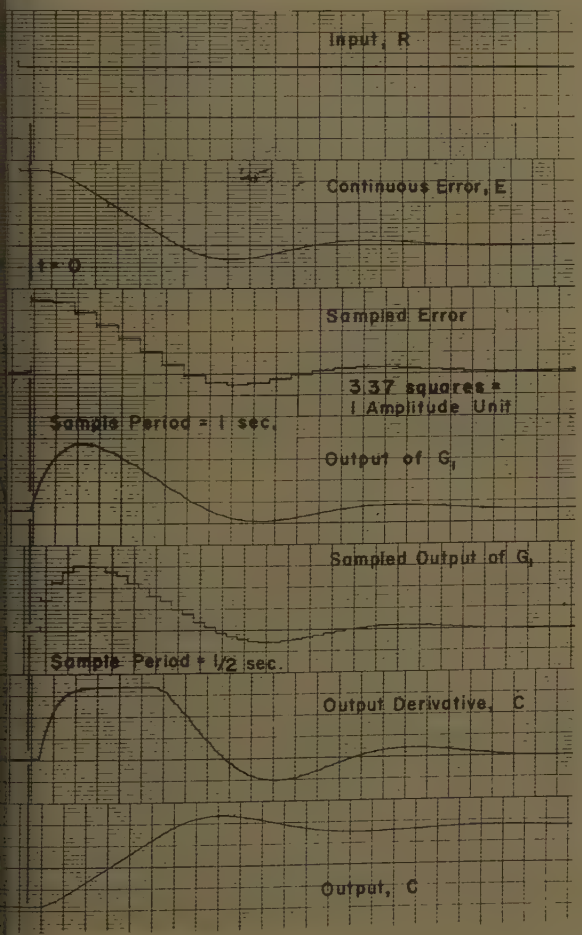


Fig. 6 (left). Approximate system response, $n = 2$, $u = \infty$, for illustration

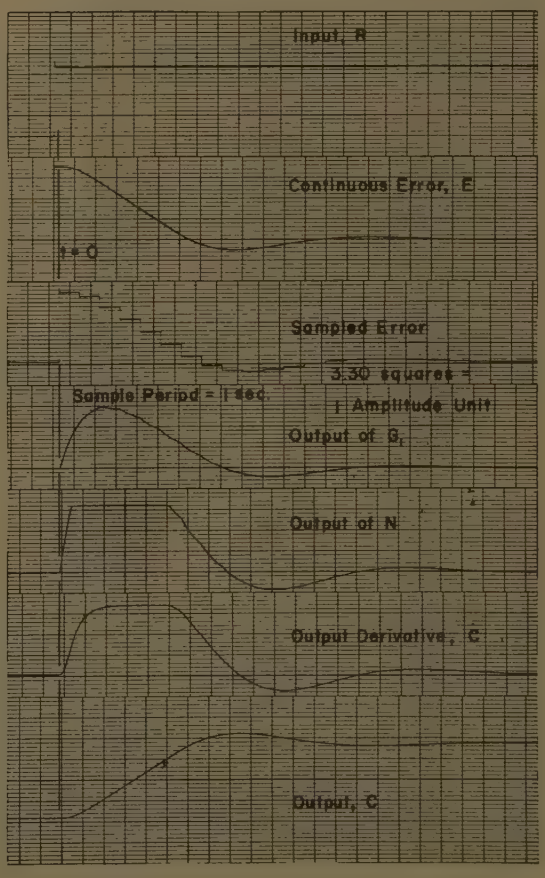


Fig. 7 (right). System response for illustration

this particular example must be generalized with care. A less severe nonlinearity, such as the saturation of a d-c generator, would tend to increase the accuracy of the approximation, while shorter time constants in the linear portion of the system would have the converse effect.

### Modifications and Extensions

The application of equations 7 and 8 to a system such as is illustrated in Fig. 1, but with a nonstep input function, a multistorage nonlinearity, and a transport delay, follows the procedures discussed for the methods developed in a previous paper.[1]

Equation 9 is equivalent to equation 8 except for the evaluation of $E(t)$ at the high sampling rate. Therefore intersample values may be investigated by varying the value of $n$ in equation 9.

A system containing time-varying parameters can be treated as suggested in reference 1, to the practical extent that the varying parameter influences just a few terms in a reduced equation, such as in equation 11.

### Conclusions

Methods for obtaining the numerical solution of nonlinear sampled-data control systems, as illustated in Fig. 1, are described. The use of these methods makes it possible to obtain solutions to important nonlinear control system problems which cannot be solved by conventional methods or those described in reference 1. For finite $n$ the solution is approximate. The methods are general in application and they permit any degree of approximation. As the accuracy of the approximation increases, the labor required to derive the solution increases, as expected.

The ease with which these methods a applied changes little with the relati complexity of the description of $N$ a the form of $G_1(s)$. Various $D_1(s)$ fu tions, however, may increase the numb of nonnegligible $\bar{d}_{nv-p}$ terms in equation thus varying the extent of one of three summations. An actual probl evaluation requires only the use of sta ard $z$-transform tables and systema calculations.

### References


1. Analysis of Nonlinear Sampled-D Control Systems, Part I, E. Kinnen, J. *AIEE Transactions*, see pp. 386–90 of this issu

2. The Analysis of Nonlinear Sampled-I Control Systems, E. Kinnen. *Ph.D. Th* Purdue University, Lafayette, Ind., 1958.

3. Digital and Sampled-Data Control Syst (book), J. T. Tou. McGraw-Hill Book Comp Inc., New York, N. Y., section 6.7, 1959.

4. Analysis of Sampled-Data Feedback trol Systems with Finite Sampling Durat J. Tou. *AIEE CP 58-801* (available on reque


## Joint Discussion

### Discussion of Papers 59-828 and 59-829

**Thomas J. Higgins** (University of Wisconsin, Madison, Wis.): The authors of these two papers have written a clear, easily followed account of an excellent numerical technique for analysis of nonlinear sampled-data systems. The numerical examples and experimental data confirm well the application and correctness of the general theory.

**Keisuke Izawa** (Tokyo Institute of Technology, Tokyo, Japan): The papers under discussion are an outstanding contribution to the theory of nonlinear sampled-data control systems. The proposed sequence method and the modified one with the introduction of multirate sampler are useful for tracing the transient responses of the control systems.

The $G_1$'s in the papers might include the equalizer to achieve better control behavior. The design of the equalizer would be of particular interest to the practicing engineer. Although the introduction of the multirate sampler simplifies the analysis it might be of great help to discuss the adequate value of $n$ of the multirate sampler.

**E. Kinnen and J. Tou:** The authors appreciate the comments made by Dr. Higgins and Dr. Izawa. The inclusion of an equalizer in $G_1$ to achieve better control behavior is certainly a valuable suggestion. In fact, work is now being undertaken to extend the techniques described in this paper to the design of equalizers, both continuous and discrete, for compensating nonlin sampled-data systems. The results wil reported in a future paper.

The second comment made by Dr. Iz brings up a good point. However, choice of a suitable value of $n$ for the titious sampler in Part II is dependent many factors, such as the properties of the sampling period $T$, and the nature of nonlinearity. A detailed discussion of point would require a whole paper. main idea is to approximate the continu input to the nonlinear element $N$ by a s case signal, which is more amenable mathematical analysis. A general st ment for the minimum value of $n$ is diffi to make. Roughly speaking, if $G_1$ is a low-pass filter, a fictituous sampling quency of five times its bandwidth w usually lead to a satisfactory result. the sampling period $T$ specified, the quate value of $n$ can thus be estimated.

# Cathodic Protection Applications at the Hanford Works


C. S. BUCHOLZ
MEMBER AIEE


THIS PAPER describes existing, presently planned, and experimental impressed-current cathodic protection (CP) installations at the Hanford Atomic Products Operation. The Hanford plants are located in the south-central part of the state of Washington. Climatic conditions are semiarid and the plant area is typical desert country. The soil is predominantly glacial deposits ranging from fine sand to gravel mixed with larger boulders. This water-washed material has a very high resistivity, from 5,000 to 100,000 ohm-centimeters, although there are local strata of hardpan and alkali of lower resistivity. In general, the soil is only mildly corrosive to ordinary materials. Most of the original cast-iron, galvanized-steel, and carbon-steel un ground piping installed in 1943 and is in good condition. As discussed he the direct burial of unprotected stain steel pipe lines has not been succes

Some serious corrosion of large vanized grounding cables has been perienced because of the wartime pedient of using available materials this case a lightly galvanized, h strength (high-carbon) steel strand.


Paper 59-821, recommended by the AIEE Che Industry Committee and approved by the Technical Operations Department for presenta at the AIEE Summer and Pacific General Me and Air Transportation Conference, Seattle, W June 21–26, 1959. Manuscript submitted M 23, 1959; made available for printing May 22,



C. S. Bucholz is with the Hanford Atomic Pro Operation, General Electric Company, Rich Wash.

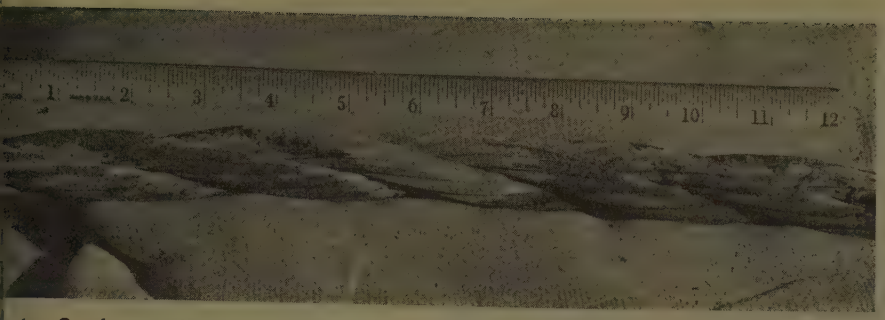

1. Steel grounding cable after burial in sandy soil for approximately 14 years. The galvanizing has been consumed in the dark areas

ical example is shown in Fig. 1. Extra-vy galvanizing is specified for new struction. Failure of underground l piping has been caused by near-by e-copper ground conductors and, for reason, copper is no longer used in the nity of other buried metals.

rocess water for the Hanford facilities pumped from the Columbia River, red, and treated. Resistivity varies h the season of the year and treatment, has an average range of 3,000 ohm-timeters at 40 F (degrees Fahrenheit) ,000 at 170 F. Sanitary water is taken n the process water supply (or pumped n wells near the river) and chlorinated. s about 3,400 ohm-centimeters at 70 F. se waters are quite aggressive to on steel.

xclusive of a few specialized applica-s, the four subjects discussed herein ntially cover the scope of CP work at nford. A general knowledge of CP ciples on the part of the reader is med.

## hodic Protection of Underground Stainless-Steel Process Lines

uried stainless-steel pipelines are used nsively for transport of liquid process erials between separations plants, te storage tanks, and other facilities. lines are from 1 to 4 inches in nominal neter and are mostly of the *18-8* les of stainless steel. All joints are lded-arc welded. Some of these ess materials are highly radioactive any leakage into the surrounding h could have serious consequences. revent such incidents, lines installed e 1948 are encased in concrete ducts teel pipe (except those carrying low-l radioactive wastes). The ducts are nged to drain into catch tanks from h any leakage can be removed safely. pproximately 5 miles of pipe for the inal separations plants were installed 3-44) directly in the earth with no ective covering or coating. Several leaks in these lines had occurred by 1947 but corrosion was not seriously considered as the cause at that time. During that same year a new line was laid as a part of a process change. The excavation was partially backfilled, and the pipe left exposed to air and moisture for about 2 months. No pressure could be maintained when testing was attempted because the new line had become literally honeycombed by corrosion. This surprising incident definitely established the fact that, under certain conditions, stainless steel does corrode rapidly in Hanford soils. Corrosion starts in small round pits 1/8 to 3/16 inch in diameter. The pits or craters, when active, contain a moist black corrosion product, and often apparently migrate down and around the pipe giving the metal a worm-eaten appearance.

After a thorough investigation of the problem, CP was recommended as the most practical method to prevent further deterioration of underground stainless lines, and late in 1947 protective systems were installed on the 5 miles of existing piping. About half of these lines are still in use, and only five leaks have been detected since the inception of the CP program. Three of these are thought to be, at least in part, caused by factors other than external corrosion, i.e., damage by heavy machinery, abnormal stress at a diversion box, and other damage to an unusually light-gage old line.

A total of approximately 15 miles of encased or bituminous-mastic-coated stainless-steel process lines has been constructed since 1948, all cathodically protected. Parallel lines are often placed in a common concrete duct and single runs are sometimes contained within a larger carbon-steel pipe. In either case, the stainless pipe is supported at intervals on insulating collars so that the metal is not in contact with any conducting media. Cathodic protection is used to obviate the possibility of corrosion in the event that process solutions or water should enter the encasements.

Anodes for these CP systems are made

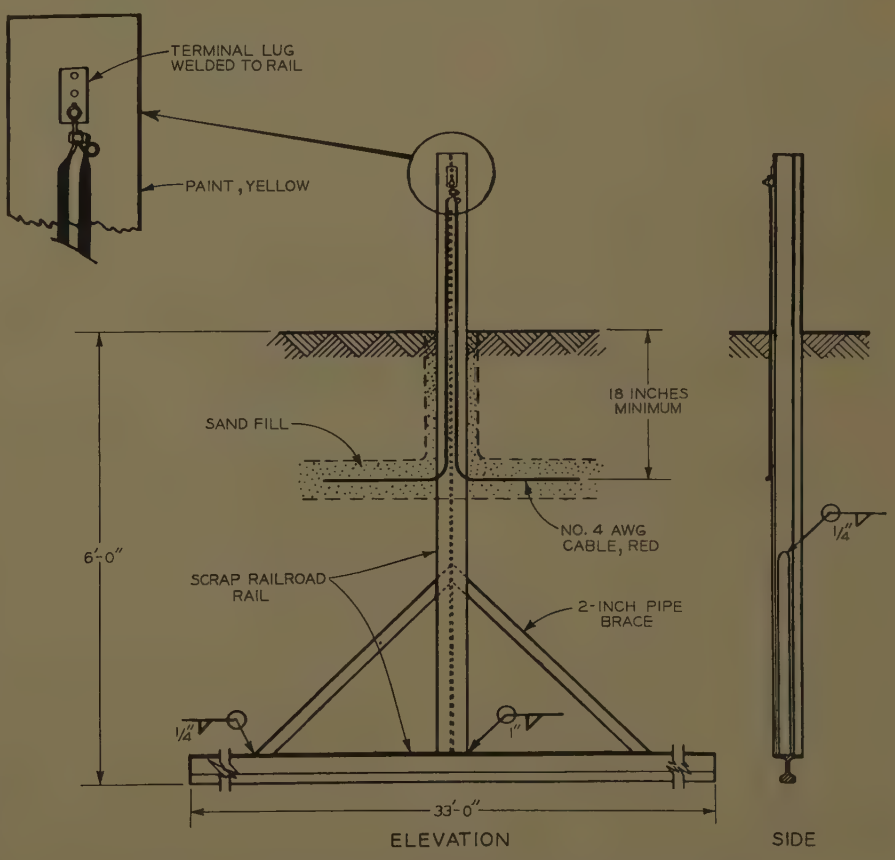


Fig. 2. Anodes used for protection of stainless-steel pipelines

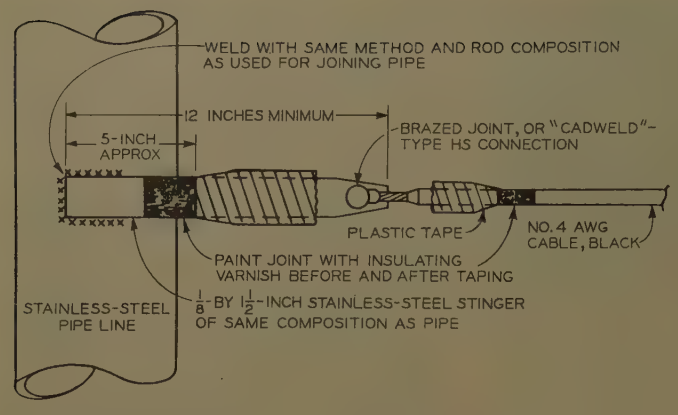


**Fig. 3 (left). Cathode connection to stainless-steel lines**

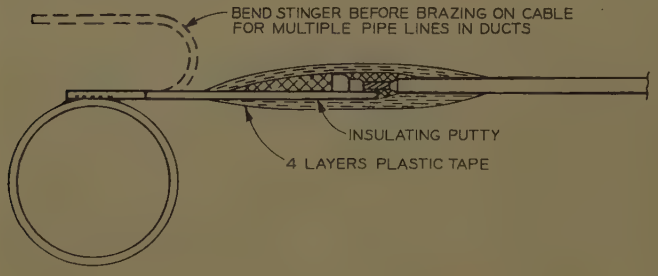


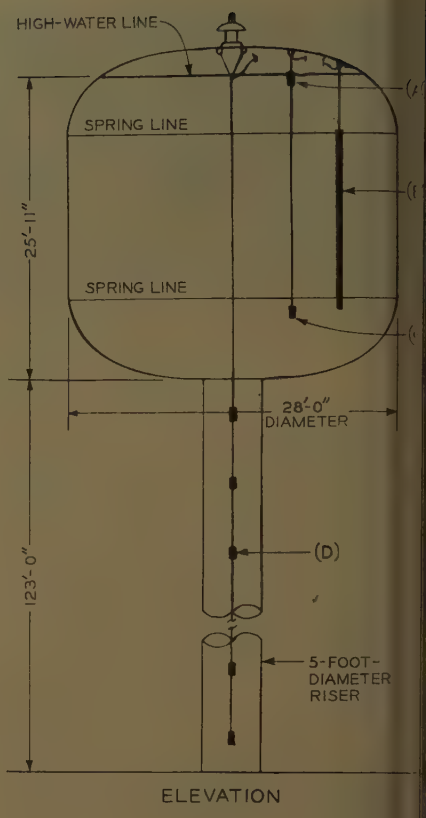


**Fig. 4 (right). Anode configuration for an elevated water-storage tank**

A—Six 1 1/2- by 12-inch top anodes
B—Six 1-inch by 15-foot main anodes on 9-foot radius
C—Six 1 1/2- by 12-inch stub anodes on 5-foot radius
D—21 1 1/2-by 12-inch riser anodes, 5-foot 6-inch spacing

from railroad rail because scrap rail is readily available and a large effective area can be obtained. A typical anode detail is shown in Fig. 2. Anodes are spaced 150 feet apart alternately on both sides of the pipeline, and the same distance laterally from the line. Close spacing is desirable in this high-resistivity soil. The method of attaching the cathode lead to lines is shown in Fig. 3. Tape is used over the copper conductor and weld material to prevent local cell action with the stainless steel. All other connections and splices are made above ground at the anode or in boxes to prevent current leakage and to provide convenient test points.

Rectifiers rated at 24 volts output are usually adequate. The current averages about 1 ma (milliampere) per square foot of bare pipe but is, of course, much less for the encased lines. A potential of not less than −0.60 volt as measured with a copper–copper-sulphate half-cell is maintained. The cell is positioned directly over the pipeline, or about 10 feet from the line where lines are less than that depth from grade.

## Water-Storage-Tank Protective System

Fig. 4 shows a CP system design for a 100,000-gallon elevated storage tank for sanitary water. This type of tank has an ellipsoidal top and bottom section and is well adapted for CP having rounded contours without sharp corners or shielded areas. Many have been erected in all parts of the United States including several others at Hanford. In the plant areas, these tanks are used for fire protection or other emergency water supply and are therefore kept completely filled.

The conventional anode layout for tanks of this kind employ a number of main anodes in the bowl and sectionalized anodes extending the full length of the riser. Except possibly for small tanks, additional stub anodes are required for the bottom area of the bowl which is inside the effective radius of the main anodes. The design shown follows these standard details.

Referring again to Fig. 4, it will be noted that the high water line is well up into the top ellipsoidal section where the effectiveness of the main anodes drops off rapidly. The mains cannot be raised because to do so would reduce the allowable 5-foot minimum spacing to the tank surfaces. Thus protection at the water line, where it is most needed, may not be adequate. In the design of the system shown, the author added short top anodes to the stub strings which reinforce the main anode current in the upper region. The additional cost for these anodes is insignificant.

The interior of the tank was paint just prior to installation of CP in Nove ber 1958. Six 1-inch-diameter by foot-long main anodes, six top and bottom 1 1/2- by 12-inch stub anodes, a 21 1 1/2- by 12-inch riser anodes, all high-silicon cast iron, were used. A CP rectifier was installed with one sect for the main and the other for the ri and stub anodes. With the addition rheostat in the stub feed, the voltage each of the three anode assemblies can individually controlled. Design an resistance, and voltage and current quirements were close to actual operat values. Data taken after the system become stabilized are shown in Table Final testing and adjustments have been completed to date because of clement weather.

## Protecting a Reactor-Containment Vessel

A common design feature of reactors be located in populated areas is the la

**Table I. Water-Storage-Tank Protective System**

| Anodes | Voltage | Total Current, Amperes | Actual Resistance, Ohms | Calcula Resistan Ohms |
|---|---|---|---|---|
| Main | 14.6 | 11.6 | 1.26 | 1.08 |
| Top and bottom stub | 10.0 | 1.1 | 9.10 | 9.50 |
| Riser | 14.9 | 7.1 | 2.10 | 1.25 |

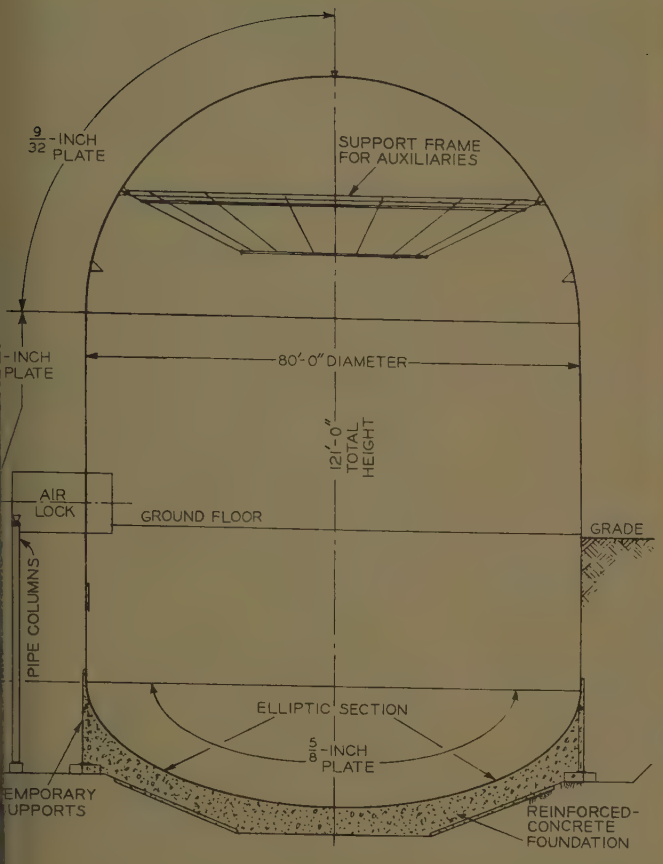


Fig. 5 (left). Section through welded-steel reactor-containment vessel

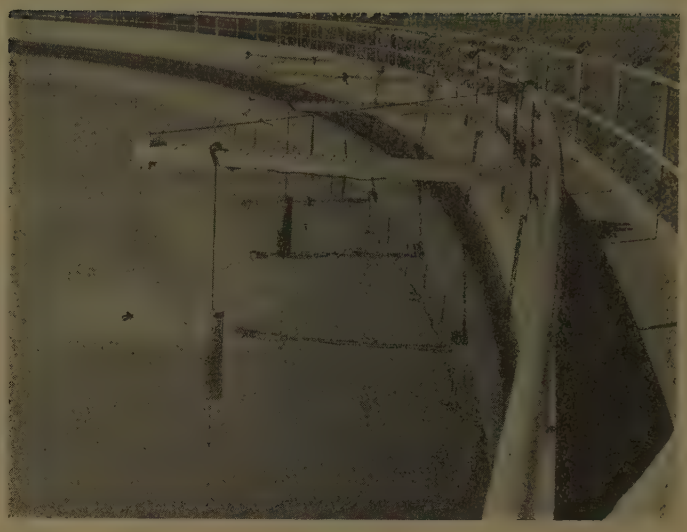

Fig. 7 (above). Experimental installation in a steel retention basin showing the wood brackets and graphite anodes

eel sphere (or similar form) entirely rrounding the reactor. The objective of course, to hold within the shell any dioactive materials that may result from reactor mishap. Because they are essure vessels, the underground portion ould be protected from corrosion.

A containment vessel for a research re-tor now under construction at Hanford shown in Fig. 5. The design does not provide for any corrosion allowance on the plate thickness. Nearly half of the structure is below grade, and the underground surfaces were covered with an asphalt-impregnated fiber membrane, 5/32 inch in thickness, applied with hot asphalt. The concrete foundation was poured after fabrication of the lower portion and after the membrane was in place.

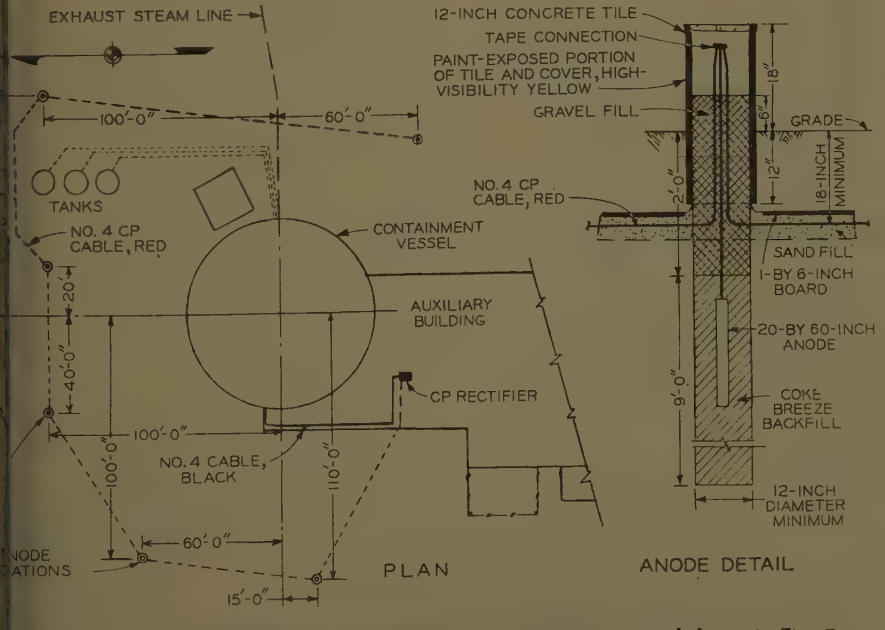


6. Layout and anode detail for protection of the containment vessel shown in Fig. 5

Cathodic protection will be applied immediately after backfilling. Current will be supplied from six 2- by 60-inch high-silicon iron anodes with coke breeze backfill, the first installation of this kind at Hanford. Graphite anodes would also be suitable for this application. The anode layout is shown in Fig. 6. Irregular anode spacing was necessary to avoid underground service lines and to provide some protection to this piping and to auxiliary tanks. A rectifier rated at 48 volts and 15 amperes will supply approximately 10 ma per square foot of metal surface assuming that the coating may, in time, become only 90 per cent effective. Fig. 6 also shows a combination anode installation and test station made from a length of 12-inch-diameter concrete tile. Sand backfill covered with creosoted wood boards, as shown, is commonly used at Hanford to provide some mechanical protection for directly buried electric cables.

No operating data for this system will be available for several months.

## Experimental Cathodic Protection Installation for Reactor-Cooling-Water Retention Basins

Effluent water from the Hanford reactors is discharged into retention basins so that, in the event of an abnormal level of radioactivity in the water, the radioactivity can be allowed to decay before the water is returned to the Columbia River. Several very large steel tanks are used for this purpose. The water is thermally hot and ordinary paint coatings are not suitable for use on the inside surfaces of these basins. Two open tanks, constructed in 1952 for use with the *105-C* re-

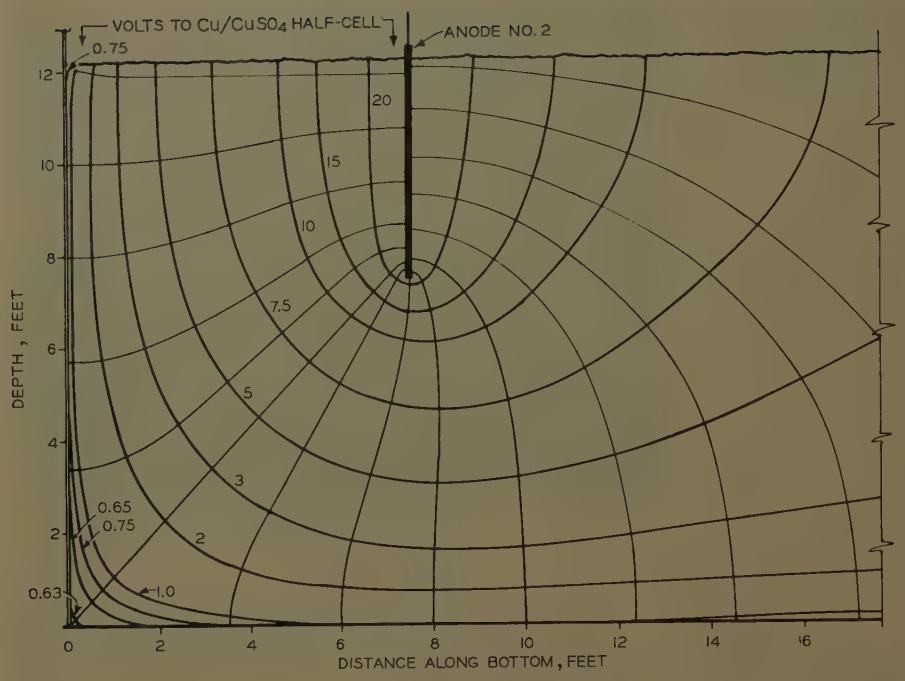


**Fig. 8. Cross section of the basin at an anode location showing equipotential and current flow lines**

Water temperature = hot
Rectifier voltage = 35
Anode current = 1.99 amperes

actor, are 330 feet in diameter, have straight 16-foot sides, and a capacity of 9 million gallons each. The original paint had begun to fail after about one year of operation.

It was then decided to investigate the possible application of CP to these basins and, in the summer of 1954, an experimental system was installed in one of the tanks to operate on a small segment of the side wall. This work was continued by the author through July of 1957. Preliminary results were discussed in an unpublished conference paper presented at the AIEE Summer and Pacific General Meeting in 1956.

Four anodes were suspended from wood brackets as shown in Fig. 7. Aluminum graphite, and high-silicon-iron anodes were tried. The last proved most satisfactory for this application. Two- by 60-inch anodes were spaced 7½ feet from the tank wall and 15 feet apart. With hot water, this spacing required 35 volts to produce a current of about 2 amperes per anode and an average of 10 ma per square foot at the protected metal. Half-cell readings at the water surface under these conditions were −0.82 volt maximum opposite an anode position and −0.70 minimum mid-way between anodes.

Tanks with the side and bottom surfaces at a right angle present a difficult problem in the protection of the extreme corner. The cross section, Fig. 8, shows the approximate current and voltage distribution and shows the serious drop in potential which occurs at the lower third of the tank wall. The lower end of the anodes are about the same distance (7½ feet) from the tank bottom as the radial spacing from the wall. Little would be gained by using longer anodes because a large part of the current would flow to the bottom in the region directly beneath them.

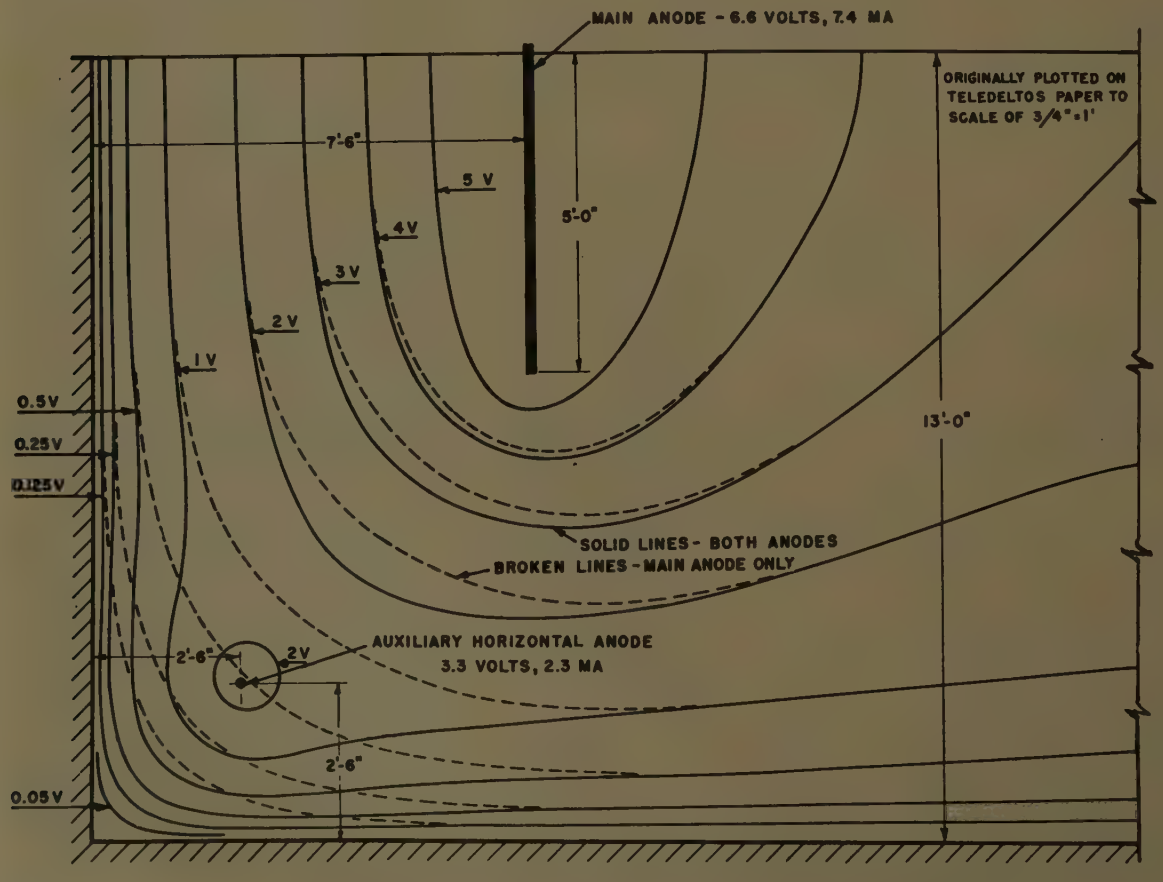


**Fig. 9. Plot conductive pap representing a s tion through t basin. The effect auxiliary anodes the potential dis bution is dem strated**

It was realized from the beginning that ie corner areas were probably not re-iving adequate current for complete otection, but it was hoped that the fects of prolonged polarization and ssibly some mineral deposition would entually force the current to pro-essively lower surfaces. This did not aterialize. There was no significant ange in the potential distribution after arly 2 years of operation.

Further effort was then made to in-stigate the degree of coroner protection means of Corrosometer probes and the e of a one-foot-square test plate. This ly confirmed what was already known, at the lower third of the wall was t receiving sufficient current. The rrosometer showed complete protection the top and half-depth probe locations t the rate of corrosion at the bottom was t much improved over that at an un-otected location. Currents to the test ate were about 6 ma per square foot at e bottom, 12 at half-depth, and 20 at the rface.

The conventional design methods for wl-shaped tanks containing quiet water appreciable mineral content cannot be plied to these basins. None of the sential factors are present, i.e., the nks have a sharp, square side-bottom tersection, much more current is re-ired to maintain the polarizing film of drogen with rapidly flowing water, and ere is little, if any, mineral deposition at e current density required for protec-n. It is quite possible that adequate rner protection could have been at-ined had any one of these factors been vorable.

Fig. 8 is a plot of the actual measured lf-cell potentials taken at various loca-ns. Curves were drawn through points equal potential. To aid in visualizing e pattern of current flow, one can draw econd set of curves which interesect the uipotential lines at right angles.

An easier method for mapping the tential field at corners, interference as, etc., which produces a reasonably curate "picture," is as follows. A tion through the current source ode) and the metal to be protected is wn on resistance paper using conduc-e paint, and a small d-c potential is plied across this analog of the anode and thode surfaces. Lines of equal po-

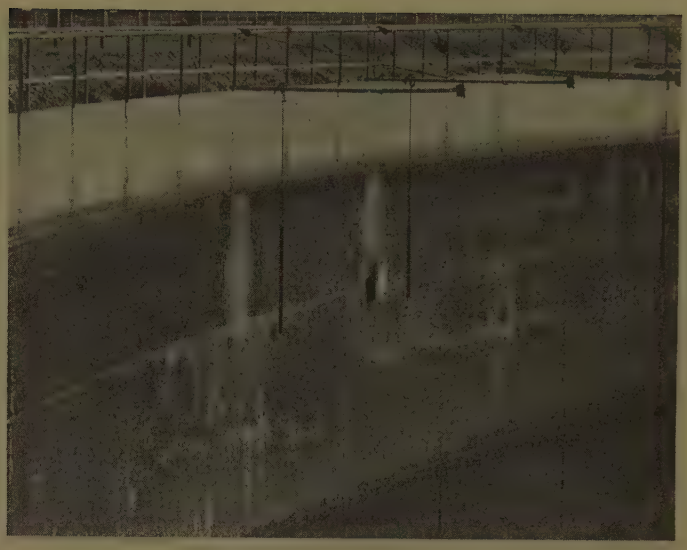

**Fig. 10. Interior side wall of the drained basin showing the mineral deposits obtained with abnormally high current**

tential can then be traced on the paper with a probe connected to a sensitive voltmeter. Fig. 9 is a plot made in this way for the same cross section. Note that the shape of the potential curves (broken lines) are almost identical with those of Fig. 8, although the numerical values now have no particular significance.

The solid curves in Fig. 9 illustrate the effect of introducing a horizontal auxiliary anode in the corner area. Many combinations of position and fraction of main anode voltage applied to the auxiliary anode are possible. The arrangement shown is the most successful of several made by the author. Note how the equipotential lines are straightened down into the coroner, which is a great improvement over the distribution with the main anode only (broken lines). Nevertheless, the extreme corner inevitably remains at a reduced potential.

Although the cost of a full-scale CP system for these tanks can be justified, the lower few inches of the side walls could not be fully protected without the application of some type of insulating coating in the corner area which largely defeats the advantages of CP. The original paint has since ceased to be of any value and other studies are being made in an effort to prolonged the serviceability of the basins. The corrosion rate is about 10 mils per year. One-eighth inch of extra plate thickness was provided in the design and thus the tanks should have a minimum life of 12 years with no protection. It has been shown that, for new basins, the cost of providing the necessary extra metal thickness for any desired life is more economical than periodic painting or the installation of CP.

The author had been curious during the course of the experimental work as to why no mineral deposits could be observed on the tank wall. At the conclusion of the work it was decided to move two of the anodes to within about 2 feet of the wall in an attempt to force a precipitate. The current from each anode at this location was increased to 3.2 amperes. The photograph, Fig. 10, was taken about 3 weeks later when the tank was drained. A heavy localized deposit of calcium carbonate had formed on the tank wall directly behind the anodes which appears on Fig. 10 as the two white rectangular areas. However, calcareous deposition occurs only at a current density of about ten times that necessary to stop corrosion.

The other irregular light-colored areas in Fig. 10 are patches of the original paint. Presumably the paint film, somewhat thicker in these areas, had not deteriorated before CP was applied, and CP had halted further breakdown of the paint. The dark surfaces in the illustration are, of course, corroded metal and all surfaces outside the influence of the protective current are uniformly of this appearance. The contrast is not as strikingly apparent as formerly because the CP installation was inoperative for several months before the photograph was taken.

# A Solid Rotor A-C Generator for High-Temperature Electrical Systems

J. T. BATEMAN
NONMEMBER AIEE

RELIABILITY has always been the primary requirement for aircraft generating systems. The rapid development of high-performance aircraft has continually demanded greater reliability along with increased operating temperatures. These two conditions are not directly compatible. As temperatures increase the choice of insulations and lubricants is narrowed to a few which, in general, have inherently lower mechanical properties than the conventional lower temperature materials. During high-temperature operation these materials, as well as the electromagnetic materials, suffer additional loss in physical and electrical properties. The desired increase in reliability must be achieved despite these obstacles introduced by the increased temperatures.

A development program aimed at generating equipment for 600 F (degrees Fahrenheit) ambient temperature has been in progress since March 1958. At the outset of this program it was recognized that the most painstaking development and application of high-temperature materials might still result in a generator which fell short of acceptable aircraft reliability. For this reason, a vital part of this development program has been the investigation of unusual types of generators where there are fewer components and where the stress of critical components is reduced.

This paper presents a brief survey of high-reliability generator configurations. The generator selected for the 600 F development program is described and its characteristics are related to conventional equipment. Bearing and insulation work on the 600 F program is described in other related papers.[1,2]

## Objectives

The 40-kva 120/208-volt 0.75-power-factor 3-phase 400-cycle 8,000-rpm generator rating that has been specified in this development program is typical of the majority of current military and commercial a-c aircraft generators. Environmental specifications reflect the more severe conditions which would be encountered in a Mach-3 aircraft.

| | |
|---|---|
| Ambient temperature | 600 F |
| Vibration | 20 *g* |
| Shock | 50 *g* |

Out of 500 hours of life, 20 hours are specified at the ultimate condition with the remainder at more conventional temperatures.

To maximize reliability under these severe environmental conditions, several additional design objectives were set.

1. Use a minimum number of parts, especially where high electrical or mechanical stresses will occur.
2. Remove all windings, rectifiers, and other electrical components from the rotor. This will also eliminate brushes, slip rings, and commutators.
3. Utilize configurations where the mechanical strength of the electromagnetic iron parts will add to the structure and ruggedness of the generator.
4. Select electromagnetic circuits which would allow rectifiers, capacitors, and other sensitive components to be relocated in a more favorable environment if necessary.

These approaches for achieving the greatest possible reliability were all tempered by the fact that lightweight design is an extremely important requirement in aircraft generating systems. The known electromagnetic configurations which would meet the high-reliability design objectives appeared to be somewhat heavier than conventional salient pole wound rotor designs. This was not considered an insurmountable problem since these high reliability configurations did not have the benefit of intensive creative design study directed toward their weight and performance optimization. With the expectation that significant improvements could be made, the investigation of new generator configurations was directed toward those having the greatest inherent reliability.

## Permanent Magnet Alternator

The removal of all windings from the rotor could be accomplished with a permanent magnet type of generator with saturating windings in the stator providing voltage control. Because the excitation system serves to depress the output voltage, this type of generator would deliver overvoltages in the event of a failure of the regulating system. If an internal fault occurred in the generator, no method short of mechanically disconnecting the generator would be certain to prevent a fire. Only magnetic materials having a high energy product would be considered for lightweight aircraft design. Above 600 F these magnet materials are gradually demagnetized.

## Inductor Alternator

The inductor alternator has already distinguished itself as a generator configuration which meets all of the design objectives for high reliability. A brushless d-c generator has been built using the basic inductor electromagnetics with only a rotating iron configuration on the rotor. The 800-cps power generated by these electromagnetics is rectified to provide 100 amperes, 30 volts direct current at the terminals of the generator. This brushless d-c generator is now in use on a modern, high-performance intercept aircraft.[3]

The basic principle of the inductor alternator in all of its varied configurations is well described in the literature.[4] In spite of this, it should be helpful to describe briefly, the double-ended, homopolar inductor configuration which is the basic design around which much of this study centered. This can be done conveniently with reference to the conventional salient pole synchronous generator pictured in Fig. 1(A). The alternately north and south magnetic poles of this rotor are induced by d-c field windings placed around each pole piece. Since these windings encircle each pole, they must rotate with the rotor and, therefore, field current from a stationary source must be supplied through some sort of sliding contacts or brushes to the rotor. This conventional generator can be converted into a homopolar inductor machine by the changes pictured in Fig. 1(B). The rotor body and the stator are lengthened, but the pole pieces themselves are unchanged. The north poles are displaced at one end and the south poles are displaced at the other end, but the angular relationship is unchanged. The modified rotor would still work with the original field coils, but this is unnecessary.

Paper 59-848, recommended by the AIEE Transportation Committee and approved by the AIEE Technical Operations Department for presentation at the AIEE Summer and Pacific General Meeting and Air Transportation Conference, Seattle, Wash., June 21–26, 1959. Manuscript submitted March 23, 1959; made available for printing April 30, 1959.

J. T. BATEMAN is with General Electric Company, Erie, Pa.

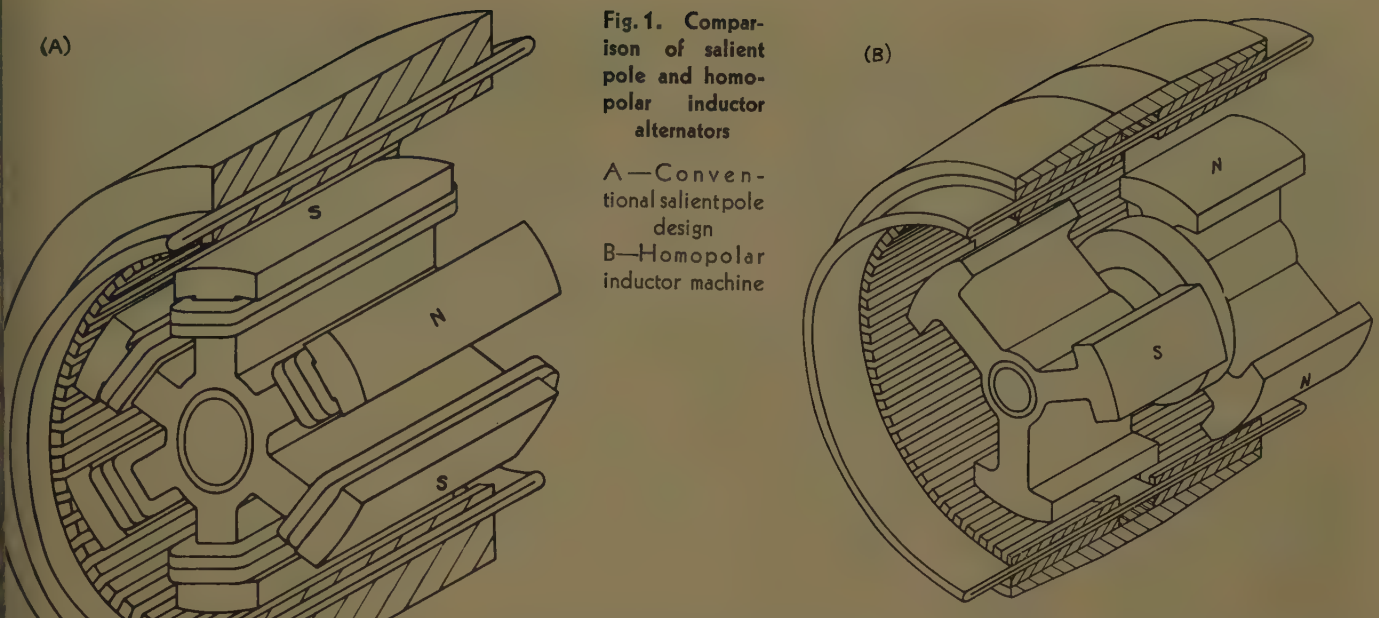


**Fig. 1. Comparison of salient pole and homopolar inductor alternators**

A—Conventional salient pole design
B—Homopolar inductor machine

l of the magnetic flux which passes from e north poles to the south poles internal the rotor must go through the center rtion of the shaft. A single, coaxial ld coil around the shaft at this point ll link all of the flux and supply all of e necessary excitation. This coil is not quired to rotate and it can therefore be ed in the stator eliminating the need for ushes or other sliding contacts.

It is evident from Fig. 1(B) that the ux must travel axially both in the center the rotor and outside the stator core. order to accommodate this flux, solid el paths are provided at both points. he coaxial coil is required to supply ly as many ampere-turns as originally pplied by two of the separate coils of g. 1(A). In the case of a 6-pole genera- r this represents a significant reduction excitation power. The sketches of Fig. might suggest that the inductor machine more than twice as large as the con- ntional machine. This is not the case. he inductor is usually heavier, but the pical increase is only about 60%. The wer excitation power requirements and mination of current collection pro- sions will actually result in a reduction system weight or volume for some appli- tions.

The actual rotor used in the 100-ampere ushless d-c generator is shown in Fig. 2, ng with the stator. The coaxial field il can be seen inside the stator. This nfiguration satisfies all of the design jectives for greater reliability. The tor has been reduced to a minimum mber of parts by the elimination of rotating field windings, topsticks, binding bands, slip rings and brushes. The stator design includes an iron frame which not only carries flux but also adds to the frame structure of the generator. Because all of the electrical circuits are located on the stator, remote location of associated rectifiers and capacitors is possible. Oil cooling may be accomplished with a simple and reliable circuit of oil tubing across the outside of the frame. For 40-kva 6-pole generators, however, the additional weight involved in the usual double-ended homopolar inductor design would indicate that improved variations of the basic configuration should be considered.

## Lundell Alternator

The weight disadvantage in the homopolar inductor generator is largely explained by the fact that the north and south poles are at opposite ends of the rotor and no part of the stator sees a full north to south variation of flux. With this half-wave flux, the stator iron is used to only one half of its capability and accordingly the machine is heavy. A rotor configuration which would present alternate north and south poles to a single stator while retaining the feature of a coaxial field coil would seem to be desirable.

The Lundell generator provides such a configuration. North and south polarities are maintained at opposite ends of the rotor through the action of a coaxial field coil. The north and south poles are not positioned at opposite ends of the rotor, however. North and south poles are extended from each end toward the center of the rotor so that north poles project between south poles and vice versa. This presents an array of alternate north and south poles to the stator and provides for a full-wave flux variation and optimum stator electromagnetic weight.

One of the many possible arrangements of Lundell electromagnetics is shown in Fig. 3. One of the marks of a brushless Lundell configuration may be seen in this sketch. Two secondary or parasitic air gaps are always required to complete the rotor flux circuit and yet allow the use of a stationary coil. In the configuration shown, flux travels along the frame and crosses one secondary air gap into the north pole end of the rotor. The flux then travels out along the cantilevered north pole fingers, emerging from the north pole faces and crossing the main air gap into the stator. The flux follows the same paths in the stator as it does in conven-

**Fig. 2. 30-volt 100-ampere d-c generator disassembled rotor and stator showing inductor construction with coaxial field coil visible in stator**

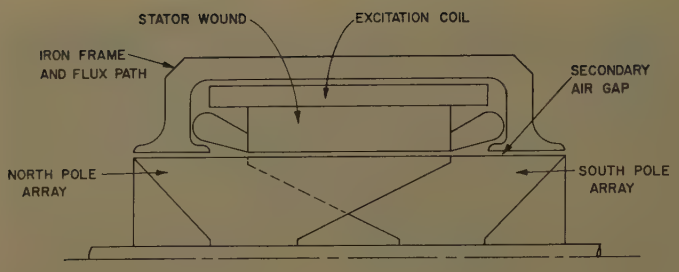


**Fig. 3. Lundell generator with rotor flux path completed behind the stator**

tional salient pole generators. Emerging from the stator, the flux crosses the main air gap into the south poles, and finally crosses the secondary air gap into the frame. Like the inductor generator, a single coaxial field coil serves to excite the entire flux path regardless of the number of poles. There are many possible combinations of pole shapes, secondary air gap locations, and flux return paths that fall in the classification of Lundell designs. This particular configuration was shown because it will assist in the understanding of a design to be discussed later.

The Lundell generator has one inherent characteristic which affects its weight as compared with conventional generators. The rotor of a Lundell generator tends to be a very closely intertwined 3-dimensional configuration where the leakage between north and south poles is about four times the rotor leakage found in conventional salient pole wound rotor generators. Part of this is due to the absence of windings on the Lundell poles so that the full mmf (magnetomotive force) exists between all north pole and south pole surfaces. If a short rotor flux circuit is designed, then the rotor leakage will be high because of the proximity of rotor parts. With this high leakage, the cross section of the rotor iron must be increased to accommodate the leakage flux and the rotor weight will be accordingly increased. If a long rotor flux circuit is designed in an effort to separate the parts and reduce the leakage, the rotor weight will still be high because of the length of the flux path. Brushless Lundell machines will generally be 30% heavier in electromagnetic weight.

The high rotor leakage also has an adverse effect on generator transient performance. Rotor leakage flux represents stored energy which will tend to cause voltage overshoots upon load removal. Rotor leakage reactance also increases the open circuit time constant of the generator. Lundell configurations clearly satisfy the design objectives for high reliability but still indicate a need for further improvement in the direction of lighter weight and improved transient performance.

## Inductor-Lundell Alternator

The diagram in Fig. 4(A) shows two homopolar inductor generators located side by side. Each generator is complete with double ended rotor, two stator sections, coaxial coil and frame. Fig. 4(B) shows these same generators combined together as an inductor-Lundell generator. The rotors of each machine are altered slightly so that the inner sets of poles will fit between each other in a Lundell manner. As the machines are combined together it will be noted that one stator section is completely eliminated along with a significant portion of the stator conductors and conductor end turns. The inductor generators when combined together in this inductor-Lundell configuration are significantly lighter than an inductor generator alone.

The inductor-Lundell configuration bears a certain resemblance to the Lundell design sketched in Fig. 3. The two parasitic air gaps have been replaced by working gaps with inductor power being generated at each end of the machine. The Lundell pole-to-pole leakage still exists and is still greater than that generated in conventional machines. However, the Lundell pole configurations naturally extend in opposite directions to minimize leakage without necessarily increasing the length and weight of rotor iron. More significantly, the effect of Lundell leakage on over-all generator characteristics is drastically reduced. The flux which leaks between Lundell poles fails to generate voltage in the center stator section and so affects generator characteristics as seen by that portion of the stator. However, this same leakage flux generates useful voltage as it completes the circu through one inductor generator, across th frame, and returns through the induct section at the other end. As seen by th inductor stator sections on each end of th generator, this leakage flux is useful flu The total effect of the Lundell leakage seen at the terminals of the inducto Lundell generator is less than half th effect seen on the characteristics of th Lundell generator. This reduction sufficient to provide acceptable machi performance under transient conditions.

While it offers promise of improved pe formance and reduced weight, the indu tor-Lundell configuration is very compl to design and analyze. The inductor a Lundell sections of the machine are ve closely interrelated. For example, th size of the induction portion is dete mined by leakage occurring between pol in the Lundell sections and the leakage the Lundell section is affected by the si of the inductor portion. There are many different parameters which mu be solved by trial and error that effecti and accurate designs cannot be obtain in a reasonable time by hand calculati The inductor-Lundell design formul have been programmed for use on International Business Machines Corpo tion *650* computer. The program corporates many loops which allow t computer to balance interrelated para eters and to investigate possible vari tions leading to the lightest design with the limits of the input requirements. T design work on the computer has sho that inductor-Lundell electromagne weights are generally less than the weig of either the basic homopolar inductor Lundell configurations for convention speeds, frequencies, and ratings. T inductor-Lundell configuration, like t basic inductor and Lundell machines, m be lighter than conventional salient po designs for many of the unusual spee ratings, and duty cycles that are specifi from time to time in aircraft applicatio

An inductor-Lundell rotor is shown Fig. 5. This rotor is from a generat which was built to the specifications of t

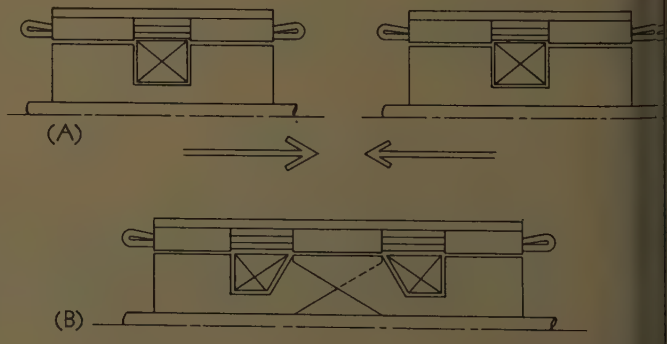


**Fig. 4. Comparison of inductor and inductor-Lundell generators**

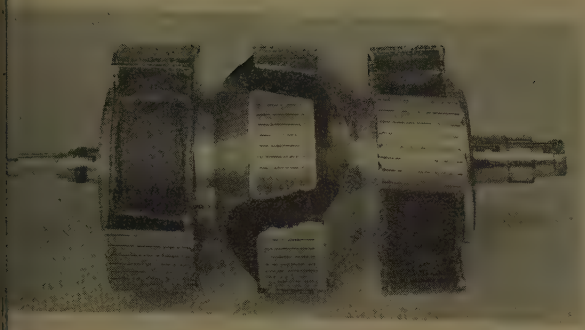

Fig. 5 (left). Inductor - Lundell rotor

Fig. 6 (right). Rotor assembled into stator

00 F development program except that igh-temperature component materials ere not used. The center Lundell sec- ions of this rotor are solid iron while the nductor sections at each end are assem- led from iron laminations. Other con- gurations are possible where laminations re used throughout. The center sec- ion of the shaft must be nonmagnetic naterial or flux will leak directly between undell poles through the shaft. mortisseur bars are included at the pole aces. The rotor as shown meets all of he design objectives for high reliability. ig. 6 shows the inductor-Lundell rotor ssembled into the oil-cooled stator.

Results of both analytical work and esting of inductor-Lundell machines have nown that electrical characteristics are mparable with conventional generators. enerator characteristics, voltage balance nder unbalanced loads, waveform, fficiency, and short-circuit capabilities ave all been better than specifications. n several respects, the dual nature of the nductor-Lundell generator is providing ew methods of design improvement hich should challenge the capabilities f conventional aircraft generator de- gns. The increase in reliability of the inductor-Lundell configuration suggests its use in many applications where extremely dependable operation is required.

## Summary

Severe environmental conditions and the continuing need for greater reliability have suggested the further development of unconventional generator configurations which have fewer components and where stress on critical components is reduced. Inductor and Lundell generators satisfy this design objective since they involve simple iron configurations on the rotor with no rotating electrical components. The homopolar inductor design in its basic form is 60% heaver in its electromagnetic weight at the most significant ratings and speeds. The basic Lundell design involves less weight penalty but has a high leakage flux in the rotor which adversely affects transient performance.

A configuration combining inductor and Lundell machines has been developed to overcome the disadvantages that these configurations exhibit separately. The inductor-Lundell combination provides generally lighter weights than either of the separate types. The Lundell leakage flux is put to work in the inductor portion of the machine and as a result, the generator characteristics compare favorably with conventional generators. The increase in reliability of the inductor-Lundell configuration suggests its use in many applications where extremely dependable operation is required.

## References

1. Bearing Systems for High-Temperature Aircraft Generators, G. D. Bradley. *AIEE CP 59-865* (available on request).

2. Generator Insulator Systems Development for Hypersonic Aircraft, W. B. Penn, R. L. Balke, F. M. Precopio. *AIEE Transactions*, pt. II (*Applications and Indusry*), vol. 78, Sept. 1959, pp. 255–59.

3. A Brushless D-C Generator for Aircraft Use, J. T. Duane. *Ibid.*, vol. 77, Nov. 1958, pp. 367–72.

4. The Theory of the Inductor Alternator, J. H. Walker. *Journal*, Institution of Electrical Engineers, London, England, vol. 89, pt. 2, 1942, pp. 227–41.

5. Short Circuit Characteristics and Load Performance of Inductor Alternators, A. Mandl. *Ibid.*, vol. 94, 1947, pp. 102–17.

6. High-Frequency Alternators, J. H. Walker. *Ibid.*, vol. 93, pt. 2, 1947, pp. 67–80.

## Discussion

**ichard T. Smith** (University of Texas, ustin, Tex.): The author is to be con- ratulated for proposing a novel solution the problem of providing reliable genera- on at high temperatures with available aterials. The new generator appears have certain components of leakage hich would be higher than for conven- onal designs. In particular, the periph- al end leakage may be quite significant, hereas, for many standard machines, is component is negligible. In addition, ie differential and belt leakages in the undell Section will be higher than for the maining sections. The author does not dicate that any special provisions are ade for quadrature axis damping. It is ear that such damping can be achieved, owever, perhaps more easily than for the nventional salient-pole construction.

**. M. Chirgwin** (Jack & Heintz, Cleveland, hio): The author states that the electromagnetic weight of the homopolar inductor alternator is 60% greater than that of a conventional wound-rotor salient-pole alternator. This seems to be a very optimistic figure. Would the author indicate whether all or part of the weight of the steel yoke was excluded in making this comparison? Further details of the applications in which the homopolar inductor alternator results in a reduction of system weight and volume would add to the interest of the paper.

When comparing the excitation requirements of the homopolar and conventional alternators, the author concludes correctly that the homopolar machine needs less excitation power, but the wording could lead to a misunderstanding of the reason for this. If both types of machines had circular exciting coils, then the power requirements would be the same; because, although a 6-pole homopolar machine needs only one third of the total ampere turns, three times as much flux must be carried by the core on which the coil is wound, and consequently the mean length of one turn of the coil is three times as great. The reason for the lower excitation power requirements of the homopolar machine is to be found solely in the more favorable geometry of the exciting coil.

Turning now to brushless Lundell-type machines, the author states that these machines are generally 30% heavier in electromagnetic weight. If this refers to the type of machine[1] shown in Fig. 3, where the flux returns through the endbells and stator housing then this figure seems to be much too low, unless the weight of endbells and housing is omitted. If it is intended to refer to those brushless Lundell machines where the flux returns through the shaft[2,3] then the figure of 30% is too high.

In the summary the author seems to imply that the electromagnetic weight of his inductor-Lundell alternator is less than 30% greater than that of a conventional machine. Would the author quote the actual figure, or otherwise clarify this point?

In defense of the brushless Lundell machine it should be pointed out that the so called secondary air gaps are effectively

in series with the main air gap to both the exciting and the armature reaction ampere turns. So these secondary air gaps are only a penalty on the design to the extent that they must for mechanical reasons be made larger than is required for electrical reasons.

The author is correct in stating that the Lundell machine has a high rotor leakage flux, but he is incorrect when he states that this leads to increased transient reactance and increased voltage overshoot on removal of load. The voltage overshoot and transient reactance depend much more on the ratio of armature reaction ampere turns to exciting ampere turns than they do on rotor leakage flux. By suitable choice of magnetic and electric loadings of the stator it is possible to attain any reasonable value of machine transient reactance. The secondary air gaps previously mentioned tend to give the machine a "naturally" low transient reactance.

### References


1. A New System of Autonomous Power Supply for Railway Passenger Cars (in Russian), G. I. Shturman, E. A. Yakubaitis, A. F. Krogeris, V. V. Apsit. *Elektrichestvo*, Moscow, U.S.S.R., 1957, no. 3, pp. 39–43.

2. A Rugged Power Team. *Machine Design*, Cleveland, Ohio, May 29, 1958, p. 43.

3. Dynamo Electric Machines, A. Bekey, H. M. Robinson. *U. S. Patent no. 2,796,542*, June 18, 1957.


**R. E. Smith, W. J. Shilling** (Westinghouse Electric Corporation, Lima, Ohio): Certainly with the ever-changing requirements of modern aircraft electrical systems, the generator design engineer must continuously evaluate the advantages and disadvantages of every generator type known, with their possible variations, and any new type which he might conceive. It is very important, however, that the major advantages of the conventional salient-pole construction be carefully considered before choosing a less conventional type.

It can be agreed that the inductor and inductor-Lundell generators weigh considerably more than salient-pole generators. It can also be agreed that the performance is comparable to salient-pole generators, but certainly not equivalent for the normal range of speed and frequency. Basically, the inductor-Lundell generator must have at least 50% more stator iron weight, stack length, and leakage reactance than a conventional salient-pole construction and the stator copper loss and stator copper weight will tend to be approximately 50% greater. The increased losses result in greater system heat generation and lower efficiency. Besides the generator weight penalty, another weight penalty also results because of additional fuel and cooling required. The increased leakage reactance increases voltage overshoots and voltage unbalance. The 50% increase in the factors previously mentioned are basic. There are, however, additional performance problems for the inductor-Lundell generators which increase these factors considerably beyond 50%.

The author indicates that the inductor-Lundell design is *less than* 30% heavier than the conventional salient-pole machine. It would appear that the inductor-Lundell design would have about half of the penalty of the straight inductor type since the inductor-Lundell stack must be increased by 50% over the salient-pole machine versus 100% increase for the inductor machine. Also, the inductor-Lundell machine described requires two stack separations. This means one more added stack separation than for the inductor generator. Thus, it would appear that since the inductor machine has about a 60% weight penalty (per the paper), the inductor-Lundell machine would generally be *more than* 30% heavier in electromagnetic weight than a salient-pole generator for normal speeds and frequencies.

Although field excitation tends to be less in the solid rotor designs, it is not necessarily true that it always will be. In the inductor-Lundell design described, twice as much stator mmf is required than in the inductor design. Thus, the ampere-turn requirement of the stator coils of the inductor-Lundell machine is the same as that for four poles of a salient-pole machine (4 coils of Fig. 1). Depending on the particular design considered, the mean-length turn of the field coil of the solid rotor machine may be greater than the length of turn in an equivalent salient-pole machine. In general, it is expected that the field excitation of a 4-pole inductor-Lundell generator will be about the same as the excitation of a 4-pole salient-pole generator for the same field copper weight. Any difference will depend upon the difference of coil mean-length turn and coil temperatures.

Another item that should be considered in the inductor-Lundell design is leakage reactance or Potier reactance. In comparing this machine with the salient-pole design, it is seen that the total stator stack is at least 50% greater in the inductor-Lundell design and hence, has inherently more leakage reactance. To evaluate this leakage reactance, assume all the poles of the inductor-Lundell design are under the middle and one end-stack only. This leaves the other end-stack with no poles under it. The reactance in the two stacks with the poles under them would be the same as that in an equivalent salient-pole machine.

In the inductor-Lundell machine more reactance is introduced because: 1. slot reactance in the stack with no poles under it; 2. leakage reactance in the stator winding at the stack separations; and 3. leakage flux in the air where the poles were removed. The last two items may be calculated by assuming the length of the straight portion of the a-c coil end extensions are increased an appropriate amount.[1] (This may be determined after considering how the reactance is determined for end extensions.) Calculations of the leakage reactance were made on a sample inductor-Lundell machine. Load tests were later run which verified these calculations so far as they can be verified by load tests. These results indicate that the designer should expect about a 160% increase in leakage reactance (2.6 times reactance of an equivalent salient-pole machine) for a well designed a-c stack. To overcome this reactance increase at overload conditions, a weight penalty is required. This leakage reactance increase will increase the problem of voltage overshoot upon load removal. The reactance increase will also adversely effect machine constants such as $X_d$, $X_d'$, $X_q'$, $X_d''$, $X_q''$, $X_2$, and $X_0$. The effect of the last two constants is to increase the voltage unbalance problems.

As the author states, the "leakage flux" in the middle stack becomes useful flux in the two end portions of the machine. This flux then is only half as effective in developing voltage as the "useful flux" is. Thus, half of this leakage flux may be considered true leakage flux. In the salient-pole design the leakage flux is carried only a short distance from one pole to the next. In the inductor-Lundell design the leakage flux must be carried the length of the rotor and back again by way of the stator. This extra length of leakage flux path means extra steel with corresponding weight penalty. The end stacks must be increased to carry leakage flux which again penalizes leakage reactance.

In regard to voltage unbalance, it appears from Fig. 5 that it would be difficult to obtain quadrature axis damping. Meeting the voltage unbalance requirements of *MIL-G-6099A* should require a considerable sacrifice in weight and size not only because of the problem of obtaining quadrature axis damping but also because of the very high leakage reactance of this type of design. Laminations might be used on the rotor to simplify application of damper bars and to reduce pole face losses. However, this would destroy the advantage of ruggedness in the solid rotor design.

With respect to reliability, certainly the elimination of brushes, brush rigging, slip rings, and commutators increases the reliability of a generator. It was for this reason that a great deal of effort has been concentrated on brushless generators with integral a-c exciters and rotating rectifiers. Removing rectifiers and windings from the rotor does not necessarily contribute to increased reliability. Our reliability information indicates that the rotating field winding is perhaps the most reliable winding in generators. One reason for this is the fact that there is only a very small voltage (1 or 2 volts) present between adjacent turns since they are wound in series on a given pole and then all poles are connected in series. Further, the normal voltage to ground is typically 30 volts. In the a-c stator, however, the voltage of the main a-c winding to ground is 170 volts peak and the voltage between turns can be 295 volts peak. Applying field windings adjacent to these high voltage stator windings might well reduce the reliability. The fact that the rotating field windings are under compression due to centrifugal force makes them much less susceptible to damaging vibration effects than a field on the stator. Rotating rectifiers have had exceptionally high reliability. In one application which has accumulated an appreciable amount of operating time, the mean-time to failure of the rectifiers is 60,000 hours based on 240,000 rectifier flight hours.

We would like to ask the author the following questions:

1. Assume, for example, a 40-kva 8,000 rpm 400-cps machine built to meet *MIL-G-6099*.
   (a). How would the inductor-Lundell generator weight compare with

conventional 40-kva brushless salient-pole air-cooled machine weighing 70 pounds with integral exciter for class *C* operating conditions?

(b). What would the excitation requirements of the inductor-Lundell machine be compared to the salient-pole machine?

(c). How would the transient voltage differ for:

1. 0 to full load to 0 load change?
2. 0 to 200% to 0 load?
3. 0 to 300% short circuit to 0 load?

The paper shows the field coils located so the rotor has to be assembled around the field coils. This will be difficult to accomplish mechanically. If the coils were to be moved behind the stator coils, what would be the effect on weight, excitation, and flux leakage?

This discussion is intended to point out at there are many major inherent adntages to the salient-pole type of genera- which have been the reason for its mary choice in the electrical industry nost since the birth of the industry. ese very important advantages should carefully considered before leaving the ient-pole generator for less conventional oes.


REFERENCE

1. ARMATURE REACTION OF SYNCHRONOUS MACHINES, P. L. Alger. *AIEE Transactions*, vol. 47, April 1928, pp. 493–513.


**J. T. Bateman:** The discussers have each indicated a willingness to give thought and consideration to new electromagnetic configurations. This is gratifying since the field of rotating electric machinery design is all too often treated as a closed book.

R. T. Smith has suggested certain components of armature leakage which would be higher in the inductor-Lundell configuration than in conventional generators. Tests of the inductor-Lundell generator have demonstrated that such additional components of leakage will amount to less than half of the total armature leakage reactance. The presence of additional leakage components does not mean that increased leakage reactance is inherent in this or any other machine configuration. This leakage reactance is determined not only by machine permeances but also by the number of turns in the armature. The designer must reduce armature turns, adding to the generator weight and size if necessary, until reactances are at acceptable levels before he can compare his design with another. The discussion given in the paper assumes generators which are designed for complete compliance with aircraft application requirements and specification *MIL-G-6099A*.

K. M. Chirgwin suggests that the reduced excitation power obtained with a coaxial coil is due only to the fact that the coil is round rather than rectangular. However, in the example he has given, the increase in area of a circular core to carry three times the flux will result in an increase of the mean length of the turn of a coil surrounding that core by a factor of 1.73 rather than 3 as he states. This significant saving in excitation coil length is one of the factors which make 6-pole and 8-pole inductor-Lundell designs attractive.

W. J. Shilling has prepared a verbal analysis of the inductor-Lundell generator which presumes to prove that the configuration cannot have the weight and performance stated in the paper. Many of his discussions are inaccurate when related to the total generator design. The difficulty with such an analysis is that the preparation a long list of design problems does not in itself disprove the fact that many complete inductor-Lundell generator designs have been developed by the author and his associates where these design problems have been met effectively to provide generator sizes, weights, and performance which are attractive in the aircraft applications for which they were developed.

# Dual-Mode Relay Servos


**R. N. BULAND**
ASSOCIATE MEMBER AIEE

**N. FURUMOTO**
NONMEMBER AIEE



THIS PAPER DESCRIBES a dual-mode servo which utilizes a relay or ntactor for both the saturated mode and e linear mode. The dual-mode servo, ich was first suggested by McDonald,[1,2] erates as an on-off or bang-bang con-ller for large amplitude errors (satura-n mode) and as a linear servo when the or approaches zero (linear mode). e saturation mode may be optimized a minimum transient response to step ction inputs by means of special non-ear circuitry which is used to determine the optimum points for control reversal, normally referred to as a switching line. The linear mode is optimized by inserting linear networks of the lead-lag variety.

The practical difficulty with dual-mode systems lies in combining the two modes while maintaining a reasonably simple and reliable design. Hopkins[3] suggested a saturated amplifier for the controller and analog-computer-type function generators for the nonlinear switching line. The relay is not usually favored because of the difficulty of obtaining reasonably linear action from such a nonlinear device. But the relay is the natural element for the saturation mode so that it is well worth the effort to explore the possibilities of a quasi-linear relay power amplifier.

The problem of combining a saturation mode switching line and a linear mode lead-lag network is also of great practical interest. Nieswander and MacNeal[4] develop the general design philosophy for combining both modes but design details are not considered. In this paper the design philosophy will be made more explicit for a particular type of servo and possibilities of combining the saturation mode switching line with the linear mode compensating network will be studied.



per 59-840, recommended by the AIEE Feedback ntrol Systems Committee and approved by the EE Technical Operations Department for pres-ation at the AIEE Summer and Pacific General eting and Air Transportation Conference, Seattle sh., June 21–26, 1959. Manuscript submitted uary 28, 1959; made available for printing June 1959.



N. BULAND is with the Aeronutronic Systems, ., Glendale, Calif. N. FURUMOTO is with the iversity of California, Berkeley, Calif.



e authors wish to acknowledge the introduction of ethod of linearizing relay servo systems by Dr. A. Wagner, former president of the H. A. gner Engineering Company, and now a professor the Technical University, Aachen, Germany, by T. F. Sturm, Vice-President of the Electronic tems Development Corporation, Ventura, if.


## Background

The relay has been used as a control element in regulators and servos for a least 30 years.[5] Probably there are more contactor controlled regulators and servos in existence than any other type. Yet it was not until the concept of optimum step function response was suggested that any real interest was shown in the technical literature.

In terms of optimum step function response, the relay servo is ideal because sudden reversals of control are required. On the other hand, the relay has the annoying habit of limit cycling when no error is present and the relay cannot follow arbitrary inputs accurately.

Shortly after World War II a method of linearizing relay servo systems was introduced at the Pacific Missile Range, then called Naval Air Missile Test Center, by Dr. H. A. Wagner and Mr. T. F. Sturm. This concept utilized feedback directly around the relay as shown in Fig. 1 in comparison to the conventional bang-bang relay servo of Fig. 2. The configuration of Fig. 1 was designed by linear theory assuming the relay was an infinite gain power amplifier. Bass[6] developed

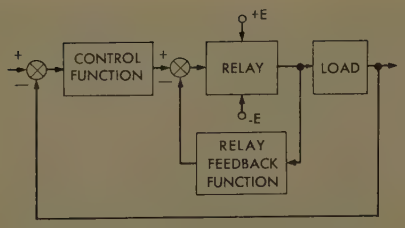


**Fig. 1. Relay servo with feedback around relay**

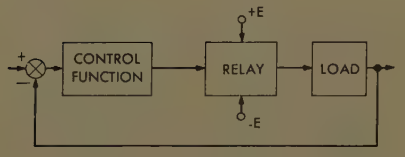


**Fig. 2. Conventional bang-bang relay servo**

several theorems to describe relay amplifier operation and suggested the possibility of dual-mode operation. More recently Gibson and Tuteur[7] analyzed a slightly different version of the relay amplifier with unity feedback around the relay.

The basis of linearization of the relay amplifier lies in defining the relay input to output relationship as a variable gain $\mu_e$ in a manner similar to describing function analysis.[8] It will be shown that when the relay amplifier feedback is not saturated $\mu_e$ approaches infinity and can be treated as a quasi-linear high-gain amplifier.

This paper will discuss the quasi-linear relay servo and will extend this concept to dual-mode operation.

## The Dual-Mode Relay Servo

The concept of dual-mode control with the configuration of Fig. 1 is that the feedback around the relay will make the system operate in a quasi-linear fashion for small error signals. For large error signals the system will act as a conventional bang-bang controller and near optimum response can be obtained by means of a switching line in the phase plane. The concept is shown in Fig. 3. Fig. 3(A) shows the generalized block diagram where

$K_\alpha G_\alpha$ = saturated mode switching network
$K_\beta G_\beta$ = linear mode stabilizing network
$K_F$ = coefficient relating the magnitude of the force, or torque, on the load to the magnitude of the relay output
$K_M G_M$ = dynamics of unalterable load

For small motions it will be shown that the transfer function for the system approaches the linear system shown in Fig. 3(B). For large motions the relay feedback becomes saturated and the system acts as a conventional bang-bang system as shown in Fig. 3(C). Each of the two modes will be discussed separately.

### Quasi-Linear Mode

The quasi-linear mode depends upon the extent to which the relay power amplifier of Fig. 4 is linearized. For practical implementation of the relay power amplifier, a voltage amplifier with gain $-K_E$ is inserted as a summing point and to decrease the effective system dead space. The amount of amplification required is a function of the type, i.e., 2- or 3-position polarized relay, and quality of the relay being used and the positioning accuracy required of the system. In this study, only the 2-position relay with hysteresis will be analyzed.

The quasi-linear operation of the relay is based upon the assumption that the relay may be replaced by a gain $\mu_e$ such that

$$\mu_e(t)=\frac{E_R(t)}{e(t)}$$

where $e(t)$ and $E_R(t)$ are the instantaneous input and output of the relay. Thus $\mu_e$ is an inverse function of $e$.

Referring to Fig. 4(A), the relationship of $E_R$ to $\alpha$ is found to be

$$\frac{E_R}{\alpha}=\frac{-1}{\frac{1}{\mu_e K_E}+K_B G_B(s)} \qquad (1)$$

Because in the quasi-linear mode the error signal $e$ is always small, it can be assumed that $1/\mu_e K_E$ is negligible, resulting in

$$\lim_{e\to 0}\frac{E_R}{\alpha}=\frac{-1}{K_\beta G_\beta(s)} \qquad (2)$$

The relay power amplifier thus acts in a linear manner for small error signals. As a result, the relay with its feedback network can be replaced by a linear transfer function which is merely the negative reciprocal of the transfer function of the feedback loop.

As a partial verification of equation 2 it can be shown that the average steady-state output for the 2-position relay servo is identical to a linear system with the same $K_\beta G_\beta$. For a 3-position relay the results are identical except for a small offset caused by relay dead space. The particular case to be investigated is for $G(\beta)=(1+\tau_D s)^{-1}$. The steady-state response of the relay power amplifier to a step of $\alpha$ will be determined by equation 2 and by a detailed investigation of the relay output signal.

From the preceding equation, the steady-state response to a step input for a linear system and $\mu_e \to \infty$ is:

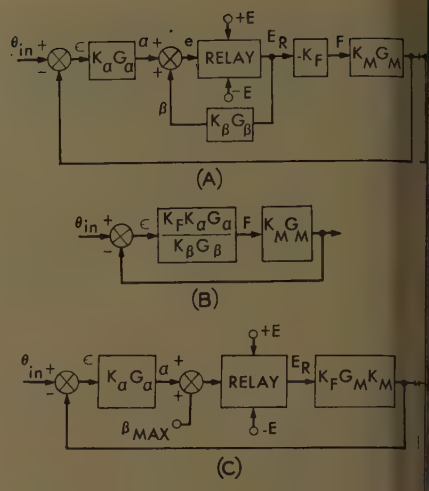


**Fig. 3. A—Dual-mode relay servo. B Quasi-linear mode, small motions. C Saturated mode, large motions**

$$E_{Rss}=\lim_{s\to 0} s\cdot\frac{(1+\tau_D s)}{K_\beta}\cdot\frac{|\alpha|}{s}=-\frac{|\alpha|}{K_\beta}$$

In the Appendix, a detailed investigation of the voltages of the relay power amplifier yields the following two voltage relationships:

$$\left(EK_\beta+\frac{\Delta h}{2}+\alpha\right)(1-e^{-\Delta t_1/\tau})=\Delta h$$

$$\left(EK_\beta+\frac{\Delta h}{2}-\alpha\right)(1-e^{-\Delta t_2/\tau})=\Delta h$$

where $\Delta h$ is the width of the hysteresis zone as shown in Fig. 4(B).

If the average output voltage on the relay arm is defined as

$$E_{Rss}=\frac{\Delta t_1 E-\Delta t_2 E}{\Delta t_1+\Delta t_2}$$

and the values for $\Delta t_1$ and $\Delta t_2$ from equation 4 are substituted in equation 5, $E_{Rss}$ becomes

$$E_{Rss}=\frac{E\left[\ln\left(1-\frac{\Delta h}{EK_\beta+\frac{\Delta h}{2}+\alpha}\right)-\ln\left(1-\frac{\Delta h}{EK_\beta+\frac{\Delta h}{2}-\alpha}\right)\right]}{\ln\left(1-\frac{\Delta h}{EK_\beta+\frac{\Delta h}{2}+\alpha}\right)+\ln\left(1-\frac{\Delta h}{EK_\beta+\frac{\Delta h}{2}-\alpha}\right)}$$

Now, $\Delta h << EK_\beta$ and $\ln(1+x)$ can represented by a power series

$$\ln(1+x)=x-\frac{1}{2}x^2+\frac{1}{3}x^3-\ldots,\quad -1<x\leq$$

If $x<<1$, then the higher order terms can be neglected and $E_{Rss}$ becomes

$$R_{ss}=\frac{-1}{K_\beta+\frac{\Delta h/2}{E}}|\alpha|$$

nce $\Delta h<<E$,

$$R_{ss}=-\frac{1}{K_\beta}|\alpha| \tag{7}$$

s previously obtained, i.e., the steady sponse to a step input of $\alpha$ is the same s the average response to a constant in- ut of $\alpha$.

From equation 6 it can be seen that ie system is linear in the steady-state se as long as the following relationship olds

$$|\alpha|\ll|EK_\beta|-\left|\frac{\Delta h}{2}\right| \tag{8}$$

hen $|\alpha|=|EK_\beta|-|\Delta h/2|$, the system is the saturated mode.

At steady-state conditions the relay mplifier tends to oscillate about the ysteresis zone. The period and ampli- de of the oscillation will depend upon ie parameters of the system. The gain, , can be found for this condition to be

$$=\frac{\pi EK_e}{\Delta h}$$

or a practical situation $\mu_e$ will be in the der of 10,000.

### ATURATED MODE

The saturated mode will be designed to btain near optimum response to step nction inputs. In geneal the number of versals of control for an optimum satu- ted response will be $N-1$ where $N$ is the der of the differential equation describ- g the load.[9] However, Chang[10] utilized e dead space of a 3-position relay con- ol to allow the higher order transients to

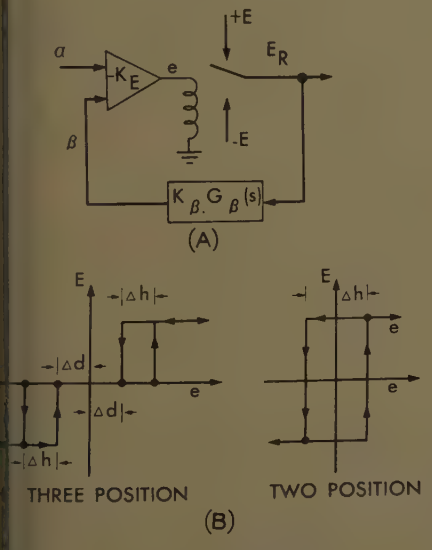


**3. 4. A—Relay power amplifier. B—Relay characteristics**

die out during the switching sequence and effectively reduce the system to a second order system so that only one switching curve was required.

The procedure in this paper will be to design a single switching line which will approximate the first switching curve for the particular load function under consideration. The system will be designed to have a linear region about the switching line and about the zero error or terminal point. This linear region will be relied upon to compensate for any other switching curves that may be required by the criteria of reference 9 and for the fact that a switching line will be utilized rather than the actual switching curve. In other words, a lead network will be used to approximate the optimum switching curve.

For a second order system conventional phase plane techniques can be employed to determine the optimum switching curve[11] as shown in Fig. 5. The switching curve may be approximated by a straight line but then an optimum response is obtained for only one value of step input amplitude. The quasi-linear mode is relied upon to minimize the error in switching. The instrumentation of the straight line is, of course, much simpler than the curve for the switching line.

$$[\epsilon+T_L\dot{\epsilon}]=\epsilon[1+T_Ls]$$

The switching line circuit can be inserted in the feedback or the forward path of the servo. The forward path is the more difficult problem because the switching circuit must be approximated by a lead-lag network

$$\frac{1+T_Ls}{1+\tau s}\epsilon$$

The additional lag makes the system third order, and two switchings are required for an optimum response. Again the quasi-linear zone is utilized to minimize this additional error.

For servos of higher order the single switching line is still useful but the width of the quasi-linear region becomes of increasing importance and the transient time will not approach the optimum as closely.

## Basic Design

The design of the dual-mode relay servo can be described, with the aid of Fig. 3, in the following steps:

1. The quasi-linear mode is designed by conventional linear techniques so that

$$\frac{\theta_0}{\theta_{in}}=K_LK_MG_LG_M \tag{9}$$

$$\frac{\theta_0}{\theta_{in}}=\frac{K_LK_MG_LG_M}{1+K_LK_MG_LG_M} \tag{10}$$

where

$$K_L=\frac{K_\alpha K_F}{K_\beta} \tag{11}$$

$$G_L=\frac{G_\alpha}{G_\beta} \tag{12}$$

2. The boundary between the saturation mode and the quasi-linear mode is determined when

$$\beta_{max}=\alpha$$

but

$$\beta_{max}=K_\beta E$$

and

$$\alpha=K_\alpha\epsilon$$

after all transients have died out so that all derivatives of $\epsilon$ are zero then

$$|\epsilon_{LM}|=\frac{K_\beta}{K_\alpha}|E| \tag{13}$$

where

$\epsilon_{LM}$ = the minimum saturated mode error
$E$ = maximum magnitude of $E_R$

as shown by equation 8. The linear limit will depend upon the quality of the relay, character of $G_\alpha$ and $G_\beta$ and the derivatives of $\epsilon$.

For preliminary design $\epsilon_{LM}$ will be utilized as a measure of the quasi-linear region. From equation 13 it is seen that

$$\epsilon_{LM}=f(E)$$

but $E$ is also constrained by the output response

$$\theta_0=K_MG_MK_FE_R \tag{14}$$

Thus the speed of response is directly related to the magnitude of $K_F$ and $E_R$ or $E$ for the saturated mode. Normally it is desirable to make $K_F$ and $E$ as large as possible in order to minimize response time. Also $K_\beta$ and $K_\alpha$ are constrained by the quasi-linear gain $K_L$ and by $K_F$. Combining equations 11 and 13

$$\frac{\epsilon_{LM}}{E}=\frac{K_F}{K_L} \tag{15}$$

which defines the fraction of the linear range

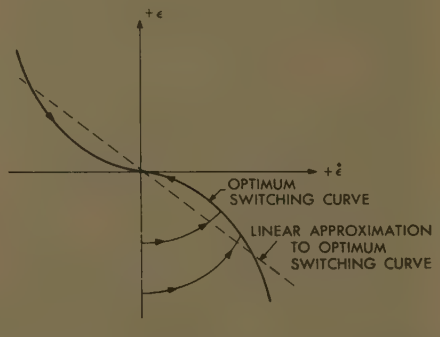


**Fig. 5. A phase-plane plot of the optimum switching curve for a second-order bang-bang servo system**

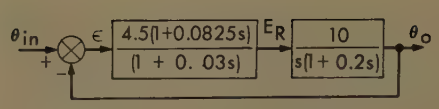


Fig. 6. Linear design

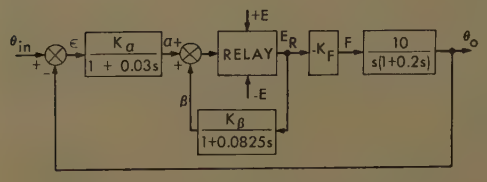


Fig. 7. Quasi-linear relay servo

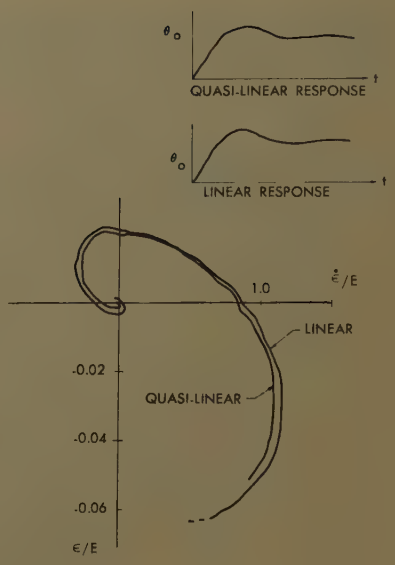


Fig. 8 (right). Comparison of quasi-linear and linear systems for small magnitude inputs ($\theta_{in}=0.3\epsilon_{LM}$)

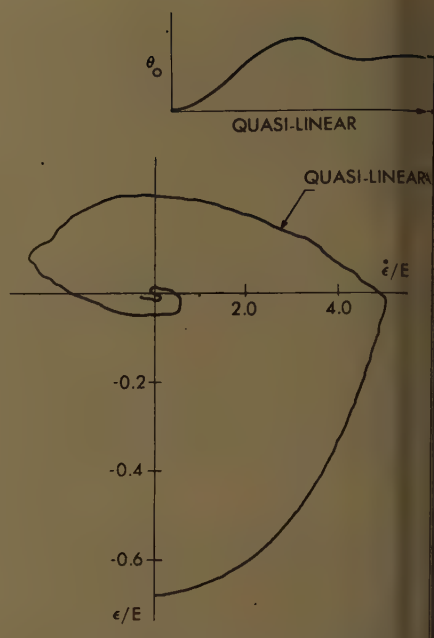


Fig. 9. Quasi-linear system response f large magnitude inputs ($\theta_{in}=3\epsilon_{LM}$)

with respect to the maximum relay output.

3. The saturation mode switching line is defined by $G_\alpha$ and will normally have the form

$$G_\alpha=\frac{1+T_Ls}{1+\tau_1 s} \tag{16}$$

where $\tau_1$ is chosen to be a part of $G_L$ if this is possible. $T_L$ is chosen to be a best fit to the optimum first switching line.

4. The final step is to choose $G_\beta$ from equations 12 and 16

$$G_\beta=\frac{G_\alpha}{G_L} \tag{17}$$

and choosing either $K_\beta$ or $K_\alpha$ arbitrarily so that the other can be found from equation 11. As a final step the analysis should be reviewed to determine where simplifications can be made.

## Example Problem

To demonstrate the dual-mode relay servo design, a second order servo was designed and tested by means of an analog computer. The unalterable element of the system was

$$K_MG_M=\frac{10}{s(1+0.2s)}$$

### The Quasi-Linear Mode

The first step was to design a linear system which had acceptable transient characteristics. The linear system had the form shown in Fig. 3(B). The system was designed for a damping coefficient of 0.5 and an undamped natural frequency of 20 radians per second. It was found that

$T_L=0.0825$

$\tau_1=0.03$

$K_L=4.5$

and

$$\frac{\theta_0}{\epsilon}=\frac{45.0(1+0.0825s)}{s(1+0.2s)(1+0.03s)}$$

as shown in Fig. 6. The quasi-linear relay is shown in Fig. 7 where

$K_L=4.5$

$$G_L=\frac{1+0.0825s}{1+0.03s}$$

and

$$G_\alpha=\frac{1}{1+0.03s}$$

$$G_\beta=\frac{1}{1+0.0825s}$$

The next step in the design is to determine the magnitudes of $K_F$ and E. For the system being designed, which was built up on an analog computer, the maximum $E$ was $\pm 50$ volts, the maximum $K_F$ is $\pm 1$. If these values are used, then

$$\frac{\epsilon_{LM}}{50}=\frac{1}{4.5}=0.22$$

or $\epsilon_{Lm}$ is 22% of $E$. This is a quite acceptable linear zone and has been found to operate quite satisfactorily although Hopkin, in Reference 3, recommended a minimum linear region in order to sharpen the saturated mode response.

For comparison purposes $K_\alpha$ was set at 4.5 and thus

$K_\beta=1.0$

This system was then compared to the equi alent linear system. In Fig. 8 the tw systems are compared for a step input

$\theta_{in}=0.3\epsilon_{LM}$

The response of the quasi-linear system shown for

$\theta_{in}=3\epsilon_{LM}$

in Fig. 9. The response is by no mea optimum although the per cent oversho is about the same as for the linear model.

### Saturated Mode Design

The saturation mode switching line mu be computed to determine $G_\alpha$. From t work done on the quasi-linear system seems that a suitable form for $G_\alpha$ wou be

$$G_\alpha=\frac{1+T_Ls}{1+0.03s}$$

The saturation mode system is shown Fig. 10. The best linear switching li approximation to the optimum switchi curve was found by the method of ref ence 12 to be

$\epsilon+0.075\dot{\epsilon}=0$

or

$T_L=0.075$ sec.

### Dual-Mode Design

The two modes can now be combin It was previously determined that

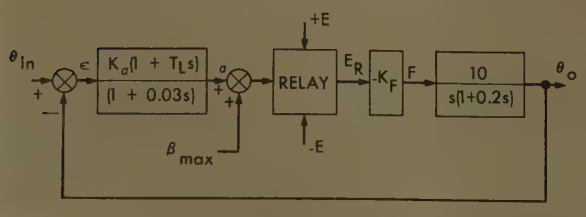


Fig. 10 (left). Saturation mode

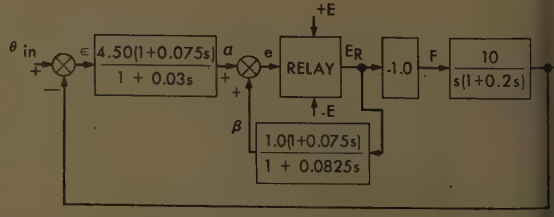


Fig. 11 (right). Final design, Case 1

. 12. Family of ponses for dual- node relay servo

—Case 1 conditions
—Case 2 conditions
—Case 3 conditions

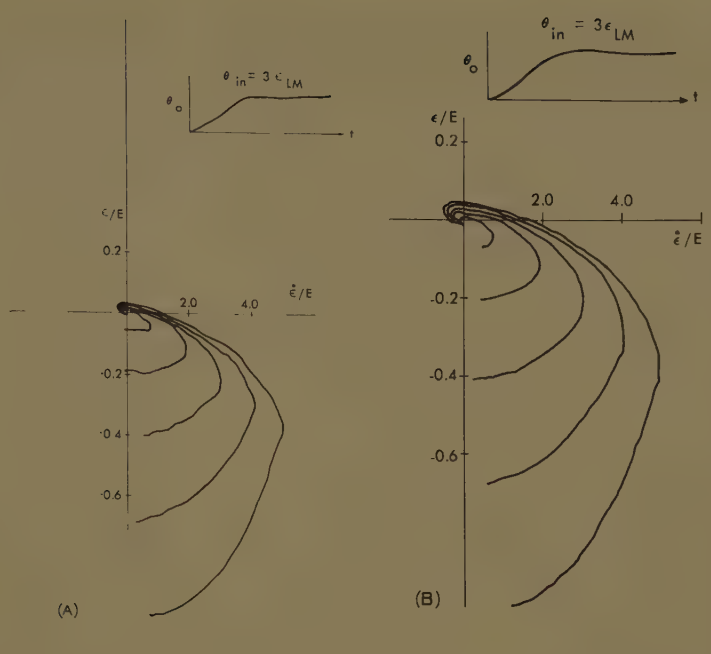


$$=\frac{1+0.0825s}{1+0.03s}$$

m the quasi-linear design, and that

$$=\frac{1+0.075s}{1+0.03s}$$

m the saturated mode design for the merator and the quasi-linear design for denominator. Thus $G_\beta$ is defined as

$$=\frac{1+0.075s}{1+0.0825s}$$

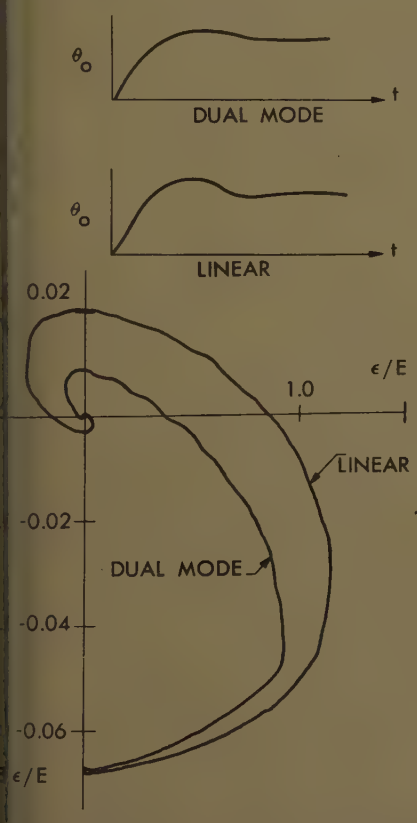


**13. Response of dual mode and linear ems to small magnitude input and Case 1 conditions**

All that remains is to choose $K_\alpha$ and $K_\beta$, keeping the ratio fixed at 4.5. Experiments indicate that large values of $K_\alpha$ and $K_\beta$ would be more desirable because the effects of relay dead space is reduced. However, in order to determine the effect, two values of $K_\alpha$ and $K_\beta$ will be investigated.

Case 1. $K_F=1$ $K_\alpha=4.5$ $K_\beta=1.0$
Case 2. $K_F=1$ $K_\alpha=0.45$ $K_\beta=0.1$

The final design for Case 1 is shown in Fig. 11. A family of phase-plane responses to different amplitude steps are shown in Figs. 12(A) and 12(B). The transient response is shown for

$\theta_{in}=3\epsilon_{LM}$

In order to determine the effect of a narrower linear band, Case 3 was investigated:

Case 3. $K_F=0.1$ $K_\alpha=4.5$ $K_\beta=0.1$

Thus $K_L$ is unchanged, but the ratio

$$\frac{\epsilon_{LM}}{E}=0.022$$

or $\epsilon_{LM}$ is only 2.2% of $E$. The phase plane for a family of inputs is shown in Fig. 12(C). The transient response is shown for

$\theta_{in}=3\epsilon_{LM}$

The response is much slower because the forcing function has been reduced by a factor of 10 but the switching is much sharper as would be expected, because of the smaller linear region.

The response of the dual-mode relay servo for the Case 1 gains is compared to the linear system response in Fig. 13 for a small amplitude input

$\theta_{in}=0.3\epsilon_{LM}$

It is seen that the dual-mode response to small amplitude inputs does not compare to the linear as well as the quasi-linear response did in Fig. 8. However, the overshoot has been reduced and the over-all response time is about the same.

The frequency response of the dual mode servo with Case 1 gains was also investigated briefly. Fig. 14 shows the input and output for

$\theta_{in}=0.3\epsilon_{LM}$

at 3 cycles per second, and

$\theta_{in}=3\epsilon_{LM}$

at 1 cycle per second.

## Discussion

The theory for dual-mode servos has been developed in the literature to a considerable extent and experimental models have been built to demonstrate the theory. Yet very little work has been devoted to developing practical circuitry for dual-mode servos. In other words, the dual-mode servo is, at present, an

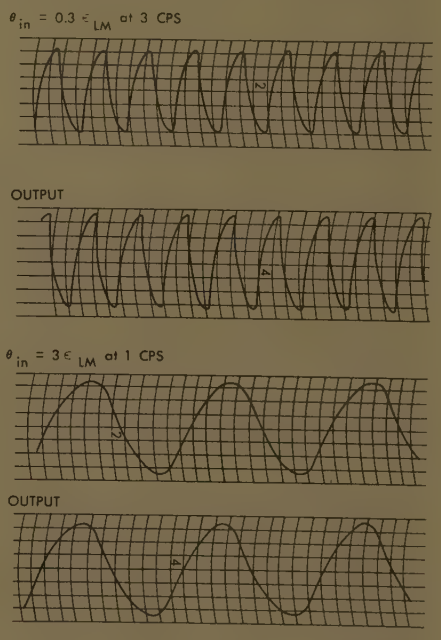


**Fig. 14. Frequency response of dual-mode relay servo**

interesting laboratory gadget but not a practical engineering reality. It is hoped that this paper will help to rectify this situation by demonstrating an approach which does not sacrifice design simplicity to achieve dual-mode operation.

The dual-mode servo proposed is not an optimum system by any single criteria, but it does give satisfactory response which approaches the optimum as specified by several criteria. It is felt that this is a desirable feature because servos in general must give satisfactory service to arbitrary inputs, not just one special kind. If, on the other hand, the special case does develop in which the servo must be designed for only one type of input, the design procedure outlined is sufficiently flexible to emphasize the response characteristics to the particular type of input desired.

The design of the saturated mode switching line is straightforward for a second order system but becomes a tedious computation for third order and an almost impossible problem for orders above third except by using a large scale computer. When using a computer to design the switching line for a high order system, the quasi-linear mode will modify the transient markedly and should be programmed on the computer. The width of the quasi-linear zone may be of first order importance in such a design.

The design of the quasi-linear mode is straightforward linear design. Unfortunately the deviation of the quasi-linear system from the linear is difficult to predict. Work needs to be done in this area so that the action of the relay power amplifier can be more accurately predicted. At present the gain characteristics of the relay power amplifier can be described for only a few special cases. In this paper the average gain $\mu_e$ was derived for the steady-state condition when the input was a constant and when $G_\beta$ is a lag term. Reference 7 considered the same situation when $G_\beta$ was unity. Describing functions can be used if the relay feedback loop is sufficiently insensitive to high frequencies, with $G_\beta$ a low pass filter, but not in general. Thus the relay power amplifier is known to work and linear analysis is satisfactory to describe the quasi-linear relay servo to a first approximation. For a more detailed analysis, simulation seems to be the best tool.

It should be noted that the concept of feedback around an on-off device can be applied, with good results, to devices more complicated than a relay. For example, a pulse coder can be built with feedback around the coder. This feedback will linearize the average coder output with respect to the input and the feedback link can be designed to generate a lead to provide stability for the over-all system.

For applications where the signal-to-noise ratio is low, the quasi-linear relay servo can be utilized to advantage by using a relay with dead zone. The dead zone is adjusted to encompass the high-frequency noise and the system will not respond to the noise. The signal, on the other hand, will activate the system whenever the dead space is exceeded. This system is particularly effective if $G_\beta$ is a low pass filter. The relay amplifier is a lead network.

It is felt that the dual-mode relay servo has many applications which are not being exploited. The advantages of light weight and circuit simplicity should not be overlooked by the servo engineer.

## Conclusions

A design concept has been developed for a dual-mode relay servo which employs linear networks in both the saturated mode and the linear mode. The linear mode employs a quasi-linear relay amplifier. It is concluded that:

1. This design provides near optimum step response in the saturated mode and near linear response in the quasi-linear mode with no additional complexity beyond a lead lag network.

2. Linear theory can be used in designing the quasi-linear relay servo with very good results.

3. The relay amplifier is an excellent device for obtaining high power amplification without sacrificing the simplicity of the relay or the advantages of linear design techniques.

## Appendix. Development of Quasi-Linear Relay Amplifier Equations

The relay amplifier is shown in Fig. 4(A). For the 2-position relay case the feedback voltage $\beta$ is approaching either $+$ or $-K_\beta E$. However $e$ is a function of $\beta$ and limits $\beta$ to a range of values determined by the hysteresis zone, $\Delta h$, of the relay.

Consider the case when

$$G_\beta = \frac{1}{1+\tau_b s}$$

and $\alpha$ is a step function. The history of $e$ and $E_R$ are shown in Fig. 15. The analysis will be piecewise linear beginning a new time sequence with each switching of $E$.

For the $t_{(0)}$ time sequence $e$ initial equals $\alpha$ and

$$E_R = -E$$

Then

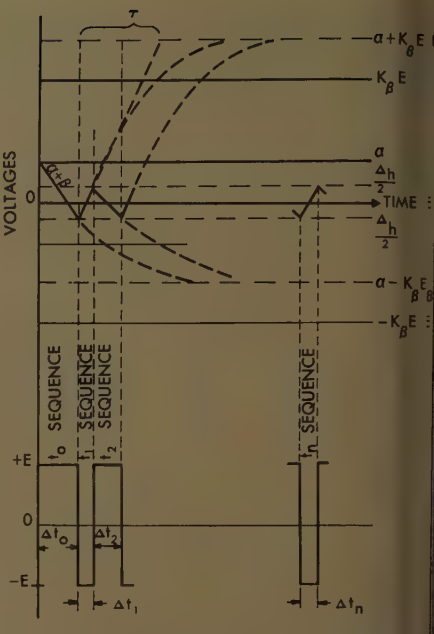


**Fig. 15. Steady-state response of the 2 position relay power amplifier to a step inpu**

$$e = \alpha - K_\beta E(1-e^{t_{(0)}/\tau_b}) \qquad (18$$

when $e$ equals $-\Delta h/2$ the relay contac reverse and the $t_{(1)}$ sequence beings

$$e_{(1)} = \alpha - \beta_{(0)} e^{-t_{(1)}/\tau_b} + K_\beta E(1-e^{-t_{(1)}/\tau_b}) \qquad (19$$

where

$$\beta_{(0)} = \alpha + \frac{\Delta h}{2} \qquad (20$$

at time $\Delta t_1$ in the $t_{(1)}$ sequence the value $e$ has increased to

$$e = \frac{\Delta h}{2}$$

and the relay contacts reverse again so th

$$E_R = -E$$

and

$$e_{(2)} = \alpha - \beta_{(1)} e^{-t_{(2)}/\tau_b} - K_\beta E(1-e^{-t_{(2)}/\tau_b}) \qquad (2$$

where

$$\beta_{(1)} = \alpha - \frac{\Delta h}{2} \qquad (2$$

at time $\Delta t_2$ in the $t_{(2)}$ sequence $e$ is again $-\Delta h/2$ and the third sequence begins and identical to the first. Thus the relay h gone into a limit cycle limited by t hysteresis band.

Now in time $\Delta t_1$ $e$ has increased by $\Delta h$ on

$$\Delta h = e_n(\Delta t_1) - e_n(0) \qquad n = 1, 2, 3, \ldots$$

combining equations 19 and 20

$$\Delta h = \alpha - \left(\alpha + \frac{\Delta h}{2}\right) e^{-\Delta t_1/\tau_b} + K_\beta E(1-e^{-\Delta t_1/\tau_b}) + \frac{\Delta h}{2} \qquad (2$$

$$\Delta h = \left(\frac{\Delta h}{2} + K_\beta E + \alpha\right)(1-e^{-\Delta t_1/\tau_b})$$

o

$\Delta h = e_{2n}(\Delta t_2) - e_{2n}(0) \quad n = 1, 2, 3, 4, \ldots$

nbining equations 21 and 22

$$\Delta h = \alpha - \left(\alpha - \frac{\Delta h}{2}\right) e^{-\Delta t_2/\tau_b} - K_\beta E(1 - e^{-\Delta t_2/\tau_b})$$

$$\Delta h = \left(\frac{\Delta h}{2} + K_\beta E - \alpha\right)(1 - e^{-\Delta t_2/\tau_b}) \quad (24)$$

Equations 23 and 24 are equation 4 of the t.

t should be noted that $\Delta t_1$ and $\Delta t_2$ are ost equal when $\alpha$ is small compared to $E$ but when

$$= K_\beta E - \frac{\Delta h}{2}$$

n $\Delta t_1$ approaches zero while $\Delta t_2$ ap- aches $\infty$ and the system enters the urated zone.

The analysis for the 3-position relay servo ows the same form but is complicated the dead zone, the configuration of the network, and whether or not the relay grounded in the dead zone position. e 3-position relay will always have a itioning error related to one half the d space of the relay.

For the 2-position relay when $\alpha$ is small pared to $K_\beta E$ the relay error voltage essentially a sawtooth wave while $E_R$ square wave. The period of the oscilla- tion is determined by $\tau_b$, $K_b$, $K_e$, and $E$. If the first harmonic of $E_R$ and $e$ are utilized, a describing function can be generated.

$$E_R \text{ (1st harmonic)} = \frac{4E}{\pi} \cos \omega t$$

$$e \text{ (1st harmonic)} = \frac{4}{\pi 2} \frac{\Delta h}{K_e} \cos \omega t$$

Then

$$\mu_e = \frac{E_R}{e} = \frac{\pi E K_e}{\Delta h}$$

For some typical values let

$E = 50$ volts

$\Delta h = 0.5$ volt

$K_e = 25$

Then

$\mu_e = 7{,}800$

which is sufficiently close to $\infty$ for a practical case.

## References


1. Nonlinear Techniques for Improving Servo Performance, **D. McDonald.** *Proceedings*, National Electronics Conference, Chicago, Ill., vol. 6, 1950, pp. 400–21.

2. Multiple Mode Operation of Servomechanisms, **D. McDonald.** *Bulletin S-3*, Cook Research Laboratories, Chicago, Ill., 1951.

3. A Phase-Plane Approach to the Compensation of Saturating Servomechanisms, **A. M. Hopkin.** *AIEE Transactions*, vol. 70, pt. I, 1951, pp. 631–39.

4. Optimization of Nonlinear Control Systems by Means of Nonlinear Feedbacks, **R. S. Nieswander, R. H. MacNeal.** *Ibid.*, pt. II (*Applications and Industry*), vol. 72, Sept. 1953, pp. 262–72.

5. Automatic Voltage Regulators, Application to Power Transmission Systems, **C. A. Nickle, R. M. Carothers.** *Ibid.*, vol. 47, July 1928, pp. 957–74.

6. Equivalent Linearization, Nonlinear Circuit Synthesis, and the Stabilization and Optimization of Control Systems, **R. W. Bass.** *Proceedings*, Symposium on Nonlinear Circuit Analysis, Brooklyn Polytechnic Institute, New York, N. Y., Oct. 1956.

7. The Response of Relay Amplifiers with Feedback, **J. E. Gibson, F. B. Tuteur.** *AIEE Transactions*, vol. 76, pt. II, Nov. 1957, pp. 303–07.

8. A Frequency Response Method for Analyzing and Synthesizing Contractor Servomechanisms, **R. J. Kochenberger.** *Ibid.*, vol. 69, pt. I, 1950, pp. 270–84.

9. An Investigation of the Switching Criteria for High Order Contractor Servomechanisms, **I. Bogner, L. F. Kazda.** *Ibid.*, vol. 73, pt. II, July 1954, pp. 118–27.

10. Optimum Switching Criteria for Higher Order Contractor Servo with Interrupted Circuits, **S. S. L. Chang.** *Ibid.*, vol. 74, pt. II, Nov. 1955, pp. 273–76.

11. Differential Equations with a Discontinuous Forcing Term, **D. W. Bushaw.** *Report no. 469*, "Experimental Towing Tank," Stevens Institute of Technology, Hoboken, N. J., Jan. 1953.

12. Optimum Switching of Third Order Position Relay Servos for Step Inputs, **R. N. Buland.** *M. S. Thesis*, University of California, Berkeley, Calif., June 1955.


# Constant-Frequency A-C Power Using Variable Speed Generation


**R. D. JESSEE**
ASSOCIATE MEMBER AIEE

**W. J. SPAVEN**
NONMEMBER AIEE


HE USUAL approach to provide a constant-frequency alternating-cur- t electric power system is to drive a erator at constant speed, thus pro- ing output power at constant fre- ncy. Numerous methods have been ised for obtaining constant frequency er from a generator running at var- le speeds. Analysis of these systems e shown the vast majority of these hods to be impractical for one reason nother, the usual problem being that excess amount of power is required for erator excitation.

Development of switching semiconduc- s has opened the way to new methods obtaining constant frequency electric er from variable speed generators. he unique system which is described, generator produces voltage which ies in frequency with the generator speed. The generator output power is directed into an efficient switching converter which changes the form of the voltage, resulting in output voltage of a lower frequency. By varying the rate of switching in the converter as the generator speed changes, the frequency of the output voltage from the converter may be kept constant within desired limits. Voltage regulation may be accomplished in the usual manner, by controlling the generator field current.

### Variable-Speed Constant-Frequency System

The variable-speed constant-frequency electric power system is shown in block diagram form in Fig. 1. The generator develops substantially a sine wave voltage at a frequency proportional to the generator speed. The minimum operating frequency of the generator is chosen to be several times higher than the desired system frequency. The electric power developed by the generator is transferred to the switching frequency converter, where periodic switching converts the frequency of the generated voltage to a lower frequency. The fundamental frequency of the converter output voltage (and therefore the system voltage) is the difference between the generator frequency and the switching frequency of the converter. Because the converter output voltage is derived from a periodic switching operation, this voltage contains high frequency components which may be undesirable if applied to the load. For


Paper 59-810, recommended by the AIEE Rotating Machinery Committee and approved by the AIEE Technical Operations Department for presentation at the AIEE Summer and Pacific General Meeting and Air Transportation Conference, Seattle, Wash., June 21–26, 1959. Manuscript submitted March 23, 1959; made available for printing April 29, 1959.



R. D. Jessee is with Westinghouse Electric Corporation, Lima, Ohio. W. J. Spaven is with Walter Kidde & Company, Inc., Bellville, N. J.



The authors wish to acknowledge the contributions of R. F. Blake, E. Demers, and C. C. Ware co-inventors of the basic frequency conversion methods. Acknowledgement is also made of independent work in a similar area by the Canadian Westinghouse Company.

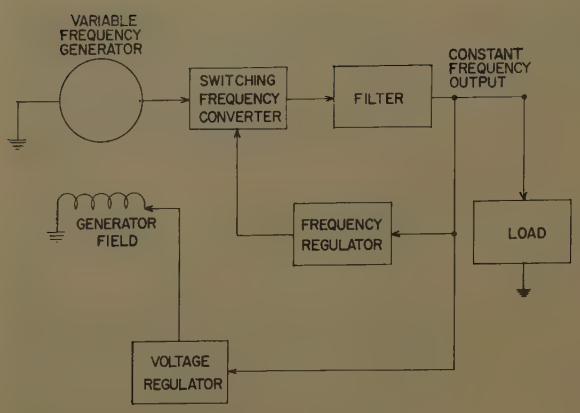


Fig. 1 (left). System diagram

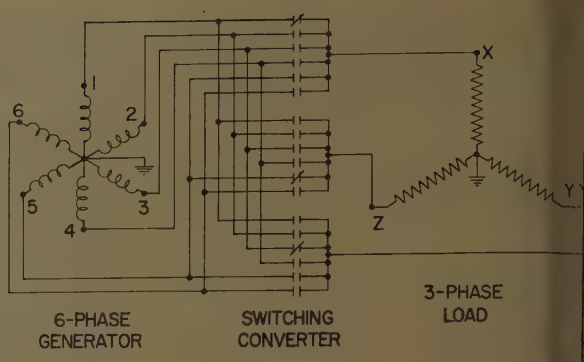


Fig. 2 (right). Schematic diagram of power circuits through switches of converter

this reason, a filter is included in the system to prevent these high frequency voltages from reaching the load.

The system frequency is kept constant by controlling the switching rate of the converter to maintain a constant difference between the switching frequency and the generator frequency despite changes in generator speed. The switching frequency is controlled by means of a frequency regulator which senses the system frequency and provides an error signal to the switching frequency converter. The converter corrects its switching frequency to reduce the error signal and thereby keep the system frequency within desired limits.

Changes in generator speed and in load cause changes in excitation requirements in the generator for constant system voltage. Voltage regulation is accomplished by a voltage regulator which senses the system voltage and adjusts the generator field current to the value required to maintain the desired system voltage.

## Method of Frequency Conversion

The method of frequency conversion to be discussed has many variations. All these variations give duplicate or similar results so far as output voltage is concerned. There are, however, numerous design considerations which must not be overlooked in coosing a particular switching method for an electric power system. For the purpose of this presentation, it appears logical to choose the method which is most straightforward and understandable, even though it may not be best from the standpoint of design.

Consider the system shown in Fig. 2. This system consists of a 6-phase generator connected to a 3-phase load through an array of 18 switches. In this case, the filter is considered part of the load. The action of the switches is to connect the load to three of the six phases for a prescribed time, then to advance to the next set for an equal time interval, and again advance, etc.

For example, at some time the load point $X$ is connected to generator terminal 1, while $Y$ is connected to 3, and $Z$ to 5. At the switching instant, the three switches making the connections just described open, and three others connect $X$ to 2, $Y$ to 4, and $Z$ to 6. Terminal $X$ is then connected in sequence to 3, 4, 5, 6, etc., for equal time intervals, while $Y$ is connected to 5, 6, 1, 2, etc., and $Z$ to 1, 2, 3, 4, etc.

The result of this switching action may be seen in Fig. 3, which shows all six phase voltages of the generator. Superimposed on these is one phase of the load voltages which is a result of switching that load from generator terminal 1 to 2 to 3 to 4, etc. It can be seen that this load voltage is predominantly a sine wave with high frequencies superimposed on it. The fundamental component of the load voltage is drawn into the figure for clarity. The frequency of the load voltage is determined by the frequency of the generator voltage and the switching frequency. It is shown in Appendix I that the load voltage frequency is the difference between generator and switching frequencies.

In order to make it legible, Fig. 3 shows only phase one of the three load voltages. However, the other two phases can be drawn in and their fundamentals will be displaced 120 and 240 degrees from the wave form shown.

The voltage appearing on one phase of the load is derived in Appendix I, equation 23 and is expressed as

$$V_x=\frac{3E}{\pi}\left[\cos(\alpha-\beta+60°)-1/5\cos(5\alpha+\beta-60°)+1/7\cos(7\alpha-\beta+60°)-\ldots\right]$$

where $\alpha$ is proportional to the switching frequency, $\beta$ is proportional to the generator frequency, and $E$ equals the maximum value of the generator voltage. Inspection of this equation shows that the fundamental frequency of the load voltage is equal to the difference between the generator frequency and the switching frequency. Therefore, if the generator frequency changes, the output frequency may be kept constant by maintaining a constant difference between the generator frequency and the switching frequency.

This load voltage equation also offers valuable information about the undesirable high-frequency voltages. The lowest frequency undesirable voltage is defined by either the second or third term of the equation, depending on the generator and switching frequencies. For example, suppose the desired output frequency is 400 cycles per second (cps), from a 1,600 cps generator. Since the output frequency is the difference between generator and switching frequencies, the switching frequency, $f_s$, can be either 2,000 cps or 1,200 cps. If $f_s=2{,}000$ cps, the second and third terms of the equation yield $5(2{,}000)+1{,}600=11{,}600$ cps, and $7(2{,}000)-1{,}600=12{,}400$ cps respectively. The lowest undesirable frequency is $(11{,}600/400=29)$ times the fundamental. If $f_s$ is 1,200 cps, the second term yields $5(1{,}200)+1{,}600=7{,}600$ cps, and the third term $7(1{,}200)-1{,}600=6{,}800$ cps. The lowest undesirable frequency here is $(6{,}800/400=17)$ times the fundamental.

The figures in the example indicate that for a given generator design it is desirable to switch at a frequency higher than that of the generator because this results in higher minimum undesirable frequencies. Of course, the higher the frequency of the


Fig. 3. Voltage waveforms of circuit on Fig. 2, showing output voltage superimposed on six generated voltages

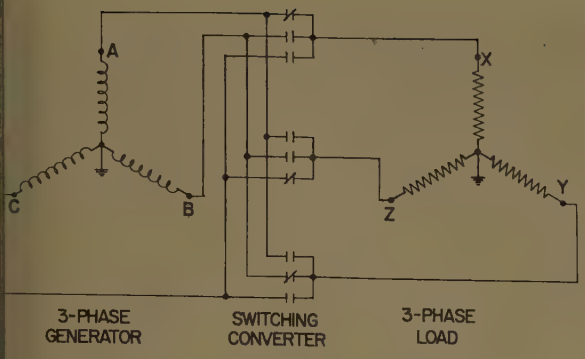


Fig. 4 (left). Schematic diagram of power circuits through switches of converter (simplified system)

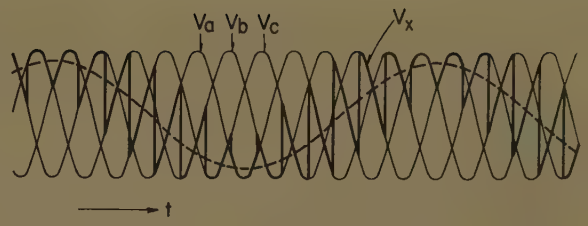


Fig. 5. Voltage waveforms of circuit of Fig. 4, showing output voltage superimposed on three generated voltages

undesirable voltage the easier will be the problem of filtering it. Another important consideration is that both the generator frequency and the switching frequency be made as high as practical in order to keep the filtering problem to a minimum.

In Appendix I the 3-phase output voltages are given in equations 23, 24, and 25. The fundamental frequency component of these voltages is given in the first term of each equation.

$$V_{xf}=\frac{3E}{\pi}\cos(\alpha-\beta+60°)$$

$$V_{yf}=\frac{3E}{\pi}\cos(\alpha-\beta+180°)$$

$$V_{zf}=\frac{3E}{\pi}\cos(\alpha-\beta-60°)$$

It will be noted from these equations that each of the three voltages is displaced 120 degrees from the other two. In this respect, the output voltages are normal for a 3-phase generating system.

Again referring to the equations of the fundamental frequency voltages, assume that the switching frequency is higher than the generator frequency. This results in the value of $(\alpha-\beta)$ being positive. In this case, $V_x$ is 60 degrees ahead of the reference, $V_y$ is 180 degrees ahead of the reference, and $V_z$ is 60 degrees behind the reference. Therefore, the sequence of the output voltages is $V_z$, $V_y$, $V_x$. If, however, the generator frequency be higher than the switching frequency, the value of $(\alpha-\beta)$ is negative; and $V_x$ is 60 degrees behind the reference, $V_y$ is 180 degrees behind the reference, while $V_z$ is 60 degrees ahead of the reference. The sequence of this mode of operation is $V_x$, $V_y$, $V_z$, opposite to that of the previous case. This is an important characteristic in some applications of this system. Appendix III describes one such application.

## Switching Frequency Converter Variations

It has already been stated that there are many possible variations on the basic system described. One which provides simplification in the switching circuits should be considered and is shown in Fig. 4. The switch operation is the same as for the previous case with the exception that there are only half as many switches in this system. Load point $X$ is switched from $V_a$ to $V_b$ to $V_c$, etc. at equal time intervals. It can be shown that the voltage appearing on the load may be expressed as

$$V_x=\frac{3\sqrt{3}E}{2\pi}[\cos(\alpha-\beta-60°)+1/2\cos(2\alpha+\beta-120°)+1/4\cos(4\alpha-\beta-60°)+1/5\cos(5\alpha+\beta-120°)+1/7\cos(7\alpha-\beta-60°)+1/8\cos(8\alpha+\beta-120°)+\ldots]$$

The load voltages $V_y$ and $V_z$ are similar to $V_x$ but displaced 120 and 240 degrees respectively. Inspection of the equation of load voltage for this case reveals the load voltage contains all the frequencies present in the 6-phase generator system. In addition, lower frequency voltage components are present as seen in the second and third terms of the equation. Because of these lower frequency voltage components, this system requires more filtering for comparable quality output. Therefore, the system requirements must be considered before the switching method is fixed. For some applications, the switching method of Fig. 4 is advantageous; for example, where sine wave output is not a requirement, or where a large number of switches is more objectionable than is the resulting increase in filter weight. The unfiltered output voltage waveform is shown in Fig. 5.

The simplest form that this method of frequency conversion can take is shown in Fig. 6 where a single-phase voltage is switched to the load in alternating polarity. Here again the load voltage contains a component of voltage which has a frequency equal to the difference between generator frequency and switching frequency. This voltage may be expressed as

$$V_L=\frac{2E}{\pi}[\cos(\alpha-\beta)+\cos(\alpha+\beta)-1/3\cos(3\alpha-\beta)-1/3\cos(3\alpha+\beta)+1/5\cos(5\alpha-\beta)+1/5\cos(5\alpha+\beta)+\ldots]$$

Inspection of this equation shows that, in addition to the fundamental frequency component, there exists a voltage component of equal magnitude at a relatively low frequency; the sum of the generator and the switching frequencies. This is, of course, quite objectionable because this component is extremely difficult to filter out in a practical power system. Fig. 7 shows the waveform of the load voltage.

Fig. 8 shows a comparison of the frequencies present in the output voltages of the three different switching methods shown in Figs. 2, 4, and 6. Figures 8(A) and 8(B) show the relative magnitudes of the various voltage components and their frequencies for the system using the 6-phase generator. Figs. 8(C) and 8(D) show the same for the 3-phase generator switched with nine switches. Figs. 8(E) and 8(F) show the same data for the single-phase case. From this compari-

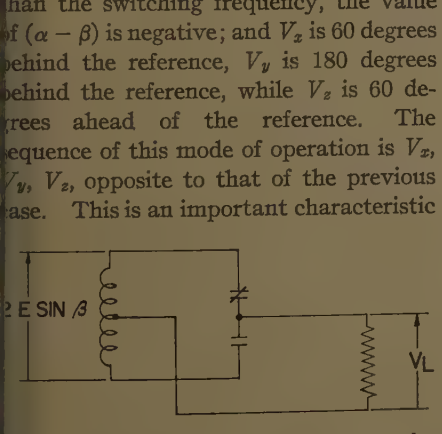


Fig. 6. Schematic diagram of basic single-phase switching circuit

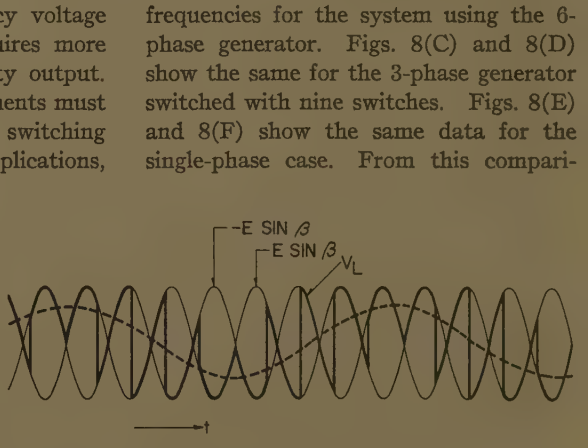


Fig. 7. Voltage waveforms of circuit in Fig. 6

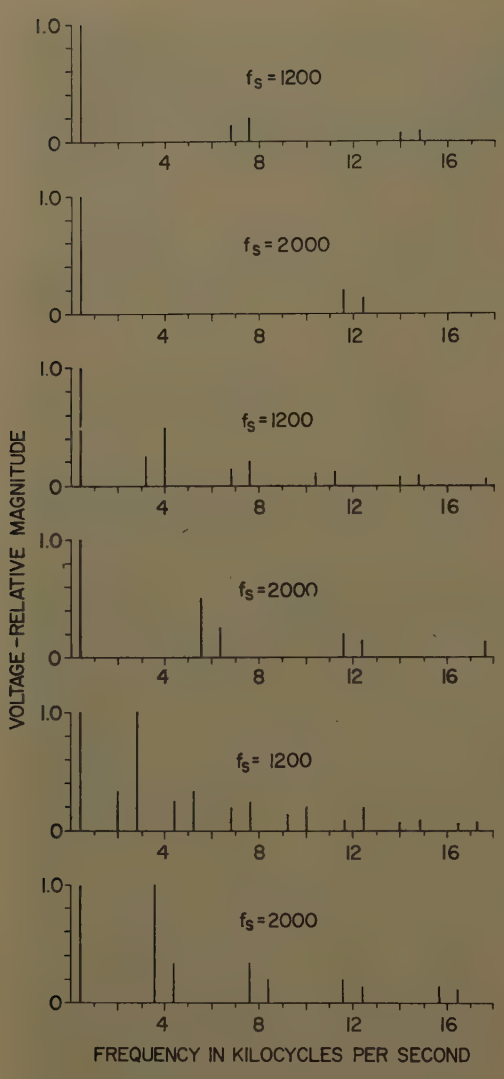


**Fig. 8 (left). Frequency spectra of converter output voltages with generator frequency = 1,600 cps**

A and B—System of Fig. 2
C and D—System of Fig. 4
E and F—System of Fig. 6

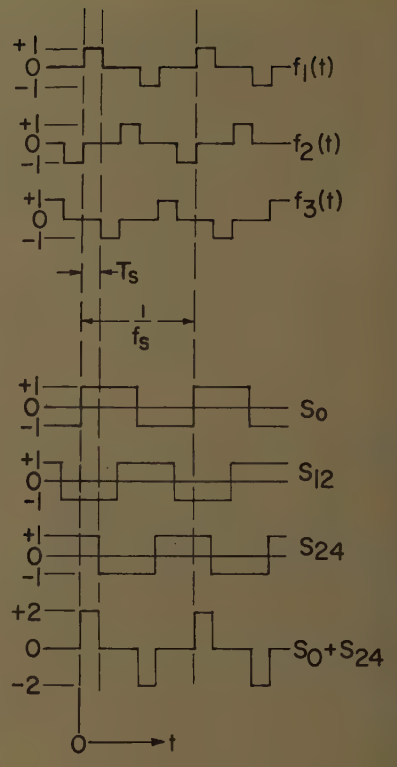


**Fig. 9 (right). Time varying functions describing converter switching**

A—Switching functions
B—Derivation of switching functions from basic square waves

son it is seen that the 6-phase switching method gives the best wave form of the three. The wave form could be further improved by switching more phases, but the obvious objection is that more switches are required—an undesirable feature from the standpoint of cost and reliability.

## Switching Semiconductors

Several methods are available for using semiconductors as switches. Some of these methods and semiconductors used are discussed briefly in Appendix II.

## Application

The most obvious application for this frequency conversion method is that of obtaining constant frequency power from a variable speed generator. This has already been discussed. The accuracy to which the output frequency may be held constant is a function of the frequency reference used. By incorporating a reference of high accuracy into the frequency regulator, an electric power system having precise frequency may be built. Fig. 12 gives the estimated weight per kva rating for this type of system.

Appendix III describes a system which is an important application of this method of frequency conversion. In this system, the frequency converter is used to supply controlled frequency excitation power to the generator. The power required from the frequency converter depends on the speed range of the generator. In a system having a narrow speed range, precise frequency output power in relatively large ratings may be obtained with a frequency converter having a low rating.

## Conclusions

A method for obtaining constant-frequency alternating-current electric power from a variable speed generator has been described. This is accomplished through use of switching circuits which are naturally bilateral, without previous rectification. This allows operation over a wide range of load power factors because there is always a low-impedance path between the load and the generator regardless of the direction of current flow.

One of the major advantages in using this system is that the only moving part required is the generator rotor. The absence of mechanical devices is indicative of lower maintenance requirements.

Because the system frequency is controlled by electrical means much faster than mechanical control, frequency transients caused by changes in generator speed are quite small and very short in duration. This is an important consideration in many applications.

By use of semiconductors which are presently available, it is practical to build electric systems in small ratings up to several kilovolt-amperes having precise frequency control. As the development of higher power semiconductors progresses, much higher power ratings will become feasible.

## Appendix I. Output Voltage Calculations

The output voltage to the load may be expressed mathematically and is developed here. In Fig. 2 each load phase is sequentially connected to each of the generator phases for equal time intervals. The sequence is $V_1$, $V_2$, $V_3$, $V_4$, $V_5$, $V_6$, etc., as indicated by Fig. 3. In the 6-phase generator, each phase is displaced from adjacent phases by 60 degrees and

$$V_1 = -V_4 \quad (1)$$

$$V_2 = -V_5 \quad (2)$$

$_3 = -V_6$ (3)

y use of equations 1, 2, and 3 it is evident at an equivalent sequence can be written $V_1$, $-V_5$, $V_3$, $-V_1$, $V_5$, $-V_3$ etc., in hich $V_2$, $V_4$, and $V_6$ are expressed in terms $-V_5$, $-V_1$, and $-V_3$. The load voltges may be expressed in terms of $V_1$, $V_3$, id $V_5$ and three functions of time as

$$_x = V_1 f_1(t) + V_3 f_2(t) + V_5 f_3(t) \quad (4)$$

$$_y = V_1 f_3(t) + V_3 f_1(t) + V_5 f_2(t) \quad (5)$$

$$_z = V_1 f_2(t) + V_3 f_3(t) + V_5 f_1(t) \quad (6)$$

here $f_1(t)$, $f_2(t)$, and $f_3(t)$ are the required nctions of time shown in Fig. 9(A). The alue of $f_1(t)$ is $(+1)$ for the first time interal (from $t=0$ to $t=T_3$), zero for the next vo intervals, $(-1)$ for the fourth, zero for he following two, etc. The values of $f_2(t)$ nd $f_3(t)$ follow a similar pattern, but are ifted in time as shown in Fig. 9(A). By spection of Fig. 9(A) it is seen that equaon 4 has values of $V_x$ equal to $V_1$ during he first interval, $-V_5$ during the second, $_3$ during the third, etc., resulting in the equired sequence. The values of $V_y$ and $_z$ follow the same sequence but are disaced in time.

It is more convenient to express $f_1(t)$, $(t)$, and $f_3(t)$ in terms of square-wave time nctions. Fig. 9(B) shows three unit quare waves, $S_0$, $S_{12}$, and $S_{24}$: displaced 120 egrees from each other. It is also shown hat the sum of two square waves $(S_0+S_{24})$ esults in the waveform of $f_1(t)$, but with vice the magnitude. Therefore,

$$(t) = (1/2)(S_0 + S_{24}) \quad (7)$$

$$(t) = (1/2)(S_{12} + S_0) \quad (8)$$

$$(t) = (1/2)(S_{24} + S_{12}) \quad (9)$$

quations 1, 2, and 3 may now be written terms of the square wave functions.

$$_x = (1/2)[(S_0 + S_{24})V_1 + (S_{12} + S_0)V_3 + (S_{24} + S_{12})V_5] \quad (10)$$

$$_x = (1/2)[S_0(V_1 + V_3) + S_{12}(V_3 + V_5) + S_{24}(V_5 + V_1)] \quad (10A)$$

$$_y = (1/2)[(S_{24} + S_{12})V_1 + (S_0 + S_{24})V_3 + (S_{12} + S_0)V_5] \quad (11)$$

$$_y = (1/2)[S_0(V_3 + V_5) + S_{12}(V_5 + V_1) + S_{24}(V_1 + V_3)] \quad (11A)$$

$$_z = (1/2)[(S_{12} + S_0)V_1 + (S_{24} + S_{12})V_3 + (S_0 + S_{24})V_5] \quad (12)$$

$$_z = (1/2)[S_0(V_5 + V_1) + S_{12}(V_1 + V_3) + S_{24}(V_3 + V_5)] \quad (12A)$$

hese equations are general expressions for he load voltages where $V_1$, $V_3$, and $V_5$ are he instantaneous voltages at the generator erminals.

If the generator output is a set of balanced nusoidal voltages

$$_1 = E \sin \beta \quad (13)$$

$$_3 = E \sin (\beta - 120°) \quad (14)$$

$$_5 = E \sin (\beta + 120°) \quad (15)$$

here $\beta = 2\pi f_g t$, $f_g$ is the generator frequency, is time, and $E$ is the maximum value of enerated voltage.

$$V_1 + V_3 + V_5 = 0$$

Therefore, equation 10(A) may be written

$$V_x = -(1/2)[S_0 V_5 + S_{12} V_1 + S_{24} V_3] \quad (16)$$

Substituting equations 13, 14, and 15

$$V_x = -(E/2)[S_0 \sin(\beta + 120°) + S_{12} \sin \beta + S_{24} \sin(\beta - 120°)]$$

But

$$\sin(\beta + 120°) = \frac{\sqrt{3}}{2} \cos \beta - \frac{1}{2} \sin \beta$$

and

$$\sin(\beta - 120°) = -\frac{\sqrt{3}}{2} \cos \beta - \frac{1}{2} \sin \beta$$

Therefore

$$V_x = \frac{E}{2}\left[(S_{24} + S_0)\frac{\sqrt{3}}{2} \cos \beta + (S_0 + S_{24} - 2S_{12})\frac{1}{2} \sin \beta\right] \quad (17)$$

The square wave functions $S_0$, $S_{12}$, and $S_{24}$ may be expressed in the form of Fourier series[1] as

$$S_0 = (4/\pi)[\sin \alpha + (1/3)\sin 3\alpha + (1/5)\sin 5\alpha + (1/7)\sin 7\alpha + \ldots] \quad (18)$$

$$S_{12} = (4/\pi)[\sin(\alpha - 120°) + (1/3)\sin 3(\alpha - 120°) + (1/5)\sin 5(\alpha - 120°) + (1/7)\sin 7(\alpha - 120°) + \ldots]$$

$$S_{12} = (4/\pi)[\sin(\alpha - 120°) + (1/3)\sin 3\alpha + (1/5)\sin(5\alpha + 120°) + (1/7)\sin(7\alpha - 120°) + \ldots] \quad (19)$$

$$S_{24} = (4/\pi)[\sin(\alpha + 120°) + (1/3)\sin 3(\alpha + 120°) + (1/5)\sin 5(\alpha + 120°) + (1/7)\sin 7(\alpha + 120°) + \ldots]$$

$$S_{24} = (4/\pi)[\sin(\alpha + 120°) + (1/3)\sin 3\alpha + (1/5)\sin(5\alpha - 120°) + (1/7)\sin(7\alpha + 120°) + \ldots] \quad (20)$$

where $\alpha = 2\pi f_s t$, and $f_s$ is the switching frequency.

The functions required in equation 17 are

$$(S_{24} - S_0) = \sqrt{3}(4/\pi)[\sin(\alpha + 150°) + (1/5)\sin(5\alpha - 150°) + (1/7)\sin(7\alpha + 150°) + \ldots] \quad (21)$$

$$(S_0 + S_{24} - 2S_{12}) = -3(4/\pi)[\sin(\alpha - 120°) + (1/5)\sin(5\alpha + 120°) + (1/7)\sin(7\alpha - 120°) \ldots] \quad (22)$$

Substituting equations 21 and 22 into equation 17,

$$V_x = \frac{E\sqrt{3}}{2} \cdot \frac{4}{\pi} \cdot \frac{\sqrt{3}}{2}\Big[\frac{1}{2}\cos(\alpha - \beta + 60°) - \frac{1}{2}\cos(\alpha + \beta + 240°) + \frac{1}{5}\cdot\frac{1}{2}\cos(5\alpha - \beta - 240°) - \frac{1}{5}\cdot\frac{1}{2}\cos(5\alpha + \beta - 60°) + \frac{1}{7}\cdot\frac{1}{2}\cos(7\alpha - \beta + 60°) - \frac{1}{7}\cdot\frac{1}{2}\cos(7\alpha + \beta + 240°) + \ldots\Big] + \frac{E}{2}\cdot\frac{1}{2}(-3)$$

$$\frac{4}{\pi}\Big[\frac{1}{2}\cos(\alpha - \beta - 120°) - \frac{1}{2}\cos(\alpha + \beta - 120°) + \frac{1}{5}\cdot\frac{1}{2}\cos(5\alpha - \beta + 120°) - \frac{1}{5}\cdot\frac{1}{2}\cos(5\alpha + \beta + 120°) + \frac{1}{7}\cdot\frac{1}{2}\cos(7\alpha - \beta - 120°) - \frac{1}{7}\cdot\frac{1}{2}\times \cos(7\alpha + \beta - 120°) + \ldots\Big]$$

$$V_x = (3E/\pi)[\cos(\alpha - \beta + 60°) - (1/5)\cos(5\alpha + \beta - 60°) + (1/7)\cos(7\alpha - \beta + 60°) - \ldots] \quad (23)$$

By a similar derivation it can be shown that

$$V_y = (3E/\pi)[\cos(\alpha - \beta + 180°) - (1/5)\cos(5\alpha + \beta + 180°) + (1/7)\cos(7\alpha - \beta + 180°) - \ldots] \quad (24)$$

and

$$V_z = (3E/\pi)[\cos(\alpha - \beta - 60°) - (1/5)\cos(5\alpha + \beta + 60°) + (1/7)\cos(7\alpha - \beta - 60°) - \ldots] \quad (25)$$

In this analysis the time required to switch from one phase to the next is neglected, for to include it would unnecessarily complicate the expressions. In any final design of a system this switching time must be considered because this represents commutation and causes short interruptions resulting in voltage spikes which must be controlled. However, this is not an extremely difficult problem to overcome.

## Appendix II. Switching Devices

The power handling capability of the variable-speed constant-frequency system is integrally related to the development of high-power switching devices. Transistors are available in both germanium and silicon materials, but it appears that the inherent higher voltage capability of silicon offers the greater possibility for this application. Silicon transistors are currently available in ratings of 5 amperes peak 300 volts; and a 15-ampere peak 200-volt unit is soon to be released.

A typical circuit using the transistor as a switching device is shown in Fig. 10. While the transistor itself is not a bilateral device, its use in a rectifier bridge as shown makes it essentially so, and as such is capable of switching alternating currents as well as

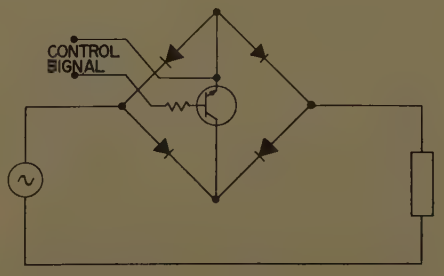


**Fig. 10. Bilateral transistor switch**

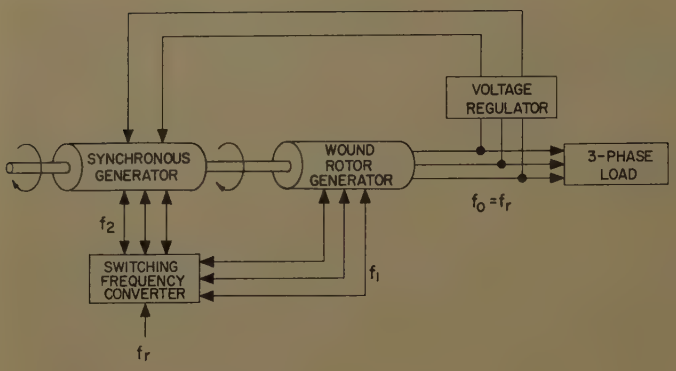


Fig. 11. System diagram of frequency converter used in excitation system for precise frequency system

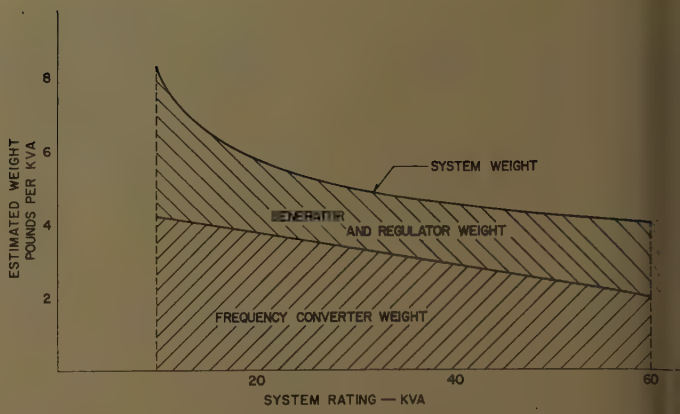


Fig. 12. Estimated weight versus rating of system shown in Fig. 1

direct currents. The switch is turned on and off by means of control current applied to the base of the transistor.

Several manufacturers have made available multiple-junction semiconductor devices[2,3] which exhibit characteristics similar to those of the thyratron. One such device is known as a trinistor. While these devices are not directly interchangeable with transistors, control circuits[2] which permit the use of trinistors as bilateral alternating current switches are available and may be used in the frequency converter. Trinistors in ratings of 300 volts and average current of 15 amperes are currently available, and much higher ratings are soon to be available.

## Appendix III. An Additional Electric Power System

One important application of the frequency changer described is in the system shown in Fig. 11 in block diagram form. This system is comprised of a voltage-regulated wound-rotor induction generator receiving its excitation power from a synchronous generator through the static-frequency changer. The wound-rotor machine and the synchronous machine are driven from a common shaft and have the same number of poles. Therefore, if both machines received direct-current excitation they would generate voltages of the same frequency.

Three-phase voltage applied to the rotor of the wound-rotor generator sets up a magnetic field which rotates around the rotor. In this respect the machine acts as a transformer, inducing in the phase windings a voltage proportional to the rotor input voltage. When the rotor of the machine is mechanically driven the angular velocity of the field is changed by an amount equal to the speed of mechanical rotation.

In other words, if the magnetic field rotates at an angular velocity of $\omega_1$ with respect to the rotor, and the rotor is driven at a speed of $\omega_2$, the speed of the field with respect to the stator phase windings will be $\omega_1+\omega_2$. Therefore, the frequency of the output voltage is proportional to $\omega_1+\omega_2$.

The 3-phase voltage applied to the rotor is supplied by the exciter system which comprises the synchronous generator and the switching frequency converter. The synchronous generator, when mechanically driven, produces voltage at a frequency, $f_2$, proportional to the shaft speed. The output voltage is applied to the switching frequency converter where it is switched at a constant reference frequency, $f_r$. As previously described, the resulting output voltage from the frequency converter is at a frequency equal to the difference between input frequency and the switching frequency. Therefore

$$f_1 = f_r - f_2$$

Since $\omega_1$, the angular velocity of the magnetic field with respect to the rotor, is produced by a voltage at a frequency of $f_1$, it follows that $\omega_1$ is proportional to $f_1$, and the frequency of the system output voltage is

$$f_0 = f_1 + f_2$$

or

$$f_0 = (f_r - f_2) + f_2$$

therefore

$$f_0 = f_r$$

Thus the system frequency is maintained constant and equal to the reference frequency, $f_r$, despite changes in shaft speed. With proper control $f_r$ may be maintained constant within limits as precise as one part in 100,000; and, therefore, the output frequency will remain within these same limits.

The ability of the switching frequency converter to put out power of either positive- or negative-sequence at a frequency proportional to the deviation from nominal speed is a very important characteristic of this system. This enables the magnetic field supplied by the excitation system to rotate in either direction with respect to the rotor and thus maintain a constant system frequency, at speeds both greater and less than nominal. It will be noted that when the generator speed is at its nominal value, the excitation system must supply direct current excitation. The switching frequency converter may do this very readily becaue this is the result of switching the converter input voltage at its natural frequency; i.e., when $f_2 = f_r$, $f_1 = 0$.

It should be noted that while the system output power is derived from shaft rotation, power must be supplied via the switching frequency converter. When the shaft speed is at nominal value, only direct current excitation is required. When the speed deviates from nominal, part of the power is supplied through transformer action in the wound-rotor generator. As the speed deviation increases, the power required from the excitation system increases. The power handling capacity of the switching frequency converter and the synchronous generator, therefore, is a direct function of the speed range.

## Nomenclature

$E$ = maximum voltage of generator
$f_g$ = generated voltage frequency
$f_0$ = system output frequency (Fig. 11)
$f_r$ = reference frequency (Fig. 11)
$f_s$ = switching frequency
$f_1$ = frequency converter output frequency (Fig. 11)
$f_2$ = synchronous generator frequency (Fig. 11)
$f_1(t), f_2(t), f_3(t)$ = functions of time defined by Fig. 10(A)
$S_0$, $S_{12}$, $S_{24}$ = square wave functions of time defined by Fig. 10(B)
$t$ = time
$T_s$ = conducting time interval of each switch
$V_a$, $V_b$, $V_c$ = instantaneous terminal voltage of 3-phase generator
$V_x$, $V_y$, $V_z$ = output voltages of switching frequency converter
$V_1$ through $V_6$ = instantaneous terminal voltages of 6-phase generator
$\alpha = 2\pi f_s t$ = time varying angle of switching operation
$\beta = 2\pi f_g t$ = time varying angle of generator voltage
$\omega_1$ = angular velocity of magnetic field with respect to rotor
$\omega_2$ = angular velocity of rotor

## References


1. Higher Mathematics for Engineers and Physicists (book), I. S. Sokolinkoff, E. S. Sokolnikoff. McGraw-Hill Book Company, Inc., New York, N. Y., 1941, chap. II.

2. Notes on the Application of the Silicon Controlled Rectifier. *Application Engineering Bulletin*, no. ECG-371-1, General Electric Company, Schenectady, N. Y., Dec. 1958.

3. High Current Trinistors, F. S. Stein, E. W. Torok. *CP58-1397* (available on request).

4. The Rectifier Calculus, W. Melvin Goodhue. *AIEE Transactions*, vol. 59, 1940, pp. 687–91.

# Discussion

**rt V. Hoard** (Boeing Airplane Company, attle, Washington): This is a very rthwhile paper which describes another y of obtaining constant frequency from a riable speed generator. However, some ditional data on the system, if included the discussion, will improve its value to e industry. What is the minimum and ximum shaft speed which was used when termining the estimated weight versus ing values shown on Fig. 12 of the paper the 60-kva generator? What over-all iciency can be expected for this 60-kva nerator at rated load and power factor minimum and at maximum shaft speed, suming the generator has the capabilities meeting present military specifications? A switching frequency of 2,000 cycles per cond rather than 1,200 cycles per second suggested by the authors as providing gher undesirable frequencies and therefore sier filtering. However, this will increase e number of switching times in each cond, and will increase the switching losses d the duty on each semiconductor. Con- ering these factors and the need for pre- nting semiconductor failures during ab- rmal overloads, faults and transient over- ltages, what do they estimate to be neces- ry derating factors in the semiconductors provide for reliable operation in the gen- tor?

**M. Chirgwin and L. J. Stratton** (Jack Heintz, Inc., Cleveland, Ohio): The thors are to be congratulated on their niconductor frequency changer and on the nple mathematical treatment of it that cy have developed. In this mathematical atment the question of commutation s been ignored in order to keep the alysis simple, and this is entirely justifi- e. It is unfortunate, however, that no ntion has been made of the problems commutation, since until these problems ve been overcome no frequency changer ving a substantial power rating can be nsidered successful. We, therefore, sub- the following discussion of the problems commutation as they appear to exist in s frequency changer.

n order to illustrate the problems of mmutation in this frequency changer an alogy with a rotating machine having a mmutator will first be developed. The erator frequency-changer combination wn in Fig. 2 of the paper can be repre- ted by a 2-pole direct-current generator ving a 6-phase star winding connected to a gment commutator. This machine is ated at 1,600 revolutions per second. ree brushes ($X$, $Y$, $Z$) spaced 120 degrees rt are provided which feed the power the 3-phase load. These brushes not stationary in space but rotate at revolutions per second against or in same direction as the machine. See . 13. With the directions shown in this re, the voltage of the brush is a positive ximum when it is at the top of the com- tator, is zero when it is on either hori- tal center line, and is a negative maxi- m when it is at the bottom of the com- tator.

he mathematical treatment given in the er requires that the micas and the brushes of this analogy both have negligible width and that commutation be instantaneous. Obviously, in an actual frequency changer the commutation cannot be instantaneous, so let us assume for the moment that the brushes of the analogy have some width. There is now an overlap in time between the currents carried by the incoming and outgoing windings. This is using the "make before break" technique which is used in most commutation problems.

Consider first the conditions that exist when a brush is located on the horizontal center line under the south pole (dotted in Fig. 13). This brush short-circuits segments 5 and 6. The voltages of these segments at the instant shown in Fig. 13 are: $-0.5V_1$ and $+0.5V_1$ respectively; where $V_1$ is the line to neutral voltage. The voltage that is short-circuited by the brush is the difference of these two or $V_1$ volts, and is in a direction to cause current to flow out of segment 6 into segment 5. That is in the direction required to transfer the out flowing load current from segment 5 to segment 6, (provided the speed of rotation of the brush is less than that of the commutator). As in any commutation process, this transfor of current will be opposed by the leakage inductance of both of the windings so that the transfer will take a certain time for completion. If the width of the brush is correctly chosen, the transfer will be just complete when segment 5 breaks contact with the brush, and perfect commutation results.

Since the time required for commutation varies directly with the load current but the voltage causing commutation remains fixed, it is necessary to vary the width of the brush (overlap time) with the load current to ensure perfect commutation.

In addition, the magnitude of the voltage between adjacent commutator segments which is the voltage causing commutation varies (sinusoidally) with brush position being a maximum on the horizontal line and zero at the top and bottom of the commutator, so it is also necessary to vary the overlap time with brush position in order to achieve perfect commutation.

If steps were taken to ensure the correct variation of overlap time with load current and brush position, then perfect commutation would be possible for an outflowing load current and for all positions of the brush under the south pole. When we consider conditions under the north pole, however, we find the direction of the voltage that is short-circuited by the brush is such as to oppose the transfer of current, and commutation cannot be accomplished without sparking. If the direction of rotation of the brushes is opposite to that of the commutator then the situation is unchanged because the direction of motion of the brushes on the commutator is unchanged.

Returning now to the semiconductor frequency-changer, it appears that by using the "make before break" technique satisfactory commutation could be achieved for half the time by varying the overlap in an appropriate manner, but for the other half of the time some external means of forcing the commutation would be necessary.

Another way of dealing with the situation that has been used where small powers are involved is to employ a "break before make" switching sequence. With this approach the energy stored in the inductance of the coil is dissipated (in an arc for example) each time a switch is opened. If the switch used is the bilateral transistor switch shown in Fig. 10 of the paper, then the energy stored in the inductance of the coil appears as heat in the transistor. When the power rating of the frequency changer becomes large, this extra heat in the transistor is objectionable because of the reduction in efficiency and because of the de-rating of the transistor. We find with a normal design of the generator this extra loss can be equal to the normal transistor losses, which means the power rating of the transistor is reduced to about one half normal.

We would be interested to know if a "break before make" technique is used in this frequency changer and if so how much the transistors must be de-rated; or whether some external means of commutation are employed.

It should be pointed out that the commutation difficulties described do not occur with all semiconductor frequency changers. A frequency changer using silicon controlled rectifiers as the switching device has been developed by the discussers.

This frequency changer is described in a paper entitled "Precise Frequency Power Generation from an Unregulated Shaft," by K. M. Chirgwin and L. J. Stratton, which is scheduled for presentation at a forthcoming AIEE meeting. Also, a paper[1] describing the application of the frequency changer to an aircraft variable-speed constant-frequency generating system was published recently.

The silicon controlled rectifier used in this frequency changer cannot be turned off by the control circuit. Because of this, commutation is very similar to that occurring in a normal (diode) rectifier circuit, where the firing of the incoming controlled

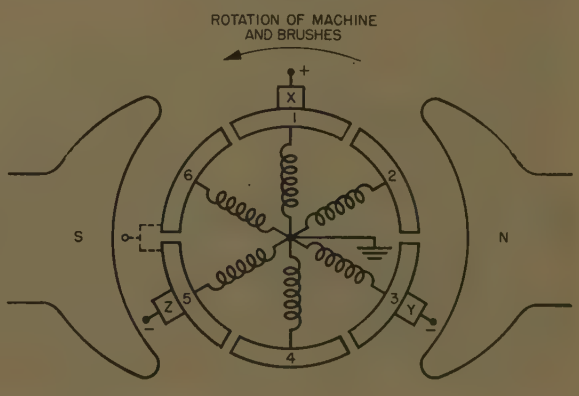


**Fig. 13. Rotating machine analogy of the frequency changer and generator**

rectifier causes the load current to transfer from the outgoing to the incoming controlled rectifier. The length of the overlap period automatically adjusts to the time required to complete the transfer.

The frequency changer has further advantages in that controlled rectifiers presently are available in higher power ratings than transistors (they may always be so[2,3]), and in that it has the capability of voltage regulation within itself; a characteristic that seems to be absent in the authors' frequency changer.


REFERENCES

1. VARIABLE-SPEED CONSTANT-FREQUENCY GENERATOR SYSTEM FOR AIRCRAFT, **K. M. Chirgwin, L. J. Stratton.** *AIEE Transactions*, pt. II (*Applications and Industry*), vol. 78, Nov. 1959, pp. 304–10.

2. PNPN SWITCHES, **J. M. Goldey.** *CP58-1359* (not available).

3. See reference 3 of the paper.

4. VARIABLE-SPEED SYNCHRONOUS-FLUX GENERATOR, **V. DeBiasi.** *Space/Aeronautics*, New York, N. Y., Apr. 1959.


**R. D. Jessee** and **William J. Spaven:** The commutation problem pointed out by Messrs. Chirgwin and Stratton is one of which we are aware. Semiconductor switches have the characteristics of faster turn-on than turn-off. Therefore, the normal mode of operation of the frequency converter described allows some overlap in switching; i.e., one set of switches turns on before the previous set turns off. This type of operation causes a short circuit on the generator through the switches each time the switches operate. As pointed out, this type of operation requires some derating of the semiconductor switches. As a set of switches completes the turn-off operation, the short circuit is removed and the result is a transient voltage of very short duration; a spike. By delaying the turn-on, the overlap may be eliminated and therefore short-circuiting of the generator does not occur. Instead, the generator terminals are opened momentarily, interrupting the current flow. This, of course, causes voltage spikes but without the short-circuiting of the generator through the switches.

In order that the switches may operate efficiently, the voltage spikes must not appear on the switches. The voltage spikes may be suppressed by providing a path for the current between the generator and the switches. By use of energy storage circuits, we have been successful in limiting the spikes appearing at the switches on models built and tested. Apparently very little de-rating of semiconductors is required because of commutation.

The questions raised by Mr. Hoard pertain to the design of specific apparatus. While the intent of the paper was to present the principles of a method for accomplishing frequency conversion, the questions raised are pertinent to the application of the principles described. Fig. 12 was intended to give a rough estimate of the weight of a constant-frequency electric power system having a two-to-one speed range. The estimate was based on experience in electric conversion equipment and aircraft generator manufacture.

Because the generator currents are continually switched, the root-mean-square values of these currents are increased for a given power output. For this reason, the generator efficiency can be expected to be somewhat lower than for a constant-speed synchronous generator. Further, efficiency depends on the specific design employed in the generator and switching circuits. Calculations indicate a generator efficiency in the order of 80% in this system.

In the final design of a system using a frequency converter as described here, the actual generated and switching frequencies are subject to several compromises. There are limitations to not only the switching frequency but also generator speed and therefore, generator frequency. More phases may be used in generation, and by so doing, the lowest frequency of undesirable voltage components may be increased in proportion. This will result in a compromise where the generator and switching frequencies may be lowered and at the same time gain high-frequency undesirable voltage components with reduced amplitude. This type of design could work in favor of both generator and frequency converter. Of course, any such compromise must consider the number of switches which must be added in order to accomplish the final configuration. In considering de-rating for semiconductors, all operating conditions must be considered. The power loss caused by switching will be approximately the same for each switching operation at any particular load. Therefore the switching losses will vary approximately with the switching rate.

# Characteristics and Measurement of Ripple in Aircraft Electric Power Systems


OSCAR MARKOWITZ
MEMBER AIEE



**Synopsis:** This paper describes the work accomplished at NADEVCEN (the Naval Air Development Center) to develop definition of frequency characteristic of ripple and to provide guidance in the voltage measurement of ripple. Factors influencing the unpredictable variations in ripple measurements are recognized and noted for guidance. Frequency characteristic data of ripple accumulated from various aircraft d-c power sources formed the basis for the developed limits recommended to be integrated into military specifications.


RIPPLE in aircraft electric systems, like other aircraft electric system characteristics, has been taken for granted. Its existence has been known and limits delineated in various military specifications[1–4] as a maximum peak from an average assumed to be the d-c level. Tremendous increases in the sophistication and performance of military electronic equipment has forced the need to know more about the characteristics of ripple. This paper deals primarily with various aspects of ripple, its measurement and development of definition for the frequency characteristics of the ripple.

The peak value of ripple as a characteristic is not as valuable to equipment designers as the voltage at any given frequency within the frequency spectrum of that ripple. Previous efforts to determine this frequency spectrum characteristic of power system ripple have been fragmentary.[5] In a sincere effort to determine susceptibility to ripple, some equipment designers have superimposed single-frequency a-c components on the d-c input to their equipment. By varying the a-c component in amplitude and frequency, they have evaluated the sensitivity of their equipment to the a-c component. The missing link in this type of evaluation was a knowledge of the limits of frequency characteristic ripple obtained in power systems. Assumptions have been made in the past that a specified peak value of ripple could be coincident of a same maximum amp


Paper **59-879,** recommended by the AIEE Transportation Committee and approved by the AIEE Technical Operations Department for presentation at the AIEE Summer and Pacific General Meeting and Air Transportation Conference, Seattle, Wash., June 21–26, 1959. Manuscript submitted March 24, 1959; made available for printing April 22, 1959.



OSCAR MARKOWITZ is with the United States Naval Air Development Center, Johnsville, Pa.



The laboratory work in obtaining measurements and pictures of ripple was accomplished by Howard Ireland. The laboratory work in obtaining data for the frequency characteristics of ripple was accomplished by Henry Kunicki. The author gratefully acknowledges the information he received on ripple of various equipments from the Naval Air Center at Patuxent River, Md. The author also wishes to thank the many engineering groups who have been extremely co-operative in establishing limits for aircraft electric system characteristics and the author's investigation of electric systems-utilization equipment compatibility problems. Illustrations are official photographs of the United States Navy.

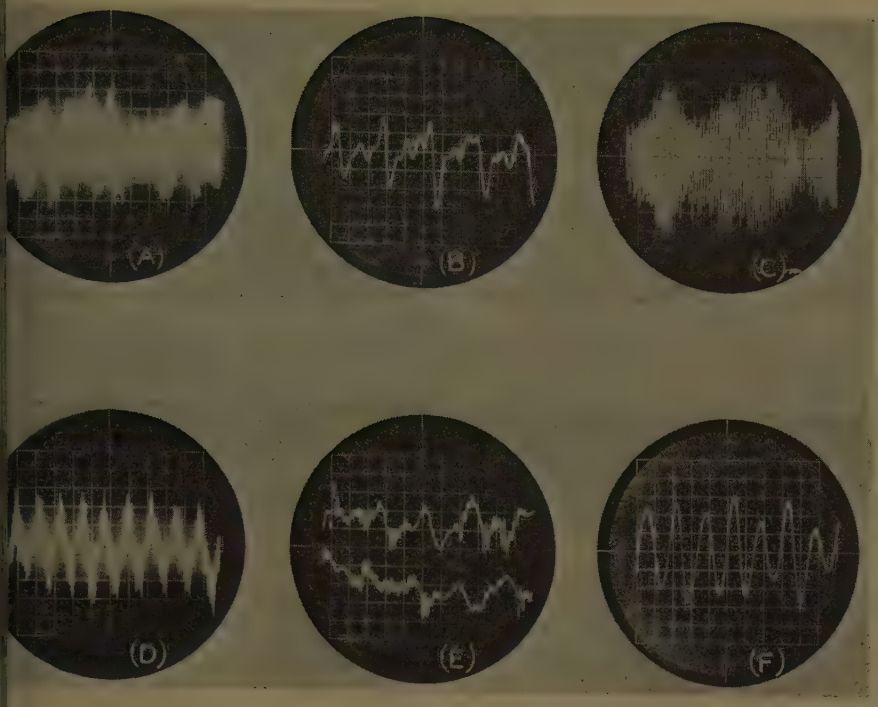


1. Sample oscillograms of d-c generator ripple. Generator: Manufacturer D, 200 amperes, 4,000 to 8,000 rpm

4,000 rpm, no load, 360 mechanical ees of generator rotation, 2 milliseconds per division, 0.5 volt per division
4,000 rpm, no load, bar to bar, 100 oseconds per division, 0.5 volt per division
8,000 rpm, no load, 360 mechanical ees of generator rotation, 750 micro- nds per division, 0.5 volt per division
D—4,000 rpm, full load, 360 mechanical degrees of generator rotation, 2 milliseconds per division, 0.2 volt per division
E—4,000 rpm, full load, bar to bar, 100 microseconds per division, 0.2 volt per division
F—6,000 rpm, no load, bar to bar, 50 microseconds per division, 0.5 volt per division

Table I. Maximum Peak Ripple Obtained From Various Equipments

| Manufacturer | Equipment | Ampere Rating | Volts Ripple |
|---|---|---|---|
| G | Unregulated TR | 200 | 2.0 |
| G | Unregulated TR | 100 | 1.3 |
| G | Unregulated TR | 50 | 4.5 |
| G | Unregulated TR | 25 | 5.8 |
| B | Unregulated TR | 100 | 1.1 |
| B | Unregulated TR | 50 | 1.15 |
| A | Unregulated TR | 100 | 1.3 |
| A | Unregulated TR | 50 | 1.0 |
| C | Unregulated TR | 100 | 1.25 |
| J | Unregulated TR | 200 | 2.45 |
| B | Regulated TR | 50 | 1.8 |
| E* | Regulated TR | 50 | 0.6 |
| H | Regulated TR | 200 | 2.4 |
| I | Regulated TR | 50 | 2.45 |
| B | Generator | 200 | 1.53 |
| B | Generator | 300 | 0.69 |
| D | Generator | 200 | 1.4 |
| D | Generator | 400 | 1.33 |
| F | Generator | 400 | 0.85 |

* Environmental evaluation not completed.

*Note:* Volts ripple is the maximum peak ripple voltage ± from the d-c average measured for all conditions of operations.

at any frequency from close to direct ent to well above the audio spectrum. assumption has forced severe filter lties on some equipment. NADEVCEN e an investigation to provide a basis lineating the frequency characteristic pple.

## uencing Factors of Ripple

present aircraft and missiles d-c power otained directly from d-c generators batteries and indirectly through trans- er rectifiers from a-c power systems. paper considers the ripple in 28-volt ower systems, including d-c genera- and transformer rectifiers.

pple in d-c generators is primarily due ommutation at the armature. The tion of flux across the pole faces, pole le, and of winding to winding give rise he lower frequency components. g at the commutator gives rise to higher frequency components. The g is function of design (effectiveness x shift compensation as a function of , load, service condition of commuta- nd brushes, and filter. Input speed tions can shift the lower frequency components but has relatively little effect on the higher frequency components due to arcing. A battery placed across the generator is very effective in reducing the peaks of ripple above the average d-c level.

The fundamental aspect of ripple in transformer rectifiers (TR) is related to flow of current only occurring during the peak of each sine wave. The conduction angle for each phase of a 6-phase half-wave TR is 60 degrees, 30 degrees each side of the sine-wave peak. Practical considerations result in distortion of each 60-cycle sine-wave peak and in variations in d-c component from one sine wave peak to the next through the six making up 360 degrees of the fundamental frequency. Thus the TR ripple is affected from its theoretical limits by the variation between rectifiers, phase-to-phase transformation, and windings. Extreme emphasis placed on minimum weight for aircraft TR's has further emphasized internal phase to phase variations and no-load to full-load variations. These factors become more acute for regulated transformer rectifiers since regulation is usually obtained by varying the conduction angle for each rectifier from 60 degrees to some value less than 60 degrees. The a-c power source can affect ripple with unbalanced voltages between phases and when the source impedance is relatively high in relation to the TR conduction angle load currents. The power source can further influence the ripple when nonlinear loads on the same source influence a-c waveform in the region of the TR conduction angle. It has been recognized that a TR in itself is a nonlinear load on the a-c power system and does increase the harmonic content of the a-c power. With the narrowing of the conduction

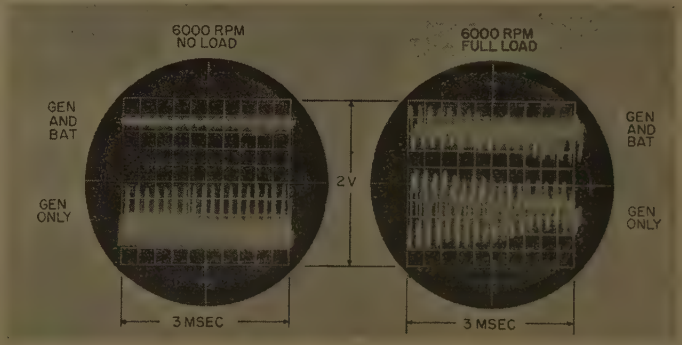


Fig. 2. Influence of a battery on d-c generator ripple. Generator: Manufacturer B, 200 amperes d-c

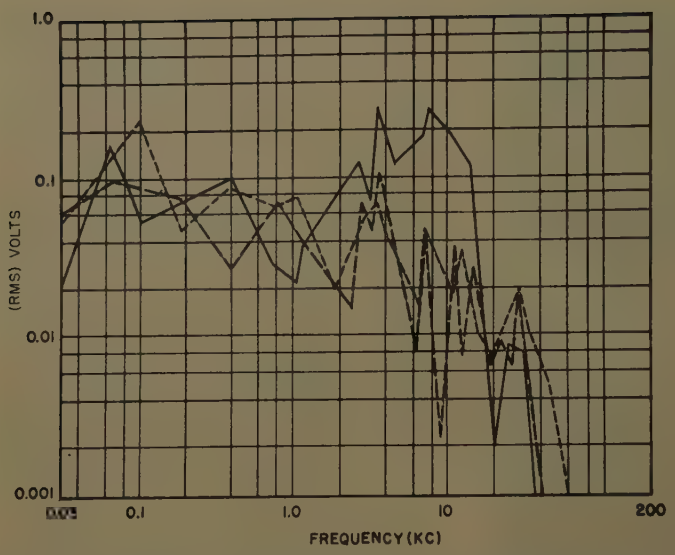


**Fig. 3. Frequency characteristics of ripple from a 300-ampere generator. Manufacturer A**

—— No load
— — Half load
– – – Full load

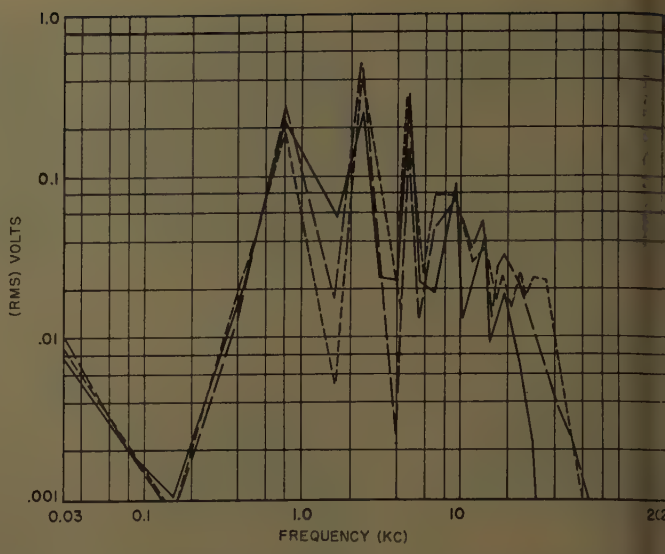


**Fig. 5. Frequency characteristics of ripple from a 100-ampere 6-pha unregulated TR. Manufacturer A, 3-volt input balanced**

—— No load
— — Half load
– – – Full load

angle in regulated units, the influence on harmonics becomes progressively worse. Increased a-c source impedance for a given TR load also correspondingly increases influence on harmonics. Voltage modulation,[6,7] which can ride through a TR and become part of the ripple is also found in a-c systems. Thus minimum ripple from a TR can be achieved only by both good design with close production control and careful application considerations.

## Measurement of Ripple

Measurement of ripple in d-c power systems for aircraft has been in the past predicated on the need to know how far the ripple caused voltage to leave the average d-c level, and is referred to in the aircraft power field as a maximum ripple voltage. It has been specified and measured in military specifications[1–4] as a maximum peak voltage. This is contrasted to other fields where ripple is considered in terms of per cent. The per cent figure is confused, since it is obtained for other power fields[8] by comparing the rms value of ripple to average d-c value and for electronic fields[9] as the total of plus and minus peak deviations compared to the average d-c value. The various methods of measurement cannot be correlated for aircraft d-c systems, since the ripple is almost always a very complex wave. Other factors that have entered into the confusion of ripple measurement are as follows:

1. Peak-to-peak voltmeters have been confused with peak reading voltmeters. The peak reading voltmeter reads only the voltage from an a-c zero to the peak going in the positive direction for one polarity connection and from a-c zero to the peak going in the negative direction for t opposite polarity connection. The zero may or may not coincide with t average direct voltage. The peak-to-pe reading voltmeter measures the span voltage between the negative ripple pe value and the positive ripple peak value.

2. Time constants of peak reading peak-to-peak instruments vary over co siderable limits. Short-duration peaks wi random or relative long duration of occurrence is often obtained in genera ripple. In many instruments, unless t voltage to be measured reoccurs on a cyc basis of high enough repetition rate, t readings do not reflect the maximum pea

3. It is not always clear when using vacuum-tube voltmeter that the act reading obtained is a function of avera rms, or peak of the input wave. T confusion is compounded when the me scale is marked as a reading not corresponding to the function of measurement. a sine wave, if the function of measurem is known, conversion can be obtain With a complex wave, if the meter is calibrated in terms of the function measurement, reading cannot always corrected by conversion factors.

4. When using a peak reading me care should be exercised that the accur is valid for the low voltages norma encountered in ripple, 0.1 to 5 vo Many instruments use diodes in their inp When input voltages are measured wh are in the same order of magnitude as conduction knee of the diode, then reading lies somewhere between the p and average values. This uncertainty be eliminated if the ripple is amplified the order of 100 volts and the peak rea divided by the amplification factor.

In order to obtain repeatable result voltage measurements of TR ripple, effect of a-c source upon ripple, and

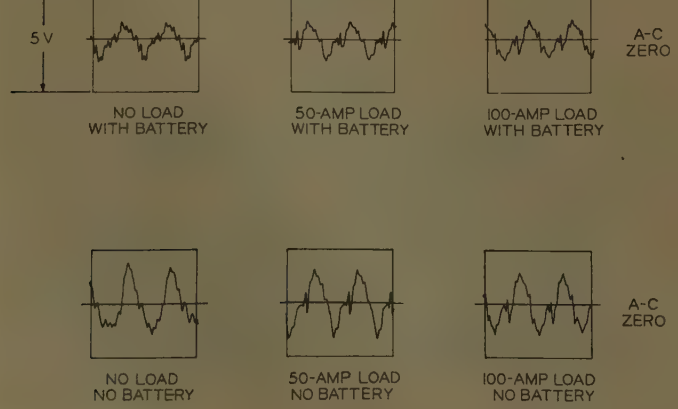


**Fig. 4. Influence of a battery on TR ripple. Battery: 24 volts, 36 ampere-hours. TR: Manufacturer A, 100 ampere, unregulated 6-phase**

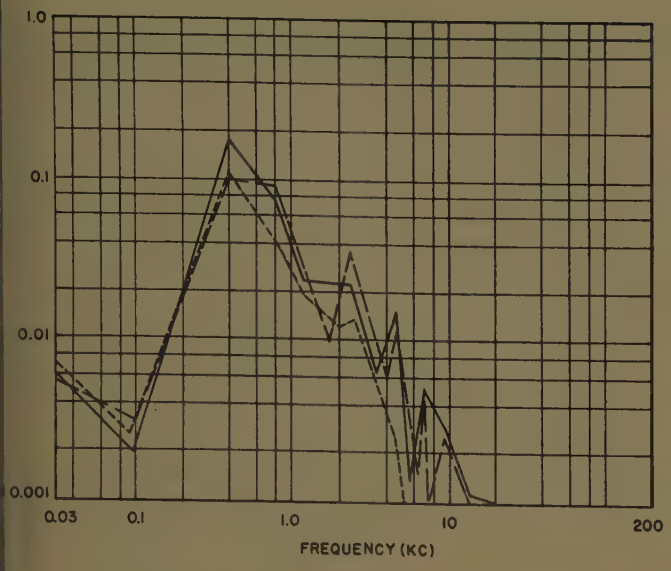


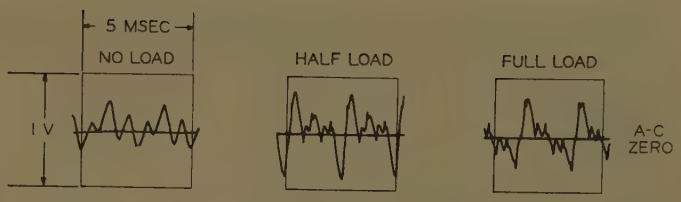


**Fig. 6 (left). Frequency characteristic of ripple from a 50-ampere 6-phase regulated TR. Manufacturer E**

——— No load
— — Half load
– – – Full load

**Fig. 7 (above). Ripple from a 50-ampere 6-phase regulated TR. Manufacturer E: Ripple filter choke input with 1,500-microfarad capacity**

fect of the TR upon a-c source, wave-rm should be recognized. To allow nsistent ripple voltage measurements, least 360 mechanical degrees of gen-ator rotation and at least 0.1 second of R operation should be considered in e measurement.

Frequency characteristics of ripple ve been measured at NADEVCEN using nducted radio-interference techniques. ilitary specification[10] for such measure-ents start at 140 kc and go up in fre-ency. Frequency characteristics of ple picks up where conducted radio terference stops (140 kc) and goes down frequency to 30 cps (cycles per second). he lower 30-cps limit is based on the neral lack of frequency components low 30 cps, the limitation of available struments to measure conducted inter-rence below 30 cps, and the limits of frequency characteristics of voltage modulation established for a-c systems.[6]

A screen room was used for all frequency characteristics measurements. Generators are driven with the generator mounting pad face coincident with the wall of the screen room. This allows the heavy drive to remain outside the screen room. The mechanical arrangements of loading and power leads were consistent with established conducted radio interference measurements techniques. Due to the low frequencies measured and extremely low impedance sources, standardizing impedance (stabilizing) network could not be used. Measurements in the range of 30 cps to 15 kc were made with a *NM-40A* Radio Interference Field Intensity Meter. Measurements in the range of 14 kc to 140 kc were made with a *URM-6* Radio Interference Field Intensity Meter. Both instruments are manufactured by Stoddart Aircraft Radio Company. As a check on the measurements, for each frequency that was measured a sine wave of corresponding frequency was substituted from an oscillator. The sine wave was varied until its output provided a reading identical to the ripple measurement. The voltage of this sine wave was read independently and compared with the voltage read for ripple in the test set.

**ble II. Source Influence Upon Ripple of anufacturer "G" 100 Amp Unregulated Transformer-Rectifier**

| Input | Additional A-C System Load | TR Load | Ripple Plus | Ripple Minus |
|---|---|---|---|---|
| kva a-c.. | None | 0 | 0.40 | 0.20 |
| enerator, | None | 10 | 1.10 | 1.50 |
| 3 manu- | None | 50 | 1.25 | 1.10 |
| facturer | None | 100 | 1.35 | 0.90 |
| kva a-c.. | None | 0 | 0.33 | 0.25 |
| enerator, | None | 10 | 1.90 | 2.10 |
| 3 manu- | None | 50 | 1.80 | 1.50 |
| facturer | None | 100 | 1.80 | 1.90 |
| | Manufacturer *A*,.. | 0 | 0.35 | 0.20 |
| | 200-ampere unregulated TR | 10 | 1.65 | 1.85 |
| | with 50-ampere load | 50 | 1.50 | 1.35 |
| | | 100 | 1.50 | 1.50 |
| | Manufacturer *I*,.. | 0 | 0.30 | 0.20 |
| | 50-ampere regulated TR with | 10 | 2.90 | 5.70 |
| | 50-ampere load | 50 | 2.10 | 5.40 |
| | | 100 | 1.90 | 4.80 |

c input maintained at 115 volts 400 cps.
*tes:* Data for this table were obtained from the val Air Test Center, Patuxent River, Md.
pple is peak voltage measured from d-c average.

## Test Data and Discussions

Fig. 1 shows oscillograms of ripple from a d-c generator. These oscillograms are fairly characteristic of ripple obtained from aircraft d-c generators. There is some variation in ripple with different input speeds. Variation in ripple due to load change is very pronounced in both peak values and frequency content.

An aircraft battery placed across a d-c generator lowers the ripple to quite a degree. The battery is not quite as effective for the full-load operation as for the light-load operation. The oscillogram shown in Fig. 2 illustrates the effect of a battery upon ripple.

The military specification for d-c generators[2] limits peak ripple voltage to 1.5 volts. The co-ordinating military specification for regulators[3] permits the generator peak ripple voltage to increase to 2.1 volts due to the regulator. Tests made in NADEVCEN laboratory failed to reveal any significant change in ripple due to the addition of a regulator. The peak ripple data shown in Table I for representative d-c generators were obtained using carbon pile regulators qualified to *MIL-R-6809*.[3]

**Table III. 50-Ampere Regulated Transformer-Rectifier Influence on Input A-C Waveform**

| Harmonic | 30-Kva Generator: Manufacturer B, Per Cent Harmonic With No Load on Generator | 30-Kva Generator: Per Cent Harmonic With Fully Loaded Manufacturer B TR on Generator | 15-Kva Generator: Manufacturer B, Per Cent Harmonic With No Load on Generator | 15-Kva Generator: Per Cent Harmonic With Fully Loaded Manufacturer E TR on Generator |
|---|---|---|---|---|
| 2 | | 0.71 | | 0.29 |
| 3 | 0.25 | 0.66 | 0.12 | 1.34 |
| 4 | | 0.66 | | 0.60 |
| 5 | 0.6 | 5.20 | 1.85 | 2.90 |
| 6 | | | | 0.22 |
| 7 | | 1.55 | 1.65 | 1.34 |
| 8 | | 0.89 | | 0.52 |
| 9 | 0.2 | 0.60 | | 1.34 |
| 10 | | | | 0.84 |
| 11 | | 2.20 | 0.39 | 1.00 |
| 12 | | | | 0.63 |
| 13 | | | | 1.26 |
| 14 | | | | 0.42 |
| 15 | 0.26 | 0.53 | | 1.00 |
| 16 | | | | 0.62 |
| 17 | | 1.50 | | 0.35 |
| 19 | | | | 0.52 |
| 20 | | 0.89 | | |
| 23 | | 0.97 | 0.6 | 0.6 |
| 30 | | 0.71 | | |

An aircraft battery placed across a d-c generator lowers the ripple to quite a degree. The battery is not quite as effective for the full-load operation as for the light-load operation. The oscillogram shown in Fig. 2 illustrates the effect of a battery upon ripple.

The military specification for d-c generators[2] limits peak ripple voltage to 1.5 volts. The co-ordinating military specification for regulators[3] permits the generator peak ripple voltage to increase to 2.1 volts due to the regulator. Tests made in NADEVCEN laboratory failed to reveal any significant change in ripple due to the addition of a regulator. The peak ripple data shown in Table I for representative d-c generators were obtained using carbon pile regulators qualified to *MIL-R-6809*.[3]

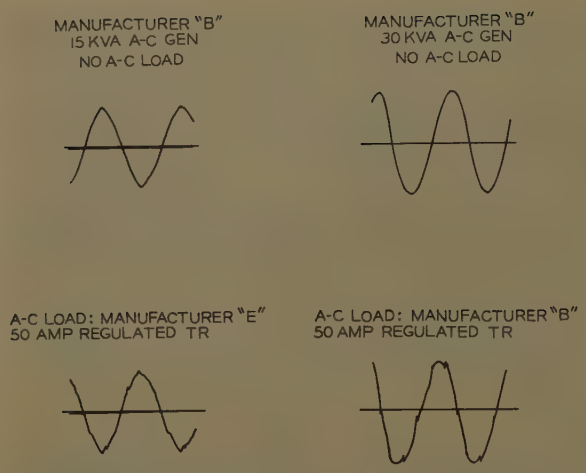


**Fig. 8. Regulated TR influence on input a-c waveform**

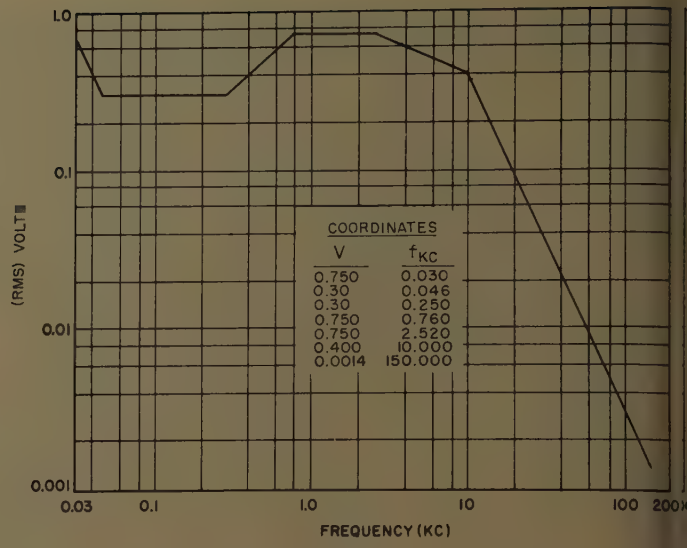


**Fig. 9. Recommended limits for the frequency characteristics of ripple**

A representative frequency characteristic of ripple for a d-c generator is shown in Fig. 3. It should be noted that all the frequency characteristic curves are representative of the maximum readings during one set of operating conditions only at the corresponding frequencies and do not show the readings obtained at frequencies other than the maximum points. Most of the readings obtained for frequencies other than the maximum points were below the 0.001-volt level.

Fig. 4 is illustrative of ripple obtained from an unregulated TR. The addition of a battery across the TR has little effect except at the no-load operation. The effect is much less than when a battery is placed across a generator. However, for TR's with higher ripple voltage the battery has a corresponding increasing influence in reducing ripple. Table I lists peak readings of ripple obtained from various TR units. These readings for TR's are the maximum obtained with different environments and loads.

The effect of unbalance in the a-c input to a TR on the frequency characteristic is shown in Fig. 5. The 800-cycle component due to the 3-volt input unbalance has increased from a negligible value for balanced input to one of the largest components. The unbalance was a 3-volt spread between the highest and lowest line to neutral voltages. The same TR with no input unbalance showed an almost identical frequency characteristic with the exception of the 800-cps component. Regulated TR's have inherently high output ripple in some cases measuring as high as 18 volts. Use of a filter becomes a necessity to reduce the ripple to acceptable limits. The frequency characteristic of one such well filtered regulated TR is shown in Fig. 6. An oscillogram of ripple from the same unit is shown in Fig. 7.

The TR, when used in air-borne electric systems, is usually a reasonable percentage of load on the a-c generator. Being a heavy nonlinear load there is an effect on a-c waveform. The waveform distortion in turn affects ripple. Table II shows the different ripple reading obtained with a given TR and different generators. This table illustrates how the addition of other nonlinear loads on the a-c generator further increases the ripple. Fig. 8 shows the effect on a-c source waveforms of regulated TR's. Table III shows the harmonic analysis of the waveforms shown in Fig. 8. The two regulated TR's had different methods of obtaining regulation. Manufacturer *B* provided the control in the input transformer while manufacturer *E* provided control by switching impedances in series with the output of the transformer. The effect upon a-c waveform was much greater when the control was integral with the input transformer.

## Conclusions and Recommendations

From independent studies it has been concluded that many air-borne utilization equipment are at the threshold of ripple tolerance when the peak ripple voltage goes above 1.5 volts. Most utilization equipments desire peak values of ripple below the 1.5-volt limit. However, present state of the art in a-c power equipment with reasonable care in design, quality control, and proper application can only confine ripple to the maximum limit of 1.5 volts. Measurement of the peak ripple voltage must be made with extreme caution. It is usually best to monitor and check the measurement with an appropriately calibrated oscilloscope capable of appropriate sweeps and having a minimum frequency response between 10 cps and 100 kc.

The study made and the data obtained at NADEVCEN indicate that realistic limits shown in Fig. 9 can be established for the frequency characteristic of ripple. These limits bridge the gap between the lower end of conducted radio interference and the upper end of frequency characteristics of a-c modulation.

Ripple measured during laboratory testing cannot be considered as an absolute value but only an indication to assist in the final application of the TR to an airborne electric system. The final application has to consider both the influence of TR upon a-c system waveform and the influence of the a-c system waveform upon ripple.

The following recommendations are made:

1. The maximum peak ripple voltage be established as 1.5 volts maximum deviation from the d-c average voltage.

2. Measurements of ripple be made with due cautions presented in this paper and be monitored with an appropriate oscilloscope.

3. The frequency characteristic of ripple shown in Fig. 9 be established as maximum limits and be integrated into appropriate specifications.

4. Measurement of ripple and application of TR's be made with due cognizance of the TR's influence upon a-c system waveform and the a-c system waveform's influence upon ripple.

## References

1. GENERAL SPECIFICATION FOR AIRCRAFT CONVERTERS. *Military Specification no. MIL-C-7115E*. Bureau of Aeronautics, Washington, D. C., Jan. 2 1957.

2. GENERAL SPECIFICATION FOR AIRCRAFT ENGIN

IVEN DIRECT CURRENT 30 VOLT GENERATOR. *litary Specification no. MIL-G-6162-A1*, Sept. 9, 55.

GENERAL SPECIFICATION FOR DIRECT CURRENT NERATOR 30 VOLT VOLTAGE REGULATOR. *litary Specification no. MIL-R-6809*, July 14, 50.

CHARACTERISTICS OF AIRCRAFT ELECTRIC WER. *Military Specification no. MIL-E-7894A*, y 17, 1955.

THE NATURE OF VOLTAGE RIPPLE ON D-C GENERATORS, **F. N. Collamore.** *AIEE Transactions*, pt. II (*Applications and Industry*), vol. 73, Jan. 1955, pp. 390–93.

6. DEVELOPMENT OF DEFINITIONS FOR VOLTAGE MODULATION CHARACTERISTICS IN 380- TO 420-CYCLES-PER-SECOND AIRCRAFT ELECTRIC SYSTEMS, **Oscar Markowitz.** *AIEE Transactions*, pt. II (*Applications and Industry*), vol. 75, Sept. 1956, pp. 193–97.

7. VOLTAGE MODULATION ON AIRCRAFT POWER SYSTEMS, **R. E. Klokow, C. F. Yoke.** *AIEE Transactions*, pt. II (*Applications and Industry*), vol. 76, Nov. 1957, pp. 314–19.

8. AMERICAN STANDARD DEFINITIONS OF ELECTRICAL TERMS (book). AIEE sect. 65.11.260.

9. FUNDAMENTALS OF ENGINEERING ELECTRONICS, **William G. Dow.** John Wiley & Sons, Inc., New York, N. Y., 1937, p. 508.

10. AIRCRAFT ELECTRICAL AND ELECTRONIC EQUIPMENT INTERFERENCE LIMITS AND TESTS. *Military Specification No. MIL-I-6181B*, May 29, 1953.

## Discussion

**W. Colehower** (The Martin Company, Baltimore, Md.): Paragraph 2, under the heading Measurement of Ripple: Consistent ripple measurements of TR operation need only require measurement over a time interval of 1 cycle rather than 1 second. Generator ripple measurements, as proposed, are limited to 360 mechanical degrees, which would be 0.02 second for a generator at 3,000 rpm. A 400-cps TR measurement should be for 1/17 second and a 3,200-cps TR measurement for only 0.31 millisecond. These are comparable intervals and should include all nonrepeatable characteristics.

In Table I, manufacturer *A*, 100-ampere rating 1.3-volt ripple (assumed maximum deviant from average d-c) does not agree with Fig. 4 (2.0 volts).

**Oscar Markowitz:** The measurement of ripple must include any subharmonics and the voltage modulation components which are inherent with a-c power sources. Examination of Figs. 5 and 6 shows that the frequency components below the 1-cycle interval start to increase as frequency goes to 100 cps. Reference 6 indicates that the low-frequency components due to modulation may reach a maximum about 10 cps. Thus the interval of ripple measurement should observe a 10-cps component (0.1 second).

Fig. 4 is an artist's sketch of the actual oscillogram. Measurements made from the oscillogram show agreement within instrumentation error (±5%). This agreement also considers that the data were obtained from different units. The data of Table I were obtained from a unit undergoing qualification tests at one government activity. The oscillogram for Fig. 4 was obtained from a different unit at a second government activity.

# Nuclear Radiation and Electronic Equipment

J. R. CRITTENDEN
ASSOCIATE MEMBER AIEE

NUCLEAR radiation causes material degradation through several processes. Ionizing radiations, the charged particles, and gamma rays cause organic materials to change chemically and electrical conductivity to increase. Energetic neutrons displace atoms by knocking them out of their position in the structure of the material; and the displaced atoms, as charged particles, also cause ionization and secondary displacements. Less energetic neutrons may be absorbed by a nucleus. The new isotope may be unstable and decay in any of several processes such as fission, alpha, beta, or gamma emission, each of which may cause ionization. Material degradation then is caused by ionization, displacement, and transmutation which are observed as chemical changes and increased conductivity.

Increased conductivity is a function of the current carriers available and their ability to move. (Mobility is a characteristic of the material under consideration.) Ionization generates large numbers of current carriers (electrons and ions or holes). The degree of ionization is a direct function of the intensity of the nuclear flux. The increase in electrical conductivity is thus related to the intensity of the nuclear flux as illustrated in Fig. 1.[1]

Chemical changes, on the other hand, are a function of the time integral of the dose-rate. Ionization, displacement, and transmutation are discrete events. For a given flux intensity (dose-rate) the number of events per unit time can be calculated. Because the reaction during an event can "go" in any of several processes, it is difficult to define the number

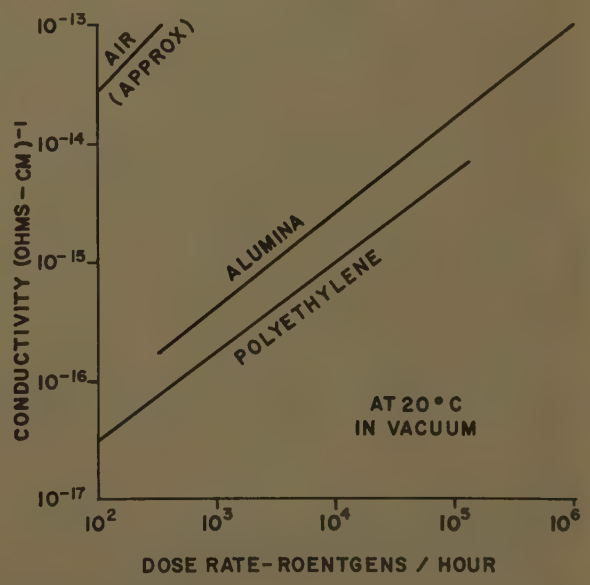


**Fig. 1. Variation of conductivity as a function of dose rate**

Paper 59-873, recommended by the AIEE Air Transportation Committee and approved by the AIEE Technical Operations Department for presentation at the AIEE Summer and Pacific General Meeting and Air Transportation Conference, Seattle, Wash., June 21–26, 1959. Manuscript submitted March 23, 1959; made available for printing May 28, 1959.

J. R. CRITTENDEN is with General Electric Company, Owensboro, Ky.

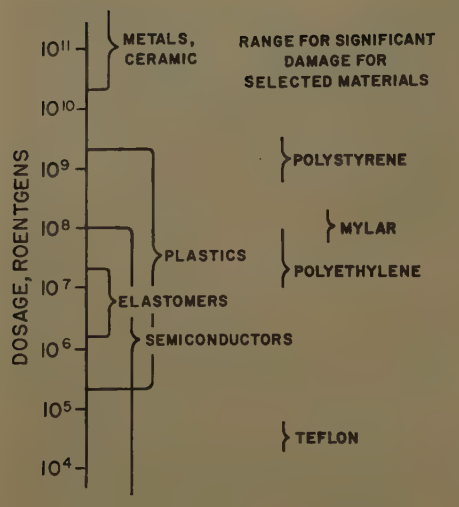


Fig. 2 (left). Scale of relative tolerance of materials

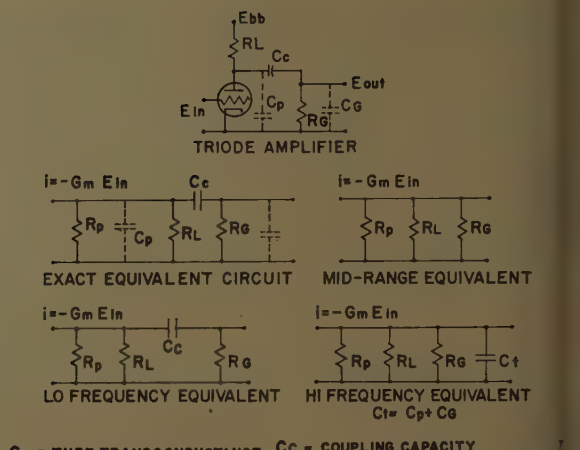


Fig. 3 (right). Electronic amplifier and equivalent circuits

of events required to bring about a specific effect, but a range of the time integrals of dose-rate (dose) can be determined. Fig. 2 illustrates the range of doses to obtain an effect for several materials.[2] As only a small portion of the induced changes revert, chemical changes are permanent in contrast to the transient conductivity changes.

Chemical changes and increased conductivity in electronic equipment can result in failure or malfunction. A simple audio amplifier may be used to demonstrate radiation effects in electronic component. Fig. 3 shows an amplifier and its equialent circuits. As indicated by the equivalent circuit, the transfer function of the amplifier, the ratio of the output signal to the input signal, $E_{out}/E_{in}$, is determined by the operating characteristics of the vacuum tube and its associated resistors and capacitors. The use of equivalent circuitry implies that the characteristics of the components remain constant. In practice, these values may vary; but the designer, through experi

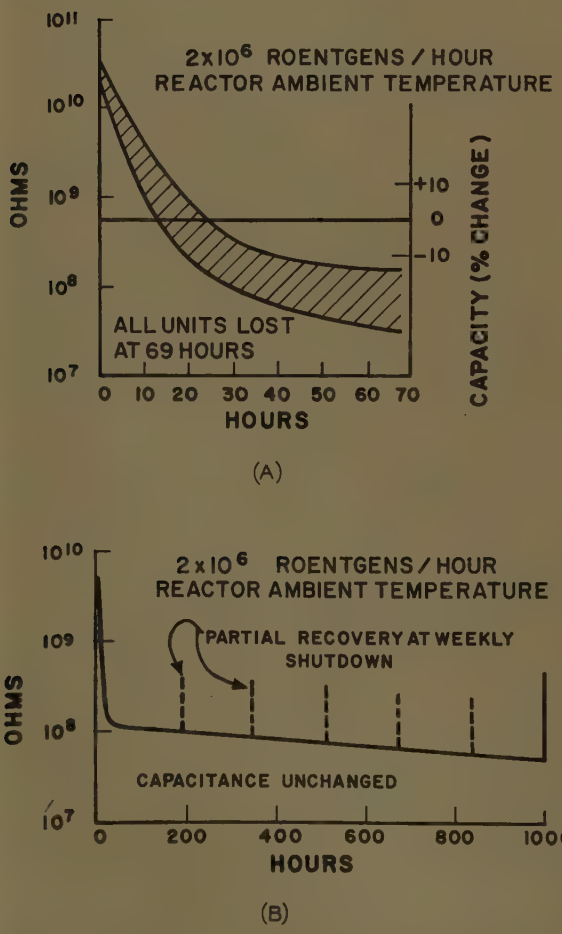


Fig. 4. (A) Resistance and capacitance of Teflon capacitors. (B) Resistance of Mylar-film capacitors

Fig. 5 (right). Typical behavior of resistors irradiated in the Oak Ridge National Laboratory (ORNL) graphite reactor at reactor ambient temperature. Total integrated dose: $2 \times 10^9$ roentgens

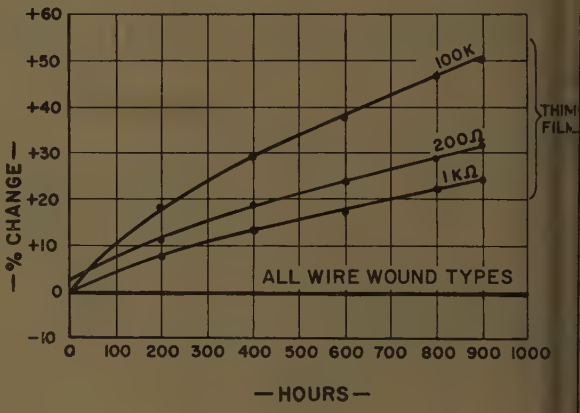


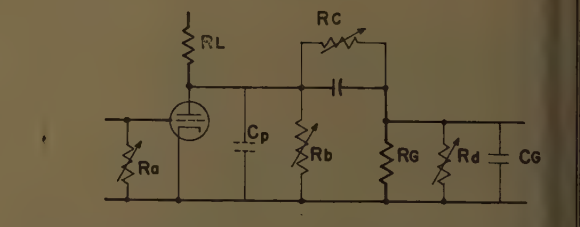


Fig. 6 (right). Electronic amplifier showing radiation-induced current paths

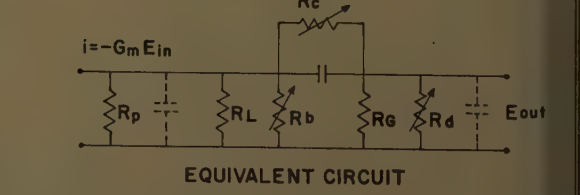

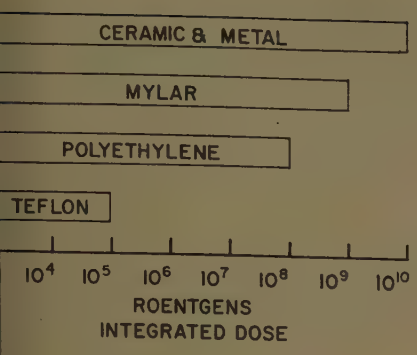


**Fig. 7 (left). Life expectancy of amplifier containing various materials**

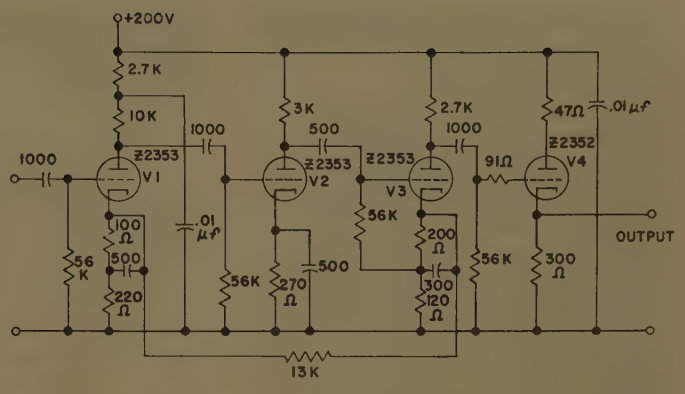


**Fig. 8 (right). Radiation tolerant amplifier**

ce, has learned to accommodate the consistencies. The problem is to evalte the radiation-induced changes and arn to accommodate them.

The amplifier depicted in Fig. 3 has ree elements which will be considered: e capacitor, the resistor, and the vacm tube. A number of studies on the lerances of vacuum tubes to nuclear diation have been reported.[3–5] Several pes were found which are essentially affected by radiation to doses which ceed the life expectancy of the other plifier components. Wire wound restors are also insensitive to nuclear diation. Large value capacitors are parently the most sensitive component. Fig. 4 shows the characteristic behavior two commercial capacitor types. The havior of capacitors having Mylar and flon dielectrics illustrate the effect of clear radiation; that is, large changes of sulation resistance, dielectric conducity, and little or no change of capaciice. As noted in Fig. 2, Teflon is quite sceptible to radiation damage whereas ylar is not so easily affected. Both pacitor types were exposed to the same vironment and in sufficient quantity achieve reliable results.

The behavior of resistors is shown in g. 5. Wire wound devices are not riously affected, but in the thin-film rieties the effect of displacements is to stort the film causing a reduction in nductor cross-sectional area. As illusted in the figure, resistance values inased. It is advantageous to use wire ound devices when the required values d sizes are available. (Because they e temperature sensitive and vary with e, carbon composition resistors are not nsidered for this application.)

The foregoing data indicate the effects duced by nuclear radiation on the comnents of the amplifier circuit. Fig. 6 ows the initial circuit modified by the riables caused by nuclear radiation d the modified equivalent circuit.

It should be noted that catastrophic lure of the amplifier occurs when a capacitor develops a short circuit. The same rule is true for the tube or the resistors; that is, drastic nonreversible changes are considered component failure and will cause amplifier failure. As they may be accommodated in the circuit design, repeatable or reversible changes do not necessarily constitute component failure.

Analysis of the equivalent circuit in Fig. 6 indicates that the radiation-induced current paths do not appreciably alter the amplifier's transfer function except at low frequencies. Should the input resistor paralleling $R_a$ have a high ohmic value, it is possible to obtain some attenuation of the input signal; or should resistor $R_g$ of the amplifier have a high value, the parallel stray leakage may cause some attenuation. The more important leakage path shunts the coupling capacitor. The coupling capacitor is often called the blocking capacitor as one of its purposes is to restrict direct-current flow. When the blocking capacitor conducts, the d-c voltage level at the amplifier output is increased. Normal amplifier design assumes that no direct current flows through the coupling capacitor. $R_g$ values are usually greater than $10^5$ ohms. It can be seen from the data in Fig. 4 that capacitor shunt resistance may decrease to $10^7$ ohms or less. The grid-leak resistor and the blocking-capacitor leakage resistance form a voltage divider which applies a d-c voltage to the amplifier output or to the next stage of the circuit. The magnitude of the d-c voltage is a function of the resistance ratio $R_c/R_g$. As $R_c$ may be as low as $10^6$ ohms and $R_g$ is frequently $10^6$ ohms or more, it is possible to apply 50% of the plate voltage at the amplifier output. Although the a-c fed into the amplifier may not be seriously distorted by its action, the variable d-c voltage at the output will change the operation of succeeding equipment.

Radiation then has two effects on electronic equipment: to cause transient amplifier malfunction or to cause catastrophic failure through drastic component change.

The preceding discussion has assumed specific and constant environmental conditions. These conditions are representative only. Each application will present new and different conditions which may vary with time and include other environmental stresses such as temperature extremes.

The problems associated with designing and developing radiation tolerant equipment begin with the environment. The range of dose-rates to be expected and the duration of each must be established or predicted. The equipment life-expectancy should be specified. Maintenance procedures should be described. Only when the environmental specification has been written and the life requirement and maintenance procedure agreed on, can the initial electronic design begin. Material choice is limited by the maximum dose-rate and the life required. System design is restricted by the materials and techniques which can be used.

This design procedure dictates a series of compromises. The cost of a completely inorganic system is exorbitantly high, and it is difficult to obtain good performance while meeting minimum weight and volume requirements. The normal array of components contains materials known to be sensitive. Selection of components constructed of more tolerant materials still does not give unlimited life. Even though a satisfactory life expectancy may be obtained, performance and size may be unsatisfactory.

To demonstrate, again consider the amplifier of Fig. 3. Fig. 7 indicates the probable life expectancy for electronic equipments containing the indicated materials. While is is not possible to predict the interaction of several materials and combined stresses using the available data, the analogy with the weakest link of a chain is applicable. Long life may be realized in many instances, but the weak material will always limit the life of its component.

For operation at a low dose-rate, only a few limitations apply. It may be feasible to use Teflon. As lifetime requirements increase, even at very low dose-rates, the weak materials begin to drop out. If high temperatures are expected life is considerably shortened. At high dose-rate only inorganic systems will give acceptable life-expectancies.

Materials are not the only limitation. Circuit design is restricted. Transient conductivity limits the maximum resistor value which is also restricted by the larger changes of high value resistors.

Fig. 8 is the schematic of an amplifier designed to tolerate high dose-rates for one thousand hours or more.[6] Note the low resistor and capacitor values; 56 kilohms and 0.01 microfarad maximum. There are no organic materials used. The amplifier has a gain of 40 decibels from 10 kc to 1,500 kc over a wide temperature range and will meet military specifications. It is an excellent example of the application of the points presented in this discussion of nuclear radiation effects on electronic components.

Suggestions for designing radiation-tolerant electronic amplifiers are given as follows:

1. Keep resistance values low.
2. Use materials compatible with the environment.
3. Avoid large capacitor values.
4. Keep the circuit simple.
5. Design the system with these restrictions in mind.

## References


1. Conductivity Induced in Solid Insulatin Materials During Gamma Irradiation, G. Huth. *Technical Report no. 58-331*, Genera Electric Company, Cincinnati, Ohio, 1958.

2. Estimated Radiation Stability of Aircra Components, C. G. Collins, et al. *APEX 35* General Electric Company, 1958.

3. The Effect of In-Pile Radiation of th G. E. Ceramic Triode, J. R. Crittenden. *APE 347*, General Electric Company, 1958.

4. Electron Tubes for Critical Enviro ments, W. H. Kohl, P. Rice. *WADC TR 57-43* Stanford Research Institute, Stanford, Cali 1958.

5. Effects of Nuclear Radiation on Ele tronic Components, E. R. Pfaff, R. D. Shelto *WADC TR 57-361*, Admiral Corporation, Ne York, N. Y., 1958.

6. Design and Development of 600° F. Pul Preamplifiers for Nuclear Environmen W. Frisby, E. Palmer. General Electric Compan Burlington, Vt., May 1959. (Personal Commu cation)


# Reliability Analysis for Aircraft Generators


J. T. DUANE
ASSOCIATE MEMBER AIEE

L. J. YEAGER
ASSOCIATE MEMBER AIEE


EVER-INCREASING reliability wherever economically justifiable long has been an important objective for the designers of all electric equipment. Rough yardsticks—such as service life, maintenance costs, and complaint charges—have been used as measures of success in the attainment of this objective, but precise, quantitative indices of reliability have been lacking in many cases. This lack of emphasis on the quantitative evaluation of product reliability may have been justifiable in the past, but the situation is changing rapidly. In particular, components for aircraft and missile applications will be required more and more frequently to attain specified levels of reliability. This will be necessary because performance requirements in such applications require that components be pushed to the extremes of their capabilities. In addition, the dollar and time investment required to bring a modern, air-borne weapons systems to an operational status, coupled with the vital importance of such systems performing their assigned tasks, makes it imperative that all components not only meet specified performance standards, but that they do so reliably and consistently.

Equipment failures are not individually predictable, but they are subject to analysis using the tools of mathematical statistics. For this reason, statistical techniques play an important part in any study of system or component reliability. However, the problem is not simply a mathematical one. The statistical analysis must be closely coupled with a clear understanding of actual behavior of the equipment to which the reliability analysis is to be applied. The discussion presented here proposes to consider the problem of reliability evaluation in terms of its application to rotating electric machinery used in aircraft and missiles. Particular attention is paid to equipment required to repetitively complete missions of specific length during a relatively long service life. In addition, emphasis is placed on equipments which exhibit wear characteristics such that the likelihood of failure varies with the length of time which the equipment has been in service.

Much has been written in the technical literature concerning reliability, but there still seems to be a need for industry-wide agreement on a precise definition of the meaning of the numerical value of reliability associated with specific pieces of equipment. This problem of definition is considered here in some detail and a specific form of definition is proposed for use.

## Definition of Reliability

It is generally agreed that reliabili may be defined as the probability that given component or system will succes fully perform some assigned task witho departing from predetermined perfor ance limits. Such a definition is gene and useful, but it leaves much unsaid. implies a careful description of t assigned task and the conditions und which it is to be performed. Formulati this sort of description is in itself a maj problem. If the assigned task is to performed repetitively, additional co plications arise when the probability successful completion is not the same each attempt. It is essential that such problems be resolved if a number to represent reliability and mean t same thing to all who use it.

### Environment

In any actual application the reliabili of a component may be determined observation of its performance. If large number of items are observed ove long period of time, sufficient data will


Paper 59-888, recommended by the AIEE Transportation Committee and approved by AIEE Technical Operations Department presentation at the AIEE Summer and Pa General Meeting and Air Transportation C ference, Seattle, Wash., June 21–26, 1959. Ma script submitted March 25, 1959; made avail for printing April 23, 1959.



J. T. Duane and L. J. Yeager are with the Gen Electric Corporation, Erie, Pa.



The authors would like to express their appre tion to E. G. Bianco and D. A. Wilhelmson their guidance and assistance in the preparatio this paper and review of the manuscript. T would also like to acknowledge the extensive of unpublished General Electric Company n and reports written by E. G. Bianco, P. Gunt and J. A. Zoellner.

btained to permit a statistical deter-
ination of the component's reliability.
he specific manner in which such data
ay be used to calculate reliability will de-
nd on other facets of the definition, but
will suffice for the moment to state that
can be calculated on the basis of field
ata. The reliability determined on the
asis of actual operating data will be re-
rred to here as "operational reliability."
here are other ways in which reliability
n be determined and defined, but it is
portant to remember that operational
liability is the single end result of any
orthwhile reliability program. It is the
ly index that counts once the equip-
ent is in service.

Unfortunately, an accurate determina-
on of operational reliability cannot be
ade until the equipment has been in
rvice for some time. As weapons sys-
ms become more sophisticated, it be-
mes increasingly important that the
ganization responsible for the develop-
ent of the system insure in advance that
e completed system will meet a specified
lue of operational reliability. In order
do this the systems manager requires
at the suppliers of subsystems and com-
nents deliver products of specified
liability. This is most effectively ac-
mplished by making product reliability
part of the suppliers contractual com-
itments. The time lag required for the
curate determination of operational
liability makes it an unsatisfactory
dex for vendor supplied components.
ndors want some means for demon-
rating that they have met their com-
tments and are entitled to payment,
hile the purchaser wants assurance
at the items he buys will do the job ex-
cted of them.

The need for an index of reliability
ior to operational use leads to the defi-
ion of a different type of reliability
hich will be referred to here as "sim-
ted-service reliability." Such an alter-
tive definition should not be considered
the establishment of a different index
performance, but rather as explicit
ognition of the fact that no test
gram short of actual operational use
n completely determine the operational
iability of a product. Simulated-serv-
reliability can be defined as an index
product performance which is the best
ailable approximation to operational
iability that can be determined in a
atively short time using existing (or
dily obtainable) test facilities. It is
portant to remember that this is at best
y an approximation to the real thing.
s the responsibility of individuals pre-
ing and issuing specifications on reli-
ability to specify test conditions and techniques that are as close to actual operation conditions as is economically feasible. Only then will simulated-service reliability provide useful predictions of product performance in actual service.

Operating conditions encountered by a product in aircraft service depend on a number of variables. Some of these are independent and some are interrelated, but most can vary over relatively wide ranges. Any single operating condition can be considered as a single point in a mutidimensional stress space where each dimension represents one of the variables or parameters which can affect the performance or life of the equipment in question. Many parameters are required to completely describe any actual operating condition, but it is difficult to visualize any situation involving more than three dimensions. A stress-space diagram for a hypothetical and highly simplified application is shown in Fig. 1. This represents an application where temperature may vary between −50 and 200 C (degrees centigrade), loads between 50 and 100%, and vibration levels between 3 and 6 times the acceleration of gravity. Such an application is therefore represented by the indicated volume on Fig. 1. This alone would not be enough to completely define the application. In addition, a complete description would require a probability density function to define the likelihood of the operating point falling within any incremental element of the indicated volume. This would make a complicated picture by itself, but it is easy to think of additional parameters such as time, vibration frequency, and altitude which should be added to make the representation complete.

Statistical techniques can be developed to analyze the stress-space representation of an application and relate it to the laboratory performance of a product when subjected to the same stresses. These techniques require the statistical evaluation of all of the interrelationships between the various stresses which may be exerted. Methods of this type would obviously be quite sophisticated and expensive to employ. They may in time be developed to the point where they can be used effectively in evaluating the simulated-service reliability of air-borne rotating machines, but that day does not seem to be here yet.

Historically, specifications for aircraft equipment have been written to require experimental demonstration of ability to perform at a limited number of points in the anticipated stress-space representation of the actual application. The points

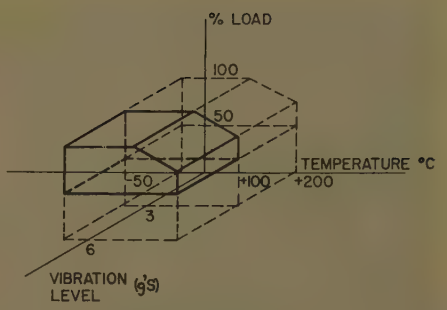


**Fig. 1. Simplified stress-space representation of hypothetical aircraft generator environment**

selected were those which experience and intuition suggested as the most severe. Some parameters such as vibration, acceleration, fungus, and humidity have been assumed to have effects relatively independent of all the others, and have been tested separately. Experience has shown assumptions of this type to be valid and, in addition, they are frequently necessary because of the limitations of existing test facilities. Specifications of this type have proved practical, and are frequently required by the economics of a given situation. They will probably continue in use.

Simplification and approximation are necessary in order to permit laboratory determination of simulated service reliability. The trend in recent years has been to increase the number of points used to simulate the actual application stress space in the laboratory. This trend probably will and should continue. However, it is important that this not be overdone. Increased complexity of test methods for reliability are justifiable only to the extent that they provide better correlation between simulated service reliability and operational reliability. It is important that adequate records be maintained on both types of reliability so that the correlation between the two may be continually evaluated.

### Time Variation of Failure Rate

Exact definition of reliability requires a decision as to whether the numerical value of the probability of successful operation refers to the completion of a single mission (one cycle of operation) or to completion of the total design life. For aircraft and other weapons systems designed for repeated use it seems most logical to specify the probability of completing a single mission. In other words, the most important question is whether or not the system will successfully accomplish its assigned task when called upon to do so. This is the definition chosen for this discussion.

Once reliability is defined in terms of mission completion another question

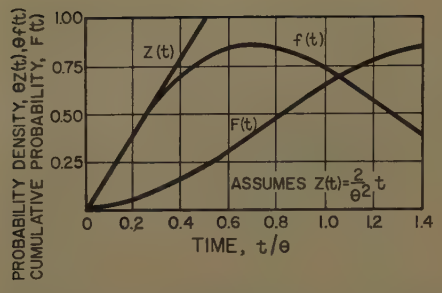


**Fig. 2. Typical statistical functions for failure rate analysis**

arises. Is the probability of successful mission completion as high for a component nearing the end of its design life as for a brand new unit? The most intuitively appealing answer to this question is negative. Most people feel they take a greater risk of breakdown trouble when they start a trip in a car with 90,000 miles on the speedometer than when they start out in a new car. However, this intuitive approach is not entirely satisfactory. On some types of equipment the probability of failure is no higher for units 1,000 hours old than it is for new units. On other types of equipment the probability of failure increases materially with the age of the item.

Since there is a possibility that the probability of successful mission completion will vary with age, provision should be made for time variation in any complete definition of reliability. This situation makes it desirable to introduce the tools of mathematical statistics. Statistical techniques for the analysis of reliability are available in the literature,[1] and need not be developed here. However, it will be helpful to introduce and define certain functions which are useful in the formulation of exact definitions for reliability.

The first and most familiar function in the analysis of failure phenomena is the probability density function of failure $f(t)$. This function represents the density of the probability of failure as a function of time. The integral of $f(t)$ over any time interval represents the probability of failure within that interval. Since the probability of failure at some time is unity

$$\int_0^\infty f(t)dt = 1.0 \tag{1}$$

The cumulative distribution function of failures $F(t)$, represents the probability of failure at some time prior to the time $t$. The cumulative distribution may be obtained by integration of $f(t)$

$$F(t) = \int_0^t f(t)dt \tag{2}$$

The probability of survival to time $t$ is denoted $G(t)$ and may be expressed as

$$G(t) = 1 - F(t) \tag{3}$$

One other function which will prove useful later is the conditional probability density of failure $z(t)$. This is the probability density of failure at time $t$, given the condition that the item is alive at $t$

$$z(t) = \frac{f(t)}{G(t)} \tag{4}$$

Complete specification of any one of these functions, $f(t)$, $F(t)$, or $z(t)$, permits the determination of all the others. Fig. 2 pictures $f(t)$, $F(t)$, and $z(t)$ for the special case where $z(t)$ is a linear function of time. The expected life of the item described by these curves is equal to the mean of $f(t)$ or the expected time to failure $T_m$

$$T_m = E[t] = \int_0^\infty tf(t)dt \tag{5}$$

It has already been stated that reliability is to be defined as the probability of successfully completing a single mission. This necessarily assumes that the item in question be alive at the beginning of the mission. If the mission is $h$ hours long and begins at time $t$, the probability of the item having failed at some time prior to the end of the mission will be $F(t+h)$. The probability of its having failed prior to the start of the mission is $F(t)$ so that the probability of an item failing in the $h$ hours starting at time $t$ will be $F(t+h)-F(t)$. This probability, divided by the probability of being alive at the start of the mission, yields the probability that the item will fail during the mission on the condition that it is alive at the start. For example, if only one-third of the original units are alive at $t$, then an expected mortality of 10% of the original units is equivalent to 30% of the survivors

$$F(h|t) = \frac{F(t+h)-F(t)}{G(t)} = \frac{F(t+h)-F(t)}{1-F(t)} \tag{6}$$

The notation $F(h|t)$ is to be taken as the probability of $h$ (failure during the next $h$ hours) on the condition $t$ (being alive at time $t$).

It is now possible to define the reliability $r(h|t)$ as the probability of completing an $h$ hour mission if alive at $t$

$$r(h|t) = 1 - F(h|t) = \frac{1-F(t+h)}{1-F(t)} \tag{7A}$$

$$r(h|t) = \frac{G(t+h)}{G(t)} \tag{7B}$$

At this point it would be possible to select as a definition of reliability the minimum value which $r$ will be allowed to assume during the design life of the equipment. For many, but by no means all, equipments $r$ will be a minimum when $t$ is maximum. In such cases reliability will be at a minimum when the equipment has completed its design life and is ready for removal for overhaul or replacement. If the scheduled operating time to replacement is $T_r$, reliability might be defined as

$$R_d(h|T_r) = \frac{G(T_r+h)}{G(T_r)} \tag{8}$$

While this $R_d$ reliability is a possible choice for an exact definition, it does have some drawbacks. These can best be seen by considering the use to which component reliability data will be put. The primary purpose for establishing component reliability is to insure an acceptable system reliability. If no redundancy exists in the system, its reliability will be equal to the product of the reliability values for the components. If we denote the probability of successful completion of an $h$ hour mission for the system, as $r(h|t)$, and the reliability of the $i$th component as $r_i\ (h|t-T_i)$, system reliability may be written as

$$r(h|t) = r_1(h|t-T_1)r_2(h|t-T_2)\ldots r_s(h|t-T_s) \tag{9A}$$

$$r(h|t) = \prod_{i=1}^{s} r_i(h|t-T_i) \tag{9B}$$

In equation 9, $s$ is the number of components in the system and $T_i$ is the time of the most recent installation of a new item for the $i$th component. Inclusion of $T_i$ makes the expression general enough to allow for continued maintenance and replacement.

It should be apparent from equation 9(B) that the system reliability may vary with time. For the special case where all $i$ components have minimum reliability at maximum age $(t-T_i=T_{ri})$, and maximum reliability at $t=T_i$ the minimum and maximum values of $r$ may be established as

$$r_{\min} = \prod_{i=1}^{s} r_i(h|T_{ri}) \tag{10A}$$

$$r_{\max} = \prod_{i=1}^{s} r_i(h|0) \tag{10B}$$

For any system with a fixed replacement or maintenance schedule for all components there will exist minimum and maximum values of $r$. There is some possibility that $r$ will take on values anywhere between its minimum and maximum values. This situation is pictured in Fig. 3 which shows a plot of a possible probability density function of $r$ denoted as $p(r)$. It seems reasonable to expect that for systems with large numbers of components, $p(r)$ is not apt to be hi

values of $r$ very far removed from some
an value. Even without proof of this
umption, it is possible to state that the
st likely or expected value of $r$ will be
resented by the first moment of the
ction $p(r)$. If reliability is to be de-
ed for a system used in large numbers
h each system including many com-
nents, the expected value of $r$ will give
excellent approximation to the reli-
lity of a single system selected at ran-
n from the group at any arbitrary time.
One of the theorems of mathematical
tistics states that the expected value of
unction which is equal to the product
several other independent functions is
product of the expected values of the
er functions

$$]=R_e \tag{11}$$

$$=\prod_{i=1}^{s} E[r_i(h|t-T_i)] \tag{12}$$

Thus, it seems reasonable to define
reliability for any single component
he expected value of its instantaneous
ability. Expected value for compo-
t reliability may be evaluated in the
owing manner.

Consider a situation where a single
nponent in a given system is observed
ough $N$ replacements. The data ob-
ed in such an observation will be
istically equivalent to a situation
re $N$ components are all placed on
at the same time. Since some of the
nponents will fail during the test, more
nponent-hours will be accumulated
ng earlier portions of the service life.
s will weight the expected reliability
avor of "low-time" reliabilities. The
tive weight (probability density) of
value of reliability is just the number
omponents still operating at the time
ciated with that reliability, divided
the total component-hours accumu-
d during the test. For this type of
the number of components alive at
time $t$ will be $NG(t)$ as long as $t<T_r$.
reliability for any component will be
n by equation 7(B) as a function of
. At any time $t(0<t<T_r)$ the in-
taneous component reliability will be
) and the probability density of
rving this reliability will be

$$=\frac{NG(t)dt}{\int_0^{T_r} NG(t)dt}\,\frac{1}{dt} \tag{13}$$

he product of $p(r)$ and $r$ integrated
the limits $-\infty$ to $+\infty$ is equal to the
moment of $p(r)$ or the expected value
. For the situation considered
$p(r)$ is zero for $t<0$ and $t>T_r$ so that
possible to make a change in variable
integrate over the limits $t=0$ to $t=T_r$.

Thus the expected value of instantaneous reliability $R_e$ for a component will be

$$R_e=\int_0^{T_r} r_1(h|t)\frac{G(t)}{\int_0^{T_r}G(t)dt}\,dt \tag{14}$$

but

$$r(h|t)=\frac{G(t+h)}{G(t)} \tag{7B}$$

and

$$R_e=\frac{\int_0^{T_r}G(t+h)dt}{\int_0^{T_r}G(t)dt} \tag{15}$$

The development of equation 15 was in terms of a system with no redundant components. If system failure requires the failure of two or more components, the system reliability as given by equations 9 will involve some sums of component reliability values. The same analysis will still apply since the expected value of a function equal to the sum of several other independent functions will be the sum of the expected values of the other functions.

Equation 15 is a mathematical statement of an exact definition of reliability which states that reliability is the mean value observed in service (or on test) of successfully completing a single mission. In the authors' opinion, this $R_e$ reliability is the most realistic definition to use for the specification of component reliability. It is preferable to the minimum or $R_d$ reliability. It should be noted that if the failure characteristics (the form of the $z(t)$ function) are known, equivalent performance may be obtained by specifying either $R_d$ or $R_e$, but the numerical values of the two will frequently be different.

When operational reliability is considered, the superiority of the $R_e$ definition becomes more apparent. To determine the $R_e$ value of operational reliability it is necessary to observe a number of systems in operation over a period of many times the replacement life of the component in question. If each mission observed is classed as either a successful one or a failure, the $R_e$ value of operational reliability will be simply the ratio of successful missions to total missions. A similar determination of $R_d$ value of operational reliability would necessitate first determining at what component age the highest percentage of components (of that age) were failing and then calculating the $R_d$ reliability as the ratio of successful missions to total missions for components of that age.

Either the operational or simulated service values of reliability as defined here will depend not only on the failure characteristics of the equipment and the mission life but also the scheduled replacement time. Thus maintenance and replacement policy may have an important effect on the reliability obtained from a given component. For some items it may be possible to set up inspection procedures which will warn of incipient deterioration and in effect insure as-good-as-new condition for a component which has been in service for some time. Periodic inspection in this case may have somewhat the same effect as reducing replacement life. All of these factors can be important in establishing operational reliability and it is therefore important that they be fully considered in specifying programs for the measurement of simulated-service reliability.

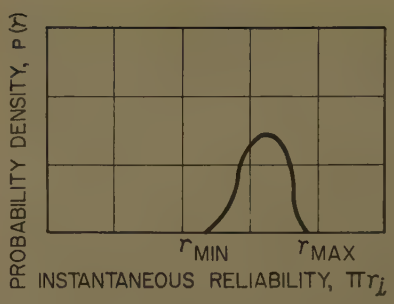


**Fig. 3. Typical probability density distribution of system reliability**

## Wear-Out Phenomena

Before considering methods for the measurement of simulated-service reliability, it will be helpful to consider in some detail the nature of the time dependence of failure rates. Much work has been done on the analysis of reliability problems for situations where failures are randomly distributed. The assumption of random failure distribution has been justified on the basis of statements that any other types of failure are due to deficiencies in the design or application of the system or its components.[2] A truly random failure distribution presupposes the absence of any significant fatigue or wearout effects. While this may be a valid assumption in some situations, the authors do not feel that it is appropriate for a general analysis of rotating electrical machinery reliability.

Analysis of various failure rates is most easily accomplished by use of the conditional probability density of failure $z(t)$. The other distribution functions of equations 1, 2, and 3 may be rewritten in terms of $z(t)$ by recognizing that

$$f(t)dt=-d[G(t)] \tag{16}$$

and from equation 4

Table I. Minimum Value of Generator Reliability $R_{dw}$ of 1,000-Hour Life Machine Operating in 4-Hour Missions

| | Reliability, $R_{dw}$ | | | |
|---|---|---|---|---|
| $\theta$ | M = 1 | M = 2 | M = 3 | M = 4 |
| 1,000 | 0.9960 | 0.9931 | 0.9880 | 0.9840 |
| 1,100 | 0.9963 | 0.9935 | 0.9910 | 0.9890 |
| 1,200 | 0.9966 | 0.9945 | 0.9929 | 0.9922 |
| 1,300 | 0.9969 | 0.9952 | 0.9944 | 0.9944 |
| 1,400 | 0.9972 | 0.9959 | 0.9955 | 0.9958 |
| 1,500 | 0.9974 | 0.9964 | 0.9964 | 0.9968 |
| 1,600 | 0.9975 | 0.9968 | 0.9970 | 0.9976 |
| 1,700 | 0.9977 | 0.9972 | 0.9975 | 0.9981 |
| 1,800 | 0.9978 | 0.9975 | 0.9979 | 0.9985 |
| 1,900 | 0.9979 | 0.9978 | 0.9983 | 0.9988 |
| 2,000 | 0.9980 | 0.9980 | 0.9985 | 0.9990 |

$$\int_0^t z(t)dt = -\ln G(t) \tag{17}$$

$$G(t) = \exp\left[-\int_0^t z(t)dt\right] \tag{18A}$$

$$f(t) = z(t)\exp\left[-\int_0^t z(t)dt\right] \tag{18B}$$

$$F(t) = 1-\exp\left[-\int_0^t z(t)dt\right] \tag{18C}$$

In addition, the function $z(t)$ is useful because it may be conveniently determined from life-test data. Differentiation of equation 17 gives

$$z(t) = -\frac{d[\ln G(t)]}{dt} \tag{19}$$

or

$$z\left(t+\frac{\Delta t}{2}\right) \cong \frac{\ln G(t) - \ln G(t+\Delta t)}{\Delta t} \tag{20}$$

If a large sample of components is placed on test at time $t=0$, and $n_s(t)$ represents the number of units still alive at time $t$

$$G(t) = \frac{n_s(t)}{n_s(0)} \tag{21}$$

and

$$z\left(t+\frac{\Delta t}{2}\right) \cong \frac{\ln n_s(t) - \ln n_s(t+\Delta t)}{\Delta t} \tag{22}$$

Given a sufficiently large sample, the function $z(t)$ may be plotted from life-test data using equation 22.

In the analysis of life-test data it is frequently helpful to fit the observed data to some statistical distribution function which can be conveniently treated by analytical methods. Many different functions have been used for this purpose, but one of the most general and widely applicable was proposed by Weibull.[3] The Weibull distribution is particularly useful for failures caused by fatigue or wearout effects. It may be written as

$$z_w(t) = \frac{m}{\theta^m}t^{m-1} \tag{23}$$

Substitution into equations 18 yields

$$G_w(t) = \exp\left[-\left(\frac{t}{\theta}\right)^m\right] \tag{24A}$$

$$f_w(t) = \frac{m}{\theta^m}t^{m-1}\exp\left[-\left(\frac{t}{\theta}\right)^m\right] \tag{24B}$$

$$F_w(t) = 1-\exp\left[-\left(\frac{t}{\theta}\right)^m\right] \tag{24C}$$

The mean life of components subject to Weibull distributed failures ($T_{mw}$), may be calculated as

$$T_{mw} = \int_0^\infty tf_w(t)dt \tag{25A}$$

$$T_{mw} = \theta\left(\frac{1}{m}\right)! \tag{25B}$$

If failures are distributed in accordance with Weibull's function, the minimum $R_d$, and expected, $R_e$, values of reliability may be written with the aid of equations 8 and 15 for the case $m \geq 1$:

$$R_{dw}(h|\,T_r) = \exp\left[\frac{T_r{}^m - (T_r+h)^m}{\theta^m}\right] \tag{26}$$

$$R_{ew} = \frac{\int_0^{T_r}\exp\left[\left(\frac{t+h}{\theta}\right)^m\right]dt}{\int_0^{T_r}\exp\left[\left(\frac{t}{\theta}\right)^m\right]dt} \tag{27}$$

where the subscript $w$ implies restriction to the Weibull distribution. While equation 26 may be solved directly for $\theta$ when $R_{dw}$, $T_r$, $h$, and $m$ are known, equation 27 presents more of a problem and in general can be best handled by trying values of $\theta$ and solving for $R_{ew}$. In either case, numerical solutions may be readily obtained with today's digital computing equipment. As an example, Table I shows values of $R_{dw}$ obtained for various values of $\theta$ and $m$ when the application requires 1,000 hour life equipment to perform successive 4-hour missions. Table II shows similar results for the $R_{ew}$ reliability.

In the special case where $m=1$, the Weibull distribution reduces to the well-known exponential distribution which describes the situation where failures are randomly distributed. In this case the mean life is also the mean-time-between-failures and is equal to $\theta$. Also, since failure rate is not time dependent, the $R_d$ and $R_e$ reliability values are identical.

The Weibull distribution is important in the analysis of reliability for rotating machinery because it provides a good description for the failure of machine components. Failure rates for bearings, brushes, insulation systems and structural parts can all usually be correlated with the Weibull distribution. Fig. 4 shows results obtained by testing to failure (under standard conditions) 40 samples of a single insulation system. These data were

Table II. Expected Value of Generat Reliability $R_{ew}$ of 1,000-Hour Life Machi Operating in 4-Hour Missions

| | Reliability, $R_{ew}$ | | | |
|---|---|---|---|---|
| $\theta$ | M = 1 | M = 2 | M = 3 | M = |
| 1,000 | 0.9960 | 0.9966 | 0.9969 | 0.99 |
| 1,100 | 0.9964 | 0.9971 | 0.9975 | 0.99 |
| 1,200 | 0.9967 | 0.9975 | 0.9980 | 0.99 |
| 1,300 | 0.9969 | 0.9979 | 0.9984 | 0.99 |
| 1,400 | 0.9971 | 0.9981 | 0.9987 | 0.99 |
| 1,500 | 0.9973 | 0.9983 | 0.9989 | 0.99 |
| 1,600 | 0.9975 | 0.9985 | 0.9991 | 0.99 |
| 1,700 | 0.9976 | 0.9987 | 0.9992 | 0.99 |
| 1,800 | 0.9978 | 0.9988 | 0.9993 | 0.99 |
| 1,900 | 0.9979 | 0.9989 | 0.9994 | 0.99 |
| 2,000 | 0.9980 | 0.9990 | 0.9995 | 0.99 |

analyzed in accordance with equation and the resulting $z(t)$ plotted in a no dimensionalized form. In this case t data suggest a Weibull failure distributi with $m=3$.

In spite of the fact that most generat components tend to exhibit Weibull d tributed failures with $m>1$, there is assurance that failure rates for compl generators will be Weibull distribut The act of combining components int generator system introduces the pos bility of additional failures due to int actions which may be random in natu These would correspond to the rand failures discussed by Wilson.[2]

One excellent source of failure r information is field service experien Fig. 5 shows plots of $z(t)$ for four differ types of aircraft generators and start manufactured by the authors' compar Failure data was obtained from field ports and analyzed by the methods equation 22. Each curve represents class of machines and includes more th one model. The a-c generator curve Fig. 5 did exhibit a slight "infant mort ity" effect, but the infant mortality per was eliminated from the analysis to p vide a consistent picture of the init failure rate effects without considerat of infant mortality. Failure data

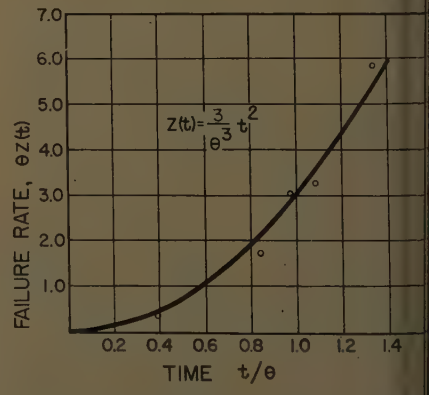


Fig. 4. Failure rate analysis based laboratory insulation system tests

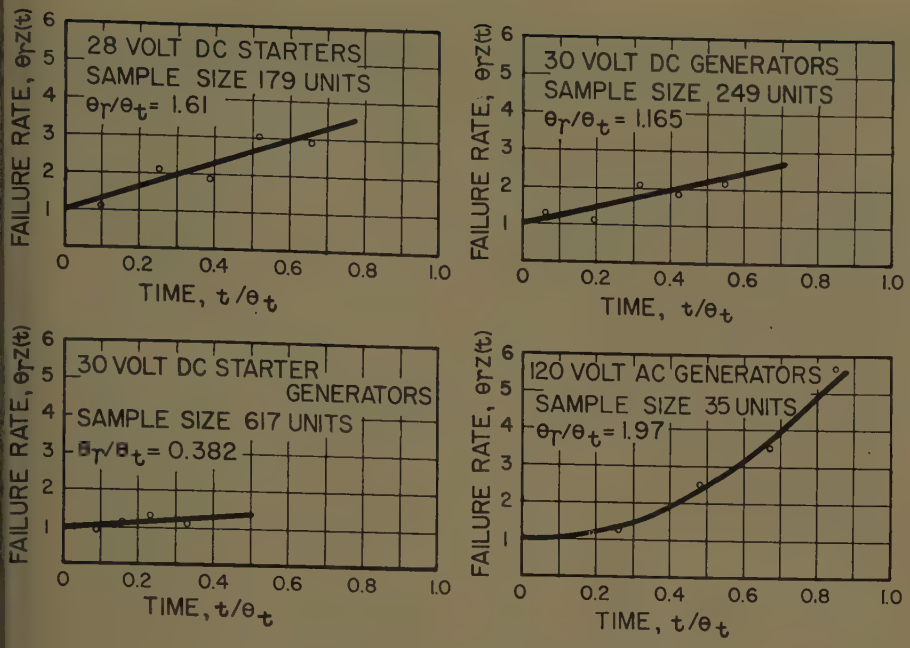


**Fig. 5. Field service data on generator failure rates**

to prepare Fig. 5 included machine removals during ground check-out and inspection and therefore the curves are not suitable for numerical evaluation of in-flight reliability. However, they do accurately portray the time-dependent nature of $z(t)$.

Particularly significant in Fig. 5 is the fact that in no case did the equipment show a zero value for $z(0)$, and in each case $z(t)$ was in increasing function of time. The Weibull distribution is nonzero at $=0$ only for the case $m=1$, and in this case $z(t)$ does not increase with time. Since the data of Fig. 5 can not be satisfactorily correlated with the Weibull distribution, some other distribution is needed. A convenient solution is offered by Flehinger and Lewis.[1] They suggest a distribution of the form

$$f(t)=\frac{1}{\theta_r}+\frac{m}{\theta_t{}^m}\,t^{m-1} \qquad (28)$$

This can be recognized as a combination of two different modes of the Weibull function. The other pertinent distributions can be written

$$G_f(t)=\exp\left[-\frac{t}{\theta_r}-\left(\frac{t}{\theta_t}\right)^m\right] \qquad (29A)$$

$$f_f(t)=\left[\frac{1}{\theta_r}+\frac{m}{\theta_t{}^m}\,t^{m-1}\right]\exp\left[-\frac{t}{\theta_r}-\left(\frac{t}{\theta_t}\right)^m\right] \qquad (29B)$$

$$F_f(t)=1-\exp\left[-\frac{t}{\theta_r}-\left(\frac{t}{\theta_t}\right)^m\right] \qquad (29C)$$

Mean life for items subject to this $z_f$ failure distribution are given as[1]

$$T_{mf}=\int_0^\infty \exp\left[-\frac{t}{\theta_r}-\left(\frac{t}{\theta_t}\right)^m\right]dt \qquad (30)$$

Closed form evaluation of equation 30 is not practical, but it can be evaluated numerically when the parameters $\theta_r$, $\theta_t$, and $m$ are specified. Fig. 6 shows the ratio $T_{mf}/\theta_t$ as a function of $\theta_t/\theta_r$ for the case $m=2$. Note that this distribution also reduces to the exponential distribution for the special case $m=1$.

The $z_f$ failure distribution leads to reliability expressions similar to equations 26 and 27 if $m>1$

$$R_{df}(h|\,T_r)=\exp\left[\frac{T_r{}^m-(T_r+h)^m}{\theta_t{}^m}-\frac{h}{\theta^r}\right] \qquad (31)$$

$$R_{ef}=\frac{\int_0^{T_r}\exp\left[-\frac{t+h}{\theta_r}-\left(\frac{t+h}{\theta_t}\right)^m\right]dt}{\int_0^{T_r}\exp\left[-\frac{t}{\theta_r}-\left(\frac{t}{\theta_t}\right)^m\right]dt} \qquad (32)$$

Again, equations 31 and 32 are best evaluated numerically. Fig. 7 shows a graphical representation of the relationship between $R_{ef}$ and the parameters $\theta_r$ and $\theta_t$ for equipment with a 1,000-hour replacement life and a 4-hour mission life.

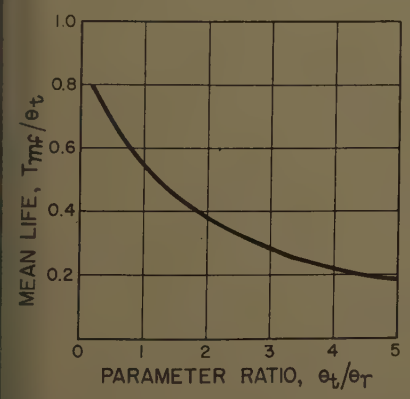


**Fig. 6. Mean life determination for Flehinger-Lewis distribution failures**

## Reliability Testing

Determination of simulated-service reliability requires some measuring technique which is presumably based on the testing of samples selected from a large population. To the extent that operational environment can be simulated, a large sample could be set in operation and observed over a long enough period of time to satisfy all interested parties that the ratio of successful operational cycles to total attempted cycles provides a valid measure of reliability. This would probably be an inelegant, uneconomical, and inaccurate approach to the problem. Fortunately, statistical theory provides more efficient test methods.

Maximum efficiency in testing of this type will be obtained by the use of the techniques of sequential analysis. The theory of sequential analysis is available elsewhere,[4] and need not be repeated here. It will suffice to point out that sequential analysis provides a method for determining whether or not one or more parameters of a distribution function describing a population lie within acceptable limits. For reliability testing, the parameters to be evaluated will be the coefficients and exponents in the functional representation of $z(t)$. It is necessary that the form of $z(t)$ be known or assumed, but it is possible to assume forms of wide generality. The general procedure for determination of reliability will be as follows if the form of $z(t)$ is known.

1. From the specified reliability figure determine the extreme values which the unknown parameters in the function $z(t)$ may assume without resulting in a reliability below the specified value.

2. Design and conduct a test to insure within a specified confidence level that each of the unknown parameters of $z(t)$ lies in a region acceptable by the standards established in step 1.

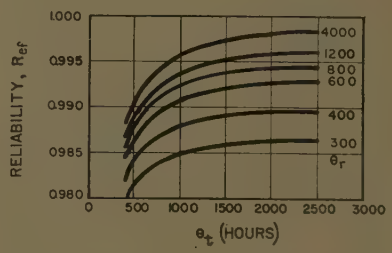


**Fig. 7. Failure parameter determination for $R_{ef}$ reliability where mission length is 4 hours, service life is 1,000 hours, and m=2**

For most generator components being tested separately under controlled conditions, the Weibull distribution may be assumed. In these cases, the nature of failure mechanisms will usually permit predetermination of the value of the exponent $m$. In such cases, the test procedure need consider only a single parameter.

## Single Parameter Tests for Weibull Distribution

General techniques for the sequential analysis of test results are described by Wald,[4] and the specific example of a sequential analysis procedure for the Weibull distribution with $m=1$ is given by Wilson.[2] This portion of the discussion considers the more general case of sequential analysis testing equipment known to have Weibull distributed failures where the exponent $m$ is known but may have any real value. It is important to note that the test procedure can only determine that $\theta$ (in the function of equation 23) is not less than some limiting value $T_1$. The numerical value of this limit on $\theta$ must be established for a given reliability by a separate analysis using equation 27 or Table II.

Operating environment and the actual mechanics of equipment operation during the test must also be established separately. Since the test considered here is intended to evaluate the equipment's failure rate throughout the entire service life, expected mission length will not necessarily be an important factor in establishing test conditions. In addition, an exact definition of what constitutes failure must be established. Once these steps have been taken, sequential analysis provides ground rules for determining whether the test should continue or be stopped with either acceptance or rejection of the equipment on test. In order to formulate the criteria for acceptance or rejection, four numbers must be established:

$\alpha$ = the risk of rejecting equipment which is actually acceptable, i.e., has higher $\theta$ than allowable minimum

$T_0$ = some value of $\theta$ higher than the minimum acceptable value

$\beta$ = the risk of accepting equipment which should actually be rejected

$T_1$ = the minimum acceptable value of $\theta$

The test is formulated in terms of the hypothesis that $\theta \geq T_0$. The equipment is rejected if test results indicate $\theta \leq T_1$ and it is accepted if $\theta \geq T_0$. No decision can be made as long as results indicate $T_1 < \theta < T_0$. Minimum acceptable reliability determines the value of $T_1$ and the allowable risk of accepting substandard performance establishes $\beta$. Thus, $T_1$ and $\beta$ are properly considered test parameters to be specified by the equipment purchaser since they determine his risk and minimum equipment performance. The $\alpha$ risk is the equipment suppliers risk and should usually be specified by him. The parameter $T_0$ is set up to define a region of no decision and does not affect minimum performance limits. It should usually be set at a value intermediate between the minimum acceptable and design objective values of $\theta$ and can therefore best be established by the group responsible for the design of the equipment.

Sequential analysis limits are established in terms of the probability that actual test results would have been observed if $\theta = T_0$ and the same probability if $\theta = T_1$. These may be denoted $P_{0n}$ and $P_{1n}$ respectively. The probability that $n$ failures will occur at the times $t_1, t_2, \ldots t_n$ if $\theta = T_0$, with $f(t)$ given by equation 24(B) is $P_{0n}$

$$P_{0n} = \prod_{i=1}^{n} f(t_i, T_0) \tag{33A}$$

$$P_{0n} = \prod_{i=1}^{n} \frac{m}{T_0^m} t_i^{m-1} \exp\left[-\left(\frac{t_i}{T_0}\right)^m\right] \tag{33B}$$

$$P_{1n} = \prod_{i=1}^{n} \frac{m}{T_1^m} t_i^{m-1} \exp\left[-\left(\frac{t_i}{T_1}\right)^m\right] \tag{33C}$$

$$\frac{P_{1n}}{P_{0n}} = \left(\frac{T_0}{T_1}\right)^{mn} \prod_{i=1}^{n} \exp\left[t_i^m \left(\frac{1}{T_0^m} - \frac{1}{T_1^m}\right)\right] \tag{34}$$

Derivation of test limits is given by Wald.[4] If

$$B < \frac{P_{1n}}{P_{0n}} < A \tag{35}$$

the test is continued with no decision. If

$$\frac{P_{1n}}{P_{0n}} \geq A \tag{36}$$

the test is terminated with rejection of the equipment and the conclusion $\theta < T_1$. If

$$\frac{P_{1n}}{P_{0n}} \leq B \tag{37}$$

the test is terminated with acceptance and the conclusion that $\theta > T_0$. The limits $A$ and $B$ are fixed by the risks $\alpha$ and $\beta$

$$A = \frac{1-\beta}{\alpha} \tag{38A}$$

$$B = \frac{\beta}{1-\alpha} \tag{38B}$$

Substituting equations 33 and 34 into 35, taking the natural logarithm and rearranging puts the inequality in a more convenient form

$$\frac{\ln B + nm \ln\left(\frac{T_1}{T_0}\right)}{\left(\frac{1}{T_0^m} - \frac{1}{T_1^m}\right)} > \sum_{i=1}^{n} t_i^m > \frac{\ln A + nm \ln\left(\frac{T_1}{T_0}\right)}{\left(\frac{1}{T_0^m} - \frac{1}{T_1^m}\right)} \tag{39}$$

Equation 39 permits continuous decisions to accept, reject, or continue testing as each failure occurs. Violation of the left-hand inequality indicates an accept decision and violating the right hand inequality indicates a reject decision.

If the exponent $m$ is not known for sure it may be desirable to provide for evaluation of results in terms of multiple limits. For each value of $m$ and the specified reliability, there will correspond a limiting value of $\theta$. Thus the same set of test results may be evaluated for several values of $m$ with a requirement that acceptance be indicated in each case before the equipment is finally accepted.

Single-parameter sequential-analysis testing can be extremely useful in the evaluation of motor and generator components. However, the data presented in Fig. 5 show that complete machines do not conform to the Weibull distribution. In order to accurately measure reliability for complete machines, some more sophisticated techniques will be required.

## Two Parameter Testing

It has already been pointed out that actual machines conform to the more complex distribution used by Flehinger and Lewis (equation 28). In this case also it seems reasonable to assume that the value of $m$ can be predetermined. If this is done, there are still two parameters which must be considered ($\theta_r$ and $\theta_t$). Equation 32 or Fig. 7 may be used to translate specified reliability into a set of allowable values for the coefficients $\theta_r$ and $\theta_t$. If $\theta_r$ is plotted versus $\theta_t$, there will be some region on the plot where the specified reliability will be obtained. In this case a test is required which will assure that the actual values of $\theta_r$ and $\theta_t$ will define a point within the acceptable region on the $\theta$ plane. Such a test is referred to as a test of a composite hypothesis.

Sequential analysis techniques have been developed for the testing of a composite hypothesis.[4] However, the mathematics involved in formulating tests for a composite hypothesis based on the $f(t)$ given by equation 29(B) become very complicated. At the present time the authors are unable to offer any pro-

tical solution to the formulation of such a test. In spite of this situation, some method is needed for the measurement of reliability for equipment with failures distributed in accordance with equation 28.

There seem to be at least four approaches which might be taken for reliability evaluation of equipment where failure distribution is governed by two parameters.

1. Develop the mathematical techniques and tabulations of appropriate functions to permit the use of conventional sequential analysis methods for the tests of the composite hypothesis.

2. Arbitrarily assume that the failure distribution conforms to some simpler function such as the Weibull distribution with $m=1$ or 2.

3. Assume that the coefficient $\theta_r$ is based on random effects which are not influenced by design and may be considered fixed and known for any given class of equipment. This assumption reduces the problem to a single parameter test to determine the value of $\theta_t$.

4. Assume that the coefficient $\theta_t$ can be accurately determined by separate tests on machine components (bearings, insulation, etc.) under ideal conditions. The test problem would then reduce to a single parameter test to measure the random failure rate contribution due to $\theta_r$.

The first of the foregoing approaches is probably the best, but it can not be counted on until it is proved practical. The second is an undesirable but immediately available solution which has already seen some use and will probably see much more. The third approach is equally unattractive and it would be very difficult to justify on a logical basis. Number four is probably the most desirable alternative to the first approach. It would seem to provide for the full consideration of fatigue or aging effects and yet still permit measurement of any random failure phenomena which may be present. Selection of an efficient and practical method for measuring two parameter failure rates to determine reliability (approach number 1) is not a simple task. There does not seem to be any good method available now, and considerable effort will probably be required before one can be developed.

Tests in accordance with the fourth of the foregoing approaches can be formulated in the following manner. Assume generator failure characteristics can be described by $z_f(t)$ as given by equation 28 and that separate tests on the component parts of the generator have established the values of $m$ and $\theta_t$. Let the value of $\theta_t$ so determined be $T_t$. From equation 32 or Fig. 7 determine the minimum value of $\theta_r$ which will give the necessary reliability and call this $T_1$. At the same time select values for $\alpha$, $\beta$, and $T_0$ as described for single parameter tests (where $T_0$ is greater than $T_1$ but less than the design objective value of $\theta_r$). Since this is actually a single parameter test, the limits of equations 35, 36, and 37 will still apply, but the ratio $P_{1n}/P_{0n}$ will be more difficult to handle. However, the ratio can be written using equation 29(B)

$$\frac{P_{1n}}{P_{0n}} = \frac{P_{1(n-1)}}{P_{0(n-1)}} \frac{f_f(T_1, T_t, t_n)}{f_f(T_0, T_t, t_n)} \tag{40A}$$

$$\frac{P_{1n}}{P_{0n}} = \frac{P_{1(n-1)}}{P_{0(n-1)}} \left[ \frac{\frac{1}{T_1} + \frac{m}{T_t^m} t_n^{m-1}}{\frac{1}{T_0} + \frac{m}{T_t^m} t_n^{m-1}} \right] \times \exp\left[ t_n \left( \frac{1}{T_0} - \frac{1}{T_1} \right) \right] \tag{40B}$$

Thus, if a number of units are placed on test; accept, reject, or continue decisions can be made each time a failure occurs. Each new failure becomes the $n$th failure and the accumulated operating time on the failed unit is $t_n$. Using $t_n$ and the previous test results, equation 40(B) can be used to determine $P_{1n}/P_{0n}$. Equations 35, 36, and 37 provide the basis for a decision.

Predetermination of test time required to evaluate equipment in accordance with equation 40(B) is not a simple problem. Considerable work will have to be done before test organizations can do an efficient job of scheduling and cost estimating for such tests. Some comfort may be gained from the fact that if the anticipated value of $\theta_r$ is much lower than $T_t$, a convenient approximation results from considering $T_t$ to be infinite. In such a case, tests of the ratio given by equation 40(B) will proceed much as if they were determined by the inequality of equation 39 (with $m=1$). Thus, some insight may be gained as to the most effective scheduling for, and probable duration of the test program.

Up to this point, infant mortality (a high, but rapidly decaying initial value of $z(t)$) has not been included in this analysis. This has been partially because of a desire to limit the length of the discussion, but more importantly it is due to the authors' opinion that it is conservative to ignore infant mortality in the definition and measurement of reliability. It is felt that extra, early failures will result in a greater reduction in the $R_e$ value of simulated-service reliability than in the $R_e$ value of operational reliability. Infant failures will automatically be included in any measurement of operational reliability and they must be fully considered in the equipment manufacturers' design and inspection testing. However, since they occur early in the service life, they will have less effect on operational reliability than on the value determined by simulated life test.

## Conclusions

Measurement and analysis of equipment reliability is a broad and complex field. Although much work has already been done, it still represents an extremely fertile field for future work. Of particular importance in providing a sound basis for future reliability work is the accumulation of extensive failure data on systems, machines and machine components. A fund of records permitting the determination of both operational and simulated-service reliability for many different items should prove invaluable in establishing better test methods and conditions.

This discussion has dealt primarily with problems in the definition and measurement of reliability. In these areas several specific conclusions are drawn:

1. Operational reliability and simulated-service reliability are two different things and should be clearly recognized as such. They should be as close together as possible, and the responsibility for the degree of agreement between them must lie with the specification which establishes the methods of measurement.

2. Reliability for an item which must operate for several missions should be defined as the expected value of the probability that it will successfully complete a randomly selected mission ($R_e$).

3. Typical aircraft rotating machines exhibit a conditional probability density of failure which increases with time and is nonzero at $t=0$.

4. Efficient and economical test methods are available for reliability testing of items (such as machine components) which are known to follow single parameter failure laws. Considerable work will be required to develop equally effective methods for testing complete machines where two parameters are of importance.

5. Until efficient test procedures are available for evaluation of the composite hypothesis required by two parameter failure distributions ($z_f$), an alternative test method is needed. In this situation the recommended approach is to measure fatigue and wear-out effects by separate component tests and use this information to establish single parameter sequential tests on the complete machine to measure the random failure rate $\theta_r$.

## Nomenclature

$A$ = upper limit for probability ratio in sequential analysis

$B$ = lower limit for probability ratio in sequential analysis
$E$ = expected value of a function
$F$ = probability of failure
$G$ = probability of survival
$R$ = reliability or probability of successful performance
$T$ = time (fixed value)
$f$ = probability density of failure
$m$ = exponent in failure distribution
$n$ = number of samples or number of failures in a test
$p$ = probability density (general)
$r$ = reliability (instantaneous value)
$s$ = number of components in a system
$t$ = time (variable)
$z$ = conditional probability density of failure
$\alpha$ = risk of rejecting good equipment
$\beta$ = risk of accepting inadequate equipment
$\theta$ = parameter in failure distribution

SUBSCRIPTS

0 = design value (greater than acceptable minimum)
1 = specified minimum
$d$ = minimum value
$e$ = expected value
$f$ = arising from Flehinger-Lewis failure distribution
$m$ = mean value
$r$ = coefficient associated with random failure rate or removal time
$s$ = survivors
$t$ = coefficient associated with time varying rate
$w$ = associated with Weibull failure distribution

## References


1. TWO-PARAMETER LIFETIME DISTRIBUTIONS FOR RELIABILITY STUDIES OF RENEWAL PROCESSES, G. J. Flehinger, P. A. Lewis. *Journal of Research and Development*, International Business Machines Corporation, New York, N. Y., vol. 3, no. 1, Jan. 1959, pp. 58–73.

2. RELIABILITY EVALUATION OF AIRCRAFT AND MISSLE EQUIPMENT, I. THEORY OF SMALL SAMPLE METHODS, B. J. Wilson. *AIEE CP 58-913*, 1958.

3. A STATISTICAL DISTRIBUTION FUNCTION OF WIDE APPLICABILITY, W. Weibull. *Journal of Applied Mechanics*, American Society of Mechanical Engineers, New York, N. Y., vol. 18, 1951, pp. 293–97.

4. SEQUENTIAL ANALYSIS (book), A. Wald, John Wiley & Sons, Inc., New York, N. Y., 1947.


# Computer Evaluation of High-Temperature Aircraft A-C Electrical System Designs


W. E. SOLLECITO
ASSOCIATE MEMBER AIEE

D. A. SWANN
ASSOCIATE MEMBER AIEE



**Synopsis:** This paper describes a design and analog computer study of a high-temperature aircraft a-c electrical system. The study includes an extensive, nonlinear representation of the a-c alternator and shows the effects of temperature, load, and regulator and exciter nonlinear behavior on system stability and transient performance. Torque-limiting techniques are evaluated and a computer approach for study of the reactive load division loop is developed.


REGULATION of alternator voltage by means of feedback techniques has been practiced successfully for many years.[1–7] Basically, such systems consist of an alternator, an exciter, a reference source, and regulating networks as shown in Fig. 1. The alternator supplies the a-c electric power, the exciter provides the control signal power level, the reference sets the output voltage level, and the regulating networks provide system stability and dynamic control.

Compared with currently available equipment, early components were bulky, heavy, low in power level, and slow in speed of response. As the components improved, so did system performance. Availability of good low-temperature (−65 to +250 F [degree Fahrenheit]) components and subcomponents allows system designs which are attractive from a size, weight, cost, and performance viewpoint.

For high-temperature systems (−65 to +775 F), the picture changes greatly. Components and subcomponents are either in the development or predevelopment stage, the expected size, weight, and cost are high, the expected range of subcomponent values is small, and the performance characteristics are limited. From a systems point of view the net effect is threefold:

1. Because of size, weight, and power requirements, component higher frequency capabilities are reduced and single-ended saturated gain characteristics are imposed. These tend to degrade system response time.

2. Available compensation network time constants are presently lower-limited in the 0.5-second region which tends to limit the system loop gain and thereby tends to degrade system accuracy.

3. The large change in temperature causes a correspondingly large change in component parameters which increases the system stability problem.

The design approach must necessarily be one which tends to minimize the deleterious effects of parameter variation and provides a stable system whose dynamic performance is commensurate with the availability of equipment and the size and weight requirements of the system.

## System Design

In designing this system, an approximate linear analysis was used to indicate favorable design areas which were then analyzed in a more exact, nonlinear fashion by means of the analog computer. The extensive alternator equations used are shown in Appendix I, the computer setup for this study is described in Appendix II, and the alternator linearization equations are shown in Appendix III.

The over-all system performance specs


Paper 59-907, recommended by the AIEE Air Transportation Committee and approved by the AIEE Technical Operations Department for presentation at the AIEE Summer and Pacific General Meeting and Air Transportation Conference, Seattle, Wash., June 21–26, 1959. Manuscript submitted March 23, 1959; made available for printing May 15, 1959.



W. E. SOLLECITO and D. A. SWANN are with the General Electric Company, Schenectady, N. Y.



The authors wish to acknowledge the assistance and guidance given to this project by their associate engineers. In particular, they express appreciation to Dr. R. T. Smith for an understanding of machine behavior, F. P. deMello for an understanding of the reactive load division problems in parallel operation, Dr. K. G. Black for numerous consultations, R. E. Anderson for equipment analysis, and F. J. Ellert for detailed calculations.


Fig. 1. Basic electrical system

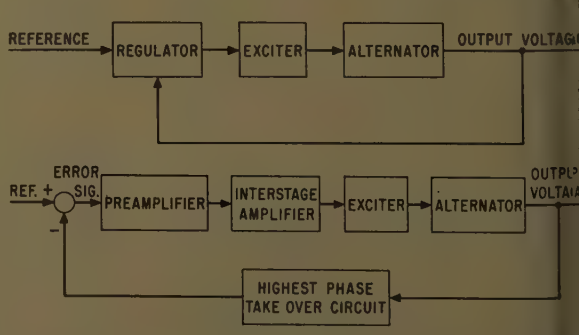


Fig. 2. Amplification stages required to supply appropriate power levels

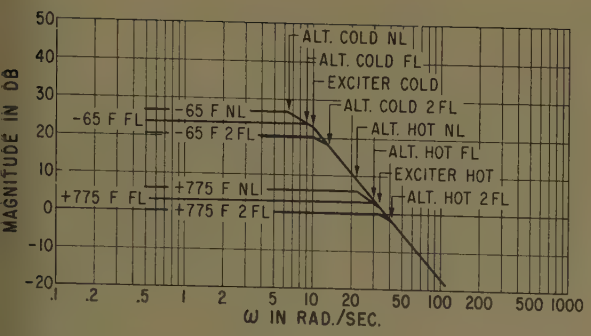


**Fig. 3. Effect of temperature and load on the linearized alternator and exciter time constants and gains**

fications require that the system maintain at least ±0.5% accuracy from no load to 0.75 pf (power factor), lagging full load, and have as short recovery and settling times as possible over the temperature range −65 to +775 F.

The alternator must be capable of delivering 2-pu (per unit) 0.75-pf lagging load at 600 F external temperature which produces approximately 775 F in the control system. At this temperature it must also be capable of delivering 3-pu fault current into a zero-impedance balanced 3-phase fault. These conditions impose an alternator field current requirement which acts as a power requirement on the exciter. To obtain this exciter output power from a low-power-level error signal, two additional stages of amplification are required as shown in Fig. 2. With this configuration as a starting point, compensation networks must be designed to provide adequate system performance under changes of temperature and load.

For this particular program, a solid-rotor-design (with no brushes or rotating windings) 3-phase 400-cycle alternator, a similar rotating exciter, and magnetic amplifiers were used.

Because the exciter and alternator have copper windings whose resistance varies with temperature, the time constants and gains of the exciter and alternator vary by a factor of approximately $3^1/_3$ under changes of temperature from −65 to 775 F. The time constant and gain of the alternator is further changed by a factor of approximately 2 due to load changes from no load to twice full load. The linearized effects of load and temperature on the cascaded exciter-alternator are shown in Fig. 3.

Examination of Fig. 3 shows that temperature and load changes cause more than a 20-to-1 gain change and shifts two time constants as much as 7 to 1 in the cascaded exciter-alternator transfer functions. To help offset these effects on system performance, a control signal proportional to alternator field current can be fed back to the interstage amplifier. This signal is returned to the interstage amplifier because of power level considerations. Use of $I_{fd}$ for minor loop feedback compensation offers the advantage that this same signal can also be used in the torque-limiting technique discussed in a later section. Assuming that some form of series compensation will be used, the block diagram of the voltage regulator loop takes the form shown in Fig. 4.

Use of $I_{fd}$ as a feedback signal causes the alternator gain change due to load changes to appear in $K_L$ which is the incremental gain between alternator field current and alternator output voltage. The load change effect on the alternator time constant still remains in the minor loop. The revised temperature-load effects on the exciter-alternator combination are shown in Fig. 5.

To stay within the approximate component requirements that

1/500 second<time constants<1/2 second

the feedback compensation network was selected as

$$H(s)=\frac{0.09(s/2.2+1)}{(s/500+1)}$$

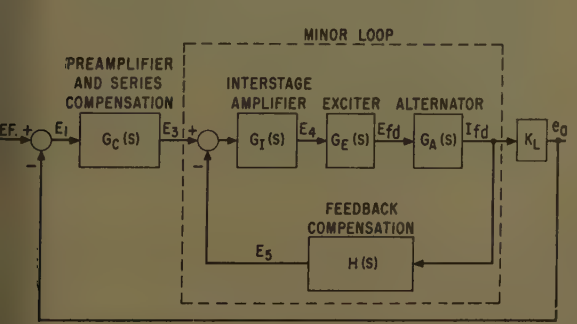


**Fig. 4 (left). Block diagram of complete voltage regulator loop with alternator field-current feedback compensation**

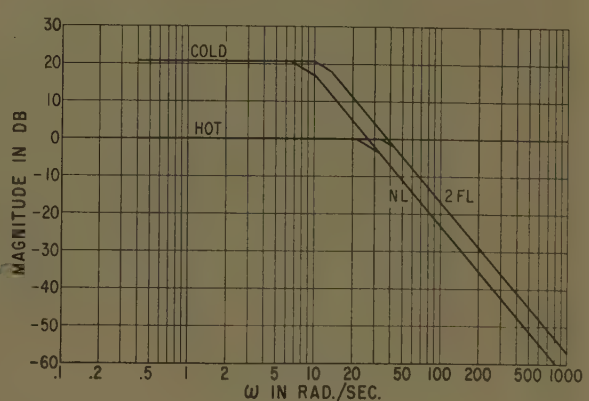


**Fig. 5 (right). Effects of temperature and load on $I_{fd}/E_4 = G_E(s)\,G_A(s)$ of Fig. 4**

Fig. 6 shows the stability characteristics of the minor loop. It is common design practice to maintain stable minor loops so that in the event of major loop failure, the minor loop does not experience destructive behavior. Fig. 7 shows a plot of the minor loop forward and inverse feedback transfer characteristics which are used to obtain the approximate closed minor loop transfer characteristics shown in Fig. 8. The net effect of the feedback compensation is to reduce the effects of temperature and load changes that the major loop experiences and to shift these changes to regions that are fairly well above and below the desired range of major loop crossover frequencies.

To allow adequate system loop gain, a series compensation network (including the preamplifier) was selected as

$$G_c(s)=\frac{38.6(s/17+1)}{(s/2.2+1)(s/500+1)}$$

The over-all forward transfer characteristics are shown in Fig. 9. For changes in temperature from −65 to 775 F and load changes from no load to twice full load, the over-all regulating system has a phase margin from 40 to 60 degrees, a crossover frequency from 50 to 100 radians per second, and a loop gain in excess of 100.

## Component Nonlinear Characteristics

The major types of nonlinearities encountered in this system are saturation and single-ended operation (a component produces an output for only one polarity of input signal). Alternator saturation provides a powerful means for limiting the output voltage rise after a heavy load or fault has been removed. In the steady-state loaded condition, $I_{kd}=0$ and $I_{fd}$ is greater than no-load $I_{fd}$ by an amount depending on $i_d$. At the time of load switching, $i_d$ changes instantly and the total flux linkages remain constant, therefore, $I_{fd}$ and $I_{kd}$ experience negative steps or jumps. The $I_{kd}$ jump decays rapidly to zero in the subtransient interval whereas

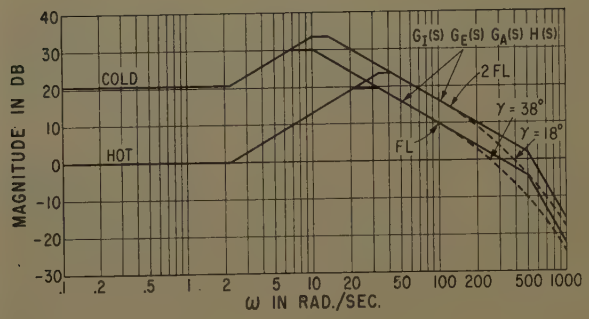


Fig. 6 (left). Minor loop stability analysis

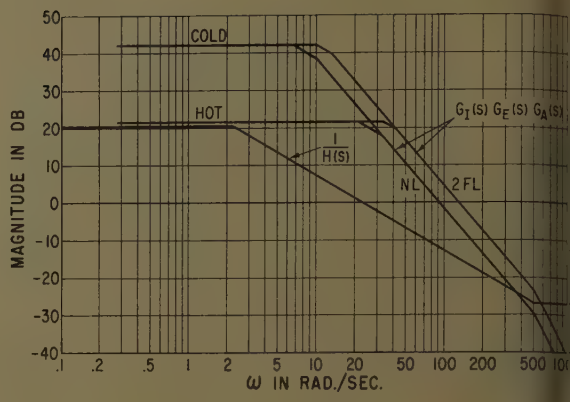


Fig. 7 (right). Minor loop transfer functions

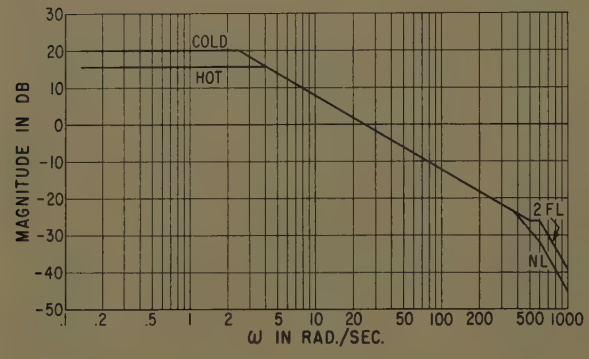


Fig. 8 (left). Closed minor loop transfer function

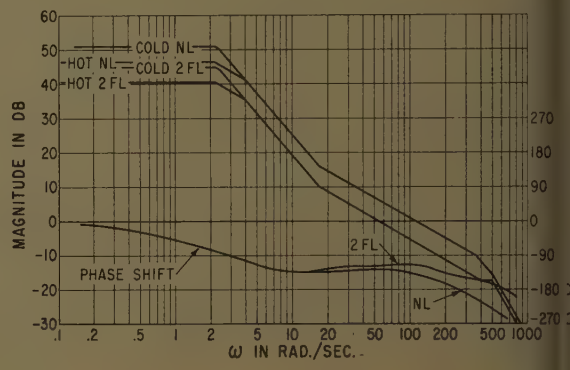


Fig. 9 (right). Bode diagram of entire forward transfer function

$I_{fd}$ tends to rise to its previous value if the alternator field voltage is unchanged. The regulating loop takes action to reduce $E_{fd}$ to the proper no-load value. Depending on the relative speed of response of the regulating loop and the field time constant, $I_{fd}$ tends to rise and then fall to its steady-state no-load value. This variation in $I_{fd}$ is shown in Fig. 10. As $I_{fd}$ changes, $\Psi_{md}$ changes in accordance with the saturation curve. If saturation is heavy, the change in $\Psi_{md}$ for a given change in $I_{fd}$ is less than when saturation is light. Since the output voltage varies with $\Psi_{md}$, saturation is very effective in limiting the output voltage rise during the transient interval. The same type of behavior is experienced upon load application except that the directions are reversed. This behavior can be seen in the computer runs of Figs. 11 and 12.

Because of size and weight considerations, the interstage amplifier and the rotating exciter are single-ended and voltage-limited. These nonlinearities have a major effect on lengthening system response time. The effects of single-ended versus double-ended operation of the interstage amplifier are shown by comparison of Fig. 11 with Fig. 12. In double-ended operation the interstage amplifier negative saturation is set equal to its positive saturation level.

The output of a device depends on its dynamic characteristics and the size of the driving signal. The driving signal is limited by the saturation characteristics of the driver. For example, the time it takes $I_{fd}$ to reach a given value depends on the time constant and gain of the machine and the value of applied $E_{fd}$. When the system is hot, resistances are at a maximum and require highest voltages to produce required currents in the system. Therefore, voltage saturation in the interstage amplifier and exciter have the greatest effect on the system response at high temperatures and increasing voltage conditions. When the system is cold, the voltage levels to produce the required system currents are at a relatively low level. Therefore, the single-ended characteristics have a major effect under low temperatures and decreasing voltage conditions.

Single-ended operation and saturation produce the effect of a decrease in gain because a given input produces a smaller-than-linear output. The system tends to be slower for lower system gains. therefore these nonlinear effects increase the time for disturbances to settle out.

(The system block diagram and computer setup for this study are shown in Figs. 19 and 20, discussed in Appendix II.)

## Torque-Limiting Techniques

The load- and fault-handling requirements on the system at high temperatures set the power and voltage capability requirements of the exciter. At low temperatures, these exciter capabilities are sufficient to produce high-current lev in the alternator. These high-curre levels can produce excessive torques the drive. Because signals proportion to developed torque are difficult obtain, current level signals are used limit developed torque. This porti of the study was concerned with the re tive merits of alternator field current lim ing versus load current limiting in effe ing torque limiting. (The block diagra of the $I_{fd}$ torque-limiting circuitry shown in Fig. 19 of Appendix II. T $i_a$ torque-limiting circuitry is similar cept that $i_a$ replaces $I_{fd}$.)

The system transient responses w obtained for application of unity faults. Fig. 13 shows a typical compu recording for application and removal c fault. At the high temperature, exci saturation is effective in limiting the tra

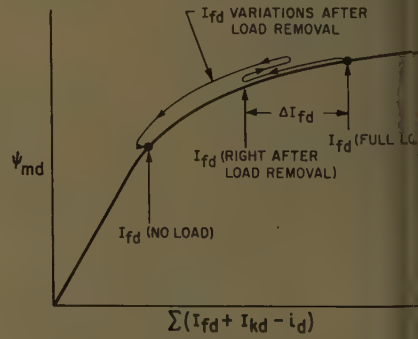


Fig. 10. Variation of $I_{fd}$ after load remo

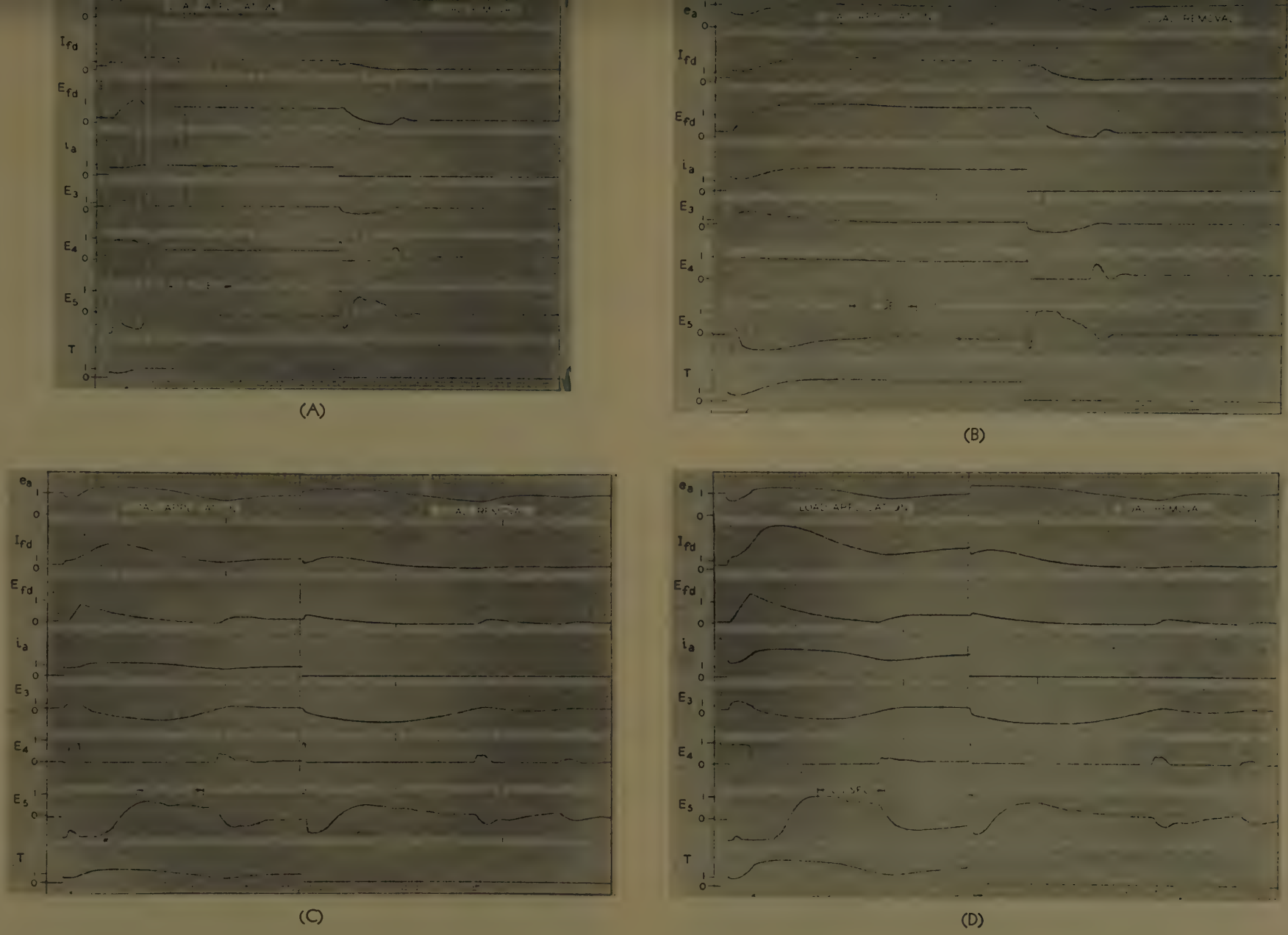


**Fig. 11. System responses in pu for single-ended interstage amplifier**

A—+775 F, 1 pu, 0.75-pf load B—+775 F, 2 pu, 0.75-pf load C—−65 F, 1 pu, 0.75-pf load D—−65 F, 2 pu, 0.75-pf load


Fig. 12. System responses in pu for double-ended interstage amplifier

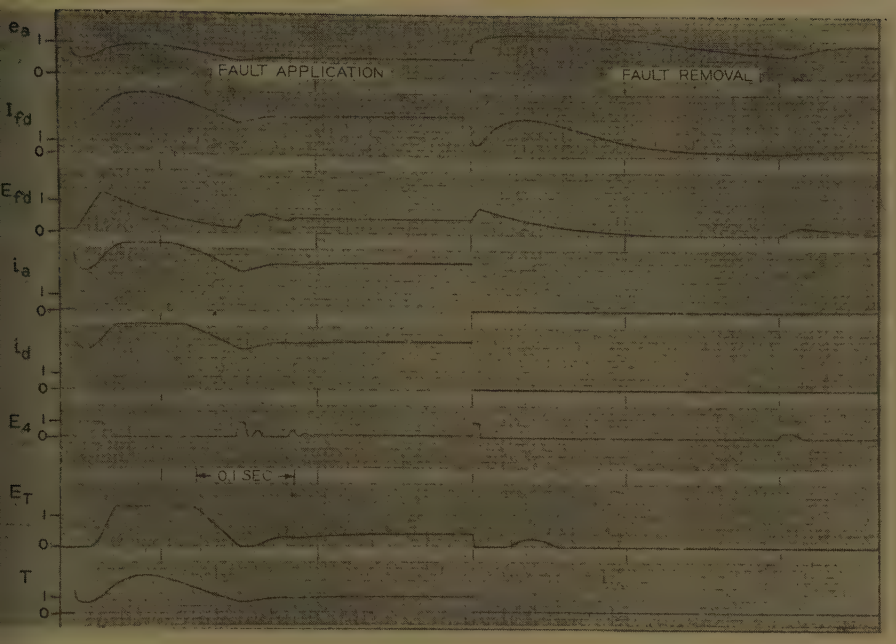


ig. 13. System responses in pu at −65 F for 0.2-pu 1-pf balanced 3-phase fault application and removal

ient torque. From a steady-state view-oint, the high-temperature condition is ne of the worst cases because of high nachine losses. From a transient view-oint, the low-temperature condition is ne of the worst cases because of the ex-iter capabilities. Figs. 14 and 15 show teady-state and peak torques, load cur-ent, and load voltage as a function of alanced 3-phase resistive fault. These gures show that $I_{fd}$ limiting is more ffective in limiting transient torque eaks. The torque peak occurs within .15 second after application of a fault nd may or may not have serious conse-uences on the drive. Since $I_{fd}$ is used n the regulating loop, this same signal neasurement can be used to effect torque miting.

## Reactive Load Division Loop

At the time this paper was written, nly a limited amount of work had been one with the reactive load division loop power angle oscillation loop). A brief nearized analysis indicated that the ossibility of power angle instability xisted in the system. A detailed simula-ion approach for studying the reactive oad division loop was developed and this pproach is presented in Appendix IV.

## Conclusions

This paper describes the analysis and esign of a high-temperature voltage-egulating system. The study is based n the characteristics of a high-tempera-ure alternator and control components at their present stages of development. The net effect of the high-temperature range is to restrict the range of component dynamic characteristics and to cause large changes in exciter and alternator transfer characteristics upon change of temperature and load. The effect of these changes can be minimized by use of negative alternator field current feedback.

The establishment of torque limiting by use of excitation system control shows promise. It is possible to reduce steady-state maximum torques to permissible values and to reduce maximum transient torques to short durations. However, evaluation against drive transient capabilities must be made before final selection of a method can be made. At present, for the two methods studied here, use of field current is preferable to use of armature current for control of maximum torques.

Simultaneous component nonlinearities were included in detail. Double-ended component operation can effect a major reduction in system response time upon application and removal of load.

A simulation approach was developed for study of the reactive load division loop.

In a voltage-regulating system, the disturbance is a step change in load. Since the characteristics of the power elements are known, it should be possible to apply nonlinear control design techniques to optimize the system response with respect to settling time and maximum deviation from rated voltage. Because of present component limitations, such optimization is impractical for high-temperature systems but should be considered for low-temperature systems and for high-temperature systems of the future. A promising new control component in this respect is the controlled rectifier. Its use should allow significant system accuracy and response improvements.

## Appendix I

### Nomenclature

$e$ = phase voltage
$i$ = phase current
$r$ = phase resistance
$I$ = field and amortisseur currents
$R$ = field, amortisseur, and load resistance
$a$ subscript = refers to armature
$d$ subscript = refers to the direct axis
$q$ subscript = refers to the quadrature axis
$f$ subscript = refers to the field winding
$k$ subscript = refers to amortisseur winding
$o$ subscript = denotes base value
$E_{fd}$ = field terminal voltage
$X_{ad}$ = direct-axis mutual reactance
$X_{aq}$ = quadrature-axis mutual reactance

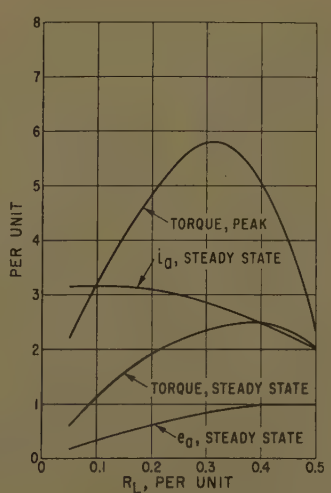


Fig. 14. Field-current torque-limiting curves

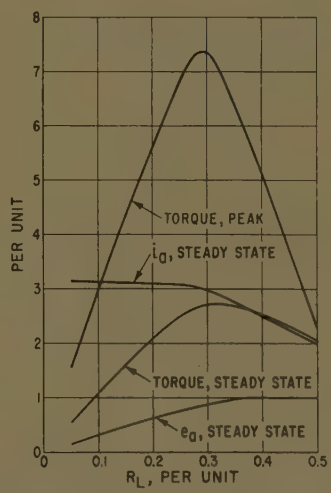


Fig. 15. Load-current torque-limiting curves

$X_l$ = armature leakage reactance
$X_f$ = field leakage reactance
$X_{kd}$ = amortisseur direct-axis leakage reactance
$X_{kq}$ = amortisseur quadrature-axis leakage reactance
$X_d$ = stator direct-axis self-reactance
$X_q$ = stator quadrature-axis self-reactance
$X_{ffd}$ = field direct-axis self-reactance
$X_{kkd}$ = amortisseur direct-axis self-reactance
$X_{kkq}$ = amortisseur quadrature-axis self-reactance
$X_{fkd}$ = mutual reactance between field and direct-axis amortisseur winding
$X_d'$ = direct-axis transient reactance
$X_d = X_{ad} + X_l$
$X_q = X_{aq} + X_l$
$X_{ffd} = X_{ad} + X_f$
$X_{kkd} = X_{ad} + X_{kd}$
$X_{kkq} = X_{aq} + X_{kq}$
$X_d' = X_{ad}X_f/X_{ad} + X_f + X_l$
$X_L$ = load reactance
$R_L$ = load resistance
$\Psi_{md}$ = direct-axis mutual flux linkages
$\Psi_{fd}$ = total field flux linkages
$\Psi_d$ = direct-axis flux linkages
$\Psi_q$ = quadrature-axis flux linkages
$\Psi_{kd}$ = total direct-axis amortisseur flux linkages
$\psi_{kq}$ = total quadrature-axis amortisseur flux linkages
$\theta$, = load power-factor angle
$\delta$ = rotor power angle
$\omega$ = angular frequency
$s$ = differential operator $d/dt$
$t$ = time
$T$ = air-gap torque
$E$ = signal voltage
$Q$ = reactive load kilovolt-amperes (kva)
$T_D$ = drive torque kva
$e_b$ = bus voltage

## Normalized Synchronous Alternator Equations for Balanced 3-Phase Load

The following general alternator equations are used to obtain a detailed representation of the alternator.[4,5] All coefficients are in pu values. Field voltage equation:

$$E_{fd} = R_{fd}I_{fd} + s\Psi_{fd} \quad (1)$$

Amortisseur voltage equations:

$$0 = R_{kd}I_{kd} + s\Psi_{kd} \quad (2)$$

**Table I. Alternator Parameters Used in This Study**

| | Temperature, F | | |
|---|---|---|---|
| | 775 | 77 | −65 |
| $R_{fd}$ | 0.0092 | 0.0038 | 0.0028 |
| $r$ | 0.049 | 0.020 | 0.015 |
| $R_{kd}$ | 0.15 | 0.062 | 0.045 |
| $R_{kq}$ | 0.20 | 0.083 | 0.061 |
| $X_l$ | 0.15 | 0.15 | 0.15 |
| $X_f$ | 0.21 | 0.21 | 0.21 |
| $X_{ad}$ | 1.9 | 1.9 | 1.9 |
| $X_{aq}$ | 1.15 | 1.15 | 1.15 |
| $X_{kd}$ | 0.068 | 0.068 | 0.068 |
| $X_{kq}$ | 0.073 | 0.073 | 0.073 |
| $X_{fkd}$ | 1.9 | 1.9 | 1.9 |
| $X_{ffd}$ | 2.1 | 2.1 | 2.1 |
| $X_d$ | 2.1 | 2.1 | 2.1 |
| $X_q$ | 1.3 | 1.3 | 1.3 |
| $X_{kkd}$ | 2.0 | 2.0 | 2.0 |
| $X_{kkq}$ | 1.2 | 1.2 | 1.2 |
| $X_d'$ | 0.35 | 0.35 | 0.35 |

$$0 = R_{kq}I_{kq} + s\Psi_{kq} \quad (3)$$

Armature voltage equations:

$$e_a = s\Psi_d - \omega\Psi_q - ri_d \quad (4)$$

$$e_q = s\Psi_q + \omega\Psi_d - ri_q \quad (5)$$

Flux-linkage equations:

$$\Psi_{fd} = \Psi_{md} + X_fI_{fd} + (X_{fkd} - X_{ad})I_{kd} \quad (6)$$

$$\Psi_{kd} = \Psi_{md} + X_{kd}I_{kd} + (X_{fkd} - X_{ad})I_{fd} \quad (7)$$

$$\Psi_{kq} = (X_{aq} + X_{kq})I_{kq} - X_{aq}i_q \quad (8)$$

$$\Psi_d = \Psi_{md} - X_li_d \quad (9)$$

$$\Psi_q = X_{aq}I_{kq} - (X_{aq} + X_l)i_q \quad (10)$$

$\Psi_{md}$ = nonlinear function of $[\Sigma(I_{fd} + I_{kd} - i_d)]$ (11)

Load equations:

$$e_d = R_Li_d + \frac{X_L}{\omega_o}si_d - X_Li_q \quad (12)$$

$$e_q = R_Li_q + \frac{X_L}{\omega_o}si_q + X_Li_d \quad (13)$$

$$e_a^2 = e_d^2 + e_q^2 \quad (14)$$

$$i_a^2 = i_d^2 + i_q^2 \quad (15)$$

Torque equations:

$$T = i_q\Psi_d - i_d\Psi_q \quad (16)$$

$$Q = i_d\Psi_d + i_q\Psi_q \quad (17)$$

## Per-Unit Quantities

To achieve the benefits of standardization, pu quantities are used in the machine equations. Per-unit quantities involve expressing the equation coefficients in terms of their respective bases. Unfortunately, there are several available basic approaches to defining pu values.[1,3,4] This situation effects a loss of some of the benefits of standardization.

For this study, the pu system is based on maintaining the same pu power in all windings, reciprocal mutual reactances, and use of peak values of voltage and current.

Armature circuit base values:

$kva_{ao}$ = base armature kva = volt-ampere rating of alternator = 40 kva

$e_{ao}$ = base armature voltage = rated peak phase voltage = 170 volts

$i_{ao}$ = base armature current = rated peak phase current = 157 amp (amperes)

$Z_{ao} = \frac{e_{ao}}{i_{ao}}$ = base armature circuit impedance = 1.08 ohms

$f_o$ = rated line frequency = 400 cycles per second

$\omega_o = 2\pi f_o = 2{,}512$ radians per second

$\omega = 1$ at synchronous speed

$\Psi_{ao} = \frac{e_{ao}}{\omega_o}$ = base armature flux linkages = 0.068 weber-turn

Field circuit base values:

$kva_{fdo}$ = base field kva = $kva_{ao}$

$I_{fdo} = \frac{i_{ao}X_{ad}}{X_{afd}}$ = base field current = $X_{ad}I_{fd}$ (no load) = 4.75 amp

$E_{fdo} = \frac{kva_{fdo}}{I_{fdo}}$ = base field voltage = 8,420 volts

$Z_{fdo} = \frac{E_{fdo}}{I_{fdo}}$ = base field impedance = 1,770 ohms

$\Psi_{fdo} = \frac{E_{fdo}}{\omega_o}$ = base field flux linkages = 3.37 weber-turns

Direct-axis amortisseur circuit base values:

$kva_{kdo}$ = base direct-axis amortisseur kva = $kva_{ao}$

$I_{kdo} = \frac{i_{ao}X_{ad}}{X_{akd}}$ = base direct-axis amortisseur current

$E_{kdo} = \frac{kva_{kdo}}{I_{kdo}}$ = base direct-axis amortisseur voltage

$Z_{kdo} = \frac{E_{kdo}}{I_{kdo}}$ = base direct-axis amortisseur impedance

$\Psi_{kdo} = \frac{E_{kdo}}{\omega_o}$ = base direct-axis amortisseur flux linkages

Quadrature-axis amortisseur circuit base values:

$kva_{kqo}$ = base quadrature-axis amortisseur kva = $kva_{ao}$

$I_{kqo} = \frac{i_{ao}X_{aq}}{X_{akq}}$ = base quadrature-axis amortisseur current

$E_{kqo} = \frac{kva_{kqo}}{I_{kqo}}$ = base quadrature-axis amortisseur voltage

$Z_{kqo} = \frac{E_{kqo}}{I_{kqo}}$ = base quadrature-axis amortisseur impedance

$\psi_{kqo} = \frac{E_{kqo}}{\omega_o}$ = base quadrature-axis amortisseur flux linkages

The coefficient values in Table I are in pu. The machine saturation curve is shown in Fig. 16. Rated no-load armature voltage without machine saturation requires a field current of 2.5 amp.

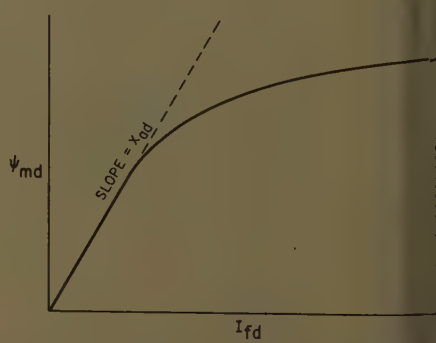


**Fig. 16. Machine no-load saturation curve**

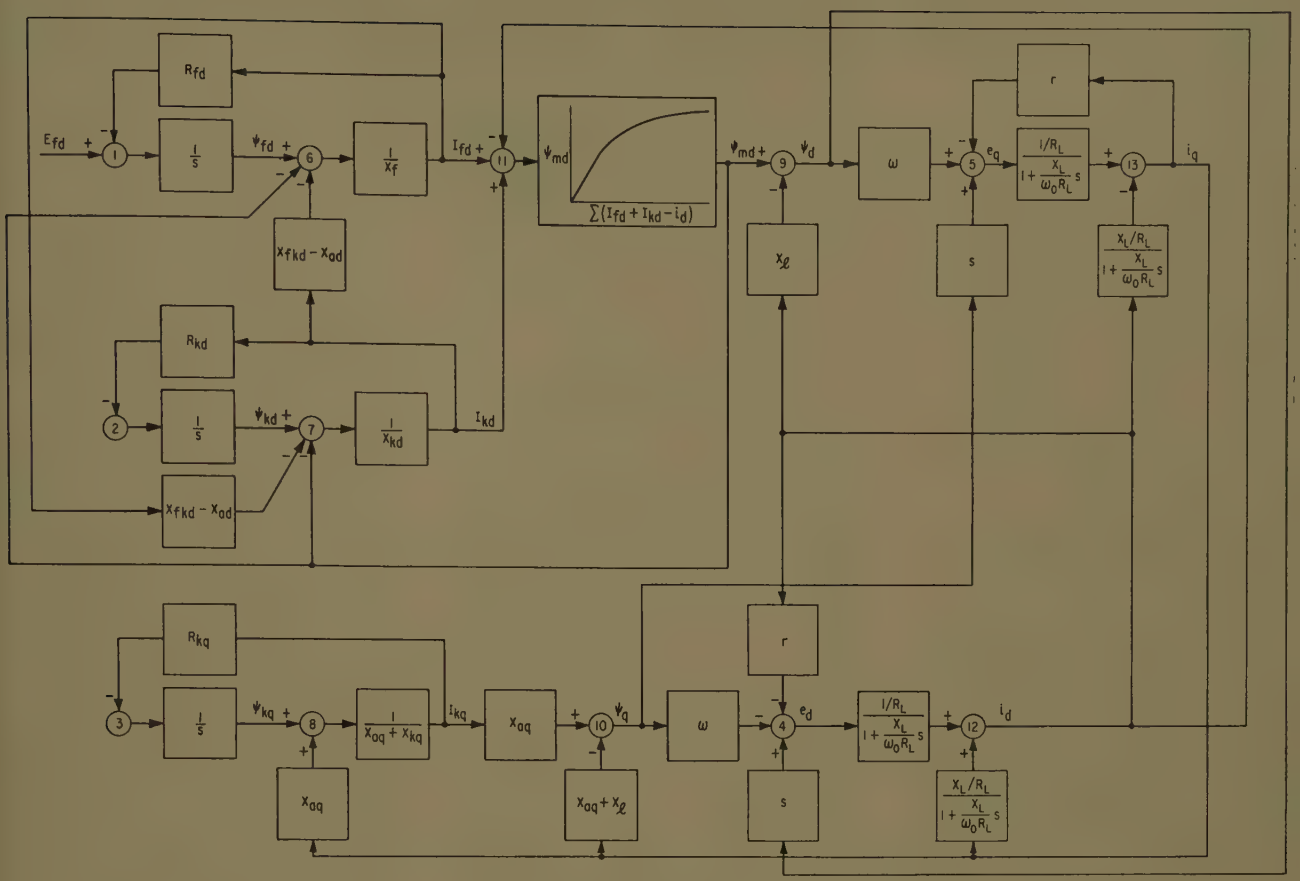


**Fig. 17. Complete synchronous alternator block diagram with balanced 3-phase load**

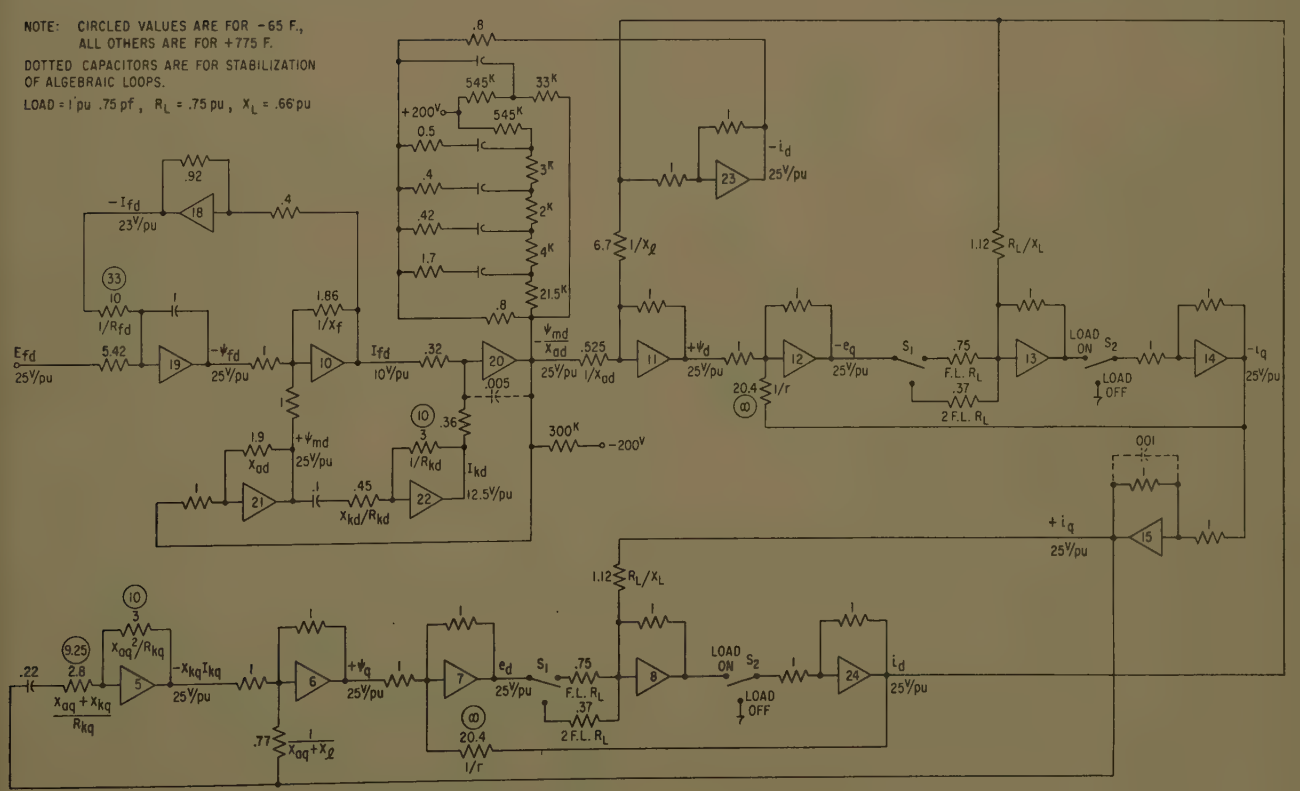


**Fig. 18. Computer diagram of alternator**

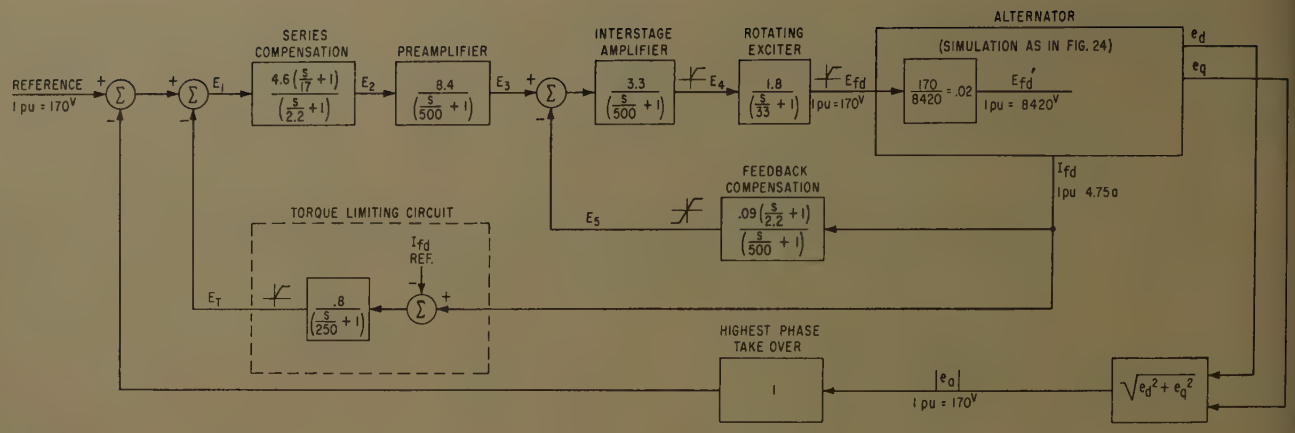


Fig. 19. Block diagram of closed-loop system with $I_{fd}$ torque limiting at 775 F

## Appendix II

### Computer Simulation of Alternator with Balanced 3-Phase Load

The synchronous alternator equations are represented in block diagram form in Fig. 17. The number at each summation point refers to the respective alternator equation in Appendix I. Although there are several forms of the block diagram which represent the simultaneous solution of the alternator equations, the one shown utilizes the output voltages to generate the load currents. This makes it possible easily to simulate heavy load or no load on the alternator (corresponding to an $R_L$ change from a very small value to infinity).

A disadvantage of representing the alternator on the analog computer in the form shown by the block diagram of Fig. 17 is that two differentiations are required to generate $s\Psi_d$ and $s\Psi_q$. Fortunately, as recommended in other work,[4] it was experimentally determined that these two terms can be neglected in this study without significant consequence. Further simplification arises by neglecting the very small terms $(X_{fkd}-X_{ad})I_{fd}$, $(X_{fd}-X_{ad})I_{fd}$, $(X_L/\omega_0)\,si_d$, and $(X_L/\omega_0)\,si_q$ in equations 6, 7, 11(B), and 11(C).

Fig. 18 shows the analog computer simulation of the alternator shown in the block diagram of Fig. 17. A double-pole double-throw switch, $s_2$, has been incorporated to facilitate instantaneous application and removal of load. The inclusion of this switch allows the computer to develop its own initial conditions, either with or without load, after which the load may be changed and the resulting transient observed. Switch $s_1$ provides a convenient method of changing the load which is to be applied and removed.

The computer has been time-scaled t
incorporate a 250-to-1 time scale expansion
This computer time scale provides sufficien
spread between the system time constant
and the necessary stabilizing capacitor tim
constants in the algebraic loops to mak
the effect of the latter negligible. Th
stabilizing capacitors are shown dotte
in the computer diagram. The magnitud
scaling of the computer is indicated on th
computer diagram by the number of volt
which equal 1 pu for each variable.

Computer results obtained from th
alternator simulation were checked agains
actual machine test data and showe
excellent agreement.

### Simulation of Voltage Regulator System with Torque Limiting

Fig. 19 shows the block diagram of th
closed-loop system as designed earlier i
this paper, and Fig. 20 above the computd

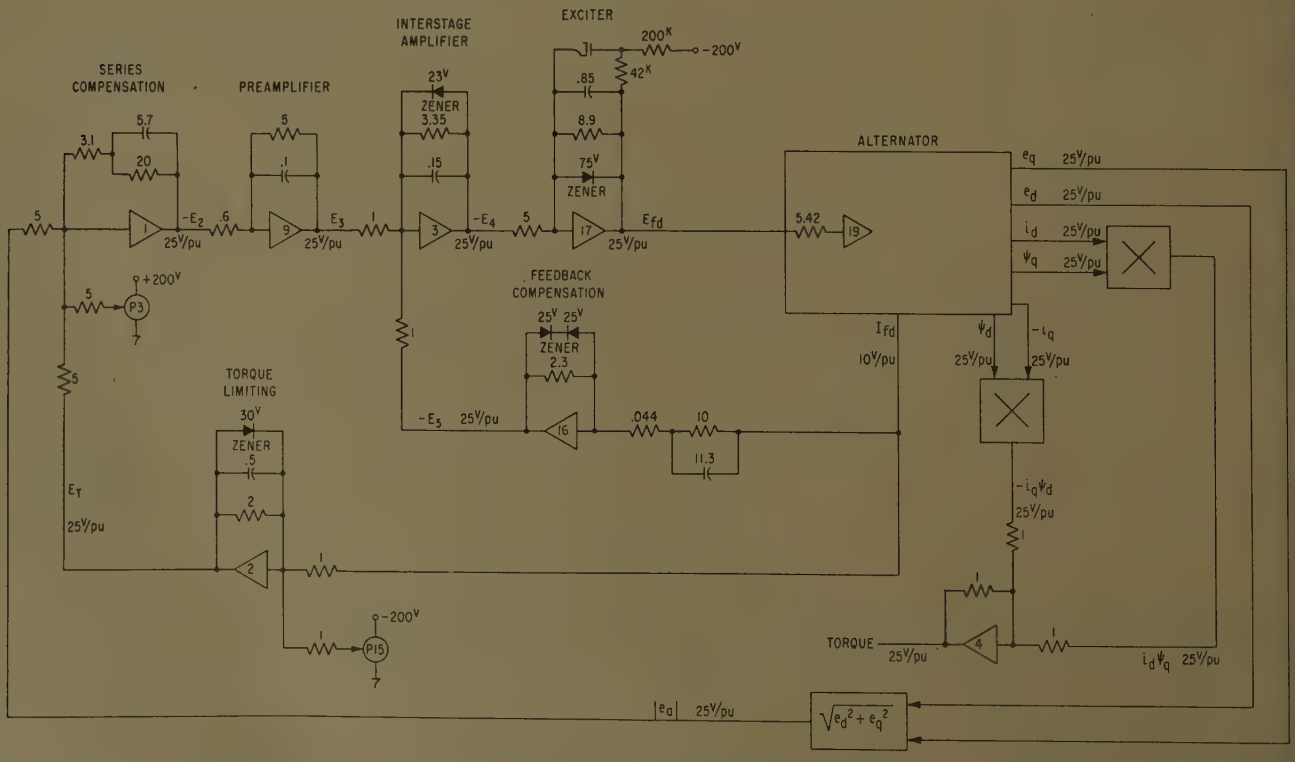


Fig. 20. Computer diagram of closed-loop system shown in Fig. 19

**Table II. Alternator Transfer Function Without Saturation**

| No Load | Full Load (0.75 PF Lagging) | Twice Full Load (0.75 PF Lagging) |
|---|---|---|
| $\frac{4.16}{\left(\frac{s}{11}+1\right)}$ | $\frac{1.39}{\left(\frac{s}{25.3}+1\right)}$ | $\frac{0.84}{\left(\frac{s}{35.3}+1\right)}$ |

**Table III. Alternator Transfer Functions at 775 F With Saturation**

| No Load | Full Load (0.75 PF Lagging) | Twice Full Load (0.75 PF Lagging) |
|---|---|---|
| $\frac{1.68}{\left(\frac{s}{22}+1\right)}$ | $\frac{1.01}{\left(\frac{s}{30}+1\right)}$ | $\frac{0.79}{\left(\frac{s}{42}+1\right)}$ |

diagram. A scale factor has been included at the input to the alternator to convert from the 170-volt base used throughout the loop to the 8,420-volt base of the alternator field.

The output of the torque-limiting circuit, $E_T$, is single-ended and is therefore zero for values of $I_{fd}$ less than the $I_{fd}$ reference. Under normal load operation this circuit is essentially inoperative. The gain and reference of the torque-limiting circuit were adjusted experimentally to provide maximum torque limiting without introducing limit cycle oscillations or violating the 3-pu fault-current requirement.

The simulation of the closed-loop system with $I_{fd}$ torque limiting is shown in Fig. 18. The time and magnitude scaling are the same as in Fig. 18. Torque limiting was also studied using $i_a$ feedback instead of $I_{fd}$. The $i_a$ is generated by obtaining $\sqrt{i_d^2+i_q^2}$ with a function generator and this signal is fed into amplifier *2* in place of $I_{fd}$. The gain and reference of this torque-limiting circuit were also adjusted for maximum torque limiting without introducing limit cycle oscillations or violating the 3-pu fault-current requirement.

To observe the torque which the drive would experience under various transient conditions, torque was generated from equation 16 using the multipliers indicated.

## Appendix III

### Alternator Linearized Transfer Function Equations

Under the assumptions of no saturation in the machine, a constant-speed drive, negligible $s\Psi_d$, $s\Psi_q$, $(X_L/\omega_0)si_d$, $(X_L/\omega_0)si_q$ terms, and negligible amortisseur effects, the normalized alternator and load equations (see Appendix I) become:

$$E_{fd}=R_{fd}I_{fd}+s\Psi_{fd} \tag{18}$$

$$e_a=-\Psi_q-ri_d \tag{19}$$

$$e_q=\Psi_d-ri_q \tag{20}$$

$$\Psi_{fd}=X_{ffd}I_{fd}-X_{ad}i_d \tag{21}$$

$$\Psi_d=X_{ad}I_{fd}-X_di_d \tag{22}$$

$$\Psi_q=-X_qi_q \tag{23}$$

$$\Psi_{md}=X_{ad}(I_{fd}-i_d) \tag{24}$$

$$e_d=R_Li_d-X_Li_q \tag{25}$$

$$e_q=R_Li_d+X_Li_q \tag{26}$$

$$e_a^2=e_d^2+e_q^2 \tag{27}$$

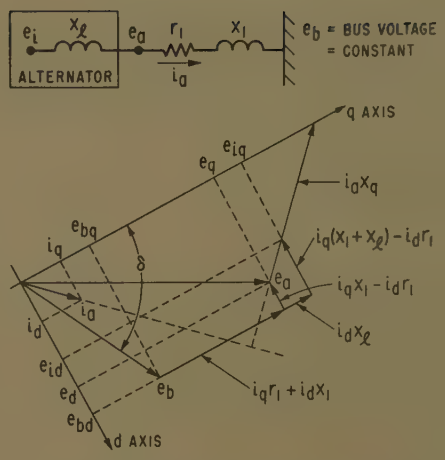


**Fig. 21. Alternator connected to infinite bus through line impedance**

For small changes about a steady-state operating point these equations become:

$$\Delta e_d=X_q\Delta i_q-r\Delta i_d \tag{28}$$

$$\Delta e_q=X_{ad}\Delta I_{fd}-X_d\Delta i_d-r\Delta i_q \tag{29}$$

$$\Delta e_d=R_L\Delta i_d-X_L\Delta i_q \tag{30}$$

$$\Delta e_q=R_L\Delta i_q+X_L\Delta i_d \tag{31}$$

$$\Delta E_{fd}=\frac{R_{fd}}{X_{ad}}\left\{s[X_{ad}\Delta I_{fd}-(X_d-X_d')\Delta i_d]\times\frac{X_{ffd}}{R_{fd}}+X_{ad}\Delta I_{fd}\right\} \tag{32}$$

$$e_{as}\Delta e_a=e_{ds}\Delta e_d+e_{qs}\Delta e_q \tag{33}$$

Equation 33 is obtained by expanding equation 34 and neglecting the second-order effects.

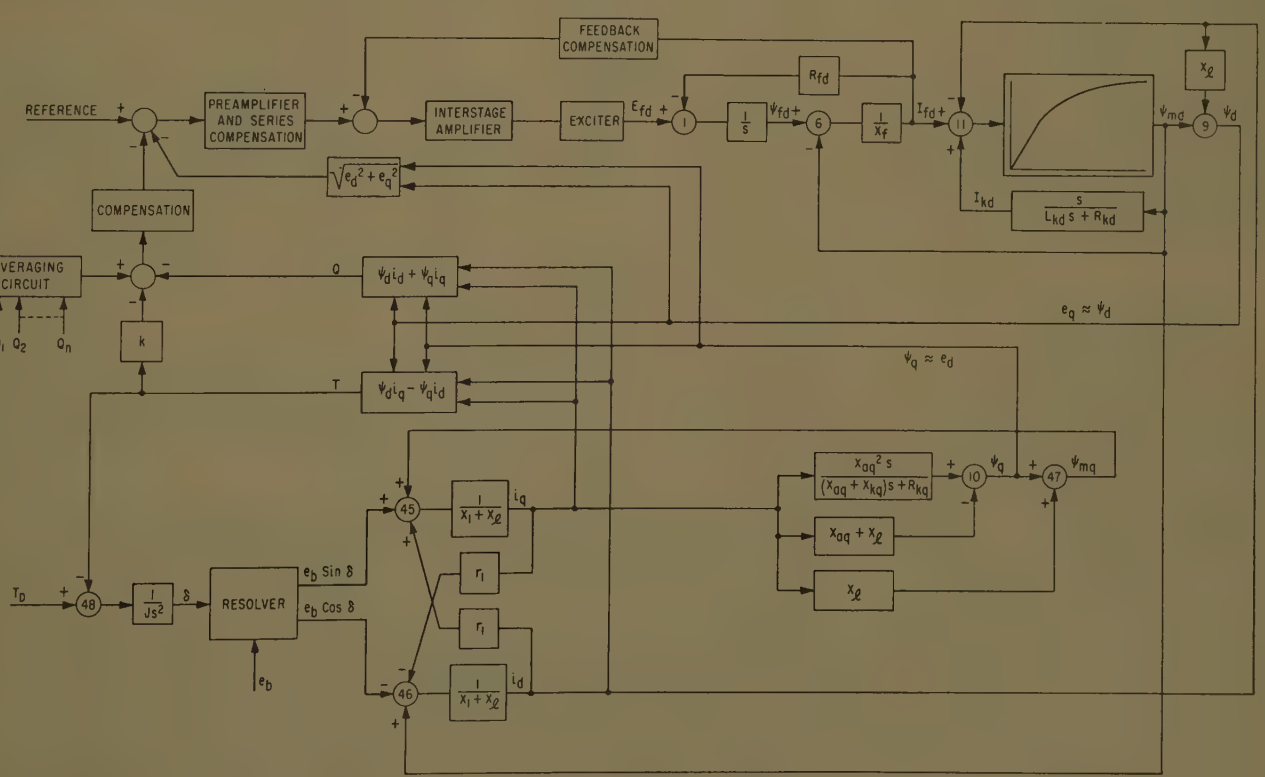


**Fig. 22. Reactive load division simulation block diagram**

$$(e_{as}+\Delta e_a)^2=(e_{ds}+\Delta e_d)^2+(e_{qs}+\Delta e_q)^2 \quad (34)$$

Combination of equations 28 through 33 yields the alternator linearized transfer function (developed by Dr. K. G. Black):

$$\frac{\Delta e_a}{\Delta E_{fd}}=\frac{K_L\Delta I_{fd}}{\Delta E_{fd}}=\frac{K_1}{T_{dz}'s+1} \quad (35)$$

where

$$K_1=\frac{e_{ao}X_{ad}}{E_{fdo}R_{fd}}\left\{\frac{e_{qs}}{e_{as}}[X_L(X_L+X_q)+R_L(R_L+r)]\times\frac{e_{ds}}{e_{as}}[X_qR_L-X_Lr]\right\}\Big/(R_L+r)^2+(X_L+X_q)(X_L+X_d) \quad (36)$$

$$T_{dz}'=\left[\frac{(R_L+r)^2+(X_L+X_d')(X_L+X_q)}{(R_L+r)^2+(X_L+X_d)(X_L+X_q)}\right]T_{do}' \quad (37)$$

$$T_{do}'=\frac{X_{ffd}}{\omega_oR_{fd}} \quad (38)$$

Here $e_{as}$, $e_{ds}$, and $e_{qs}$ are the pu steady-state values calcuable from the steady-state vector diagram. The alternator parameters are in pu values obtained from Table I. Equation 35 yields the alternator transfer function whose gain and time constant have physical dimensions because in equation 36 the ratio of the base values, $e_{ao}/E_{fdo}$, is included and in equation 38, $\omega_o$ is introduced.

At +775 F, use of equations 35 through 38 yields the alternator transfer functions shown in Table II.

Saturation has a major effect on the machine characteristics in that it reduces the machine gain and time constant. The saturation effect is greatest at no load and becomes less as load is increased. For the machine under consideration, the responses to small changes were obtained from the computer setup shown in Appendix II. The results are shown in Table III.

The linearized alternator transfer functions used in Fig. 3 are those corresponding to those of Table III which were obtained by measurement on the computer.

# Appendix IV

## Reactive Load Division Loop Simulation

When operating alternators in parallel, the electrical system must insure proper division of reactive load between machines whereas the drive system must insure proper division of real load between machines. Alternator characteristics are such that while delivering a given average kva to the load, a sizable reactive kva can oscillate between alternators while the bus voltage remains invariant at its normal level. The reactive load division loop must provide stabilizing signals which insure proper division of reactive load among alternators without reactive load oscillations.

The following analysis (developed by F. P. deMello) provides a means for simulating the reactive load division loop during parallel operation of alternators.

In parallel operation, machines tend to pair off and exchange load. The behavior of one machine is the mirror image of its partner and the bus voltage remains invariant. A load stability study can therefore be made by considering one machine against an infinite bus which is located at the electrical center between machines.

The circuit diagram in Fig. 21 shows the situation where the lines between the alternator and bus have an impedance inserted for purposes of generality. The vector diagram for this situation is also shown in Fig. 21. For purposes of simpler presentation, the assumption is made that the small alternator internal resistance, $r$, is negligible or that it can be lumped with the line resistance to produce $r_1$. Here $e_t$ is the alternator air-gap voltage while $X_1$ is the line reactance. The equations for this configuration become:

$$e_{bd}=e_b\sin\delta=e_d+i_qX_1-i_dr_1 \quad (39)$$

$$e_{bq}=e_b\cos\delta=e_q-i_dX_1-i_qr_1 \quad (40)$$

$$e_{id}\approx-\Psi_{mq} \quad (41)$$

$$e_{iq}\approx\Psi_{md} \quad (42)$$

$$e_q\approx\Psi_d \quad (43)$$

$$e_d\approx-\Psi_q \quad (44)$$

$$e_{bd}=-\Psi_{mq}+(X_1+X_l)i_q-i_dr_1 \quad (45)$$

$$e_{bq}=\Psi_{md}-(X_1+X_l)i_d-i_qr_1 \quad (46)$$

$$\Psi_{mq}=\Psi_q+X_li_q \quad (47)$$

$$\delta=\frac{1}{Js^2}(T_D-T) \quad (48)$$

These equations, in conjunction with equations 1, 6, 9, 10, and 11 of Fig. 17 and the regulating loop diagram of Fig. 4, allow generation of the block diagram shown in Fig. 22. In this diagram, $T_D$ can be inserted as a constant or as a time-varying function, depending on the drive characteristics. The reactive load signal, $Q$, is compared with the average reactive load supplied to the bus per machine. The difference signal is used to control the reactive load that the alternator supplies to the bus. The compensation network and a portion of the real load signal, $T$, are used for stabilization purposes. At the time of writing this paper, this simulation had not been verified by test.

# References


1. Synchronous Machines—Theory and Performance (book), C. Concordia. John Wiley & Sons, Inc., New York, N. Y., 1951.

2. Parallel Operation of Airplane Alternators, D. W. Exner. *AIEE Transactions (Electrical Engineering)*, vol. 62, Dec. 1943, pp. 755–60.

3. A Basic Analysis of Synchronous Machines—Part I, W. A. Lewis. *Ibid.*, pt. II (*Power Apparatus and Systems*), vol. 77, Aug. 1958, pp. 436–56.

4. Analog Computer Representations of Synchronous Generators in Voltage-Regulation Studies, M. Riaz. *Ibid.*, vol. 75, Dec. 1956, pp. 1178–84.

5. *Discussion* by C. H. Thomas of reference 4, pp. 1182–84.

6. Analog Computer Representation of Alternators for Parallel Operations, L. V. Boffi, V. B. Haas, Jr. *AIEE Transactions*, pt. II (*Communication and Electronics*), vol. 76, May 1957, pp. 153–58.

7. Random Paralleling of Aircraft Alternators, F. P. deMello, H. M. Rustebakke. *Ibid.*, pt. II (*Applications and Industry*), vol. 77, Nov. 1958, pp. 322–30.


# Discussion

**Thomas J. Higgins** (University of Wisconsin, Madison, Wis.): This clearly written, well-integrated paper evidences the values of analytic design procedures in the solution of a problem of considerable current interest in practice. It would be of interest to see the details of a study which encompass, for low-temperature systems, the optimization remarked in the closing paragraph of the body of the paper.

**Richard T. Smith** (University of Texas, Austin, Tex.): The equations used to represent the alternator are those previously developed to describe a salient-pole synchronous machine. However, construction of the inductor-type alternator[1] indicates that these equations should adequately define performance. While it is easily possible to account for saturation effects in greater detail, it was thought that such refinements were premature. In fact, it is clear that the performance equations are presently of limited utility, mainly because of the inaccuracies of the parameters characterizing the system. Nevertheless, it is gratifying to note that computers are permitting, economically, a more and more accurate determination of these parameters.


Reference

1. A Solid Rotor A-C Generator for High Temperature Electrical Systems, J. T. Bateman. *AIEE Transactions*, see pp. 400–05 of this issue.


**W. E. Sollecito and D. A. Swann:** We wish to thank the discussers for their comments on our paper.

The nonlinear optimization work that Dr. Higgins would like to see is presently being carried on at the authors' company. The work remains to be completed and then the results published.

We are in agreement with Dr. Smith's observations.

# An Elementary Design Discussion of Thermoelectric Generation

E. W. BOLLMEIER
ASSOCIATE MEMBER AIEE

AT THE PRESENT TIME, many electric power sources of unconventional nature are being pursued vigorously in research and development. One of these, thermoelectric generation, has enjoyed renewed interest because of the development of semiconductor thermoelectric materials yielding efficiencies which are now practical for some devices and encouraging for others.

Semiconductor thermoelectric materials of practical use today have multiplied thermoelectric heat conversion efficiencies by a factor of 10, approximately, compared with metal thermocouples. This remarkable increase has brought thermoelectric conversion to a point of potential competition with electromechanical or other conversion for some applications. However, large-scale economic competition remains dependent on significantly higher materials efficiency attainment. At today's state of the art, the uses to which thermoelectric generating devices are suited are those which value some feature more highly than maximum economy or which utilize very low-cost heat.

This paper seeks to acquaint the reader with the elementary problems of thermoelectric generation and some of the solutions devised. Consideration is also given to the advantages and disadvantages of thermoelectric generation for uses which may appear desirable at the present state of the art.

## A Composite View of Thermoelectric Generation

Fig. 1 presents a simplified view of thermoelectric generation as a complete, useful system. The usual elements of a useful heat energy conversion system are apparent.

1. Heat input.
2. Conversion apparatus.
3. Heat rejection.
4. Output control.

These same four elements of a useful system may be readily compared to the 1. burner, 2. boiler-turbine-generator, 3. condenser, and 4. control system of a conventional steam generating system. Similar problems and similar general solutions apply equally to both, although the elements are physically different.

The major difference between conventional electromechanical generation and thermoelectric generation is that the boiler-turbine-generator conversion devices are replaced by one unit, the thermopile.

The thermopile, being a static device, avoids many mechanical problems inherently. However, substantial new problems appear as the struggle for realization of the semiconductor materials efficiency in practical generators is carried out.

## Thermocouple Fundamentals

According to the relationships established and expanded upon by Fritts, Ioffe, and others, the Seebeck emf (electromotive force) $E_{sc}$ or open-circuit voltage of a thermocouple is equal to the sum of the two thermocouple element voltages obtained by integrating the Seebeck coefficient $S$ with respect to temperature between hot-junction temperature $T_h$, and cold-junction temperature $T_c$.[1,2]

$$E_{sc}=\int_{T_c}^{T_h} S_p dT-\int_{T_c}^{T_h} S_n dT \qquad (1)$$

The Seebeck coefficients of semiconductor materials are in general quite temperature-dependent. For accuracy in calculation of $E_{sc}$, the integral in equation 1 must be used, but for simplification of the expressions to follow, average values of Seebeck coefficient multiplied by $(T_h-T_c)$ will be used rather than the integral.

Connecting a thermopile of open-circuit voltage $V_g$, and resistance $R_g$, into a circuit of resistance $R_L$, the current in the circuit and power output may be defined by:

$$I=\frac{V_g}{(R_g+R_L)} \qquad (2)$$

$$P_o=\frac{V_g^2 R_L}{(R_g+R_L)^2} \qquad (3)$$

The internal resistance $R_g$ of a thermopile is the sum of the element resistances. Like Seebeck coefficient, the resistivity of semiconductor materials is temperature-dependent. The calculation of thermopile resistance, therefore, should be made by the integral

$$R_g=N\left[\frac{1}{A_p}\int_{T_c}^{T_h}\rho_p\frac{dx}{dT}dT+\frac{1}{A}\int_{T_c}^{T_h}\rho_n\frac{dx}{dT}dT\right] \qquad (4)$$

where

$N$ = number of couples
$A$ = element area
$\rho$ = electrical resistivity

Equation 4 can be evaluated when the variation of resistivity with temperature and temperature distribution within the thermocouple material are known. The following expression which defines the relation of $R_g$ to $R_L$ at the condition of maximum efficiency:

$$R_g=\frac{R_L}{\sqrt{1+Z\frac{(T_h+T_c)}{2}}} \qquad (5)$$

where $Z$, figure of merit

$$=\frac{(S_p-S_n)^2}{(\sqrt{k_n\rho_n}+\sqrt{k_p\rho_p})^2} \qquad (6)$$

where $Z$ is available plotted as a function of temperature for both $P$ and $N$ materials, the average $Z$ value over the temperature range encountered may be used in equation 5. $Z_{avg}$ is determined by:

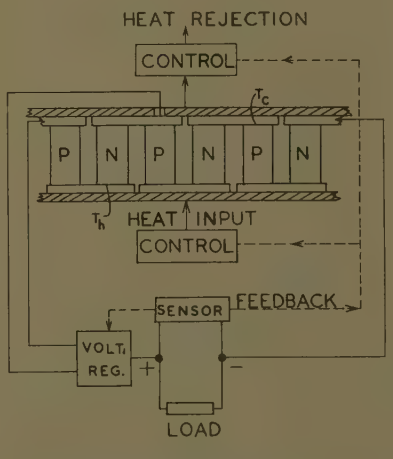


**Fig. 1. Composite view of thermoelectric generation**

Paper 59-867, recommended by the AIEE Air Transportation Committee and approved by the AIEE Technical Operations Department for presentation at the AIEE Summer and Pacific General Meeting and Air Transportation Conference, Seattle, Wash., June 21–26, 1959. Manuscript submitted March 24, 1959; made available for printing April 22, 1959.

E. W. Bollmeier is with the Minnesota Mining and Manufacturing Company, St. Paul, Minn.

The author wishes to express his appreciation to Mr. E. J. Levin, Mr. W. G. Krawczak, and Mr. R. A. Elm for their contributions to the contemporary state of the art in thermoelectric generation. He also gratefully acknowledges the orientation provided by Dr. R. W. Fritts in successful use of the products of his semi-metals research.

$$Z_{avg}=\frac{\int_{T_c}^{T_h} Z_p dT+\int_{T_c}^{T_h} Z_n dT}{2(T_h-T_c)} \quad (7)$$

It may also be shown for maximum efficiency that the cross-sectional areas of the thermocouple elements are related as follows when $L_n=L_p$, which is usually desirable in thermopile design:

$$\frac{A_n}{A_p}=\sqrt{\frac{k_p\rho_n}{k_n\rho_p}} \quad (8)$$

With $A_n/A_p$ established and thermocouple resistance $R_c=R_g/N$ known for any proposed thermopile design, approximation of the length to area ratios for the $P$ and $N$ thermocouple legs may be made through the relations:

$$\frac{L_n}{A_n}=\frac{R_g/N}{\rho_n+\frac{(\rho_p A_n)}{A_p}} \quad \text{When } L_n=L_p \quad (9)$$

$$\frac{L_p}{A_p}=\frac{R_g/N}{\rho_p+\frac{(\rho_n A_p)}{A_n}} \quad \text{When } L_n=L_p \quad (10)$$

The physical size and weight of the thermocouple elements can be varied without affecting thermopile electrical design characteristics, so long as the ratios of $L/A$ are observed. The final choice of exact $L$ and $A$ dimensions may be made on the basis of mechanical feasibility and available heat flux.

Thermocouple operating efficiency is expressed as the ratio of useful power delivered, $I^2R_L$, to the rate of heat input to the thermocouple. Rate of heat input is made up of loss rate by thermal conduction from hot junction to cold junction, input rate to drive the thermoelectric cycle at the Carnot efficiency established by $T_h$ and $T_c$ and half the $I^2R$ loss of the thermocouple material circuit. The expression for maximum conversion efficiency is given by the following relation, subject to the conditions that optimum $A_n/A_p$ ratio exists and that optimum efficiency match between $R_g$ and $R_L$ has been established:

$$\eta g(\max)=\frac{T_h-T_c}{T_h}\,\frac{\sqrt{1+Z(T_h+T_c)/2}-1}{\sqrt{1+Z(T_h+T_c)/2}+\frac{T_c}{T_h}} \quad (11)$$

For best efficiency it becomes apparent from examination of the efficiency equation 11 and the definition of $Z$ in equation 6 that the $K\rho$ product of the thermocouple materials, and the cold-junction temperature $T_c$ must be minimized and Seebeck coefficient and hot-junction temperature $T_h$ maximized. Since for most electrical conductors and semiconductors, reduction in thermal conductivity is accompanied by approximately proportional increase in electrical resistivity, reducing the $k\rho$ product while maintaining or increasing $S$ is a difficult materials research problem.

Today's practical semiconductor thermoelectric materials, such as the p- and n-type lead tellurides, have $k\rho$ products ranging up to 10 times those of metals. Fortunately, conversion efficiency improves with the square of Seebeck coefficient and inversely with the first power of the $k\rho$ product. Thus, the tenfold advantage in semiconductor Seebeck coefficient over those of metals yields a tenfold improvement in efficiency over metals, in spite of the higher semiconductor $k\rho$ products. Further reference to Fritts[1] is recommended for his broad consideration of p- and n-type lead telluride thermocouple design.

## Thermopile Configuration

Physical arrangement of a thermopile structure is primarily dependent upon:

1. Heat-source energy density and configuration.
2. Radiator absorption capacity and configuration.
3. Heat losses and surface transfer rates.
4. Mechanical and electrical design feasibility.

Heat-source energy density has inherent bearing upon thermopile configuration because of the direct relation between energy density and size of heat source. The heat source must be designed to the thermopile's heat input requirements and should be of the minimum area necessary to accommodate the number of elements of the required $L/A$ ratio in a mechanically and thermodynamically feasible arrangement. It is fundamental that heat insulation losses will be minimized if a maximum of the heat conducting path from source to radiator is made up of thermoelectric material. Available heat-source energy density and transfer rates to the thermopile hot junctions determine whether or not this ideal can be approached.

Assuming complete coverage of the heat source with thermoelectric material, configuration and type of heat source determine the degree of insulation heat loss to be combated. If the heat source were in the form of a thin slab, it might be covered with close-packed parallel elements having a very short heat-transfer path between elements from hot to cold junction. If the heat source were long and cylindrical, it might be covered with radially arrayed elements which present a small area of nonelement heat conducting path near the source but increasing with radial distance. A third heat-source configuration is the sphere, surrounded by elements extending to a spherical radiator.

The configuration choice of the thermopile design engineer is thus controlled by the factors of feasible heat-source configuration; energy density of source and minimum heat-leakage path.

Considering the spherical configuration concept, and a form of heat energy of given energy density per unit volume, it becomes apparent that a spherical heat-source configuration will contain maximum energy per unit of surface area compared to cylindrical or slab-source configurations. In heat sources where the rate of energy liberation per unit volume is low, a problem of mismatch between high source area and low thermoelectric material area may occur. Any source configuration other than spherical will present greater surface area for the same rate of energy liberation and same energy density.

The insulation heat loss of the spherical concept thermopile is proportional to the mean area $A_m$ of the insulation body. $A_m$ is characterized by the following relation, assuming negligible heat transfer from elements to insulation along their length:

$$A_m=\sqrt{(A_s-A_{tm})(A_E-A_{tm})}$$
$$=\sqrt{(\pi D_s^2-A_{tm})[\pi(D_s+2t_i)^2-A_{tm}]} \quad (12)$$

where

$A_s$ = source area
$A_e$ = insulation exterior area
$A_{tm}$ = total cross-sectional area thermoelectric material, assuming constant element diameters
$t_i$ = insulation thickness

In the range of $t_i=D_s$ and $A_{tm}=D_s^2/2$, the $A_m$ relation simplifies to:

$$A_m=\pi\frac{\sqrt{17}}{2}D_s^2$$

Thus, it is shown for the spherical configuration that insulation heat loss is proportional to the square of heat source diameter in a one-dimensional ratio area of mechanical feasibility.

Similar relationships can be shown for other thermopile configurations, but it may be shown that insulation heat loss for all configurations will vary exponentially greater than unity with heat-source size.

## Heat-Source Discussion

In the case of combustible fuel sources—whether or not coupled with

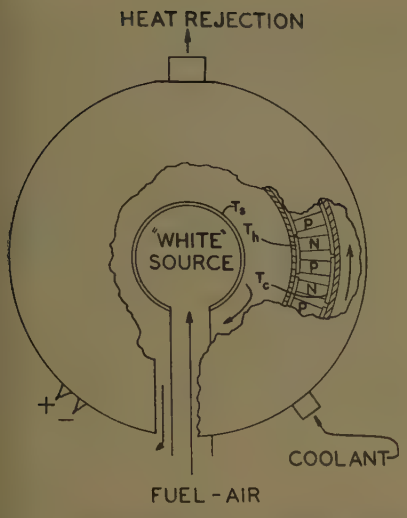


**Fig. 2. Incandescent heat source, spherical configuration**

heat-transfer mediums—uniform hot-junction temperature, combustion efficiency, and flue losses present major problems which can be attacked in four ways:

1. High energy density incandescent combustion system.
2. High-temperature closed-cycle condensing-vapor boiler system.
3. Flue gas to fuel, air heat exchanging.
4. Nuclear-energy heat sources.

The high energy density incandescent combustion system (Fig. 2) is one which seeks to transfer energy to the hot junction by radiation in preference to convection and conduction. Theoretical consideration of this system shows advantages from the standpoints of combustion efficiency, maximum energy density (minimum size), and low thermal inertia. Incandescent sources designed to transfer heat appreciably by radiation offer advantage also in designing for uniformity of hot-junction temperature, a task extremely difficult with gas convection or conduction transfer.

High-temperature condensing-vapor boiler systems (Fig. 3) offer advantages of hot-junction temperature uniformity and high heat-transfer rates at lower temperatures than required by fluid conduction or convection. This may be important in protecting thermoelectric materials which could be damaged easily by accidental overfiring of a direct flame heated thermopile. Temperature uniformity can be obtained by heating the pile with condensing vapor while energy is stripped from the heat source over a fair range of temperature approaching boiler temperature. The problems of closed-cycle high-temperature boilers are primarily those of containing the most probable candidates, such as mercury, protecting against overpressure, and minimizing thermal inertia for control purposes.

In regard to heat exchanging between flue gas and incoming fuel–air mixtures, greater advantage can be gained if flue gas stack draft can be used to provide the pressure necessary to the exchanger. Since electric power is available at rather low efficiency from the pile, use of electric output for powering inefficient accessories may yield insignificant improvement in over-all efficiency, particularly in small output generators.

The nuclear heat source is one of inherent practicality for thermoelectric generation. Nuclear sources, deriving energy from radioactive decay (in the case of isotopes) or fission (in the case of reactors), have no problem of flue gas loss to hamper over-all efficiency. The nuclear heat source has exceptional watt-hours of energy content per unit weight, compared to all other heat sources—an advantage for long life generator service in remote areas, in space, or in locations where air is not available for combustion. The nuclear source inherently minimizes a number of problems for the thermopile design engineer. Because it needs no physical connection with the pile exterior for flue gas discharge and fuel inlet, heat conducting members other than thermoelectric material or thermal insulation can be essentially eliminated. The disadvantages of nuclear sources for many ordinary uses today are cost and availability. Yet they are indispensable for those uses demanding maximum watt-hours per pound or where periodic refueling is impossible.

Much remains to be known regarding long-term radiation effects on semiconductor thermopiles. Insufficient knowledge is available to state effects on all semiconductors though it has been predicted by Fritts and others that crystal lattice damage should annal out rapidly at the thermopile operating temperatures involved.

The SNAP III nuclear-fueled generator reported on by Anderson, Barmat, and the author operated without measurable deterioration of thermoelectric properties since fueled on January 7, 1959, to the present. No great significance can be drawn from this except to note that the source external radiation level was low, very little neutron emission was involved and no damage of the doped lead telluride elements was expected, nor has it occurred.[3] Significant studies of radiation damage to n and p doped lead telluride materials are now being conducted by a number of firms active in nuclear technology.

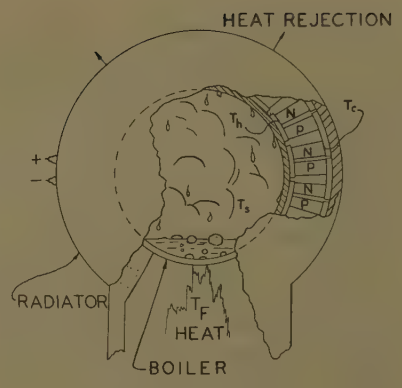


**Fig. 3. Closed boiler heat source**

## Designing with Semiconductor Thermoelectric Materials

Prime semiconductor material factors influencing thermopile design are:

1. Stability and strength.
2. Contact resistance.
3. Sublimation.
4. Oxidation and contamination.

Designing with materials at elevated temperatures involves compromises resulting from the temperature dependency of most material properties. The same problems apply to semiconductor thermoelectric materials in general, though the discussion following is based on the result of experience with p and n doped lead tellurides.

Semiconductors of thermoelectric value are, in general of brittle nature and poor in tension, but of good strength in compression. Table I gives the physical properties data of p and n doped lead telluride.

The strength properties of these materials suggest that the pile structure should be so designed as to limit thermocouple stresses to compression. This compromise imposes limitations, but at the same time aids in the solution of another problem, that of contact resistance.

Contact resistance may be minimized for doped lead telluride materials through the employment of bonded or soldered connection at the cold end and pressure contact at the hot junction. Elements may be formed with integrally bonded contacts

**Table I. Typical Physical Properties, Cast and $H_2$ Annealed Doped Lead Telluride**

| | |
|---|---|
| Tensile strength, pounds per square inch | >1,000 |
| Compressive strength, pounds per square inch | >10,000 |
| Young's modulus, pounds per square inch | $2\times10^6$ |
| Density, grams per cubic centimeter | 8.15 |
| Thermal expansion coefficient, per degree C | $18\times10^{-6}$ |
| Thermal conductivity, per centimeter per degree C | 0.02 watts |

for use at either the cold or hot end. However, the difficulty of forming elements with bonded connections at both ends makes engineering consideration of an all-bonded connection scheme impractical at today's state of the art. In usual practice, the cold-end connection is made by soldering of the semiconductor element to a metal contacting cap. The hot-end connection is satisfactorily made by compressively loading the element against the hot-junction connecting shoe shared by its companion element of opposite polarity. Constructions utilizing bonded hot-junction contacts are possible, but unnecessary except where pressure loading is undesirable or inconvenient. Flat-module pile constructions may face mechanical problems in compressive element loading because of the bending strength of the hot and cold-end plates. In such designs, bonded hot-junction contacts and soldered cold contacts may be exploited to some advantage. Atmospheric pressure contact loading of an evacuated flat pile module may also be exploited, but contacting pressure is limited to values considered insufficient at today's state of the art.

Pressure-loaded elements assure that electrical continuity will be maintained even though some sublimation may occur at the highest temperature portion of the elements. Sublimation may be regarded as an operating life design problem at temperatures in excess of 1,000 F (degrees Farenheit), and although it may be minimized by providing the elements with a coating or cover that restricts diffusion of material away from the hot junction, pressure contacting assures maximum reliability.

The factors of oxidation and poisoning of doped lead tellurides are also temperature-dependent in large degree. Both p and n lead tellurides can be used in extended air exposed service up to 500 F. However, beyond that point oxidation of the material becomes significant and hermetic sealing is required. Since operating temperatures above 500 F are desirable for maximum Carnot efficiency and the material is capable of stable operation in excess of 1,000 F with long life, hermetic sealing is indicated for maximum over-all efficiency designs.

Oxidation above 500 F may be eliminated as a problem in thermopile design by providing a reducing, inert, or high-vacuum atmosphere within the hermetically sealed enclosure. A reducing atmosphere protects both the element material and all electrical contact surfaces against oxidative degradation. While high vacuum may also provide oxidation protection, it also raises the curve of sublimation rate versus temperature. The increased structural, mechanical, and material problems created by designs which seek to maintain high vacuum over a long life are difficult to solve and costly. High-vacuum environment does have the advantage of lowering losses through most thermal insulation materials which might be used in pile design. However, over-all efficiency gain through use of vacuum is complex and questionable after consideration of the problems of increased sublimation.

Contamination of most thermoelectric materials at elevated temperatures is a problem of which the thermopile designer must be constantly aware. Contamination may result from the diffusion of a number of metals, such as zinc and copper, into the material or from reaction with a large group of active elements and radicals. Diffusion of contaminants into the thermoelectric material results predominately in lowered Seebeck coefficient, whereas reactive contamination causes increased contact resistance or sublimation rate. The best guide for safety in design is experimental testing of contamination by materials apt to come in intimate contact with the thermoelectric material at elevated temperatures.

In general, hydrogen or methane is desirable as an atmospheric environment for doped lead telluride above 500 F. Such reducing atmospheres serve to protect against oxidation or reactive contaminants that may diffuse in gaseous state to the materials. Materials such as iron, molybdenum, alumina, carbon, and mica are safe for direct contact at elevated temperature. Aluminum, tin, copper, and steel are satisfactory construction materials at the cold end of the pile where solid or gaseous diffusion proceeds at negligible rates. Thermal insulations should in general be regarded as suspect until it has been experimentally determined that they are inert at elevated temperatures. Insulation surface coatings or binders may also cause contamination.

## Thermopile Structure Design

Until thermoelectric materials significantly beyond the present 8 to 11% efficiency range are available, the thermoelectric device engineer's lot will be one of limited ability to compromise. His first problem today is tolerable output energy cost and his second is one of heat transfer—too much and too little.

As material conversion efficiencies improve, thermopile design problems decline at a considerably higher rate, particularly those of heat transfer. At the pres state of the materials art, 90 to 95% of th heat energy entering the thermopile mus be transferred through and rejected fo 5 to 10% conversion to electric energy Thermal design problems and electrica design problems are in the same approxi mate ratio: 90 to 10. The developmen engineer's ingenuity is, therefore, taxed i the thermal direction, rather than in th electrical direction in his quest for maxi mum practical attainment of today' materials efficiencies. The following dis cussion is thus oriented.

### The Hot End

Regardless of pile configuration, th hot-end problem, is one of minimum im pedance to heat transfer from source wa to thermoelectric element, in order tha source wall temperatures may be kept be low safe levels for practical materials c construction. In addition, the elemen must be electrically insulated from th source (if conductive) and its neighbors but joined electrically to its companion ele ment of opposite polarity. Solution to th simultaneous problems of low impedanc to heat flow and reliable electrical insula tion of the interface between element ho junction connecting shoe and heat-sourc wall appears best found in the area of high density vitrified ceramic materials Heat-flow impedance at this interface i the sum of the interface and insulatio thermal resistances. The electrical insula tion thermal resistance, proportional t thermal conductivity and thickness, reduced by use of thin vitreous coating on the element hot-junction connectin shoes. Also, by use of such bonded coa ings, one mechanical interface betwee shoe and source wall is eliminated.

The pressure contact between elemen and hot junction shoe is a lesser proble of thermal impedance not only becaus it is a single interface, but also becaus sufficient plastic flow does take place i lead telluride thermoelectric material a temperatures over 900 F to produce par tial, mechanically bonded contact to th hot-junction shoe. Reducing atmosphere encourage this bonding by reducing a operating temperature the oxides tha may be present on the interface material This reduction of interface oxides by re ducing atmosphere may be observed i the drop of internal resistance observed i the first few hours of operation of a pres sure-contacted doped lead tellurid thermopile. It has been noted that th thermal impedances of all the mechanica interfaces between heat source and radia tor are lowered by internal gas pressur and raised with vacuum. Gas molecule

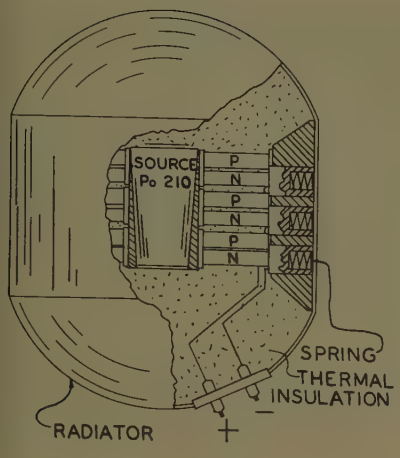


**Fig. 4. SNAP III generator, 3M-1 thermopile**

aid the transfer of heat across dry mechanical interfaces, thus lowering interface themal impedance.

### Between the Ends

As previously considered in the section on configuration, thermal insulation losses can be best limited by covering the source wall area with a maximum of thermoelectric material. Where a match can be designed between thermal watts needed per unit area of element and thermal watts available per unit area, this ideal can be approached according to the ingenuity of the designer in shaping elements for close packing and arranging hot junction connecting shoes. Usually, the 1-to-1 area match ideal cannot be realized for reasons of configuration, mechanical design feasibility, or cold-end transfer capacity.

### The Cold End

Cold-end thermal impedance, like that of the hot end must be minimized while reliable electrical insulation is maintained between elements and radiator wall. Fig. 4 illustrates one scheme of cold-end design for pressure-contacted elements.

The design of Fig. 4 utilizes a bonded metallic cold-end element contact. This contact member is in mechanical contact with a pressure applying member which is electrically insulated from the radiator hardware by means of a thin coating. Other schemes of greater or fewer mechanical interfaces may be readily devised depending on configuration, radiator wall area available per element, necessity of hermetic sealing and cost. The required features of any pressure-contacted element cold-end design are 1. reliable electrical insulation and 2. mechanical flexibility in the thermal path from element to radiator wall sufficient to permit individual element differential movement under spring loading.

The design of Fig. 4 aids electrical insulation reliability by avoiding compressive loading of the electrical insulation. It provides mechanical flexibility in the cold junction thermal path through the sliding fit between the pressure-applying member and the radiator wall. Thermal impedance of this mechanical interface is reduced by its relatively large area and a grease-like coating applied to the interface at assembly. Other schemes involving flexible metallic bellows, diaphragms, etc., may have advantages dependent upon obtainable areas, thicknesses and thermal conductivities of the interfaces, electrical insulation, and hardware involved.

Heat transfer from the radiator wall to the available heat sink is a complex subject which may be attacked in a number of ways with or without liquid or gaseous transfer mediums. Since the transfer rate of all heat-transfer methods—convection, conduction and radiation—is proportional to area, it is advantageous to design for maximum radiator area consistent with other problems. Generator designs for use in space environment face limitations in radiator area and weight. These limitations raise the temperature driving force necessary for the required radiation heat dump rate, with resultant lowering of generator Carnot efficiency. The spherical and cylindrical generator configurations have the inherent advantage of higher external area than flat configurations for the same area of thermoelectric material. The thermopile designer may find it often to his advantage to utilize cylindrical or spherical configuration to ease the problem of cold-end heat transfer, and at the same time benefit from the structural strength, minimum weight and reduced difficulty of hermetically sealing "round" configurations.

## Output and Control

The problem of output control is essentially one of heat input and radiator rejection rate control. The ability to control thermal input varies with type of heat source from moderate for direct fired to not-at-all for nuclear isotope sources. Less variation exists in ability to control heat rejection rates. Also the problem of thermal inertia in thermoelectric generation at the present state of the art makes output response to load changes sluggish.

Inertia can be reduced by shrinking element size while holding $L/A$ constant for any generator design, provided that source energy density and all heat transfer rates can be increased proportionately. These provisions are increasingly difficult as size of element goes down. Where fast response to load change is needed, the best solution may be found in the use of an electric accumulator between generator and load or by control switching of a reserve portion of the pile to match the load. Like most of the designer's problems, control response will be aided by the reduction of weight which will be made possible by higher efficiency materials.

The difficulty of rapid response control of thermoelectric generators typical of today's state of the art is such that they should be considered best suited to stable or slowly varying loads, except where battery accumulators can be used for instantly available reserve power.

Because of the fact that thermocouples are inherently low-voltage high-current devices, the problem of designing to high-voltage low-current loads becomes difficult. Since high-voltage low-current output requirements lead to high generator internal impedance design, the number of thermoelectric elements goes up and their $L/A$ ratio becomes high. As the $L/A$ ratio goes up, elements become long and thin, thus creating problems of mechanical strength for the designer and making element fabrication difficult. As design power goes up, the problem resolves itself since most electric power is utilized at under 200 volts, regardless of amperage. It may be stated as a generalization that generator designs for output characteristics of less than 10 watts and more than 10 volts would be simplified, if static d-c to d-c voltage conversion were used to achieve design output voltage. Prospective users of thermoelectric generation at low power levels should consider the voltage problem in their system design and strive for voltage-to-current

**Table II. Operational Characteristics of the 3M-1 Thermopile**

| | Initial* | At Source Half-Life |
|---|---|---|
| Thermal input, watts | 96 | 48 |
| Fueling, curies | 3,000 | 1,500 |
| Dose rate, generator surface, milliroentgens per hour | 700 | 350 |
| Dose rate, at 1 meter, milliroentgens per hour | 7 | 3.5 |
| Hot junction temperature, degrees F | 1,100 | 720 |
| Cold junction temperature, degrees F | 400 | 170 |
| Electrical output, watts | 5.3 | 2.4 |
| Voltage at maximum efficiency | 3.0 | 2.4 |
| Over-all efficiency, % | 5.5 | 5.1 |
| Watt-hours, first half-life | = 8,000 | |
| Watt-hours/pound, first half life | = 1,600 | |

* Estimated. Actual fuel load was initially at half-life values.

ratios of less than unity if possible in the 10- to 50-watt ranges.

### The SNAP III Generator

The SNAP III nuclear-fueled generator, Fig. 4, is a working example of practical thermoelectric generation.[3,4] It utilizes a type *3M-1* thermopile of cylindrical concept built so as to receive a tapered cyclindrical isotope (polonium 210) container as its heat source. Since the SNAP III was designed to demonstrate feasibility of thermoelectric power supply for space vehicles, heat rejection is by radiation only. The design of this thermo electric generator established many of the concepts outlined here. Its operational characteristics are given in Table II. The thermoelectric element and thermopile specifications are as follows:

THERMOELECTRIC ELEMENT SPECIFICATIONS

Material: p and n doped lead telluride
$A_n/A_p$ ratio: 0.89
$L$, element length: 1.0 inch
$R_{pn}$, resistance per couple: 0.07526 ohm
$E_{sc}$, couple voltage: 190 millivolts
Segmentation: n yes, p no

THERMOPILE SPECIFICATIONS

$T_h$, temperature, hot junction: 1,100 F
$T_c$, temperature, cold junction: 400 F
$P_o$, power output: 5 watts
$V_g$, voltage output, maximum efficiency: 2.8 volts d-c
$R_I$, internal resistance: 2.03 ohms
$R_L$, load resistance, maximum efficiency: 2.12 ohms
Number of couples: 27
Heat source: polonium 210, 138-day half-life
Diameter: 4.75 inches
Height: 5.5 inches
Weight: 5 pounds

This generator is working proof of practical thermoelectric power. It should be noted that the efficiency attained was the result of a combination of good efficiency thermoelectric materials, substantial design and a 100% thermally efficient heat source. The demonstrated efficiency may be debated from the standpoint of economics, but it remains a tribute to those who brought about its existence. This same group has since built and operated an advanced design generator of greater than 7% over-all efficiency.

### Conclusions

The problems confronting the development and design of thermoelectric generators which extract maximum usefulnes from today's semimetal thermoelectri materials have been presented. Th discussion of these problems serves onl to define their probable boundaries. Th solutions suggested indicate only that th problems have been attacked, not solved

An example has been given as proo that the concepts defined herein hav been reduced to practice and tha thermoelectric generation is practica today for many applications which ar difficult or uneconomical to accomplis with conventional power-generatio methods.

### References


1. DESIGN PARAMETERS FOR OPTIMIZING TH EFFICIENCY OF THERMOELECTRIC GENERATOR UTILIZING P-TYPE AND N-TYPE LEAD TELLURIDE R. W. Fritts. *AIEE Transactions*, pt. I (Com munication and Electronics), vol. 78, Nov. 195 pp. 817–20.

2. THERMOELECTRIC GENERATORS, A. F. Ioffe *Izvest Akudemii Nauk SSSR*, Moscow, USSR no. 1, Jan. 1956.

3. SNAP III—PRACTICAL POWER FROM RADIO ISOTOPES, M. Barmat, G. M. Anderson, E. W Bollmeier. *Nucleonics*, New York, N. Y., vol. 1 no. 5, 1959.

4. STATUS REPORT ON THERMOELECTRICITY, H F. Straus, B. B. Rosenbaum, P. Maycock. *Memo randum Report 901*, Naval Research Laboratory Washington, D. C., Feb. 1959, p. 21.


# New Materials for Transformer-Rectifier Unit in High-Temperature Aircraft


J. G. HOOP
MEMBER AIEE

D. K. McILVAINE
MEMBER AIEE


AIRCRAFT operating at multi-Mach speeds and high altitudes subject some portions of the electric systems to severe environmental changes. A program is underway to develop a suitable system including an a-c generator with constant-speed drive, a contactor, a circuit breaker, a current transformer, and a transformer-rectifier unit for conversion to direct current. Development and selection of materials for use in the transformer-rectifier are covered in this paper.


Paper 59-883, recommended by the AIEE Air Transportation Committee and approved by the AIEE Technical Operations Department for presentation at the AIEE Summer and Pacific General Meeting and Air Transportation Conference, Seattle, Wash., June 21–26, 1959. Manuscript submitted March 24, 1959; made available for printing April 23, 1959.



J. G. HOOP and D. K. MCILVAINE are with the Westinghouse Electric Corporation, Lima, Ohio.



This work was done at Materials Engineering, Research Laboratory, and Aircraft Equipment Department of Westinghouse Electric Corporation. Air Force Contract No. *AF33(600)35489* with North American Aviation.


### Environment

Electric equipment operated at a 315 C (degrees centigrade) ambient temperature in the low-density air at 80,000 feet altitude may develop hot spots several hundred degrees above the ambient. Storage of aircraft at temperatures far below freezing subjects the electric equipment to moisture condensation and produces pronounced changes in the electrical and mechanical properties of the materials. The materials to be used in this program are evaluated and chosen on the basis of their individual properties and on their compatibility with the other materials. In general, only in organic materials can be expected to have any appreciable life at the higher temperatures to be encountered.

### Performance

The transformer-rectifier unit being developed for high-temperature service is to convert power from a 200-volt 3 phase 400-cycle supply to give a 28 volt d-c output at 50-ampere load. A radio noise filter network is to be provided. Electrical performance of this unregulated lightweight transformer-rectifier unit restricts the minimum num

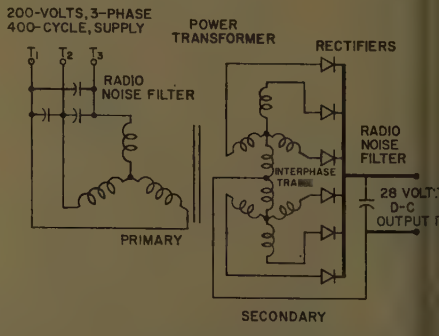


**Fig. 1. Circuit of 50-ampere transformer rectifier power supply**

Fig. 2. Test core assembly

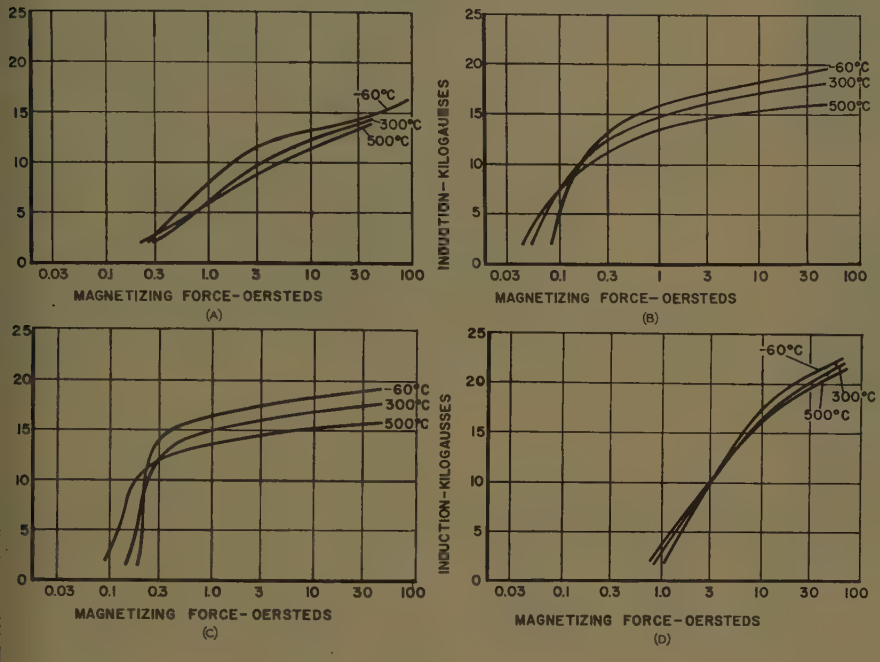


Fig. 3. Magnetization curves

A—4.7% silicon unoriented iron 0.014-inch thick
B—3% silicon oriented iron 0.012-inch thick
C—3% silicon oriented iron 0.004-inch thick
D—27% cobalt oriented iron 0.025-inch thick

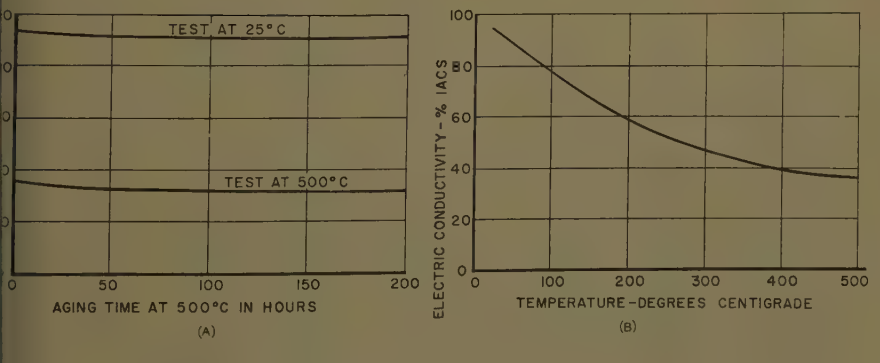


Fig. 4. Conductivity tests of no. 17 AWG copper wire with 0.006-inch nickel plate

A—Versus aging time at 500 C
B—Versus temperature

ber of phases to six. Mechanical considerations discourage the use of a higher number. Regulation and efficiency requirements eliminate consideration of bridge-type circuits with high-temperature rectifiers because of the double voltage drop thus introduced.

## Circuit

Fig. 1 shows a 6-phase double-Y connection with an interphase transformer which permits two rectifiers to operate in parallel at all times, thus reducing the rectifier loading and transformer secondary kilovolt-ampere rating. Although delta-primary connections are preferred for rectifier applications on the basis of a-c harmonic considerations, the Y connection was chosen for this relatively low-power unit because it maintains the output voltage better under a single-phase fault condition. With only two secondary windings per phase, the coil build-up is held to a minimum, and interleaved windings are easily made. Consequently, a low leakage reactance is obtained. Radio noise filtering, as shown, is achieved by straight capacitance filter networks across the input and output circuits. This form was chosen to obtain minimum weight and complexity.

## Magnetic Materials

Choice of a core material from the presently available ferromagnetic alloys called for further investigation of their properties over the broad temperature range to be encountered in service. Special core assemblies suitable for use in an oven were prepared by the steps shown in Fig. 2. Magnetization curves at 500 C, 300 C, and −60 C are given in semilogarithmic plots for 4.7% silicon unoriented iron in Fig. 3(A), 3% silicon oriented iron in Fig. 3(B), (C) for heavy and thin gages respectively, and 27% cobalt oriented iron in Fig. 3(D). Even under heavy magnetizing forces the 4.7% silicon unoriented iron achieves only moderate induction. The 3% silicon oriented iron in both the heavy and thin gages attains a higher maximum induction, but it is quite temperature sensitive except in the region where the curves cross at an induction of about 10 kilogausses. Curves for the 27% cobalt oriented iron show it to be the least temperature sensitive and capable of higher maximum induction than the others. The fact that a relatively high magnetizing force is required with this latter material is not a serious disadvantage for application in this program because the

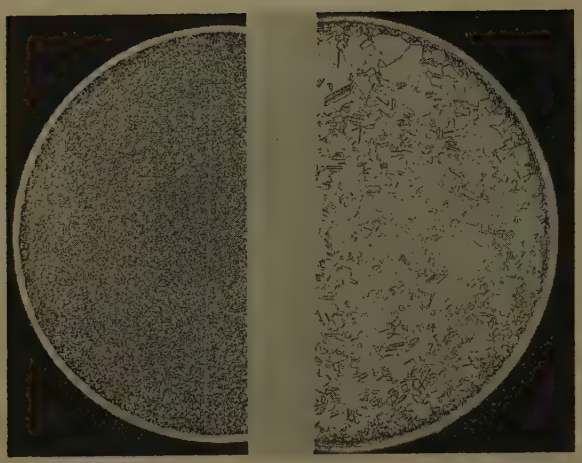

Fig. 5 (left). Effect of temperature aging on nickel-plated copper

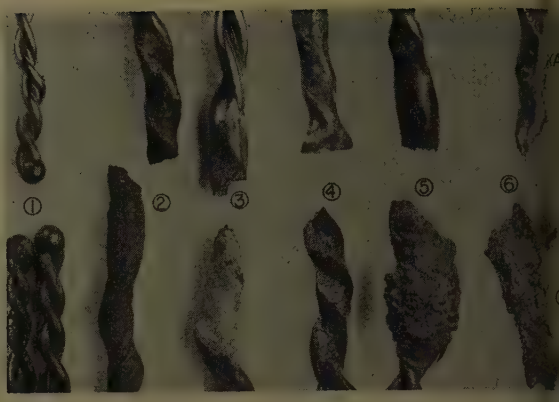


Fig. 6 (right). Effect of temperature aging on conductor joints

Fig. 7 (left). Electric connection—welding bead

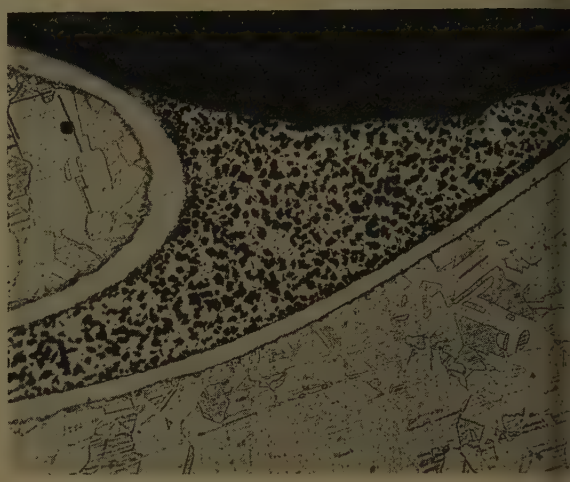

Fig. 8 (right). Electrical connection—photomicrograph of brazed joint

higher induction contributes to weight reduction. However, it should be noted that if a nuclear environment were present, a material with cobalt should not be used because it becomes activated.

## Wire

Because the expected service life at high temperature is only 20 hours, a high degree of oxidation resistance is not required in the magnet wire to be employed in the transformer windings. Tests indicate that copper wire is adequately protected when covered by a 0.0006-inch plating of nickel. The relatively minor effect of 500 C aging in air on the electric conductivity of this type of wire is shown in Fig. 4(A). The bottom curve in that figure and the one in Fig. 4(B) serve to illustrate the fact that copper, like all other common conductors, has a temperature coefficient which causes its conductivity to decrease to less than half of its room temperature value when heated to 300 C. Photomicrographs from etched cross sections of nickel-plated copper wires before and after aging for 200 hours at 500 C give a visual picture in Fig. 5 of the metallurgical effects. In the left-hand view, the outer layer of nickel covers an inner copper core made fine grained by its process of production. High-temperature aging produced an increase of grain size by recrystallization in the copper core of the right-hand view. It also left a thin reacted layer under the nickel coating. Any deterioration in the layer copper beneath the nickel constitut such a small portion of the total cro section that the effect on over-all co ductivity is small, as was shown in Fi 4(A). The evaluation of other conduct materials indicates that silver and alum num may be considered as alternates, b

**Table I. Magnet Wire**

Copper, 0.0006-Inch Nickel Plate, 400 C Insulation

| Wire Gage | Wire Diameter | | | Bare Copper Resistance Ohms/M-ft. | | | Plated Wire Resistance Ohms/M-ft. | | |
|---|---|---|---|---|---|---|---|---|---|
| | Bare | Plated | Insulated | −55 C | +20 C | 400 C | −55 C | +20 C | 400 |
| 6 | 0.1620 | 0.1633 | 0.1700 | 0.28 | 0.40 | 0.98 | 0.28 | 0.39 | 0.9 |
| 7 | 0.1443 | 0.1456 | 0.1520 | 0.35 | 0.50 | 1.24 | 0.35 | 0.49 | 1.2 |
| 8 | 0.1285 | 0.1298 | 0.1360 | 0.44 | 0.63 | 1.56 | 0.44 | 0.62 | 1.5 |
| 9 | 0.1144 | 0.1157 | 0.1216 | 0.56 | 0.79 | 1.97 | 0.56 | 0.79 | 1.9 |
| 10 | 0.1019 | 0.1032 | 0.1090 | 0.70 | 1.00 | 2.49 | 0.69 | 0.99 | 2.4 |
| 11 | 0.0907 | 0.0920 | 0.0975 | 0.89 | 1.26 | 3.14 | 0.88 | 1.25 | 3.1 |
| 12 | 0.0808 | 0.0821 | 0.0873 | 1.12 | 1.58 | 3.96 | 1.11 | 1.55 | 3.9 |
| 13 | 0.0720 | 0.0733 | 0.0783 | 1.41 | 2.00 | 4.98 | 1.40 | 1.98 | 4.7 |
| 14 | 0.0641 | 0.0654 | 0.0702 | 1.78 | 2.52 | 6.29 | 1.77 | 2.50 | 6.2 |
| 15 | 0.0571 | 0.0584 | 0.0631 | 2.24 | 3.18 | 7.92 | 2.22 | 3.16 | 7.7 |
| 16 | 0.0508 | 0.0521 | 0.0566 | 2.83 | 4.02 | 10.0 | 2.80 | 3.98 | 9.9 |
| 17 | 0.0453 | 0.0466 | 0.0510 | 3.56 | 5.05 | 12.6 | 3.52 | 4.98 | 12.5 |
| 18 | 0.0403 | 0.0416 | 0.0458 | 4.50 | 6.39 | 15.9 | 4.44 | 6.30 | 15.7 |
| 19 | 0.0359 | 0.0372 | 0.0413 | 5.67 | 8.05 | 20.0 | 5.59 | 7.93 | 19.7 |
| 20 | 0.0320 | 0.0333 | 0.0371 | 7.12 | 10.1 | 25.2 | 7.02 | 9.93 | 24.8 |
| 21 | 0.0285 | 0.0298 | 0.0335 | 9.02 | 12.8 | 31.9 | 8.84 | 12.5 | 31.3 |
| 22 | 0.0253 | 0.0266 | 0.0302 | 11.4 | 16.2 | 40.3 | 11.2 | 15.9 | 39.6 |
| 23 | 0.0226 | 0.0239 | 0.0273 | 14.3 | 20.3 | 50.6 | 14.0 | 19.6 | 49.2 |
| 24 | 0.0201 | 0.0214 | 0.0247 | 18.2 | 25.7 | 64.0 | 17.7 | 25.1 | 62.3 |
| 25 | 0.0179 | 0.0192 | 0.0224 | 22.8 | 32.4 | 80.8 | 22.2 | 31.5 | 78.4 |
| 26 | 0.0159 | 0.0172 | 0.0203 | 28.9 | 41.0 | 102 | 27.9 | 39.6 | 98.6 |
| 27 | 0.0142 | 0.0155 | 0.0183 | 36.2 | 51.4 | 128 | 34.9 | 49.6 | 123 |
| 28 | 0.0126 | 0.0139 | 0.0166 | 46.0 | 65.3 | 163 | 44.2 | 62.7 | 156 |
| 29 | 0.0113 | 0.0126 | 0.0152 | 57.2 | 81.2 | 202 | 54.7 | 77.4 | 194 |
| 30 | 0.0100 | 0.0113 | 0.0138 | 73.2 | 104 | 260 | 69.6 | 98.6 | 246 |

Fig. 9 (left). Coating tower for magnet wire

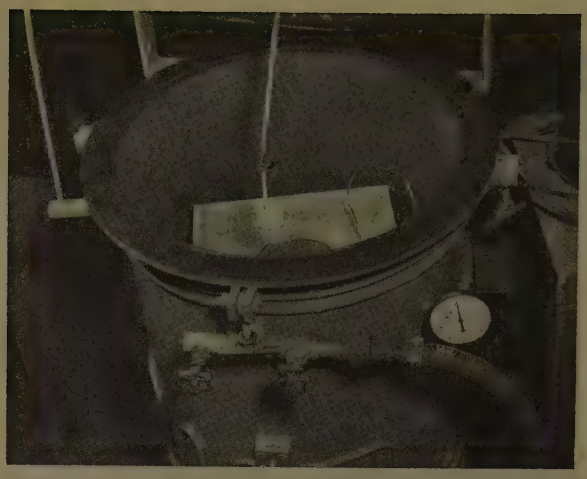

Fig. 10 (right). Vacuum impregnating furnace for insulating compounds

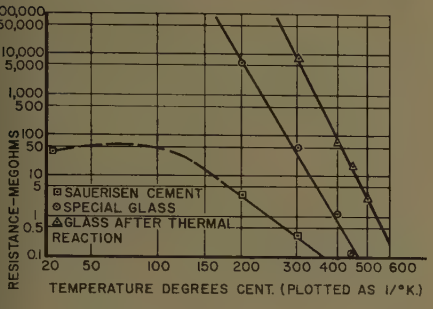


Fig. 11 (left). Insulating compounds resistivity versus temperature, potted test coils, vacuum impregnated

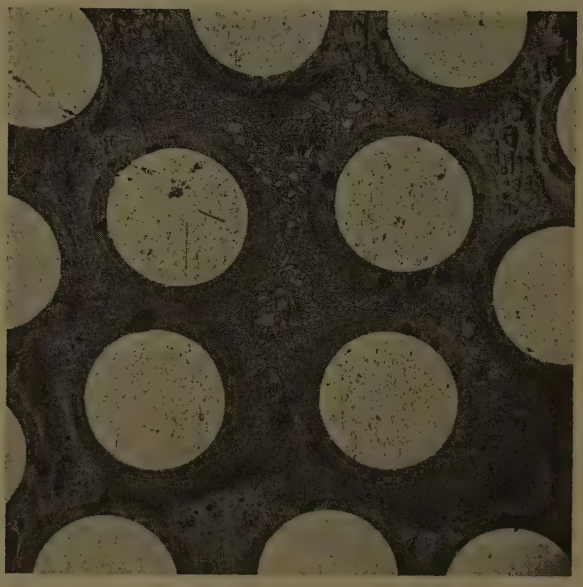

Fig. 12 (right). Insulating compound reacted in electric winding

silver will be more costly and aluminum connections are more difficult.

## Joints

A variety of techniques have been tried for producing twisted conductor joints as shown in Fig. 6. Row (A) illustrates the condition of electric joints before test and row (B) the change caused by aging 100 hours at 540 C. These specimens were prepared by 1. arc welding in inert gas, 2. brazing with 72% silver and 28% copper, 3. brazing with 50% silver, 16% zinc, 18% cadmium, and 16% copper, 4. brazing with 50% silver, 34% copper, and 16% zinc, 5. brazing with 80% copper, 15% silver, and 5% phosphorus, and 6. brazing silver with 80% copper, 15% silver, and 5% phosphorus. The welded junctions deteriorated very little as a result of aging. A photomicrograph in Fig. 7 shows the general good condition of the weld bead and its junction with the conductor which was protected by the nickel coating extending intact into the bead. The brazing alloys containing phosphorus deteriorated badly, but the high silver alloys produced a good joint. A photomicrograph from a section of the fourth joint, as shown in Fig. 8, is typical of the better brazed joints.

## Wire Insulation

Successful wire insulation for coating of nickel-plated copper must produce a suitable adherent insulating layer on the final conductor in order to be capable of withstanding deformation associated with the winding process and also retain good properties when heated in the finished winding. The desired combination of properties has been attained by the use of an inorganic pigment in a resin coating on the magnet wire. The first four columns in Table I give the nominal diameters of "bare," "plated," and "insulated" wires of this type for a range of sizes from 6–30 (American Wire Gage).

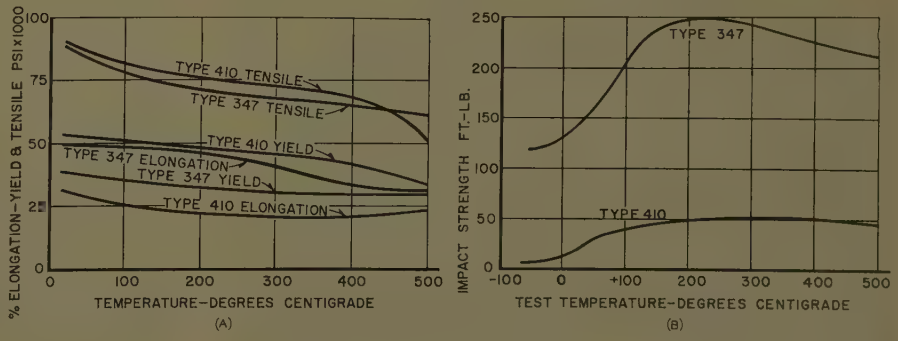


Fig. 13. Structural materials

A—Mechanical properties versus temperature
B—Impact strength versus temperature for stainless steel

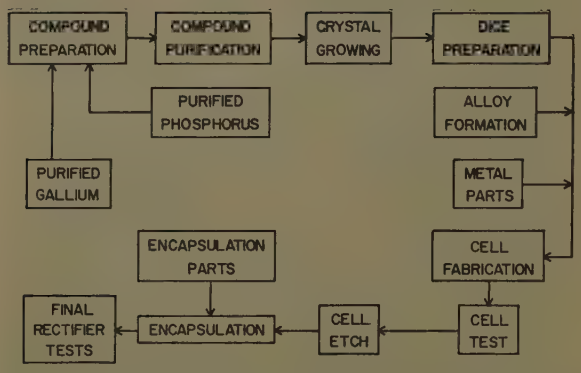


**Fig. 14. Semiconductor crystals development flow chart for gallium phosphide rectifiers**

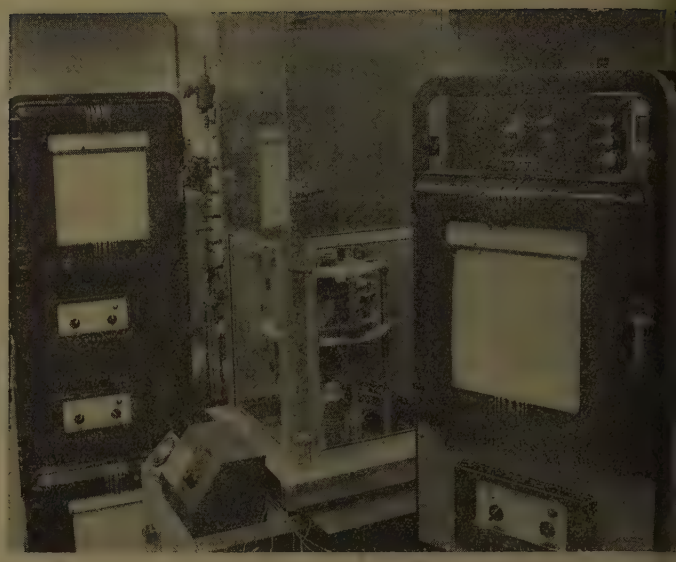

**Fig. 15 (right). Crystal pulling furnace**

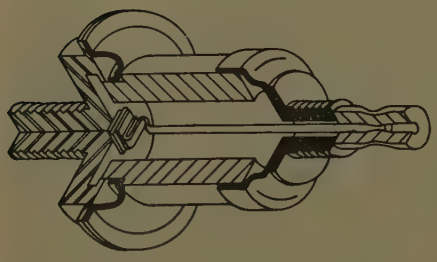

**Fig. 16. High-temperature rectifier device configuration**

In the remaining columns the tabulation shows a comparison of bare and nickel-plated wire resistances at temperatures of −55 C, +20 C, and 400 C. It may be noted that the plated wire has an appreciably lower resistance than the corresponding bare wire in the higher gages. This is due to the fact that the same nominal gage size has been here assigned to wires with the same copper cross section. The change in resistance between −55 C and +400 C is more than threefold. Application of this type of wire insulation has been done in an experimental enameling tower whose bottom or entering end appears in Fig. 9. Heating a winding of wire so coated breaks down and drives off a portion of the resin to leave a deposit forming an inorganic coating on the wire.

Subsequent vacuum impregnation with glass in a furnace of the type shown in Fig. 10 produces a solid winding structure impervious to penetration by moisture. Impregnation involves a preliminary heating under vacuum in the upper furnace section, a dip into molten glass, and retraction into the upper hot zone where admission of inert gas or air forces molten glass into the winding's voids. Simple glasses formed of low melting oxides penetrate best during impregnation because they are more fluid than those with higher melting points. However, the lower melting point glasses generally have lower volume resistivity at a given temperature than do those with higher melting points. Special glass mixtures have been devised which react upon further heating and yield a higher resistivity. In Fig. 11 the effect of such a reaction on resistivity at elevated temperatures is shown by circles for measurements taken before and by triangles for measurements taken after the extended heating. The increase in resistivity at 400 C, for example, is one-hundredfold. The curve represented by squares gives the resistivity values for a common commercial cement, as a comparison. Wires embedded in the reacted compound are shown in Fig. 12.

## Structural Materials

Structural members need to maintain good mechanical properties over the full range of temperatures to be encoun

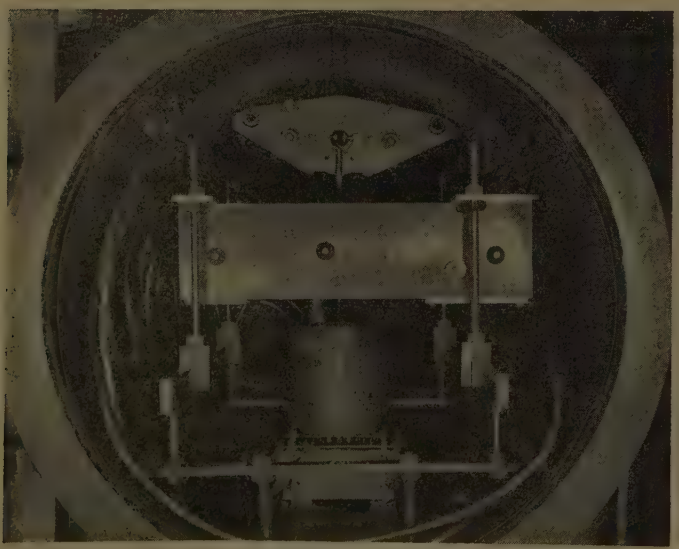

**Fig. 17. Vacuum furnace for coating metal foil**

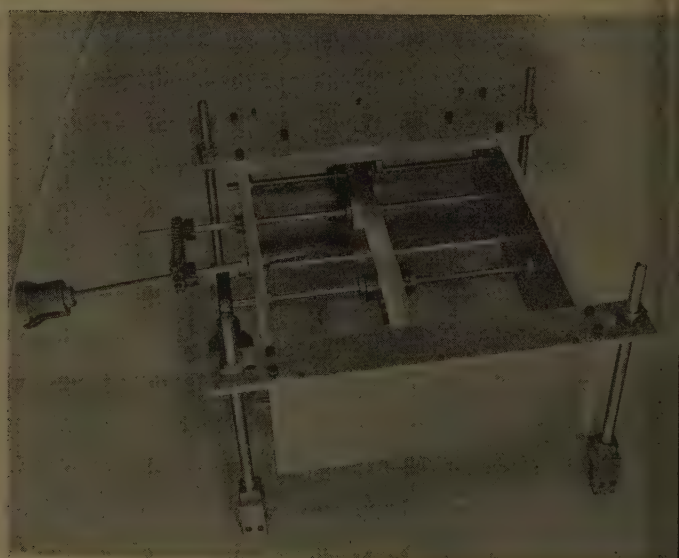

**Fig. 18. Foil reeling fixture**

Fig. 19 (left). Foil winder for condenser assembly

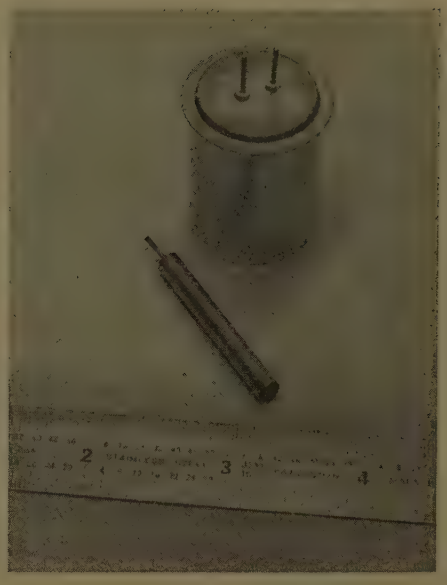

Fig. 20 (right). Capacitor encapsulations

tered. The elongation, yield, and tensile strengths of two typical alloy steels are shown in Fig. 13(A). Impact strengths of the same alloys, austenitic type *347* and martensitic type *410*, are given in Fig. 13(B). The advantage of the type *347* alloy steel is particularly evident in its superior impact strength at low temperatures.

## Rectifiers

Semiconductors to be considered for use as high-temperature rectifiers need to be capable of operation at temperatures even higher than the maximum ambient in order to compensate for extra losses produced by the higher forward voltage drop found in this class of materials. Rectification at temperatures above the 315 C ambient has been observed in gallium arsenide, gallium phosphide, and silicon carbide. Gallium phosphide has been given prime consideration for this particular application because it has a relatively low forward drop of about 2 volts at 500 C, its maximum operating temperature is less limited than is the gallium arsenide which has a ceiling of about 400 C, and when compared with silicon carbide, it has a lower forward drop and better low-temperature performance.

The semiconducting compound gallium phosphide presents all the production problems involved in making device-grade germanium and silicon rectifiers, plus the additional problems that two elements rather than one are involved and the high-temperature reaction pressure at formation of the compound is over 10 atmospheres. The requirements for large crystals with a high degree of perfection to be formed from two very pure elements with exact stoichiometry of the compound call for extreme care throughout the manufacturing processes represented by the flow chart appearing in Fig. 14. Equipment used for growing single crystals from a pool of molten gallium phosphide is shown in Fig. 15. The induction heating coil is at the bottom of the enclosure, and the magnetic suspension drive is visible at the top of the window. The desired degree of perfection has not yet been achieved in all the steps for production of gallium phosphide rectifiers. However, the form of a finished unit is shown by the phantom view in Fig. 16.

## Capacitor

High-temperature capacitors need a dielectric material structurally able to withstand wide temperature changes while maintaining usable dielectric characteristics. Vacuum deposited quartz on thin aluminum foil is a good combination which also has the advantage of producing a low bulk factor in the finished capacitor. A 12-microfarad unit may occupy a volume as small as 2 cubic inches.

The vacuum chamber used to coat foil for production of this type of capacitor is shown in Fig. 17. Inside the cylindrical shield at the bottom is a tantalum crucible from which quartz is continuously evaporated when heated by electron bombardment. To replace quartz evaporated from the crucible, a feed mechanism at the top of the chamber introduces more through a tube, as it is needed. Manipulation of the foil to be double coated is performed by a mechanism in the central rectangular framework. A detail view of it is given in Fig. 18. The mechanical driving of the left-hand coupler is done by a shaft extending through a vacuum seal at the rear of the chamber.

Capacitors are produced by concentric winding of two double quartz coated strips with a slight offset to provide a portion at each end for attaching leads. The motorized winder used for this operation appears in Fig. 19. Two forms of

Fig. 21. Testing high-temperature capacitors

encapsulation for the finished capacitors are shown together with a scale to gage their size in Fig. 20. The vacuum-tight metal enclosures have high-alumina insulated terminals for connection of external leads. Checking capacitance of finished units over a wide temperature range is done with the bridge-type instrument appearing at the left of Fig. 21 while connected to the bank of four thermally insulated test chambers. Over the −50 to +450 C range, the capacitance temperature coefficient is about 0.01% per degree centigrade.

## Conclusion

The evaluation of these materials and components indicates a successful transformer-rectifier power supply can be built with the circuit configuration described.

# Trends in Ground Bed Design for Cathodic Protection of Underground Structures

A. P. LANDRY
ASSOCIATE MEMBER AIEE

I. N. HOWELL, JR.
ASSOCIATE MEMBER AIEE

CATHODIC protection of underground structures for the mitigation of corrosion to those structures has long been an established means for controlling corrosion. It is interesting to note that this paper deals primarily with a relatively new technique in the field of corrosion, proposed originally by the man given credit in "Who's Who" for the development of cathodic protection. This man, Mr. R. J. Kuhn, a consulting engineer in New Orleans, La., has made several contributions in the field of corrosion control. The original idea of cathodic protection is one of impressing a direct current in such a way as to counteract the tendency of the galvanic or man-made electric currents which tend to leave the underground structures, thereby counteracting the loss of metal through the electrochemical process known as corrosion or electrolysis.

Cathodic protection of underground structures using galvanic anodes composed of zinc or magnesium has many applications in industry today. When protection requirements of the structure exceed that available from galvanic anodes, a method using an impressed current must be employed. The anode material can then be any expendable metal desired. The conventional distributed anode type of ground bed, in which manufactured anodes are placed in a suitable horizontal array near the surface of the earth, is in wide use today. Anodes commonly used in the conventional ground bed are graphite and high-silicon cast iron.

Southern Bell Telephone and Telegraph Company installed the first ground bed for protection of underground cable sheaths in New Orleans in 1931. It was a conventional ground bed using graphite anodes. Seven more conventional ground beds were installed in the period from 1931 to 1951.

Since Southern Bell has invested more than five million dollars in underground cables in the New Orleans area, and 92% of the cables have lead sheaths, the problem of cathodic protection is an important one. Fig. 1 shows the number of sections of underground cable which had to be replaced in the period from 1951 to 1955. These sections failed because of sheath breaks due to corrosion and had to be replaced with new cable. The cost of the replacement cables is also shown in Fig. 1. Since the total cost of replacing corroded sections exceeded 216,000 dollars for this period, efforts were made to speed up the cathodic protection program as much as possible. Nine more conventional ground beds were installed in this period.

## Experience with Conventional Ground Beds

Efforts to speed up the cathodic protection program were hampered by certain characteristics of the conventional ground bed. Considerable engineering and survey time was consumed in finding locations suitable for construction of the ground bed and the obtaining of the necessary right-of-way.

Close co-ordination was essential with other utilities having underground structures in the area. Extensive tests with New Orleans Public Service, Inc., and Sewerage & Water Board of New Orleans were required with each new installation. These joint tests were used to determine the extent of influence from the ground bed, and the amount of drainage required to offset this influence. Costs involved in making the joint tests ran high; as high as 3,900 dollars in total cost on a particular ground bed installation.

Another factor of importance was the fact that so much of the rectifier output was required for drainage on structures other than the one under primary consideration. As much as 36% of the rectifier current output was required to offset undesirable influences to other structures. This meant higher operating costs and shorter life ground beds than otherwise required.

It had been found through experience that if a minimum horizontal separation of 150 feet was maintained between the ground bed and other structures, under

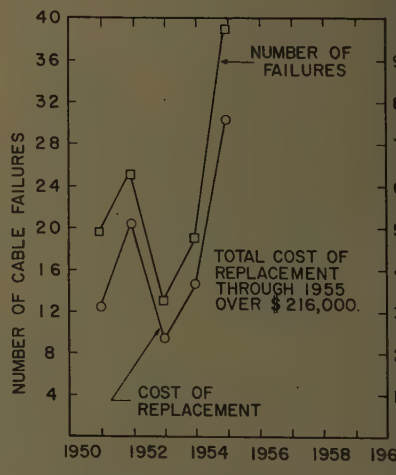


**Fig. 1. Cable failures and cost of replacement since 1951 for New Orleans, La.**

Paper 59-820, recommended by the AIEE Chemical Industry Committee and approved by the AIEE Technical Operations Department for presentation at the AIEE Summer and Pacific General Meeting and Air Transportation Conference, Seattle, Wash., June 21–26, 1959. Manuscript submitted March 19, 1959; made available for printing May 22, 1959.

A. P. LANDRY and I. N. HOWELL, JR., are with Southern Bell Telephone and Telegraph Company, New Orleans, La., and Atlanta, Ga., respectively.

The authors wish to thank all who co-operated in the preparation of this paper.

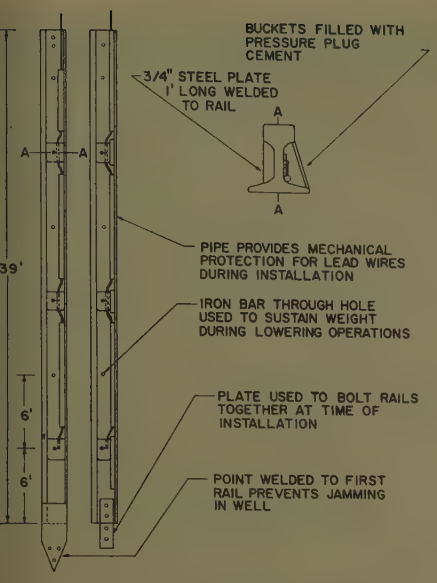


**Fig. 2. Rail anode fabrication details**

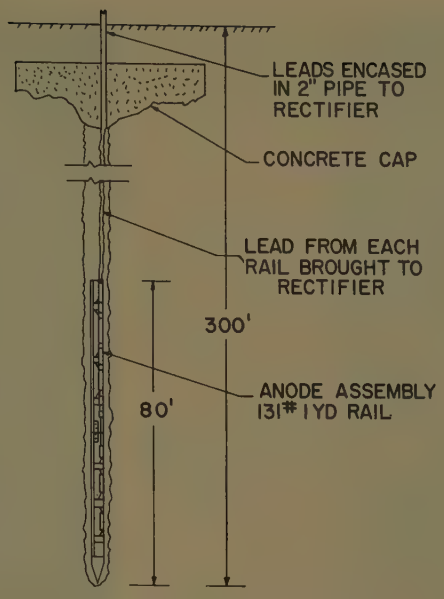


**Fig. 3. Deep ground bed installation**

irable influences could be reduced to negligible values with a drainage current not to exceed 10 amperes. It is, of course, obvious that this separation, while being sufficient in New Orleans, may not be enough in other areas. These criteria would, of necessity, have to be determined for any specific application by tests. Serious consequences could otherwise result. These separation criteria were substantiated by joint tests made by Southern Bell and New Orleans Public Service, Inc., in 1956. The results of these tests are shown in the Appendix.

During 1955 and early 1956, a total of 13 additional shallow ground bed sites were located. This seemed to have exhausted the supply of available locations.

## Deep Vertical Ground Bed

The idea for the deep vertical type of ground bed was obtained from Mr. R. J. Kuhn, Consulting Engineer, and Mr. S. E. Trouard,[1] New Orleans Public Service, Inc. The deep ground bed had been used successfully for cathodic protection of steel gas mains in areas where conventional ground beds proved impracticable. The ground bed as used by New Orleans Public Service, Inc., was essentially composed of used rail in a well 8 inches in diameter by 250 feet deep.

The basic design as used by New Orleans Public Service, Inc., was adapted for application to Southern Bell requirements. The size of the anode material was increased to compensate for larger current drains (about 10 amperes) required. Other changes were made to facilitate the fabrication and handling of the anode by a local contractor.

Fig. 2 shows general fabrication details of the rail anode assembly as used by Southern Bell. Two 39-foot used rails weighing 130 pounds per yard are employed. One anode lead from each rail is brought to the ground surface. Each lead is attached to the rail in three places. Each point of attachment is protected by a welded bucket filled with pressure plug cement, and a tar sealing compound is poured after heating. Each lead is threaded through metallic pipe welded the length of the rail for mechanical protection during installation. The lead from the first rail is threaded through the pipe on the second or top rail at the time of installation.

A cone-shaped point is welded to the first rail to avoid possible jamming in the well during the lowering operation. The two rails are bolted together with steel joint plates at the time of installation.

**Fig. 4. Rail anode showing cone point**

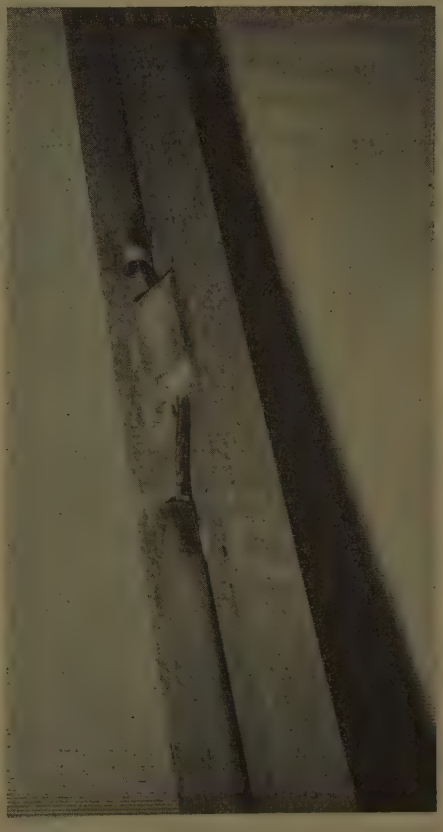

**Fig. 5. First rail connection**

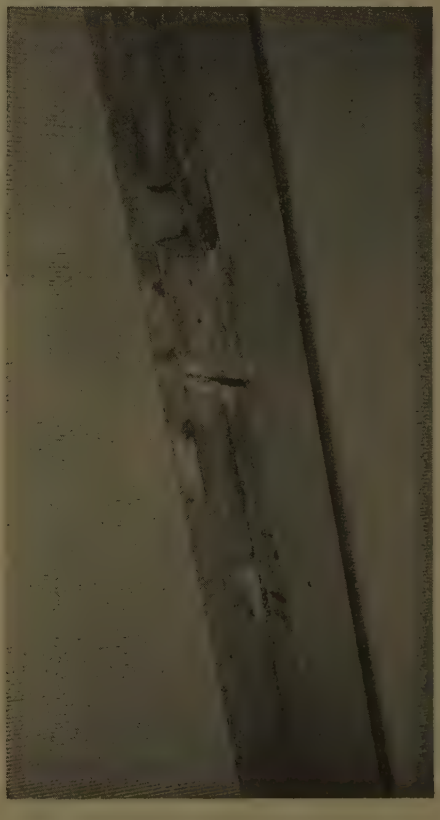

**Fig. 6. Second rail connection**

Fig. 7 (left). Drill rig

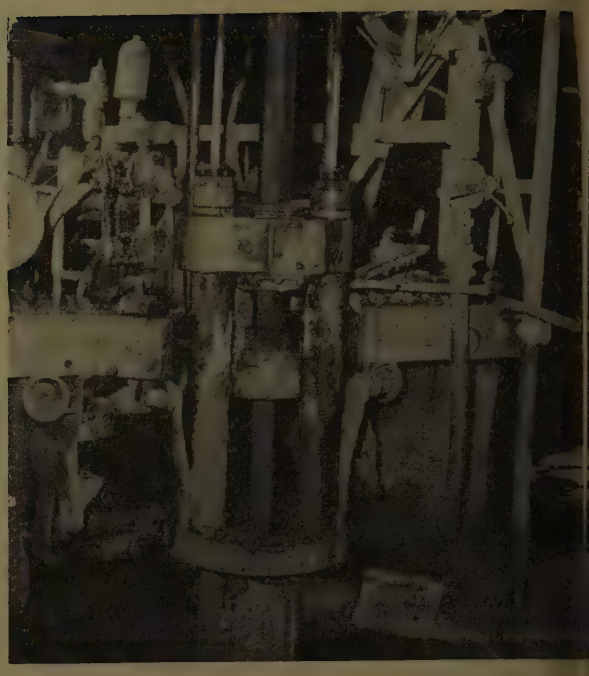

Fig. 8 (right). Close-up of drill rig

Fig. 9 (left). End of lowered first rail

Fig. 10 (right). Joining rails

This forms a completed anode assembly approximately 80 feet long, weighing about 3,500 pounds.

The completed assembly is lowered into a well 10 inches in diameter by 300 feet deep drilled by a local contractor. Fig. 3 shows a typical ground bed installation. Since the well has no casing, the lowering operation takes place immediately after drilling is completed. The hole will usually remain open somewhat in excess of 6 hours which permits adequate lowering time. The assembly is lowered with galvanized steel strand which is cut off and dropped into the well after completion. Tests were made in 1956 to determine if the steel strand had any undesirable influence; none was detected.

No special backfill is used in addition to the regular amount of drilling mud used by the contractor in his drilling operations. The hole closes in of its own accord in a day or so.

Figs. 4–11 show equipment and installations. The estimated useful life of this ground bed is calculated on the basis of failure after two thirds of the metal is consumed. For current densities used (8 to 10 amperes per ground bed), a useful life of 10 to 13 years is expected.

Total cost of the installed anode assembly is approximately 1,200 dollars. The cost of a shallow ground bed of equal life would cost approximately 1,000 dollars, plus an undetermined amount spent on co-ordinated tests.

A cost breakdown showing the various costs involved in fabrication and installation of the deep vertical ground bed is shown in the Appendix.

## Results Using Vertical Ground Bed

Fig. 12 shows the number of cable failures since 1951. The curve shows a marked decline in the period after 1955. The number of failures has decreased from 39 in 1955 to a total of 3 for 1958. The use of the deep ground bed has enabled the cathodic protection program to proceed with minimum delay and achieve these results.

Ground bed resistances have been quite satisfactory. There has been a

Fig. 11 (left). Rectifier installation

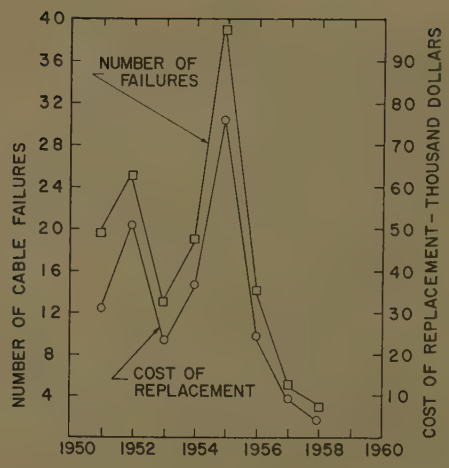


Fig. 12 (right). Cable failures and cost of replacement

evidence of gas blocking in approximately 3 years of operation. Table I shows some typical values of over-all circuit resistance for conventional and deep ground beds.

Ground bed resistances in New Orleans have been extremely satisfactory. It would be appropriate, when locating beds of this type in other areas, to make soil resistivity tests by vibro-ground, earth resistivity megger, or other satisfactory means to the expected drilling depth so that depth selection might be made to facilitate an economical and satisfactory installation. No tests of this type were made, however, in the New Orleans installations since it was well known from existing data what the results should be.

**Table I. Typical Circuit Resistances for Conventional and Deep Ground Beds**

| Ground Bed Designation | Type | Over-all Circuit Resistance (Ohms) |
|---|---|---|
| Richard & Eighth | Conventional | 1.28 |
| Franklin & Perry | Conventional | 0.62 |
| 5th & Ave. "K" | Conventional | 1.33 |
| Aviators & Bancraft | Conventional | 0.89 |
| Clara & Jena | Conventional | 1.07 |
| Ave. "K" & 8th | Conventional | 1.73 |
| St. Charles C.O. | Conventional | 0.80 |
| Rayne & Van | Conventional | 1.55 |
| 5th & Belanger | Conventional | 1.15 |
| Toulouse & Bourbon | Conventional | 1.17 |
| Maple & Oak | Deep | 0.46 |
| Coliseum & Joseph | Deep | 0.39 |
| Dorgenois & Columbus | Deep | 0.35 |
| Monroe & Solon | Deep | 0.45 |
| Coliseum & Louisiana | Deep | 0.38 |
| Burgundy & Floor | Deep | 0.39 |
| Painters & Benefit | Deep | 0.31 |
| Romap & Spain | Deep | 0.36 |
| Marais & Montegut | Deep | 0.33 |
| Erato & Roman | Deep | 0.62 |

## Deep Ground Bed Using High-Silicon Cast Iron

A new anode assembly has been developed and is being installed by Southern Bell using high-silicon cast iron. The new assembly is designed with a useful life of indefinite length (calculated in excess of 100 years). The cost of the completed assembly is 45% that of the rail and total weight is 500 pounds or 15% the weight of the complete rail assembly.

The fabrication details are shown in Fig. 13. Four 3-inch-diameter 60-inch-long high-silicon cast iron anodes are strapped to a length of channel iron which has been painted with a coal tar enamel. The channel iron is intended to hold the assembly in a vertical array during lowering and until the hole settles in around the anodes. The assembly is lowered into a 10-inch-diameter 200-foot-deep well, with a 1/2-inch manila rope. This avoids placing undue strain on lead connections and also insures electrical remoteness of the ground bed.

The anode assembly using high-silicon cast iron appears to offer a ground bed of equal electrical performance at lower initial cost, lower maintenance costs, and much longer useful life. From the data available at the present time, it appears that the high-silicon cast-iron assembly has advantages which make it preferable to the rail assembly.

## Other Deep Ground Bed Designs

Interstate Oil Pipe Line Company in Shreveport, La., has developed and has used a deep ground bed of graphite rods with backfill at depths up to 250 feet. General details are shown in Fig. 14. Thirty-three, 3-inch by 60-inch graphite rods are assembled to form a continuous anode 175 feet in length. The anode is centered in an $8^5/_8$-inch casing filled with coke-breeze backfill. The anode leads are brought to the surface; one from the top of the graphite anode assembly and one from the casing. Expected life is over 20 years at currents of approximately 30 amperes. Ground bed resistances of less than 1 ohm are reported.

Fig. 15 shows how Interstate plans to use a ground bed using high-silicon cast-iron anodes. A coke-breeze backfill will be used.

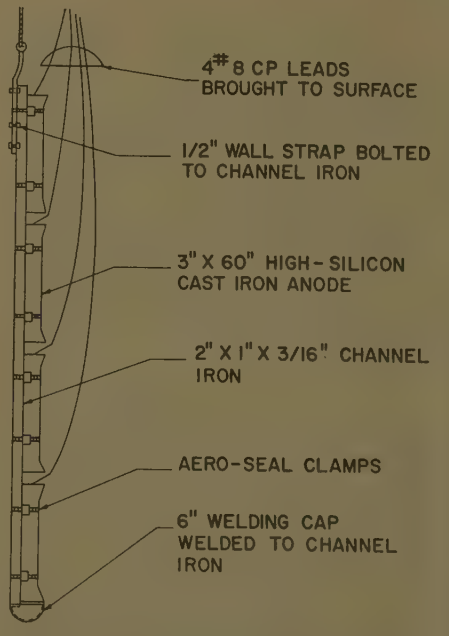


Fig. 13. High-silicon cast iron anode

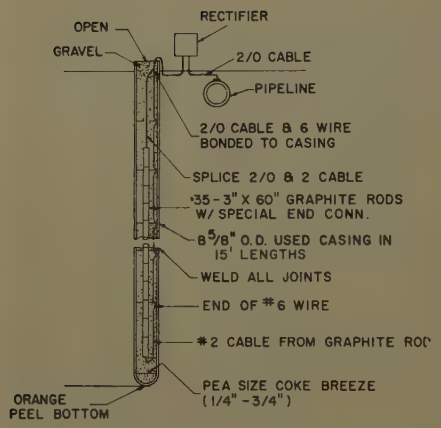


**Fig. 14. Installation by Interstate Oil Pipe Line Company using graphite anodes**

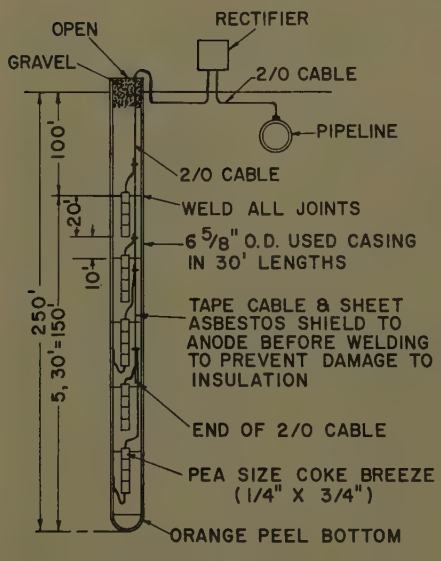


**Fig. 15. Installation by Interstate Oil Pipe Line Company using high-silicon cast iron anodes**

The Chesapeake and Potomac Telephone Company has installed four deep ground beds in the vicinity of the Pentagon Building in Washington, D. C. The anode assembly used is shown in Fig. 16. Two 3-inch by 60-inch high-silicon cast-iron anodes are held together by a collar and short piece of steel strand. One anode lead is brought to the surface. The assembly is lowered into a 100-foot well using manila rope. No special backfill was used.

The four deep ground beds are augmented by duct-type high-silicon cast-iron anodes. Total expected delivery is 32.7 amperes at 25 volts which is 83% voltage capacity and 71% current capacity of the silicon rectifier used. Overall circuit resistance is 0.77 ohm.

The Willmut Gas and Oil Company in Mississippi has used deep ground beds backfilled at depths of 350 feet.[2] The anode assembly is made up of high-silicon cast-iron anodes attached to a 1-inch metallic pipe used to lower the anodes into the well. A coke-breeze backfill is pumped through the pipe until it flows from the top of the hole. The pipe is then removed by means of a loose coupling at the anode assembly to achieve electrical remoteness of the ground bed. Two main header wires are brought to the surface. Anode to earth resistances of less than 1 ohm have been achieved with no evidence of gas blocking after 1 year of operation.

The method developed by Steele and Associates, Inc., of Atlanta, Ga., makes use of high-silicon cast-iron anodes in a 6-inch-diameter by 200-foot-deep well. The anodes are strapped to a 3/4-inch plastic pipe as shown in Fig. 17. The plastic pipe is used to lower the anodes and to pump backfill of standard drilling mud, bentonite clay, aqua gel, or equivalent, into the well. The plastic pipe, which assures electrical remoteness of the ground bed, is left in the well in the event it becomes necessary to break gas blocking at some future date. This remoteness which is achieved is a relative quantity and refers to other installation techniques which may involve the use of metallic stranded cable or metallic pipe for lowering the assembly into place. Steele and Associates feel that this plastic pipe, which is left in the ground, may be used to flush the anode installation for purposes of breaking any gas blocking should it occur at some future date. Some 50 installations of similar nature have now been installed by these engineers.

## Conclusions and Trends

Many problems which have been encountered when applying cathodic protection to underground structures have been alleviated by the use of the deep vertical ground bed. Extensive, coordinated tests with other utilities were made unnecessary by mutual agreement since the adverse influence on other structures are undetectable with present instrumentation. The deep ground bed using high-silicon cast iron has a very long useful life, and does away with expensive ground bed replacements. The use of backfill in higher resistance soils has been successful in lowering ground bed resistances to quite acceptable values.

As more experience is gained with the newer designs of deep ground beds, it is expected that improvements and refinements will be made. As improved anode materials and drilling techniques

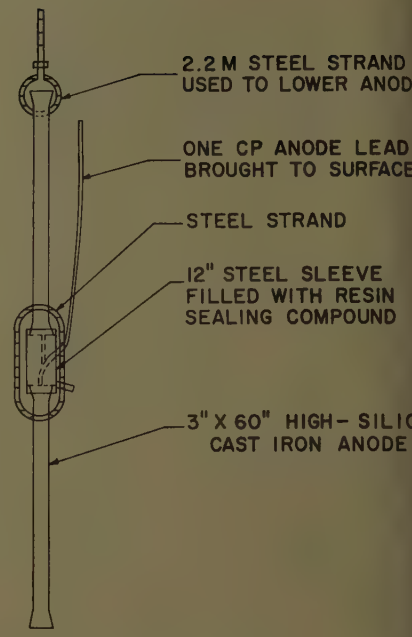


**Fig. 16. Anode assembly used by the Chesapeake & Potomac Telephone Company**

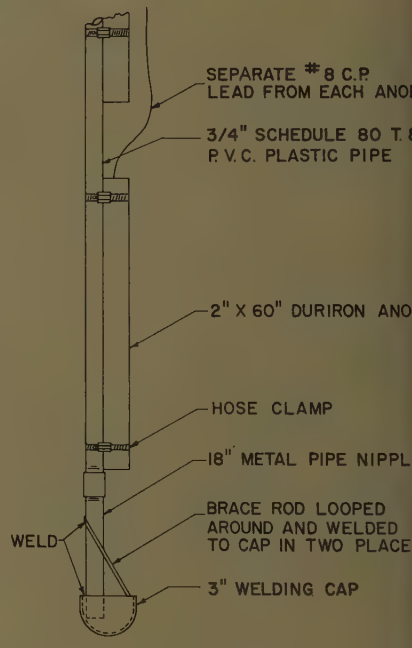


**Fig. 17. Steele & Associates, Inc., anode assembly**

are developed, deep ground beds should become attractive for application of cathodic protection where it is not practical at the present time. The deep ground bed has answered a real need in New Orleans and will continue to serve well in the years to come.

## Appendix

The following table lists the cost of major items involved in the fabrication and installation of the deep ground bed using rail. Figures are approximate and reflect (h

average of figures which have been encountered in the past.

**Typical Costs of Rail Ground Bed**

| | |
|---|---|
| 3,300 pounds used steel rail | $ 330.00 |
| 700 feet no. 6-type *RR* wire | 210.00 |
| Fabrication charges | 170.00 |
| 350 feet 10*M* galvanized steel cable | 30.00 |
| Pipe, miscellaneous steel, etc. | 70.00 |
| Labor and equipment for lowering anode into well | 90.00* |
| Anode well (10 inches diameter by 300 feet deep) | 300.00 |
| Total | $1,200.00 |

* This item is variable over wide ranges due to dependence on completion of drilling operation by well contractor.

Fig. 18 shows a plot of the results obtained in tests performed jointly by Southern Bell Telephone and Telegraph and New Orleans Public Service, Inc. As indicated in Fig. 18 two ground beds were installed in a vacant lot; one a deep ground bed using a rail anode assembly, the other a test ground bed composed of steel rods 5/8 inch diameter.

Voltage gradient measurement were made using two copper sulfate half-cells. Readings were taken with one half-cell held stationary at a remote location while the other half-cell was moved to various locations throughout the area. Readings were recorded with the rectifier on and with rectifier off for both the conventional ground bed and the deep ground bed. The difference between the "rectifier on" readings and "rectifier off" readings is plotted as a function of distance in Fig. 18. The data recorded for the deep ground bed did show some slight variations, but they were negligible when plotted on the scale used.

The change in earth potential due to the conventional ground bed is appreciable up to distances of 150 feet, while the changes due to the deep ground bed are negligible at all distances.

**Fig. 18. Plot of results using two ground beds**

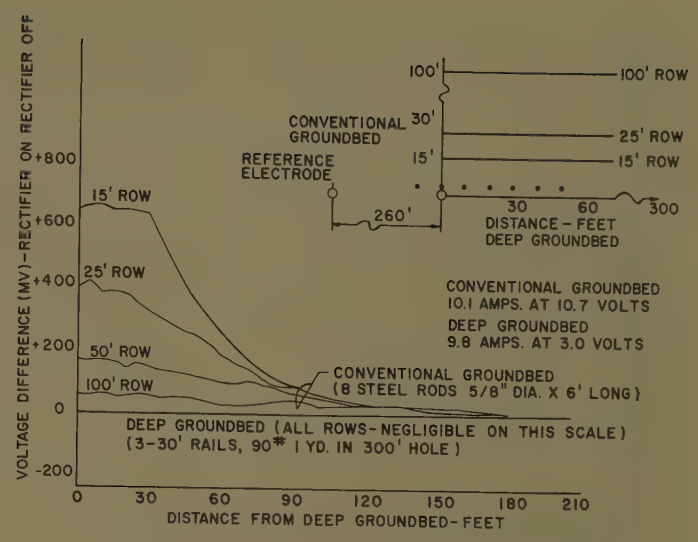


## References


1. Cathodic Protection of the Coated Steel Gas Main Distribution System in New Orleans, S. E. Trouard. *Corrosion*, Houston, Tex., vol. 13, no. 3, Mar. 1957, pp. 21–31.

2. Impressed Current Anodes Installed and Backfilled at Depth of 350 Feet, J. F. Tatum. *Corrosion*, Houston, Tex., vol. 14, no. 4, Apr. 1958, pp. 98–100.

3. Deep Ground Beds for Line Protection, R. L. Bullock. *Pipe Line Industry*, Houston, Tex., vol. 9, no. 4, Oct. 1958, pp. 40–44.


## Discussion

**G. P. Miles** (Interstate Oil Pipe Line Company, Shreveport, La.): In reading and commenting on this paper, I found many points of agreement and many new ideas which may be useful in the design of future deep ground bed installations. There are several other points which need clarification and still others with which I am not in agreement.

First, let us consider some of the advantages listed for deep ground beds. The authors listed the elimination of right-of-way problems and extensive co-ordinated tests with other utilities as major advantages. I am in full agreement with the first and in partial agreement with the second.

Though the elimination of right-of-way problems is certainly a major advantage for utility companies in congested areas, an advantage of even greater importance is the adaptability of these ground beds to high resistance soil. The use of deep ground beds has afforded an economical method of applying cathodic protection to bare pipe lines which were heretofore considered impractical to protect due to their location in ultrahigh-resistance surface soil. Their adaptability to this type of soil makes it possible to install low-resistance ground beds at any of the scattered locations of electric power along pipe lines. Interstate presently has 13 cathodic protection rectifier–deep ground bed units in service. Many of these installations are in soil of 100,000 ohms per centimeter and all are operating at below 1 ohm total circuit resistance with the exception of one which is 3 ohms.

Another extremely important advantage of deep ground beds is the extensive protective current spread obtained. Protection from deep ground beds in many cases is equal to three times the pipeline surface area which could be protected from a normal ground bed with equal current output.

In regard to the elimination of extensive interference surveys, interference is minimized, but the need for such surveys is not eliminated. Remember that all ground beds act differently and the elimination of interference surveys based on the results of one or a 100 tests can mean serious and costly damage. The reported test of interference using two copper sulfate half-cells leaves much to be desired. Interference tests conducted in areas where potentially interfering metallic conductors are not present seem baseless. Possibly, these tests were performed with interfering elements present; however, the magnitude of potential damage from improperly bonded interfering metallic masses is such that this point cannot be taken lightly.

Two excerpts from the Interstate papers referenced by the authors need comment. First, it was stated that the life of Interstate's deep ground beds is over 20 years. This is correct though the 20 years, which is a conservative estimate, is based on a current output of from 40 to 60 amperes rather than the 30 amperes stated.

Further, it was correctly stated that Interstate plans to use a deep ground bed using high-silicon cast iron anodes. This ground bed has been installed. However, it was of an experimental nature. Due to the erratic results reported for this material by others, we plan to proceed cautiously, watching results, evaluating data, and proving their worth before proceeding with additional ground beds of this material.

While on the subject of high-silicon cast-iron anodes, the reference to a ground bed life "calculated in excess of 100 years" is certainly something to think about. Using a manufacturer's literature, I once calculated a normal ground bed life in excess of 50 years for an area where galvanic anodes were being expended in 3 to 4 years. These calculations were filed away without being quoted, with the notation "FANTASTIC." Aren't we buying a pig in a poke or trying to make good on the lifetime guarantee of a fountain pen, when we let our enthusiam run away with us?

This paper by Mr. Landry and Mr. Howell has performed a service to pipeline and utility-corrosion engineers by combining many deep ground bed designs in current use into one composite paper. It is my opinion that the widespread use of the deep vertical-type cathodic protection ground bed has been one of the most significant developments in the field of cathodic protection during the last 5 or more years. The further exploration and development of this useful tool of corrosion control offers a challenge to all whose job is the protection of buried metallic structures.

**Lyle R. Sheppard** (Shell Pipeline Corporation, Houston, Tex.): The paper by Landry and Howell on deep ground beds is a very good summary of the recent work. However, I believe several points of ground bed design have not been pointed out, and thus without their consideration, the anticipated favorable results may not always be attained.

1. An anode at the surface of the earth has approximately twice the electrical resistance to earth as the same anode, in the same resistivity soil, at great depths in the earth.

The soil in the New Orleans area is uniform to great depths. The average surface-ground bed circuit resistance of the ten beds given is 1.159 ohms. That of the ten deep beds is 0.404 ohm, or approximately 35% of the surface beds. This effect of geometry accounts, in part at least, for the success of deep anodes in high resistance soil.

2. The deep anode as designed is effectively a single anode, thus, the resistance of mutual interference is less than that of several shallow anodes having the same anode surface. Approximately 30% of the surface ground bed resistance above is due to mutual interference.

3. Bentonite backfill is shown in Fig. 9 around high-silicon cast-iron anodes. This would accentuate the surface corrosion of the anodes. High-silicon cast-iron anodes are essentially "oxygen"-type anodes, the same as graphite, and should have coke-breeze backfill to take the anode corrosion away from the anode surface.

4. The resistances of the individual leads to various parts of the deep anode should be equalized by insertion of additional resistances, in order that the anode will be uniformly consumed without "necking."

**A. P. Landry** and **I. N. Howell, Jr.:** The authors are grateful for Mr. Sheppard's and Mr. Miles' comments and additional points of ground bed design contained in their discussions. In reference to Mr. Sheppard's comments, the phenomenon of the anode to earth resistance varying with the anode depth has been discussed in the literature.[1] Bentonite backfill referred to by Mr. Sheppard has been in use for some time now by many users of high-silicon cast iron anodes. The general feeling is that as long as current discharge per unit area of the high-silicon cast iron anodes is not excessive, there should be no appreciable increase in surface corrosion attributable to the bentonite backfill. It is also thought that the water holding properties of the bentonite will tend to retain the moisture around the anode and prevent a possible increase in resistance due to "drying out process" around the anode.

The use of compensating resistances in the anode leads to make the current discharge the same for all sections of the rail anode is not considered necessary for the following reasons. Since a lead is brought from each rail and each lead is attached to the rail at three locations, the maximum difference in anode lead length would be approximately 24 feet. The resistance of 24 feet of no. 6 wire is of such small proportions, its effect can be safely neglected. An additional factor to consider is that if necking does occur, the three lead contact points will insure continued consumption of metal with little increase in circuit resistance.

Mr. Miles has made reference in his discussion to the interference tests described in the paper. The results of these tests, which were made in the low-resistance soil in New Orleans and shown on the potential profile plot (Fig. 18), indicated that relatively steep potential gradients are produced by the conventional ground bed. The data taken for the deep ground bed show no appreciable potential gradient. No excessive current flow can be induced on an interfering metallic structure if there is no appreciable potential gradient to cause this current flow. Other tests not discussed in the paper have been conducted for the expressed purpose of determining the influence of a deep ground bed (operating at approximately 10 amperes) on all underground metallic structures in the vicinity. These tests, without exception, indicated no appreciable adverse effects on any underground structure.

The deep ground bed using high-silicon cast iron anodes has been modified slightly eliminating all local fabrication. Each anode is lowered into the well using its individual lead and is suspended at the desired depth from this lead. This greatly facilitates and expedites the placing of the ground bed by the contractor. It was not the authors' intent to convey the impression that "indefinite life" was the main consideration in the use of high-silicon cast iron for the anode material. Other equally important considerations are reduced cost, reduced weight and size, and elimination of local fabrication intervals. At the same time, published laboratory and field measurements indicate that a service life can be expected which far surpasses the expected life of the rail anode. The actual extent to which anode life will be extended can be determined only by the results of data obtained over a long period of time.


REFERENCE

1. DEEP GROUND BEDS FOR CATHODIC PROTECTION, S. E. Trouard, E. A. Wagner, Jr. *AIEE Transactions*, pt. II (*Applications and Industry*), vol. 78, Nov. 1959, pp. 278–85.


# Temperature Prediction in Thermal-Lag Equipment


P. B. RICHARDS
NONMEMBER AIEE


IN MISSILE applications, electric equipment is required to function for a relatively short period of time in a hot ambient atmosphere, but is deprived of external cooling media such as air or oil. The dependability of the equipment depends on its ability to absorb its own heat losses or to transmit these losses by conduction to cooler surroundings. The general purpose of this paper is to present a method for predicting simultaneously the transient temperatures in two heat-generating solids such that both materials store some heat, while some heat is transmitted from one to the other and thence possibly to a third region at a fixed temperature. In particular, mean transient temperatures are predicted in the field winding and laminations of an a-c generator which is bolted to a support, but otherwise insulated from the ambient atmosphere. Application of this method to temperature prediction in solid-state devices is natural.


Paper 59-913, recommended by the AIEE Air Transportation Committee and approved by the AIEE Technical Operations Department for presentation at the AIEE Summer and Pacific General Meeting and Air Transportation Conference, Seattle, Wash., June 21–26, 1959. Manuscript submitted March 23, 1959; made available for printing May 4, 1959.



P. B. RICHARDS is with the General Electric Company, Philadelphia, Pa. This paper is the outgrowth of work performed while the author was with the Research and Development Department of Jack and Heintz, Inc.


## Statement of Problem

The significant heat losses in the rotor (Fig. 1) are the winding $I^2R$ loss in the coil and the pole face loss in the iron. It will be assumed that no heat is transmitted across the air gap, hence the aforementioned losses must be stored either in the rotor coil and iron or transmitted along the shaft to the mounting pad (support). The machine is completely insulated from the hot atmosphere by necessity, so the mounting pad is the only available heat sink.

The energy balance can be expressed by the following equations

$$Q_c = Q'_c - Q_{cl} \quad (1$$

$$Q_l = Q'_l + Q_{cl} - Q_{lp} \quad (2$$

where

$Q_c$ = heat absorbed by coil
$Q'_c$ = heat generated by coil ($I^2R$ loss)
$Q_{cl}$ = heat conducted from coil to lamination
$Q_l$ = heat absorbed by lamination
$Q'_l$ = heat generated in lamination (pole face loss)
$Q_{lp}$ = heat conducted from lamination to pad

These quantities of heat are expressible in terms of the time $t$, mean temperature $T(t)$, mass $M$, specific heat $C$, and thermal resistance $R$ as follows:

$$Q_c = M_c C_c \frac{dT_c}{dt} \quad (3$$

$'_c = A + B\,T_c$, $A$, $B$ constants (4)

$$_{cl} = \frac{T_c - T_l}{R_{cl}} \quad (5)$$

$$_l = M_l C_l \frac{dT_l}{dt} \quad (6)$$

$$'_l = Q_{PF} = \text{constant} \quad (7)$$

$$_{lp} = \frac{T_l - T_p}{R_{lp}} \quad (8)$$

here the subscripts $c$, $l$, $p$ denote coil, aminations, and pad respectively, $R_{cl}$ the thermal resistance between the coil nd the laminations, $R_{lp}$ the thermal resistance between the laminations and ad, and $Q_{PF}$ the pole face losses.

Substituting these expressions in the nergy balance formulas, two simultaneous ifferential equations are obtained for $_c(t)$ and $T_l(t)$:

$$M_c C_c \frac{dT_c}{dt} = A + BT_c - \frac{(T_c - T_l)}{R_{cl}} \quad (9)$$

$$M_l C_l \frac{dT_l}{dt} = Q_{PF} + \frac{T_c - T_l}{R_{cl}} + \frac{T_p - T_l}{R_{lp}} \quad (10)$$

ubject to the initial conditions

$$_c(0) = T_0$$

$$_l(0) = T_0, \qquad T_0 = \text{constant}$$

## olution

Equations 9 and 10 are readily solved y the Laplace transform method, assumng the material thermal properties are onstant. The procedure will be explained in sufficient detail to permit numerical calculation of solutions.

The equations are first simplified by the otation

$$_c(t) = y(t) \qquad T_l(t) = x(t)$$

$$= M_c C_c \qquad a_3 = \frac{1}{R_{cl}}$$

$$= B - \frac{1}{R_{cl}} \qquad a_4 = A \quad (11)$$

$$= M_l C_l \qquad b_3 = -\left(\frac{1}{R_{cl}} + \frac{1}{R_{lp}}\right)$$

$$= \frac{1}{R_{cl}} \qquad b_4 = Q_{PF} + \frac{T_p}{R_{lp}}$$

$$y'(t) - a_2 y(t) - a_3 x(t) = a_4$$

$$x'(t) - b_2 y(t) - b_3 x(t) = b_4$$

he Laplace transforms of $x$ and $y$ are

$$\{x\} = \frac{A_1 p^2 + B_1 p + C_1}{A_2 p^2 + B_2 p + C_2} = \frac{N(p)}{D(p)} \quad (12)$$

$$\{y\} = \frac{A_1^0 p^2 + B_1^0 p + C_1^0}{A_2 p^2 + B_2 p + C_2} = \frac{N^0(p)}{D(p)} \quad (13)$$

**Fig. 1. Cross section of rotor**

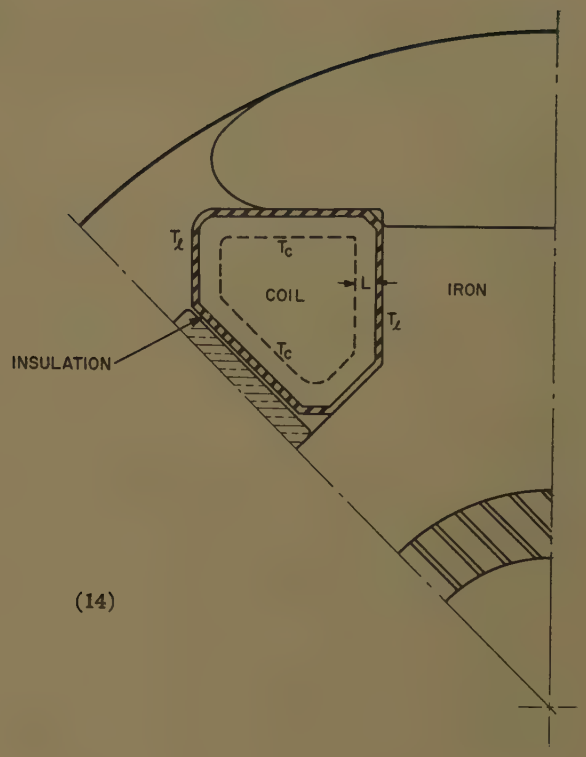


where

$$\begin{aligned}
A_1 &= a_1 b_1 T_0 \\
B_1 &= a_1 b_4 + T_0(a_1 b_2 - a_2 b_1) \\
C_1 &= a_4 b_2 - a_2 b_4 \\
A_1^0 &= a_1 b_1 T_0 = A_1 \\
B_1^0 &= a_4 b_1 + T_0(a_3 b_1 - a_1 b_3) \\
C_1^0 &= a_3 b_4 - a_4 b_3 \\
A_2 &= a_1 b_1 \\
B_2 &= -(a_1 b_3 + a_2 b_1) \\
C_2 &= a_2 b_3 - a_3 b_2
\end{aligned} \quad (14)$$

Using Pipes' transform pair #52,[1] the inverse transforms of equations 12 and 13, the desired solutions $T_c(t)$ and $T_l(t)$, are given by the Heaviside Expansion Formula

$$x(t) = \frac{N(0)}{D(0)} + \sum_{r=1}^{2} \frac{N(p_r)e^{p_r t}}{p_r D'(p_r)} = T_l(t) \quad (15)$$

$$y(t) = \frac{N^0(0)}{D(0)} + \sum_{r=1}^{2} \frac{N^0(p_r)e^{p_r t}}{p_r D'(p_r)} = T_c(t) \quad (16)$$

provided $p_r$, $r = 1, 2$, are distinct nonzero roots of $D(p) = 0$, and

$$D'(p_r) = \left.\frac{dD}{dp}\right|_{p = p_r} \neq 0$$

These temperatures will stabilize with time; i.e., become asymptotic to some finite value, provided the roots $p_r$ of $D(p) = 0$ are real and negative. Requirements for this condition will now be obtained.

### Temperature Stabilization Criterion

For

$$D(p_r) = A_2 p_r^2 + B_2 p_r + C_2 = 0$$

the roots are given by

$$p_r = \frac{-B_2 \pm \sqrt{B_2^2 - 4A_2 C_2}}{2A_2} \quad (17)$$

From equations 14 and 11, assuming $M_c \neq 0$, $M_l \neq 0$, $0 < R_{cl} < \infty$, $0 < R_{lp}$, it is apparent that both roots will be real and distinct, for

$A_2 > 0$,

$$\begin{aligned}
B_2^2 - 4A_2 C_2 &= (a_1 b_3 + a_2 b_1)^2 - 4a_1 b_1 (a_2 b_3 - a_3 b_2) \\
&= (a_1 b_3 - a_2 b_1)^2 + 4a_1 a_3 b_1 b_2 > 0
\end{aligned}$$

Since there can be no complex roots, any nonstabilization will be of the nature of increasing temperatures.

It is shown in the Appendix that a necessary and sufficient condition for the stabilization of temperature is

$$B < \frac{1}{R_{cl} + R_{lp}} \quad (18)$$

that is, if, and only if, the rate, with respect to temperature, at which heat is generated in the coil is less than the thermal conductance (reciprocal of thermal resistance) from the coil to the pad, then the temperatures in the machine will stabilize with time.

This rate will be the product

$B = I^2 b$

$I$ = current (constant)

$b$ = rate at which electrical resistance $R$ changes with temperature ($R = a + bT_c$)

The temperatures will stabilize at the finite values

$$T_l(\infty) = \frac{N(0)}{D(0)} = \frac{C_1}{C_2}$$

$$T_c(\infty) = \frac{N^0(0)}{D(0)} = \frac{C_1^0}{C_2}$$

### Calculation of Solutions

Calculation of equations 15 and 16 is straightforward and easy to program for a

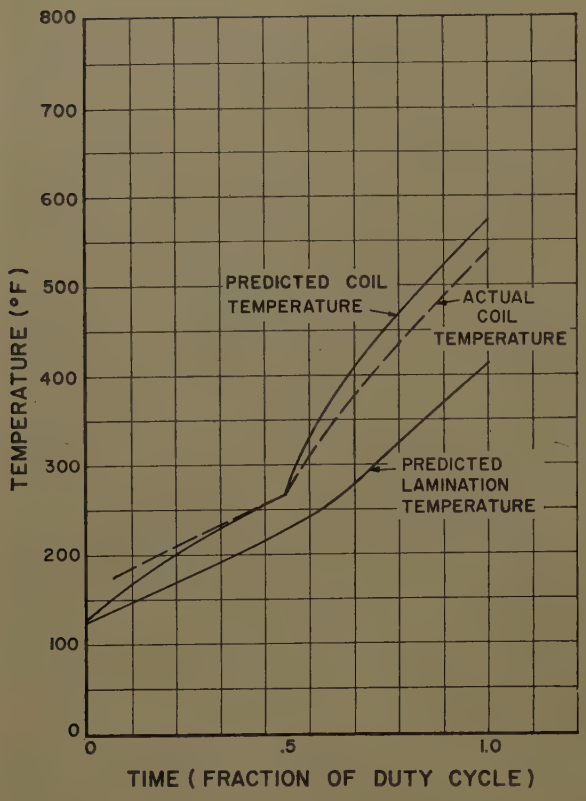


Fig. 2 (left). Temperatures in thermal-lag generator. Initial temperature 125 F. Pad temperature: 125 F, first half of duty cycle; 150 F, final half of duty cycle

Fig. 3 (right). Temperatures in thermal-lag generator. Initial temperature: 160 F. Pad temperature: 250 F, first half of duty cycle; 325 F, final half of duty cycle

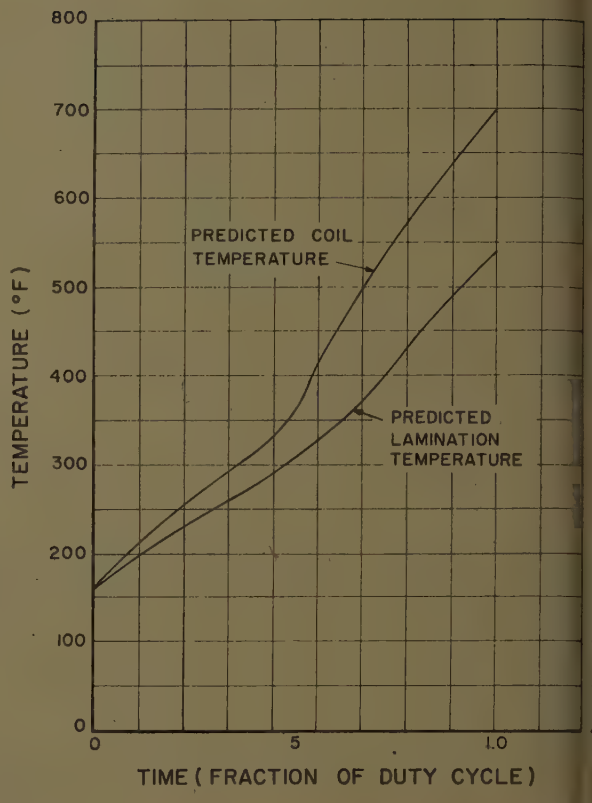


digital computer once the constants in equations 14 and 11 are determined. Of these, only $R_{cl}$ is likely to cause trouble in a rotating machine.

By definition (equation 5), $R_{cl}$ is the thermal resistance between the isotherm which denotes the average temperature $T_c$ in the coil and the isotherm which represents the average temperature $T_l$ in the laminations. For all practical purposes, however, the resistance within the lamination is negligible,[2] so the isotherm $T_l$ coincides with the boundary separating the coil from the laminations (Fig. 1). The coil is surrounded by electrical insulation whose thermal resistance is easy to compute. The remaining resistance is that in the coil between the isotherm $T_c$ and the surrounding insulation. Denote this resistance by $R_c$. Then

$$R_c = \frac{L}{KA}$$

where $L$ is the distance from this isotherm $T_c$ to that portion of the outer edge of the coil through which heat is transmitted $K$ is the thermal conductivity of the coil

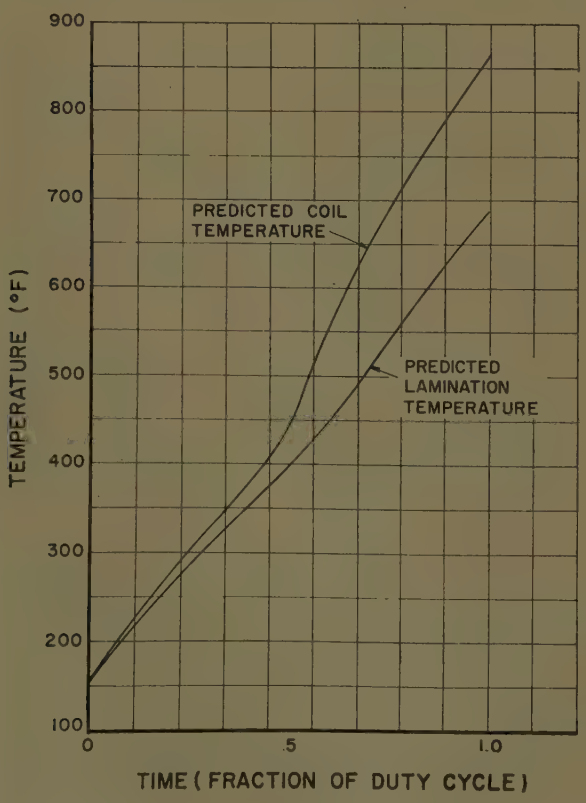


Fig. 4 (left). Temperatures in thermal-lag generator. Initial temperature: 160 F. Pad temperature: 500 F

Fig. 5 (right). Temperatures in thermal-lag generator. Initial temperature: 160 F. Generator perfectly insulated from pad

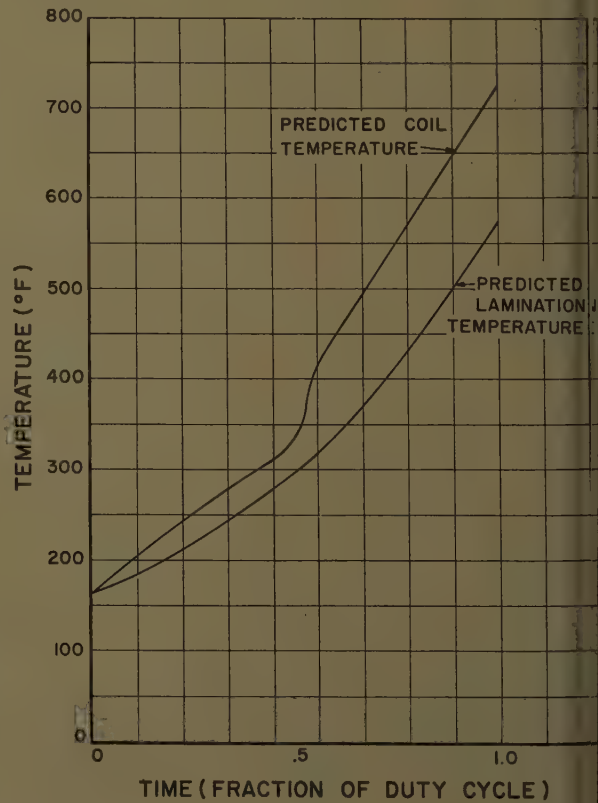

and $A$ is the surface area through which heat is transmitted from the isotherm $T_c$ to the edge of the coil. Equations 3 and 4 suggest that the distance $L$ be defined as follows:

Consider the entire mass $M_c$ of the coil concentrated at the isotherm $T_c$ at a distance $L$ from the outer heat transfer surfaces of the coil such that the total moment $L\,M_c$ is equal to the total moment of the individual masses in the coil with respect to these same surfaces. Since the coil is homogeneous, picture the coil as consisting of $n$ equal masses $m_k$. Then $M_c = n\,m_k$ and

$$L = \frac{\sum_1^n x_k m_k}{M_c} = \frac{\sum_1^n x_k}{n}$$

where $x_k$ is the shortest distance from any point, mass, in the coil to the heat transfer surface. $L$ can be calculated by placing a small grid over a print of the coil cross section and simply counting the number of nodal points at one unit distance from the heat transfer surface, then the number at two units, and so on.

Using this method of calculating $L$, solutions of equations 15 and 16 have been computed on the International Business Machines Corporation *650* digital computer for a pad-mounted a-c generator operated under typical missile conditions: half-load for the first half of the duty cycle, followed by full-load for the last half of the duty cycle. The generator is insulated from the pad, drive end, by gasket material. The theoretical solutions are plotted in Fig. 2 as predicted coil and predicted lamination temperature, under the conditions

$T_0 = 125$ F (degrees Fahrenheit), initial temperature
$T_p = 125$ F, first half of duty cycle
$T_p = 150$ F, last half of duty cycle

To verify this analysis, a generator was tested under the same conditions as were used in obtaining the predicted temperatures. The average coil temperature was calculated from the measured field resistance. This temperature is plotted in Fig. 2 as actual coil temperature. Agreement between theory and experiment is within 6%. Satisfied that this theoretical analysis is sufficiently accurate to predict temperatures, a series of solutions were calculated to determine the effect of pad temperature.

Fig. 3 indicates the predicted coil and lamination temperatures for the generator just discussed, but with

$T_0 = 160$ F, initial temperature
$T_p = 250$ F, first half of duty cycle
$T_p = 325$ F, last half of duty cycle

Fig. 4 indicates the predicted coil and lamination temperatures for the same generator, but with

$T_0 = 160$ F, initial temperature
$T_p = 500$ F, entire duty cycle

indicating that with a pad temperature of 500 F, coil temperature is dangerously high for the final 20% of the duty cycle. Fig. 5 indicates the predicted coil and lamination temperatures for the same generator, but with

$T_0 = 160$ F, initial temperature
$R_{lp} = \infty$, generator perfectly insulated from pad

These temperatures are 130 F cooler than when the pad is at 500 F, and only about 30 F hotter than when the pad is at 325 F. One would thus expect that insulation is the solution to high pad temperatures, but this is not practical. Mechanical requirements limit the amount of insulation that can be used between the generator and the pad, while a very large increase in insulation is required to appreciably reduce the coil temperature.

## Summary

Two simultaneous differential equations are derived and solved for the transient temperatures in two heat-generating solids such that both materials store some heat, while some heat is transmitted from one to the other and thence possibly to a third region at a fixed temperature. Conditions are determined under which the temperatures will stabilize with time. To demonstrate the theory, temperatures are predicted in the field winding and laminations of an a-c generator which is bolted to a support, but otherwise insulated from the ambient atmosphere. Measured temperatures agree within 6% with predicted temperatures.

The theory can be extended to any number of heat-generating regions, and therefore can be applied to solid-state devices.

## Appendix. Proof of Stabilization Criterion

If

$$B < \frac{1}{R_{cl} + R_{lp}}$$

then

$$B < \frac{1}{R_{cl}}$$

and

$$B_2 = -a_1 b_3 - a_3 b_1 = M_c C_c \left(\frac{1}{R_{cl}} + \frac{1}{R_{lp}}\right) - M_l C_l \left(B - \frac{1}{R_{cl}}\right) > 0$$

Also

$$C_2 = a_2 b_3 - a_3 b_2 = -\frac{[B(R_{cl} + R_{lp}) - 1]}{R_{cl} R_{lp}} > 0$$

then

$$A_2 C_2 > 0$$

and

$$B_2 > \sqrt{B_2^2 - 4A_2C_2}$$

Hence, from equation 17, it is clear that $p_r < 0$, $r = 1, 2$ and stabilization follows.

Next consider the case

$$B > \frac{1}{R_{cl} + R_{lp}}$$

then

$$C_2 < 0$$

hence

$$A_2 C_2 < 0$$

and

$$|B_2| < \sqrt{B_2^2 - 4A_2C_2}$$

Hence from equation 17 it is clear that one of the roots $p_r$ will be positive, and the temperatures will never stabilize.

This will occur, for example, if the machine is perfectly insulated from the pad ($R_{lp} = \infty$), since, in general, $B$ is a positive quantity.

Finally, if

$$B = \frac{1}{R_{cl} + R_{lp}}$$

it is readily apparent that $C_2 = 0$, implying, by equation 17, that one root $p_r$ will vanish. This necessitates another form for the solutions than the Heaviside Expansion Formula (equations 15 and 16). Indeed, for $C = 0$, instead of equation 12, write

$$L\{x\} = \frac{A_1 p_2^2 + B_1 p}{p(A_2 p + B_2)} + \frac{C_1}{p(A_2 p + B_2)}$$

and by transform pair #9,[1] the inverse transform of $x$ diverges linearly with time. The same will be true for $L\{y\}$. Thus the stabilization criterion equation 18 is established.

## References

1. Applied Mathematics for Engineers and Physicists (book), L. A. Pipes. McGraw-Hill Book Company, Inc., New York, N. Y., 1946.

2. Progress in the Thermal Design of Oil-Cooled Rotating Electrical Machines, P. B. Richards. *AIEE Transactions*, pt. II, (*Applications and Industry*), vol. 77, Nov. 1958, pp. 330–34.

# Application of Switching Transistors and Saturable Reactors in a High-Performance Servo

FRED B. COX
STUDENT MEMBER AIEE

PAUL R. JOHANNESSEN
ASSOCIATE MEMBER AIEE

THE PURPOSE of this paper is to demonstrate that the performance of instrument servos can be improved by the exclusive use of magnetic devices and transistors to perform the functions of amplification, modulation, and demodulation. Substitution of solid-state devices for electronic amplifiers and mechanical choppers not only increases the efficiency, the reliability, and the durability of the system but also minimizes its size and weight.

Successful use of magnetic amplifiers as servo units has been reported in numerous papers (see, for example, references 1 and 2) but the drift and slow response of conventional 60- and 400-cps (cycles per second) amplifiers prohibit their use in many applications. Furthermore, it is customary to drive the magnetic stage with an electronic preamplifier in order to achieve adequate gain because of the drift problems encountered in cascading two magnetic-amplifier stages. The use of a high-frequency supply voltage has been shown to overcome many of the inherent limitations of a magnetic amplifier.[3] The push-pull amplifier, however, is electrically inefficient because the output circuit dissipates power when the error signal is zero. Power-switching transistors, driven by a magnetic amplifier, have been suggested as a solution to the problem of inefficiency.[4] These ideas, together with many others, however, are as yet unproved as a means of improving over-all servo performance.

## The System

A block diagram of the high-performance position servo is shown in Fig. 1, and a schematic diagram of the electric circuits is shown in Fig. 2. The system was designed with no particular application in mind, but every attempt was made to determine an "upper bound" on the performance that might be expected from such a servo. In particular, the system parameters were chosen for maximum bandwidth and velocity constant. Other desirable characteristics, such as negligible drift, short settling time after slew, high efficiency, and insensitivity to small changes in the system carrier frequency follow from the inherent properties of the system components.

The servo amplifier consists of a 2-stage transistor common-emitter voltage amplifier, a magnetic amplifier, and a push-pull switched-transistor power amplifier. The class *A* transistor amplifiers are necessary to achieve the desired loop gain because of the low-voltage amplification of the magnetic and power stages.

The magnetic amplifier is designed to furnish current pulses, the widths of which are proportional to the control signal, to the bases of the power transistors. The magnetic-amplifier supply voltage, furnished by a simple d-c to a-c converter, is a 5-kc square wave, and, because an output pulse occurs on each half-cycle of the supply, the pulse repetition rate is 10 kc. The output polarity reverses on each half-cycle of the 400-cps system carrier. Depending upon the load requirements, the magnetic amplifier must supply from 200- to 500-milliampere peak current to the *H-6* power transistors. The quiescent power dissipation of the magnetic stage is therefore substantially lower than it would be if the magnetic amplifier were used to drive the motor.

Output pulses from the magnetic amplifier control the polarity of the transistor bases with respect to ground, and therefore control the flow of current to the load. Because current flows in the transistors only when an error signal appears in the loop, the efficiency of the power stage is enhanced, and heating in the motor windings is kept to a minimum.

Because it is desirable that the motor control voltage be sinusoidal, a 2-microfarad capacitor is connected across the control windings. The tank circuit, consisting of the capacitor in parallel with the winding inductance and resistance, is tuned for resonance at the 400-cps system carrier frequency. Thus all harmonics of the 10-kc repetition frequency and higher harmonics of the 400-cps carrier are filtered out so that only the information component of voltage is retained.

Minor-loop feedback from an a-c tachometer is used to achieve the desired bandwidth. To obtain a high velocity constant, the tachometer is effectively decoupled from the system for constant motor speeds by a high-pass filter in the feedback loop. To avoid the use of a band-pass filter, the tachometer signal is demodulated prior to filtering by a keyed phase-sensitive magnetic demodulator. A transistor emitter-follower amplifier is used to isolate the demodulator output.

Fig. 2 shows that position and acceleration errors are summed at the input of the emitter-follower isolation amplifier. It is necessary to tie the two error channels together at this point because of the impedance-matching problems associated with the following stage. The high-pass filter has no effect upon the position error signal, however, because it is a modulated 400-cps signal from a synchro coupled to the motor shaft. Thus, summation of the two voltages is effectively performed at the input of the keyed magnetic modulator.

To sum the a-c position and the d-c acceleration errors, a keyed modulator is used. The modulator samples during a short interval of time (50 microseconds) on each half-cycle of the system carrier. In the interval between samplings, the output voltage is maintained constant by a pulse-stretching circuit. The output, therefore, is a 400-cps square wave whose amplitude is proportional to the difference between the synchro voltage and the filtered, demodulated tachometer voltage.

## System Performance

The system described in the preceding section has been built and tested. Results of these tests are summarized briefly as follows:

Velocity constant—approximately 9,500 seconds$^{-1}$.

Torque constant—0.17 ounce-inch per milliradian, referred to the motor shaft. (This applies to a Kearfott *R801-1A* 2-phase motor-rate generator.)

Paper 58-89, recommended by the AIEE Feedback Control Systems Committee and approved by the AIEE Technical Operations Department for presentation at the AIEE Winter General Meeting, New York, N. Y., February 2–7, 1958. Manuscript submitted October 29, 1957; made available for printing March 31, 1959.

FRED B. COX and PAUL R. JOHANNESSEN are with Massachusetts Institute of Technology, Cambridge, Mass.

The work reported in this paper was supported in part by Project *7668-R*, Servomechanisms Laboratory, Massachusetts Institute of Technology, under contract no. *AF 33(616)-3950* with the Weapons Guidance Laboratory, Wright Air Development Center.

Open-loop gain crossover frequency—230 radians per second.

Settling time for 1-degree step input (referred to the motor shaft)—approximately 20 milliseconds. (Settling time is the time required for oscillation of the response to decrease to less than 5% of the final value.)

The closed-loop sinusoidal frequency response is plotted in Fig. 3. These results were obtained for an input signal corresponding to a 1-degree peak displacement at the motor shaft. Because equipment was not available to obtain modulation frequencies above 50 cps, exact determination of the resonant frequency and the peak magnitude ratio was not possible. The system step response is shown in Fig. 4.

## System Components

The units comprising the major components of the servo electrical system are described in the following paragraphs.

### Magnetic Amplifier

The magnetic amplifier, shown in detail in Fig. 5, serves as the controller for the push-pull transistor output stage. This amplifier is quite similar to the one described by Fischer[3] and consists of two half-wave phase-reversible push-pull units operating side by side, so that an output

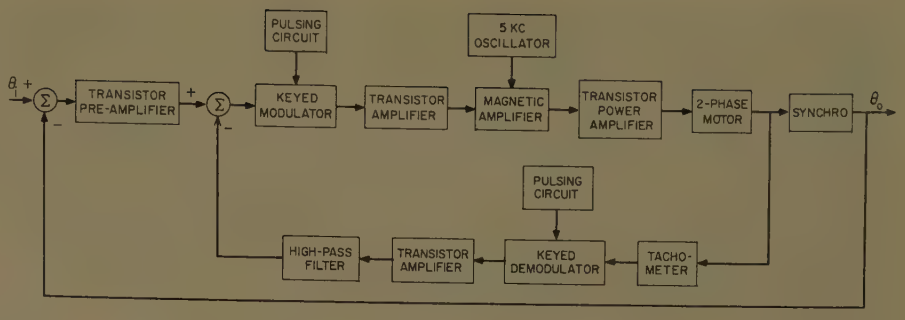


**Fig. 1. Schematic diagram of the servo**

signal occurs on each half-cycle of the supply voltage.

The supply voltage $e_g$ is 5 kc and square-wave, obtained from a conventional transistor d-c to a-c converter.[5] The high-frequency supply is used in order to minimize the phase lags introduced by the magnetic amplifier. A square-wave supply is recommended rather than a sinusoidal supply because a sinusoidal voltage will allow the output rectifiers to conduct at the beginning and end of each control half-cycle with a resulting loss of gain.

Operation of the unit may be understood with the aid of Fig. 5. From this diagram it is seen that the winding polarities are such that a positive control signal $e_c$ opposes the bias voltage in core IV and aids the bias voltage in core I. Similarly, a positive control voltage opposes the bias in core III and aids the bias in core II. Therefore, when $e_{g1}$ is negative and the associated rectifier is nonconducting, a positive control signal resets the flux of core I to a lower level than that of core IV. The same action takes place between cores II and III when $e_{g2}$ is negative.

When $e_{g1}$ is positive, the flux of cores I and IV is driven toward saturation. As a result of the difference in flux levels in the two cores, core IV reaches saturation sooner than core I and a step of voltage, $e_o = -e_{o2}$, appears across the output transformer. When core I saturates, the net output voltage drops to zero. The same sequence of events occurs for cores II and III on the next half-cycle, and the net output is therefore a series of pulses at a repetition rate of 10 kc. The polarity of the output pulses is determined by the polarity of the control signal, and no out-

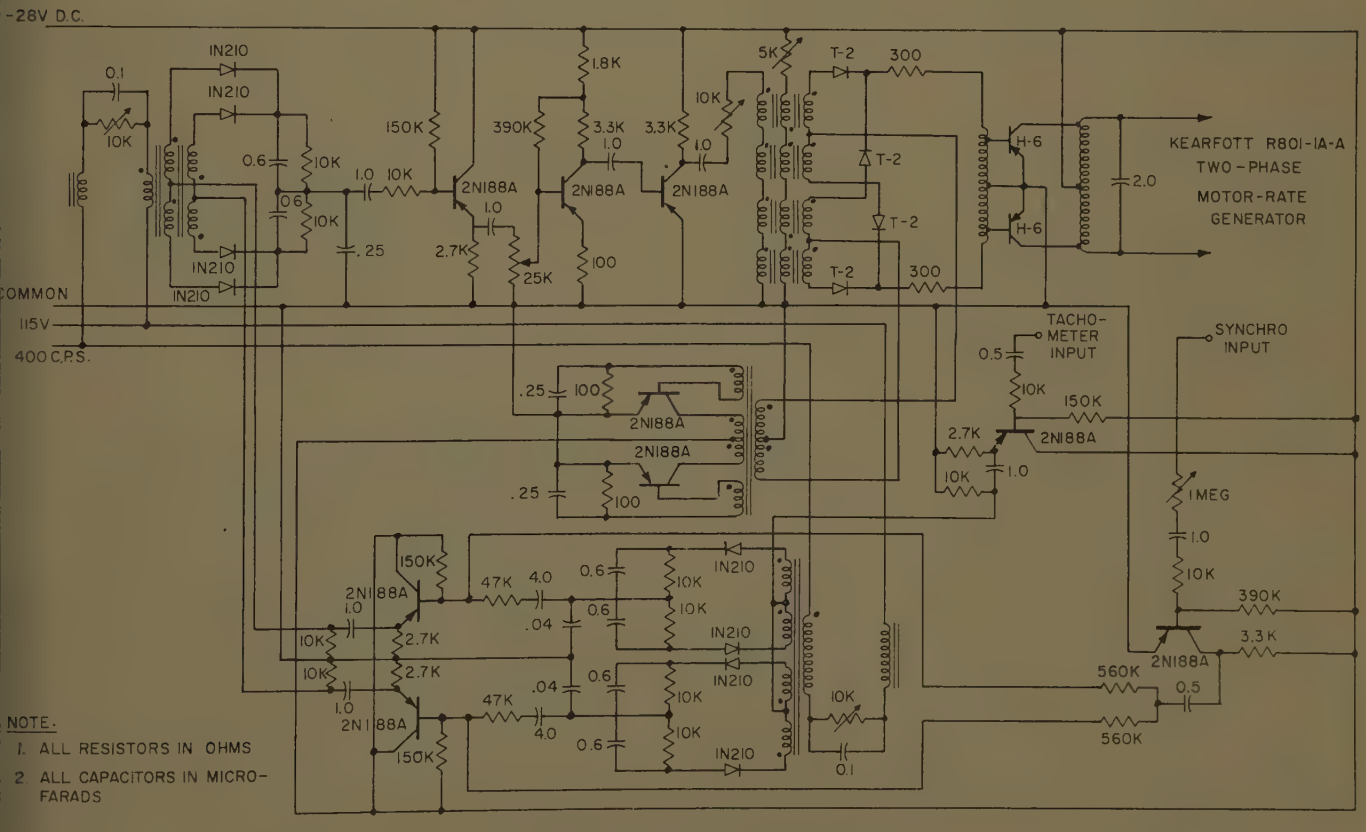


**Fig. 2. Electric circuit diagram**

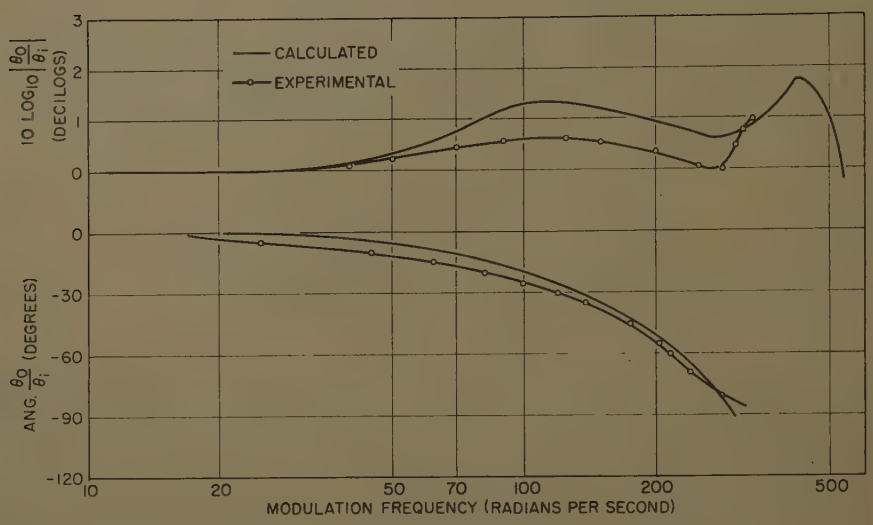


Fig. 3. Frequency response of the servo

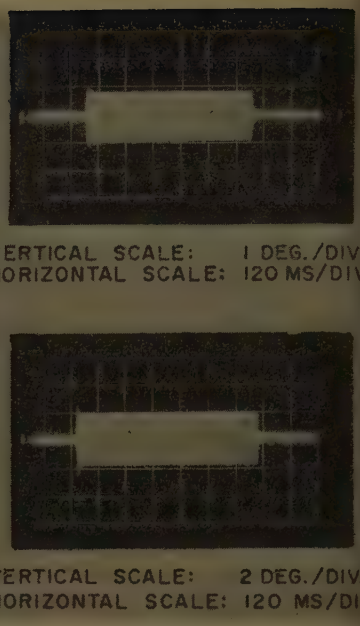


Fig. 4. Transient response of the servo

put occurs for a zero control signal because both cores saturate simultaneously.

The operation described gives rise to a dual-carrier system consisting of the system 400-cps carrier signal and the 10-kc repetition frequency of the output pulses. Both the 400-cps carrier and the error signal acting as amplitude modulation upon it act as modulation to vary the width and polarity of the high-frequency output pulses from the magnetic amplifier. Fig. 6 illustrates the ideal magnetic-amplifier output for a 400-cps signal input.

The transfer function for the magnetic amplifier is derived in the Appendix and is given approximately in the form

$$G_{MA}(S)=K_{MA}\frac{1}{\tau_{MA}S+1} \qquad (1)$$

This approximation characterizes the unit as having a single time constant rather than a fixed time delay of one half-cycle of the supply voltage. That this representation is valid may be seen by computing the phase lag introduced by a pure transportation delay at a signal frequency of 300 radians per second:

$$\frac{\pi\times 300}{2\pi\times 5{,}000}\times 57.2=1.7^\circ$$

By way of comparison, the phase lag at a signal frequency of 300 radians per second of a similar unit utilizing a 400-cps carrier would be

$$\frac{\pi\times 300}{2\pi\times 400}\times 57.2=21.5^\circ$$

These figures show that the objectionable time delay of the magnetic amplifier has practically been eliminated. Another advantage of the high-frequency supply is that any output of the amplifier due to unbalance in the components consists of harmonics of the 10-kc repetition frequency. Since the motor responds only to a 400-cps signal, this drift in the magnetic amplifier does not result in drift of the output position.

The maximum range of linear control with regard to the supply voltage is obtained when the cores are normally excited. (Normal excitation is defined a the supply voltage amplitude necessar to change the core flux from minus to plu saturation in a period of one half-cycle.)

Because the supply voltage is usuall set for normal excitation of the cores, th peak current in the output circuit may b adjusted for the desired value by the serie resistor $R_s$. The peak current is dete mined by the base drive necessary t switch the transistors for the largest loa expected. In this case, 200 milliampere was sufficient. Total dissipation in th magnetic amplifier under quiescent con ditions was 2 watts.

## Transistor Power Amplifier

The magnetic amplifier is coupled the transistor power stage through a 3 1 stepdown transformer as shown in Fi 7. The transformer windings are n isolated because the current-resistan

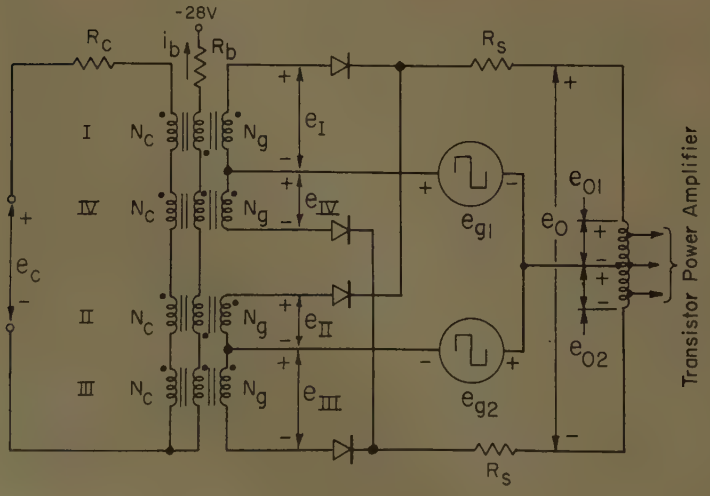


MAGNETIC AMPLIFIER CORERS
MAGNETICS INC. #5000-2A ORTHONOL
CONTROL WINDING 100 TURNS #36 WIRE
BIAS WINDING 100 TURNS #36 WIRE
GATE WINDING 400 TURNS #36 WIRE
COUPLING TRANSFORMER
MAGNETICS INC. #50168-2A ORTHONOL
PRIMARY 840 TURNS #35 WIRE CENTER-TAPPE
SECONDARY 280 TURNS #35 WIRE CENTER-TAPPE
RECTIFIERS
TRANSITRON TYPE T-2

Fig. 5. Magnetic amplifier

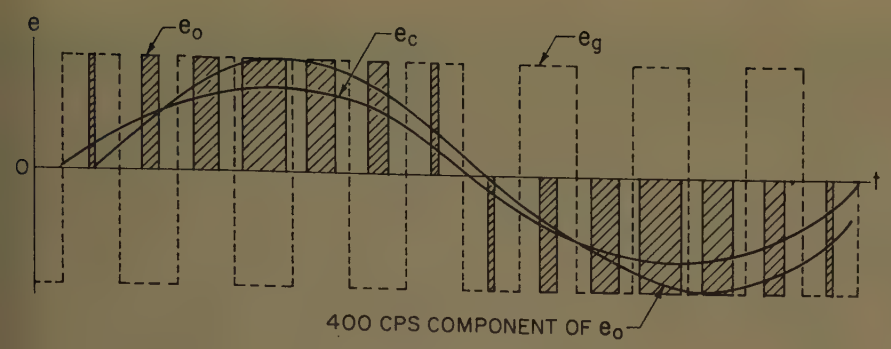


**Fig. 6. Magnetic amplifier output for a sinusoidal input**

drop in the windings due to the exciting current and the quiescent current in the magnetic-amplifier output circuit provide a positive bias on the transistor bases. This positive bias, for the p-n-p transistor, serves to prevent current flow from emitter to collector under zero-signal conditions.

When a step of voltage appears across the coupling transformer $e_o = e_{o1}$, the base transistor $A$ is pulsed positive with respect to its emitter, and the base of transistor $B$ is pulsed negative with respect to its emitter. If sufficient base drive is provided by the magnetic amplifier, the voltage across the emitter-collector junction of transistor $B$ will drop to almost zero while transistor $A$ will remain cut off. Transistor $B$ is again switched off when the net magnetic-amplifier output drops to zero.

Analysis of the power stage is complicated by the tuned network load. In fact, it is not possible to derive a transfer function for the output amplifier alone because the output impedance changes radically as the transistors are switched on and off. An approximate transfer function from magnetic-amplifier input to power amplifier output which checks well with experimental data for small signals may, however, be derived from the following considerations.

The transistor power amplifier operates in one of the two states: 1. both transistors nonconducting, and 2. one transistor conducting and the other transistor nonconducting. In state 1, the output impedance is high, whereas in state 2 the output impedance is low. Because the ON time is proportional to the signal amplitude, the amplifier impedance is predominantly high for small-loop error signals. Furthermore, the transistors are current-limited, so that for small signals the load is driven by a current pulse of roughly constant amplitude. In this case the amplifier may be represented as a current source. Such an assumption represents the worst possible case from a dynamic standpoint.

The transfer function given in equation 2 follows from the foregoing discussion.

$$\frac{e_{m(S)}}{e_{b(S)}} = K_M G_{MA}(S) K_{PA}(S) \qquad (2)$$

$K_{PA}(S)$ is determined from the impedance loading the assumed output current source and is of the form

$$K_{PA}(S) = \frac{1}{TS+1}$$

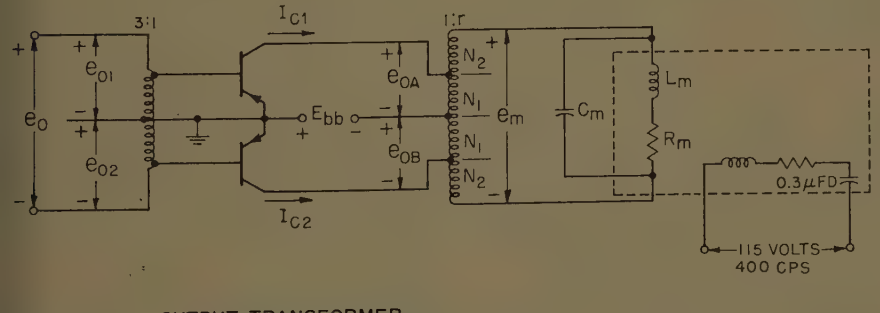


OUTPUT TRANSFORMER
ARNOLD ENGINEERING CO. #5233-D2 DELTAMAX
$N_1$ = 200 TURNS #30 WIRE
$N_2$ = 400 TURNS #30 WIRE
TRANSISTORS
HONEYWELL H-6
SUPPLY VOLTAGE
28 VOLTS DC

**Fig. 7. Transistor power amplifier**

However, the tuned motor represents a low $Q$ tank circuit so that the following approximation is valid over a fairly large range of signal frequencies:

$$K_{PA}(S)\epsilon^{-\zeta S}.$$

where $L_m/R_m \leq \zeta \leq 2L_m/R_m$ and $L_m$ = inductance of the motor control windings, and $R_m$ = equivalent stalled-rotor-resistance. This approximation provides a conservative prediction of the forward loop phase lag, and is therefore used in the analysis.

## Compensation

To improve the performance of the servo, three basic types of compensation were initially considered: 1. viscous-coupled inertia damper, 2. lead network, and 3. tachometer feedback.[6]

Equalization by means of an inertia damper coupled to the load has the advantage that both high velocity and torque constants are obtainable, plus a wide bandwidth.[8] The damper, however, draws power from the load, under transient conditions, which has two degrading effects. First, it decreases acceleration capabilities of the motor and, second, it produces a long, nonlinear oscillating transient following a large step input. By declutching the damper during slew, these difficulties can be overcome. The complexity of such a system, however, prompted investigation of a simpler solution.

The lead network is a simple means of increasing the allowable gain-crossover frequency. If the motor time constant is sufficiently long (small motor damping), the allowable velocity constant is also improved over the uncompensated system. The torque constant for the system employing lead network equalization is low, but this may be improved by the use of an integral network. The integral network increases only the "static" torque constant however, since it is effective only at quite low frequencies and is ineffective in offsetting dynamic changes in the load torque. To avoid this difficulty, a combination of tachometer and network compensation was used.

Tachometer feedback has the advantage of effectively increasing the motor

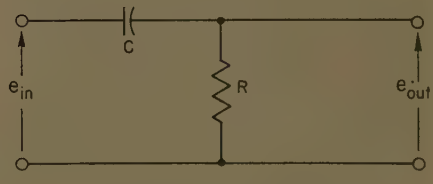


**Fig. 8. High-pass filter**

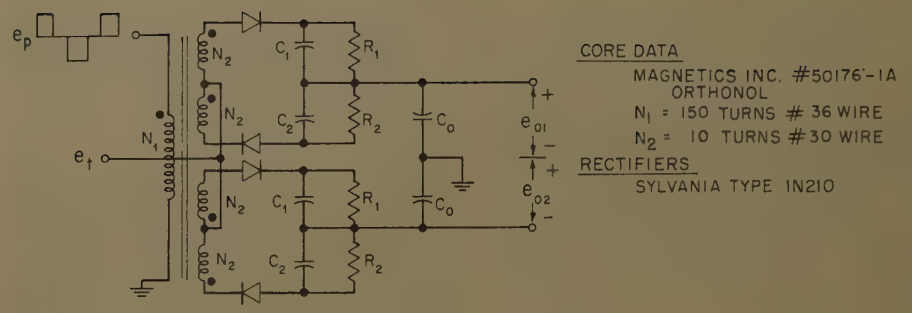


Fig. 9. Magnetic demodulator

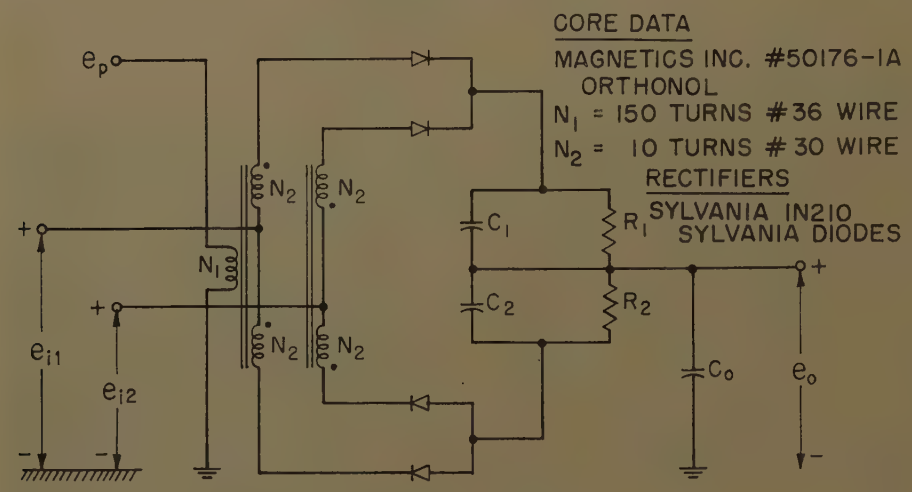


Fig. 10. Magnetic modulator

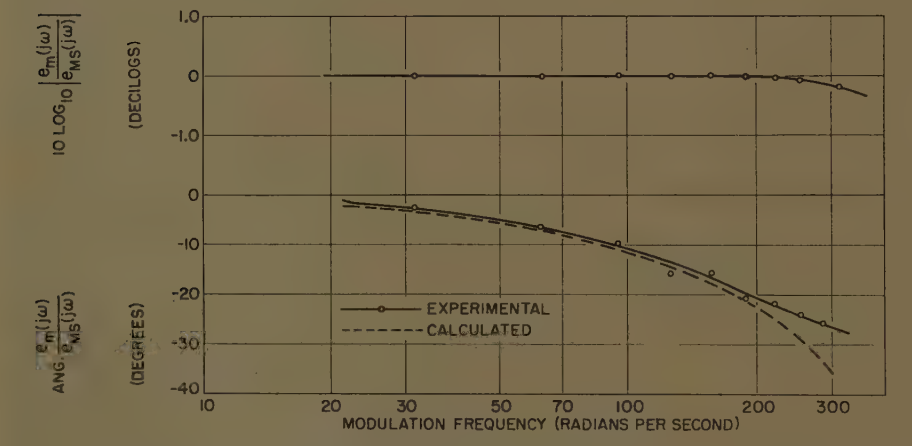


Fig. 11. Comparison of calculated and measured frequency response of the modulator, magnetic amplifier, and power amplifier

damping without drawing power from the load. As a result, the time constant of the motor is effectively reduced so that the open-loop gain and the bandwidth of the system may be increased. The low-frequency gain may be further increased by passing the tachometer signal through the simple high-pass filter shown in Fig. 8 provided the tachometer signal is a d-c voltage. If the tachometer signal is a-c, demodulation and remodulation are required. The transfer function of the high-pass filter is

$$\frac{e_{out}(S)}{e_{in}(S)} = \frac{S}{S+\omega_f} \qquad (3)$$

where $\omega_f = 1/RC$(resistance-capacitance). Hence, it may be seen that for a constant motor speed (ramp input), the tachometer is effectively decoupled from the system so that the velocity constant is much higher than for tachometer feedback without high-pass filtering

## Modulator and Demodulator

The magnetic-keyed, phase-sensitive sampling units used to demodulate and remodulate the tachometer output are basically identical to the device described by Mark, et al.[9] To reduce the phase lags introduced by these units, their respective inputs are sampled on each half-cycle of the 400-cps system carrier.

The demodulator is shown in Fig. 9 the modulator in Fig. 10. The sampling modulator not only sums the a-c error signal and d-c tachometer signal but also rejects any quadrature signal that may be present in the error voltage. The modulator also introduces a constant 90 degree phase shift of the error signal. These effects are the result of the sampling being performed at the peak of the 400-cp reference voltage wave.

The transfer functions of the demodulator and of the modulator can be approximated by a simple time delay of 1/4 cycle of the system carrier frequency, and are therefore of the form

$$G_{DS} = K_{DS}\epsilon^{-(\pi/2\omega_c)S} \qquad (4$$

$$G_{MS} = K_{MS}\epsilon^{-(\pi/2\omega_c)S} \qquad (5$$

Both $K_{DS}$ and $K_{MS}$ are dependent upon the output capacitance $C_o$ and the keying pulse amplitude. Selection of these values for this particular application is discussed in reference 9.

## Analysis of the Servo

As previously shown, the time delay of the magnetic amplifier using a 5-kc supply is negligible. The effects of the amplifier time constant $\tau_{MA}$ may also be made negligible by proper adjustment of the control resistance.

For small $R_c$ value, amplifier gain is high, but the time constant also assumes a large value. If $\tau_{MA}$ is made suitably large, however, the modulating signals are essentially shifted by a constant 90 degrees, and this phase lag may be cancelled by shifting the reference phase of the motor by 90 degrees. For a large value of $R_c$, both the amplifier gain and time constant are small, so that either extreme can lead to a suitable design. The relative merits of these extremes are discussed more fully in reference 10.

Use of the transfer functions obtained in the previous section yields the open-loop transfer function of the forward transmission (excluding the motor dynamics and neglecting $\tau_{MA}$) in the form

$$G_f(S) = K\epsilon^{-(\pi/2\omega_c+\xi)S} \qquad (6$$

The validity of this approximation is confirmed by the experimental data plotted in Fig. 11.

The effect of the modulator, aside from the constant attenuation $K_{MS}$, is to introduce a time delay of 1/4 cycle of the carrier frequency in the position loop. Because the modulator and demodulator sample at almost the same

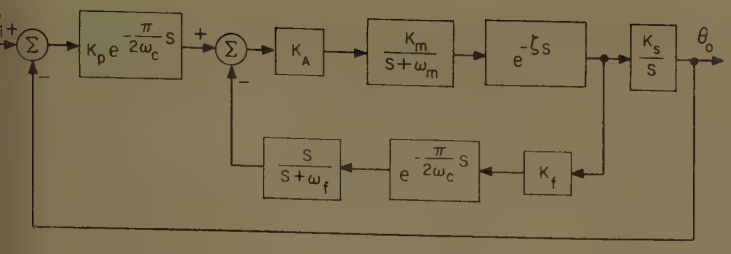


Fig. 12 (above). Mathematical model of the system

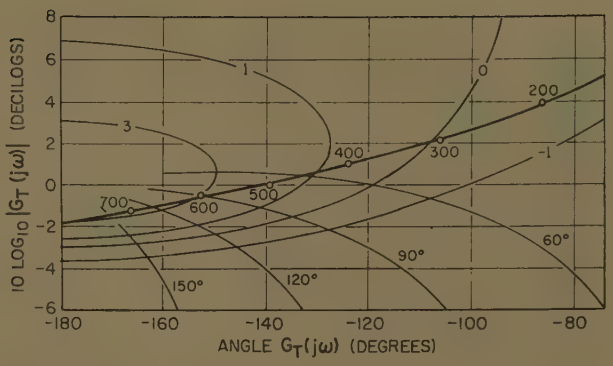


Fig. 13 (right). Nichols plot for the tachometer loop

ime, the modulator introduces a neg-gible time delay of the tachometer gnal in addition to that already intro-uced by the demodulator. Summation f position and acceleration error is herefore effectively performed at the nodulator output terminals except for he demodulator attenuation. With $K_{MS}$ umped into $K_A$ and the transportation ag of the modulator acting only upon he position error, the system may be epresented by the block diagram of ig. 12.

The open-loop transfer function for his mathematical model is

$$G(S)=(K_pK_s/K_f)\frac{S+\omega_f}{S^2}W_T(S) \qquad (7)$$

where $W_T(S)$ is the closed-loop weighting unction of the tachometer loop, given by

$$W_T(S)=\frac{G_T(S)}{1+G_T(S)} \qquad (8)$$

nd

$$G_T(S)=K_AK_mK_f\frac{\epsilon^{-(\pi/2\omega_c+\zeta)S}}{S+\omega_f} \qquad (9)$$

For the type of motor driving stage sed in this system, the motor damping s extremely small for low-shaft velocities. Hence, $\omega_m \approx 0$, and

$$G_T(S)\approx K_AK_mK_f\frac{\epsilon^{-(\pi/2\omega_c+\zeta)S}}{S+\omega_f} \qquad (10)$$

A Nichols chart plot for the tachometer loop is shown in Fig. 13 for $\omega_f=100$ radians per second. The open-loop transfer function, obtained from this plot and equation 7, is shown in Fig. 14. The effect of the time delay present in the power stage and in the demodulator is apparent from Fig. 13, which shows the low rate of attenuation and rapid phase shift with increasing frequency. The tachometer loop was adjusted for a resonant frequency of 700 radians per second with a peak closed-loop magnitude ratio of 3.8 decibels.

The effect of the narrow resonant peak of $W_T(S)$ on the system open-loop transfer function may be seen in Fig. 14 by the deviation of the actual magnitude from that of the logarithmic asymptotes. The rapid phase shift with almost no attenuation at frequencies between 300 and 700 radians per second requires that the gain crossover be made very near the corner frequency of the high-pass filter.

Fig. 1 shows a comparison of the calculated and the experimental closed-loop frequency response of the system. The experimentally determined magnitude ratio is seen to be somewhat less than the predicted value. Although equipment was not available for obtaining signal frequencies above 314 radians per second, comparison of the results indicates that the resonant frequency is between 350 and 400 radians per second and that the peak magnitude ratio $M_p$ is between 1.5 and 2.0.

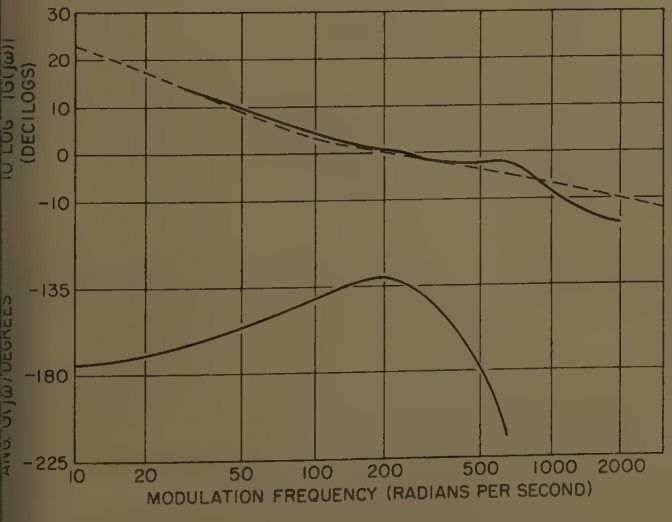


Fig. 14. Attenuation and phase diagram for the mathematical model

## Appendix

The following derivations are based upon a new method of magnetic-amplifier analysis proposed by Johannessen.[11] The procedure is based upon representation of the half-cycle averages of the terminal variables of a basic single-core amplifier, shown in Fig. 15, in matrix form. (In Fig. 15, the core is represented by an ideal reactor shunted by a linear magnetizing resistance $R_M$. This assumption is discussed in detail in reference 11, pages 9–15, and experimental confirmation of its validity has been obtained by Knutrud.[12])

Once the terminal variables are established, this basic element may be interconnected with other basic circuits to yield the multicore amplifier configuration under consideration. The difference equation[13] for the multicore amplifier is then obtained from matrix manipulations.

The 4-core amplifier used in the system is redrawn in Fig. 16 for convenience in

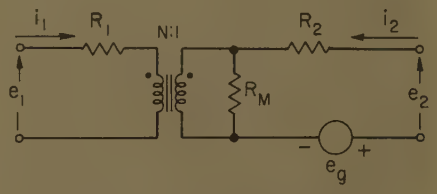


Fig. 15. Basic amplifier circuit

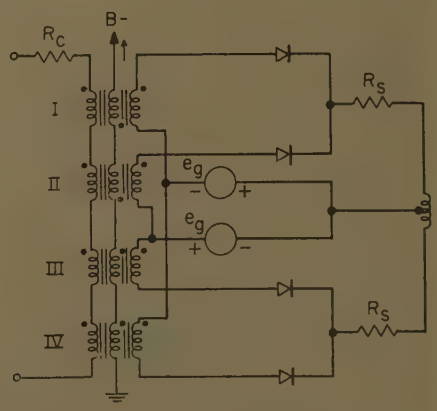


Fig. 16. Full-wave amplifier

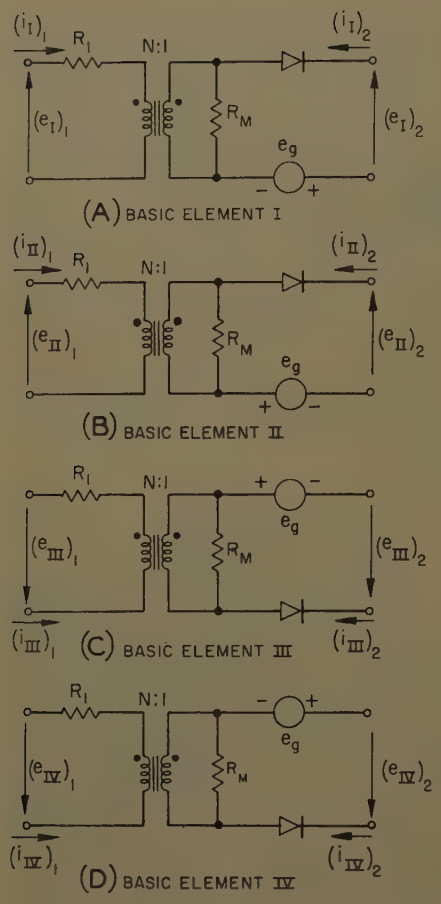


**Fig. 17. Basic elements of the full-wave amplifier**

separating the device into four basic elements. These four single-reactor elements are shown separately in Fig. 17 in order to define the reference polarities of the circuit variables.

The voltage source $e_g$ is a symmetrical square wave, and hence has no d-c component. It therefore functions merely as a synchronous switch to bias the rectifier in the reverse direction on one half-cycle (termed the control period) and in the forward direction on the next half-cycle (termed the gate period). If the above condition is fulfilled and if the amplitude and the frequency of $e_g$ do not fluctuate, then the supply voltage does not enter into the relations between the terminal variables.

In Fig. 18, elements I and II are combined to form a 2-core, half-wave amplifier, and elements III and IV are combined in a similar manner. It is evident from the polarity of the supply voltages that a control period of element I corresponds to a gating period of element II. Similarly, a control period of element IV corresponds to a gating period of element III.

The two half-wave amplifiers of Fig. 18(A) and (B) are combined in Fig. 19 to form the desired full-wave amplifier. Because the input terminals of the full-wave amplifier are connected in series and the output terminals are connected in parallel, it is convenient to use a hybrid matrix in which the input voltage and output current are used as the dependent variables. In the following equations, the variable quantities represent the Laplace transforms of the half-cycle averages of voltages and currents.

Each basic element of Fig. 17 may be presented in matrix form by

$$\|\alpha_j\| = \|H_j\| \ \|\beta_j\| \ (j = \text{I, II, III, IV}) \qquad (11)$$

where

$$\|\alpha_j\| = \begin{Vmatrix} (E_j)_1{}^c \\ (E_j)_1{}^g \\ (I_j)_2{}^c \\ (I_j)_2{}^g \end{Vmatrix} \text{ and } \|\beta_j\| = \begin{Vmatrix} (I_j)_1{}^c \\ (I_j)_1{}^g \\ (E_j)_2{}^c \\ (E_j)_2{}^g \end{Vmatrix} \qquad (12)$$

The superscripts $c$ and $g$ refer to the control and gating periods respectively.

The basic circuit of Fig. 15 shows the series resistor in the output circuit $R_2$ as a linear element. This resistor must be modified to take into account the diode in the output circuit of the actual elements shown in Fig. 17. In the following equations, the term $R_b$ is defined as the diode reverse resistance plus the resistance of the core winding, and $R_f$ is defined as the diode forward resistance plus the resistance of the core winding. Thus, $R_f$ replaces $R_2$ when $e_g$ is in such a direction that the rectifier is conducting, and $R_b$ replaces $R_2$ when $e_g$ is in such a direction that the rectifier is nonconducting.

Because the basic elements are identical, the $\|H_j\|$ matrix is the same for any value of $j$. With the modifications explained in the above paragraph taken into account, the network matrix is given by

$$\|H_I\| = \begin{Vmatrix} (R_1+N^2R_3) & 0 & NR_3/R_b & 0 \\ -N^2R_3' & R_1 & -NR_3'/R_b & 0 \\ -NR_3/R_b & 0 & R_3/R_MR_b & 0 \\ NR_3'/R_f & 0 & R_3'/R_fR_b & 1/R_f \end{Vmatrix} \qquad (13)$$

where

$$R_3 = R_MR_b/(R_M+R_b)$$

$$R_3' = R_3/z$$

$$z = \epsilon^{(\pi/\omega_a)S}$$

$\omega_a$ = frequency of the supply voltage $e_g$.

Because of the symmetry which exists between the interconnection consisting of elements I and II and the interconnection consisting of elements III and IV, it is apparent that for any equation involving only elements I and II, an identical equation (except for a change of capital subscripts) may be written involving only elements III and IV. In the following steps, therefore, only equations necessary to obtain relations for the half-wave amplifier of Fig. 18(A) will be written explicitly. The terminal quantities of the final interconnection ($e_1$, $i_1$, $e_2$, and $i_2$ in Fig. 19) will then be obtained by addition of the two identical matrices for the half-wave amplifiers of Fig. 18.

Consideration of the relative polarity of the supply voltages in Fig. 18(A) yields the following relations:

$$\begin{aligned} (I_I)_1{}^c &= (I_{II})_1{}^g \\ (I_I)_1{}^g &= (I_{II})_1{}^c \\ (E_I)_2{}^c &= (E_{II})_2{}^g \\ (E_I)_2{}^g &= (E_{II})_2{}^c \end{aligned} \qquad (14)$$

If the transformation matrix

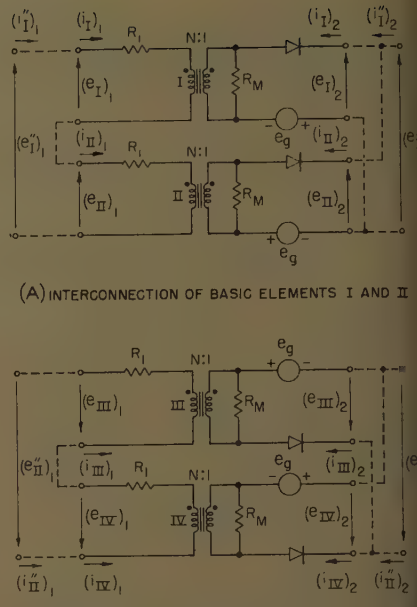


**Fig. 18. Interconnections to form two half wave amplifiers**

$$\|T\| = \begin{Vmatrix} 0 & 1 & 0 & 0 \\ 1 & 0 & 0 & 0 \\ 0 & 0 & 0 & 1 \\ 0 & 0 & 1 & 0 \end{Vmatrix} \qquad (15$$

is defined, it may be seen that

$$\|\beta_{II}\| = \|T\| \ \|\beta_I\| \qquad (16$$

From Fig. 18(A), the following relation may be written:

$$(E_I'')_1 = (E_I)_1{}^c + (E_{II})_1{}^g \qquad (17$$

$$(I_I'')_2 = (I_I)_2{}^c + (I_{II})_2{}^g \qquad (18$$

The following transformation of variable is now made:

$$\|\alpha_{II}\| = \|T\| \ \|\alpha_{II}'\| \qquad (19$$

where

$$\|\alpha_{II}'\| = \begin{Vmatrix} (E_{II})_1{}^g \\ (E_{II})_1{}^c \\ (I_{II})_2{}^g \\ (I_{II})_2{}^c \end{Vmatrix} \qquad (20$$

Equation 11 (for $j$=II) may now be written as

$$\|T\| \ \|\alpha_{II}'\| = \|H_I\| \ \|T\| \ \|\beta_I\| \qquad (21$$

but, since the transformation matrix is equal to its inverse, equation 21 may be premultiplied by $\|T\|$ with the result

$$\|\alpha_{II}'\| = \|T\| \ \|H_I\| \ \|T\| \ \|\beta_I\| \qquad (22$$

It is seen that the addition of equations 11 (for $j$=I) and 22 yields the desired matrix for the double-primed terminals.

$$\|\alpha_I''\| = \|H_1\| + \|T\| \ \|H_I\| \ \|T\| \ \|\beta_I\| = \|H\| \ \|\beta_I\| \qquad (23$$

where

$$\|H\| = \|H_I\| + \|T\| \ \|H_I\| \ \|T\| \qquad (24$$

and

$$\|\alpha_I''\| = \|\alpha_I\| + \|\alpha_I'\| = \begin{Vmatrix} (E_I)_1^c + (E_{II})_1^g \\ (E_I)_1^g + (E_{II})_1^c \\ (I_I)_2^c + (I_{II})_2^g \\ (I_I)_2^g + (I_{II})_2^c \end{Vmatrix} = \begin{Vmatrix} (E_I'')_1^c \\ (E_I'')_1^g \\ (I_I'')_2^c \\ (I_I'')_2^g \end{Vmatrix}$$

When the matrix transformation and addition indicated in equation 24 is performed, the following network matrix for the 2-core amplifier is obtained as

$$\|H\| = \begin{Vmatrix} (2R_1+N^2R_3) & -N^2R_3' & NR_3/R_b & -NR_3'/R_b \\ -N^2R_3' & (2R_1+N^2R_3) & -NR_3'/R_b & NR_3/R_b \\ -NR_3/R_b & NR_3'/R_f & (1/R_f+R_3/R_MR_b) & R_3'/R_fR_b \\ NR_3'/R_f & -NR_3/R_b & R_3'/R_fR_b & (1/R_f+R_3/R_MR_b) \end{Vmatrix} \quad (25)$$

If the first two rows and the second two rows respectively of $[\alpha_I'']$ are added, there results

$$(E_1'')_1 = m(I_1'')_1 + n(E_1'')_2 \quad (26)$$

$$(I_1'')_2 = p(I_1'')_1 + q(E_1'')_2 \quad (27)$$

where

$$(E_k'')_r = (E_k'')_r^c + (E_k'')_r^g \quad (k = I, II)$$

$$(I_k'')_r = (I_k'')_r^c + (I_k'')_r^g \quad (r = I, 2)$$

$$m = 2R_1 + N^2(R_3 - R_3')$$

$$n = N/R_b(R_3 - R_3')$$

$$p = N(R_3'/R_f - R_3/R_b)$$

$$q = 1/R_f + R_3/R_MR_b + R_3'/R_fR_b$$

It should be remembered at this point that an identical set of equations exists for the variables $(E_{II})_1$ and $(I_{II}'')_2$. From Fig. 18, it may be seen that

$$(I_{II}'')_1 = -(I_1'')_1 \quad (28)$$

and from Fig. 19 that

$$(I_1'')_1 = I_1 \quad (29)$$

Hence, the network matrices for the double-primed terminals of the half-wave circuits of Fig. 18(A) and (B) may be written as

$$\begin{Vmatrix} (E_I'')_1 \\ (I_I'')_2 \end{Vmatrix} = \begin{Vmatrix} m & n \\ p & q \end{Vmatrix} \begin{Vmatrix} (I_1'')_1 \\ (E_I'')_2 \end{Vmatrix} \quad (30)$$

$$\begin{Vmatrix} (E_{II}'')_1 \\ (I_{II}'')_2 \end{Vmatrix} = \begin{Vmatrix} -m & n \\ -p & q \end{Vmatrix} \begin{Vmatrix} (I_1'')_1 \\ (E_{II}'')_2 \end{Vmatrix} \quad (31)$$

Consideration of Fig. 20 leads to the following equations:

$$(E_I'')_2 = -(I_I'')_2R_s + E_2 \quad (32)$$

$$(E_{II}'')_2 = -(I_{II}'')_2R_s - E_2 \quad (33)$$

Substitution of equation 32 into 30 and equation 33 into 31 yields

$$\begin{Vmatrix} (E_I'')_1 \\ (I_1'')_2 \end{Vmatrix} = \begin{Vmatrix} A & B \\ C & D \end{Vmatrix} \begin{Vmatrix} I_1 \\ E_2 \end{Vmatrix} \quad (34)$$

$$\begin{Vmatrix} (E_{II}'')_1 \\ (I_{II}'')_2 \end{Vmatrix} = -\begin{Vmatrix} A & B \\ C & D \end{Vmatrix} \begin{Vmatrix} I_1 \\ E_2 \end{Vmatrix} \quad (35)$$

where

$$A = m - \frac{npR_s}{1+qR_s}$$

$$B = n - \frac{ngR_s}{1+qR_s}$$

$$C = \frac{p}{1+qR_s}$$

$$D = \frac{q}{1+qR_s}$$

Subtraction of equation 35 from equation 34 yields the network matrix for the full-wave amplifier:

$$\begin{Vmatrix} E_1 \\ I_2 \end{Vmatrix} = 2\begin{Vmatrix} A & B \\ C & D \end{Vmatrix} \begin{Vmatrix} I_1 \\ E_2 \end{Vmatrix} \quad (36)$$

$$E_1 = (E_I'')_1 - (E_{II}'')_1$$

$$I_2 = (I_I'')_2 - (I_{II}'')_2$$

To relate the output voltage to the control voltage, the load characteristics must be known. If it is assumed that the input impedance to the following stage is a linear resistance $R_T$, then

$$I_2 = -E_2/R_T \quad (37)$$

Substitution of equation 37 into the network matrix and elimination of $I_1$ from the two equations yields the desired transfer function.

The resulting transfer function may be simplified if it is assumed that the diode reverse impedance $R_b$, is infinite. In this case, the transfer function obtained from equations 36 and 37 becomes

$$E_2(S) - 2\sigma\epsilon^{-(\pi/\omega_a)S}E_2(S) = -(2\gamma\sigma/N)\epsilon^{-(\pi/\omega_a)S}E_1(S) \quad (38)$$

or

$$\frac{E_2(S)}{E_1(S)} = -\frac{2\gamma\sigma}{N}\,\frac{\epsilon^{-(\pi/\omega_a)S}}{1-2\sigma\epsilon^{-(\pi/\omega_a)S}} \quad (39)$$

where

$$\sigma = \frac{N^2R_M}{R_c+2N^2R_M}$$

$$R_c = 4R_1$$

$$\gamma = \frac{R_T}{R_f+R_s+2R_T}$$

The difference equation may be obtained by taking the inverse Laplace transform of equation 38. The result of this operation is

$$E_2(n+1) - 2\sigma E_2(n) = -(2\gamma\sigma/N)E_1(n) \quad (40)$$

Equation 39 is somewhat inconvenient for the purpose of servo analysis because of the delay term in the denominator. Since $\pi/\omega_a \ll 1$, the exponential term may be approximated by the first two terms of a series expansion:

$$\epsilon^{-(\pi/\omega_a)S} \approx \frac{1}{(\pi/\omega_a)S+1}$$

Equation 39 then becomes

$$G_{MA}(S) = \frac{E_2(S)}{E_1(S)} = -\frac{2\gamma\sigma}{N(1-2\sigma)}\,\frac{1}{\frac{(\pi/\omega_a)}{1-2\sigma}S+1} \quad (41)$$

Equation 41 represents the amplifier by a single time constant and neglects the inherent transportation lag of one half-cycle of the supply voltage, which is assumed to be negligible.

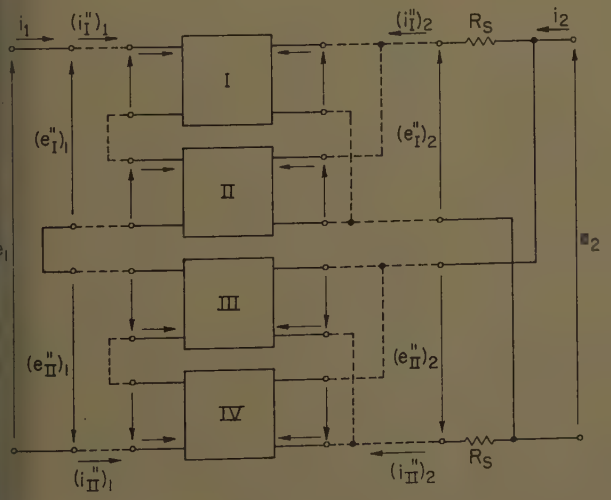


Fig. 19. Full-wave amplifier as an interconnection of four basic elements

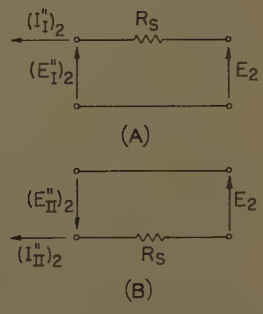


Fig. 20. Relationships at the output terminals

## References


1. Application of a Magnetic Amplifier to a High Performance Instrument Servo. P. R. Johannessen. *Technical Report 7002-10*, Massachusetts Institute of Technology, Cambridge, Mass., May 1955.

2. An Improved Servo Amplifier, C. W. Lufcy, A. E. Schmidt, P. W. Barnhardt. *AIEE Transactions*, pt. I (*Communication and Electronics*), vol. 71, Sept. 1952, pp. 281–89.

3. A Five-Kilocycle Magnetic Amplifier for Servo-motors, D. G. Fischer. *M.S. Thesis*, Massachusetts Institute of Technology, Aug. 1956.

4. Power Switching Transistors in Servo Amplifiers, S. E. Beckjord. *Technical Report 7002-13*, Massachusetts Institute of Technology, June 1956.

5. A Switching Transistor D-C to A-C Converter Having an Output Frequency Proportional to the D-C Input Voltage, G. H.

Royer. *AIEE Transactions*, pt. I (*Communication and Electronics*), vol. 74, July 1955, pp. 323–33.

6. Comparison of Three Basic Types of Compensation of Electric Servomechanisms, George Biernson. *Engineering Memorandum no. 27, DIC Project 6506*, Massachusetts Institute of Technology, May 1952.

7. Damper Stabilized Servo Data Repeater, J. E. Ward. *Report 7138-TM-3*, Massachusetts Institute of Technology, July 1955.

8. A Study of a Dual-Mode Damper-Stabilized Servo, James R. Kaiser. *Technical Report 7002-16*, Massachusetts Institute of Technology, June 1956.

9. Magnetically Keyed, Phase-Sensitive Demodulators, Robert B. Mark, Wheeler X. Johnson, Paul R. Johannessen. *AIEE Transactions*, pt. I (*Communication and Electronics*), vol. 76, Mar. 1957, pp. 1–6.

10. Application of Switching Transistors and Saturable Reactors in a High-Performance Servo, Fred B. Cox, Jr. *M.S. Thesis*, Massachusetts Institute of Technology, Sept. 1957.

11. Analysis of Magnetic Amplifiers, P. R. Johannessen. *Memorandum 7668-M-235R*, Massachusetts Institute of Technology, July 2, 1957.

12. Analysis and Design Procedure for a Two-Stage Magnetic Amplifier, T. Knutrud. *M.S. Thesis*, Massachusetts Institute of Technology, June 1956.

13. Analysis of Magnetic Amplifiers by the Use of Difference Equations, P. R. Johannessen. *AIEE Transactions*, pt. I (*Communication and Electronics*), vol. 73, 1954 (Jan. 1955 section), pp. 700–11.

# Rapid Transit Is Expanding in Chicago

STANLEY D. FORSYTHE
NONMEMBER AIEE

MAN is that inexplicably complex creature who confidently expects to fly to the moon in the next decade and yet spends more time between home and work now than he did a decade ago.

When the mayors of some of the world's largest cities were asked by the Citizens' Budget Commission of New York, N.Y., to name the worst problems facing their cities, finance, taxation, and transportation and traffic were almost unanimously selected.[1]

A Chicago, Ill., planner has estimated that it takes 5,000,000 square feet of off-street parking space to handle the automotive traffic brought in by a single new expressway lane, implying that the mammoth road building programs under way will help provide facilities to carry vehicles in motion, but will not solve the problem of providing for these vehicles at rest.

Every city in the United States underwrites its rapid transit system to some degree, and those now without rapid transit but planning such facilities for the future, will underwrite these operations to a greater degree than most of the existing systems enjoy.

There would seem to be a common denominator to these rather unrelated statements. It is this: A modern well-designed, adequate rapid transit system can contribute substantially to solving the mayors' problems, can contribute substantially to minimizing the need for mammoth downtown parking facilities, and can, in general, improve the attractiveness of urban living. More and more it is being recognized throughout the United States that a rapid transit system is a very valuable municipal asset which should be considered in much the same light as are other municipal assets such as highways, sewers, water, lighting, fire protection, and police protection. In San Francisco, Calif., for example, legislation is being prepared which would provide the necessary measure of public support for a rapid transit system that is estimated will cost ultimately $1,700,000-000. It will serve a population estimated at 7,000,000 by 1990 and a territory of approximately 7,500 square miles. A somewhat similar program is under way in Los Angeles and a number of other cities throughout the country are taking tentative steps in this direction. Therefore, since every rapid transit system on the North American continent in operation or under consideration is supported or planned to be supported to a greater or less degree by the municipality which it serves, it is not too radical to say that any large city can have just as fine a rapid transit system as its citizens desire.

Chicago planners and government officials are awake to this possibility and the city is becoming increasingly aware of the value of its rapid transit system. As this awareness grows, another decade should see tremendous changes and significant enlargement of the existing system which, during the last 40 of its 55 years of private operation, was financially unable to make any sizable extensions. This prediction is based on what has been done during the last decade, what is being done at present, and what is being actively planned for the near future. In each of these phases, there has been and will be increasing participation by the citizenry as a whole.

Practically all of the elevated system that the Chicago Transit Authority took over in 1947 was installed in the few years between 1893 and 1907. That it was well conceived and well built is borne out by the use to which it is still being put today. But the city has grown so greatly both in population and area that rapid transit routes in some important instances do not extend far enough to serve sizable residential, commercial, and manufacturing centers, and in other instances are nonexistent.

The cost of underground tubes is prohibitively expensive and they must be confined to those areas where no other type of right-of-way is available. The outmoded elevated structures erected around the turn of the century depress property values and discourage substantial additions to this type of right-of-way. There remains, however, the unparalleled opportunity to incorporate rapid transit into urban highway plans and this possibility is being actively considered in connection with every expressway which is planned for the Chicago area. In addition, there is gradually emerging a realization that railroad rights-of-way furnish well-protected traffic-free arteries that may also, in certain instances, accommodate rapid transit facilities a great benefit to the municipality. A look at a railroad map of any large city will show how much comparatively lightly used right-of-way of this type exists. The rapidly changing attitude of railroad officials towards this possibility makes it a particularly attractive one to explore when rapid transit routes are being sought.

When the Chicago Transit Authority took over the existing rapid transit system late in 1947, the rapid transit company had only four pieces of equipment less than 30 years old, and no multiple-unit door-control operation. In addition, there were far too many stations for true rapid transit service, and the cost of maintaining and operating these stations 24 hours a day was a very heavy burden. At that time the number of employees per vehicle amounted to 3.2. Today Chicago has 474 lightweight high-speed multiple-unit door-control cars (with 130 more on order), and the multiple

Paper 56-837, recommended by the AIEE Land Transportation Committee and approved by the AIEE Technical Operations Department. Manuscript submitted June 26, 1956; made available for printing April 3, 1959.

Stanley D. Forsythe is with the Chicago Transit Authority, Chicago, Ill.

nit door control has been installed on nore than 400 of the older all-steel cars. Approximately 25 stations have been liminated, fare collection on the trains as been instituted during the hours of ghter traffic, and several terminal loops ave been installed to replace stub-end perations with their attendant operating osts. The skip-stop system in wide use n the entire system has substantially in-reased the operating speed of all trains. The result of this and other kindred hanges has been to reduce the number of mployees per vehicle to 2.4. All this as been accomplished with but one ignificant change in the existing routes: he opening of the Dearborn Street Sub-vay. This change provided a more direct lowntown delivery for the Logan Square Branch extending approximately 5 miles northwest from the Loop.

All urban transportation systems have een drastic changes in revenue passengers during the last decade. The Chicago Transit Authority was no exception. However, the way in which rapid transit iding continued, and even increased lightly, during this period greatly en-couraged those who feel that rapid transit s an important asset to Chicago's well-eing. While revenue rides on the sur-ace system declined from 641,600,000 in 950 to 510,600,000 in 1955 (a decrease of pproximately 20%), the rapid transit iding increased from 110,600,000 to 112,-00,000. This is a very modest increase, ut a very significant one in view of the act that there was no change in the erritory directly served by the rapid ransit system during these years.

During this 6-year period the car-miles er employee on the entire system in-reased from 8,750 to 10,800, or 23%. The corresponding increase on the Rapid Transit Division was from 9,150 to 12,250, r 34%.

The revenue rides per employee on the ntire system increased from 38,300 to 1,500, or 10.5%. The corresponding ncrease on the Rapid Transit Division as from 25,200 to 31,800, or 26%.

These figures are measures of operating fficiencies and illustrate what is being one in rapid transit service to reduce osts with modern facilities and tech-iques.

Much more can be done and is being lanned in this area. A further and more mplete modernization of rolling stock, ubstitution of high-speed grade-separated rivate rights-of-way for obsolete elevated ructures and ground-line operation, mplified fare-collection techniques, mod-n maintenance facilities, and other re-ted activities will tend to decrease the operating costs of rapid transit operation further.

It was stated earlier that any large city have as fine a rapid transit system as its citizens desire.

The preceding figures indicate that even today, modern rapid transit operation can be in the same cost bracket as bus operation on city streets, but that the capital cost remains a burden. This suggests that cities and rapid transit operators might co-operate to their mutual advantage on a "we'll build it, you operate it" basis. The value that the San Francisco planners place on this type of public works is clearly indicated by the sources of funds suggested to finance their $1.7 billion rapid transit program, the first stage of which is estimated to cost $875,000,000. They feel that the need for rapid transit in this area is such that they would provide over $30,000,000 of public support per year for the next 30 years to serve the bonded indebtedness of the first stage. This public support would come from property tax, retail sales tax, gasoline tax, and payroll tax. In addition, a proportion of bridge tolls is included. The possibility of state or federal aid has been discussed, but the planners prudently refrain from recommending a definite proportion of support from these sources.

It is clearly intended, however, that the citizens acting through either an authority or a district (probably the latter in this instance) will finance and build the rapid transit facilities and that the operation of these facilities will be supported by the revenues. That degree of support could revolutionize the activities of many large American urban areas, and the planners are to be commended for their vision.

The rapid transit incorporated in the median strip of the Congress Street or West Route Expressway, opened in June 1958, utilizes welded rails on heavily ballasted track with long radius curves to permit a speed of operation limited only by the distance between stops. Attractive island-type stations are connected by covered ramps to adjacent bridges carrying cross-traffic over the expressway. This route, extending approximately 10 miles west from the Loop, largely replaces an older route that combined elevated and ground-line operation using some of the oldest equipment on the system. It has a new downtown delivery which, instead of using the elevated Loop, combines with the Logan Square Branch and operates through the Dearborn Street Subway. It will be extremely interesting to see the effect on traffic volume of new equipment, new right-of-way, and a greatly reduced running time.

The Northwest Route Expressway, extending from a point just west of the Loop to the northwest city limits, was originally designed without provision for rapid transit. In the last several years, however, the highway designers have become convinced that rapid transit in the median strip is a vital necessity in order to relieve the expressway of some of its automobile traffic. Therefore, the plans were altered to include a 2-track rapid transit line with island platform stations approximately every 7/10ths of a mile. This line extends northwest from the Logan Square terminal for a distance of approximately $7\frac{1}{2}$ miles. It was installed in accordance with the formula that has been used by the city and the Chicago Transit Authority since the inception of the Authority whereby the city installs all of the fixed transportation equipment and the Chicago Transit Authority repays the city in monthly payments over a period of approximately 30 years without interest charges. The cost of the right-of-way and stations is not included in the amount repaid to the city.

As the last three miles of this extension provide extremely light traffic for normal rapid transit operation, the Authority suggested to the city that the Authority be relieved of any repayment for the cost of fixed transportation equipment until the revenues justify such payments.

Another significant improvement in rapid transit service concerns the west end of the Lake Street Branch. The outermost $2\frac{1}{2}$-mile section of this line, which serves the west side of Chicago and the village of Oak Park, involves 22 grade crossings. Immediately to the north of the Chicago Transit Authority right-of-way is an elevated 6-track right-of-way belonging to the Chicago North Western Railroad. The railroad has indicated its willingness to lease two tracks to the Chicago Transit Authority and the various governmental and highway agencies interested in this $2\frac{1}{2}$-mile stretch have indicated their approval of the project and their willingness to share in the expense of eliminating these 22 grade crossings at an estimated total cost not to exceed $4,000,000. This would substantially improve the rapid transit service on this branch as well as immeasurably improve street traffic conditions through the affected area. There will also be a notable improvement in abutting property values. It is expected that work on this project can be completed 18 months after agreements are signed.

The South Route Expressway starts from a point just west of the Loop and, after a short swing to the east, generally parallels State Street south from the Loop to 99th Street where the highway divides. One branch will serve Beverly Hills and Morgan Park to the southwest while the other branch will serve the Lake Calumet industrial district to the southeast. Here, too, it is being planned that a median strip of sufficient width for rapid transit operation will be provided throughout the entire length of the expressway. It is felt that rapid transit operation should be provided in that part of the expressway nearest the central business district at the earliest opportunity and extended south as far and as quickly as circumstances permit. The south end of the State Street Subway would be only slightly more than $1^1/_2$ miles from a convenient point of access to this median strip, or a shorter connection could be made farther south to the south-side elevated structure.

Another opportunity for an important median strip rapid transit operation will arise when the the crosstown expressway is built. This is planned to extend 7 miles in a north-south direction, approximately $3^1/_2$ miles west of and paralleling State Street, from the Northwest Expressway on the north to the Southwest Expressway on the south. Rapid transit operation on this expressway which would intersect every rapid transit branch except the North-South and Ravenswood as well as 30-section line, half-section line, and diagonal streets, would furnish an excellent north-south trunk line by-passing the central business district but linking a number of outlying commercial, residential and manufacturing districts.

From the viewpoint of a mass transit operator, it is extremely gratifying to see how rapidly highway planners and city officials have come to realize the invaluable role that rapid transit plays in the big team job of moving people. As this realization grows and larger segments of cities' populations learn how much rapid transit can be provided for a comparatively little expenditure as compared with highway construction, one can expect to see greatly expanding rapid transit facilities in many American cities.

## Reference

1. *American City*, New York, N. Y., Apr. 1956.

# Analysis of A-C Servomotors Operated from Unbalanced Nonsinusoidal Voltage Sources and Nonlinear Discontinuous Source Impedances

E. R. LIND
ASSOCIATE MEMBER AIEE

N. L. SCHMITZ
MEMBER AIEE

MANY ANALYTICAL studies directed at the predetermination of output characteristics of a-c servomotors have been based on the assumptions of constant-source impedance and sinusoidal excitation. Under these assumptions, the method of symmetrical components serves admirably, particularly when steady-state characteristics are desired, and in cases where the duration of the mechanical transients makes the electrical transients insignificant.

In recent years, the use of devices such as chopper modulators, magnetic amplifiers, and gaseous tubes in servomechanism design has caused a-c servomotors to be subjected to new modes of operation. These devices may produce nonsinusoidal waveforms which are supplied through constant impedance amplifiers to the servomotor. In other cases the waveform is nonsinusoidal and the output impedance of the amplifier is nonlinear. With thyratrons or magnetic amplifiers, the output impedance is essentially zero during conduction and approaches open-circuit conditions during the nonconducting period. In addition, the waveform may have either an average value (d-c level), or the direct current may be superimposed on sine-wave excitation to produce some desired dynamic effect.

A considerable volume of literature has appeared concerning magnetic materials, thyratrons, semiconductor devices, etc. Much study has gone into these special devices but there is a serious lack of information available on the performance of a-c servomotors when operated in conjunction with these nonlinear devices.

Methods outlined in this paper circumvent the limitations of the method of symmetrical components and permit analysis of systems wherein source impedances are discontinuous functions of current and time. Electromotive force (emf) sources may be either sinusoidal or nonsinusoidal.

Paper 59-1157, recommended by the AIEE Feedback Control Systems Committee and approved by the AIEE Technical Operations Department for presentation at the AIEE Fall General Meeting, Chicago, Ill., October 11–16, 1959. Manuscript submitted March 20, 1959; made available for printing August 7, 1959.

E. R. LIND is with the General Electric Company, Ithaca, N. Y., and N. L. SCHMITZ is with the University of Wisconsin, Madison, Wis.

## General Relationships

To specify completely the performance of a motor it is necessary to employ a physical representation in terms of the self and mutual operational impedances instead of the conventional steady-state equivalent circuit. This has been done in the classic paper by H. C. Stanley[1]. Stanley's equations can be rewritten in the following form to facilitate solution:

$$-\frac{dI_\alpha}{dt} = -\frac{V_\alpha}{L_S} + \frac{R_S}{L_S} I_\alpha + \frac{M}{L_S}\frac{di_\alpha}{dt}$$

$$-\frac{dI_\beta}{dt} = -\frac{V_\beta}{L_S} + \frac{R_S}{L_S} I_\beta + \frac{M}{L_S}\frac{di_\beta}{dt}$$

$$\frac{di_\alpha}{dt} = -\frac{M}{L_R}\frac{dI_\alpha}{dt} - \frac{M}{L_R}\omega_0 I_\beta - \frac{R_R}{L_R} i_\alpha - \omega_0 i_\beta$$

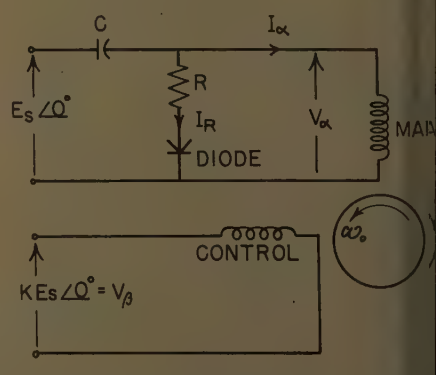


**Fig. 1. Phase shift and damping circuit for servomotor**

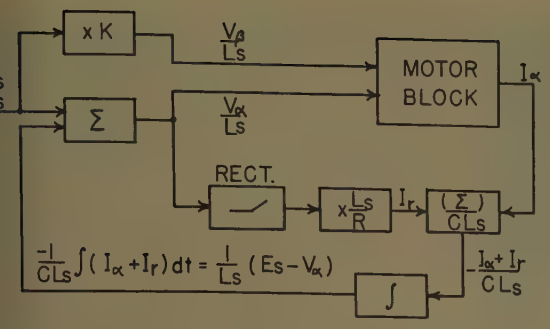


**2. Analog computer representation of nonlinear impedance in main phase**

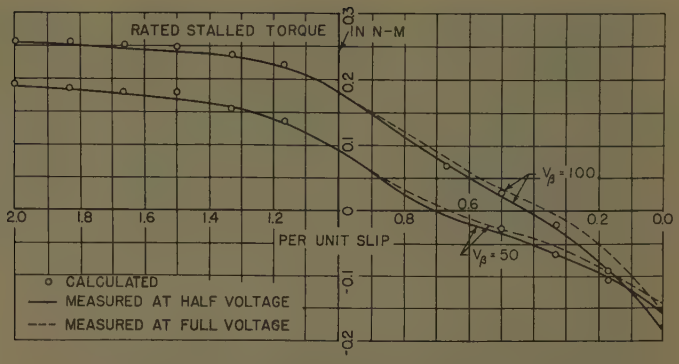


**Fig. 3. Slip torque characteristics of servomotor excited through nonlinear impedance**

$$=\frac{M}{L_R}\omega_0 I_\alpha-\frac{M}{L_R}\frac{dI_\beta}{dt}+\omega_0 i_\alpha-\frac{R_R}{L_R}i_\beta$$

hese equations have been widely used onjunction with operational methods obtain transient solutions to a wide iety of problems involving constant edances. With balanced sinusoidal itation, these equations are greatly plified by considerations of symmetry. following section sets forth methods olving these equations simultaneously h additional relationships describing variation of source impedances with rent or time.

## nputer Representation of Motor nd Source Impedances

n analog computer solution of this e of problem involves two parts. t 1 relates the motor torque and cur- t quantities to its input voltages. t 2 of the solution solves for the im- ssed voltages of the motor in terms of source emf's and impedances as well as or currents.

art 1, motor representation, is general. t 2, source representation, is necessarily developed with regard to the nature of the specific system in which the motor is to be applied. In this paper, part 2 is illustrated through application to a typical diode damping circuit (see Fig. 1).

## Illustrative Application

Part 1 of the computer solution is developed as shown in Appendix I. With this representation of the motor available it appears possible in the majority of cases to program the nonlinear portion of the circuit to supply the proper terminal voltages to the motor block of part 1. For the circuit of Fig. 1, this can be done in the following manner.

From an examination of the external circuits of Fig. 1, the potential drop across the phase-shift capacitor can be written as:

$$E_S-V_\alpha=\frac{1}{C}\int_0^t(I_\alpha+I_R)dt$$

also

$$I_R=\frac{V_\alpha}{R}\qquad V_\alpha>0$$

$$I_R=0\qquad V_\alpha\leq 0$$

From Appendix I, the terminal input voltages to that portion of the computer which represents the motor are $V_\alpha/L_S$ and $V_\beta/L_S$.

Hence:

$$\frac{1}{L_S}(E_S-V_\alpha)=\frac{1}{CL_S}\int_0^t(I_\alpha+I_R)dt$$

and

$$I_R=\frac{V_\alpha/L_S}{R/L_S}\qquad V_\alpha>0$$

$$I_R=0\qquad V_\alpha\leq 0$$

The program for this nonlinear external circuitry is represented in Fig. 2. The nonlinear element, the diode, is represented by a Philbrick half-wave rectifier unit. Only the $I_\alpha$ motor current is necessary to complete this program and this is obtained from the motor block.

The only adjustment required is the setting of the two $\omega_0$ constants to correspond to the desired speed, as shown in Appendix I. The circuit of Fig. 1 was

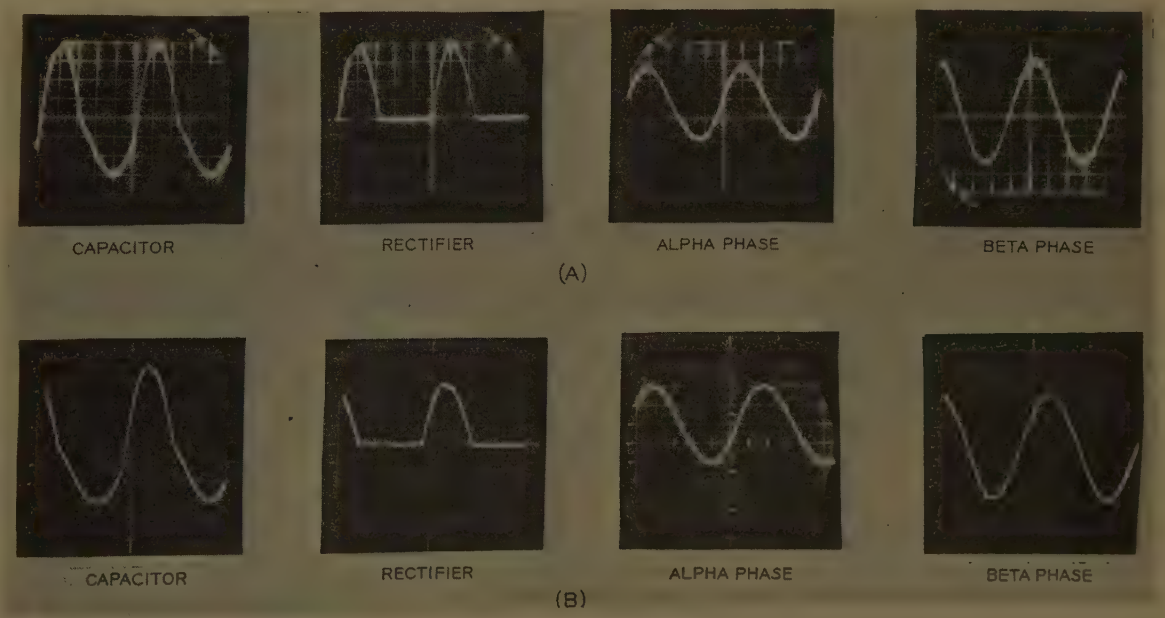


**4. Comparison computer (A) experimental (B) nt waveforms onlinear driving it. Horizontal s in A differ om those in B**

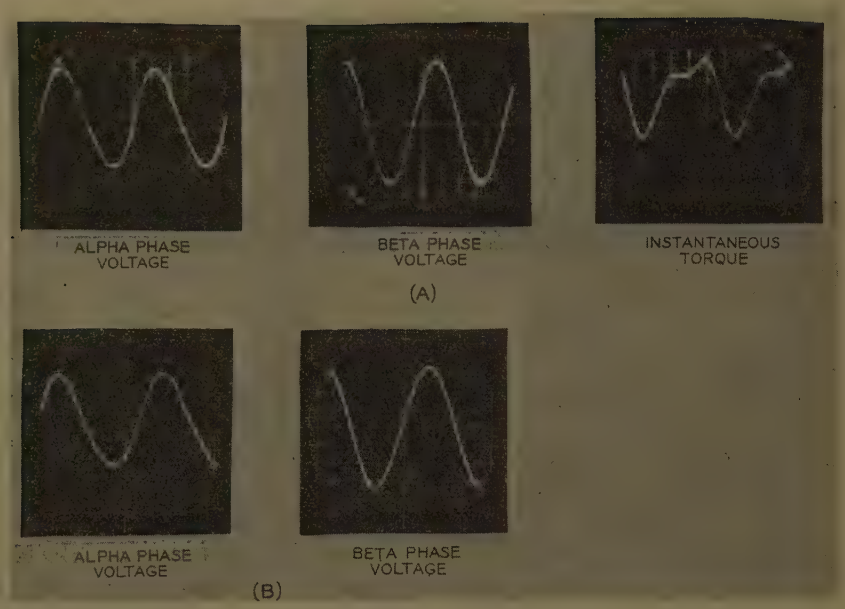


**Fig. 5. Comparison of computer (A) and experimental (B) torque and voltage waveforms for nonlinear driving circuit. Horizontal scales in A differ from those in B**

thoroughly investigated in the laboratory and then simulated on the Wisconsin-Philbrick analog computer.

## Comparison of Experimental and Computer Results

The physical constants of the experimental circuits are presented in Appendix II, along with the scaling factors used by the authors on a fast-time computer having a 1-ms (millisecond) time base. The static slip-torque curves for the experimental and computer results are presented in Fig. 3.

The dashed curves represent the original experimental data measured with full excitation. When the computer solution was compared with these experimental results, a large discrepancy was noted in the small slip region. A careful re-examination of the experimental results revealed that both the direct component and the a-c exciting component of current in the main phase increase as slip becomes small. Also, the phase shift between currents in the main and control phases becomes very small as slip decreases. These factors suggested the possibility of magnetic saturation. A second experimental curve was run with excitation voltages all reduced by a factor of 2. These new test data were scaled to represent full voltage operation and excellent agreement with the computer solution was achieved.

Figs. 4 and 5 present a comparison of the various waveshapes from the computer solution and the physical setup in the laboratory. Again, the correlation is excellent. Instantaneous torque waveform could not be recorded in the laboratory.

## Conclusions

The analysis of 2-phase servomotors excited through stator impedances which are nonlinear discontinuous functions of time and current can be accomplished through the use of the analog computer. The simple study presented herein illustrates the basic approach. More complicated studies can now be undertaken with confidence in the computer representation.

In addition, although the computer studies presented in this paper were limited to steady-state conditions, this same basic program can be readily adapted for transient studies by replacing the two $\omega_0$ coefficient units with multipliers. This would permit a rigorous solution for the transient response of a complete carrier servomechanism, either with linear or nonlinear amplifiers.

The complexity of the motor representation makes the exact study of large or complicated servo systems difficult. D tailed representation of the motor ca however, help establish more accurate the parameters to be used in the simplifie "transfer function" of the motor und any condition of excitation.

## Appendix I

The analog computer representation of 2-phase servomotor is presented in Fig. This circuit is based on the physical repr sentation of the motor, not on an equivale circuit. The equations presented earl will give the rotor and stator currents f the applied stator voltages, whether sin soidal excitation is applied or not. T torque is found from the general expressi for torque in terms of the space rate change of flux linkages. Thus torque comes:

$$T = M(I_\beta i_\alpha - I_\alpha i_\beta)$$

This is instantaneous torque and will subject to fairly violent variations if t inputs are unbalanced. The average torc may be found by putting this instantane torque through a lag unit having unity g and a very long time constant.

## Appendix II

The motor used for the studies und taken in this paper is a Diehl-type *FPE 11*, 115-volt 60-cycle-per-second 2-phase watt servomotor. This machine was fou to have quite linear characteristics over normal operating range.

The values of the motor and circ parameters and an explanation of the va ous symbols used in the program are p sented in Appendix III.

The actual rotor currents may be found applying the inverse transformations fr Stanley's paper. Thus, the rotor curre $i_1$, $i_2$ become:

$$i_1 = i_\alpha \cos \omega_0 t + i_\beta \sin \omega_0 t$$

$$i_2 = -i_\alpha \sin \omega_0 t + i_\beta \cos \omega_0 t$$

Using these physical constants in c junction with the previously presented ferential equations yields a very unwieb set of coefficients. A set of scale fact which were found to yield a very desira set of equations for computer representati are:

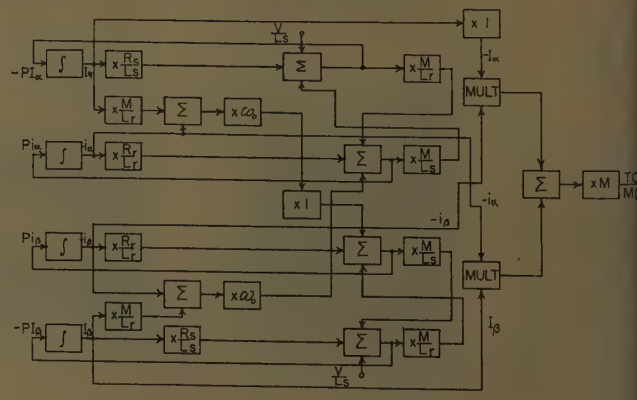


**Fig. 6. Computer representation of 2-phase servomotor**

$=0.01t'$
$_\alpha=0.01\ I_\alpha'$
$_\beta=0.01\ I_\beta'$
$_R=0.01\ I_R'$
$_\alpha=0.01\ i_\alpha'$
$_\beta=0.01\ i_\beta'$
$_0=100\ \omega_0'$
$V_\alpha=V_\alpha'$
$V_\beta=V_\beta'$
$E_S=E_S'$

## Appendix III. Nomenclature

$_R=684$ ohms, rotor-phase resistance
$_R=2.84$ henrys, total rotor-phase inductance
$M=2.59$ henrys, mutual inductance per phase
$L_S=2.84$ henrys, total stator-phase inductance
$R_S=317$ ohms, stator-phase resistance
$R=333$ ohms, rectifier dropping resistor
$C=7$ microfarads, phase-shift capacitor
$\omega_0=$output speed
$V_\alpha=$main-phase stator voltage
$V_\beta=100\ K$; $K=1, 1/2$, control-phase stator voltage
$E_S=100$ volts, circuit input reference voltage
$I_\alpha=$main-phase stator current
$I_\beta=$control-phase stator current
$I_R=$rectifier current
$i_\alpha, i_\beta=$transformed rotor-phase currents

## References


1. An Analysis of the Induction Machine, H. C. Stanley. *AIEE Transactions*, vol. 57, 1938, pp. 751–57.

2. Alternating Current Control of the Half-Wave Bridge Magnetic Amplifier, T. Bernstein, N. L. Schmitz. *Ibid.*, pt. I (*Communication and Electronics*), vol. 75, Sept. 1956, pp. 433–38.

3. Operating Characteristics of 2-Phase Servomotors, R. J. W. Koopman. *Ibid.*, vol. 68, pt. I, 1949, pp. 319–29.

4. Analysis of AC Servomotors Operated from Unbalanced, Non-Sinusoidal Voltage Sources and Nonlinear Discontinuous Source Impedances, E. R. Lind. *Ph.D. Thesis*, University of Wisconsin, Madison, Wis., 1958.


## Discussion

. M. Saunders and A. M. Hopkin (University of California, Berkeley, Calif.): nalog computer representations for servootors, with one exception,[1] have not reived much attention in the recent technical terature although two papers on analog mputer studies of the transient response induction motors did appear about fifteen ears ago.[2,3] Considering these three pubcations, the authors, in limiting themselves the steady-state case, have not made a ery strong contribution to the literature.

The use of direct and quadrature axis mponents and cross-field theory for solvg servomotor problems in the time domain as the distinct advantage over the use of symmetrical components and the revolving field theory in that the equations governing the behavior of the induction machine are expressed in real rather than in complex variables. Thus the use of direct and quadrature axis components lead directly to a solution under dynamic conditions when the variables are functions of time. In general, it may be said that the price paid for obtaining the solution in real time is that simultaneous solution of the equations of motion is not as simple and straightforward as the use of the equivalent circuits which come from the symmetrical component and revolving field theory. In the authors' case it seems regrettable to pay the price of complexity without obtaining a solution valid for transient excitations.

On the other hand, the symmetrical component method yielding, as it does, equivalent circuits is admirably adapted to the solution of steady-state problems even with nonzero source impedances or even nonsinusoidal excitation. In the case of nonzero source impedances one must develop the proper sequence network quantities representing the source impedances and include them as part of the positive and negative sequence networks. For nonsinusoidal excitation one must resolve the nonsinusoidal waveform into its component harmonics by a suitable Fourier analysis and then consider the response of the network to each harmonic successively. Generally speaking, in contrast with the authors' case, the excitation of 2-phase servomotors is such that nonharmonic sources only appear in the control phase and not in the

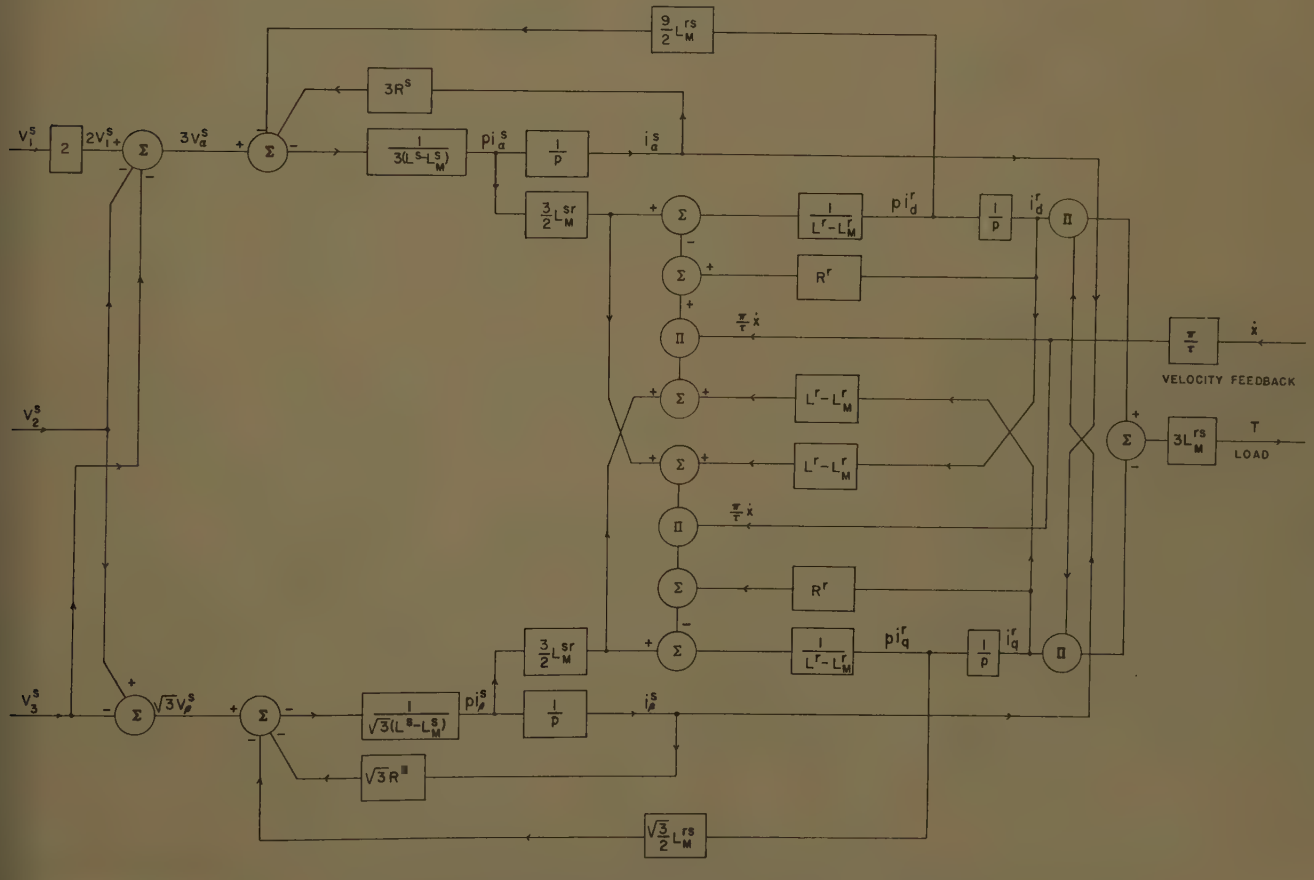


**Fig. 7. Analog computer representation for a 3-phase induction motor**

reference phase. Under such conditions the harmonic torque produced will have a single-phase motor characteristic (i.e., zero torque at zero speed). Further, the harmonic torques will be multiplied by $1/n^2$ at the very least. Considering the fact that the harmonic content of the voltage at the motor terminals is apt to be very low in amplitude for all components except the fundamental, only the fundamental component of the nonsinusoidal waveform needs to be considered since it is the only one which will produce an average torque. Of much more importance than the amplitudes of the harmonics is the phase shift of the fundamental component with respect to the fundamental component of the reference phase. We have found that with magnetic amplifier excitation of the control phase this effect is equally as important as the amplitude effect of the fundamental and is much more significant than the harmonic content. It is not clear in the paper if this phase shift effect is considered.

Unless saturation effects are to be considered, we can see little merit in using the direct and quadrature axis method for steady-state solutions. In the case of saturation, Slemon[4] points out that the use of direct and quadrature components on the stator and backward and forward components on the rotor yields a very satisfactory method of coping with the problem. It appears that in this particular case an analog computer representation could not be effected without the use of gyrators.

The White and Woodson[1] representation for the 2-phase servomotor is about as elemental as one can expect to achieve, and does cover not only the steady-state but the dynamic case where any time-varying excitation may be applied. Fig. 7 shows an analog computer representation for a 3-phase induction motor which will also yield dynamic as well as steady-state solutions.[5]

In some respects the elegance of an analog computer solution is measured by the number of components used to achieve the final result. In the authors' case it would take seven amplifiers, four integrators, and four multipliers to yield a dynamic solution. In the White and Woodson case the figures are 5, 4, and 6 respectively (although the discussers believe that the number of multipliers in their case could be cut to 4) and in the case of the 3-phase machine representation of Guilford and Saunders the figures are 6, 4, and 4 respectively. Even so, the use of an analog computer for 2-phase servomotors is a formidable operation and in most system studies is just not necessary.

One final note of caution: Not all servomotors are as free of space harmonics as the one shown in this paper. Erroneous results would tend to show up when the servomotor was rich in space harmonics and would tend to produce cusps in the speed-torque curve not predicted by the analog computer solution for the fundamental.

A basic weakness of the analog computer approach to problems is in the tendency of people to set up the computer before they have sufficient information concerning the true nature of the process being represented. In this case, the overlooking of saturation effects in the machine resulted in a discrepancy between computed and test data. The meaningful way to eliminate the discrepancy would have been to modify the computer representation to give a more realistic behavior of the model. The discussers note with distress that the authors eliminated the discrepancy by modifying the actual test procedure to give a less realistic measure of the motor behavior.

## References


1. Electromechanical Energy Conversion (book), **D. C. White, H. H. Woodson.** John Wiley & Sons, Inc., New York, N. Y., 1959, pp. 486–95.

2. Transient Performance of Induction Motors, **F. J. Maginniss, N. R. Schultz.** *AIEE Transactions*, vol. 63, Sept. 1944, pp. 641–46.

3. Electromechanical Transient Performance of Induction Motors, **C. N. Weygandt, S. Charp.** *Ibid.*, vol. 65, 1946, pp. 1000–09.

4. Equivalent Circuits for Single-Phase Motors, **G. R. Slemon.** *Ibid.*, pt. III (*Power Apparatus and Systems*), vol. 74, 1955 (Feb. 1956 section), pp. 1335–43.

5. Applications of Electromagnetic Field Theory to Induction Machines, **E. C. Guilford, R. M. Saunders.** *AIEE CP 58-201* (available on request).


**N. L. Schmitz and E. R. Lind:** Mr. Hopkin and Mr. Saunders seem to feel that the method of steady-state symmetrical components can be used to solve all steady-state induction motor problems; even those in volving nonzero source impedances whic are variable discontinuous functions o current and time. The authors do no agree with this.

It has been pointed out by the discusser that steady-state symmetrical component can be used to solve a variety of problem involving steady-state periodic voltages an constant linear impedances. This class problem is investigated in some detail i reference 4 of the paper. Their suppositio is applied conventionally to cases involvin nonsinusoidal impressed emf's in one or bot stator phases and in combination with d excitation. The fact that their suppositi proved inadequate in the solution of th more general problem involving variab discontinuous source impedances led to th method reported in the paper.

The authors concur in the comments r lating to harmonic torques caused by no sinusoidal excitation through fixed stat impedances. This aspect of inductio motor operation is considered in some d tail in reference 4. Figs. 8(A) an (B) (Figs. 4–7 and 4–8 of referen 4) show the speed-torque character tics of a servomotor obtained with sin voltage excitation in the main phase and variable length constant-amplitude volta pulse in the control phase. In one case t pulse was started at the maximum of t sine voltage, while in the other the pulse w centered in order to keep its fundamen component in quadrature with the sis voltage. Speed-torque curves were co puted using steady-state symmetrical co ponents and correlated to test resul This technique represents a possible a proach to the analysis of motor performan with magnetic amplifiers but it is n recommended by the authors. The disco tinuous nature of the output impedance the magnetic amplifier is not accounted in this method. Also the effect of mot load variations upon output voltage is n included.

The authors have not as yet evolve computer program for determining the p formance of a servomotor when opera with a magnetic amplifier. We note t the discussers have not disclosed a solut to this problem using either steady-st

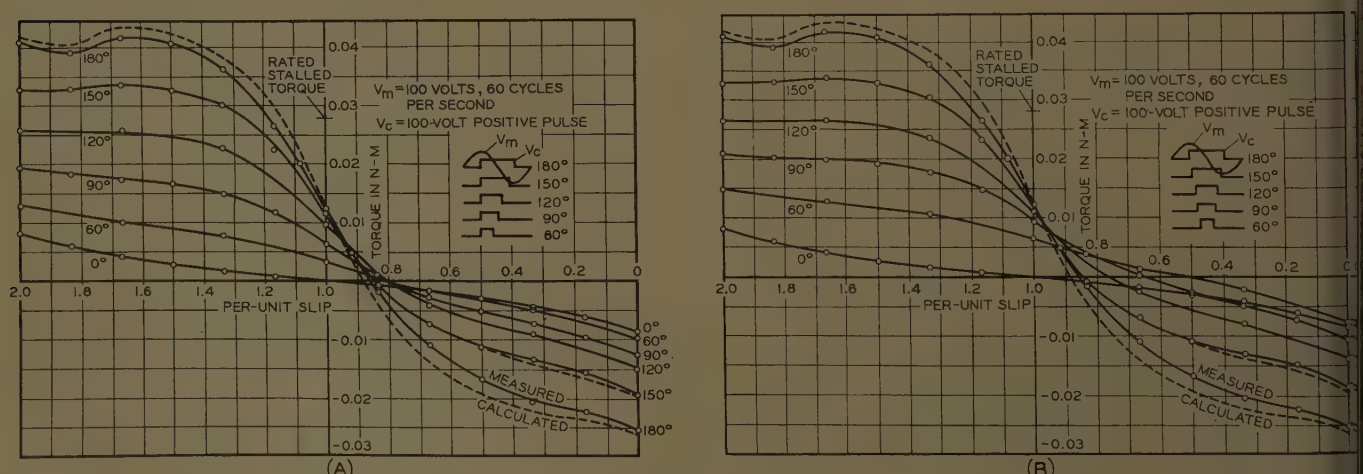


**Fig. 8. Slip-torque characteristics with variable length, rectangular voltage pulses on control phase and sine-wave voltage on main phas**

A—Leading edge of pulse fixed B—Fundamental component of pulse in quadrature with main-phase voltage

symmetrical components or an analog computer. This is perhaps one of the more promising areas for further investigation.

Further investigations have already indicated the feasibility of introducing multipliers, as suggested under the "Conclusions" section of the paper, for solution of transient problems. Before condemning the analog computer solution to a problem because of torque discrepancies of the order of 0.02 per unit resulting from magnetic saturation, it is perhaps advisable to inquire into the purposes of an analog computer solution. It is our belief that one of the prime merits of a fast-time computer is that of being able to observe immediately the results of changes in one or more parameters. Having established the magnitude of discrepancy introduced by certain assumptions and localized it to these assumptions, the investigator is then free to proceed with an awareness of the possible effects upon his results. The reduced voltage test reported in Fig. 3 localizes the discrepancy observed between the full-voltage test and computed results. Since the error was small (probably less than one-third that which could have resulted had not precise torque-measuring equipment and temperature-control procedures been used), it was not considered desirable to introduce variable inductance parameters to account for saturation. It is hoped that the authors' method of localizing the source of the relatively small discrepancy caused by saturation did not unduly distress our other readers.

# A Suppressed-Carrier Signal Generator for Servosystem Instrumentation

P. J. POLLARD
ASSOCIATE MEMBER AIEE

**Synopsis:** This paper describes a method of obtaining a sinusoidal suppressed carrier voltage using two synchros connected in such a way as to eliminate the need for slip rings. The result is a relatively simple and maintenance-free signal generator that is capable of producing modulation frequencies as high as 500 cps (cycles per second).

ONE OF THE more widely accepted methods of generating a suppressed carrier signal for the analysis of servosystems is the use of "synchros." Briefly the synchro is an electromechanical device that generates a suppressed carrier signal when properly excited and rotated at some constant velocity. Being a rather rugged mechanical device, maintenance is an extremely small factor for most applications and the operation of the synchro within its limits requires nothing more than a small d-c motor as a driver. Although synchros may be used at higher carrier or excitation frequencies, the modulating frequency is a function of the speed of rotation and the latter is materially limited. This limitation corresponds to a modulating frequency of approximately 40 cps for most commercial synchros.

The advantages of using synchros, as previously pointed out, prompted the development of a method of extending the modulation frequency range. The result was the electromechanical signal generator shown in Fig. 1. The two outstanding features of this unit are:

1. It may be rotated at speeds as high as 15,000 rpm (modulating frequency is proportional to rotational speed).
2. Two cycles of the modulating frequency per revolution are obtained.

The word "cascaded" has been adopted as signifying the mechanical and electrical coupling of synchros in such a manner as to increase the initial or fundamental modulating frequency by a factor dependent upon the number of synchros cascaded. Thus with two synchros, twice the fundamental modulating frequency is obtained for the same synchro shaft speed; with three, three times the fundamental modulating frequency results; etc.

## Voltage Relations in a Synchro

Before considering cascaded synchros, it is best to review briefly the equations involved with one synchro. It may be seen from Fig. 2 that the output voltage of each winding is determined by the cosine of the angle between the magnetic axis of the rotor and the axis of each stator winding. Equations for each stator winding voltage can be written by inspection, and the line-to-line voltage is the sum of the stator winding voltages between the line terminals. For an input voltage of

$$e_{in} = E \sin \omega_c t \qquad (1A)$$

and making the proper assumptions as to reference and polarity, the following equations can be written for the phase voltages.

$$e_1 = kE \sin \omega_c t \cos (\theta + 180) \qquad (1)$$

$$e_2 = kE \sin \omega_c t \cos (\theta + 60) \qquad (2)$$

$$e_3 = kE \sin w_c t \cos (\theta - 60) \qquad (3)$$

where $E \sin \omega_c t$ = excitation voltage on rotor, $k$ = transformation ratio of rotor to stator, and $\theta$ = angle between rotor and stator.

The line-to-line voltages are:

$$e_{1-2} = e_1 + e_2 = kE \sin \omega_c t \cos (\theta + 120) \qquad (4)$$

$$e_{2-3} = e_2 + e_3 = kE \sin \omega_c t \cos \theta \qquad (5)$$

$$e_{1-3} = e_1 + e_3 = kE \sin \omega_c t \cos (\theta - 120) \qquad (6)$$

The angular displacement is related to the angular velocity by the expression $\omega_m = d\theta/dt$. Thus, for a constant angular velocity $\omega_m$, equation 5 may be rewritten as

$$e_{2-3} = kE \sin \omega_c t \cos \omega_m t$$

which can be expanded into the form

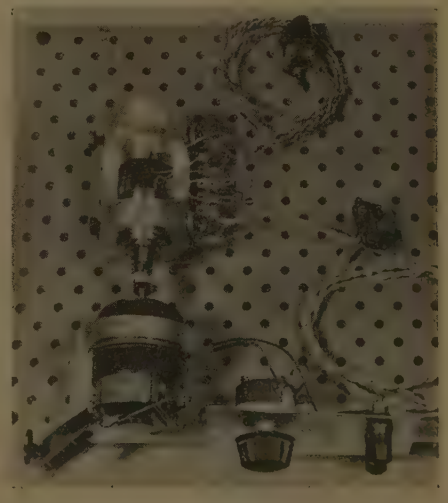

**Fig. 1. Electromechanical signal generator with d-c motor as driving source and potentiometer as speed control**

Paper 59-1153 recommended by the AIEE Feedback Control Systems Committee and approved by the AIEE Technical Operations Department for presentation at the AIEE Fall General Meeting, Chicago, Ill., October 11–16, 1959. Manuscript submitted April 10, 1959; made available for printing August 19, 1959.

P. J. POLLARD is with Sylvania Electric Products, Inc., Detroit, Mich., and was formerly with Chrysler Corporation, Detroit, Mich.

Credit for the idea of coupling two synchros as a method of eliminating slip rings should go to D. Prichard. The author would also like to express appreciation for the technical assistance of B. Horner and L. Stopke for development of this instrument, and to Mr. Prichard for all experimental test work.

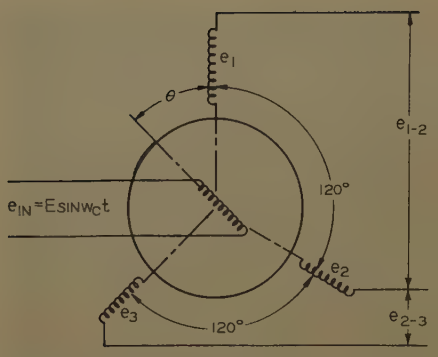


**Fig. 2. Electrical schematic of synchro having a 3-phase stator and a single-phase rotor**

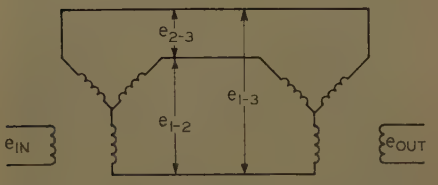


**Fig. 3. Electrical schematic of two synchros cascaded**

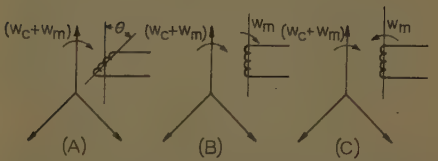


**Fig. 4. Vector diagrams illustrating frequency relationships on cascaded synchros**

A—Rotor fixed at angle 0, 3-phase stator excitation frequency $(\omega_c+\omega_m)$

B—Rotor angular velocity equal to $\omega_m$ and in the same direction as the 3-phase stator excitation sequence

C—Rotor angular velocity equal to $\omega_m$ and in the opposite direction to the 3-phase stator excitation sequence

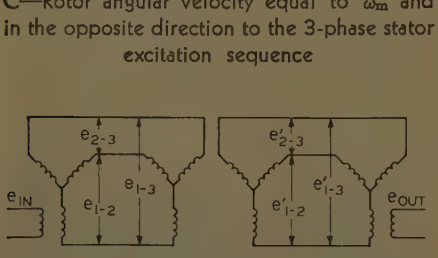


**Fig. 5. Electrical schematic of three synchros cascaded**

$$e_{2-3}=1/2kE[\sin(\omega_c+\omega_m)t+\sin(\omega_c-\omega_m)t] \quad (7)$$

Substitution and expansion of the other line-to-line voltages will produce the same terms with the addition of a phase angle term. From this it can be seen that in its idealized state, the synchro produces a suppressed carrier modulated signal.

## Cascading Synchros

Assuming the manufacturer's rating on synchro speed is to be respected, some method of circumventing this speed limitation was needed to extend the modulating frequency range. The solution was found in the system referred to as cascaded synchros.

The electrical configuration for cascading synchros is illustrated in Fig. 3. For an input signal as expressed by equation 1(A), the three output voltages of the first synchro would be equal to those expressed by equations 4, 5, and 6, respectively. As pointed out previously, equations 4, 5, and 6 may be rewritten as

$$e_{1-2}=kE\sin\omega_c t\cos(\omega_m t+120)$$

$$e_{2-3}=kE\sin\omega_c t\cos\omega_m t$$

$$e_{1-3}=kE\sin\omega_c t\cos(\omega_m t-120)$$

Expanding these equations

$$e_{1-2}=1/2kE[\sin\{(\omega_c+\omega_m)t+120\}+\sin\{(\omega_c-\omega_m)t-120\}] \quad (8)$$

$$e_{2-3}=1/2kE[\sin(\omega_c+\omega_m)t+\sin(\omega_c-\omega_m)t] \quad (9)$$

$$e_{1-3}=1/2kE[\sin\{(\omega_c+\omega_m)t-120\}+\sin\{(\omega_c-\omega_m)t+120\}] \quad (10)$$

Upon examination of the sidebands as shown in equations 8, 9, and 10, it may be seen that both the upper and lower sidebands fulfill the time and space requirements for a 3-phase system. This fact is the basis upon which cascading synchros has been developed. When the stator of a synchro is excited with a 3-phase current the output of the rotor of the synchro will be a constant amplitude signal in which the phase relationship between the output and the input is dependent upon the rotor position. Thus, considering the 3-phase input signals of the form $\sin(\omega_c+\omega_m)t$ and $\sin(\omega_c-\omega_m)t$ to the stator of the second synchro, the output voltage would be given by the expression

$$e_{out}=\frac{3}{4}E[\cos\{(\omega_c+\omega v_m)t\pm\alpha\}+\cos\{(\omega_c-\omega_m)t\mp\alpha\}] \quad (11)$$

where $\alpha$ is the angular position of the rotor of the second synchro with respect to its stator

At this point, the relationship of the 3-phase excitation voltage and the resultant induced voltage in the rotor winding should be studied. To simplify the explanation, only the upper 3-phase sideband will be considered. The results obtained from this will be equally applicable to the lower sideband. From the vector diagram of Fig. 4(A), the rate of change of flux linking the rotor winding and thus the frequency of the induced voltage is seen to be a function of $(\omega_c+\omega_m)$ and $\theta$. If the rotor winding is rotated at the same angular velocity and in the same

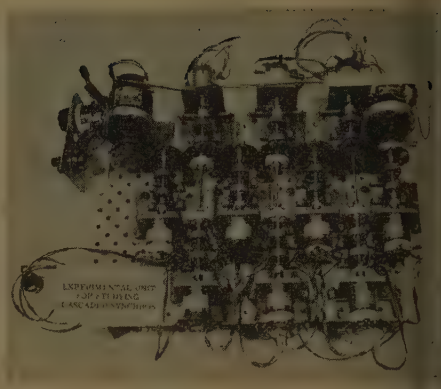

**Fig. 6. Experimental model used for the study of cascading synchros**

direction as the 3-phase vectors, Fig. 4(B), the resultant change in flux linking the rotor winding due to the factor $\omega_m$ becomes zero and the frequency of the resultant induced voltage will be a function of $\omega_c$. However, if the rotor winding is rotated in the opposite direction to that of the 3-phase vectors Fig. 4(C), the rate of change of flux linking the rotor winding becomes a function of $(\omega_c+2\omega_m)$. Thus by rotating the second synchro at the same angular velocity as the first and in the proper direction with respect to the rotation of the 3-phase vectors, the resultant output voltage will be

$$e_{out}=\frac{3}{4}E[\cos(\omega_c+2\omega_m)t+\cos(\omega_c-2\omega_m)t] \quad (12)$$

It is obvious from equation 12 that the desired doubling of the modulation frequency has been attained. It is interesting to note that the relative position of the rotor of the second synchro with respect to the rotor of the first simply determines the phase relationship of the output of the first synchro with that of the second. Thus, mechanical alignment of the respective rotors is not necessary. To cascade more than two synchros using this system, differential synchros must be used. Referring to Fig. 5 and considering an input voltage equal to $E\sin\omega_c t$, the voltages $e_{1-2}$, $e_{2-3}$, and $e_{1-3}$ will be the same as equations 8, 9, and 10. From the previous explanation given for cascading synchros, it may be seen that the output voltages will be

$$e'_{1-2}=\frac{3}{4}kE[\cos\{(\omega_c+2\omega_m)t+120\}+\cos\{(\omega_c-2\omega_m)t-120\}] \quad (13)$$

$$e'_{2-3}=\frac{3}{4}kE[\cos(\omega_c+2\omega_m)t+\cos(\omega_c-2\omega_m)t] \quad (14)$$

$$e'_{1-3}=\frac{3}{4}kE[\cos\{(\omega_c+2\omega_m)t-120\}+\cos\{(\omega_c-2\omega_m)t+120\}] \quad (15)$$

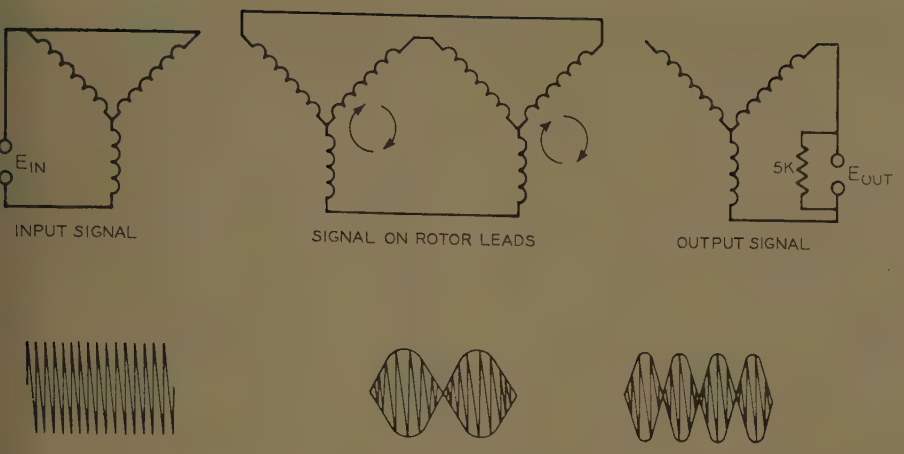


**Fig. 7. Wiring diagram and corresponding waveform configurations for two synchros cascaded**

This, then, becomes the 3-phase excitation for the third synchro. If the third synchro is rotated in the proper direction with respect to the 3-phase excitation, the output voltage will be

$$e_{out}=\frac{9}{8}E[\sin(\omega_c+3\omega_m)t+\sin(\omega_c-3\omega_m)t] \quad (16)$$

The primary limitations of the number of synchros that may be practically cascaded are the bulkiness of the resulting system, brush noise and speed regulation.

## Eliminating Synchro Slip Rings

Cascading synchros had provided a method of extending the modulating frequency range but the limitations mentioned previously were considered too severe. These limitations were inflicted by the mechanical arrangement necessary; i.e., a number of synchros coupled together as shown in Fig. 6. As a result, the problem was again considered but this time with the idea of eliminating, rather than circumventing, the speed limitation of the synchro. It is evident from the previous discussion that the maximum obtainable speed of a synchro will determine its maximum modulating frequency. Since the primary factor in establishing this maximum speed rating is the slip ring and brush assembly, efforts were directed toward eliminating the latter in order that higher synchro speeds could be practically attained. Reviewing the method of cascading synchros as illustrated in Fig. 3, it may be seen that the two 3-phase stators are electrically connected. If the single-phase rotor winding and 3-phase stator winding of each synchro were interchanged; i.e., if the single-phase winding would be made the stator and the 3-phase winding would be made the rotor, operation of the synchro should not be affected. Since the rotors are mechanically coupled to a common shaft, it would then be possible to connect electrically the two 3-phase windings without the use of slip rings. The signal generator of Fig. 1 was made from two standard differential synchros (*15CDx4*) connected as shown in Fig. 7. A sleeve-type coupling was used to couple mechanically the two rotors, and lead wire was clamped along the common shaft to connect electrically the rotor windings. The resultant rotor assembly was then aligned in a cradle mount which held the two stators. Thus, the only speed limitation remaining was that of alignment and dynamic balancing. Since these could be controlled without too much difficulty a practical high-frequency suppressed-carrier signal generator was obtained.

## Effect of Angular Velocity on Sideband Amplitudes

The block diagrams of Figs. 8(A) and 8(B) illustrate the instrumentation of typical Vickers electrohydraulic open-loop and closed-loop servosystems respectively. In the closed-loop system, the control signal (output of the servosystem analyzer) must be added to the feedback signal or signals. Thus, an important factor concerning the signal source when used to instrument a closed-loop servosystem is its amplitude-versus-frequency characteristic over the range to be studied. Equations 4, 5, and 6, that have been used thus far as expressing the output of a synchro, although a simplification of the true output, have been sufficiently accurate for the preceding analysis. However, a more rigorous derivation of the latter must be carried out if the amplitude versus modulating frequency characteristics of a synchro are to be understood. Thus, for an input signal given by

$$e_{in}=\sin\omega_c t \quad (1A)$$

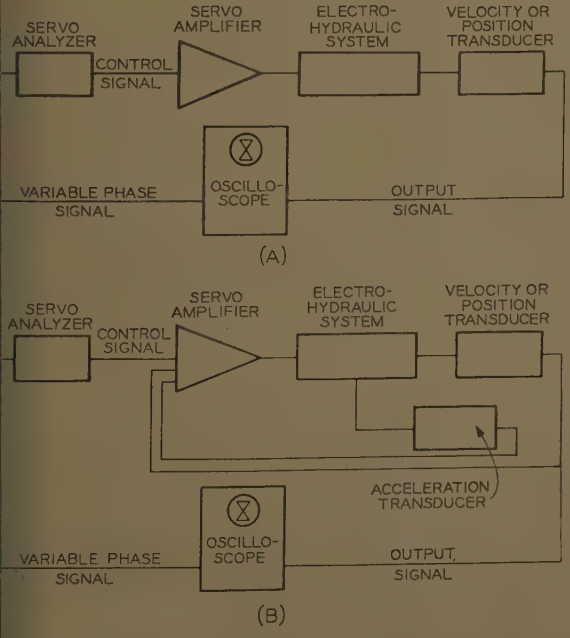


**Fig. 8 (left). Block diagrams illustrating standard instrumentation for electrohydraulic servosystems**

A—Open-loop instrumentation
B—Closed-loop instrumentation

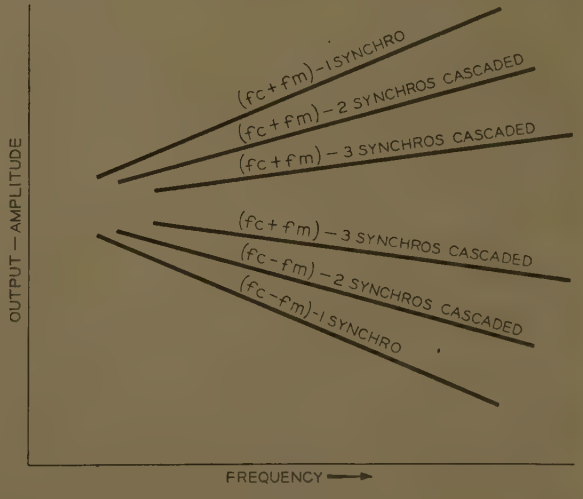


**Fig. 9 (right). Curves illustrating the effect of cascading synchros on the output amplitude of the upper and lower sidebands**

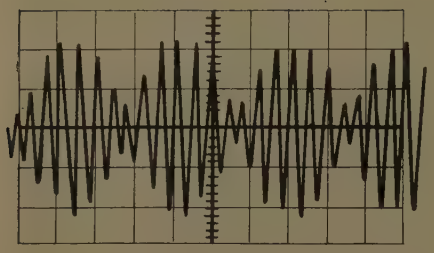

**Fig. 10. Oscillogram of suppressed-carrier signal-generator output waveform frequency = 5,000 cps, modulating frequency = 500 cps, output voltage = 180 volts peak-to-peak**

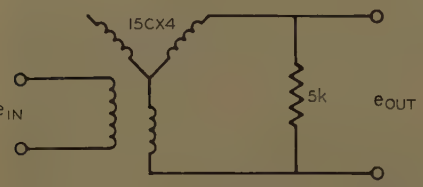


**Fig. 11. Ketay 15CX4 synchro with a 5-kilohm load at a carrier frequency of 400 cps. See Table I**

the instantaneous flux produced would be

$$\varphi = \Phi \cos \omega_c t \tag{17}$$

where $\varphi$ is the instantaneous value of flux produced by the excitation voltage and $\Phi$ is the maximum value of flux produced by the excitation voltage.

The flux linking the secondary windings of the synchro is a function of the rotor (primary) position with respect to the stator (secondary), thus

$$\varphi' = \Phi \cos \omega_c t \sin \theta \tag{18}$$

where $\varphi'$ is the instantaneous value of flux linking the secondary. Considering the synchro as rotating at some constant angular velocity equation 18 may be expressed as

$$\varphi' = \Phi \cos \omega_c t \sin \omega_m t \tag{19}$$

The voltage induced in the secondary winding under these conditions would be

$$e_{out} = kN \frac{d\varphi'}{dt} \tag{20}$$

where $k$ is a constant, $N$ the number of turns enclosed, and $d\varphi'/dt$ the time rate of change of flux linking the secondary. By substituting equation 19 in equation 20, the induced voltage may be expressed as

$$e_{out} = kN \frac{d}{dt} (\Phi \cos \omega_c t \sin \omega_m t)$$

$$= kN\Phi(\omega_m \cos \omega_c t \cos \omega_m t - \omega_c \sin \omega_c t \sin \omega_m t) \tag{21}$$

Expanding and simplifying equation 21

$$e_{out} = kN\Phi[1/2\ \omega_m\{\cos(\omega_c - \omega_m)t + \cos(\omega_c + \omega_m)t\} - 1/2\ \omega_c\{\cos(\omega_c - \omega_m)t - \cos(\omega_c + \omega_m)t\}]$$

$$= kN\Phi\pi\,[(f_c + f_m)\cos(\omega_c + \omega_m)t - (f_c - f_m)\cos(\omega_c - \omega_m)t] \tag{22}$$

It should be noted that sideband unbalance is a function of synchro speed, rather than modulating frequency. Thus in cascading synchros, the sideband unbalance characteristic changes as shown by the curves of Fig 9. If this device is to be effective in providing reliable instrumentation for closed-loop servosystems, the characteristics of the feedback elements must be considered in reference to those of the signal generator More specifically, if these characteristics differ from those of the driving signal as shown in Fig. 9, an error will result as expressed by

$$\%_{error} = \frac{f_m}{f_c}\left(1 - \frac{1}{N}\right) \times 100 \tag{23}$$

where $N$ is the number of synchros cascaded.

## Performance of Signal Generator

Figs. 10–14 indicate the performance of a signal generator. To establish a reference for comparison purposes, the characteristics of one synchro (*15Cx4*) were determined for rated excitation voltage and frequency are presented in Fig. 11 in outline form (also see Table I). The carrier phase shift refers to the phase shift occurring between the input and output terminals of the synchro with the rotor adjusted for maximum output. This position is also used to determine the

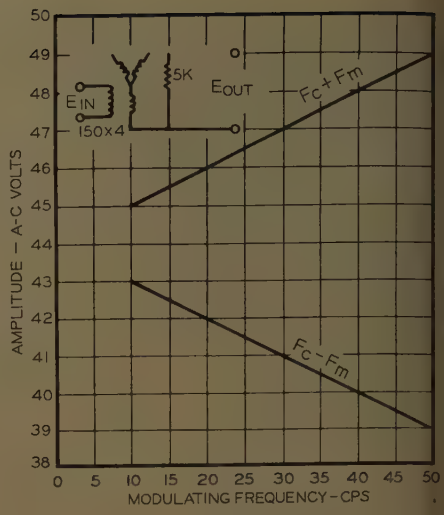


**Fig. 13. Curve illustrating the effect of modulating frequency on the sideband amplitudes in the output of a Ketay 15CX4 synchro**

Constants: excitation voltage = 110 volts, excitation frequency = 400 cps, output load resistance = 5 kilohms. Voltage measurements were made using the General Radio Wave Analyzer

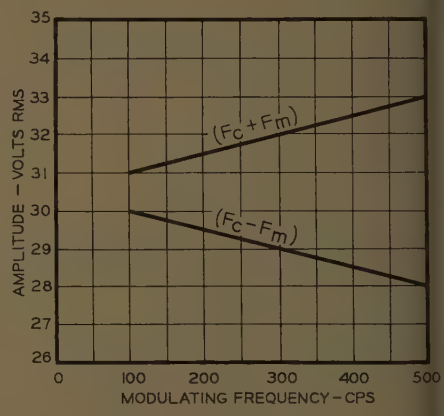


**Fig. 14. Curve illustrating the effect of modulating frequency on the sideband amplitudes in the output of the suppressed-carrier signal generator**

Constants: excitation voltage = 90 volts rms, excitation frequency = 5 kc, output load resistance = 5 kilohms

**Table I. Characteristics of One Ketay 15CX4 Synchro with a 5-Kilohm load at a Carrier Frequency of 400 Cps**

| | |
|---|---|
| *Statically*: | |
| Gain | 0.77 |
| Null | 51 millivolts |
| Harmonic components | |
| $2f_c$ | −43 db |
| $3f_c$ | −49 db |
| $5f_c$ | −61 db |
| *Dynamically*: | |
| Modulating frequency | 40 cps |
| Harmonic components | |
| $(f_c + 2f_m)$ | −36 db |
| $(2f_c + f_m)$ | −44 db |
| $(3f_c + 2f_m)$ | −47 db |
| $(3f_c + f_m)$ | −47 db |


**Fig. 12. Suppressed carrier signal generator with 5-kilohm load at carrier frequency of 5 kc. See Table II**

Table II. Characteristics of Suppressed Carrier Signal Generator with 5-Kilohm Load at Carrier Frequency 5 Kc

| | |
|---|---|
| *Statically*: | |
| Gain | 0.71 |
| Null | 80 millivolts |
| Carrier phase shift | 9 degrees |
| Harmonic components | |
| $2fc$ | 38 db |
| $3fc$ | 48 db |
| *Dynamically*: | |
| Modulating frequency | 100 cps |
| Harmonic components | |
| $2fc+fm$ | 38 db |
| $3fc+fm$ | 48 db |

harmonic components. The information of decibels (db) to facilitate comparing the operation of the subject generator to the normal operating characteristics of a synchro. Statically, the reference for the decibel ratios was the carrier frequency component present in the output with the synchro rotated to its maximum output point. Dynamically, the reference was the mean of the upper and lower fundamental sideband components at the modulating frequency indicated. The curves in Figs. 11 and 12 and Tables I and II illustrate the sideband output characteristics of a standard synchro in comparison to that of the signal generator developed. The oscillogram in Fig. 10 was taken to show the output waveform of this generator at a modulating frequency of 500 cps.

## Appendix I

From Fig. 11 it can be seen that the total voltage induced into the secondary at any instant will be equal to the voltage induced by each phase of the 3-phase excitation source. Considering the angular position of the synchro rotor with respect to phase 1, a general equation for the output voltage $e_{out}$ may be written as

$$\begin{aligned} e_{out} &= kE[\sin\theta \sin\varphi + \sin(\theta-120)\sin(\varphi-120) + \sin(\theta+120)\sin(\varphi+120)] \\ &= 1/2\, kE[\cos(\theta-\varphi)-\cos(\theta+\varphi)+\cos(\theta-120-\varphi+120)-\cos(\theta-120+\varphi-120)+\cos(\theta+120-\varphi-120)-\cos(\theta+120+\varphi+120)] \\ &= 1/2\, kE[2\cos\theta\cos\varphi+4\sin\theta\sin\varphi-\cos\theta\{\cos(\varphi+240)+\cos(\varphi-240)\}+\sin\theta\{\sin(\varphi+240)+\sin(\varphi-240)\}] \\ &= 1/2\, kE[2\cos\theta\cos\varphi+4\sin\theta\sin\varphi+\cos\theta\cos\varphi-\sin\theta\sin\varphi] \\ &= 1/2\, kE[3\cos\theta\cos\varphi+3\sin\theta\sin\varphi] \\ &= \frac{3}{2}kE\cos(\varphi-\theta) \end{aligned}$$

In the case of a synchro having a 3-phase carrier excitation expressed by

$$e = \sin\omega_c t$$

$$e' = \sin(\omega_c t+120)$$

$$e'' = \sin(\omega_c t-120)$$

and rotating at an angular velocity $\omega_m$, the output voltage would be

$$e_{out} = \frac{3}{2}kE[\cos(\omega_c-\omega_m)t]$$

In the case of a synchro having a 3-phase excitation expressed by

$$e = \cos(\omega_c+\omega_m)t$$

$$e' = \cos[(\omega_c+\omega_m)t+120]$$

$$e'' = \cos[(\omega_c+\omega_m)t-120]$$

and rotating at an angular velocity $\omega_m$, the output voltage would be

$$e_{out} = \frac{3}{2}kE[\sin(\omega_c-\omega_m)t]$$

## Appendix II

From equation 22, the sideband amplitudes of a synchro may be represented as $k'(f_c+f_m)$ and $k'(f_c-f_m)$, respectively. Furthermore the sideband amplitude of the output of cascaded synchros would be $k''(f_c+f_m/N)$ and $k''(f_c-f_m/N)$ respectively, where $N$ represents the number of synchros cascaded. If the factors $k'$ and $k''$ were made equal and opposite, as in the case of negative feedback around a servoloop, the difference signal remaining would be $kf_m(1-1/N)$ and $-kf_m(1-1/N)$, respectively. Using zero modulating frequency as a reference amplitude, the per cent error introduced by the difference in the two signals would be

$$\%_{error} = \frac{f_m}{f_c}\left(1-\frac{1}{N}\right)\times 100$$

# Control by Stochastic Adjustment

J. E. BERTRAM
ASSOCIATE MEMBER AIEE

**Synopsis:** This paper is concerned with the problem of designing an "adaptive controller" for the control of a certain class of dynamic processes. In general, these processes consist of a dynamic element governed by a nonstationary, linear differential equation. It is assumed that the designer knows only the form of the differential equation and bounds on the parameter variations but not the exact equations. A further complication of the problem is that all measurements of the state variables of the process are obscured by additive noise.

Control is exerted by means of a piecewise continuous signal which can change only at "sampling instants." The problem is to design a controller, on the basis of this meager information, which is capable of generating an input sequence that will take the process to equilibrium with zero steady-state error from any initial state. A controller capable of achieving this performance in a stochastic sense is shown to consist of a very simple multifeedback arrangement in which the only unconventional element is a time-varying gain element.

A PARTICULAR CLASS of problems of engineering and economic importance is the control, over a certain time interval, of a dynamic process such as a chemical reactor or missile. In general, the solution of this problem results in a system which has the schematic form of Fig. 1. The function of the controller is to maintain the state, $\mathbf{x}(t)$, of the process being controlled, at or near, in some sense, to an abritrary reference state, $\mathbf{x}^r$. Control action is effected by the control variable, $m(t)$, the input to the dynamic process, which is generated in the controller. Thus, the design of the controller consists of building into it some knowledge of the dynamics of the process so that, on the basis of the desired state $\mathbf{x}^r$ and the feedback information concerning the state of the process, it is possible to generate an "intelligent" control signal, $m(t)$.

In a large number of systems the dynamic behavior of the process is adequately described or approximated by an ordinary differential equation relating the state variables and the input or control variable. In most of the so-called optimal systems, the design of the controller requires a precise knowledge of the differential equation of the process if the overall system is to perform in the manner desired. This is unfortunate, for experience has shown that, while the designer

Paper 59-1156, recommended by the AIEE Feedback Control Systems Committee and approved by the AIEE Technical Operations Department for presentation at the AIEE Fall General Meeting, Chicago, Ill., October 11–16, 1959. Manuscript submitted February 20, 1959; made available for printing August 6, 1959.

J. E. BERTRAM, with Columbia University, New York, N. Y., when this work was done, is now with Research Center, International Business Machines Corporation, Yorktown Heights, N. Y.

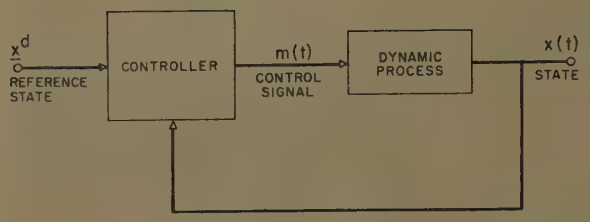


Fig. 1. (left). Control system

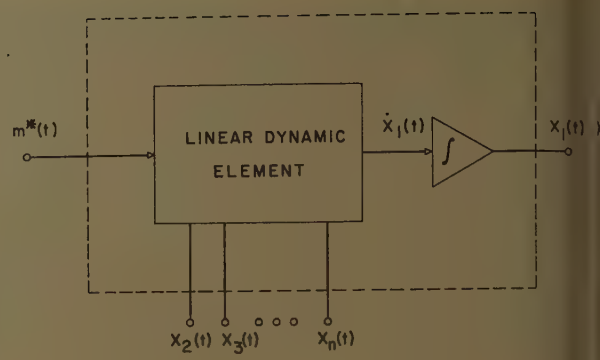


Fig. 2. (right). Dynamic process

may know the order and form of the equation, he seldom knows with any precision the exact values of the parameters. Even when measurements are made and precise estimates of the parameters are obtained prior to designing the controller, it has been found in most applications that these parameters change appreciably during the life of the system either because of aging of certain critical components or because of environmental changes.

In the past few years a considerable effort has been made to develop control-system design methods which do not require that the designer have a precise a priori knowledge of the dynamics of the process.

These efforts, in general, have been based more on intuition than on analysis. Usually the procedure has been to select some criterion of performance which is readily measurable, perform this measurement continuously on the system, and utilize the measurement to adjust certain free parameters in the controller in order to achieve the desired performance. Examples of such systems are found in the work of Draper and Li, Burt,[1] Cosgriff,[2] and also Anderson and Aseltine.[3] Kalman[4] has suggested a somewhat different approach to the problem which is applicable to the control of any dynamic process which is adequately described by an ordinary, linear, differential equation which changes slowly with time. In his system, the process dynamics are estimated from input–output measurements and on the basis of these estimates the controller parameters are calculated and adjusted in compliance with some performance criterion. In other words, the standard design procedure is mechanized. At various times these systems have been classified as "self-adjusting," "self-optimalizing," or "adaptive." In the following these terms are considered as synonymous.

In each of the systems mentioned before it is assumed that any time variation in the process parameters is slow in comparison with either the response time of the process or the measurements and adjustment time of the controller. Furthermore, since the dynamic performance of these systems with the self-adjustment loops is described by nonlinear differential or difference equations, little is known about the transient behavior. In those systems which have been built[3,4] it has been found that satisfactory performance has required the introduction of a disturbance or test signal in order to insure a minimum signal-to-noise ratio in the measurements. This signal limits the steady-state accuracy of the system.

This paper is concerned with a different approach to the adaptive control problem. The methods employed are strongly motivated by and are closely related to an area of current interest in mathematical statistics called stochastic approximations. In their pioneering paper, Robbins and Monro[5] give an algorithm for stochastically converging on the solution, $x$, of the equation $M(x)=\alpha$, where $M(x)$ is the expected value of the response of an experiment to the input $x$. (It is assumed that the function $M(x)$ is unknown to the experimenter.) Thus, the problem is to find that input $x$ which on the average yields the output $\alpha$. Their results have been extended by numerous authors.[6–8] A point of view which is of particular interest in adaptive control systems was suggested by Dvoretzky.[9] He considered the stochastic approximation method as a convergent deterministic procedure with a superimposed random element or noise. The adaptive-control problem of this paper is viewed in a similar way.

## Statement of the Problem

The dynamic process to be controlled is illustrated in Fig. 2. The following assumptions concerning the process are made:

1. It is assumed that the input, $m^*(t)$, generated in the controller, is sampled-and-held so that it is piecewise constant. That is, between successive sampling instants the signal is held constant at the value of the function at the previous sampling instant. Thus:

$$m^*(t)=m^*(kT),\ kT\leq t<(k+1)T,\qquad k=0,\ 1,\ 2,\ \ldots \quad (1)$$

where the sampling period, $T$, is a positive constant and the point, $t=kT$, is called the $k$th sampling instant. (Frequently it will be convenient to write $f(k)$ rather than $f[kT]$.)

2. The state variables of the dynamic process denoted by $x_1,\ x_2,\ x_3,\ \ldots,\ x_n$ are observed or measured only at the same sampling instants ($t=0,\ T,\ 2T,\ \ldots$). The state of a dynamic element at any instant of time is a set of numbers which completely summarize that past history of a dynamic element which is necessary to a determination of its future behavior. To be specific, if one thinks of the element as being simulated on an analog computer, then the voltages at the outputs of the integrators form such a set. (The number of integrators needed to simulate an $n$th order differential equation is exactly $n$ and no more.) Since the simulation of a dynamic element is not unique, it follows that the state variables are not unique. However, in the present case it is assumed that the state variables have been selected so that all $n$ of them are physically accessible to measurement. A discussion of how this condition may be relaxed is found in reference 10.

3. It is assumed that in the process of performing the observation or measurement a random element (noise) is added to the state variable so that:

$$y_i(t)=x_i(t)+n_i(t),\ i=1,\ 2,\ \ldots,\ n \quad (2)$$

where $y$ is the observation, $x$ is the true state value, and $n$ is the noise.

4. The dynamic process contains an integrator so arranged that if the differential equations describing the process are written in normal form,[11] then the derivatives of the state variables with respect to time are functions only of the state variables $x_2$, $x_3,\ \ldots,\ x_n$, the input $m^*$, and time, so that

$$\dot{x}_i(t)=\sum_{j=2}^{n} a_{ij}(t)x_j(t)+d_i(t)m^*(t),\qquad i=1,\ 2,\ \ldots,\ n \quad (3)$$

Consequently, equation 3 is such that the only equilibrium states for $m^*=0$ are:

$$x_1=x_1^r \text{ (an arbitrary constant)}$$
$$x_i=0,\ i=2,\ 3,\ \ldots,\ n \quad (4)$$

The restrictions to sampling which are inherent in assumptions 1 and 2 only tend to simplify the problem without any real loss in generality. Assumption 3 merely states a condition which is always present in the physical world. On the other

and, 4 somewhat limits the applicability
the result, but fortunately this re-
ricted class includes a large number of
ysical problems. Actually this as-
mption may be relaxed considerably;
the present paper this has not been
ne so that the mathematical arguments
ay be kept simple in order not to obscure
e motivation and methods employed.

The problem now is to determine under
hat conditions, if any, it is possible to
sign a controller which will generate a
ntrol sequence $m(0)$, $m(1)$, ... which
ill take the process from any initial
ate $\mathbf{x}(0)$ to a desired equilibrium state
in some optimal fashion. Further, it is
sired to use a simple controller and one
hich can be designed from as little a
iori knowledge concerning the time-
rying parameters and the noise, $n_i$,
possible.

The state of the art at the present time
not at the point where a unique best
lution is possible. This paper presents
solution which satisfies most of the con-
tions of the problem and has the po-
ntial of satisfying many more.

## escription of Over-All System

If the state variables are observed only
the sampling instants, $t=0, T, 2T, \ldots,$
en the solution of equation 3 will yield
e difference equation:

$$k+1)=\Phi_k\mathbf{x}(k)+\mathbf{d}_k m^*(k) \quad (5)$$

ere $\mathbf{x}(k)$ is an $n$-dimensional vector
th components $(x_1, x_2, \ldots, x_n)$ denoting
e state of the process at the $k$th sam-
ng instant; $\Phi_k$ is an $(n\times n)$ square
trix which represents the transforma-
n of the state at the $k$th to $(k+1)$th
mpling instant in the absence of an
ut; $\mathbf{d}_k$ is an $n$ vector which represents
effect on the state at the $(k+1)$th in-
nt of a unit step-control signal applied
the $k$th instant; and $m^*(k)$ is a scaler
oting the value of the $k$th control
nal.

The adaptive controller suggested in this
per is a simple device which generates
control signal $m^*(k)$ by weighting the
ference between the desired equilibrium
te $\mathbf{x}^r$ and the observed state vector $\mathbf{y}(k)$
the time-varying gain $\mathbf{a}_k$. Thus:

$$(k)=\mathbf{a}_k'[\mathbf{x}^r-\mathbf{y}(k)] \quad (6)$$

ere $\mathbf{a}_k'$ is the transpose of vector $\mathbf{a}_k$
e observed state vector $\mathbf{y}(k)$ is actually
sum of a noise vector $\mathbf{n}(k)$ and the
ual state vector $\mathbf{x}(k)$.

$$)=\mathbf{x}(k)+\mathbf{n}(k) \quad (7)$$

Equations 5, 6, and 7 describe the over-
system shown in Fig. 3. To obtain

Fig. 3. Linear system

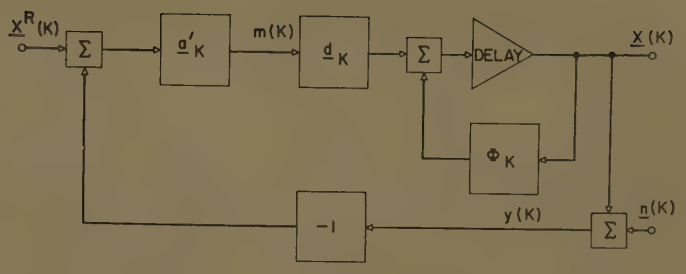


the over-all difference equation describing the behavior of this system at sampling instants, substitute equations 6 and 7 into 5 and find:

$$\mathbf{x}(k+1)=(\Phi_k-\mathbf{d}_k\mathbf{a}_k')\mathbf{x}(k)+\mathbf{d}_k\mathbf{a}_k'\mathbf{x}^r-\mathbf{d}_k\mathbf{a}_k'\mathbf{n}(k) \quad (8)$$

The problem now is to show that under conditions which are reasonable in practice, $\mathbf{x}(k)$ in some sense tends to the desired equilibrium state, $\mathbf{x}^r$. Rather than investigate equation 8 for all $\mathbf{x}^r$, it is easier to subtract $\mathbf{x}_k{}^r$ from both sides of 8, and letting $\mathbf{e}(k)=\mathbf{x}(k)-\mathbf{x}^r$, find conditions under which $e(k)$ tends to zero as $k$ becomes large. This result can be written:

$$\mathbf{e}(k+1)=(\Phi_k-\mathbf{d}_k\mathbf{a}_k')\mathbf{e}(k)-(\Phi_k-I)\mathbf{x}^r-\mathbf{d}_k\mathbf{a}_k'\mathbf{n}(k) \quad (9)$$

where $I$ denotes the identity matrix (unity on the diagonal, zero elsewhere). However, from condition 4, which is explicitly stated in equations 3 and 4, the term

$$(\Phi_k-I)\mathbf{x}^r=0 \quad (10)$$

From equation 3 the first column of the matrix $\Phi_k$ contains only zeros except for the $\Phi_{11}$ term which is always unity. Consequently the matrix $(\Phi_k-I)$ has only zeros in the first column. From equation 4 the equilibrium reference vector $\mathbf{x}^r$ has all components equal to zero except $x_1{}^r$ which is arbitrary. That is:

$$\mathbf{x}^r=\begin{bmatrix} x_1{}^r \\ 0 \\ \vdots \\ 0 \end{bmatrix} \quad (11)$$

As a result, the product of equation 10 is identically equal to zero and equation 9 is simply:

$$\mathbf{e}(k+1)=(\Phi_k-\mathbf{d}_k\mathbf{a}_k')\mathbf{e}(k)-\mathbf{d}_k\mathbf{a}_k'\mathbf{n}(k) \quad (12)$$

## Conditions for Convergence

The conditions for convergence of equation 12 may be stated formally as follows:

In the equation the expected or mean value of the norm of $\mathbf{e}(k)$ denoted by $E||\mathbf{e}(k)||$ tends to zero as $k\to\infty$

$$\lim_{k\to\infty} E(||\mathbf{x}(k)-\mathbf{x}^r||)\to 0 \quad (13)$$

if the following conditions are satisfied:

1. The norm

$$\|\Phi_k-\mathbf{d}_k\mathbf{a}_k'\|<\mu_k \quad (13A)$$

where $\mu_k$ is a sequence of positive numbers satisfying

$$\prod_{k=0}^{\infty}\mu_k=0 \quad (13B)$$

and such that the partial products of equation 13(B) are uniformly bounded.

2. The $\mathbf{n}(k)$ for $k=0, 1, 2, \ldots$ are random vectors which are statistically independent of the dynamic system and such that the expected value of their norm is finite:

$$E(\|\mathbf{n}(k)\|)<\infty \quad (13C)$$

3. The infinite sum:

$$\sum_{k=0}^{\infty} E(\|\mathbf{d}_k\mathbf{a}_k'\|)E(\|\mathbf{n}(k)\|) \quad (13D)$$

is finite.

The proof and application of this result require at least an elementary understanding of the concept of norm. The norm of a vector $\mathbf{y}$ written as $||\mathbf{y}||$ is a scaler quantity denoting in some sense the magnitude or length of $\mathbf{y}$. Examples of a norm are:

$$\|\mathbf{y}\|_1=\sum_{i=1}^{n}|y_i| \quad (14A)$$

$$\|\mathbf{y}\|_2=\left[\sum_{i=1}^{n}(y_i{}^2)\right]^{1/2} \quad (14B)$$

or

$$\|\mathbf{y}\|_3=\max_i(\alpha_i|y_i|) \quad (14C)$$

where $\alpha_1, \alpha_2, \ldots, \alpha_n$ are a set of positive numbers.

It is readily verified that each of these norms has the properties that:

$$\|\mathbf{x}+\mathbf{y}\|\leq\|\mathbf{x}\|+\|\mathbf{y}\| \quad (15A)$$

$$\|c\mathbf{y}\|=|c|\ \|\mathbf{y}\| \quad (15B)$$

$\|\mathbf{y}\|>0$ if $\mathbf{y}\neq 0$

$\|\mathbf{y}\|=0$ if, and only if, $\mathbf{y}=0$ (15C)

($\mathbf{y}=0$ implies that every component of $\mathbf{y}$ is zero)

In defining matrix norms it is natural to impose the same conditions and possibly a few others;[11] that is:

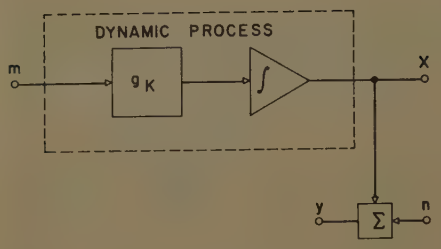


Fig. 4. Example 1

$$\|A+B\| \leq \|A\| + \|B\| \tag{16A}$$

$$\|\alpha A\| = |\alpha| \, \|A\| \tag{16B}$$

where $\alpha$ is a scaler, and

$$\|A\| \neq 0 \text{ unless } A = 0 \tag{16C}$$

A particular matrix norm will be said to be consistent with a given vector norm if for every $A$ and $\mathbf{x}$:

$$\|A\mathbf{x}\| \leq \|A\| \, \|\mathbf{x}\| \tag{16D}$$

Matrix norms which satisfy equations 16(A), 16(B), and 16(C) and which are consistent respectively with the vector norms of equation 14 are:

$$\sum_{i=1}^{n} \sum_{j=1}^{n} |a_{ij}| \tag{17A}$$

$$\left[ \sum_{i=1}^{n} \sum_{j=1}^{n} (a_{ij})^2 \right]^{1/2} \tag{17B}$$

Either

$$\max_i \left( \sum_{j=1}^{n} \frac{\alpha_i}{\alpha_j} |a_{ij}| \right) \tag{17C}$$

or

$$\max_j \left( \sum_{j=1}^{n} \frac{\alpha_j}{\alpha_i} |a_{ij}| \right)$$

The proof of equation 13 is quite straightforward using the concept of norm and will be presented here because it illustrates the applicability and limitations of the result.

The first step is to take the norm of equation 12 and use equations 15(A) and 16(D) to obtain:

$$\|\mathbf{e}(k+1)\| < \|\phi_k - \mathbf{d}_k \mathbf{a}_k'\| \, \|\mathbf{e}(k)\| + \|\mathbf{d}_k \mathbf{a}_k'\| \, \|\mathbf{n}(k)\| \tag{18}$$

Next take the ensemble average or expected value of equation 18. Letting $V_k = E(\|\mathbf{e}(k)\|)$ and $\sigma_k = E(\|\mathbf{d}_k \mathbf{a}_k'\|) E(\|\mathbf{n}(k)\|)$ and using condition 13(A):

$$V_{k+1} < \mu_k V_k + \sigma_k \tag{19}$$

is found, a first-order difference equation. Upon successively iterating equation 19, let

$$b_{km} = \prod_{j=m}^{k} \mu_j = \mu_m \mu_{m+1} \cdots \mu_k$$

then:

$$V_{k+1} < b_{k0} V_0 + \sum_{i=0}^{k} b_{k,i+1} \sigma_i \tag{20}$$

where $b_{k,k+1} = 1$. From equation 13(B) as $k \to \infty$ for any finite $m$, $b_{km} = 0$ so that the first term on the right in equation 20 goes to zero as $k \to \infty$. To show that the second term also goes to zero as $k \to \infty$, break it into two partial sums:

$$\sum_{i=0}^{k} b_{k,i+1} \sigma_i = \sum_{i=0}^{m} b_{k,i+1} \sigma_i + \sum_{i=m+1}^{k} b_{k,i+1} \sigma_i \tag{21}$$

for any finite $m$, it follows from equation 13(B) that as $k \to \infty$, each term in the first sum of equation 21 goes to zero. Further, from 13(B) all partial products of $b_{ij}$ are uniformly bounded by some finite positive constant. Since from equations 13(C) and 13(D)

$$\sum_{k=0}^{\infty} \sigma_k < \infty$$

it is possible to choose an $m$ in equation 21 so that:

$$\sum_{i=m+1}^{k} b_{k,i+1} \sigma_i < \epsilon$$

for any positive $\epsilon$. Therefore, it has been shown that in the limit as $k \to \infty$, $V_k$ converges to zero.

Note that in control systems one is generally interested in designing systems which are asymptotically-stable-in-the-large (i.e., for any initial state $\mathbf{x}(0)$ the norm of the solution $\mathbf{x}(k)$ tends to the equilibrium point as $k \to \infty$). In this case however, the best solution achieved is that the expected value of the norm, $E(\|\mathbf{x}(k) - \mathbf{x}^r\|) \to 0$ as $k \to \infty$. Roughly speaking, this means that $\mathbf{x}(k)$ generally converges to $\mathbf{x}^r$ but it is not an absolute certainty. While this limitation is not desirable, it seems to be the best that can be achieved for the generality of the present case.

To illustrate how this result is applied to the design of a particular system, consider the following first-order example.

## Example 1

For the dynamic process of Fig. 4, it is desired to determine an input sequence $m(0)$, $m(1)$, ... which will bring an arbitrary initial state $x(0)$ to the desired state $x^r$. The process consists of an integrator preceded by a time-varying gain element $g(t)$. The only a priori information available to the designer is that these variations are bounded by the positive constants $\alpha_1$ and $\alpha_2$ such that $\alpha_1 < g(t) < \alpha_2$.

The differential equation describing the process is:

$$\frac{dx}{dt} = g(t) m(t) \tag{22}$$

Since the input is a piecewise constant signal (defined by equation 1), the difference equation relating the state variable $x$, and the input $m$ at sampling instants is

$$x(k+1) = x(k) + d_k m(k) \tag{23}$$

where

$$d_k = \int_{kT}^{(k+1)T} g(\tau) d\tau$$

Consequently, $\alpha_1 T < d_k < \alpha_2 T$.

The observation of the state variable $y(k)$ is a linear combination of the actual state variable $x(k)$ and a random element or noise, $n(k)$. The only information available about this noise is that its expected value or mean is zero, while the variance is bounded by a positive constant. That is $E[n(k)] = 0$ while $E(n(k)^2) < \infty$ for all $k$.

From this information it is possible to generate an input sequence $m(0)$, $m(1)$, ..., which insures convergence in the sense described by simply multiplying the difference between the desired state $x^r$ and the observation $y(k)$ by the time-varying gain $a_k = A/(1+k)$ where $A > 0$, and using the result as a control signal. Otherwise choice of $A$ speeds the convergence.

To see that this simple strategy works write the difference equation of the complete system of Fig. 5.

$$(x(k+1) - x^r) = \left(1 - \frac{A}{1+k} d_k\right)(x(k) - x^r) - \frac{A}{1+k} d_k n(k) \tag{24}$$

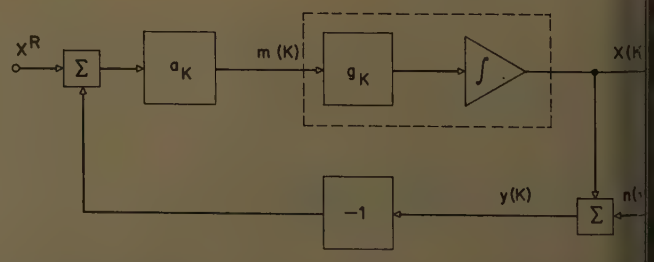


Fig. 5. The system

n the first-order system the state vector as only one component. If it is desired o obtain convergence in the mean square, $^2$ can be used rather than the norm $x$ or this example. If the system is to converge in the mean square:

$$\lim_{k\to\infty} E((x(k)-x^r)^2)\to 0$$

hen it follows from equations 13(A)–(D) hat, first:

$$\left(1-\frac{A}{1+k}\,d_k\right)^2<\mu_k \qquad (25A)$$

where $\mu_k$ is a sequence of positive numbers uch that

$$\prod_{k=0}^{\infty}\mu_k=0 \qquad (25B)$$

A necessary and sufficient condition[12] hat the infinite product:

$$\prod_{k=0}^{\infty}\left(1-\frac{A}{1+k}\,d_k\right)=0$$

s that the infinite sum

$$\sum_{k=0}^{\infty}\frac{A}{1+k}\,d_k=\infty$$

Obviously this condition is satisfied since

$$Ad_k<\alpha_2 TA$$

nd

$$\sum_{k=0}^{\infty}\frac{1}{1+k}=\infty$$

Second, it is also necessary that

$$\sum_{k=0}^{\infty}E\left(\left(d_k\frac{A}{1+k}\right)^2\right)E(n(k)^2)<\infty \qquad (25C)$$

e finite. By assumption $E\ (n(k)^2)$ is inite and $d_kA<\alpha_2TA$ which is finite. It ollows that equation 25(C) is less than

$$C\sum_{k=0}^{\infty}\frac{1}{(1+k)^2}<\infty \qquad (26)$$

where $C$ is a finite positive constant, since he infinite sum of equation 26 is kown to e finite.

Thus in this system with the gain, $g(t)$, arying in an unknown but bounded ashion, and with the feedback measureents obscured by noise, it is possible o generate a control or input sequence $n(0)$, $m(1)$, ..., which takes an initial tage, $x(0)$, to the desired state $x^r$ in the tochastic sense (i.e., $E(x(k)-x^r)^2\to 0$ as $\to\infty$) without the steady-state variance f error usually associated with noise in a ystem.

Note that to satisfy equation 25(A) and B) the time-varying gain cannot tend to ero too rapidly, but in order to satisfy 5(C) its square must tend to zero fast enough that its infinite sum is finite. A sequence which satisfies these two conditions is classified as type $1/k$.

## Comparison

As a comparison of this design method with that of conventional sampling systems, consider the previous example with $T=1$ second, $g(t)=10$; $E(n(kT)^2)=\sigma^2$, and the noise, $n(kT)$, "sampled white."[13]

If this system is designed in the conventional way for "finite settling time" in the absence of noise, the controller is a constant gain, $a(k)=0.1$. In the presence of noise, the variance of the system error for all $k$ is $E(x(k)-x^r)^2=\sigma^2$.

In comparison, if the method of this paper is used and the controller gain $a(k)$ is made equal to $0.1/(1+k)$, then the variance of system error as a function of $k$ is:

$$E(x(k)-x^r)^2=\frac{\sigma^2}{1+k}$$

Thus for all $k>1$ the variance of the latter system error is less than one-half that of the conventional sampling system and, further, it tends to zero with large $k$.

## Practical Considerations

First, since $a(k)\to 0$ as $k\to\infty$, it would seem that such a system would only be useful as a one-shot device. To get around this difficulty and permit continuous performance, it is necessary to add an element to the controller which starts the sequence $a(k)$ over again when a change in the reference state occurs. If the reference state, $x^r$, changes infrequently, that is, at a rate which is much slower than the relative convergence rate of the system, then the performance is the same as that previously described. If the input changes are rapid, then the present system is not adequate for the task.

A second and more serious problem concerns the effect of a disturbance at the input of the integrator. With such a disturbance it is not possible to achieve convergence in the sense of

$$\lim_{k\to\infty} E(x(k)-x^r)^2\to 0$$

nor could such convergence be obtained by any other scheme as long as the control effort is restricted to manipulating the input, $m(t)$.

To illustrate the effect of such a disturbance assume that in the previous example a disturbance $q(t)$ is added to the input of the integrator The equation governing the dynamic element now takes the form:

$$\dot{x}=d(t)m^*(t)+q(t)$$

so that the difference equation relating input and output at sampling instants is:

$$x(k+1)=x(k)+d(k)m^*(k)+q'(k)$$

where

$$d(k)=\int_{kT}^{(k+1)T}d(\mu)d\mu$$

and

$$q'(k)=\int_{kT}^{(k+1)T}q(\mu)d\mu$$

Using the controller of the previous section, the system equation now takes the form

$$e(k+1)=(1-a(k)d(k))e(k)-a(k)d(k)n(k)+q'(k) \qquad (27)$$

This equation without the disturbance is equation 24.

From equation 27 it can be seen that for a constant disturbance $q(t)=Q$, $(q'(k)=QT)$ the system is such that the deviation $e=x-x^r$ grows without bound. The expression for this deviation due to the disturbance alone $(n(k)=e(0)=0)$ is:

$$e(k+1)=\sum_{j=0}^{k}f_{k,j+1}q'(j)$$

where $f_{k,j+1}=[1-a(j+1)d(j+1)]\ldots[(1-a(k)d(k)]$. For $a(k)$ of the form $A/_{(1+k)}$ the infinite sum:

$$\lim_{k\to\infty}\sum_{j=0}^{h}f_{k,j+1}=\infty$$

does not exist.

If the disturbance, however, is random, independent of the observation noise and the state of the dynamic process, has mean $E(q'(k))=0$, and has a variance $E(q'(k)^2)$ which is finite; then the effect is quite different. Letting $U_k=E(e(k)^2)$, $\sigma_k=E[a(k)d(k)(n(k))]$, and $Q(k)=E(q'(k)^2)$ the following is obtained:

$$V_{k+1}<\mu_kV_k+\sigma_k+Q_k$$

where $\mu_k<(1-a(k)d(k))^2$. Successively iterating from $k=0$, find:

$$V_{k+1}<b_{k,0}\,V_0+\sum_{j=0}^{k}b_{k,j+1}\sigma_j+\sum_{j=0}^{k}b_{k,j+1}Q_{(j)}$$

where $b_{k,j}$, as previously defined, is the product $\mu_j\mu_{j+1}\ldots\mu_k$.

From previous results it is known that that the first two terms on the right of equation 28 tend to zero as $k$ becomes large. The third term:

$$\sum_{j=0}^{k}b_{k,j+1}Q_{(j)}<C\sum_{j=0}^{k}b_{k,j+1}<\infty$$

Table I. Transient Response

| K | $g_K$ | $n_K$ | x(K) A=1 | =1/4 | =1/8 | =1/16 | =1/32 |
|---|---|---|---|---|---|---|---|
| 00000 | +000.000 | +000.000 | +020.000 | +020.000 | +020.000 | +020.000 | +020.000 |
| 00001 | +007.978 | +005.600 | +020.000 | +020.000 | +020.000 | +020.000 | +020.000 |
| 00002 | +006.162 | +006.920 | −184.256 | −031.064 | −005.532 | +008.185 | +007.233 |
| 00003 | +009.569 | −006.600 | +116.834 | −012.465 | −006.066 | +005.908 | +004.508 |
| 00004 | +009.984 | −004.051 | −234.792 | +002.738 | −001.016 | +006.266 | +004.925 |
| 00005 | +011.038 | +004.957 | +100.319 | +003.558 | +000.565 | +006.123 | +004.788 |
| 00006 | +007.541 | −001.986 | −132.090 | −001.141 | −000.958 | +004.520 | +003.444 |
| 00007 | +008.460 | −001.419 | +036.438 | −000.158 | −000.495 | +004.662 | +003.329 |
| 00008 | +002.193 | −000.822 | −005.888 | +000.318 | −000.206 | +004.525 | +003.185 |
| 00009 | +007.079 | +001.004 | −004.048 | +000.352 | −000.171 | +004.543 | +003.144 |
| 00010 | +003.025 | +004.612 | −001.654 | +000.085 | −000.253 | +004.240 | +002.940 |
| 00011 | +014.123 | −001.698 | −002.549 | −000.269 | −000.418 | +004.067 | +002.798 |
| 00012 | +003.027 | +003.099 | +002.905 | +000.362 | −000.078 | +003.765 | +002.709 |
| 00013 | +013.308 | +002.469 | +001.390 | +000.143 | −000.173 | +003.685 | +002.618 |
| 00014 | +011.929 | +007.207 | −002.561 | −000.524 | −000.467 | +003.386 | +002.292 |
| 00015 | +013.674 | −001.439 | −006.520 | −001.948 | −001.185 | +003.014 | +001.786 |
| 00016 | +007.618 | +001.268 | +000.736 | −001.176 | −000.886 | +003.182 | +001.766 |
| 00017 | +008.093 | −006.611 | −000.218 | −001.187 | −000.908 | +002.963 | +001.676 |
| 00018 | +013.308 | +006.405 | +003.033 | −000.259 | −000.461 | +003.098 | +001.823 |
| 00019 | +014.335 | −003.320 | −003.945 | −001.395 | −001.010 | +002.715 | +001.443 |
| 00020 | +006.795 | +003.327 | +001.537 | −000.505 | −000.602 | +002.720 | +001.531 |
| 00021 | +012.860 | −000.055 | −000.115 | −000.745 | −000.717 | +002.552 | +001.428 |
| 00022 | +015.716 | −006.001 | −000.010 | −000.622 | −000.658 | +002.524 | +001.376 |
| 00023 | +013.888 | +006.038 | +004.284 | +000.560 | −000.064 | +002.482 | +001.582 |
| 00024 | +010.177 | +003.307 | −001.949 | −000.435 | −000.514 | +002.287 | +001.294 |
| 00025 | +010.352 | −004.780 | −002.525 | −000.740 | −000.662 | +002.153 | +001.172 |
| 00026 | +014.999 | −005.483 | +000.500 | −000.168 | −000.381 | +002.111 | +001.266 |
| 00027 | +000.628 | +001.337 | +003.375 | +000.646 | +000.041 | +002.066 | +001.418 |
| 00028 | +010.096 | +006.403 | +003.265 | +000.634 | +000.037 | +002.053 | +000.414 |
| 00029 | +010.699 | +001.017 | −000.221 | +000.000 | −000.252 | +001.973 | +001.238 |
| 00030 | +000.607 | −005.761 | −000.514 | −000.093 | −000.287 | +001.812 | +001.186 |
| 00031 | +008.674 | −005.834 | −000.387 | −000.063 | −000.272 | +001.818 | +001.191 |
| 00032 | +006.511 | −003.290 | +001.353 | +000.348 | −000.058 | +001.869 | +001.273 |
| 00033 | +014.695 | +003.883 | +001.747 | +000.498 | +000.026 | +001.935 | +001.298 |
| 00034 | +010.031 | +004.248 | −000.759 | +000.010 | −000.191 | +001.810 | +001.154 |
| 00035 | +012.777 | −005.281 | −001.789 | −000.303 | −000.340 | +001.708 | +001.054 |
| 00036 | +008.128 | +004.080 | +000.792 | +000.206 | −000.084 | +001.755 | +001.151 |
| 00037 | +003.438 | +004.985 | −000.307 | −000.035 | −000.197 | +001.709 | +001.077 |
| 00038 | +002.497 | +002.969 | −000.742 | −000.150 | −000.252 | +001.673 | +001.042 |
| 00039 | +008.466 | +001.857 | −000.888 | −000.196 | −000.275 | +001.645 | +001.025 |
| 00040 | +000.491 | −000.172 | −001.099 | −000.287 | −000.318 | +001.613 | +000.986 |
| 00041 | +003.201 | +000.023 | −001.083 | −000.285 | −000.317 | +001.612 | +000.986 |
| 00042 | +006.401 | +001.572 | −001.000 | −000.280 | −000.314 | +001.587 | +000.981 |
| 00043 | +006.114 | −001.749 | −001.087 | −000.329 | −000.338 | +001.520 | +000.956 |
| 00044 | +004.179 | +001.869 | −000.684 | −000.255 | −000.301 | +001.540 | +000.963 |
| 00045 | +006.860 | −003.499 | −000.797 | −000.294 | −000.319 | +001.490 | +000.947 |
| 00046 | +006.121 | +000.347 | −000.141 | −000.149 | −000.247 | +001.513 | +000.971 |
| 00047 | +013.767 | −003.001 | −000.169 | −000.156 | −000.248 | +001.479 | +000.960 |
| 00048 | +001.020 | −000.839 | +000.759 | +000.075 | −000.129 | +001.593 | +000.997 |
| 00049 | +008.793 | −002.077 | +000.761 | +000.079 | −000.127 | +001.599 | +000.997 |
| 00050 | +000.686 | +000.559 | +000.997 | +000.168 | −000.077 | +001.611 | +001.009 |

since the infinite sum of the $b_{k,j+1}$'s is finite.

### Transient Behavior

While it has been shown that $x(k)$ converges to the desired state $x^r$ in the mean square as $k\to\infty$, nothing has been said about the rapidity or lack of it in the convergence. From equation 20 in the absence of noise (i.e., $n(k)=0$), it can be seen that $V_k$, the variance of the system error, is less than

$$b_{ko}=\prod_{j=0}^{k}\mu_j$$

times the variance of the initial error. Therefore a fast transient response requires that $b_{ko}$ tends to zero quickly with $k$. In the previous example, with

$$\mu_k \geqq \left|1-\frac{A}{1+k}\,Tg(k)\right|^2$$

it is apparent that this result depends on getting $\mu_k$ very small (i.e., $\mu_k<1$) as quickly as possible. This depends on $g(k)$ and $AT$ but since only $AT$ is commandable it seems that the best one can do is choose $AT$ so that $\mu_k$ is less than unity for all $k$. (Note that as $k\to\infty$, $\mu_k\to 1$.) This choice depends on the bounds $\alpha_1$ and $\alpha_2$ on $g(k)$. However, any particular transient response depends on the exact gain sequence, $g(k)$, and the noise, $n(k)$, so that often another choice of $A$ which leads to $\mu_k$ being greater than unity for small $k$, yields better results.

In Table I, the transient performance of the system described, with an initial state $x(0)=20$, sampling period of $T=1$ second, and the noise and gain sequences tabulated, is shown. The terms in the gain sequence are confined to the range, $0.1<g(k)<16$, while the noise $n(k)$, is uniformly distributed in the range from $-8$ to $+8$ (i.e., $E[n(k)]=0$, $E[n(K)]^2=4/3$). The response is tabulated for $A=1$, 1/8, 1/16, and 1/32. The latter two choices insure that $\mu_k$ is always less than unity, but the fastest convergence is obtained with $A=1/8$.

## Example 2

Example 2 is similar to example 1 except that it is of second order rather than first order (see Fig. 6).

The information available to the designer is the following:

1. The time-varying gain $\alpha<g_k<\beta$ where $\alpha$ and $\beta$ are positive numbers.
2. The noise vector $\mathbf{n}(k)$ is such that $E(\|\mathbf{n}(k)\|)<\infty$ for all $k$.
3. The parameter, $a$, is positive.

Using the vector norm 15(C) and its consistent matrix norm 17(C), it can be shown that $a_{ik}=A_i/(1+k)^2$, where $A_i$ is a positive constant, satisfies equations 13(A)–(D), and thus insures that:

$$E(\|\mathbf{x}(k)-\mathbf{x}^r\|)\to 0$$

in the limit as $k\to\infty$. As before, the transient behavior is closely related to the choice of $A_i$.

## Conclusions

This paper presents a method for designing a control system when the process being controlled has the following properties:

1. Parameters varying in a bounded fashion.
2. The measurements of the state variables are obscured by additive noise.

The controller required to insure sta-

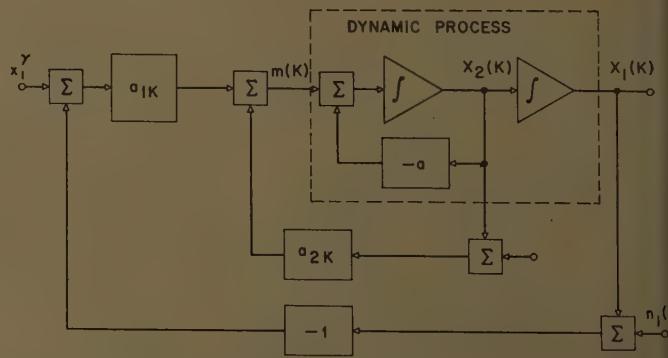


Fig. 6. Example 2

lity in a stochastic sense is conventional
xcept for time-varying gain elements.
It is hoped that the present discussion
ill help in developing the design of con-
ol systems in which the a priori knowl-
lge of the description of the process is
eager and measurement is difficult.

## eferences


SELF OPTIMIZING SYSTEMS WITH RANDOM PUTS, E. G. C. Burt. *Report*, Seminar on Non-near Control Problems, Department of Engi-ering, Cambridge University, Cambridge, Eng-nd, Sept. 1954, pp. 88–89.

SERVOS THAT USE LOGIC CAN OPTIMIZE, R. Cosgriff. *Control Engineering*, New York, . Y., Sept. 1955, pp. 133–35.

3. A SELF-ADJUSTING SYSTEM FOR OPTIMUM DYNAMIC PERFORMANCE, G. W. Anderson, J. A. Aseltine. *Convention Record*, Institute of Radio Engineers, New York, N. Y., pt. 4, 1958, pp. 182–90.

4. DESIGN OF A SELF-OPTIMIZING CONTROL SYSTEM, R. E. Kalman. *Transactions*, American Society of Mechanical Engineers, New York, N. Y., vol. 80, 1957, pp. 468–78.

5. A STOCHASTIC APPROXIMATION METHOD, H. Robbins, S. Monro. *Annals of Mathematical Statistics*, East Lansing, Mich., vol. 22, 1951, pp. 400–07.

6. ON THE STOCHASTIC APPROXIMATION METHOD OF ROBBINS AND MONRO, J. Wolfowitz. *Ibid.*, vol. 23, 1952, pp. 457–61.

7. APPROXIMATION METHODS WHICH CONVERGE WITH PROBABILITY ONE, J. R. Blum. *Ibid.*, vol. 25, 1954, pp. 737–44.

8. MULTIDIMENSIONAL STOCHASTIC APPROXIMATION METHODS, J. R. Blum. *Ibid.*, pp. 737–44.

9. ON STOCHASTIC APPROXIMATION, A. Dvoretzky. *Proceedings*, Third Berkeley Symposium on Mathematical Statistics and Probability, University of California, Berkeley, Calif., vol. 1, 1957, pp. 39–51.

10. GENERAL SYNTHESIS PROCEDURE FOR COMPUTER CONTROL OF SINGLE-LOOP AND MULTILOOP LINEAR SYSTEMS, R. E. Kalman, J. E. Bertram. *AIEE Transactions*, pt. II (*Applications and Industry*), vol. 77, 1958 (Jan. 1959 section), pp. 602–09.

11. THE APPROXIMATE SOLUTION OF MATRIX PROBLEMS, A. S. Householder. *Journal*, Association for Computing Machinery, Baltimore, Md., vol. 5, no. 3, July 1958.

12. THEORY AND APPLICATION OF INFINITE SERIES (book), Knopp. Hafner Publishing Company, New York, N. Y., 1947, pp. 218–26.

13. SAMPLED-DATA CONTROL SYSTEMS (book), J. R. Ragazzini, G. Franklin. McGraw-Hill Book Company, Inc., New York, N. Y., 1958, chap. 10.


# The Effect of Elevated Temperature on Flash-Welded Aluminum-Copper Joints


C. R. DIXON
ASSOCIATE MEMBER AIEE

F. G. NELSON
NONMEMBER AIEE


BOTH ALUMINUM and copper have high conductivity and hence are xcellently suited for use as electric onductors. Since both metals are widely sed, connections between them fre-uently have to be made. The most ommon type of connection is the bolted oint, as when an aluminum bus bar is olted to a copper stud. Although this ype of connection is satisfactory, fre-uently a more efficient and less bulky onnection, with better appearance, can e made by flash welding, as illustrated Fig. 1.

The quality of flash welds is dependent n certain conditions during the welding peration. As a result of important im-rovements in techniques, especially in ne forging mechanism and in the die esign of the welding equipment, flash elding is now used commercially in an creasing number of applications in which onnections have to be made between uminum and copper. The improve-ents provide 1. rigid support of the eces at the ends during joining, 2. rge increase of velocity of the platen at e time of upset, and 3. control of time change from flashing to upsetting dur-g the flash-welding operation. These ree improvements make it possible to tain welds of high quality. Further-ore, the die not only rigidly supports the aterial but uses the energy of motion to ear off the upset metal.

While it was possible that extreme temperature conditions might be harmful to the joints, it was believed that the conditions that would exist in normal service would not be harmful. Some tests to evaluate the effects of elevated temperatures were reported several years ago, using joints made before the present improved techniques were available.[1] In the investigation now being described, the improved techniques have been used. From tests of almost 500 joints, the effects of heating on tensile strength, ductility, resistance to impact, and electrical resistance were determined.

## Welding Procedure and Materials

A general view of the 250-kva flash welder that was used is shown in Fig. 2. A close-up of the dies, indicating the pinching-off action at the weld, is shown in Fig. 3. An oscillogram of the operation during the controlled change of platen movement, when the velocity of the platen changes from 0.125 inch per second to 13.7 inches per second, is shown in Fig. 4, together with traces for voltage and current.

Joints were prepared consisting of commerically pure aluminum bar, 1/4 by $1^1/_2$ inches, flash welded to copper bar of the same size.

The conditions under which the welds were made are shown in Fig. 5. Before making any welds to be tested, the setup of the welding machine was checked by

**Fig. 1. Stator of large generator containing flash-welded aluminum-copper joints. Arrows indicate one of 24 groups of welds; note bend near one weld**

**Fig. 2. Flash-welding machine, 250 kva**


Paper 59-1162, recommended by the AIEE Electric Welding Committee and approved by the AIEE Technical Operations Department for presentation at the AIEE Fall General Meeting, Chicago, Ill., October 11–16, 1959. Manuscript submitted April 8, 1959; made available for printing August 6, 1959.



C. R. DIXON is with Alcoa Process Development Laboratories, and F. G. NELSON is with Alcoa Research Laboratories, both in New Kensington, Pa.

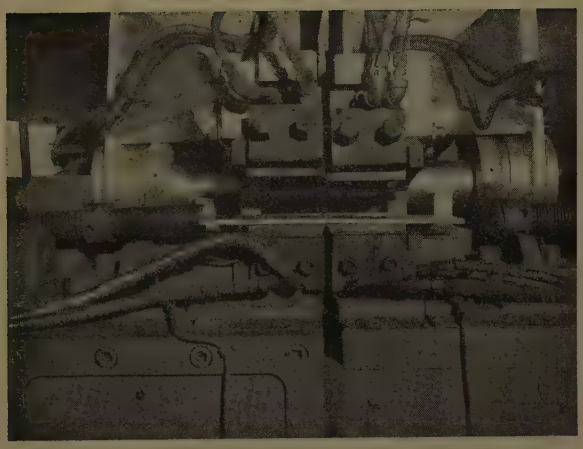

Fig. 3 (left). Pinch-off dies in flash - welding machine

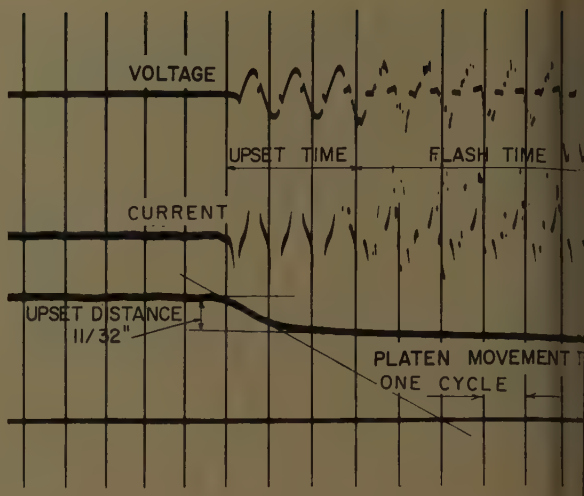


Fig. 4 (right). Oscillogram indicating speed of platen during flash welding

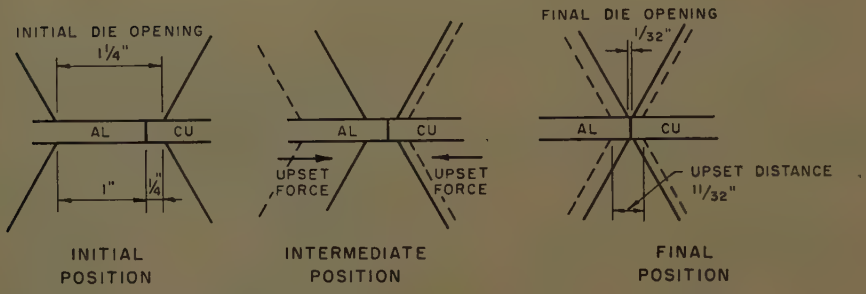


Fig. 5. Conditions used in flash welding 1/4-inch by $1\frac{1}{2}$-inch bars

Flashing distance = 7/8 inch
Flashing time = 7 seconds
Flashing velocity = 0.125 inch per second
Force time delay = 0.032 second
Upset time = 0.049 second
Maximum upset velocity = 13.7 inches per second

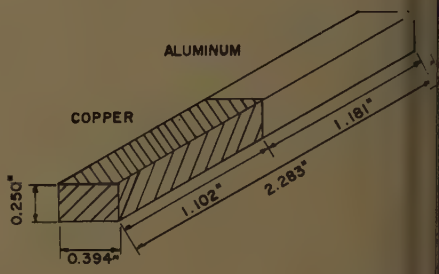


Fig. 6. Cantilever-beam impact test specimen of flash-welded aluminum-copper joint

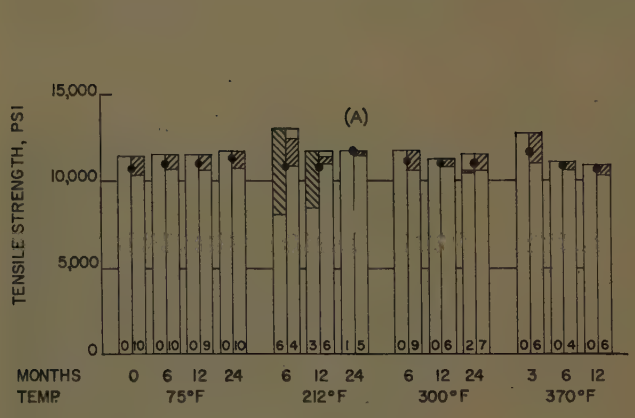


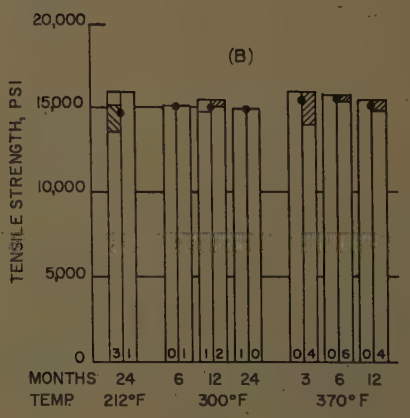


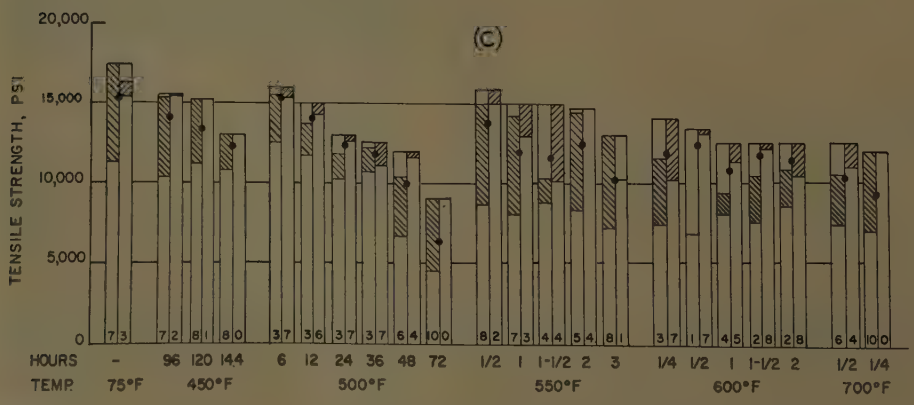


Fig. 7. Tensile strengths at room temperature after indicated exposures for group (A); group B (B); and group C (C)

Key:
A = range for specimens that failed at weld
B = range for specimens that failed in aluminu
C = range for all specimens
D = average for all specimens
E = number of specimens that failed at weld
F = number of specimens that failed in aluminu

## Table I. Average Results of Tensile Tests

| Heating Conditions | | Tensile Strength, Psi | Location of Failure, No. at Weld per Total No. | Extension in 2 Inches, %* |
|---|---|---|---|---|
| Temperature, F | Time, Months | | | |
| **Group A** | | | | |
| 75 | 0 | 11,000 | 0/10 | |
| | 6 | 11,200 | 0/10 | |
| | 12 | 11,200 | 0/9 | |
| | 24 | 11,500 | 0/10 | |
| 212 | 6 | 11,000 | 6/10 | 6.9 |
| | 12 | 11,000 | 3/9 | 8.7 |
| | 24 | 12,000 | 1/6 | 21.0 |
| 300 | 6 | 11,400 | 0/9 | |
| | 12 | 11,200 | 0/6 | |
| | 24 | 11,100 | 2/9 | 9.8 |
| 370 | 3† | 11,800 | 0/6 | |
| | 6† | 11,000 | 0/4 | |
| | 12† | 10,900 | 0/6 | |
| **Group B** | | | | |
| 212 | 24 | 14,800 | 3/4 | 7.7 |
| 300 | 6 | 15,200 | 0/1 | |
| | 12 | 15,100 | 1/3 | 11.5 |
| | 24 | 15,000 | 1/1 | 17.0 |
| 370 | 3† | 15,500 | 0/6 | |
| | 6† | 15,600 | 0/6 | |
| | 12† | 15,200 | 0/4 | |

| Heating Conditions | | Tensile Strength, Psi | Location of Failure, No. at Weld per Total No. | Extension in 2 Inches, %* |
|---|---|---|---|---|
| Temperature, F | Time, Hours | | | |
| **Group C** | | | | |
| 75 | | 15,400 | 7/10 | 9.3 |
| 450 | 96 | 14,000 | 7/9 | 10.3 |
| | 120 | 13,300 | 8/9 | 5.5 |
| | 144 | 12,200 | 8/8 | 5.2 |
| 500 | 6 | 15,400 | 3/10 | 13.5 |
| | 12 | 14,200 | 3/9 | 13.5 |
| | 24 | 12,500 | 3/10 | 14.2 |
| | 36 | 11,900 | 3/10 | 14.5 |
| | 48 | 10,100 | 6/10 | 10.9 |
| | 72 | 6,500 | 10/10 | 4.0 |
| 550 | 1/2 | 13,900 | 8/10 | 11.9 |
| | 1 | 12,000 | 7/10 | 8.6 |
| | 1½ | 11,700 | 4/8 | 7.4 |
| | 2 | 12,600 | 5/9 | 10.4 |
| | 3 | 10,500 | 8/9 | 13.1 |
| 600 | 1/4 | 12,100 | 3/10 | 10.0 |
| | 1/2 | 12,500 | 1/8 | 7.5 |
| | 1 | 10,800 | 4/9 | 14.9 |
| | 1½ | 11,800 | 2/10 | 16.0 |
| | 2 | 11,500 | 2/10 | 10.2 |
| 700 | 1/12 | 10,300 | 6/10 | 9 7 |
| | 1/4 | 9,400 | 10/10 | 6.6 |

* Includes only those that failed at weld.

† Intermittent instead of continuous heating; total time at temperature.

qualification tests in which sample welds were required to withstand bending 90 degrees around a 3/4-inch mandrel without failure.

The joints consisted of three groups. Groups *A* and *B* were welded at the same time, the only difference being that the aluminum bar used for group *A* had been annealed while that used for group *B* was in an intermediate strain-hardened temper. The third group, *C*, was welded some 2 years later using bar similar to that used for group *B*.

## Test Procedures

Joints from groups *A* and *B*, as shown in Table I, were tested either after holding at room temperature or after heating continuously at temperatures of 212 or 300 (degrees Fahrenheit) for different periods, including some as long as 2 years. In addition, some were heated intermittently at 370 F for a total time at temperature of 1 year. Joints from group *C* were heated continuously at temperatures of 450 to 700 F for periods ranging from a few minutes to 6 days.

All tests were made at room temperature. They included tensile and impact tests, electrical resistance measurements, and metallographic examinations.

Tensile tests were made of specimens consisting of the full section of the bar. As a measure of ductility, the extension, in per cent, of a 2-inch gage length centered across the weld was determined.

Impact test specimens 0.250 by 0.394 inch as in Fig. 6 were machined without notches and were tested as cantilever beams in an Izod machine of 50-foot-pound capacity. The aluminum end of the specimen was gripped in the vise with the joint at the edge of the jaws. The copper end was struck on a 0.394-inch face by the pendulum so that an original surface was subjected to maximum tension.

Electrical resistance measurements were made in which current was passed through the length of the specimen, including the layer of intermetallic compound. The potential drops were measured over 2- and 4-inch gage lengths, using an L-and-N-type *K-2* potentiometer.

Metallographic examination of some

## Table II. Results of Impact Tests

| Heating Conditions | | Total No. of Tests | Complete Fractures | | |
|---|---|---|---|---|---|
| Temperature, F | Time | | No. | Range of Values, Foot-Pounds | Average Value, Foot-Pounds |
| **Groups A and B, Time in Months** | | | | | |
| 75 | 0 | 9 | 0 | | |
| | 6 | 9 | 1 | 2.3 | 2.3 |
| | 12 | 9 | 1 | 3.2 | 3.2 |
| | 24 | 9 | 2 | 6.6–6.6 | 6.6 |
| 212 | 6 | 9 | 2 | 2.4–3.7 | 3.0 |
| | 12 | 9 | 1 | 0.9 | 0.9 |
| | 24 | 9 | 1 | 1.6 | 1.6 |
| 300 | 6 | 9 | 2 | 2.9–7.7 | 5.3 |
| | 12 | 9 | 0 | | |
| | 24 | 9 | 2 | 2.4–8.0 | 5.2 |
| 370 | 3* | 9 | 3 | 3.7–12.1 | 7.2 |
| | 6* | 9 | 0 | | |
| | 12* | 9 | 1 | 1.6 | 1.6 |
| **Group C, Time in Hours** | | | | | |
| 75 | | 4 | 2 | 1.5–8.0 | 4.8 |
| 450 | 96 | 9 | 5 | 0.5–6.0 | 2.4 |
| | 120 | 9 | 9 | 0.5–7.5 | 2.3 |
| | 144 | 9 | 5 | 0.3–2.5 | 1.3 |
| 500 | 6 | 9 | 3 | 2.1–2.5 | 2.2 |
| | 12 | 9 | 2 | 1.3–4.1 | 2.7 |
| | 24 | 9 | 2 | 2.5–3.3 | 2.9 |
| | 36 | 9 | 1 | 1.1 | 1.1 |
| | 48 | 9 | 3 | 1.0–8.5 | 4.1 |
| | 72 | 9 | 6 | 1.0–4.5 | 2.9 |
| 550 | 1/2 | 9 | 1 | 4.8 | 4.8 |
| | 1 | 9 | 0 | | |
| | 1½ | 9 | 2 | 0.5–2.5 | 1.5 |
| | 2 | 9 | 1 | 1.5 | 1.5 |
| | 3 | 9 | 1 | 1.0 | 1.0 |
| 600 | 1/4 | 9 | 2 | 2.5–5.5 | 4.0 |
| | 1/2 | 9 | 1 | 0.5 | 0.5 |
| | 1 | 9 | 1 | 2.2 | 2.2 |
| | 1½ | 9 | 0 | | |
| | 2 | 9 | 2 | 0.2–1.8 | 1.0 |
| 700 | 1/12 | 9 | 3 | 0.8–2.0 | 1.6 |
| | 1/4 | 9 | 5 | 1.0–5.1 | 2.5 |

* Intermittent instead of continuous heating; total time at temperature.

**Table III. Electrical Resistance of 1/4- by 1 1/2-Inch Flash-Welded Aluminum-Copper Joints**

| Heating Conditions | | Electrical Resistance, Microhms, Gage Length | |
|---|---|---|---|
| Temperature, F | Time | 4 Inches | 2 Inches |
| **Groups A and B, Time in Months** | | | |
| Room temperature | | 10.0 | 5.0 |
| 212 | 24 | 10.1 | 5.0 |
| 300 | 24 | 9.9 | 4.8 |
| 370 | 12* | 10.0 | |
| **Group C, Time in Hours** | | | |
| Room temperature | | 9.8 | 4.8 |
| 450 | 144 | 9.7 | 4.8 |
| 500 | 72 | 9.8 | 5.0 |
| 550 | 3 | 9.8 | 4.8 |
| 600 | 2 | 9.7 | 4.7 |
| 700 | 1/4 | 9.8 | 4.8 |

* Intermittent instead of continuous heating; total time at temperature.

of the welds was made in which the thickness of the layer of intermetallic compound was determined.

## Results and Discussion

The results of tensile tests are summarized in Table I and in Fig. 7.

In about 40% of the tests, failure occurred in the aluminum and, therefore, the actual strengths of the welds were not determined, only the maximum stress that they withstood before the specimens failed. The average strength of all of the specimens was 11,900 psi (pounds per square inch), but for the reason just stated the actual average strength of the welds must have been even higher.

In groups *A* and *B* (Table I and Figs. 7(A) and (B)) there was obviously no significant decrease in the strength of the specimens as a result of heating. It will be noted that in both groups the slight decreases in strengths with increases in length of heating period at the highest temperature (370 F) are not an indication of loss of strength of the welds, since none of the failures in these tests occurred at welds. Since very few of the specimens in groups *A* and *B* failed at the welds, the higher strengths in group *B* reflect the higher strength of the aluminum bar in those specimens.

In group *C* (Table I and Fig. 7(C)), the percentage of failures at the welds was larger than in groups *A* and *B*. This is true regardless of whether or not the joints were heated. Also, heating at the various conditions caused decreases in strengths of the specimens. Decreases of this kind were expected because such heating would anneal the aluminum which, in this group of specimens as mentioned previously, was in a strain-hardened temper. When the decreases that occurred were accompanied by definite increases in the proportion of failures at the welds, and when the strengths became less than that of thoroughly annealed aluminum, then there was distinct evidence that the heating was detrimental to the welds. For the heating conditions investigated, the percentage of failures at the weld did not increase significantly until the specimens had been heated 120 hours at 450 F, 48 hours at 500 F or 1/4 hour at 700 F. The average tensile strength did not decrease to less than 10,000 psi until the specimens had been heated 72 hours at 500 F or 1/4 hour at 700 F. In general, the scatter or spread of strengths was no greater for the exposed specimens than for those that were not heated, but the lowest individual strengths encountered for exposures of 48 hours or more at 500 F and for all times at higher temperatures were considerably below 10,000 psi.

In general, the extension values obtained in the tensile tests are in agreement with the foregoing observations.

The results of the impact tests are summarized in Table II. Values are shown only for those tests in which complete fracture occurred, because it is only under such conditions that the results have quantitative meaning.

Complete fracture occurred in only about one-fourth of the tests, and in those cases it was at the weld. Generally, the percentage of complete fractures tended to decrease with increase in temperature. Although the average impact values were generally lower for the specimens that had been heated than for the specimens that had not been heated, the number of specimens that actually

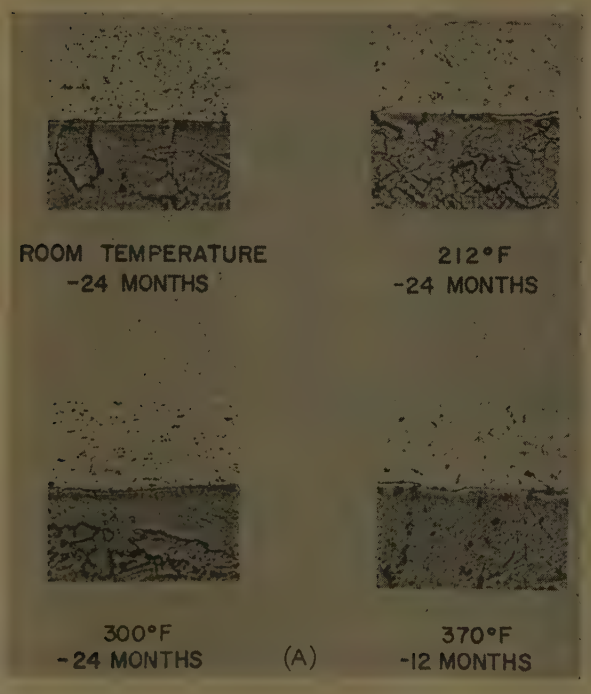


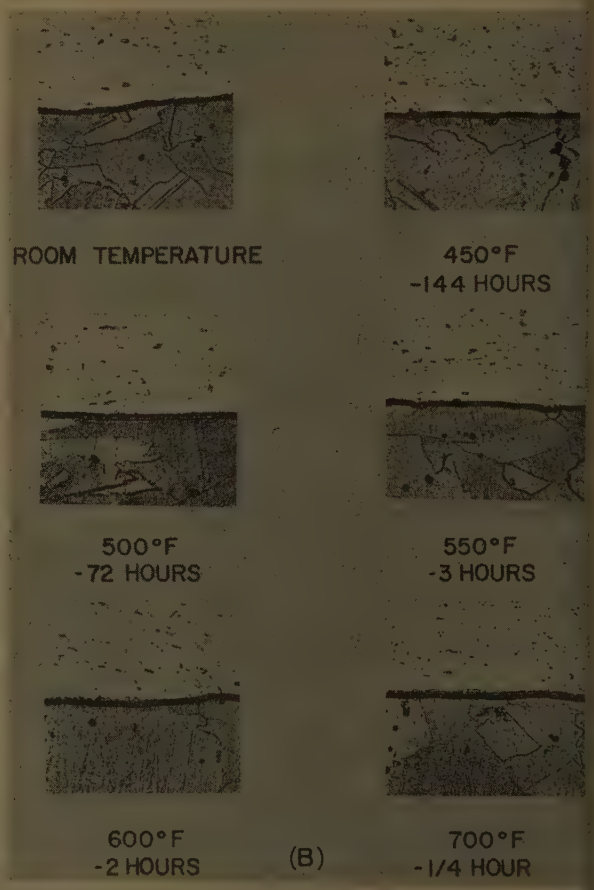


**Fig. 8. Etched cross sections of joints after heating, 500×**

A—Groups A and B
B—Group C

fractured at the welds was so small, and the number of specimens in which the welds withstood the impact blow was so large, that the values themselves are not significant in evaluating the effects of heating.

The measurements of electrical resistance at room temperature after heating for the longest period of time at each temperature are listed in Table III. The data show no trend toward an increase in resistance with increase in temperature or time of heating. Furthermore, the resistance of a 2-inch gage length was almost exactly half that of a 4-inch gage length. If the thickness of the layer of intermetallic compound had been increased by the heating, the resistances would have increased and the resistance for a 2-inch gage length would have been more than half of those for a 4-inch gage length. This would also be the case if any discontinuities, such as separation at the intermetallic layer, had been caused by heating.

Photomicrographs of welds subjected to each of the temperatures for the longest periods are shown in Fig. 8 There is little if any significant increase in thickness of the interfacial layer with increase in temperature or length of heating period. The thickness of this layer generally was 0.00015 inch or less.

## Conclusions

Improved techniques have been developed by which flash-welded joints between aluminum and copper can now be made commercially. The average strengths of the welds are at least 10,000 psi when heated as high as 300 F for 2 years, 370 F for 1 year, 450 F for 144 hours, 500 F for 36 hours, 600 F for 2 hours, or 700 F for 5 minutes. The strengths of individual welds, however, may drop below 10,000 psi when joints are heated 48 hours or more at 500 F, or when heated for shorter times above that temperature.

There was no evidence of embrittlement at any of the heating conditions used.

## Reference

1. Preventing Embrittlement in Copper-to-Aluminum Weld Joints, C. L. Carlson, R. M. Leedy. *Product Engineering*, New York, N. Y., Oct. 1955, pp. 172–73.

## Discussion

**Thomas B. Correy** (Hanford Atomic Products Operation, General Electric Company, Richland, Wash.): The subject matter is very well prepared and the duration of the tests long enough to provide accurate vital information on the joining of aluminum to copper by the flash-welding process. This information is very vital as portions of the electrical industry are moving rapidly into the use of aluminum for windings in motors, generators, and transformers.

There is one portion of the tensile test data that the authors neglected to discuss. What causes the high weld failure rate for the 212 F test? Other alloys of aluminum have displayed brittle failure of flash-welded joints at a critical temperature somewhat higher than this. This condition should be explained, as windings are subject to temperatures of this order of magnitude and under mechanical stress.

**C. R. Dixon** and **F. G. Nelson:** The authors thank Mr. Correy for his complimentary remarks and admit that he has asked a very pertinent question concerning the data presented.

Efforts were made to determine the reason for the relatively high number of failures in the welds of group *A* that were subjected to a temperature of 212 F. The fractured specimens were examined and both the fractured surfaces and the metallurgical structure appeared normal. The only conclusion the authors can reach is that this was simply the result of random selection of specimens. Experience with similar flash-welded joints in current-carrying circuits in Alcoa plants where they have been in use at temperatures near 212 F has given us confidence in the behavior of flash-welded joints at this temperature.

# Transient Response and the Stabilization of Feedback Amplifiers

J. H. MULLIGAN, JR.
MEMBER AIEE

ANY VACUUM-tube or transistor amplifier is continuously subjected to random current and voltage disturbances of varying peak amplitude and waveshape. Thermal noise is a common example of such excitation. The importance of this interfering effect, as far as the circuit designer is concerned, depends to a large extent upon the relative magnitudes of the desired signals for which the amplifier is designed as compared to the strength of the response produced by the system to the random excitation.

In a passive network or a nonfeedback amplifier, the transient response to an impulse or step function consists of constants and/or exponentially damped terms, and, as a consequence, one may predict accurately the response of any applied signal be it desired or undesired. In a feedback amplifier, on the other hand, possibilities exist, in general, for the production of terms in the transient response whose amplitudes continue to increase with time until such values are reached that the nonlinear input-output characteristics of the vacuum tubes or transistors limit further growth. At such times, it is possible for the response to bear little relation to the excitation which initiated it. Because of the continual excitation by thermal noise pulses and similar internally generated signals, an amplifier with no external signal applied can produce an appreciable output with no apparent input because of the presence in its transient response of terms which increase exponentially with time.

Amplifiers and other dynamic systems can accordingly be classified as stable or unstable, respectively, depending on the nature of their transient response. In this paper a stable system is considered to be one in which any disturbance which decays with time and ultimately dies out produces a response which decays with time and ultimately dies out. The principal concern here is with the process of stabilizing an unstable feedback amplifier. Stated in other terms, the problem considered is one of determining what modifications are needed in a feedback amplifier design in order to change the

Paper 59-1151, recommended by the AIEE Feedback Control Systems Committee and approved by the AIEE Technical Operations Department for presentation at the AIEE Fall General Meeting, Chicago, Ill., October 11–16, 1959. Manuscript submitted March 23, 1959; made available for printing July 31, 1959.

J. H. Mulligan, Jr., is with New York University, New York, N. Y.

transient response so that it contains no terms whose amplitudes increase indefinitely with time. In terms of the complex frequency plane, the stabilization problem consists of insuring that all roots of the characteristic equation of the amplifier lie in the interior of the left half plane.

The stabilization problem for feedback amplifiers is not a new one by any means. The question has been considered at length in terms of Nyquist polar diagrams as well as in terms of plots of the gain and phase characteristics of the return ratio, or loop gain, as functions of frequency. H. W. Bode[1] has given an elegant solution to the stabilization problem in terms of an "ideal gain characteristic." This loop gain function calls for a constant gain up to a certain frequency, and a constant phase shift equal to 180 degrees minus a prescribed "phase margin" beyond, until the gain has dropped a prescribed amount (called the "gain margin") below unity. Design control is relaxed above the frequency at which this occurs. The characteristic is "ideal" in the sense that it achieves the maximum amount of feedback over a prescribed frequency range that can be attained with the given tubes or transistors in an absolutely stable amplifier whose phase shift does not exceed a fixed amount in the frequency interval in which design control is maintained.

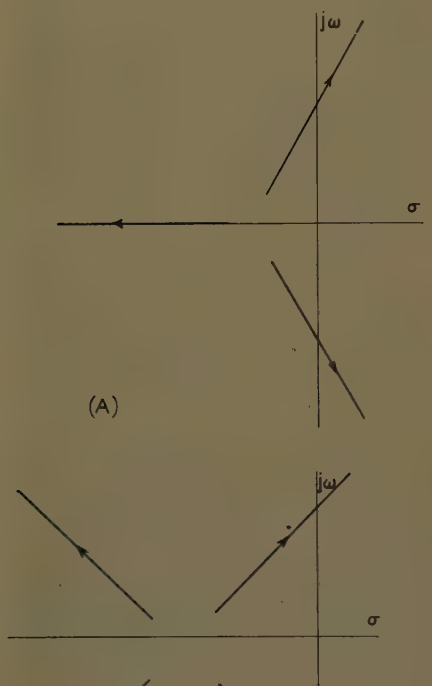


**Fig. 1. Asymptotes approached by loci of closed loop poles as mid-band open loop gain is increased indefinitely**

A—For an amplifier with three more poles than zeros in T(s)
B—For an amplifier with four more poles than zeros in T(s)

Duerdoth[2] has shown, however, that if one relaxes the Bode condition of constant phase shift in the region just outside the pass-band, the loop gain attainable over the useful frequency band can be increased and adequate protection against oscillation which might result from component variation can still be provided. Other investigators have considered the stabilization problem, also from the frequency response viewpoint, with various special design requirements in mind such as the one of obtaining a maximal flatness closed-loop gain response.

The two quantities, gain margin and phase margin, are included in all the approaches to the stabilization problem based on the frequency response viewpoint. Some success has been attained in relating frequency response data to certain aspects of the transient response.[3,4] Gain margins and phase margins are still established to a large extent, however, on a rule-of-thumb basis in the formulation of design requirements rather than being amenable to a direct analytical determination from a knowledge of the transient performance desired from the amplifier to be designed.

It is recalled that the stabilization problem arises in the first place because the transient response is not satisfactory, viz. not all of the roots of the characteristic equation lie in the left half plane. It is profitable, therefore, to consider the stabilization of feedback amplifiers directly in terms of the transient response desired. That is to say, it is of value to study the problem without recourse to frequency response data and, in particular, to think in terms of a performance criterion for stabilization different from a gain margin plus a phase margin. A similar approach has been utilized in connection with the design of servomechanisms, but the results obtained cannot be applied directly to the general feedback amplifier problem because of a fundamental difference in the elements which find principal application in the two classes of systems.

In servomechanisms, the time constants, or frequency response characteristics, associated with the mechanical elements employed represent a fundamental limitation to the speed of system response. The limitations of vacuum tubes and transistors which arise from parasitic capacitances and the variation of parameters with frequency are of negligible importance when these elements are employed in servomechanism systems. This occurs because the time constants associated with these devices are so much less than those associated with the response of the necessary mechanical elements that their limitations are virtually nonexistent by comparison. On the other hand, the so-called asymptotic characteristics of tubes and transistors (their limiting performance at high frequencies) impose serious constraints on pole and zero locations in the complex plane that may be realized in feedback or nonfeedback amplifiers. Taking these extra constraints into account is an important feature of a design procedure for the feedback amplifier problem.

The principal purpose of this paper is to describe an approach to the stabilization of feedback amplifiers which is based on the direct control of the transient response to a step function input. The minimum rate at which the overshoots at succeeding maxima of the step function response are attenuated is taken as a design criterion for stabilization and the direct determination of element values from the specified attenuation is shown in illustrative examples.

## Stabilization Philosophy Based on Transient Response

### Root Loci and Dominant Response

In the stabilization philosophy based on the direct control of transient response, the requirements calling for a given phase margin and a preassigned gain margin are replaced by either a statement of the minimum rate at which the overshoots at the succeeding maxima of the step-function response are to be attenuated or, alternatively, a specification of the maximum per-cent overshoot that will be permitted in the step-function response. For either one of these two time-response design criteria to have practical usefulness, one must have reason to believe that the step-function response characteristics of common feedback amplifiers are sufficiently similar so that the proposed criteria are both meaningful and applicable.

Two factors considered together indicate that the transient response approach to the stabilization problem should be valuable in the design of a large class of vacuum-tube and transistor feedback amplifiers. The first factor is concerned with the location of the poles of the

closed-loop transfer function of a feedback amplifier. Root locus techniques introduced by Evans[5] predict an asymptotic movement of the closed-loop poles along radial lines having equal angular displacement and a center located in the left half plane as the mid-band return ratio (or loop gain) is increased without limit. The detailed form of the loci depends on the specific positions of the poles and zeros of the return ratio function $T(s)$, but the asymptotic behavior for large values of $T(0)$ has the general form depicted in Fig. 1. The movement of the poles away from one another with increased $T(0)$ is suggested from the figure.

This behavior suggests the second factor of importance, namely the applicability of the dominant-term approximation to the step function response introduced previously by the author.[6] In the reference cited, it was shown that under suitable conditions of separation among the poles in the complex frequency plane, the normalized time response can be well approximated at the first maximum and beyond by a constant term plus a single exponentially damped sinusoid. In general, although not always, the pair of complex poles located nearest to the imaginary axis in the complex frequency plane will produce the dominant term in the time response. The approximation to the actual time response given by the dominant term theory is improved as the separation among poles increases. By consideration of the root loci asymptotes obtained from the open-loop transfer functions of common vacuum-tube and transistor feedback amplifiers and the corresponding pole movements which are implied, one is led to the conclusion that the dominant term theory should have wide application in the approximation of the transient response of such amplifiers. A design criterion for stabilization based on the form of time response obtained using the dominant-term approximation should, therefore, have considerable utility.

## Underlying Principles

For a dynamic system having a transfer function consisting of a single pair of complex poles as depicted in Fig. 2, the first maximum in the time response to a step function excitation occurs at a value $t_{max}$ expressed by

$$\beta_1 t_{max} = \pi \tag{1}$$

and the deviation ($\gamma$) from unity at the first maximum of the normalized time response is[6]

$$\gamma = \epsilon^{-\pi \cot \psi_1} \tag{2}$$

The quantities $\beta_1$ and $\psi_1$ are shown in Fig. 2. For a pole-zero configuration to which the dominant term theory is applicable (detailed conditions relating to the degree of approximation involved are given in reference 6) but which is otherwise arbitrary, the extreme values of the time response, local maxima and minima, occur at times given approximately by

$$\beta_1 t = h\pi - \lambda_1 \tag{3}$$

and the corresponding deviations from unity in the normalized response are approximately given by equation 4. (See equations 23 and 40 of reference 6 for the approximations associated with equations 3 and 4.)

$$\gamma_h = (-1)^{w+h+1} M_1 \epsilon^{\lambda_1 \cot \psi_1} \epsilon^{-h\pi \cot \psi_1} \tag{4}$$

where $w$ is the number of real zeros in the right half plane and $h = b, b\text{-}1, b\text{-}2, \ldots, b$ being the integer (positive, negative, or zero) for which $b\pi - \lambda_1$ has its smallest non-negative value. $M_1$ is the coefficient of the term $\sin(\beta_1 t + \lambda_1 + \psi_1)$ in the normalized time response. It is equal to the quotient of the product of length factors due to zeros divided by the product of length factors due to poles. All poles and zeros in the pattern except the pole at $-\alpha_1 - j\beta_1$ are considered; the factor for any element, pole or zero, is equal to the ratio of the distance in the complex plane from the element to $-\alpha_1 + j\beta_1$ divided by the distance from the origin to the element. Each directed distance from a pole or zero to $-\alpha_1 + j\beta_1$ may be viewed as a complex number. $\lambda_1$ is found by summing the angles of the complex numbers associated with the directed distance from each pole and zero to $-\alpha_1 + j\beta_1$, a plus sign being used with angles associated with zeros and a minus sign being employed for the angles associated with poles. The pole at $-\alpha_1 - j\beta_1$ is not included in this calculation.

By examination of equation 4, it is seen that the ratio of the deviations from unity in the normalized time response to two successive extreme values is

$$\eta = \left| \frac{\gamma_{h+1}}{\gamma_h} \right| = \epsilon^{-\pi \cot \psi_1} \tag{5}$$

If there are no zeros in the right half plane and $b = 1$, which is common for simple pole-zero patterns, then the first maximum occurs at $t_{max}$ where

$$\beta_1 t_{max} = \pi - \lambda_1 \tag{6}$$

and the fractional overshoot at the first maximum is

$$\gamma_1 = M_1 \epsilon^{\lambda_1 \cot \psi_1} \epsilon^{-\pi \cot \psi_1} \tag{7}$$

The quantity $M_1 \epsilon^{\lambda_1 \cot \psi_1}$ is a function not only of the pole angle of the dominant pair of poles but also of the location of the other poles and zeros relative to $-\alpha_1 \pm j\beta_1$. It has been defined as an "overshoot factor," and graphs have been provided for its direct computation from pole-zero locations.[6] It is noted by comparison of equations 1 and 6 as well as equations 2 and 7 that in systems where the dominant-term theory applies, the effect of adding other poles and zeros to the simple system of two complex poles is but to change both the magnitude and the time of occurrence of the first maximum, leaving the shape of the curve essentially unchanged. These matters are considered at length in the reference cited.

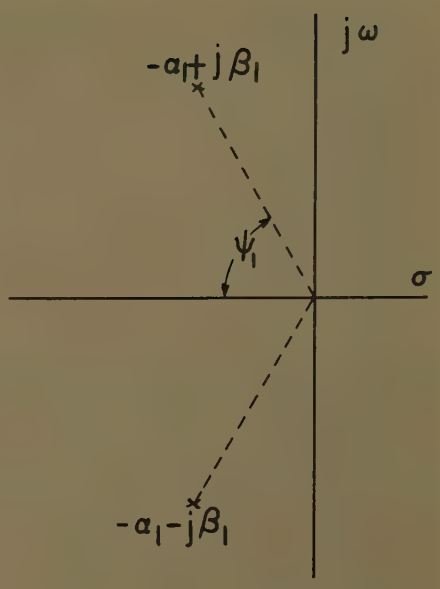


**Fig. 2. Pole pattern for a system having a transfer function containing two complex poles illustrating notation used in text**

## Stabilization Design Criterion

Equation 5 provides a logical design criterion for the stabilization of feedback amplifiers. For a system to be stable it is necessary that $\eta < 1$, or that $\psi_1 < \pi/2$. Furthermore, the time taken for the step-function transient to be completed to an arbitrarily assigned degree; i.e., the time taken for the value of overshoot at a local maximum to become less than a stated value, is not only a measure of the stability of the amplifier but one which is acceptable from an intuitive standpoint. $\eta$ will be specified, therefore, as a stabilization design criterion based on the control of transient response; a design philosophy will be outlined whose use will permit achieving a pair of dominant poles with the angle $\psi_1$ once the angle has been determined from an acceptable value of $\eta$. It is to be noted also, however, that equation 7 for the overshoot at the first maxi-

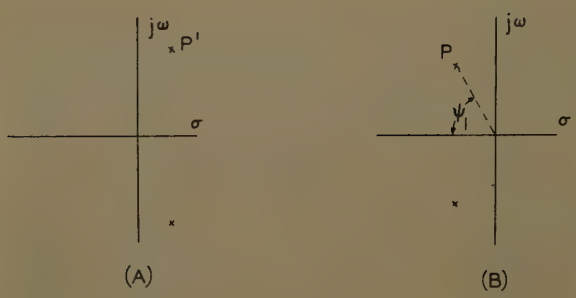


**Fig. 3. The feedback amplifier stability problem may be viewed as that of shifting the position of the complex pole at P′ (and its conjugate) in (A) to point P in (B)**

mum contains the expression for $\eta$ as a factor. Specification of the overshoot at the first maximum thus provides an acceptable alternative design criterion for stabilization although the geometry of the final closed-loop pole-zero pattern then enters the design process through the quantities $M_1$ and $\lambda_1$. In many simple feedback amplifier configurations (where the excess of poles over zeros is three or four, for example), the overshoot factor $M_1 \epsilon^{\lambda_1} \cot \psi_1$ is frequently approximately unity so that $\eta$ is essentially equal to $\gamma_1$, the percent overshoot at the first maximum.

A statement of the stabilization problem can now be made in terms of the complex frequency plane. Suppose that an amplifier has been designed to meet various performance requirements and it is found to have two complex poles in the right half plane as depicted in Fig. 3(A). Furthermore, suppose the circuit designer desires that the step-function transient response should have a maximum overshoot of a prescribed percent or that the damped sinusoidal dominant transient should decay at a certain minimum rate. In effect, the designer wishes to achieve the condition pictured in Fig. 3(B), a condition in which the dominant pole pair ($P$ in the second quadrant) has an angle $\psi_1$ determined from either the overshoot or attenuation requirement. (Note that the two are related; see equations 5 and 7.) The amplifier design must be altered in such a manner that with the desired mid-band return ratio unchanged, point $P'$ in Fig. 3(A) moves to $P$ in Fig. 3(B). To illustrate the process involved in the shift of dominant pole position, let the closed-loop transfer function be written in the form of equation 8. (This can be done only for a certain class of feedback amplifiers.)

$$G(s) = k \frac{T(s)}{1+T(s)} \tag{8}$$

where $T(s)$ is the return ratio for zero reference for one of the active elements in the amplifier and $k$ is independent of $s$. The poles of $G(s)$ are located at those values of $s$ which result in the equality $T(s) = -1$. In order to cause the root locus to pass through point $P$, it is necessary that at point $P$

$$|T(s)| = 1 \tag{9}$$

$$\text{Angle } T(s) = \pm(2n-1)\pi, \quad n = 0, 1, 2, \ldots \tag{10}$$

In summary, the stabilization procedure based on direct control of transient response consists of choosing $\psi_1$ on the basis of overshoot at the first maximums or on the basis of the rate of attenuation of the transient, plus the subsequent imposition of the conditions 9 and 10 at a point on the radial line through the origin inclined $\psi_1$ degrees to the horizontal, Fig. 3(B). As will be evident, additional constraints can be also introduced into the design process, if desired.

The actual technique employed to effect the variation in dominant pole position depends on the specific amplifier design problem. Two practical techniques that can be employed for the purpose are the addition of corrective interstage networks and the use of local feedback around the active elements. Both methods are illustrated in the examples furnished.

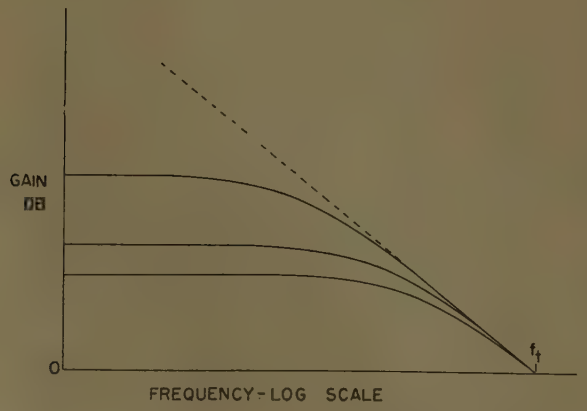


**Fig. 4. Gain characteristic of single-stage grounded cathode amplifier showing approach to asymptotic characteristic (dashed line-slope: −6 db per octave). Figure of merit frequency $f_t = g_m/2\pi C$. Increased load resistance yields higher low-frequency gain, less bandwidth, but the same asymptotic behavior at high frequencies**

## Implementation

The statement of the stabilization problem in the form previously mentioned is closely related to the problem of designing a servomechanism for a prescribed transient response, a problem for which an important body of design information exists. The contributions of Aaron, Aseltine, Chu, Russell and Weaver, and Zaborsky[7–11] are representative of the progress that has been made in this area. And yet, the feedback amplifier stabilization problem differs from the former in one crucial respect which was previously mentioned. When vacuum tubes and transistors are used as elements of feedback amplifiers, their limiting behavior at high frequencies or "asymptotic characteristics" are of paramount importance in the design process. When they are used as elements in a servomechanism system, however, the limitations of the mechanical elements virtually obscure their limitations. As a result, the addition of amplifier stages with suitable interstage networks to a servomechanism system provides the circuit designer with a considerable amount of flexibility in the realization of suitable pole-zero configurations to control transient response. In the low-frequency spectrum associated with servomechanism operation, the limit of amplification that may be added occurs primarily as a result of the undesirable effects of overloading amplifier stages or the excessive amplification of noise. In the extended frequency range in which feedback amplifiers find their usual application, however, the constraints on the pole-zero locations imposed by the properties of a tube or transistor itself are usually important design factors. In general, in terms of the active devices now available, the addition of one or more stages of amplification to an existing feedback amplifier whose return ratio characteristics are satisfactory except for the problem of stabilization and transient response can do more to complicate the design problem than to simplify it because of the additional constraints that are imposed.

If one measures the frequency response of a grounded cathode vacuum tube


**Fig. 5. Simple resistance-capacitance interstage for illustrative example**

amplifier for various values of load resistance, curves similar to those shown in Fig. 4 will result. As frequency is increased, the curves for all values of load resistance become asymptotic to the dashed line which has a slope of −6 db (decibels) per octave and crosses the zero gain level at the frequency $g_m/2\pi C$. The location of the dashed line, called the "asymptotic characteristic," is clearly dependent upon the properties of the tube and the minimum shunt capacitance associated with it. Comparable behavior is experienced in transistor amplifiers. Asymptotic characteristics are of fundamental importance in the stabilization procedures based on frequency response.[1] A convenient classification based on these characteristics may be made of the various techniques used to shift the root locus so that it passes through $P$ in Fig. 3(B) rather than through $P'$ in Fig. 3(A) for the same mid-band return ratio. The techniques may be grouped into two classes; viz. those that do not affect the asymptotic characteristic and those that degrade it. Those in the first class permit optimization of design with respect to selected parameters whereas the techniques in the second class usually permit simplifications in design or adjustment at the expense of not being able to attain the ultimate in performance. Simple examples of both methods are given in the next section.

## Illustrative Examples

In this section, three examples are considered which illustrate the use of the approach to stabilization based on time response which has been discussed. The examples have been chosen primarily for their value in illustrating the stabilization design philosophy under consideration although all are useful in practical applications.

### Shunt Capacitor-Shifted Asymptote

Consider that a 3-stage feedback amplifier having a gain given by equation 8 has been designed with interstage networks having the form shown in Fig. 5, and a return ratio function expressed by

$$T(s)=\frac{T(0)}{\left(1+\frac{s}{\rho_0}\right)^3} \tag{11}$$

with $T(0)=40$. The pole pattern for the function $T(s)$ is shown in Fig. 6(A). It is found that for $T(0)>8$, the function $1+T(s)$ has two complex roots in the right half plane, so the feedback amplifier is unstable. Assume that it is desired to stabilize the amplifier so that $\eta\leq 0.2$, that is, the deviation from unity at one local extreme value of the transient response is to be (at least ) five times the deviation at the next maximum deviation. Furthermore, it is assumed that the stabilization is to be effected by the addition of a capacitor of value $C_1$ in parallel with only one of the interstage networks shown in Fig. 5.

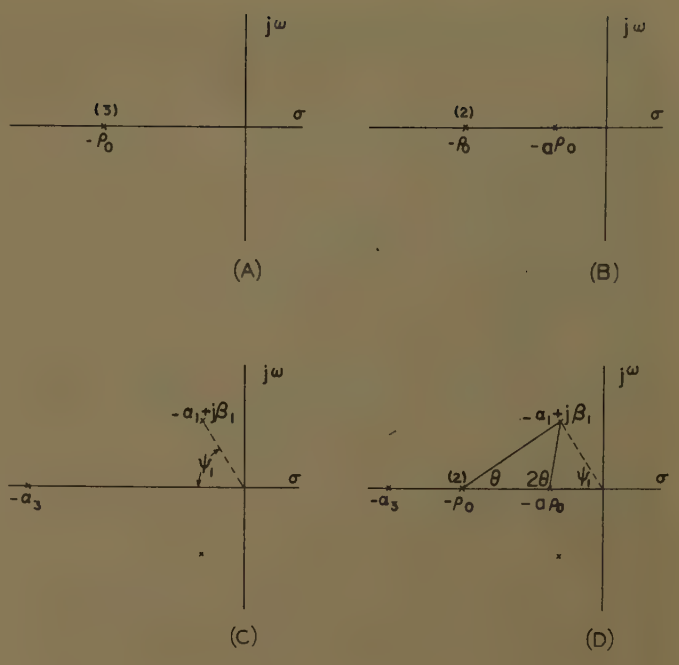


**Fig. 6. Pole patterns for illustrative example**

A—Original pole pattern of T(s)
B—Modified pole pattern caused by addition of capacitor to one stage
C—Desired roots of $1+T(s)=0$
D—Illustration of variables used in formulating design conditions

The stabilization method selected has the property of shifting the asymptote of the stage to which the capacitance is added to the left in Fig. 4. The new intersection of the asymptote for the single stage with the zero-db gain level will be at a frequency $f_1=g_m/2\pi(C+C_1)$; the composite asymptote for the whole amplifier will also be shifted to the left resulting in degradation of performance as compared to that attainable from the original structure.

The addition of capacitor $C_1$ as described produces the pole pattern for the modified return ratio function $T'(s)$ shown in Fig. 6(B) where

$$a\rho_0=\frac{1}{R(C+C_1)} \tag{12}$$

and

$$T'(s)=\frac{T(0)}{\left(1+\frac{s}{\rho_0}\right)^2\left(1+\frac{s}{a\rho_0}\right)}=\frac{a\rho_0^3T(0)}{(s+\rho_0)^2(s+a\rho_0)} \tag{13}$$

Fig. 6(C) shows the pole pattern of $G(s)$ (see equation 8), that is, the root pattern of $1+T(s)=0$ which is derived from Fig. 6(B) and meets the condition that $P$ lies on the radial line with displacement $\psi_1$ from the negative real axis. By the use of equation 5 with $\eta=0.2$, $\psi_1$ is found to be 62.9 degrees. In terms of the quantities defined in Fig. 6(D), in order to have the conditions

$$|T'(s)|=1$$

and

angle of $T'(s)=-180$ degrees

satisfied as the root locus crosses the radial line at $P$, it is necessary that

$$\sin(2\theta-\psi_1)\sin^2(\theta+\psi_1)=\frac{\sin^3\psi_1}{T(0)} \tag{14}$$

After finding $\theta$ using equation 14, the quantity $a$ is determined from the expression

$$a=\frac{1}{2T(0)\cos\theta}\,\frac{\sin^3\psi_1}{\sin^3(\theta+\psi_1)} \tag{15}$$

Knowing $R$, $C$, and $a$, the value of $C_1$ necessary to effect the desired stabilization is computed using equation 12.

It is of interest to record that

$$\alpha_1=\rho_0\frac{\sin\theta\cos\psi_1}{\sin(\theta+\psi_1)} \tag{16}$$

$$\beta_1=\rho_0\frac{\sin\theta\sin\psi_1}{\sin(\theta+\psi_1)} \tag{17}$$

and

$$\alpha_3=2\rho_0\left[1+\frac{a}{2}-\frac{\sin\theta\cos\psi_1}{\sin(\theta+\psi_1)}\right] \tag{18}$$

For $\psi_1=62.9$ degrees, and $T(0)=40$, it is found that $a=0.0105$, $\alpha_1=0.242\ \rho_0$, $\beta_1=0.473\ \rho_0$, and $\alpha_3=1.526\ \rho_0$. Fig. 6(C) is drawn to scale to show the correct relations among $\alpha_1$, $\beta_1$, and $\alpha_3$.

### Shunt Resistance Capacitance Network—Original Asymptote

The stabilization of the amplifier characterized by equation 11 will now be

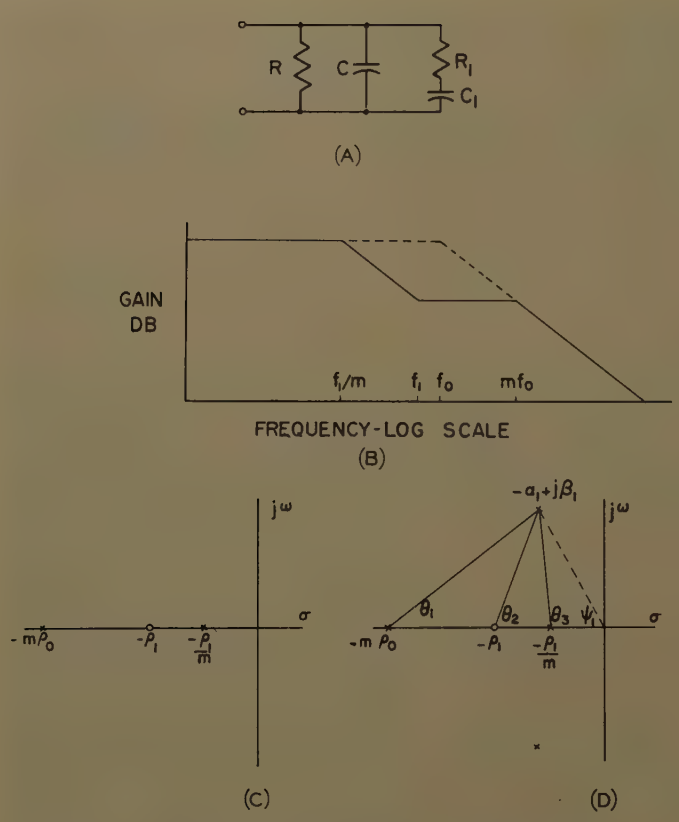


**Fig. 7. Stabilization by modification of interstage network**

A—Interstage network showing added stabilization elements $R_1$, $C_1$
B—Representative gain characteristic of single-stage amplifier using network in (A). The slope of the inclined portions of the characteristic is −6 db per octave; $f_1=\rho_1/2\pi$; see text
C—Pole pattern of T(s) using networks of (A) in three stages. Each pole and zero shown is of third order
D—Illustration of variables used in formulating design conditions

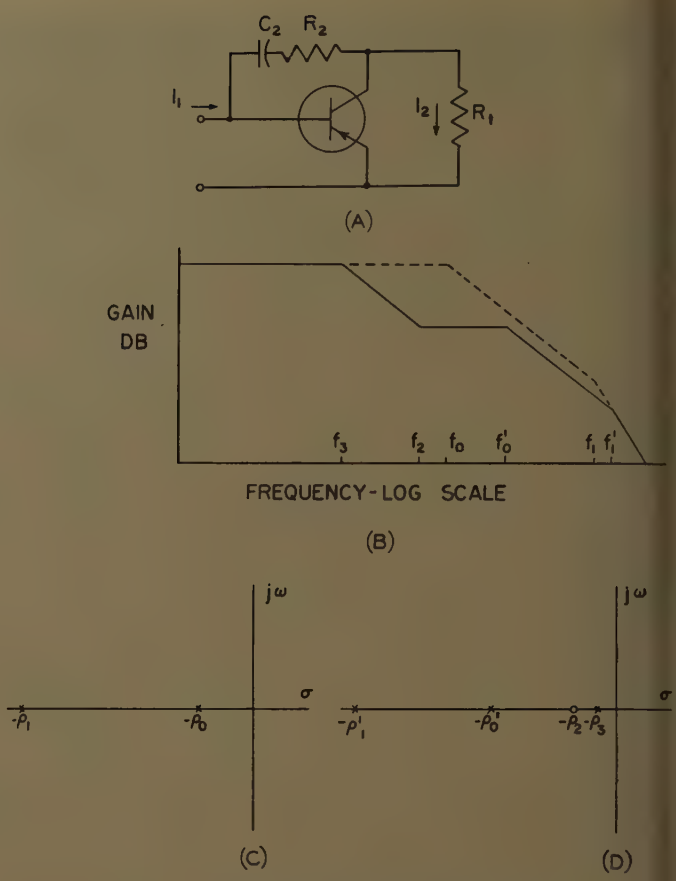


**Fig. 8. Stabilization by use of local feedback**

A—Common emitter transistor amplifier with local feedback
B—Representative current gain ($I_2/I_1$) characteristic of stage in (A). The slope of the inclined portions of the characteristic below $f_1$ is −6 db per octave; above $f_1'$ the slope is −12 db per octave; $f_1=\rho_1/2\pi$; see text
C—Pole pattern of amplifier stage without feedback
D—Pole pattern of amplifier stage with feedback; see text for values of pole and zero locations in terms of circuit elements

undertaken with the same attenuation requirement of $\eta=0.2$ but with the added stipulation that the corrective method employed must not shift the original asymptote of the amplifier.

The addition of a series combination $R_1$-$C_1$ in parallel with the interstage of Fig. 5 yields the network of Fig. 7(A). The straight line approximation to the resulting gain characteristic of a vacuum-tube amplifier using the interstage is indicated in Fig. 7(B) by the solid line; the dashed portion illustrates the variation without $R_1$-$C_1$. The slope of the characteristic is −6 db per octave. Note that the original asymptote is followed above the frequency $mf_0$. The form of constraints frequently encountered in the stabilization of amplifiers is also indicated in Fig. 7(B). Note that whereas $f_1$ may be selected arbitrarily, the other two critical frequencies are determined as soon as the value of $m$ is chosen. This behavior must, of course, be considered in the design process and represents one additional complication not present in the corresponding servomechanism transient response design problem.

The stabilization will be effected by the addition of one $R_1$-$C_1$ network to each of the three interstages represented by the characteristic of equation 11. The modified pole-zero pattern for $T(s)$ is shown in Fig. 7(C); all poles and zeros shown are third order. For convenience in the example, $m$ and $\rho_1$ have been taken the same for all networks. Once $\rho_1$ and $m$ have been determined as will be discussed, $R_1$ and $C_1$ are given by

$$R_1=\frac{R}{m-1}\,\frac{1}{1-\dfrac{\rho_1}{m\rho_0}} \tag{19}$$

$$C_1=\frac{1}{R_1\rho_1} \tag{20}$$

The return ratio with the corrective networks added is

$$T'(s)=\frac{T(0)}{\left(1+\dfrac{s}{m\rho_0}\right)^3}\,\frac{\left(1+\dfrac{s}{\rho_1}\right)^3}{\left(1+\dfrac{ms}{\rho_1}\right)^3}$$

or

$$T'(s)=\frac{\rho_0^3T(0)}{(s+m\rho_0)^3}\,\frac{(s+\rho_1)^3}{(s+\rho_1/m)^3} \tag{21}$$

The stabilization problem consists in determining what values to assign to $\rho_1$ and $m$ so that the root locus passes through the point P at $-\alpha_1+j\beta_1$ located on the dashed line making the angle $\psi_1$ with the negative real axis when the return ratio has the value $T(0)$. In the preceding example, specification of $\psi_1$ determined the quantity $a$ uniquely. Here it will be seen that unless another design condition is imposed, there is not just a single pair of values of $\rho_1$ and $m$ that satisfy the condition imposed on point P but rather a family of pairs. The choice of a particular combination of $\rho_1$ and $m$ will depend on what other features of the transient response are of interest to the designer.

In order to satisfy the condition $|T'(s)|=1$ at $-\alpha_1+j\beta_1$ in Fig. 7(D), it is nec-

sary that $\theta_1$, $\theta_2$, and $\theta_3$ satisfy the relation

$$\frac{\sin(\psi_1+\theta_1)\sin(\psi_1+\theta_2)}{\sin(\psi_1+\theta_3)} = \frac{\sin\psi_1}{\sqrt[3]{T(0)}} \tag{22}$$

or the angle of $T(s)$ to be an odd multiple of 180 degrees, the three angles ust be related as

$$-\theta_2+\theta_3 = \pm(2n+1)60 \tag{23}$$

s stated, another condition may be nposed on the variables $\theta_1$, $\theta_2$, and $\theta_3$. ssuming the additional condition to be dependent of equations 22 and 23, its ecification will permit a solution for the ree quantities. With $\theta_1$, $\theta_2$, and $\theta_3$ nown, the quantities $m$ and $\rho_1$ from hich the necessary values of $R_1$ and $C_1$ re computed (see equations 19 and 20) ay be calculated from the relations

$$= \sqrt[3]{T(0)}\,\frac{\sin(\theta_1+\psi_1)}{\sin\psi_1}\,\frac{\sin\theta_3}{\sin\theta_2} \tag{24}$$

$$= m\rho_0\,\frac{\sin\theta_1}{\sin(\psi_1+\theta_1)}\,\frac{\sin(\psi_1+\theta_2)}{\sin\theta_2} \tag{25}$$

he co-ordinates of the dominant pole re also of interest. They may be comuted from the equations

$$_1 = m\rho_0\,\frac{\sin\theta_1\cos\psi_1}{\sin(\psi_1+\theta_1)} \tag{26}$$

$$_1 = \rho_0\sqrt[3]{T(0)}\,\frac{\sin\theta_1\sin\theta_2}{\sin\theta_2} \tag{27}$$

If no specific condition is added to quations 22 and 23, one may choose $\theta_1$ sing as a guide, for example, some eneral characteristics of the transient esponse. Recall that the time at which he first maximum occurs is inversely roportional to $\beta_1$ if $\lambda_1$ remains fixed. One might want to select a value of $\theta_1$ ased on making $\beta_1$ as large as possible. f $\theta_1$ is chosen, then $\theta_3$ may be determined t once from the relation

$$\text{an}\,\theta_3 = -\frac{\sin\psi_1 - A\sin(\psi_1+\theta_1-60°)}{\cos\psi_1 - A\cos(\psi_1+\theta_1-60°)} \tag{28}$$

here

$$= \frac{\sin\psi_1}{\sqrt[3]{T(0)}\sin(\psi_1+\theta_1)} \tag{29}$$

Equation 23 may be used to determine $\theta_2$ ith $\theta_1$ and $\theta_3$ known.

By consideration of equation 27 plus he condition 23, in view of the requirement that $\theta_3 > \theta_2 > \theta_1$, which follows from ig. 7(D), it is found that $\theta_1$ cannot xceed 60 degrees and that $\beta_1$ attains its aximum value for a given $T(0)$ as $\theta_1$ pproaches this figure. To provide an idication of the relative values involved n this stabilization method, $\theta_1$ was selected s 55 degrees. $\theta_3$ and $\theta_2$ were found to be 115.0 degrees and 110.0 degrees, respectively, which then gave values of $m = 3.28$, $\rho_1 = 0.397\rho_0$, $\alpha_1 = 1.384\ \rho_0$, and $\beta_1 = 2.70\rho_0$. The values of $R_1$ and $C_1$ necessary to produce this performance can be found using equations 19 and 20 when $R$ and $\rho_0$ are known.

### Local Feedback—Original Asymptote

The common emitter transistor amplifier circuit shown in Fig. 8(A) which has been discussed by Abraham[12] and Blecher[13,14] provides an example of the way in which local feedback can be used to achieve pole-zero patterns suitable for stabilization. The straight line approximation to the current gain $I_2/I_1$ is shown in Fig. 8(B). If $R_2$ is much greater than the base resistance $r_b'$ of the transistor, then the operation with feedback is along the original asymptote beyond the frequency $f_1'$. Without feedback, the amplifier has the pole pattern shown in Fig. 8(C); with the elements $R_2$-$C_2$ added, the pattern of Fig. 8(D) results. Here again a constraint on pole-zero locations is noted. By choice of the product $R_2C_2$, the real zero ($\rho_2 = 1/R_2C_2$) can be located arbitrarily. The addition of the network $R_2C_2$ adds a pole at $-\rho_3$ and shifts the locations of the poles at $-\rho_0$ and $-\rho_1$ to $-\rho_0'$ and $-\rho_1'$. The values of $\rho_0'$, $\rho_1'$, and $\rho_3$ depend upon the choice of $R_2$ and $C_2$. Blecher[14] has given the following approximate values for $\rho_0$ and $\rho_1$, (see reference 12 for details of the approximations):

$$\rho_0 = \frac{1-a_0+\delta}{\dfrac{1+a_0m+\delta}{\omega_a}+\dfrac{1}{\omega_c}} \tag{30}$$

$$\rho_1 = \omega_a+\omega_c(1+a_0m+\delta) \tag{31}$$

If $\rho_2$ is selected to be much less than $\rho_0'$ (as given next) then the approximate locations of the poles with local feedback are given by

$$\rho_0' = \frac{1-a_0+\gamma}{\dfrac{1+a_0m+\gamma}{\omega_a}+\dfrac{1}{\omega_c}} \tag{32}$$

$$\rho_1' = \omega_a+\omega_c(1+a_0m+\gamma) \tag{33}$$

$$\rho_3 = \frac{1-a_0+\delta}{1-a_0+\gamma}\,\frac{1}{C_2R_2} \tag{34}$$

In all of these equations

$$\delta = \frac{R_1+r_e}{r_c};\quad \gamma = \frac{R_1+r_e}{R_2+r_b'};\quad \omega_c = \frac{1}{(R_1+r_e)C_c} \tag{35}$$

and $C_c$, $r_b'$, $r_e$, $r_c$, and $a_0$ are the usual transistor parameters. $m$ is the phase shift in radians by which the phase of $a$ exceeds the phase shift of an ordinary R-C network at the frequency $\omega_a$ where the amplitude of $a$ is 0.707 $a_0$. A measurement technique for the determination of $m$ has been discussed by Thomas and Moll.[15]

From the similarity of the straight line approximations of Fig. 7(B) and Fig. 8(B) and the corresponding pole-zero patterns, it is clear that one may proceed to stabilize a transistor feedback amplifier using a transient response criterion in essentially the same fashion as in the previous example. (Pederson and Ghausi[16] have used the root locus method to design a transistor feedback amplifier having a prescribed closed-loop amplitude-frequency response characteristic.) There are two complications which may arise, however. It is seen from equations 32, 33, and 35 that $\rho_0'$ and $\rho_1'$ depend on $R_2$ through the factor $\gamma$ and therefore, the locations of $\rho_0'$ and $\rho_1'$ relative to $\rho_0$ and $\rho_1$ are not as simply expressed as in the previous example. In addition, if the effect of the excess phase shift which is represented approximetly by a factor $\epsilon^{-sm/\omega_a}$ in the transfer functon is large enough, the root locus should be modified as considered by Chu.[17] It should be noted that both of these possible complications arise because of the nature of the device and the particular circuit employed; the factors arise similarly in a

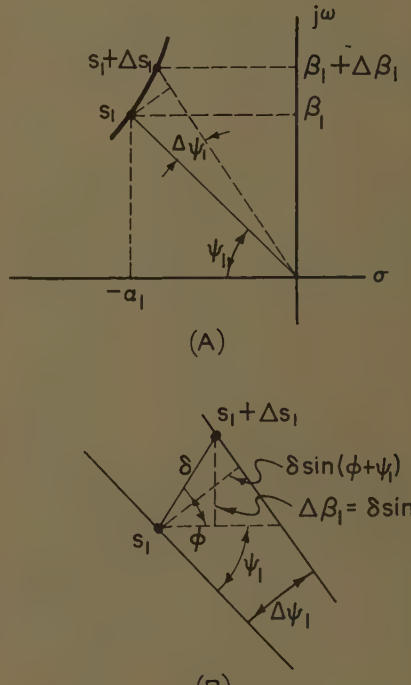


**Fig. 9. Effect of parameter variations**

A—Dominant pole at $s_1 = -\alpha_1 + j\beta_1$ and shift in pole location ($\Delta s_1$) as a result of parameter change

B—An expanded portion of (A) illustrating the geometrical relations associated with the change in dominant pole location

stabilization design procedure based on frequency response as well as in one based on transient response.

### Effect of Parameter Variations

Changes in the active as well as passive elements comprising a feedback amplifier can cause a shift in the location of the open loop, and hence closed loop, pole, and zero locations. It is of interest to consider briefly what effect these variations have on the transient response of the amplifier. Fig. 9(A) shows the variation of one dominant pole position from $s_1$ to $s_1+\Delta s_1$. Such a change might be caused by a change in magnitude of mid-band return ratio, for example, in which event the broad segment shown would be part of a root locus. In general, a change in dominant pole location causes both $\psi_1$ and $\beta_1$ to change. From Fig. 9(B) which is an expanded portion of Fig. 9(A), it is seen that if the change in dominant pole location is expressed as

$$\Delta s_1=\delta e^{j\varphi} \tag{36}$$

then

$$\Delta\beta_1=\delta \sin \varphi \tag{37}$$

and

$$\Delta\psi_1 \doteq \tan^{-1}\frac{\delta}{\beta_{01}} \sin(\varphi+\psi_1) \tag{38}$$

where $\beta_{01}$ is the magnitude of $s_1$. For small values of $\delta/\beta_{01}$, equation 38 can be written to a good approximation as

$$\Delta\psi_1 \doteq \frac{\delta}{\beta_{01}} \sin(\varphi+\psi_1) \tag{39}$$

The effect that the changes have on the stabilization design parameter $\eta$ and the time at which the first maximum occurs in the time response can be found by the use of equations 5 and 6. From the latter it is found that

$$\frac{\Delta t_{max}}{t_{max}}=-\frac{1}{1+\frac{\beta_1}{\Delta\beta_1}} \doteq -\frac{\Delta\beta_1}{\beta_1} \tag{40}$$

where changes in $\lambda_1$ have been assumed small enough to be neglected. By the use of equation 37 this becomes

$$\frac{\Delta t_{max}}{t_{max}} \doteq -\frac{\delta \sin\varphi}{\beta_1} \doteq -\frac{\delta}{\beta_{01}} \sin\varphi \csc\psi_1 \tag{41}$$

Considering equation 5, it is seen that

$$\eta+\Delta\eta=\epsilon^{-\pi \cot(\psi_1+\Delta\psi_1)} \tag{42}$$

Since cot $(\psi_1+\Delta\psi_1)$ can be expressed in the Taylor's series.

$$\cot(\psi_1+\Delta\psi_1)=\cot\psi_1-\Delta\psi_1\csc^2\psi_1+(\Delta\psi_1)^2\csc^2\psi_1\cot\psi_1+\dots \tag{43}$$

the fractional change in $\eta$ can be written approximately as

$$\frac{\Delta\eta}{\eta}=\epsilon^{\pi\Delta\psi_1\csc^2\psi_1}-1 \tag{44}$$

where only the linear term in $\Delta\psi_1$ in the series has been used. Use of equation 39 allows the change in $\eta$ to be written as a function of the change in $s_1$, viz.

$$\frac{\Delta\eta}{\eta}=-1+\epsilon^{\pi\delta/\beta_{01}\csc^2\psi_1\sin(\varphi+\psi_1)} \tag{45}$$

The changes in $t_{max}$ and $\eta$ may be related to parameter changes by application of results reported in three recent papers. Huang[18] has studied the change in closed-loop pole locations as a result of variations in open loop pole and zero locations or gain constant. Truxal and Horowitz[19] considered the sensitivity of a pole of a return difference to any parameter in the network under consideration, and their work was extended by Kuo[20] to the sensitivity of a root of a polynomial with respect to any network parameter.

Consider an amplifier characterized by equation 8. To study the effect of the variation in the magnitude of the mid-band return ratio $T(0)$ on $\Delta s_1$ and hence $\eta$ and $t_{max}$, use may be made of equation 10 of Huang's paper. In terms of the notation here, it is found that

$$\Delta s_1=-\frac{\Delta T(0)}{T(0)}\,k_{-1} \tag{46}$$

where $k_{-1}$ is the residue of the closed loop gain function at the pole $s_1$. Expression of this result in the form of equation 36 allows evaluation of equations 41 and 44 by substitution of $\delta$ and $\varphi$. Similar calculations may be made to study the effect on the transient response of other parameter variations but the detailed computation is beyond the scope of this paper.

### Conclusions

By the combination of root-locus methods and the concept of the dominance of the step-function response, it is possible to formulate a stabilization design criterion for feedback amplifiers based on direct control of the transient response. The design criterion suggested, the damping or rate of attenuation of the dominant time term in the step-function response, is a simple function of the pole angle of the dominant pair of complex poles and is also related to the maximum transient overshoot. Illustrative examples indicate how one may proceed directly from the statement of desired performance in terms of the criterion to element values in the stabilization networks.

The problem of optimizing the design of a feedback amplifier for a prescribed transient response differs from the corresponding servomechanism problem because of the constraints imposed by the characteristics of the active devices employed and their associated coupling networks. Further investigation in which design methods already known for achieving pre-scribed transient response with servo-mechanisms are coupled with the results of studies of constraints imposed on amplifier interstage pole-zero configurations by the addition of stabilization networks should be profitable in increasing the applicability of the procedure suggested. A stabilization philosophy for feedback amplifiers based directly on control of transient responses can, as it is developed further, provide the circuit designer with far greater insight into the effect of design parameters than criteria based solely on gain and phase margins.

## Appendix

### Derivation of Equations 14 and 15

In Fig. 6(D), let $\gamma$ be the angle that the directed distance from $-a\rho_0$ to $-\alpha_1+j\beta_1$ makes with the positive real axis. In order to satisfy the condition that the angle of $T'(s)$, equation 13, is equal to $-180$ degrees, it is necessary that

$$2\theta+\gamma=180 \text{ degrees}$$

or $\gamma=180-2\theta$

Thus, the supplement of $\gamma$ has the value $2\theta$ which is shown in Fig. 6(D).

Because of the condition $|T'(s)|=1$ at $s=-\alpha_1+j\beta_1$, equation 13 may be reduced to the form

$$1=\frac{T(0)}{\left[\frac{|s+\rho_0|}{\rho_0}\right]^2\frac{|s+a\rho_0|}{a\rho_0}}$$

The factors $|s+\rho_0|$ and $|s+a\rho_0|$ are recognized as the magnitudes of the directed distances from $-\rho_0$ to $-\alpha_1+j\beta_1$ and from $-a\rho_0$ to $-\alpha_1+j\beta_1$, respectively. By application of the law of sines to the triangles in the figure, it is found that

$$\frac{|s+\rho_0|}{\rho_0}=\frac{\sin\psi_1}{\sin[180-(\theta+\psi_1)]}=\frac{\sin\psi_1}{\sin(\theta+\psi_1)}$$

$$\frac{|s+a\rho_0|}{a\rho_0}=\frac{\sin\psi_1}{\sin[180-(\gamma+\psi_1)]}=\frac{\sin\psi_1}{\sin(2\theta-\psi_1)}$$

Substitution of these results in the previous expression containing $T(0)$ yields

$$\frac{\sin^2\psi_1}{\sin^2(\theta+\psi_1)}\,\frac{\sin\psi_1}{\sin(2\theta-\psi_1)}=T(0)$$

from which equation 14 follows directly.

To obtain equation 15 for $a$, the condition above derived from equation 13 may first be written as

$$a=\frac{1}{T(0)}\left[\frac{|s+\rho_0|}{\rho_0}\right]^2\frac{|s+a\rho_0|}{\rho_0}$$

$$=\frac{1}{T(0)}\,\frac{\sin^2\psi_1}{\sin^2(\theta+\psi_1)}\,\frac{|s+a\rho_0|}{\rho_0}$$

If $\rho_{01}$ denotes the magnitude of the directed distance from $-\rho_0$ to $-\alpha_1+j\beta_1$, then

$$\frac{|s+a\rho_0|}{\rho_0}=\frac{|s+a\rho_0|}{\rho_{01}}\,\frac{\rho_{01}}{\rho_0}$$

Application of the law of sines yields the equality

$$\frac{|s+a\rho_0|}{\rho_0}=\frac{\sin\theta}{\sin 2\theta}\,\frac{\sin\psi_1}{\sin(\theta+\psi_1)}$$

$$=\frac{\sin\psi_1}{2\cos\theta\sin(\theta+\psi_1)}$$

Substitution of the expression for this ratio in terms of $\theta$ and $\psi_1$ in the equation for $a$ results in equation 15, viz.

$$a=\frac{1}{2T(0)\cos\theta}\,\frac{\sin^3\psi_1}{\sin^3(\theta+\psi_1)}$$

## Derivation of Equations 22 and 24 through 28

The magnitude condition $|T'(s)|=1$ applied to equation 21 results in the following equality:

$$|s+m\rho_0|^3\,|s+\rho_1/m|^3=\rho_0{}^3T(0)\,|s+\rho_1|^3$$

An equivalent form is

$$\frac{|s+m\rho_0|}{m\rho_0}\,\frac{|s+\rho_1/m|}{\rho_1/m}=\sqrt[3]{T(0)}\,\frac{|s+\rho_1|}{\rho_1}$$

The use of the law of sines in the appropriate triangles of Fig. 7(D) allows the ratios of magnitudes to be expressed in terms of the angles $\theta_1$, $\theta_2$, $\theta_3$, and $\psi_1$ as follows:

$$\frac{|s+m\rho_0|}{m\rho_0}=\frac{\sin\psi_1}{\sin[180-(\psi_1+\theta_1)]}=\frac{\sin\psi_1}{\sin(\psi_1+\theta_1)}$$

$$\frac{|s+\rho/m|}{\rho_1/m}=\frac{\sin\psi_1}{\sin(\psi_1+\theta_3)};$$

$$\frac{|s+\rho_1|}{\rho_1}=\frac{\sin\psi_1}{\sin(\psi_1+\theta_2)}$$

Substitution of these results in the equality above changes its form to

$$\frac{\sin\psi_1}{\sin(\psi_1+\theta_1)}\,\frac{\sin\psi_1}{\sin(\psi_1+\theta_3)}=\sqrt[3]{T(0)}\,\frac{\sin\psi_1}{\sin(\psi_1+\theta_2)}$$

which may be converted directly to equation 22.

By examination of Fig. 7(D), it is seen that the law of sines may be used to express the ratio $|s+\rho_1|/|s+\rho_1/m|$ in terms of $\theta_2$ and $\theta_3$. The equality is

$$\frac{|s+\rho_1|}{|s+\rho_1/m|}=\frac{\sin\theta_3}{\sin\theta_2}$$

One may then start with the equality derived above from the condition $|T'(s)|=1$ in the form

$$\frac{|s+m\rho_0|}{m\rho_0}=\sqrt[3]{T(0)}\,\frac{|s+\rho_1|}{|s+\rho_1/m|}$$

and substitute values for the ratios in terms of the various angles in the figure to obtain

$$m\,\frac{\sin\psi_1}{\sin(\psi_1+\theta_1)}=\sqrt[3]{T(0)}\,\frac{\sin\theta_3}{\sin\theta_2}$$

This gives equation 24 for $m$, namely

$$m=\sqrt[3]{T(0)}\,\frac{\sin(\theta_1+\psi_1)}{\sin\psi_1}\,\frac{\sin\theta_3}{\sin\theta_2}$$

Suppose $\beta_{01}$ designates the distance from the origin to $-\alpha_1+j\beta_1$. Then proceeding as previously,

$$\frac{\beta_{01}}{\rho_1}=\frac{\sin\theta_2}{\sin[180-(\psi_1+\theta_2)]}=\frac{\sin\theta_2}{\sin(\psi_1+\theta_2)}$$

$$\frac{\beta_{01}}{m\rho_0}=\frac{\sin\theta_1}{\sin(\psi_1+\theta_1)}$$

whence

$$\rho_1=m\rho_0\,\frac{\sin\theta_1}{\sin(\psi_1+\theta_1)}\,\frac{\sin(\psi_1+\theta_2)}{\sin\theta_2}$$

which is equation 25.

The quantities $\alpha_1$ and $\beta_1$ can be expressed simply in terms of $\beta_{01}$ and $\psi_1$ as

$$\alpha_1=\beta_{01}\cos\psi_1$$

$$\beta_1=\beta_{01}\sin\psi_1$$

Substitution of the value for $\beta_{01}$ in terms of $m\rho_0$ gives the forms

$$\alpha_1=m\rho_0\,\frac{\sin\theta_1\cos\psi_1}{\sin(\psi_1+\theta_1)}$$

$$\beta_1=m\rho_0\,\frac{\sin\theta_1\sin\psi_1}{\sin(\psi_1+\theta_1)}=\rho_0\sqrt[3]{T(0)}\,\frac{\sin\theta_1\sin\theta_3}{\sin\theta_2}$$

These are equations 26 and 27; equation 24 for $m$ has been used in passing to the second form of the expression for $\beta_1$.

Equation 28 is derived by starting with equations 22 and 23, with $n$ taken equal to zero and the plus sign chosen in the latter, that is,

$$\theta_2=\theta_1+\theta_3-60$$

Equation 22 can now be written as

$$\frac{\sin(\psi_1+\theta_3)}{\sin(\psi_1+\theta_1+\theta_3-60)}=\frac{\sin\psi_1}{\sqrt[3]{T(0)}\sin(\psi_1+\theta_1)}=A$$

Clearly $A$ is a known quantity since $\psi$ and $T(0)$ are assigned, and it is assumed that a value has been chosen for $\theta_1$. The terms $\sin(\psi_1+\theta_3)$ and $\sin(\psi_1+\theta_1+\theta_3-60)$ may be expanded to

$$\sin(\psi_1+\theta_3)=\sin\psi_1\cos\theta_3+\cos\psi_1\sin\theta_3$$

and

$$\sin(\psi_1+\theta_1+\theta_3-60)=\sin(\psi_1+\theta_1-60)\cos\theta_3+\cos(\psi_1+\theta_1-60)\sin\theta_3$$

The previous equation,

$$\sin(\psi_1+\theta_3)=A\sin(\psi_1+\theta_1+\theta_3-60)$$

written in terms of the expansions just provided becomes

$$[\cos\psi_1-A\cos(\psi_1+\theta_1-60)]\sin\theta_3=-[\sin\psi_1-A\sin(\psi_1+\theta_1-60)]\cos\theta_3$$

This may be rewritten in the form of equation 28.

## References


1. Network Analysis and Feedback Amplifier Design ((book), H. W. Bode. D. Van Nostrand Company, Princeton, N. J., 1945.

2. Some Considerations in the Design of Negative-Feedback Amplifiers, W. T. Duerdoth. *Proceedings*, Institution of Electrical Engineers, London, England, pt. III, vol. 97, 1950, pp. 138–58.

3. A Simple Connection Between Closed-Loop Transient Response and Open-Loop Frequency Response, J. C. West, J. Potts. *Ibid.*, pt. II, vol. 100, 1953, pp. 201–12.

4. Servomechanism Transient Performance from Decibel-Log Frequency Plots, H. Harris, Jr., M. J. Kerby, E. F. VonArx. *AIEE Transactions*, vol. 70, pt. II, 1951, pp. 1452–59.

5. Control System Dynamics (book), W. R. Evans. McGraw-Hill Book Company, Inc., New York, N. Y., 1954.

6. The Effect of Pole and Zero Locations on the Transient Response of Linear Dynamic Systems, J. H. Mulligan, Jr. *Proceedings*, Institute of Radio Engineers, New York, N. Y., vol. 37, 1949, pp. 516–29.

7. Synthesis of Feedback Control Systems by Means of Pole and Zero Location of the Closed Loop Function, M. R. Aaron. *AIEE Transactions*, vol. 70, pt. II, 1951, pp. 1439–46.

8. Feedback System Synthesis by the Inverse Root-Locus Method, J. A. Aseltine. *Convention Record*, Institute of Radio Engineers, vol. 4, pt. 2, 1956, pp. 13–17.

9. Synthesis of Feedback Control System by Phase-Angle Loci, Y. Chu. *AIEE Transactions*, pt. II (*Applications and Industry*), vol. 71, Nov. 1952, pp. 330–39.

10. Synthesis of Closed Loop Systems Using Curvilinear Squares to Predict Root Location, D. W. Russell, C. H. Weaver. *Ibid.*, Jan., pp. 95–104.

11. Integrated s-Plane Synthesis Using 2-Way Root Locus, John Zaborszky. *Ibid.*, pt. I (*Communication and Electronics*), vol. 75, 1956 (Jan. 1957 section), pp. 797–801.

12. A Wide-Band Transistor Feedback Amplifier, R. P. Abraham. *Wescon Convention Record*, Institute of Radio Engineers, 1957, pt. 2, pp. 10–19.

13. Transistor Circuits for Analog and Digital Systems, F. H. Blecher. *Bell System Technical Journal*, New York, N. Y., vol. 35, 1956, pp. 295–332.

14. Design Principles for Single Loop Transistor Feedback Amplifiers, F. H. Blecher. *Transactions*, Professional Group on Circuit Theory, Institute of Radio Engineers, vol. CT-4, 1957, pp. 145–56.

15. Junction Transistor Short-Circuit Current Gain and Phase Determination, D. E. Thomas, J. L. Moll. *Proceedings*, Institute of Radio Engineers, vol. 46, 1958, pp. 1177–84.

16. The Root Locus Design of Transistor Feedback Amplifiers, D. O. Pederson M. S. Ghausi. *Wescon Convention Record*, Institute of Radio Engineers, 1958, pt. 2, pp. 87–93.

17. Feedback Control Systems With Dead-Time Lag or Distributed Lag by Root-Locus Method, Yaohan Chu. *AIEE Transactions*, pt. II (*Applications and Industry*), vol. 71, Nov. 1952, pp. 291–96.

18. The Sensitivity of the Poles of Linear, Closed-Loop Systems, R. Y. Huang. *Ibid.*, vol. 77, Sept. 1958, pp. 182–87.

19. Sensitivity Considerations in Active Network Synthesis, J. G. Truxal, I. M. Horowitz. *Proceedings*, Second Midwest Symposium on Circuit Theory, Michigan State University, East Lansing, Mich., Dec. 1956.

20. Pole-Zero Sensitivity in Network Functions, F. F. Kuo. *Transactions*, Professional Group on Circuit Theory, Institute of Radio Engineers, vol. CT-5, 1958, pp. 372–73.

# Proposed Recommended Practices for Medium-Voltage Motor Controllers for Rubber and Plastics Industries

WILLIAM S. WATKINS
MEMBER AIEE

THE RUBBER and Plastics Subcommittee of the General Industry Applications Committee is presenting for discussion the following proposed Recommended Practices, in the hope that comments from the wide circulation so provided will be helpful in attaining maximum usefulness from the specifications. Membership of the Working Group assigned to this project consists of engineers from both large and small rubber companies, electrical manufacturers, machinery builders, and consulting engineering firms. The requirements listed are a composite of the desires of the persons who apply controls to the large rubber and plastics processing machines, influenced to an appropriate degree by the manufacturers. Discussions resulting from this presentation are necessary to assure the widest possible acceptance of the proposal.

It has been a basic consideration in the deliberations of the Working Group that new standards should depart from existing standards only where absolutely necessary, and it is hoped that these proposed Recommended Practices might possibly serve as a basis for standards acceptable to the entire processing industry, with deviations only where peculiar conditions make some industries differ greatly from others. Comments will be welcomed on this general aspect as well as on the specific suitability of the recommendations.

The following is to be proposed to the AIEE Standards Committee as a "Recommended Practice" as described in Division III, Section I of the AIEE Standards Manual. It is not intended to be an AIEE Standard, and the recommendations are not mandatory or restrictive.

## Foreword

The advantages of standardization in this field have been considered at sessions of the Rubber and Plastics Subcommittee since 1948. At the 1956 conference in Akron, Ohio, it was voted that a Working Group should be appointed to draft standards for the industries, and that this group should direct its efforts first toward the problem of the medium-voltage motor controller. Progress reports were made at the 1957 and 1958 conferences, and in 1958 the subcommittee voted unanimously to support the Recommended Practices proposed by the Working Group.

Throughout the period required for the development of the Recommended Practices it has been the policy of the Working Group to invite participation by all interested engineers, and comments have been received from many who were not actually members of the group. A liaison committee representing the General Engineering Committee of the National Electrical Manufacturers Association worked closely with the AIEE group, and is proposing the incorporation of parts of these Recommended Practices as National Electrical Manufacturers Association (NEMA) standards. The Electrical Engineering Committee of the Technical Association of the Pulp and Paper Industry (TAPPI) has followed the progress of this project, and has proposed for its industry a set of Recommended Practices almost identical to these.

It has been the intent of the Working Group to make this publication as useful as possible at the earliest possible date. It is assumed that the Rubber and Plastics Subcommittee will make certain that the very latest and best thinking is incorporated into these Recommended Practices from time to time, in order to encourage rather than hinder progress.

## Section 1. General

1.1 PURPOSE The purpose of these Recommended Practices is to define and recommend specifications for medium-voltage motor controllers for application in the rubber and plastics industries, in order to promote:

(a). Safety to personnel and equipment, including the reduction of fire and accident hazards.

(b). Maximum production with minimum unscheduled shutdowns.

(c). Reduced maintenance and increased life of equipment.

(d). Clarification of needs and conditions, to reduce special engineering and chance of error in specifications.

(e). Over-all economy.

The contents of this publication are intended to bring to the attention of engineers, management, and equipment suppliers the important features necessary to meet the specific requirements of the rubber and plastics industries.

1.2 SCOPE The provisions of these Recommended Practices apply to the construction and application of controllers for motors in the medium-voltage classification (601 to 5,000 volts.)

Although many of the specifications herein have been influenced by the conditions peculiar to the processing areas of these industries, it is probable that they may be applied to all purchases of controllers for a given company in order to promote uniformity. They are intended as minimum requirements, and may be supplemented where special needs exist.

1.3 USE OF RECOMMENDED PRACTICES It is urged that users and manufacturers co-operate and mutually agree to follow these recommended practices to insure the use of proven apparatus and methods for economical and safe machine operation.

1.4 APPLICABLE STANDARDS It is assumed that apparatus will comply with the National Electrical Code and NEMA standards insofar as they are applicable.

## Section 2. Enclosure

2.1 DESCRIPTION Enclosure shall be general-purpose NEMA 1. High-voltage compartment shall be segregated. Material which will support combustion shall be kept to a minimum.

2.2 DIMENSIONS Basic enclosure shall have a height of 90 inches exclusive of mounting sills. Preferred depth is 32 inches; maximum depth is 32 inches.

2.3 POWER AND CONTROL LEADS Space for conduit or armored cable entrance shall be provided at top and bottom.

2.4 LOCATION OF RESISTORS Resistors which require ventilation shall be mounted

---

Paper 59-1112, recommended by the AIEE General Industry Applications Committee and approved by the AIEE Technical Operations Department for presentation at the AIEE Fall General Meeting, Chicago, Ill., October 11–16, 1959. Manuscript submitted June 15, 1959; made available for printing July 15, 1959.

WILLIAM S. WATKINS is with The Ohio Rubber Company, a division of Eagle-Picher Company, Willoughby, Ohio.

in a ventilated portion of the enclosure, or externally mounted.

## Section 3. Power Busses

3.1 LOCATION Busses, if specified, shall be on top of the control enclosure at the front. All manufacturers shall locate the busses in the same position so controllers of different manufacturers can be mounted adjacent to each other and the busses can be easily connected between controllers.

3.2 ENCLOSURE Bus compartment shall be isolated from the controller interior.

3.3 SPLICES Bus-bar connections shall be silver plated.

## Section 4. Isolating Device

4.1 DESCRIPTION The isolating device shall be a 3-pole gang-operated isolating switch. With compartment door open, the blades shall be visible when open, or else disconnecting-type fuses shall be furnished. Operating handle of this switch shall be outside of compartment.

4.2 PADLOCKING Provision shall be included to accommodate three padlocks for locking the switch in the open position.

## Section 5. Interrupting Rating

5.1 INTERRUPTING RATING The interrupting rating shall be at least 150,000 kva at 2,300 volts and 250,000 kva at 4,600 volts.

5.2 DESCRIPTION Power fuses, if used, shall be of the current-limiting type.

## Section 6. Contactors

6.1 DESCRIPTION Contactors shall be of the air-break type and not mechanically latched in the closed position. They shall be either removable or readily accessible.

## Section 7. Accessibility

7.1 ACCESSIBLE FROM FRONT All functioning parts of the controller shall be readily accessible for maintenance or replacement from front of the controller.

7.2 LOW-VOLTAGE PANEL Low-voltage panel shall either be front wired, hinged, or otherwise accessible for maintenance and inspection of all wiring.

7.3 TERMINAL BOARDS All terminals for outgoing low-voltage conductors to be at least 12 inches from floor and readily accessible for connection and identification. Sufficient space shall be provided for routing of customer's control wiring, segregated from high-voltage leads, to such terminals boards. On contactors, terminal boards for coil leads and control wiring shall be readily accessible.

## Section 8. Interlock Requirements

8.1 ISOLATING SWITCH AND COMPARTMENT DOOR Isolating switch must be open before any high-voltage compartment door can be opened and cannot be closed before all such compartment doors have been closed.

8.2 ISOLATING SWITCH AND CONTACTORS It shall not be possible to open or close the isolating switch while any of the line contacts are closed, or closing.

8.3 CONTACTORS The *F*, *R*, and *DB* contactors shall be mechanically interlocked. The *DB* contactor shall be preferably interlocked in most direct manner with the *F* contactor.

8.4 PROVISION FOR TESTING Provision shall be made so that controller can be operated for testing, but only with main isolating switch open. If a "Test-Normal" switch is specified, it shall be arranged to nullify control stations remote from the controller when testing and to nullify test push buttons at the controller when in "Normal position, except that all "Stop" push buttons, whether for "Normal" or "Test" operation, shall be connected in series, so as to be effective at all times. The Test switch shall also transfer the control circuit from the normal source to a test power source to be furnished by user. Test push buttons shall be located inside the controller.

8.5 TYPES OF INTERLOCKS Mechanical-type interlocks are preferred over key-type interlocks. Some means shall be provided for gaining entry to the enclosure in case a contactor should weld closed.

## Section 9. Protective Devices and Control Circuits

9.1 PROTECTIVE DEVICES Control shall include control devices such as undervoltage relay, overload relays, field application where required, etc., which are recognized as necessary for adequate protection to personnel and equipment.

9.2 EXCITATION FAILURE A field-loss relay, power-factor relay, or other effective means shall be provided to insure the shutdown of synchronous motor in the event of excitation failure. This device shall operate on loss of d-c excitation voltage or current, and shall prevent restarting until it has been manually reset. The resetting means shall be clearly marked as to function.

9.3 NUMBER OF EXTERNAL WIRES Control circuit shall be designed so that a minimum number of wires to external devices are required.

9.4 A-C CONTROL CIRCUIT. When a-c control is required, it shall be supplied by a control transformer, 220 volts secondary, on each controller. It shall be supplied from the load side of the main disconnect through its own current-limiting fuses. A-c control shall also be provided with main disconnecting means and overcurrent protection on secondary side. Provision shall be made for grounding one side of secondary of control transformer and where ground bus is specified this connection shall be made to the ground bus.

9.5 D-C CONTROL CIRCUIT When d-c control is required it shall be supplied through a disconnecting switch and fault current protective means furnished as part of the controller. When d-c excitation is required the controller shall include means for disconnecting, short-circuit protection, and adequate field discharge protection. Adequate field discharge protection is understood to include a discharge means permanently connected across the load side of the circuit protective device, in addition to any other resistors which may be connected to the field circuit on occasion by discharge clips or normally closed contacts.

9.6 EMERGENCY STOP If emergency braking is required, emergency stop switches shall break both sides of the control circuit (American Standard safety code for rubber mills and calenders *A2.1.6*). The time required between safety switch opening and braking contactor closing shall be the minimum possible.

All "Stop" push buttons, as well as all "Emergency Stop" switches, shall cause a braked stop. Means shall be provided to ensure completion of the normal braking cycle in all cases before restarting.

9.7 CONDUCTORS All control conductors shall be stranded.

9.8 UNDERVOLTAGE PROTECTION Instantaneous undervoltage protection shall be furnished unless time-delay is specified.

9.9 FUSING OF POTENTIAL TRANSFORMERS Potential transformers, if fur-

nished, shall be fused primary and secondary. Primary fuses shall be of the current-limiting type.

### Section 10. Name Plates

10.1 DESCRIPTION Permanent and legible name plates shall be provided for all devices, with designations per NEMA Standards *1 C1-3.01*.

10.2 POWER FUSE DESIGNATION Nameplate showing catalog number of power circuit fuses used shall be mounted on inside of fuse compartment door.

### Section 11. Wiring Diagram

11.1 LOCATION OF CONTACTS IN CONTROL CIRCUIT On schematic diagram, all contacts shall be on left-hand side of coils, except overload contacts and emergency stop switches which break both sides of line.

11.2 GENERAL REQUIREMENTS Wiring diagram shall include schematic and panel diagram. Each line of schematic diagram shall be numbered on left-hand side, and location of each control circuit contact on a device designated on the right-hand side adjacent to the coil. The line numbers of normally closed contacts should be underlined.

## Discussion

**E. H. Peters** (Westinghouse Electric Corporation, Chicago, Ill.) and **W. F. Gardner** (Westinghouse Electric Corporation, Akron, Ohio): In our opinion the committee accomplished what they set out to do, that is, to provide a specification that would give a standard acceptable to both users and industry. We believe most users were able to have included in the specifications the features which they desired. The features where users did not agree usually represented the result of different company practices and were recognized as such. In those cases, each user will specify the modifications he requires. Most suppliers, we believe, feel the specification is not restrictive to prevent the use of individual design initiative.

There seem to be two items however in which compromise solutions were accepted which were not entirely satisfactory to suppliers or users. These were:

1. The present bus location allows only 6 inches of space at the back of the cabinet to bring out motor leads. This is certainly the minimum acceptable. Since it appears that bus location will ultimately become a NEMA standard perhaps a better solution of this problem can be found.

2. Various methods of protection have been offered by suppliers to shut down the motor in the event of loss of field. Nothing, however, was available to protect the machine if the field circuit was open and the operator attempted to start. It was agreed that this was the operator's usual reaction if he could not find what shut the machine down. A compromise was reached whereby the field-loss relay would operate a manual reset device thereby warning the operator of the field loss.

Since the writing of these specifications a circuit has been developed which actually samples the continuity of motor field and starting resistor circuit before the main contactors can be picked up. This eliminates the necessity of having a manually reset field-loss relay and also protects the machine from incorrect wiring at the time of start up and the loss of fields due to raised brushes. As this circuit receives further field testing it should be considered as an improved feature to be included in the specifications.

**William S. Watkins:** Oral comments and the written discussion received seem to verify that the proposal is generally acceptable, with the reservation that a few points should be subjected to a little more scrutiny. Questions were raised concerning the grounding of one side of the control transformer, the location of the supply busway, and the provision for protection against lack of field continuity. These are certainly very penetrating questions, and will be studied by the Working Group before the final draft is submitted to the Standards Committee. We shall be grateful for any additional comments which may be submitted, on these and other items, to assist the group in making its decisions.

# Use of a Mathematical Error Criterion in the Design of Adaptive Control Systems

C. W. MERRIAM, III
ASSOCIATE MEMBER AIEE

**Synopsis:** Mathematical error criteria are examined in terms of the goals of an adaptive control system. For dynamic processes which contain pure-time delay, a modification of these error criteria is postulated on the basis of the time-domain concept of control developed here.

Also, the mathematical methods used in optimization are examined in terms of the feedback concept. In particular, the optimum configuration of the control system is discussed and illustrated for dynamic processes with and without pure-time delay.

THE GENERAL topic of adaptive control systems presently is of great interest to engineers who traditionally have employed the concepts and methods of feedback control. In this regard, much of the impetus stems from the observation that, even though the human lacks many attributes required of purely physical systems such as speed of response, the human does possess desirable characteristics which are as yet unattainable in a purely physical form. Many of these desirable human characteristics arise from subjective judgment and the ability to utilize *a priori* information in situations identifiable by the human as having been encountered previously.

In an effort to emulate the subjective characteristics sometimes attributed to the human, researchers have postulated classes of systems such as self-adjusting and self-organizing which broadly could be classified as adaptive. Unfortunately, very little is understood regarding human behavior. Hence, systems designed to approximate human characteristics are restricted from a philosophical standpoint by the validity of the model of the human adopted, even though the response characteristics of the resulting systems may be very acceptable from some objective viewpoint.

In order to circumvent such philosophical arguments, this paper is predicated on the use of a mathematical index of performance for the synthesis of a class of adaptive control systems. The author regards this class of adaptive control systems as particularly useful in practice because adaptation is accomplished in an optimum fashion merely by gain changes. Furthermore these gains can be computed readily so that real-time computa-

Paper 59-1158, recommended by the AIEE Feedback Control Systems Committee and approved by the AIEE Technical Operations Department for presentation at the AIEE Fall General Meeting, Chicago, Ill., October 11–16, 1959. Manuscript submitted April 8, 1959; made available for printing August 13, 1959.

C. W. MERRIAM, III, is with Massachusetts Institute of Technology, Cambridge, Mass.

This work was supported in part by the International Business Machines Company (IBM) under IBM Purchase Order No. L-R19014, and under the Massachusetts Institute of Technology DSR Project No. 7793.

tions are feasible and could be employed to make these adaptive controllers applicable in a variety of situations

## Selection of an Error Criterion

Generally speaking, performance indices may be put into two categories. The first category is defined here as the shaping of transient response characteristic without regard to the nature of the particular response desired of the system. For instance, a shaping criterion may be the specification that the closed-loop system should approximate a linear, second-order system with a given rise time, setting time, or possibly a given overshoot. Unfortunately, many systems contain time varying and nonlinear components which are not readily amenable to these simple conceptual interpretations of the second-order system. The second category is defined here as the optimum approximation of desired response signals where errors in the approximation are weighted according to an appropriate performance criterion, called an error criterion when used in this sense. Here, then, an optimum occurs when the weighted error is minimized, thereby specifying the transient response characteristics of the resulting system in addition. For this paper, only performance indices of the second category are discussed in order to avoid the inevitable limitation of attempting to specify appropriate criteria that are based on linear concepts for the design of adaptive systems which are by definition nonlinear and time varying.

Having adopted the method of designing an adaptive system by the minimization of an error criterion, the specific class of design problems which reflect the goals of an adaptive control system must be defined. Here an adaptive control system is intended to be a feedback system which is altered continuously in order to maintain optimum system response. Controller alterations are necessary when changes occur in the estimated characteristics of the controlled dynamic process and of the response desired of the system. Also, alterations are necessary when the error criterion is changed. It should be mentioned here that the scope of this paper is restricted, for the sake of brevity, by neglecting the errors which may occur in the estimation of both the characteristics of the dynamic process and of the desired response. Inclusion of such errors is a study in itself and suitable results have been obtained only when the errors occur additively in the control and response signals.

A natural starting point for the selection of an error criterion might be the use of a least-squares criterion which is traditional in approximation problems arising in many fields including numerical analysis. In particular, a valid error criterion is the integral

$$I=\int_{-\infty}^{\infty}[Q(\sigma)-q(\sigma)]^2d\sigma \qquad (1)$$

where $Q(\sigma)$ is the estimated desired system response signal, $q(\sigma)$ is the actual system response signal, and $\sigma$ is a dummy time variable defined such that the value $\sigma=t$ is present or real time. The optimum system then would be defined as that system which minimizes the integral $I$. However, because practical components have limitations, a dynamic constraint must often be placed on the class of systems which are acceptable. A mathematically convenient way to insure the avoidance of saturating the control signal $m(\sigma)$ is the addition of a second term to the integral in equation 1, thereby, obtaining

$$I_c=\int_{-\infty}^{\infty}\{\lambda(\sigma)[Q(\sigma)-q(\sigma)]^2+m^2(\sigma)\}d\sigma \qquad (2)$$

For the present, the assumption is made that the response signal $q(\sigma)$ and control signal $m(\sigma)$ are related unilaterally, as indicated in Fig. 1, by the linear ordinary differential equation

$$\sum_{u=0}^{U}a_u(\sigma)q^{(u)}(\sigma)=\sum_{u=0}^{U-1}b_u(\sigma)m^{(u)}(\sigma) \qquad (3)$$

The superscript $(u)$ indicates the $u$th derivative of the function. Generally, the multiplier $\lambda(\sigma)$ in equation 2 is treated as an independent parameter such that $\lambda(\sigma)\geqq 0$, and chosen so that $m^2(\sigma)\leqq\mathfrak{M}^2(\sigma)$ where $\mathfrak{M}(\sigma)$ is the magnitude of the control signal where saturation occurs. This treatment of $\lambda$ as a Lagrange multiplier is predicated, of course, on the proper engineering selection of the saturation level $\mathfrak{M}(\sigma)$.[1] Another interpretation of the criterion given in equation 2, however, is that the multiplier $\lambda(\sigma)$ can be determined directly from engineering considerations. A good example of this interpretation arises when the first term in equation 2 is representative of economic penalties arising from response errors and the second term in equation 2 is considered as the "cost" of control. For the purposes of this paper, no generality is sacrificed by assuming that the multiplier $\lambda(\sigma)$ is determined directly from engineering considerations.


**Fig. 1. Block diagram of controlled process**

The error criteria presented thus far have no particular reference to adaptive control and are utilized conventionally, with the proper mathematical restrictions, in the design of linear time-invariant controls which of course are the antithesis of adaptive controls.

In order to postulate modifications to these criteria that are appropriate for application to adaptive controls, an analogy to the human faced with the problem of control is convenient. In words, the human attempts to select optimally the present value of the control signal $m(t)$. This selection is based on the existing conditions in the dynamic process, on the dynamic characteristics of the process, and on the response desired of the dynamic process in the future. Note that consideration of the future is necessary when the magnitude of the control system $m(\sigma)$ is constrained mathematically as in equation 2 because the existing conditions of the dynamic process cannot be changed instantaneously. Because of the conditions in the dynamic process, the dynamic characteristics of the process, and the desired response change with time, the optimum selection of the control signal changes with time. In this sense then, it is said that the human controller used in the analogy is adaptive.

The recognition that the existing conditions in the dynamic process are an integral part of adaptive control is of paramount importance to the selction of an appropriate error criterion. In particular, there is no apparent reason for weighting errors over the interval of past time $\sigma<t$ because, having occurred previously, no control can be exerted on them. If the assumption is made that the existing conditions in the dynamic process can be measured, as is desirous in a feedback control system, the errors that occur in the past can be neglected. Measurement of the existing conditions in the process is necessary in order to specify the effects of the past history of the process on the present and future response of the process. For processes which can be represented by an ordinary differential equation of finite order, elementary theory of such equations states that the effects of past history are specified completely by the present values of a finite number of state variables, usually called initial conditions. Now with the assumption that the state variables are measured, the error criterion used for adaptive control system design in this paper is

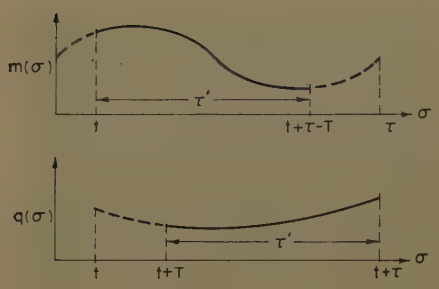


**Fig. 2. Weighting intervals for dynamic process with pure-time delay of duration T**

$$e=\int_{t}^{t+\tau}\{\lambda(\sigma)[Q(\sigma)-q(\sigma)]^2+m^2(\sigma)\}d\sigma \tag{4}$$

Note that the errors occuring in the interval of furture time $\sigma>t+\tau$ also have been neglected in equation 4. The omission of these future errors is necessary in many cases because adequate prediction or extrapolation of the desired response signal $Q(\sigma)$ may not be available. Also from a dynamic standpoint, no appreciable error is introduced into the selection of the optimum present value of the control signal $m(t)$ if the interval $\tau$ is chosen to be large in comparison to the time in which substantial transients can occur in the process. However, no particular restrictions are placed on the interval $\tau$ which is selected properly for the engineering problem at hand. For example, this interval may be chosen $\tau=\infty$ or $\tau=T_t-t$, where $T_t$ is a constant as might be appropriate for control which terminates at time $t=T_t$.

Based on the heuristic assumption of the availability of a finite number of measurements which define the state of the dynamic process, the error criterion given in equation 4 may be appropriate for the adaptive control of a dynamic process which is described by an ordinary differential equation of finite order such as the linear one given in equation 3. However, many dynamic processes of interest involve pure-time delay due to distributed parameter effects where the measurement of the present values of a finite number of variables no longer represent completely the effects of past history on the present and future response of the process. A case in point is a dynamic process which is described by the differential equation

$$\sum_{u=0}^{U}a_u(\sigma)q^{(u)}(\sigma+T)=\sum_{u=0}^{U-1}b_u(\sigma)m^{(u)}(\sigma) \tag{5}$$

A comparison of equations 3 and 5 indicates that, for the same control signal $m(\sigma)$, the response signal of equation 5 is delayed by an interval of time $T$ from that of equation 3. In addition to cases where equation 5 actually represents the dynamic process, an equation which contains pure-time delay but of low order often can be used as a good approximation to equation 3 when the order $U$ is large. Such an approximation gives rise to a definite simplification in the optimum controller.

For dynamic processes with pure-time delay, appropriate changes in the error criterion given in equation 4 are facilitated by the sketches of the control and response signals given in Fig. 2. A pure-time delay $T$ means that the segment of the control signal on the interval $t+\tau-T\leqq\sigma\leqq t+\tau$ is arbitrary in the sense that this segment does not affect the process response on the interval $t\leqq\sigma\leqq t+\tau$. Furthermore, the pure-time delay means that the control signal on the interval $t\leqq\sigma\leqq t+\tau$ does not affect the process response on the interval $t\leqq\sigma\leqq t+T$. Because the segment of the control signal on the interval $t+\tau-T\leqq\sigma\leqq t+\tau$ is arbitrary and because the segment of the response signal on the interval $t\leqq\sigma\leqq t+T$ is predetermined, a modified error criterion is postulated to be

$$e_T=\int_{t+T}^{t+\tau}\lambda(\sigma)[Q(\sigma)-q(\sigma)]^2d\sigma+\int_{t}^{t+\tau-T}m^2(\sigma)d\sigma \tag{6}$$

With a change in variables, this modified criterion can be written as

$$e_T=\int_{t}^{t+\tau'}\{\lambda(\sigma+T)[Q(\sigma+T)-q(\sigma+T)]^2+m^2(\sigma)\}d\sigma \tag{7}$$

where $\tau'=\tau-T$. This error criterion, then, weights only the portions of the signals that are meaningful, as determined from the time-domain concept developed here for adaptive control.

## Determination of the Optimum Adaptive Controller

Even though an error criterion has been chosen which appears to be applicable to some adaptive control problems, useful results will be obtained only if the optimum controller can be specified explicitly. Consideration of the mathematical methods that could be used in the determination of the optimum system can lead to involved discussions of the relative analytical and computational merits of the various methods. In order to avoid these involvements, heuristic arguments are introduced which lead naturally to the explicit determination of both the transient characteristics of the optimum system and the optimum configuration of the system components. In particular, the error criterion appropriate for the design of adaptive feedback controls has been selected by recognizing the role of the conditions existing in the dynamic process (called state of the process) and then assuming that this state could be measured. An effort to preserve a thread of unity dictates that these considerations should be reflected by the mathematical methods used in the explicit optimization. In order to emphasize concepts and not generality, the concepts are identified here by discussing the simplest possible dynamic process which is given by

$$q^{(1)}(\sigma)=b_0(\sigma)m(\sigma) \tag{8}$$

The error $e$ associated with the dynamic process described by equation 8 is given by equation 4. If the assumption is made that the multiplier $\lambda(\sigma)$ and the desired response signal $Q(\sigma)$ are given, this error is a function of the present state of the dynamic process which now is merely $q(t)$, the time $t$ where this process state variable is measured, and whatever control signal $m(\sigma)$ that is inserted into the error criterion. If a dummy variable $\mu$ is defined as the time where the state of the dynamic process is measured, the error given in equation 4 can be expressed functionally as

$$e[q(\mu),m(\sigma);\mu]=\int_{\mu}^{t+\tau}\times\{\lambda(\sigma)[Q(\sigma)-q(\sigma)]^2+m^2(\sigma)\}d\sigma \tag{9}$$

However, when equation 9 is minimized, the control signal $m(\sigma)$ is no longer arbitrary but is specified as a function of the remaining independent variable $q(\mu)$. Symbolically, the minimum error $E$ can be written as

$$E=\min_{\substack{m(\sigma)\\ \mu\leqq\sigma\leqq t+\tau}}\{e[q(\mu),m(\sigma);\mu]\} \tag{10}$$

where the minimization is performed with respect to the control signal $m(\sigma)$ over the interval $\mu\leqq\sigma\leqq t+\tau$. For minimum error, the control signal is given functionally as

$$m(\sigma)=F_\sigma[q(\mu)] \tag{11}$$

where the dummy variable $\sigma$ is treated as a parameter in the function $F$. Therefore equation 10 is rewritten as

$$E=e[q(\mu),F_\sigma[q(\mu)];\mu], \tag{12}$$

and the minimum error is seen to be a function only of the measured state of the dynamic process $q(\mu)$ and the time of measurement $\mu$. Finally then, the minimum error function is defined for the dynamic process described by equation 8 as

$$[q(\mu);\ \mu]=\min_{\substack{m(\sigma)\\ \mu\leqq\sigma\leqq t+\tau}}\left[\int_{\mu}^{t+\tau}\{\lambda(\sigma)[Q(\sigma)-q(\sigma)]^2+m^2(\sigma)\}d\sigma\right] \quad (13)$$

The reason for defining the minimum ror function $E[q(\mu);\mu]$ is that the neces- ry key step is the use of the functional quation given in equation 11 which gives ie optimum control signal. Specifically, quation 11 is a control law for a feed- ack controller when $\mu=t$ because the ptimum control signal $m(t)$ is expressed terms of the measured response signal $t$). Therefore, the optimum control gnal will be found directly when the inimum error function is found with- it the necessity of converting an ptimum transfer function into a feed- ack system, a procedure associated with e usual calculus of variations. This nversion, of course, is predicted on the sumption of linearity, and hence olates the desire for adaptability. ith the use of Bellman's "principle of ptimality," the condition for minimum ror can be shown to be

$$\min_{m(\mu)}\left\{\lambda(\mu)[Q(\mu)-q(\mu)]^2+m^2(\mu)+\frac{\partial E[q(\mu);\mu]}{\partial\mu}+b_0(\mu)m(\mu)\frac{\partial E[q(\mu);\mu]}{\partial q(\mu)}\right\}=0 \quad (14)$$

ere $E[q(t+\tau);\ t+\tau]=0$ as can be seen m equation 13 with $\mu=t+\tau$.[2,3] The thor has omitted the derivation of uation 14 because no additional con- pts pertinent to the adaptive control oblem per se are required for the rivation. In other words, equation 14 tes that the sum of the terms in the aces vanishes when the value of the ntrol signal $m(\mu)$, treated here as a rameter, is adjusted so that this sum is minimum.

The sum in the braces of equation 14 minimum when

$$\frac{\partial}{m(\mu)}\left\{\lambda(\mu)[Q(\mu)-q(\mu)]^2+m^2(\mu)+\frac{\partial E[q(\mu);\mu]}{\partial\mu}+b_0(\mu)m(\mu)\times\frac{\partial E[q(\mu);\mu]}{\partial q(\mu)}\right\}=0 \quad (15)$$

ich is satisfied when

$$m(\mu)=-\frac{b_0(\mu)}{2}\frac{\partial E[q(\mu);\mu]}{\partial q(\mu)} \quad (16)$$

bstitution of the value of $m(\mu)$ given equation 16 into equation 14 gives the dition required of the minimum error function for the dynamic process specified by equation 8 as

$$\lambda(\mu)[Q(\mu)-q(\mu)]^2+\frac{\partial E[q(\mu);\mu]}{\partial\mu}-\left\{\frac{b_0(\mu)}{2}\frac{\partial E[q(\mu);\mu]}{\partial q(\mu)}\right\}^2=0 \quad (17)$$

As noted previously, the feedback control law is given directly in terms of the minimum error function as expressed in equation 16 when $\mu=t$

Having obtained the condition that specifies the minimum error function in terms of a partial differential equation, this function is sought in explicit form. As would be the case for an unfamiliar ordinary differential equation, a power series solution could be assumed. Then the coefficients in the series could be found by direct substitution.

The solution of equation 17 is assumed to be of the form

$$E[q(\mu);\mu]=K(\mu)+K_0(\mu)q(\mu)+K_{00}(\mu)q^2(\mu) \quad (18)$$

where the $K$'s are the parameters to be determined. The series given in equation 18 is truncated at the squared term because higher order terms can be shown to be zero by the procedure that follows when applied to the more general series. Now remembering that both $q(\mu)$ and $\mu$ are treated as independent variables in the definition of the minimum error function, the partial derivatives needed for equation 17 are

$$\frac{\partial E[q(\mu);\mu]}{\partial\mu}=K^{(1)}(\mu)+K_0{}^{(1)}(\mu)q(\mu)+K_{00}{}^{(1)}(\mu)q^2(\mu) \quad (19)$$

and

$$\frac{\partial E[q(\mu);\mu]}{\partial q(\mu)}=K_0(\mu)+2K_{00}(\mu)q(\mu) \quad (20)$$

When equations 19 and 20 are substituted into equation 17, equation 17 can be rewritten by collecting terms according to their power in $q(\mu)$ such that

$$\left[K^{(1)}(\mu)+\lambda(\mu)Q^2(\mu)-\frac{b_0{}^2(\mu)}{4}K_0{}^2(\mu)\right]+q(\mu)[K_0{}^{(1)}(\mu)-2\lambda(\mu)Q(\mu)-b_0{}^2(\mu)K_0(\mu)K_{00}(\mu)]+q^2(\mu)[K_{00}{}^{(1)}(\mu)+\lambda(\mu)-b_0{}^2(\mu)K_{00}{}^2(\mu)]=0 \quad (21)$$

Because three independent parameters $K$, $K_0$, and $K_{00}$ appear in the assumed form of the minimum error function, three independent conditions are applied to equation 21. In particular, these parameters are chosen so that the three brackets in equation 21 vanish and, therefore, are given by the three ordinary first-order differential equations

$$K^{(1)}(\mu)=-\lambda(\mu)Q^2(\mu)+\frac{b_0{}^2(\mu)}{4}K_0{}^2(\mu) \quad (22)$$

$$K_0{}^{(1)}(\mu)=2\lambda(\mu)Q(\mu)+b_0{}^2(\mu)K_0(\mu)K_{00}(\mu) \quad (23)$$

$$K_{00}{}^{(1)}(\mu)=-\lambda(\mu)+b_0{}^2(\mu)K_{00}{}^2(\mu) \quad (24)$$

These parameters then are specified completely because $K(t+\tau)=K_0(t+\tau)=K_{00}(t+\tau)=0$, a condition which arises from $E[q(t+\tau);\ t+\tau]=0$ for all $q(t+\tau)$. Finally, the control law of the optimum controller is given (when $\mu=t$) from equation 16 as

$$m(\mu)=-\frac{b_0(\mu)}{2}K_0(\mu)-b_0(\mu)K_{00}(\mu)q(\mu) \quad (25)$$

However, before a detailed discussion of the properties of the optimum controller is embarked upon, the preceeding development is re-examined for the simplest case of pure-time delay in the dynamic process as given by

$$q^{(1)}(\sigma+T)=b_0(\sigma)m(\sigma) \quad (26)$$

For the error criterion given in equation 7 which applies for pure-time delay, the corresponding minimum error function can be defined as

$$E_T[q(\mu+T);\mu]=\min_{\substack{m(\sigma)\\ \mu\leqq\sigma\leqq t+\tau'}}\left[\int_{\mu}^{t+\tau'}\{\lambda(\sigma+T)\times[Q(\sigma+T)-q(\sigma+T)]^2+m^2(\sigma)\}d\sigma\right] \quad (27)$$

such that $E_T[q(t+\tau);\ t+\tau']=0$. Here the state of the dynamic process, as measured at time $\mu$ in conjunction with an appropriate computation, that specifies the effect of the past on the controllable segment $\mu+T\leqq\sigma\leqq t+\tau$ of the response signal is given by $q(\mu+T)$.

Corresponding to this minimum error function, the condition similar to equation 14 is

$$\min_{m(\mu)}\left\{\lambda(\mu+T)[Q(\mu+T)-q(\mu+T)]^2+m^2(\mu)+\frac{\partial E_T[q(\mu+T);\mu]}{\partial\mu}+b_0(\mu)m(\mu)\frac{\partial E_T[q(\mu+T);\mu]}{\partial q(\mu+T)}\right\}=0 \quad (28)$$

If the minimum error function is assumed to be of the form

$$E_T[q(\mu+T);\mu]=K(\mu)+K_0(\mu)q(\mu+T)+K_{00}(\mu)q^2(\mu+T) \quad (29)$$

the derivation from equation 15 to equation 24 can be repeated for the pure-time delay case to give the following equations which specify the parameters $K$, $K_0$, and $K_{00}$:

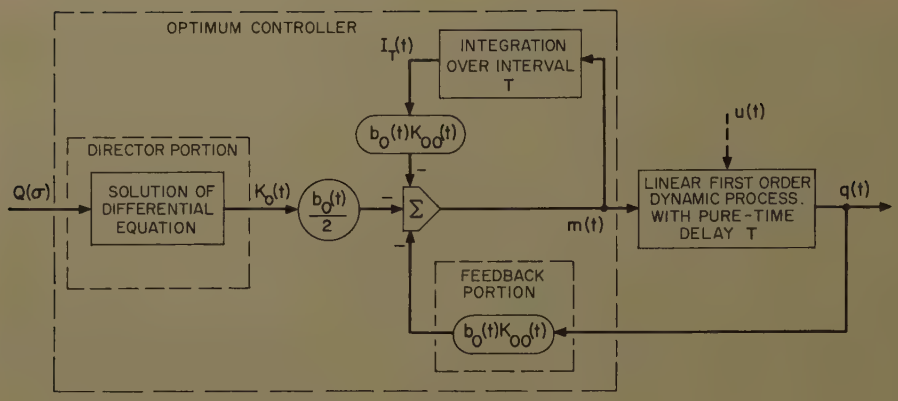


**Fig. 3. Block diagram of the optimum controller for a first-order dynamic process with pure-time delay T. Not indicated is that the parameter $K_{00}(t)$ also is the solution of a differential equation**

$$K^{(1)}(\mu) = -\lambda(\mu+T)Q^2(\mu+T) + \frac{b_0^2(\mu)}{4} K_0^2(\mu) \quad (30)$$

$$K_0^{(1)}(\mu) = 2\lambda(\mu+T)Q(\mu+T) + b_0^2(\mu)K_0(\mu)K_{00}(\mu) \quad (31)$$

$$K_{00}^{(1)}(\mu) = -\lambda(\mu+T) + b_0^2(\mu)K_{00}^2(\mu) \quad (32)$$

where $K(t+\tau') = K_0(t+\tau') = K_{00}(t+\tau') = 0$. Finally, the control law for the pure-time delay case (when $\mu = t$) which corresponds to equation 25 is

$$m(\mu) = -\frac{b_0(\mu)}{2} K_0(\mu) - b_0(\mu)K_{00}(\mu)q(\mu+T) \quad (33)$$

## Properties of the Optimum Adaptive Controller

Having derived the control law for the optimum adaptive controller, a detailed examination of the results indicates some very important properties of the optimum controller from a feedback control standpoint. Because the case with a pure-time delay of duration $T$ degenerates to the case without time delay by allowing $T \to 0$, as can be seen from equation 30 to equation 32 and equation 22 to equation 24, the discussion generally is directed to the case with the pure-time delay. From equation 33 then, the control law for the optimum controller is

$$m(t) = -\frac{b_0(t)}{2} K_0(t) - b_0(t)K_{00}(t)q(t+T) \quad (34)$$

Furthermore, for the dynamic process given in equation 26, the response of the process is

$$q(t) = \int_{-\infty}^{t-T} b_0(\xi)m(\xi)d\xi \quad (35)$$

Therefore, the measured variable $q(t+T)$ that appears in the optimum control law can be written as

$$q(t+T) = q(t) + I_T(t) \quad (36)$$

where

$$I_T(t) = \int_{t-T}^{t} b_0(\xi)m(\xi)d\xi \quad (37)$$

Finally, the optimum control law when written in terms of the measured response signal is

$$m(t) = \left[ -\frac{b_0(t)}{2} K_0(t) - b_0(t)K_{00}(t)I_T(t) - b_0(t)K_{00}(t)q(t) \right] \quad (38)$$

which can be depicted as shown in Fig. 3. In general then, the director and feedback portions of the adaptive controller are the result of continually repeated computations of the parameters $K_0(t)$ and $K_{00}(t)$ by the solving of two ordinary differential equations over a time interval $\tau'$. The remaining portion of the controller is the continuous measurement of the integral $I_T(t)$ which is required by the presence of puretime delay.

Now with reference to Fig. 3 and to the steps used in the derivation of the parameters $K_0(t)$ and $K_{00}(t)$ which appear in the block diagram, the important properties of this optimally adaptive controller can be listed as follows.

1. The controller is optimum for all initial conditions $q(t)$ which may occur because the parameters are chosen so that equation 21 is satisfied for all finite $q(t)$ by making each bracket in that equation vanish.

2. The controller is optimum for all future states of the dynamic process, as given by $q(\mu)$ at the interval $t < \mu \leqq t+\tau$, from the same reasoning used to establish th previous property. Therefore the controlle is optimum for all additive load disturbance (shown dashed in Fig. 3) that cannot b measured and possess the property tha their future is independent of their presen and past.

3. The feedback portion of the optimur controller, given by $K_{00}(t)$, is independen of the desired response $Q(\sigma)$ as can be see from equation 32.

4. The output of the director portion o the optimum controller, given by $K_0(t)$ is linear with respect to additive component in the desired response signal $Q(\sigma)$. Thi property can be seen from equation 3 and results because the parameter $K_{00}(\mu$ is merely a time varying multiplier, as i is not dependent on $Q(\sigma)$.

The first two properties of the optimum control system give rise to the concep of an optimum configuration. Becaus the feedback portion of the optimum con trol system is linear, the feedback loop, fo instance, could be replaced by an equiv alent linear compensation as indicate in Fig. 4. The system shown in Fig. has the same response signal as the sys tem shown in Fig. 3 when the initia conditions and load disturbances ar neglected. However, the configuratio shown in Fig. 3 gives minimum erro due to both initial conditions and addi tive load disturbances of the class define previously, and hence is termed th "optimum configuration." In othe words, deviation from the optimum con figuration in general causes increase error.

The second two properties of th optimum control system give rise na urally to the suggestion that the controll may have important properties for de sired response signals that can be repre sented by a sum of components. In pa ticular, here the assumption is made tha the desired response signal is

$$Q(\sigma) = \sum_{n=0}^{N} f_n(\sigma, t)Q_n(t) \quad (3$$

where the signal $Q_n(t)$ is a componen which can be extracted from $Q(t)$ by physically realizable device. The nece sity for a physically realizable device stressed here because the segment of th

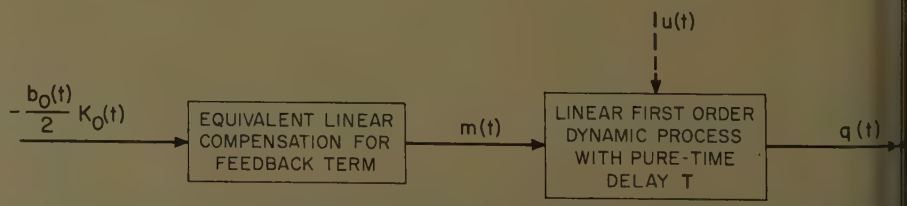


**Fig. 4. Block diagram of equivalent linear compensation which is optimum only for zero initi conditions and additive load disturbances**

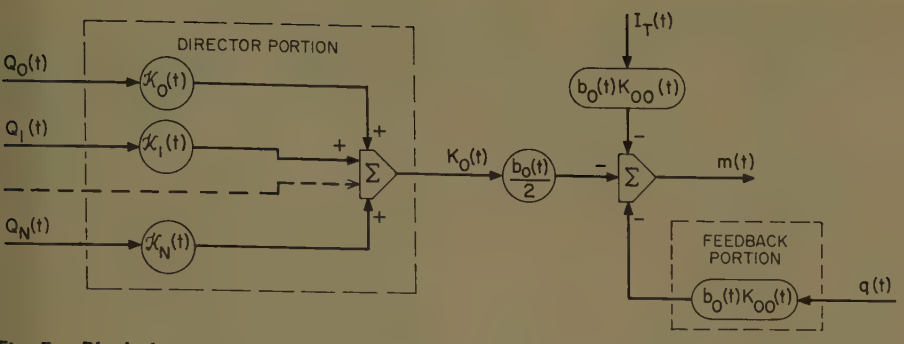


**Fig. 5. Block diagram of the optimum linearly-adaptive controller that occurs when the desired response is a sum of separable components**

desired response signal that is required for the solution of equation 31 is on an interval of future time $t+T \leqq \sigma \leqq T+\tau$. As an example in this class of signals, the desired response signal may be approximated with accuracy by a Taylor series such that $Q_n(t)=Q^{(n)}(t)$, and hence the function $f_n$ is $f_n(\sigma,t)=(\sigma-t)^n/n!$ In this example, the component extraction is accomplished by successive differentiation. Now because superposition applies to equation 31, the director output can be written in terms of the integral

$$K_0(t)=\int_t^{t+\tau'} h_T(\tau', t+\tau'-\mu)Q(\mu+T)d\mu \tag{40}$$

The impulse response function $h_T(\tau',\xi)$ is defined as the signal $K_0(\zeta)$ at $\zeta=\tau'$ caused by a unit impulse at $\zeta=\xi$ where the dummy variable $\zeta$ is defined as $\zeta=t+\tau'-$ for use in equation 31. For the class of desired response signals given by equation 39, the director output signal becomes

$$K_0(t)=\sum_{n=0}^{N} \kappa_n(t)Q_n(t) \tag{41}$$

where the no-energy storage gain $\kappa_n(t)$ is

$$\kappa_n(t)=\int_t^{t+\tau'} h_T(\tau', t+\tau'-\mu)f_n(\mu+T, t)d\mu \tag{42}$$

Therefore these gains are the solution of the differential equation

$$\kappa_n^{(1)}(\mu)=2\lambda(\mu+T)f_n(\mu+T, t)+ b_0^2(\mu)\kappa_n(\mu)K_{00}(\mu) \tag{43}$$

Fig. 5 shows that the optimum controller consists of only time varying gains, for desired response signals of the form of equation 39, and hence the optimum control system is "linearly-adaptive" to the desired response signal.

## Conclusions

The goals of this paper have been to demonstate, via the simplest problem, how the selection of an appropriate error criterion and the use of a particular method of optimization apply to the design of a class of adaptive controllers that enjoy the attributes of feedback. In particular, the design problem is restricted to a linear but time-varying first-order dynamic process that may contain a pure-time delay and to an error criterion of quadratic form. For these mathematical restrictions, the optimum controller is shown to be independent of all finite initial conditions and additive load disturbances of the class defined previously. Furthermore, the parameters which appear in the optimum controller are specified at each instant of real time $t$ as the solutions of two ordinary first-order differential equations. Finally, for these mathematical restrictions and a class of desired response signals which are a sum of separable components, the optimum control system is linear but in general time varying by virtue of the presence of time varying gains.

For the purposes of application to engineering design problems, a wide variety of transient characteristics can be obtained by the proper selection of the weighting of response errors, as given by $\lambda(\sigma)$ and $\tau$ which are identified with the problem statement. Furthermore, these linearly-adaptive controllers are particularly practical because the differential equations can be solved by either analog or digital computers at a rate high enough for many applications and because the time-varying gains are readily obtained componentry.

Fortunately the properties described here can be extended to more general problems but with varying degrees of complication, depending upon the mathematical restrictions imposed. Some important cases are:

1. For a $U$th order linear dynamic process and a quadratic error criterion, the feedback portion of the control system is specified by $U$ parameters which occur in $U$ feedback loops. However, the director is still given by one parameter. The controller parameters are specified from the solution of $2U+U!/2!(U-2)!$ simultaneous first order differential equations. The system is optimum for all initial conditions and all additive load disturbances of the restricted class defined previously. For a desired response signal of the separable class given in equation 39, the optimum system is linearly-adaptive because the director is specified by time varying gains.

2. For the restrictions of case 1 but allowing the desired response signal to have random components, minimum mean-square error in the control and response signals (the errors being caused by errors that occur in the prediction of the desired response signal over the interval of future time where response errors are weighted in the error criterion) gives rise to Wiener prediction of the desired response signal. The optimum mean-square prediction of the response signal has the separable form of equation 39 for linear lumped parameter Wiener predictors, and hence the system is linearly-adaptive as the director is again given by time-varying gains. Here each component signal $Q_n(t)$ is measured with a Wiener filter.[4,5]

3. For certain types of nonlinear dynamic processes of $U$th order such as the case where the control signal is limited in range due to saturation but where the process is otherwise linear, a quadratic form of the error criterion gives rise to an optimum control system that has $U$ feedback loops and is specified by $1+U$ parameters which are computed from $2U+U!/2!(U-2)!$ simultaneous ordinary first-order differential equations. However, the system is optimum only for the particular initial condition, additive load disturbance, and member of the ensemble of possible desired response signals for which the parameters are computed. Hence, the optimum controller is nonlinear for all classes of desired response signals. Also because an iterative procedure is required to select the proper solutions for the parameters, application to problems of various time scales generally is more limited.

4. For nonquadratic forms of the error criterion, optimization by continual computations is possible but very lengthy when load disturbances and the like are included. Hence, without the use of "quasi-optimum" techniques now being investigated, this procedure seems to have a very limited application to problems such as may arise in the chemical processing industry.

## Nomenclature

$a_u(t)$, $b_u(t)$ = parameters of the linear dynamic process
$e$ = error criterion
$f_n(\sigma, t)$ = function associated with the extrapolation of a component of the desired response signal, $Q_n(t)$
$E[q(\mu); \mu]$ = minimum error function for first-order dynamic process
$h_T(\tau', t+\tau'-\mu)$ = impulse response of the director portion of the adaptive controller
$I_T(t)$ = integral of the control signal over an interval equal to the duration of the time delay

$K(\mu)$, $K_0(\mu)$, $K_{00}(\mu)$ = parameters of the minimum error function
$\kappa_n(t)$ = no energy storage gain computed from the director equations
$m(t)$ = control signal of the dynamic process
$n$ = dummy index of summation
$q(t)$ = response signal of the dynamic process
$Q(t)$ = desired process response signal
$Q_n(t)$ = component of the desired response signal
$t$ = present time
$T$ = duration of pure-time delay
$u$ = dummy index of summation
$U$ = order of the dynamic process
$\zeta$, $\mu$, $\xi$, $\sigma$ = dummy time variables
$\lambda(\sigma)$ = weighting factor
$\tau$ = interval where process response errors are weighted
$\tau'$ = interval where process response errors are weighted for case with a pure-time delay of duration $T$
Superscript $(u)$ = $u$th derivative of function with respect to a time variable

## References


1. Analytical Design of Linear Feedback Controls (book), G. C. Newton, Jr., L. A. Gould, J. F. Kaiser. John Wiley & Sons, Inc., New York, N. Y., 1957.

2. A Class of Optimum Control Systems, C. W. Merriam, III. *Journal*, Franklin Institute, Philadelphia, Pa., Apr. 1959, pp. 267–81.

3. Dynamic Programming (book), R. E. Bellman. Princeton University Press, Princeton, N. J., 1957.

4. Extrapolation, Interpolation, and Smoothing of Stationary Time Series, with Engineering Applications (book), N. Wiener. Technology Press, Cambridge, Mass., 1949.

5. Application of Statistical Methods to Communication Problems, Y. W. Lee. *Technical Report no. 181*, Massachusetts Institute of Technology, Cambridge, Mass., 1950.


# A Method for the Symbolic Representation and Analysis of Linear Periodic Feedback Systems


EDWARD O. GILBERT
NONMEMBER AIEE


LINEAR FEEDBACK systems with periodic sampling, finite pulsing, finite pulse clamping and similar variations have been a subject of increasing interest in recent years. Applications in such important areas as digital control and time-division multiplexing have motivated continued research and development. This is particularly true for certain types of systems where the theory is extensive and well developed. Unfortunately, there are many types of systems which have received little or no attention.

It is the purpose of this paper to present methods of symbolism and analysis which handle an extensive class of new problems and present an improved treatment of many problems previously considered.

The sampled-data system is the most studied and well-known system type. Here the periodic variation appears as instantaneous periodic sampling of signals. Mathematically, this sampling is represented by multiplying signals by a periodic impulse train. The literature is extensive and includes multirate and cyclic-rate systems.[1–5] The most important tools of analysis are the $Z$-transform and modified $Z$-transform.

Farmanfarma has considered finite pulsed systems where the periodic variation is signal multiplication by a train of periodic pulses with finite width and amplitude.[6–8] The $P$-transform is defined and used in his analysis. Analysis of closed-loop systems is considerably more complicated than that of open-loop systems. Approximate methods, based on sampled-data models have been proposed by Kranc,[9] Murphy and Kennedy,[10] and Tou.[3]

Another type of periodic variation is the operation of finite pulse clamping illustrated in Fig. 1, where Fig. 1(A) shows the signal input $e(t)$ and Fig. 1(B) shows the finite pulse-clamped signal $e_c(t)$. Mathematically,

$$e_c(t) = e(t),\ nT < t \leqslant nT + t_1$$
$$= e(nT + t_1),\ nT + t_1 < t \leqslant (n+1)T \qquad (1)$$

where $T$ is the fundamental period of variation and $n$ ranges over all integers. Analysis techniques for systems with finite pulse-clamped error signals have been developed.[11]

A periodic variation which includes finite pulsing as a special case is the piecewise constant variation of parameters. Such variation can be in gains and/or time constants of control elements. An example of a parameter with a 2-interval variation is the gain:

$$K(t) = K_1,\ nT < t < nT + t_1$$
$$= K_2,\ nT + t_1 < t < (n+1)T \qquad (2)$$

where $T$ is the fundamental period. Finite pulsing obviously occurs when $K_2 = 0$. Unforced systems of this type are conveniently treated by the matrix method of Pipes.[12] The sinusoidal response of electric networks with piecewise constant variation of parameters was treated by Bennett[13] and extended by Desoer.[14] A still more complete theory of such systems has been developed by the author.[11]

All of these variations can be included in a single system. Fig. 2 shows an example of such a system where the error is finite pulse clamped, modified by digital computer with clamper, and fed into a plant ($p = d/dt$) with periodic gain variation. The finite pulse-clamped error $e_c$ is defined by equation 1 and the variable gain $K$ by equation 2. The digital computer and clamper are described by the equation:

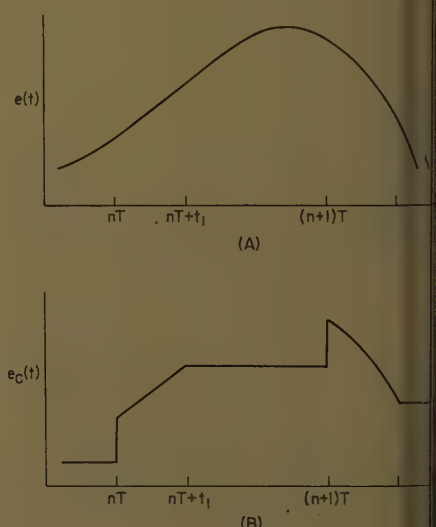


**Fig. 1. Operation of finite pulse clamping**

A—Continuous signal
B—Finite pulse-clamped signal


Paper 59-1183, recommended by the AIEE Feedback Control Systems Committee and approved by the AIEE Technical Operations Department for presentation at the AIEE Fall General Meeting, Chicago, Ill., October 11–16, 1959. Manuscript submitted March 24, 1959; made available for printing September 3, 1959.



Edward O. Gilbert is with the University of Michigan, Ann Arbor, Mich., and on leave of absence with Space Technology Laboratories Inc., Los Angeles, Calif.

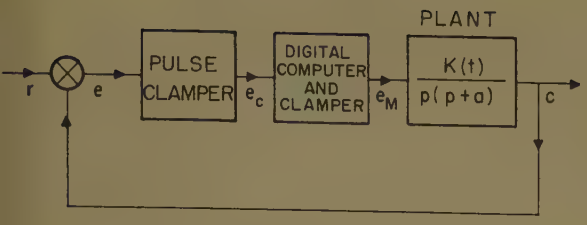


Fig. 2 (above). Example feedback system

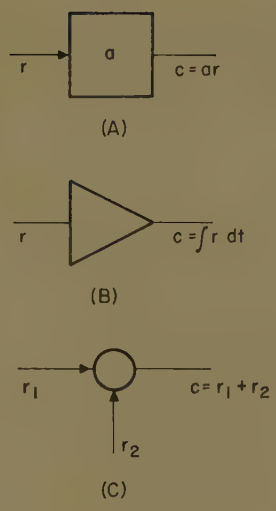


Fig. 3 (right). Basic symbolic elements

A—Multiplication by a constant
B—Integration
C—Summation

$$e_M(t)=\sum_{i=0}^{3} a_i e_c[t_2+(n-i-1)T]-\sum_{j=1}^{3} b_j e_M[t_2+(n-j)T]$$

$$nT<t\leqslant(n+1)T,\ 0<t_1<t_2<T \quad (3)$$

representing instantaneous sampling and clamping.

A typical problem in analysis would be to determine the step response of this system.

The methods of symbolism and analysis presented in this paper treat systems with any combination of the described periodic variations. The formulation is based on a state vector that completely defines the system and input behavior at all times. This state vector is defined by a series of constant coefficient differential equations and transition equations. The equations are readily obtained, from a block diagram consisting of basic symbolic elements. State vectors have been used with success in other applications by Kalman and Bertram,[15,16] Bashkow,[17] and others. The block diagram methods are in some ways similar to those of Bertram.[16]

Solution of the equations is accomplished by matrix methods. The $Z$-transformation is used to obtain the solution at the fundamental time intervals $nT$. The continuous solution in any fundamental period $nT<t\leqslant(n+1)T$ is also obtained. The methods are illustrated with examples.

## System Description

All the periodic operations already described are easily represented in block diagram form by five basic operations: multiplication by a constant, integration, summation, switching, and sampling. When every system component is described by symbols representing the basic operations, the mathematical representation in terms of a state vector readily follows.

### Invariant Components

Consider first components described by transfer functions with constant coefficients. In this case switching or sampling operations are not necessary and the component can be represented by the block diagram symbols of Fig. 3. The decomposition which results is by no means unique.

To illustrate several decompositions, consider the transfer function:

$$\frac{c}{r}=\frac{p^2+3p+2}{p^3+4.5p^2+2p}=\frac{(p+1)(p+2)}{p(p+0.5)(p+4)} \quad (4)$$

A direct decomposition is shown in Fig. 4. The correctness of this block diagram is made apparent by writing $c$ as:

$$c=(p^{-1}+3p^{-2}+2p^{-3})\bar{c}$$

where

$$\bar{c}=\frac{1}{1+4.5p^{-1}+2p^{-2}}r$$

The state vector is defined by the components $y_1$, $y_2$, and $y_3$, equal in number to the system order. The differential equations for the state variables are readily obtained by inspection. For example, the time rate of change of $y_3$ equals the sum of inputs to the $y_3$ integrator, or:

$$\dot{y}_3=-4.5y_3-2y+r$$

Similarly, $\dot{y}_2=y_3$, and $\dot{y}_1=y_2$.

The desired output $c(t)$ is given by a linear combination of the state variables. Thus:

$$c(t)=2y_1+3y_2+y_3$$

By writing the transfer function 4 as the partial fraction expansion

$$\frac{c}{r}=\frac{1}{p}+\frac{-3/7}{p+0.5}+\frac{3/7}{p+4}$$

the block diagram of Fig. 5 results. The state variables are again the integrator outputs defined by the equations:

$$\dot{y}_1=r$$

$$\dot{y}_2=-0.5y+r$$

$$\dot{y}_3=-4y_3+r$$

The output $c$ is given by:

$$c=y_1-\frac{3}{7}y_2+\frac{3}{7}y_3$$

Still another decomposition is obtained by cascading elements of the form $1/(p+a)$ and $(p+b)/(p+c)$. One such form for transfer function 4 is shown in Fig. 6. In this case the state variables are defined by:

$$\dot{y}_1=(1-0.5)y_2+(2-4)y_3+r$$

$$\dot{y}_2=-0.5y_2+(2-4)y_3+r$$

$$\dot{y}_3=-4y_3+r$$

and $c=y_1$.

These and other possible decompositions illustrate the plurality of the symbolic representations. The appropriate decomposition and corresponding state vector are determined by a number of factors. If a transfer function is of high

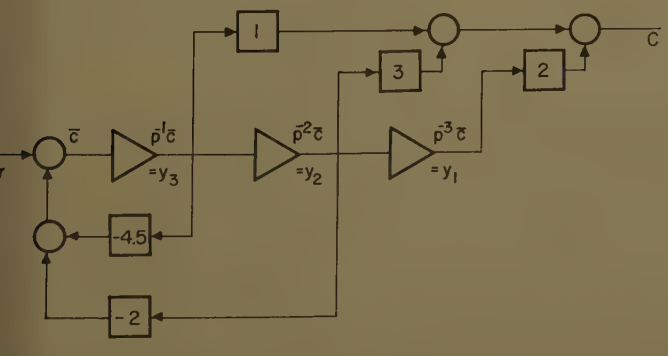


Fig. 4 (left). Direct decomposition

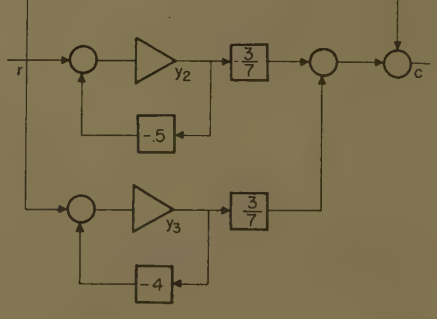


Fig. 5 (right). Partial fraction decomposition

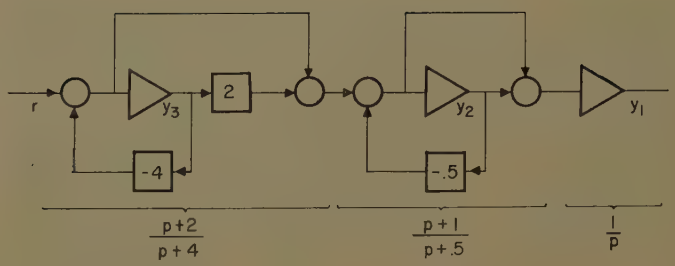


Fig. 6. Cascade decomposition

order and unfactored, the direct decomposition method is most convenient. The partial fraction representation has a computational advantage in that the differential equation for each state variable is independent of the other state variables. Often it is desirable from the standpoint of synthesis and compensation to have the state variables correspond directly to physical quantities. In control systems, this can frequently be done by using the cascade representation.

In many cases the application of physical laws leads directly to a state vector. One example occurs in electrical network analysis when dependent variables are selected as the voltages across capacitors and the currents through inductors.[17] Another example is the linearized equations for an aircraft which are a set of first-order differential equations. In these cases, the state variables represent physical quantities and transfer function derivation is superfluous.

### Switching and Sampling

Before describing the basic switching and sampling operations, the interval number and sampling number of a system will be defined. The interval number $N$ is the number of intervals of time invariant behavior in the fundamental period $T$. These intervals of invariance are specified by $0<t-nT\leq t_1$, $t_1<t-nT\leq t_2$, $\ldots$, $t_{n-1}<t-nT\leq t_N=T$. The sampling number $M$ is the number of instantaneous samples in the fundamental period $T$. Since sampling is a time variability, the sampling instants separate time invariant behavior and must occur at one or more of the values $nT$, $nT+t_1$, $\ldots$, $nT+t_{n-1}$. Obviously, $M\leq N$. Note that the time origin has been selected so that $t=nT$ separates intervals of time invariability.

To illustrate the meaning of $N$ and $M$ more fully, consider several examples. For a conventional sampled-data system with sampling at $t=nT$, $N=M=1$. For a cyclic-rate sampled-data system with five sampling instants in each fundamental period, $N=M=5$. A finite pulsed system with one pulse per period gives $N=2$ and $M=0$. For the finite pulse-clamping operation given by equation 1, $N=2$, $M=1$. As will be seen, the mixed system of Fig. 2 can have several $N$, $M$ combinations depending on the formulation chosen. It is sometimes useful to think of time invariant systems as a special case where $N=1$, $M=0$.

The $(i-1)-i$ switching operation, shown schematically in Fig. 7 by a bar switch, is defined by:

$$\begin{aligned} c&=0,\ 0<t-nT\leq t_{i-1}\\ &=r,\ t_{i-1}<t-nT\leq t_i\\ &=0,\ t_i<t-nT\leq T \end{aligned} \qquad (5)$$

Although $N$ switching operators exist, they may not all be used. An example of this is shown in Figs. 8(A) and (B) where the pulsed error:

$$\begin{aligned} e_p(t)&=e(t),\ 0<t-nT\leq t_1\\ &=0,\ t_1<t-nT\leq T \end{aligned}$$

is obtained in two different ways. Depending on the application, one formulation may be preferable to another.

The switching operations describe any piecewise constant parameter variation. The only other necessary operation is that of sampling. The sampling operator considered here differs from the usual impulse train multiplication. The new method of representation is illustrated in Fig. 9(A) for a 3-sample system where sampling occurs at $t=nT$, $nT+t_1$, and $nT+t_2$. The sampling operation, which always occurs in conjunction with integration is represented by arrow switches, as opposed to the bar switches, feeding the lower side of an integrator. The integrator equations in Fig. 9(A) are:

$$\begin{aligned} \dot{y}_1&=r_1\\ y_1(nT+)&=r\,(nT)\\ y_1(nT+t_1+)&=y_1(nT+t_1)\\ y_1(nT+t_2+)&=y_1(nT+t_2) \end{aligned} \qquad (6)$$

The first equation is the integrator differential equation; the last three equations are the reset or transition equations that specify the integrator initial condition at $t=nT+$, $nT+t_1+$, and $nT+t_2+$. For an $M$ sample system each integrator would have $M$ sample switches associated with it. To simplify the block diagrams, the sample switches will not be shown if they connect an integrator output to its lower side. This is reasonable since such

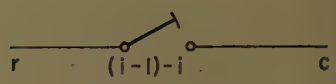


Fig. 7. Symbolic switching elements

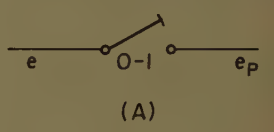


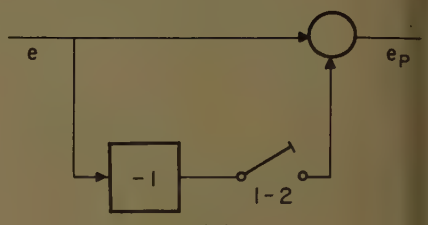


Fig. 8. Two representations of finite pulsing

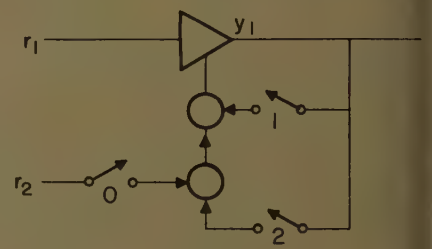


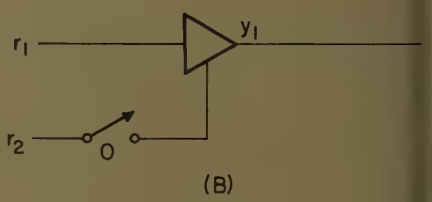


Fig. 9. Symbolic sampling elements

A—Complete form
B—Simplified form

operations give continuity in the integrator variable. Fig. 9(B) shows this simplification for the system of Fig. 9(A). Other examples are illustrated in Figs. 3, 4, 5, and 6 for invariant systems where the integrator outputs are obviously continuous.

To illustrate the use of the sampling operator consider several examples. Fig. 10(A) shows the usual way of representing linear interpolation between data points. Here:

$$r^*(t)=\sum_{n=-\infty}^{\infty} r(nT)\delta(t-nT)$$

$$c(t)=r[(n-1)T]+\frac{1}{T}\{r(nT)-r[(n-1)T]\}(t-nT),\ 0<t-nT\leq T$$

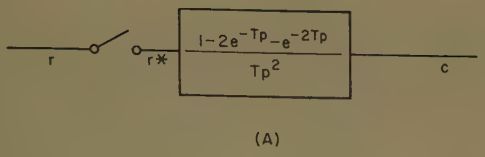


(A)

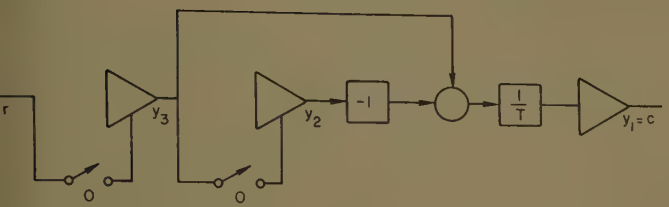


(B)

**Fig. 10. Linear interpolation device**

A—Conventional sampled-data system representation
B—New representation

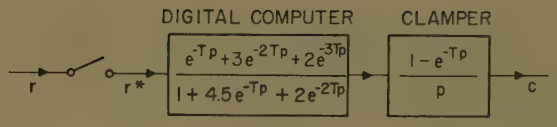


(A)

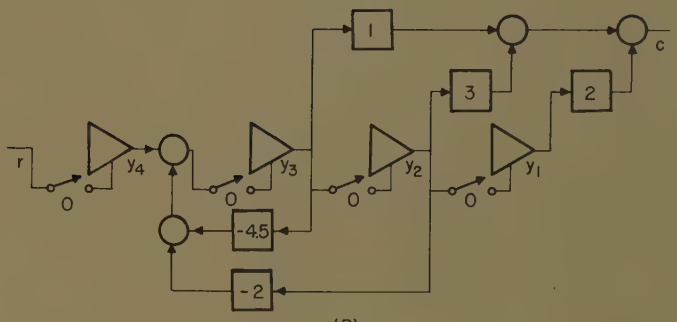


(B)

**Fig. 11. Digital computer and clamper**

A—Conventional sampled-data system representation
B—New representation

The new description, using the basic symbolism, is shown in Fig. 10(B). The variable $y_3$ is the sampled and clamped $c(t)$; $y_2$ is the sampled and clamped signal delayed by the period $T$; $y_1$ is $1/T\{r(nt)-r[(n-1)T]\}$ for $0<t-nT<T$; and therefore $y_1$ equals the desired $c(t)$ if $y_1(nT)=r[(n-1)T]$, which is the case if the system is initially at rest (say at $t=0$). The state vector formed by $y_1$, $y_2$, and $y_3$ completely describes the device. The variables are governed by the differential equations:

$$\dot{y}_1=-\frac{1}{T}y_2+\frac{1}{T}y_3$$

$$\dot{y}_2=0$$

$$\dot{y}_3=0$$

and the reset or transition equations:

$$y_1(nT+)=y_1(nT)$$
$$y_2(nT+)=y_3(nT)$$
$$y_3(nT+)=r(nT)$$

A somewhat more general example of a sampled-data system is the digital computer and clamper shown in the usual notation in Fig. 11(A) and in the new notation in Fig. 11(B). The sampled and clamped $r$ is given by the $y_4$ integrator while the digital computer program is accomplished in the remainder of the block diagram. Note that the digital computer transfer function is the same as equation 4 with $p^{-1}$ replaced by $\epsilon^{-Tp}$. For this reason, the diagram is analogous to the direct decomposition of Fig. 4. The only difference is the replacement of integrator inputs by reset operations. Other forms of decomposition are of course possible. Fig. 12 illustates the cascade decomposition analogous to Fig. 6. Other decompositions are also possible; for example, the sampling and clamping accomplished in $y_4$ could take place following the computer representation instead of preceding it. The equations for the state variables of Fig. 11(B) or Fig. 12 are easily written. For the Fig. 12 representation, the differential equations are:

$$\dot{y}_1=0$$

$$\dot{y}_2=0$$

$$\dot{y}_3=0$$

$$\dot{y}_4=0$$

and the reset or transition equations are:

$$y_1(nT+)=(1-0.5)y_2(nT)+(2-4)y_3(nT)+y_4(nT)$$

$$y_2(nT+)=-0.5y_2(nT)+(2-4)y_3(nT)+y_4(nT)$$

$$y_3(nT+)=-4y_3(nT)+y_4(nT)$$

$$y_4(nT+)=r(nT)$$

These transition equations have the same coefficients as the differential equations for the system of Fig. 6.

To represent the finite pulse-clamping operation defined in equation 1, both the switching and sampling operations are necessary. This is obvious from Fig. 13 where the 0–1 and the 1–2 interval equations for $e_c$ are:

$$e_c(t)=e(t),\ 0<t-nT\leq t_1$$
$$=y_1,\ t_1<t-nT\leq T$$

with $\dot{y}_1=0$ and

$$y_1(nT+)=y_1(nT)$$
$$y_1(nT+t_1+)=e(nT+t_1)$$

Time delay is a dynamic characteristic that can be represented when it occurs in a path containing sampling. As an example, suppose that a sampler and a clamper are followed by a time delay of $2T+t_1$, where $0<t_1<T$. The symbolic representation is shown in Fig. 14. Here $y_4$ is the sampled and clamped $r$ where it is assumed sampling occurs at $t=nT$. The $y_2$ and $y_3$ integrators provide a delay of $2T$ while the remaining delay $t_1$ occurs in the $y_1$ integrator.

This completes the symbolic description of components necessary to represent more complex systems such as the one in Fig. 2. As described earlier, this system

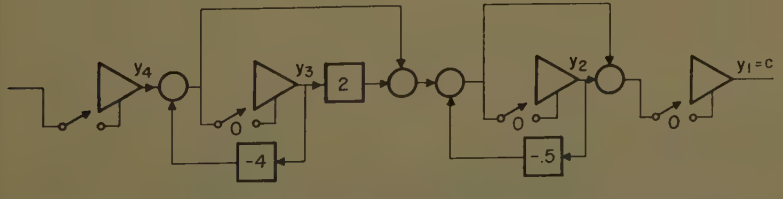


**Fig. 12. Alternative representation or digital computer and clamper**

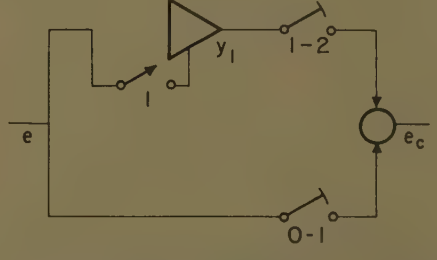


**Fig. 13. Symbolic representation of finite pulse clamping**

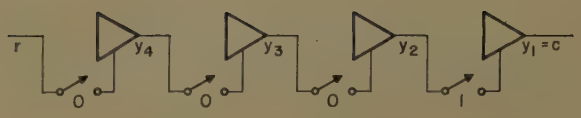


Fig. 14. Representation of a time delay

is a 3-interval 3-sample problem. The three intervals of the fundamental period are 0 to $t_1$, $t_1$ to $t_2$, and $t_2$ to $T$. The sampling occurs in the error pulse clamper at $nT+t_1$, and in the digital computer at $nT+t_2$ and $nT$. However, the sampling at $nT+t_2$ could equally well occur at $(n+1)T$ since the digital computer has constant input for $nT+t_1<t\leq(n+1)T$. This reduces the problem to a 2-interval 2-sample problem. One representation of the simplified system is shown in Fig. 15. Since there are seven state variables, two intervals, and two samples times, fourteen constant coefficient differential equations and fourteen transition equations must be written. The differential equations in interval 0–1 are:

$$\dot{y}_1=y_2$$

$$\dot{y}_2=-a_4y_2+K_1[a_3y_3+(a_2-b_2a_0)y_4+(a_1-b_1a_0)y_5+a_0y_6] \quad (7)$$

$$\dot{y}_3=\dot{y}_4=\dot{y}_5=\dot{y}_6=\dot{y}_7=0$$

and in interval 1–2 are:

$$\dot{y}_1=y_2$$

$$\dot{y}_2=-a_4y_2+K_2[a_3y_3+(a_2-b_2a_0)y_4+(a_1-b_1a_0)y_5+a_0y_6] \quad (8)$$

$$\dot{y}_3=\dot{y}_4=\dot{y}_5=\dot{y}_6=\dot{y}_7=0$$

The transition equations at $t=nT$ and $t=nT+t_1$ are:

$$y_1(nT+)=y_1(nT),\ y_1(nT+t_1+)=y_1(nT+t_1)$$

$$y_2(nT+)=y_2(nT),\ y_2(nT+t_1+)=y_2(nT+t_1)$$

$$y_3(nT+)=y_4(nT),\quad y_3(nT+t_1+)=y_3(nT+t_1)$$

$$y_4(nT+)=y_5(nT),\ y_4(nT+t_1+)=y_4(nT+t_1)$$

$$y_5(nT+)=y_6(nT)-b_1y_5(nT)-b_2y_4(nT),\quad y_5(nT+t_1+)=y_5(nT+t_1)$$

$$y_6(nT+)=y_7(nT),\ y_6(nT+t_1+)=y_6(nT+t_1)$$

$$y_7(nT+)=y_7(nT),\ y_7(nT+t_1+)=x_1(nT+t_1)-y_1(nT+t_1) \quad (9)$$

It is worthy to note that the 0–1 switch in the error pulse clamper is superfluous in this system since the sampler following operates at $t=nT$ only.

## Input Description

Up to now, input variables have been unspecified in functional form. For analysis, it will be useful to think of input quantities as additional state variables described by differential equations and, possibly, transition equations. For a deterministic input such as a step function, ramp function, general polynomial in $t$, exponential, sinusoid, or certain periodic functions, the formulation of the input state vector offers no particular difficulty. Fortunately, such inputs occur in many important response and synthesis problems. Methods for obtaining the input state variables will now be discussed.

Polynomial inputs are easily generated by the series of integrators shown in Fig. 16(A). Here:

$$\dot{x}_1=x_2$$
$$\dot{x}_2=x_3$$
$$\vdots$$
$$\dot{x}_{n-1}=x_n$$
$$\dot{x}_n=0$$

With the general set of initial conditions $x_1(0)$ $x_2(0)$, ..., $x_{n-1}(0)$, $x_n(0)$ any function of the type

$$x_1=r=r_0+r_1t+r_2t^2+\ldots+r_{n-1}t^{n-1},\ t>0$$

can be generated. Special cases are the step and ramp functions. Exponential functions are generated by the system represented in Fig. 16(B). Here:

$$\dot{x}_1=ax_1 \quad (10)$$

and with the initial condition $x_1(0)=1$,

$$x_1=r=\epsilon^{at},\ t>0 \quad (11)$$

Response to a cosine wave is obtained by setting $a=j\omega$ and taking the real part of the response. If desired, a sine and/or cosine function can be obtained from the system in Fig. 16(C). Here:

$$\dot{x}_1=\omega x_2$$
$$\dot{x}_2=-\omega x_1$$

and with the initial conditions $x_1(0)$ and $x_2(0)$:

$$r=x_1(0)\cos\omega t+x_2(0)\sin\omega t$$

Other functions that are similar or combinations of the above are readily obtained.

More general inputs are obtained using sampling and/or switching. As one example consider the symbolic diagram in Fig. 17 defining a 1-interval 1-sample system. The differential equations are:

$$\dot{x}_1=x_2$$
$$\dot{x}_2=0$$
$$\dot{x}_3=0$$

the transition equations are:

$$x_1(nT+)=x_3(nT)$$
$$x_2(nT+)=x_2(nT)$$
$$x_3(nT+)=x_3(nT)$$

and the initial conditions at $t=0$ are:

$$x_1(0)=0$$
$$x_2(0)=\frac{1}{T}$$

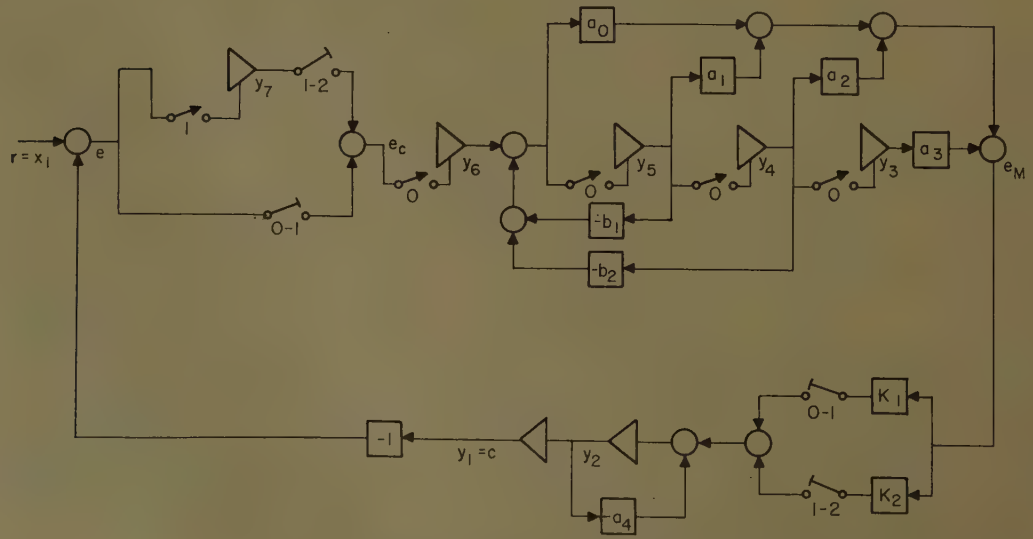


Fig. 15. The symbolic representation of feedback system example

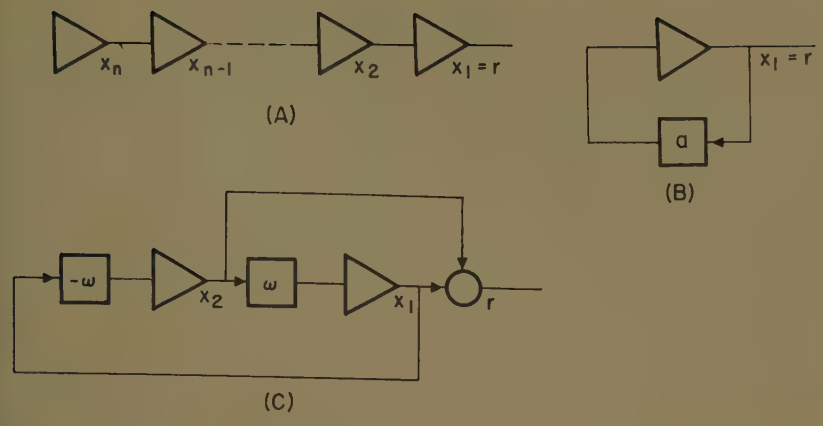


**Fig. 16. Input representation**

A—Polynomial B—Exponent C—Sinusoid

$x_3(0)=0$

For this system:

$$x_1=r=\frac{t-nT}{T},\ 0<t-nT\leq T,\ t>0$$

This is the equation for a sawtooth wave of unit amplitude and period $T$. Other periodic inputs, such as a square wave or parabolic wave, are obtainable through similar methods. These more general periodic inputs are limited in that their period or an integral multiple of it must equal the system fundamental period $T$. It is also possible to generate aperiodic functions of a more general class than defined.

## System Equations in Vector Form

By defining the input state vector in the described manner, it is now possible to state concisely equations governing system response. Assume that the system vector $\mathbf{y}$ has $k$ components $y_1, y_2, \ldots, y_k$ and that the input vector $\mathbf{x}$ has $m$ components $x_1, x_2, \ldots, x_m$. Furthermore, assume that the input and system has $N$ invariant intervals and $M$ sampling instants in the fundamental period $T$. If $\mathbf{w}$ is defined as the vector with the $m+k$ components $x_1, x_2, \ldots, x_m, y_1, y_2, \ldots, y_k$, the system is described by the $N$ vector differential equations:

$$\begin{aligned}\dot{\mathbf{w}}&=A_1\mathbf{w},\ 0<t-nT\leq t_1\\ \dot{\mathbf{w}}&=A_2\mathbf{w},\ t_1<t-nT\leq t_2\\ &\vdots\\ \dot{\mathbf{w}}&=A_N\mathbf{w},\ t_{N-1},<t-nT\leq T\end{aligned}\qquad(12)$$

and the $N$ vector transition equations:

$$\begin{aligned}\mathbf{w}(nT+)&=\bar{A}_0\mathbf{w}(nT)\\ \mathbf{w}(nT+t_1+)&=\bar{A}_1\mathbf{w}(nT+t_1)\\ &\vdots\\ \mathbf{w}(nT+t_{N-1}+)&=\bar{A}_{N-1}\mathbf{w}(nT+t_{N-1})\end{aligned}\qquad(13)$$

where $A_i$ and $\bar{A}_i$ are $(m+k)\times(m+k)$ matrices. $N-M$ of the matrices $\bar{A}_i$ are equal to the identity matrix $I$ while the remaining $M$ matrices $\bar{A}_i$ are not. Equations 12 and 13 and an initial condition on $\mathbf{w}$ at some time completely specifies the system response.

The matrices $A_i$ and $\bar{A}_i$ are easily obtained from the input and system state variable differential and transition equations. Consider the system in Fig. 15 forced by the exponential of Fig. 16(B). The differential and transition equations are given by 7, 8, 9, 10, and 11. From these the four necessary $8\times8$ matrices are:

$$A_1=\begin{array}{c}\begin{array}{cccccccc}x_1 & y_1 & y_2 & y_3 & y_4 & y_5 & y_6 & y_7\end{array}\\ \left\|\begin{array}{cccccccc}a & 0 & 0 & 0 & 0 & 0 & 0 & 0\\ 0 & 0 & 1 & 0 & 0 & 0 & 0 & 0\\ 0 & 0 & -a_4 & K_1a_3 & K_1(a_2-b_2a_0) & K_1(a_1-b_1a_0) & K_1a_0 & 0\\ 0 & 0 & 0 & 0 & 0 & 0 & 0 & 0\\ 0 & 0 & 0 & 0 & 0 & 0 & 0 & 0\\ 0 & 0 & 0 & 0 & 0 & 0 & 0 & 0\\ 0 & 0 & 0 & 0 & 0 & 0 & 0 & 0\\ 0 & 0 & 0 & 0 & 0 & 0 & 0 & 0\end{array}\right\|\end{array}\begin{array}{c}\dot{x}_1\\ \dot{y}_1\\ \dot{y}_2\\ \dot{y}_3\\ \dot{y}_4\\ \dot{y}_5\\ \dot{y}_6\\ \dot{y}_7\end{array}$$

$$A_2=\left\|\begin{array}{cccccccc}a & 0 & 0 & 0 & 0 & 0 & 0 & 0\\ 0 & 0 & 1 & 0 & 0 & 0 & 0 & 0\\ 0 & 0 & -a_4 & K_2a_3 & K_2(a_2-b_2a_0) & K_2(a_1-b_1a_0) & K_2a_0 & 0\\ 0 & 0 & 0 & 0 & 0 & 0 & 0 & 0\\ 0 & 0 & 0 & 0 & 0 & 0 & 0 & 0\\ 0 & 0 & 0 & 0 & 0 & 0 & 0 & 0\\ 0 & 0 & 0 & 0 & 0 & 0 & 0 & 0\\ 0 & 0 & 0 & 0 & 0 & 0 & 0 & 0\end{array}\right\|\qquad(14)$$

$$\bar{A}_0=\left\|\begin{array}{cccccccc}1 & 0 & 0 & 0 & 0 & 0 & 0 & 0\\ 0 & 1 & 0 & 0 & 0 & 0 & 0 & 0\\ 0 & 0 & 1 & 0 & 0 & 0 & 0 & 0\\ 0 & 0 & 0 & 0 & 1 & 0 & 0 & 0\\ 0 & 0 & 0 & 0 & 0 & 1 & 0 & 0\\ 0 & 0 & 0 & 0 & -b_2 & -b_1 & 1 & 0\\ 0 & 0 & 0 & 0 & 0 & 0 & 0 & 1\\ 0 & 0 & 0 & 0 & 0 & 0 & 0 & 1\end{array}\right\|$$

$$\bar{A}_1=\left\|\begin{array}{cccccccc}1 & 0 & 0 & 0 & 0 & 0 & 0 & 0\\ 0 & 1 & 0 & 0 & 0 & 0 & 0 & 0\\ 0 & 0 & 1 & 0 & 0 & 0 & 0 & 0\\ 0 & 0 & 0 & 1 & 0 & 0 & 0 & 0\\ 0 & 0 & 0 & 0 & 1 & 0 & 0 & 0\\ 0 & 0 & 0 & 0 & 0 & 1 & 0 & 0\\ 0 & 0 & 0 & 0 & 0 & 0 & 1 & 0\\ 1 & -1 & 0 & 0 & 0 & 0 & 0 & 0\end{array}\right\|$$

Above and to the right side of $A_1$ are the variables corresponding to the respective columns and rows of the matrix.

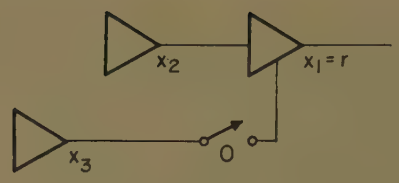


**Fig. 17. Sawtooth wave representation**

From this example, it is apparent that the matrices can be written by inspection of the system and input symbolic diagrams. A particular response problem is specified by an initial condition on $\mathbf{w}$. As an example, suppose that the system is initially at rest and the input $x_1=\epsilon^{at}$ is applied at $t=0$. Then

$$\mathbf{w}(0)=\left|\begin{array}{c}x_1(0)\\ y_1(0)\\ y_2(0)\\ y_3(0)\\ y_4(0)\\ y_5(0)\\ y_6(0)\\ y_7(0)\end{array}\right|=\left|\begin{array}{c}1\\ 0\\ 0\\ 0\\ 0\\ 0\\ 0\\ 0\end{array}\right|$$

In this example many of the matrix components are zero. Frequently, but not always, this is the case. However, the $i, j$ components of the $A$ and $\bar{A}$ matrices for $i=1$ to $m$ and $j=m+1$ to $m+k$ are always zero, since the output components $y_i$ cannot influence the input components $x_i$. This is seen by partitioning equations 12 and 13:

$$\left|\begin{array}{c}\dot{\mathbf{x}}\\ \dot{\mathbf{y}}\end{array}\right|=\left\|\begin{array}{cc}F_i & 0\\ G_i & S_i\end{array}\right\|\left|\begin{array}{c}\mathbf{x}\\ \mathbf{y}\end{array}\right|,\ i=1\text{ to }N\qquad(15)$$

$$\left|\begin{array}{c}\mathbf{x}(nT+t_i+)\\ \mathbf{y}(nT+t_i+)\end{array}\right|=\left\|\begin{array}{cc}\bar{F}_i & 0\\ \bar{G}_i & S_i\end{array}\right\|\left|\begin{array}{c}\mathbf{x}(nT+t_i)\\ \mathbf{y}(nT+t_i)\end{array}\right|$$

$i=0$ to $N-1$, $t_0=0$

The $m\times m$ matrices $F_i$ and $\bar{F}_i$ determine the input; the $k\times k$ matrices $S_i$ and $\bar{S}_i$ define the system dynamics; the $k\times m$ matrices $G_i$ and $\bar{G}_i$ are gain factors in-

dicating the effect of the input on the system; and 0 is an $m$x$k$ null matrix.

When the input cannot be expressed in components of an input state vector, separate system equations are desirable. From equation 15.

$$\dot{\mathbf{y}} = S_i\mathbf{y} + G_i\mathbf{x},\ i=1 \text{ to } N$$

$$\mathbf{y}(nT+t_i+) = \bar{S}_i\mathbf{y}(nT+t_i) + \bar{G}_i\mathbf{x}(nT+t_i),\ i=0 \text{ to } N-1 \quad (16)$$

where $\mathbf{x}$ is now a scalar input.

## System Response

### Basic Techniques

In the previous section an extensive class of periodic system response problems have been concisely formulated in the $2N$ differential and transition equations 12 and 13. The solution of these equations will now be obtained.

The basic procedure is to work from interval to interval piecing the solution together. Start at $t=nT$ where the solution, yet unknown, is $\mathbf{w}(nT)$. Application of the first transition equation gives:

$$\mathbf{w}(nT+) = \bar{A}_0\mathbf{w}(nT) \quad (17)$$

This serves as the initial condition on the first differential equation of 12 that defines the solution for $0<t-nT\leq t_1$. Thus the vector equation $d\mathbf{w}/dt = A_1\mathbf{w}$ must be solved with the initial condition $\mathbf{w}(nT+)$. This is conveniently accomplished by the Laplace transform. First define the new time scale $\tau = t-nT$ translating $t=nT$ into $\tau=0$. The problem is now stated:

$$\frac{d\mathbf{w}}{d\tau} = A_1\mathbf{w},\ \mathbf{w}(\tau)\big|_{\tau=0} = \mathbf{w}(nT+) \quad (18)$$

Using the notion $\bar{\mathbf{w}}(s) = L[\mathbf{w}(\tau)]$ to indicate the Laplace transform of $\mathbf{w}(\tau)$ with respect to $\tau$, the transform of equation 18 is:

$$s\bar{\mathbf{w}}(s) - \mathbf{w}(nT+) = A_1\bar{\mathbf{w}}(s) \quad (19)$$

Solving for $\bar{\mathbf{w}}$ and using the inverse Laplace transform gives:

$$\mathbf{w}(\tau) = L^{-1}[(sI-A_1)^{-1}]\mathbf{w}(nT+) \quad (20)$$

The matrix function $L^{-1}[(sI-A_1)^{-1}]$ deserves special notation: define the matrix time function:

$$\epsilon^{A_1\tau} = L^{-1}[(sI-A_1)^{-1}] \quad (21)$$

This function and methods for simplifying its computation are discussed in the Appendix. The solution for $0<t-nT\leq t_1$, is now completed by substituting for $\tau$ in equation 21, using equations 20 and 17. The result is:

$$\mathbf{w}(t) = \epsilon^{A_1(t-nT)}\bar{A}_0\mathbf{w}(nT),\ 0<t-nT\leq t_1 \quad (22)$$

A similar procedure is used in the second interval.

First:

$$\mathbf{w}(nT+t_1+) = \bar{A}_1\mathbf{w}(nT+t_1) \quad (23)$$

where $\mathbf{w}(nT+t_1)$ is obtained by evaluating equation 22 at $t=nT+t_1$. Defining another new time scale $\tau = t-(nT+t_1)$, the second equation of 12 becomes:

$$\frac{d\mathbf{w}}{d\tau} = A_2\mathbf{w},\ \mathbf{w}(\tau)\big|_{\tau=0} = \mathbf{w}(nT+t_1+) \quad (24)$$

Use of the Laplace transform, substitution for $\tau$, and use of equation 23 yields:

$$\mathbf{w}(t) = \epsilon^{A_2(t-nT-t_1)}\bar{A}_1\mathbf{w}(nT+t_1),\quad t_1<t-nT\leq t_2 \quad (25)$$

where

$$\epsilon^{A_2\tau} = L^{-1}[(sI-A_2)^{-1}] \quad (26)$$

Substituting in equation 25 for $w(nT+t_1)$ from equation 22 gives:

$$\mathbf{w}(t) = \epsilon^{A_2(t-nT-t_1)}\bar{A}_1\epsilon^{A_1t_1}\bar{A}_0\mathbf{w}(nT),\quad t_1<t-nT\leq t_2 \quad (27)$$

The solution for the remaining $N$-2 intervals of $0<t-nT\leq T$ is obtained in a similar manner.

The solution derived is expressed more concisely by defining the matrix time function:

$$\begin{aligned} W(\tau) &= \epsilon^{A_1\tau}\bar{A}_0,\ 0<\tau\leq t_1 \\ &\vdots \\ &= \epsilon^{A_i(\tau-t_{i-1})}\bar{A}_{i-1}\epsilon^{A_{i-1}(t_{i-1}-t_{i-2})}\cdots \\ &\qquad \bar{A}_0,\ t_{i-1}<\tau\leq t_i \quad (28) \\ &\vdots \\ &= \epsilon^{A_N(\tau-t_{N-1})}\bar{A}_{N-1}\cdots\bar{A}_0, \\ &\qquad t_{N-1}<\tau\leq t_N = T \end{aligned}$$

where of course

$$\epsilon^{A_i\tau} = L^{-1}[(sI-A_i)^{-1}] \quad (29)$$

If $M<N$, $W(\tau)$ is simpler in form since $N-M$ of the $\bar{A}_i$ equal the identity matrix. The solution $\mathbf{w}(t)$ is now easily written as:

$$\mathbf{w}(t) = W(t-nT)\mathbf{w}(nT),\ 0<t-nT\leq T \quad (30)$$

This is the equation for the solution interior to any fundamental interval.

The first step in obtaining the solution at multiples of $T$ is to evaluate equation 30 for $t=(n+1)T$ giving the vector difference equation:

$$\mathbf{w}[(n+1)T] = W(T)\mathbf{w}(nT) \quad (31)$$

Since this equation is valid for all $n$, start with $n=0$ and the known initial condition $\mathbf{w}(0)$. After $n$ applications of equation 31, it is found that:

$$\mathbf{w}(nT) = W^n\mathbf{w}(0) \quad (32)$$

where the notation $W=W(T)$ has been used. The problem of solving for $\mathbf{w}(nT)$ is now reduced to obtaining the $n$th power of $W$. This is accomplished by obtaining $\mathbf{w}^*(z)$, the $Z$-transform of $\mathbf{w}(t)$. Using equation 32, the $Z$-transform can of written:

$$\mathbf{w}^*(z) = \sum_{n=0}^{\infty}\mathbf{w}(nT)z^{-n} = \left[\sum_{n=0}^{\infty}W^nz^{-n}\right]\mathbf{w}(0) \quad (33)$$

where it is understood that $W^0=I$. But the bracketed infinite matrix series is recognized as the matrix function $[I-z^{-1}W]^{-1}$.[18] Thus:

$$\mathbf{w}^*(z) = [I-z^{-1}W]^{-1}\mathbf{w}(0) \quad (34)$$

is the closed form of the $Z$-transform. Application of the inverse $Z$-transform to equation 34 gives the desired values $\mathbf{w}(nT)$. Alternatively, the components of equation 34, ratios of polynomials in $z^{-1}$, can be divided out and the coefficient of $z^{-n}$ equated to the components of $\mathbf{w}(nT)$.

As an illustration of the method, consider the response of a first-order system to a suddenly applied sawtooth wave. The transfer function and input are defined by

$$\frac{c}{r} = \frac{1}{\frac{1}{a}p+1}$$

and

$$r=0,\ t<0$$

$$=\frac{1}{T}(t-nT),\ 0<t-nT\leq T$$

Initially the system is at rest so $c(0)=0$. Fig. 18 shows the symbolic representation of the input, identical to that of Fig. 17, and the system. By inspection of the diagram, the two required matrices:

$$A_1 = \begin{Vmatrix} 0 & 1 & 0 & 0 \\ 0 & 0 & 0 & 0 \\ 0 & 0 & 0 & 0 \\ a & 0 & 0 & -a \end{Vmatrix} \quad (35)$$

$$\bar{A}_0 = \begin{Vmatrix} 0 & 0 & 1 & 0 \\ 0 & 1 & 0 & 0 \\ 0 & 0 & 1 & 0 \\ 0 & 0 & 0 & 1 \end{Vmatrix}$$

are obtained. Since $N=M=1$, post-multiplying $e^{A_1t}$, which is evaluated in the Appendix, by $\bar{A}_0$ gives the desired:

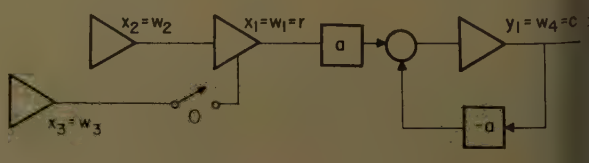


Fig. 18. Example of input and the system

$$W(\tau)=\begin{Vmatrix} 0 & \tau & 1 & 0 \\ 0 & 1 & 0 & 0 \\ 0 & 0 & 1 & 0 \\ 0 & \tau-\frac{1}{a}(1-\epsilon^{-a\tau}) & (1-\epsilon^{-a\tau}) & \epsilon^{-a\tau} \end{Vmatrix} \tag{36}$$

Evaluating equation 36 for $\tau=T$, $\mathbf{w}^*(z)$ is readily obtained from equation 34 using the initial condition:

$$\mathbf{w}(0)=\begin{vmatrix} x_1(0) \\ x_2(0) \\ x_3(0) \\ y_1(0) \end{vmatrix}=\begin{vmatrix} 0 \\ \frac{1}{T} \\ 0 \\ 0 \end{vmatrix} \tag{37}$$

Because of the zero components in $\mathbf{w}(0)$, only the second columns of $(I-z^{-1}W)^{-1}$ need be computed. Multiplication of this second column by $1/T$ then gives

$$\mathbf{w}^*(z)=\begin{vmatrix} \frac{z^{-1}}{1-z^{-1}} \\ \frac{\frac{1}{T}}{1-z^{-1}} \\ 0 \\ \frac{\left[1-\frac{1}{Ta}(1-\epsilon^{-aT})\right]z^{-1}}{(1-z^{-1})(1-\epsilon^{-aT}z^{-1})} \end{vmatrix} \tag{38}$$

Evaluating the inverse $Z$-transform of each component at $t=nT$ yields the desired solution:

$$\mathbf{w}(nT)=\begin{vmatrix} u(nT-T) \\ \frac{1}{T}\,u(nT) \\ 0 \\ u(nT)\left(\frac{1}{1-\epsilon^{-aT}}-\frac{1}{aT}\right)(1-\epsilon^{-anT}) \end{vmatrix} \tag{39}$$

where the step function $u(t)$ is zero for $t<0$ and unity for $t\geq 0$. The first three components, $x_1(nT)$, $x_2(nT)$, and $x_3(nT)$, obviously agree with specified input state vector. System response is given by the fourth component, $w_4(nT)=y_1(nT)=c(nT)$. From equations 30 and 39 the response $w_4(t)=c(t)$ for $t>0$ is:

$$c(t)=\frac{t-nT}{T}-\frac{1}{aT}+\left[\frac{1}{aT}+\left(\frac{1}{1-\epsilon^{-aT}}-\frac{1}{aT}\right)(1-\epsilon^{-anT})\right]\epsilon^{-a(t-nT)},\quad 0<t-nT\leq T \tag{40}$$

Note that the input and output values $x_2(nT)$ and $y_1(nT)$ were needed to obtain equation 40.

### Detailed Solution for N=M=2

The general method just presented has the advantage of notational simplicity. A more detailed form of the solution with some computational advantage can be obtained using the partitioned equations 15. Unfortunately, equations are excessively long and burdensome to derive if $N$ is large. For this reason only the $N=M=2$ case will be considered here. The solution for higher $N$ and $M$ would proceed in a similar manner. Actually many problems fall into $N=M=2$ class.

To obtain the desired solution, it is necessary to express $e^{A_i\tau}$ and $W(\tau)$ in partitioned form. From equations 29 and 15:

$$\epsilon^{A_i\tau}=L^{-1}\left[\begin{Vmatrix} (sI-F_i) & 0 \\ -G_i & (sI-S_i) \end{Vmatrix}^{-1}\right]$$

$$=L^{-1}\left[\begin{Vmatrix} (sI-F_i)^{-1} & 0 \\ (sI-S_i)^{-1}G_i(sI-F_i)^{-1} & (sI-S_i)^{-1} \end{Vmatrix}\right] \tag{41}$$

This is expressed more simply as:

$$\epsilon^{A_i\tau}=\begin{Vmatrix} \epsilon^{F_i\tau} & 0 \\ G_i(\tau) & \epsilon^{S_i\tau} \end{Vmatrix} \tag{42}$$

by defining

$$\epsilon^{F_i\tau}=L^{-1}[(sI-F_i)^{-1}]$$

$$\epsilon^{S_i\tau}=L^{-1}[(sI-S_i)^{-1}]$$

$$G_i(\tau)=L^{-1}[(sI-S_i)^{-1}G_i(sI-F_i)^{-1}] \tag{43}$$

where $i=1$ and 2. Substituting equation 42 and the partitioned transition matrices of 15, equation 28 then gives:

$$W(\tau)=\begin{Vmatrix} X(\tau) & 0 \\ G(\tau) & Y(\tau) \end{Vmatrix} \tag{44}$$

where

$$X(\tau)=\epsilon^{F_1\tau}\bar{F}_0,\ 0<\tau\leq t_1$$

$$=\epsilon^{F_2(\tau-t_1)}\bar{F}_1\epsilon^{F_1t_1}\bar{F}_0,\ t_1<\tau\leq T$$

$$Y(\tau)=\epsilon^{S_1\tau}\bar{S}_0,\ 0<\tau\leq t_1$$

$$=\epsilon^{S_2(\tau-t_1)}\bar{S}_1\epsilon^{S_1t_1}\bar{S}_0,\ t_1<\tau\leq T$$

$$G(\tau)=G_1(\tau)\bar{F}_0+\epsilon^{S_1\tau}\bar{G}_0,\ 0<\tau\leq t_1 \tag{45}$$

$$=[G_2(\tau-t_1)\bar{F}_1+\epsilon^{S_2(\tau-t_1)}\bar{G}_1]\epsilon^{F_1t_1}\bar{F}_0+\epsilon^{S_2(\tau-t_1)}\bar{S}_1[G_1(t_1)\bar{F}_0+\epsilon^{S_1t_1}\bar{G}_0],\ t_1<\tau\leq T$$

The solution for $t=nT$ is obtained by the $Z$-transform as before. By defining $X=X(T)$, $Y=Y(T)$, and $G=G(T)$, equation 34 becomes

$$\mathbf{w}^*(z)=\begin{vmatrix} \mathbf{x}^*(z) \\ \mathbf{y}^*(z) \end{vmatrix}=\begin{Vmatrix} (I-z^{-1}X) & 0 \\ -z^{-1}G & (I-z^{-1}Y) \end{Vmatrix}^{-1}\begin{vmatrix} \mathbf{x}(0) \\ \mathbf{y}(0) \end{vmatrix}$$

$$=\begin{Vmatrix} (I-z^{-1}X)^{-1} & 0 \\ z^{-1}(I-z^{-1}Y)^{-1}G(I-z^{-1}X)^{-1} & (I-z^{-1}Y)^{-1} \end{Vmatrix}\begin{vmatrix} \mathbf{x}(0) \\ \mathbf{y}(0) \end{vmatrix} \tag{46}$$

From this

$$\mathbf{y}^*(z)=z^{-1}(I-z^{-1}Y)^{-1}G\mathbf{x}^*(z)+(I-z^{-1}Y)^{-1}\mathbf{y}(0) \tag{47}$$

where

$$\mathbf{x}^*(z)=(I-z^{-1}X)^{-1}\mathbf{x}(0) \tag{48}$$

The forced part of the solution 47 is the first term; the part of the solution due to an initial $\mathbf{y}(0)$ is the second term, obviously zero for a system initially at rest. This equation for $\mathbf{y}^*(z)$ is correct in form for any $N$ and $M$. Higher $N$ and $M$ only result in increased complexity of the equations analogous to equation 45.

After $\mathbf{y}(nT)$ is obtained from equation 47 by the inverse $Z$-transform or component division, equations 30 and 44 can be used to write:

$$\mathbf{y}(t)=Y(t-nT)\mathbf{y}(nT)+G(t-nT)\mathbf{x}(nT),\quad 0<t-nT\leq T \tag{49}$$

Note that the input vector at $t=nT$ is required.

The complete solution described by equations 47, 48, and 49 is simple in form. For complicated systems, determination of $X(\tau)$, $Y(\tau)$, $G(\tau)$, and the $Z$-transforms may be lengthy, but the work is straightforward and systematic. To illustrate the method and allow comparison with other methods, when other methods apply, several examples will now be discussed.

## Examples

### Example I

Fig. 19 shows the symbolic representation for a sampled-data feedback system where the sampled error is clamped and fed into the transfer function $G(p)=K/p(p+a)$. This is an $N=M=1$ system and the results for the $N=M=2$ system apply by taking $t_1=T$ and $\bar{S}_1=I$. The system matrices are:

$$S_1=\begin{Vmatrix} 0 & 1 & 0 \\ 0 & -a & K \\ 0 & 0 & 0 \end{Vmatrix} \tag{50}$$

$$\bar{S}_0=\begin{Vmatrix} 1 & 0 & 0 \\ 0 & 1 & 0 \\ -1 & 0 & 0 \end{Vmatrix}$$

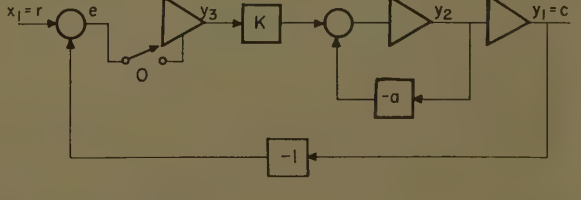


Fig. 19. Sampled-data system example

Now

$$\epsilon^{S_1\tau}=\left\|\begin{matrix}1 & \frac{1}{a}(1-\epsilon^{-a\tau}) & \frac{K}{a}\left[\tau-\frac{1}{a}(1-e^{-a\tau})\right]\\ 0 & \epsilon^{-a\tau} & \frac{K}{a}(1-\epsilon^{-a\tau})\\ 0 & 0 & 1\end{matrix}\right\| \tag{51}$$

and thus

$$Y=Y(T)=\epsilon^{S_1T}\bar{S}_0=\left\|\begin{matrix}\left\{1-\frac{K}{a}\left[T-\frac{1}{a}(1-\epsilon^{-aT})\right]\right\} & \frac{1}{a}(1-\epsilon^{-aT}) & 0\\ -\frac{K}{a}(1-\epsilon^{-aT}) & \epsilon^{-aT} & 0\\ -1 & 0 & 0\end{matrix}\right\| \tag{52}$$

Since $t_1=T$, equation 45 shows that $G=G(T)=G_1(T)+\epsilon^{S_1T}\bar{G}_0$ for $\bar{F}_0=I$. But $G_1=0$ and

$$\bar{G}_0=\left|\begin{matrix}0\\0\\1\end{matrix}\right| \tag{53}$$

Thus:

$$G=\left|\begin{matrix}\frac{K}{a}\left[T-\frac{1}{a}(1-\epsilon^{-aT})\right]\\ \frac{K}{a}(1-\epsilon^{-aT})\\ 1\end{matrix}\right| \tag{54}$$

In this case $G$ is the same for any input, so for all $r^*(z)=x_1^*(z)$, $\mathbf{y}^*(z)=z^{-1}(I-z^{-1}Y)^{-1}Gx_1^*(z)$ where it is assumed that system is initially at rest. Computation of the component $y_1^*=c^*(z)$ gives:

$$c^*(z)=\frac{K}{a^2}\frac{\{(aT-1+\epsilon^{-aT})z^{-1}+[1-(aT+1)\epsilon^{-aT}]z^{-2}\}r^*(z)}{1-\left[1-\frac{K}{a^2}(aT-1)+\left(1-\frac{K}{a^2}\right)\epsilon^{-aT}\right]z^{-1}+\left[\frac{K}{a^2}+\left(1-\frac{K}{a^2}-\frac{KT}{a}\right)\epsilon^{-aT}\right]z^{-2}} \tag{55}$$

a result easily checked with the conventional $Z$-transform theory of sampled-data systems. In the matrix method, manipulation is somewhat more complicated but not excessively so. The solution between samples, conventionally handled by the modified $Z$-transform, is given by equation 49.

## Example 2

Next consider a finite pulsed system analyzed by Farmanfarma.[8] In this system the plant input is $e=r-c$ for $0<t-n<0.6$ and zero for $0.6<t-n<1$. The plant transfer function is $G(p)=6/p(p+5)$. Fig. 20 shows the symbolic diagram for the system and input when $r=x_1=\epsilon^{at}$. Since in this case $N=2$ and $M=0$, $\bar{S}_0=\bar{S}_1=\bar{F}_0=\bar{F}_1=I$ and $\bar{G}_0=\bar{G}_1=0$. By inspection:

$$S_1=\left\|\begin{matrix}0 & 1\\ -6 & -5\end{matrix}\right\|,\quad G_1=\left|\begin{matrix}0\\6\end{matrix}\right|$$

$$S_2=\left\|\begin{matrix}0 & 1\\ 0 & -5\end{matrix}\right\|,\quad G_2=\left|\begin{matrix}0\\0\end{matrix}\right| \tag{56}$$

From equations 10 and 11, desired input is obtained when $F_1=F_2=a$. After obtaining $\epsilon^{A_1\tau}$ and $\epsilon^{A_2\tau}$ and computing $Y=\epsilon^{A_1 0.4}\epsilon^{A_2 0.6}$, it is possible to find.

$$(I-z^{-1}Y)^{-1}=\left\|\begin{matrix}\frac{1+0.0144z^{-1}}{1-0.417z^{-1}+0.0067z^{-2}} & \frac{0.1175z^{-1}}{1-0.417z^{-1}+0.0067z^{-2}}\\ (\quad) & (\quad)\end{matrix}\right\| \tag{57}$$

Only $y_1^*(z)=c^*(z)$ is of interest so the second row is not computed.

If stability is the only question, only the denominator of each component, equal to the $\det(I-z^{-1}Y)$, need be computed. In this case the system is stable since both the $z$ roots are within the unit circle. Bertram and Kalman in a discussion of Farmanfarma's paper[8] discussed this method of stability determination.

To continue with the response problem, $G$ is obtained from equation 45, which in this case is the simpler form:

$$G(\tau)=\epsilon^{S_2(\tau-t_1)}G_1(t_1)$$

where

$$G_1(\tau)=L^{-1}\left[(sI-S_1)^{-1}G_1\frac{1}{s-a}\right]$$

Carrying out the computation for $G=G(1)$,

$$G=\frac{1}{\left(\frac{a}{2}+1\right)\left(\frac{a}{3}+1\right)}\left|\begin{matrix}-0.1175a-0.432+(1+0.173a)\epsilon^{0.6a}\\ 0.0144a-0.1104+0.1353a\epsilon^{0.6\tau}\end{matrix}\right| \tag{58}$$

In this case, $G$ depends on the input indicating the greater complexity of finite pulsed systems as compared with sampled-data systems.

Assuming the system is initially at rest,

$$y_1^*(z)=c^*(z)=\frac{[-0.1175a-0.432+(1+0.173a)\epsilon^{0.6a}]z^{-1}+[0.0067+(0.0144+0.0184a)\epsilon^{0.6a}]z^{-2}}{\left(\frac{a}{2}+1\right)\left(\frac{a}{3}+1\right)(1-0.417z^{-1}+0.0067z^{-2})(1-\epsilon^{a}z^{-1})} \tag{59}$$

is obtained from equation 47. Setting $a=0$ and dividing out the polynomial gives $c(n)$ values that check with Farmanfarma's Fig. 10.[8]

## Example 3

As a final example consider the finite pulse-clamped system shown in Fig. 21. Take $T=1$ so that the plant receives the actual error for $0<t-n\leq t_1$, and the $t_1$ clamped error for $t_1<t-n<1$, where the plant has the transfer function $G(p)=2/p$. The initial conditions $x_1(0)=1$, and $y_1(0)=y_2(0)=0$ specify a step-response problem.

By inspection:

$$S_1=\left\|\begin{matrix}-2 & 0\\ 0 & 0\end{matrix}\right\|,\quad \bar{S}_0=\left\|\begin{matrix}1 & 0\\ 0 & 1\end{matrix}\right\|$$

$$S_2=\left\|\begin{matrix}0 & 2\\ 0 & 0\end{matrix}\right\|,\quad \bar{S}_1=\left\|\begin{matrix}1 & 0\\ -1 & 0\end{matrix}\right\| \tag{60}$$

$$G_1=\left|\begin{matrix}2\\0\end{matrix}\right|,\quad \bar{G}_0=\left|\begin{matrix}0\\0\end{matrix}\right|$$

$$G_2=\left|\begin{matrix}0\\0\end{matrix}\right|,\quad \bar{G}_1=\left|\begin{matrix}0\\1\end{matrix}\right|$$

$$F_1=F_2=0,\quad \bar{F}_0=\bar{F}_1=1$$

After $\epsilon^{A_1\tau}$ and $\epsilon^{A_2\tau}$ are obtained,

$$Y=\epsilon^{A_2(1-t_1)}\bar{A}_1\epsilon^{A_1t_1}A_0=\left\|\begin{matrix}\epsilon^{-2t_1}(2t_1-1) & 0\\ -\epsilon^{-2t_1} & 0\end{matrix}\right\| \tag{61}$$

is readily found. Then:

$$(I-z^{-1}Y)^{-1}=\left\|\begin{matrix}\frac{1}{1-\epsilon^{-2t_1}(2t_1-1)z^{-1}} & 0\\ \frac{-\epsilon^{-2t_1}z^{-1}}{1-\epsilon^{-2t_1}(2t_1-1)z^{-1}} & 1\end{matrix}\right\| \tag{62}$$

Stability is determined by the component denominators. In this case the system is stable for all $t_1$ except $t_1=0$, where neutral stability exists.

By equations 45 and 60,

$$G=G(1)=\epsilon^{S_2(1-t_1)}\bar{G}_1+\epsilon^{S_2(1-t_1)}\bar{S}_1G_1(t_1) \tag{63}$$

where by equation 43

$$G_1(\tau)=L^{-1}\left[\left\|\begin{matrix}\frac{1}{s+2} & 0\\ 0 & \frac{1}{s}\end{matrix}\right\|\left\|\begin{matrix}2\\0\end{matrix}\right|\frac{1}{s}\right] \tag{64}$$

Carrying out the indicated operations:

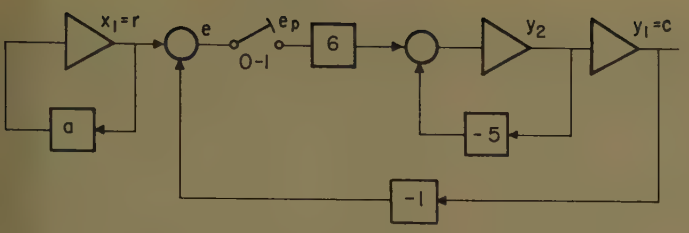


Fig. 20 (above). Finite pulsed system example

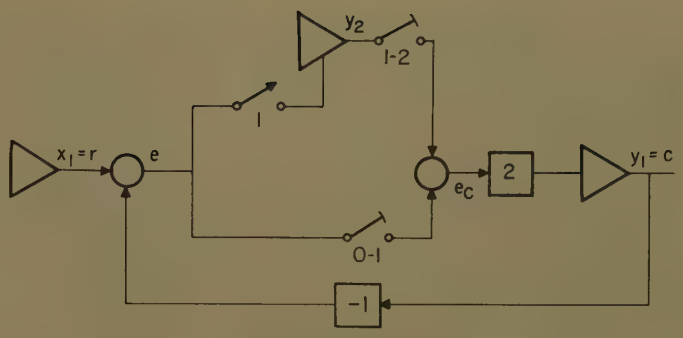


Fig. 21 (right). Finite-pulse clamped-system example

$$G=\begin{vmatrix}1-(2t_1-1)\epsilon^{-2t_1} \\ \epsilon^{-2t_1}\end{vmatrix} \quad (65)$$

Substituting in equation 47 from 62 and 65, the component $y_1^*(z)=c^*(z)$ is given by:

$$y_1^*(z)=c^*(z)=\frac{[1-(2t_1-1)\epsilon^{-2t_1}]z^{-1}}{[1-(2t_1-1)\epsilon^{-2t_1}z^{-1}](1-z^{-1})} \quad (66)$$

This result reduces to the sampled-data case when $t_1=0$ and the continuous case when $t_1=1$. Applications of the final value theorem shows that $c(\infty)=1$ as expected. The system has dead-beat response for $t_1=1/2$. More complicated examples of finite pulse-clamped systems are analyzed in a similar way.

## Conclusions

This paper presents methods of symbolic representation and analysis applicable to an extensive class of periodic linear systems. The symbolic representations are easily obtained and lead directly to a concise mathematical formulation in terms of a state vector representing both the input and system variables. System response at multiples of the fundamental period, obtained by $Z$-transform methods, is presented in a concise vector matrix notation. The usual $Z$-transform methods for stability prediction and final value determination apply. Response interior to the fundamental periods is readily obtained using time matrices and the solution at multiples of the fundamental period.

## Appendix

The matrix time function

$$\epsilon^{A\tau}=L^{-1}[(sI-A)^{-1}] \quad (67)$$

results naturally from the vector differential equation and initial condition

$$\frac{d\mathbf{w}}{d\tau}=A\mathbf{w},\ \mathbf{w}(0) \quad (68)$$

This is obvious from the Laplace transform of equation 68 which gives:

$$\bar{\mathbf{w}}(s)=(sI-A)^{-1}\mathbf{w}(0) \quad (69)$$

The computation of $\epsilon^{A\tau}$ by equation 67 is perfectly straightforward but may become lengthy if the matrix order $Q$ is high. One difficulty is the rapidly increasing complexity of matrix inversion with increasing $Q$; another problem is that the $(sI-A)^{-1}$ components, in general $Q-1$ order polynomials in $s$ divided by $Q$ order polynomials in $s$, rapidly increase in number and complexity with increasing $Q$. However, there are frequently many zero entries in the $A$ matrix. As a result, matrix inversion is less complex than expected. Also, $(sI-A)^{-1}$ typically has many components that are zero or simple in form.

In most cases the computation of $\epsilon^{A\tau}$ is greatly simplified by relating the components of $\epsilon^{A\tau}$ to the symbolic diagram. To see this, write:

$$\mathbf{w}(\tau)=\epsilon^{A\tau}\mathbf{w}(0) \quad (70)$$

obtained by applying the inverse Laplace transform to equation 69 and using equation 67. Assume that the $j$th component of $\mathbf{w}(0)$ is one and that all other components of $\mathbf{w}(0)$ are zero. Then by equation 70, the $i$th component of $\mathbf{w}(\tau)$ is the $i, j$ component of $\epsilon^{A\tau}$. In terms of the symbolic diagram, the $i, j$ component of $\epsilon^{A\tau}$ is the $i$th integrator output for unit initial condition on the $j$th integrator and zero initial condition on all other integrators. This interpretation of $\epsilon^{A\tau}$ immediately gives all the components of $\epsilon^{A\tau}$ which are zero and frequently allows simple evaluation of the remaining nonzero components.

To illustrate, consider the system in Fig. 18. Since $\epsilon^{A\tau}$ describes the system between sample intervals, neglect the sample switch. Consider first-unit initial value on $w_1$. By inspection of Fig. 18 $i$, 1 components, forming the first column of $\epsilon^{A\tau}$, are 1, 0, 0, and $1-\epsilon^{A\tau}$. For unit initial value on $w_2$, the $i$, 2 components forming the second column of $\epsilon^{A\tau}$ are $\tau$, 1, 0, and $\tau-1/a\ (1-\epsilon^{-a\tau})$. The other columns are obtained similarly. Thus:

$$\epsilon^{A\tau}=\begin{Vmatrix}1 & \tau & 0 & 0 \\ 0 & 1 & 0 & 0 \\ 0 & 0 & 1 & 0 \\ 1-\epsilon^{-a\tau} & \tau-\frac{1}{a}(1-\epsilon^{-a\tau}) & 0 & \epsilon^{-a\tau}\end{Vmatrix} \quad (71)$$

In more complicated systems, any component of $(sI-A)^{-1}$ can be obtained from the symbolic block diagram using the same basic idea. Thus the $i, j$ component to $(sI-A)^{-1}$ is the transfer function relating the $i$th integrator output to an artificial input summed in directly at the $j$th integrator output. This is made clear in Fig. 22 for the system of Fig. 4. Here the $i$, 2 components of $(sI-A)^{-1}$ are the transfer functions relating $y_i$ to the artificial input $u_2$. For example, the 3, 2 component of $(sI-A)^{-1}$ is the transfer function:

$$\frac{-2s}{s^2+4.5s+2}$$

relating $y_3$ to $u_2$.

Another method, particularly useful in approximation, is to use the infinite series representation of $\epsilon^{A\tau}$. By substitution into equations 70 and 68, it is easily shown that the infinite matrix series:

$$\epsilon^{A\tau}=I+A\tau+A^2\frac{\tau^2}{2!}+A^3\frac{\tau^3}{3!}+\ldots \quad (72)$$

is valid. When $\tau$ is small, two or three terms of this series yield a good approximation to the desired function.

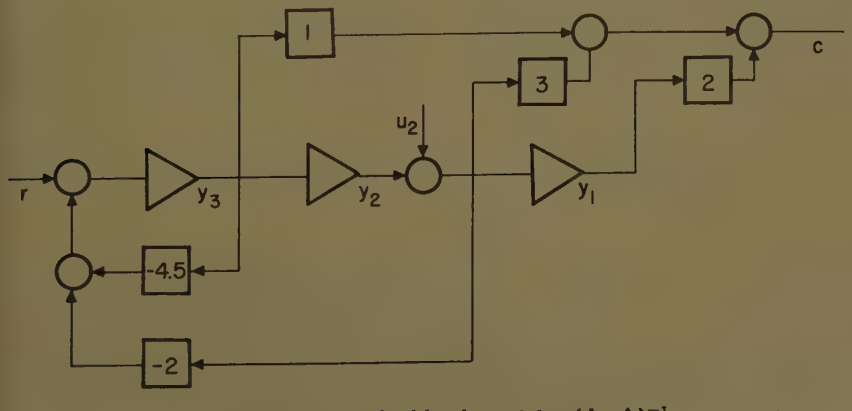


Fig. 22. Symbolic diagram method for determining $(sI-A)^{-1}$ components

## References

1. Sampled-Data Control Systems (book), **John R. Ragazzini, Gene F. Franklin.** McGraw-Hill Book Company, Inc., New York, N. Y., 1958.

2. Sampled-Data Control Systems (book), **Eliahu I. Jury.** John Wiley & Sons, Inc., New York, N. Y., 1958.

3. Digital and Sampled-Data Control Systems (book), **Julius T. Tou.** McGraw-Hill Book Company, Inc., 1959.

4. Bibliography of Sampled-Data Control Systems and Z-Transform Applications, **H. Freeman, O. Lowenchuss.** *Transactions*, Professional Group on Automatic Control, Institute of Radio Engineers, New York, N. Y., vol. PGAC-4, Mar. 1958.

5. Analysis of Cyclic-Rate Sampled-Data Feedback-Control Systems, **R. E. Hufnagel.** *AIEE Transactions*, pt. II (*Applications and Industry*), vol. 77, Nov. 1958, pp. 421–25.

6. Analysis of Linear Sampled-Data Systems with Finite Pulse Width: Open Loop, **G. Farmanfarma.** *Ibid.*, pt. I (*Communication and Electronics*), vol. 75, 1956 (Jan. 1957 section), pp. 808–19.

7. Analysis of Multiple Sampler Systems with Finite Pulse Width, Open Loop, **G. Farmanfarma.** *Ibid.*, pt. II (*Applications and Industry*), vol. 77, Mar. 1958, pp. 20–28.

8. General Analysis and Stability Study of Finite Pulsed Feedback Systems, **G. Farmanfarma.** *Ibid.*, July, pp. 148–62.

9. Additional Techniques for Sampled-Data Feedback Problems, **G. M. Kranc.** *Wescon Convention Record*, Institute of Radio Engineers, pt. 4, 1957, pp. 157–65.

10. Closed-Loop Analysis of Sampled-Data Systems with Appreciable Pulse Width, **Gordon J. Murphy, Harold B. Kennedy.** *AIEE Transactions*, pt. II (*Applications and Industry*), vol. 77, 1958 (Jan. 1959 section), pp. 659–65.

11. A Theoretical Study of Linear Dynamic Systems with Periodic, Piecewise Constant Parameters, **Edward O. Gilbert.** *Ph.D. Dissertation*, University of Michigan, Ann Arbor, Mich., Jan. 1957.

12. Four Methods for the Analysis of Time-Variable Circuits, **L. A. Pipes.** *Transactions*, Professional Group on Circuit Theory, Institute of Radio Engineers, vol. PGCT-2, no. 1, Mar. 1955 pp. 4–12.

13. Steady-State Transmission Through Networks Containing Periodically Operated Switches, **W. R. Bennett.** *Ibid.*, pp. 17–21.

14. Transmission Through a Linear Network Containing a Periodically Operated Switch, **C. A. Desoer.** *Wescon Convention Record*, Institute of Radio Engineers, pt. 2, 1958, pp. 34–41.

15. General Synthesis for Computer Control of Single-Loop and Multiloop Linear Systems (An Optimal Sampling System), **R. E. Kalman, J. E. Bertram.** *AIEE Transactions*, pt. II (*Applications and Industry*), vol. 77, 1958 (Jan. 1959 section), pp. 602–09.

16. The Effect of Quantization in Sampled-Feedback Systems, **J. E Bertram.** *Ibid.*, Sept. 1958, pp. 177–82.

17. The A-Matrix, New Network Description, **T. R. Bashkow.** *Transactions*, Professional Group on Circuit Theory, Institute of Radio Engineers, vol. PGCT-4, no. 3, Sept. 1957, pp. 117–19.

18. The Theory of Matrices (book), **C. C. MacDuffee.** Chelsea Publishing Company, New York, N. Y., 1946.


## Discussion

**E. I. Jury** (University of California, Berkeley, Calif.): The author is to be commended for the general analysis of a large class of periodic feedback systems in a unified symbolic representation. This form of representation is very useful in interpreting the steps of the mathematical formulation and is, in some cases, useful in the simulation studies of these systems. Among the important classes this method describes is the case of periodically varying parameters. This includes the category of gain, time constants, pulse duration or the sampling period, and periodic variations. This category is among the topics of recent investigation in this field and this paper appears timely and illuminating.

The analytical solution of the problem is generally based on two steps: 1. the formulation of the difference equations which describe the systems, and 2. the stability study and solutions of these equations for certain periodic or aperiodic inputs or disturbances. For the class of systems mentioned, the difference equations are generally linear with periodic coefficients and, for simpler cases, with constant coefficients.

To obtain the difference equations for these systems, the author has made use of the state vector[1] concept; however, at this point it might be well to mention that one can also arrive at this step by simple manipulation of the $p$-transform and $Z$-transform methods or by writing the difference equations in time domain if the transfer function is given (or can be easily obtained) in terms of differential equations.[2] For the solution of these difference equations, there also exist several methods, among them the $Z$-transform[3] method and the matrix form,[4] or a combination of both, as used by the author. The choice among the several methods of formulation and solution depends on the problem and on ease and convenience of arriving at the required results. However, the labor involved is more or less equal among the several methods.

I have recently proposed in a paper written with T. Nishimura the analysis of finite pulsed feedback systems with periodically varying sampling rate and pulse width. Fig. 23 illustrates the basic concepts involved in this problem. Although this case was not treated by the author, the method of the paper is applicable, for it falls under the general category $(N, M)$ with $M=0$ for this case. Our method of approach, based on the $p$-transform and $Z$-transform methods known for the conventional cases, is quite different from the method of the paper, indicating an alternate approach to analysis of the general class of $(N, M)$ systems. It might be indicated that for the simpler cases of linear sampled-data systems, the basic $Z$-transform or $p$-transform methods are easily applicable without having to use the general method of the paper. However, it is for larger values of $(N, M)$ that this method becomes more effective and useful.

Furthermore, it is worthwhile to mention that the class of systems having piecewise constant-varying sampling rate[5] shown in Fig. 24, can also be solved by minor extension of this paper's method. Further work on investigating the various sampling schemes as well as the synthesis procedure that could be tackled with this method is indeed warranted.

In conclusion, this paper represents a useful contribution to the growing area of the field and the symbolic method introduced will undoubtedly enhance the methods and techniques available for the formulation and analysis of the general class of linear periodic feedback systems.


### References

1. A Unified Approach to the Theory of Sampling Systems, **R. E. Kalman, J. E. Bertram.** *Journal*, Franklin Institute, Philadelphia, Pa., vol. 267, no. 5, May 1959, pp. 405–36.

2. The Analysis of Sampled-Data Control Systems with a Periodically Time Varying Sampling Rate, **E. I Jury, F. J. Mullin.** *Transactions*, Professional Group on Automatic Control, Institute of Radio Engineers, New York, N. Y., vol. PGAC-4, no. 1, May 1959.

3. A Note on the Operational Solution of Linear Difference Equations, **E. I. Jury, F. J. Mullin.** *Journal*, Franklin Institute, vol. 266, no. 3, Sept. 1958.

4. Theory of Time Varying Sampled-Data Systems, **B. Friedland.** *Technical Report T-19/B*, Electronics Research Laboratory, Columbia University, New York, N. Y., Apr. 1957.

5. Analysis of Aperiodically-Sampled-Data Feedback Control Systems, **R. E. Hufnagel.** *Ph.D. Dissertation*, Cornell University, Ithaca, N. Y., June 1959.


**Julius T. Tou** (Purdue University, Lafayette, Ind.): Dr. Gilbert is to be commended for his valuable contribution to the literature of

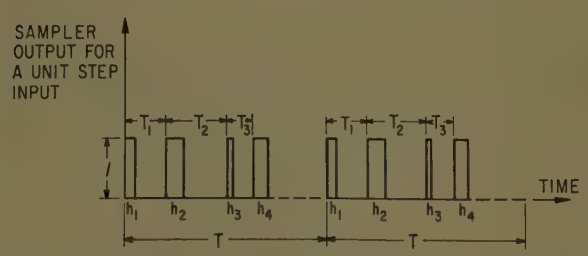


Fig. 23. Periodically time-varying sampling rate and pulse width

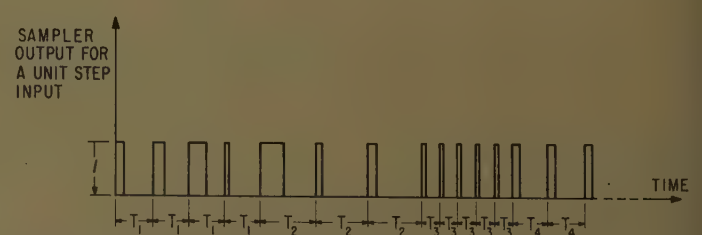


Fig. 24. Piecewise constant rate finite pulse system, settling into a fixed period

sampled-data control systems. The method presented by the author is systematic and straightforward and appears to be a better technique for analyzing finite pulsed feedback control systems by use of $Z$-transforms. However, it appears that the new symbolic representation by the author does not simplify the problem. On the other hand, the conventional symbolic representation is probably easier and simpler to use. The continuous-data part of the system and the continuous input signals can be represented by the conventional analog-computer simulation diagrams. The pulsed-data part of the system can be described by the conventional symbolic representation given in reference 3 of the paper, with each ideal sampler followed by a zero-order hold. When a sampled-data system is so represented, the state and the transition equations, like equations 8 and 9 of the paper, can readily be obtained.

It would be clearer if $t_0=0$ is added to equation 5 which defines the switching operation analytically. According to the definition of equation 5, Fig. 8(B) can represent a number of switching operations depending upon the value of $t_2$, and it is equivalent to Fig. 8(A) only if $t_2=T$.

In general, system analysis and synthesis may be carried out by two major approaches. One approach involves the determination of the transfer characteristics of the system components and the over-all transfer characteristic. This approach is usually effected by a block diagram representation and may be referred to as the block diagram approach. The other approach is based upon the characterization of a system by a number of simple first-order differential equations describing the state variables, with the initial conditions given by the transition equations. Each component of a system is decomposed into the basic mathematical elements describing it. This approach is usually effected by a state variable diagram and may be referred to as the state diagram approach.

The author has written a concise and lucid paper on the state diagram approach of the analysis of linear periodic feedback systems.

**Edward O. Gilbert:** The discussions by Professors Jury and Tou are indeed appreciated. Their discussions and recent papers,[1,2] published or submitted after submission of the author's paper, indicate high interest in more general time-variant operations.

Professor Jury is correct in pointing out the usefulness of the representation in system simulation. There is a 1-to-1 correspondence between the symbolic diagram and differential analyzer setup, including discrete components. Using this analogy, the author has successfully simulated digital computer components by approximating the sampling operation described in the paper. The method of the paper does not lead to difference equations with periodic coefficients as does the method of reference 2. The reduction of the periodic difference equations to constant coefficient difference equations[2,3] is inherent in the computation of the matrix $W(T)$. The $p$-transform and $Z$-transform methods for writing difference equations are certainly acceptable, but are more difficult to generalize to the extensive class considered in this paper. This, of course, does not invalidate the usefulness of such approaches, which for certain systems, primarily low $(N, M)$ systems, may be more desirable. The same may be said for the various techniques of solving the resulting difference equations.

Professor Tou's statement that the symbolic representation does not simplify the problem and is not necessary to readily derive the state and transition equations is only true for the simplest of systems. For example, the finite pulse-clamping operation is not easily described by conventional representations. The correction in regard to Fig. 8(B) is appreciated.


REFERENCES

1. See reference 1 of the Jury discussion.
2. See reference 2 of the Jury discussion.
3. See reference 3 of the Jury discussion.


# Executive-Controlled Adaptive Systems


ROBERT STAFFIN
NONMEMBER AIEE


THERE IS an immense body of literature on the general subject of feedback control theory. The greatest portion of this literature is devoted to the analysis and synthesis of single-loop or simple multiloop linear or piecewise-linear feedback systems. In most of this work, there is a common fundamental assumption, and that is that the designer has, or can obtain, reasonably complete knowledge of the properties of the device or process which is to be controlled. This knowledge generally consists of a fairly accurate characterization of the process or device under one set of environmental conditions, along with information indicating the manner and the limits within which the properties of the process vary with time and with different external conditions. It is the ability of closed-loop control to render the complete system relatively insensitive to inaccuracies in the characterization and to variations in the properties of the process to be controlled that has resulted in the phenonomenal growth of the field.

In this introductory era of supersonic flight, guided missiles, space travel, and complex industrial processes, the control engineer is frequently confronted with the problem of designing control systems for processes where little significant information is known about the process, where the properties of the process vary over an extraordinarily large range, and where the characteristics of the input signals change markedly with time. It is the purpose of this paper to present an approach to the design of feedback control systems which will enable the designer to cope with such situations when they arise.

## Adaptive Systems

A block diagram of a single-loop feedback system is shown in Fig. 1. The compensator can be a passive or an active network, linear or nonlinear, a digital controller, or an analog computer. If the characteristics of the process and of the input signal are known, there are numerous procedures for designing the compensator so that some desired performance is obtained. Deviations from this desired performance due to changes in the process and/or the input signal often can be made acceptably small by increasing the loop gain. If, however, the parameter variations are extremely large, the gain required to achieve the specified system performance may become so high as to be unobtainable because of noise or saturation limitations. As an alternative to increasing the gain, the transfer char-


Paper 59-1181, recommended by the AIEE Feedback Control Systems Committee and approved by the AIEE Technical Operations Department for presentation at the AIEE Fall General Meeting, Chicago, Ill., October 11–16, 1959. Manuscript submitted August 3, 1959; made available for printing August 13, 1959.



ROBERT STAFFIN is with Polytechnic Institute of Brooklyn, Brooklyn, N. Y.


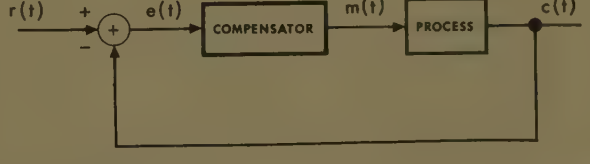


Fig. 1. General single-loop feedback system

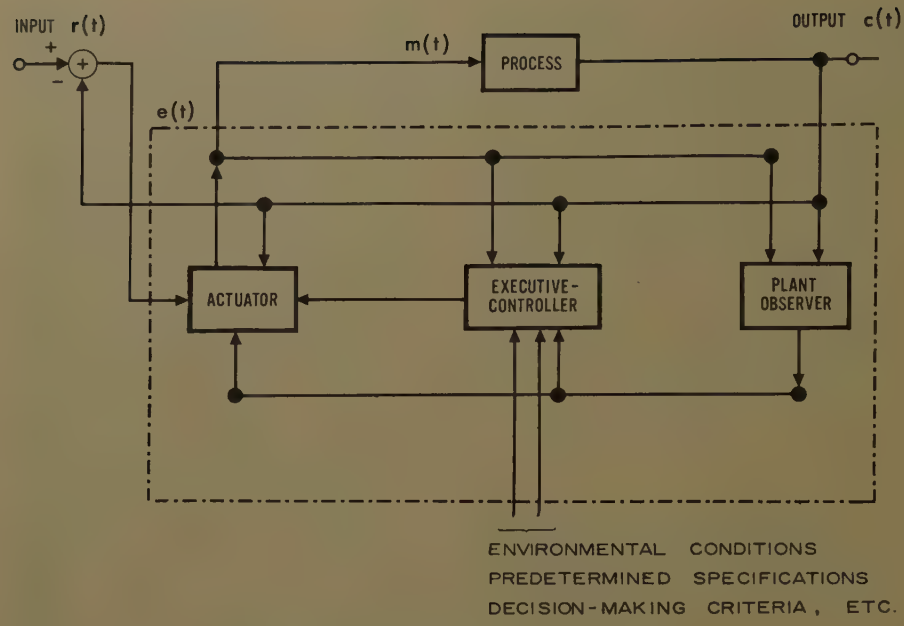


**Fig. 2. Executive-controlled adaptive system**

acteristic of the compensator can be altered. (The term "transfer characteristic" is used instead of transfer function so that linearity is not implied. If the compensator is linear, the terms are synonymous.) This type of system in which the transfer characteristic of the controller is adjusted to compensate for variations in the characteristics of the signal and/or the process is called an "adaptive system."

In the process-adaptive system[1,2] in which the compensator is designed to adjust for variations in the process, the object is essentially to maintain a relatively constant loop transmittance. In the signal-adaptive system,[3] however, the object is to maintain some specified overall performance in spite of large variations in input-signal characteristics. This latter type of adaptability therefore requires that the compensator vary the loop transmittance as the properties of the input signal change. This fundamental difference in the function of the compensator for process-adaptive and signal-adaptive systems is primarily responsible for the fact that in the past, process adaptability and signal adaptability have been treated as separate design problems.

There is, however, an approach to the design of adaptive systems which enables the designer to develop a system which can be made simultaneously signal-adaptive and process-adaptive. The resulting systems which also can be constructed as either process-adaptive or signal-adaptive are called "executive-controlled adaptive systems."[4,5]

## Executive-Controlled Adaptive Systems

In an executive-controlled system, the compensator is a computer which is divided into three basic sections, each with a sharply defined responsibility. An operations diagram for such a system, which may include either an analog, a digital, or a hybrid analog-digital computer, is shown in Fig. 2. The plant observer is responsible for the measurement of the process characteristics and for the detection of changes in significant parameters; the executive-controller is responsible for supplying the required performance information: and the actuator is charged with the computation and generation of the control signal $m(t)$. Although the actual details of each computer section are dependent upon the complexity of the control problem, the following is a general description of the operation of an executive-controlled system.

The actuator, which may range in complexity from an elaborate digital installation to a simple passive network, is designed so that its transfer characteristic is a function both of the significant process characteristics as determined by the plant observer and of the performance requirements as contained in the executive controller. For processes which vary markedly in an extreme and unpredictable manner, the required plant observer may involve a reasonably large computational facility. However, as in the examples which are presented later, a simple computer is often sufficient for handling a number of practical control problems which are commonly encountered. For processes wherein the variations are related to environmental conditions, the plant observer reduces to a set of simple environmental measuring instruments, and, in the limit, for a system which is to be solely signal adaptive, the plant-observer stage is omitted completely.

The executive-controller is responsible for supplying the actuator with performance information. In one of the examples presented later, the executive-controller appears in the form of a set of potentiometer settings. In another, it is a passive network. The actual form of the controller is strongly dependent upon the actuator which is used. As an example, the actuator of Fig. 3 is adjusted to approximately cancel the poles and zeros of the process. For this case, the executive-controller is a model of the desired forward-path transmittance. Although in general, the executive-controller can be called upon to operate on almost any performance criteria, for the purpose of this paper, the executive-controller is used exclusively to achieve a desired forward-path transmittance.

Assuming that the actuator is capable of forcing the forward path to behave as required by the executive-controller, it is

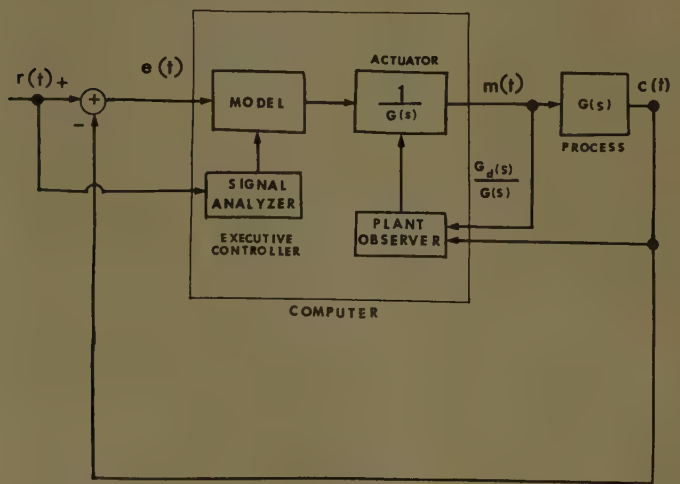


**Fig. 3. Function diagram of executive-controller and actuator**

apparent that in order to design a signal-adaptive system, it is necessary to vary the parameters of the executive-controller in accordance with the input-signal characteristics. In the system of Fig. 3, this implies that the characteristics of the model are changed as the properties of the input signal vary. For signal-adaptive systems, all signal measuring equipment is included in the executive-controller. Since the problems associated with the measurement of process characteristics are extremely challenging, and because at present, systems which adjust to extreme process variations are of primary interest, the emphasis in the illustrative examples is on process-adaptive executive-controlled systems.

## Process Measurement

If the complete executive-controlled system is to adjust automatically to extreme and unpredictable variations in the process characteristics, one section of the computer must be devoted to the continuous measurement and computation of the significant process parameters. The problems associated with this so-called plant-observer stage are enormous. Fundamentally, they fall into two categories: difficulties due to stored energy in the system, and erratic results caused by measurement noise.

Measurements are made by the plant observer over a finite interval of time. During this interval, the output of the process to be measured is not only a function of the input during the interval of measurement, but is also a function of the input for all time prior to the measurement interval. The measurement technique must be capable of taking into account this stored energy which is due to inputs prior to the measurement interval.

Measurement noise is the term applied to errors which arise either as a result of noise within the process itself or from inaccuracies in the measuring equipment. It is apparent that a measured output due to noise in the process with no corresponding input signal would yield nonsensical information about the process. Effects due to measurement noise can be minimized by artifically maintaining high signal levels or by making measurements only when the signals rise above a predetermined threshold value.

The two basic approaches to the solution of these difficulties involve systems which employ test signals as opposed to systems which compute the significant process characteristics from measurements made on the signals present during ordinary operating conditions. Systems which utilize test signals offer two advantages. First, the effects of stored energy due to prior inputs are filtered out. Second, the magnitude of the test signal can be maintained at a level high enough to eliminate most of the errors due to measurement noise. The major disadvantage associated with test-signal systems is, of course, the continual disturbance of the system by the test-signal input.

Systems that compute on the basis of signals which exist during ordinary operation are free from this disturbing feature. However, in order to insure the reliability of the measured data, measurements must be made only when the signals are above some threshold level. An unfortunate consequence of this threshold arrangement is that after periods of low signal levels, the executive-controlled system operates with stale process information. If the occasional lack of immediate information proves more disturbing than test-signal inputs, then the systems which employ test signals are preferable.

Regardless of which approach is chosen, the complexity of the plant-observer stage is dependent upon the number of process parameters which are required in order to appropriately adjust the actuator. For this reason, attempts to solve the process measurement problem in general usually result in enormous computer requirements. Fortunately, for many given practical control situations, the measurement problem can be greatly simplified. The following examples illustrate this point as well as a number of the general chraacteristics of executive-controlled adaptive systems.

## Particular Solution to the General Problem

The design of the computer for an executive-controlled system depends quite markedly on the choice of characterization for the process and for the performance specification. This characterization may be in terms of a set of difference equations, by pole-zero location, in terms of an impulse response, or by a frequency spectrum. A number of computer designs based upon these characterizations are discussed in references 1, 2, 4, and 5.

One interesting approach results from choosing a set of linear differential equations to describe the process and the required performance specification. Assuming a linear process, the process input $m(t)$ and the process output $c(t)$ can be related by a differential equation of the form:

$$\sum_{k=0}^{n} a_k p^k c(t) = \sum_{j=0}^{n} b_j p^j m(t) \qquad (1)$$

where $p=d/dt$ and the $a_k$ and $b_j$ are constants. The performance specification which, in this case, is the desired forward-path transmittance, can also be expressed in terms of a differential equation:

$$\sum_{k=0}^{n} \alpha_k p^k c(t) = \sum_{j=0}^{n} \beta_j p^j e(t) \qquad (2)$$

where $c(t)$ is now the desired process output for a given input $r(t)$, and $e(t)$ is the closed-loop error signal $r(t)-c(t)$.

If equation 2 is subtracted from equation 1 and the resultant equation solved for the actuator output $m(t)$, the transfer equation for the actuator is obtained as:

$$m(t)=\frac{1}{b_0}\sum_{k=0}^{n}\left[(a_k-\alpha_k)\frac{d^k}{dt^k}c(t)+\beta_k\frac{d^k}{dt^k}e(t)\right]-\sum_{j=1}^{n} b_j\frac{d^j}{dt^j}m(t) \qquad (3)$$

For the case when $b=0$, the equation can be solved for $dm(t)/dt$ where $m(t)$ is given to within an additive constant by:

$$m(t)=\frac{1}{b_1}\int\left\{\sum_{k=0}^{n}\left[(a_k-\alpha_k)\frac{d^k}{dt^k}c(t)+\beta_k\frac{d^k}{dt^k}e(t)\right]-\sum_{j=2}^{n} b_j\frac{d^j}{dt^j}m(t)\right\}dt \qquad (4)$$

For $b_0=b_1=0$, two integrations are required, and so on.

If equations 3 and 4 are normalized for convenience ($-1<a,\ b,\ \alpha,\ \beta<1$), one possible computer circuit for generating $m(t)$ utilizing d-c operational amplifiers and single-pole–double-throw switches or relays is shown in Fig. 4(A). The magnitudes of the $\alpha_k$, $\beta_k$, $a_k$ and $b_k$ are set on the potentiometers and the required algebraic signs are obtained by selecting the the proper switch position. It is interesting to note that in this method of realization, the executive-controller and the actuator are essentially fused together, the executive-controller taking form as a set of potentiometer settings.

Of extreme importance, however, is the fact that as long as the $a_k$ and $b_k$ correctly characterize the process the forward loop is constrained to perform in the manner described by specification equation 2. Thus, if a signal-adaptive system is desired, it is only necessary to vary the $\alpha$ and $\beta$ potentiometers in a predetermined manner as the characteristics of the input-signal change. For a process-adaptive system, the $a$ and $b$ potentiometers are

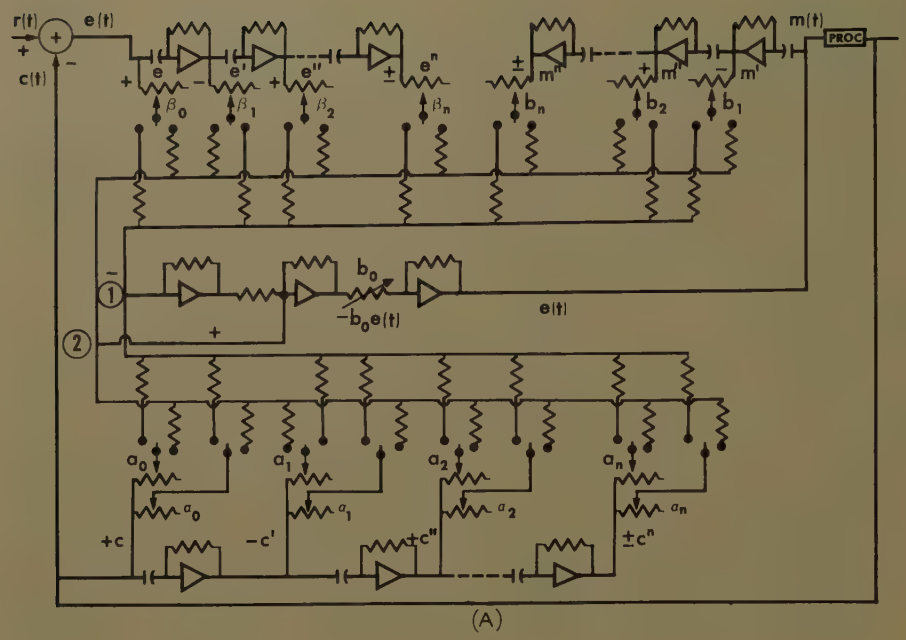


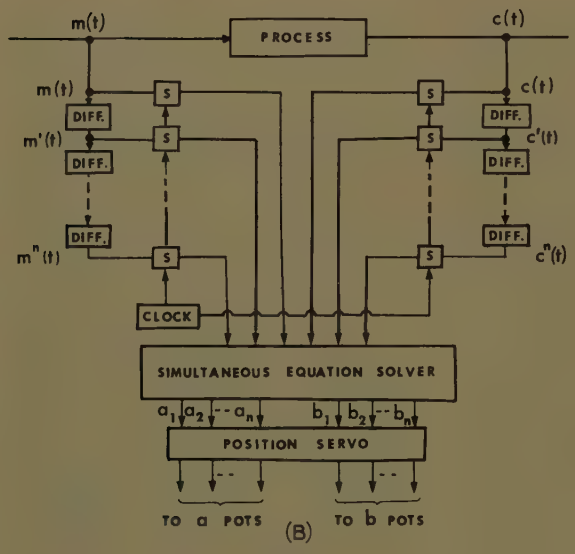


**Fig. 4. Differential equation approach**

A—Circuit diagram
B—Plant observer

adjusted in accordance with information obtained from a plant observer.

The plant observer for the actuator of Fig. 4(A) is required to supply the coefficients of the process differential equation. If the process input $m(t)$ and output $c(t)$ and all $n$ derivatives of $m(t)$ and $c(t)$ are sampled at $2(n+1)$ instants of time, then process equation 1 can be used to generate a set of linear simultaneous equations. The $a_k$ and $b_k$ are obtained from the solution of this set of equations. A block diagram of the plant observer which operates in this manner is shown in Fig. 4(B). The differentiators can be constructed from analog components, utilizing either operational amplifiers or delay-line differentiators. For the simultaneous equation solver, a digital computer would be more appropriate. The outputs from the equation solver are transformed into potentiometer settings through a positioning servomechanism.

As indicated earlier, the total installation represented by Figs. 4(A) and (B) is quite large, especially for a process which must be represented by a high-order differential equation. In addition, the utilization of a large number of differentiators in an analog computer is usually to be avoided. Fortunately, when the problem is restricted, the instrumentation can be greatly simplified. It is apparent, for example, that for linear systems, the transfer characteristic of the actuator can be writen as $G_d(s)/G(s)$ where $G(s)$ is the process transfer function and $G_d(s)$ is the desired forward-path transmittance. For simple special cases, the computer can therefore be replaced by a network realization of $G_d(s)/G(s)$, even when $G_d(s)$ or $G(s)$ are to be varied during operation. For systems, however, in which the parameter variations are extreme, the actuator must be realized, either partially or totally as shown in Figs. 4(A) and (B). (For a more detailed analysis of this and other approaches, see reference 5.)

Fortunately, the solution for a particular problem is usually much simpler than that for the general problem just discussed. This simplification is demonstrated in the next section.

## Executive-Control for Lightly Damped Varying Process

A common problem which is encountered in the design of practical control systems is one which involves process-transfer functions with one complex pole-pair close to the real frequency axis. Although the transfer function may contain additional poles and zeros as, for example, in Fig. 5(A), the behavior of the process when included in a closed loop is dominated by the poles adjacent to the $j\omega$ axis. In particular, with a relatively small loop gain, the system tends to become unstable.

If the process is fixed, the usual approach to improving the closed-loop operation is to add a compensating network with zeros in close proximity to the poles, as for example, at position $a$ in Fig. 5(A). If, however, the process poles vary in an unpredictable manner over a large region as illustrated in Fig. 5(B), it is extremely difficult, and sometimes impossible, to stabilize the system with fixed compensation without introducing undesirable effects into the over-all operation of the closed-loop system.

By applying the principles of executive-control, it is not only possible to stabilize the system, but it is also possible to maintain an approximately nonvarying, desirable, closed-loop transfer function in spite of large variations in the position of the offending pole-pair. In addition, for this problem, the executive-controller and the actuator are realizable as passive networks. This passive realization results in a relatively simple executive-controlled system.

In the actuator-controller of Fig. 3, the actuator transfer function is constructed to be $1/G(s)$, the inverse of the process-transfer function; and the executive-controller, which is responsible for achieving the specified operation, is a model of the desired forward-path transfer characteristic. For the problem under discussion, this approach is modified so that the actuator cancels only the effects due to the dominating pole-pair. Thus, if the process transfer function is:

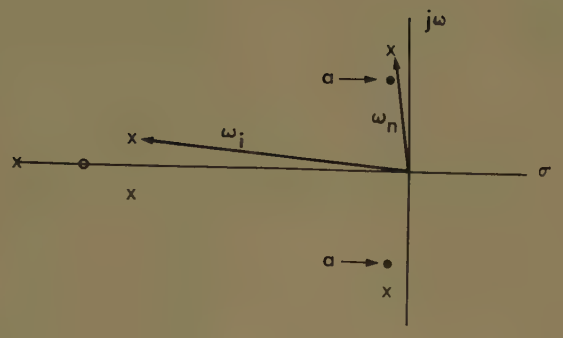


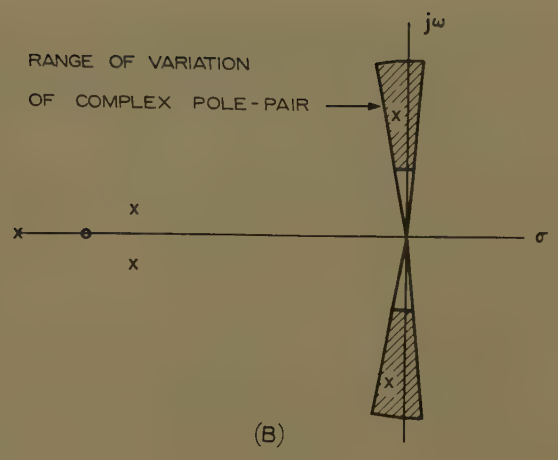


Fig. 5. S-plane diagram of pole-pair variation

$$G(s)=\frac{N(s)}{D(s)}=\frac{N(s)}{D_1(s)[s^2+2\zeta\omega_n s+\omega_n^2]} \tag{5}$$

the actuator transfer function is constructed to be:

$$G_a(s)=\frac{[s^2+2\zeta\omega_n+\omega_n^2]}{D_a(s)} \tag{6}$$

where the poles of $G_a(s)$ are added to make $G_a(s)$ realizable with a linear passive network.

Since the dominant pole-pair changes position in the $s$-plane, it is necessary for $G_a(s)$ to be variable if the offending pole-pair is to be approximately cancelled at all times. Assuming that a plant observer exists which is capable of supplying the actuator with the approximate location of the important pole-pair, and assuming that $G_a(s)$ is able to vary accordingly, the transfer function of the executive-controller can be immediately determined as:

$$G_e(s)=G_d(s)\,\frac{D_1(s)D_a(s)}{N(s)} \tag{7}$$

A block diagram of the complete system is shown in Fig. 6(A).

Since it is not necessary to cancel exactly the dominant pole-pair, $G_a(s)$ need not be continuously variable. Instead, several fixed passive networks can be employed to cover effectively the region over which the pole-pair moves. Such an arrangement is shown in Fig. 6(B). The $G_a(s)$ networks are selected by a rotary switch. The function of the plant observer in such a system is to measure the approximate pole location and to choose the appropriate switch position.

If the region of pole variation closely surrounds the $j\omega$ axis, then $\omega_n$, the resonant frequency of the dominant pole-pair, is sufficient for locating the pole position for the purposes of switching in the successive compensation networks. A plant observer capable of supplying the value of $\omega_n$ can be constructed by taking advantage of the properties of the frequency response characterization of a lightly damped process.

If, for the moment, it is assumed that in Fig. 5, $\omega_n$ is less than all other $\omega_i$ where the $\omega_i$ are the radial distances to all other poles and zeros of the process transfer function, then the frequency response of the process is of the form drawn in Fig. 7. If, in addition, $\omega_1$ and $\omega_2$ are chosen in such a manner that $\omega_1<\omega_n<\omega_2$ over the entire range of variation of $\omega_n$, and where $\omega_2<\omega_i$, then it is shown in Appendix I that:

$$\omega_n=\omega_2\sqrt{\frac{|C(\omega_2)|}{|C(\omega_2)|+|KM(\omega_2)|}} \tag{8}$$

and

$$K=\left|\frac{C(\omega_1)}{M(\omega_1)}\right|=|G(\omega_1)| \tag{9}$$

where $C(\omega_1)$ and $C(\omega_2)$ are obtained from two narrow-band filters at the process output, and $M(\omega_1)$ qnd $M(\omega_2)$ are similarly obtained with two filters at the process input. ($M(\omega)$ and $C(\omega)$ are the Fourier transforms of $m(t)$ and $c(t)$, the process input and output.)

A straightforward analog computer

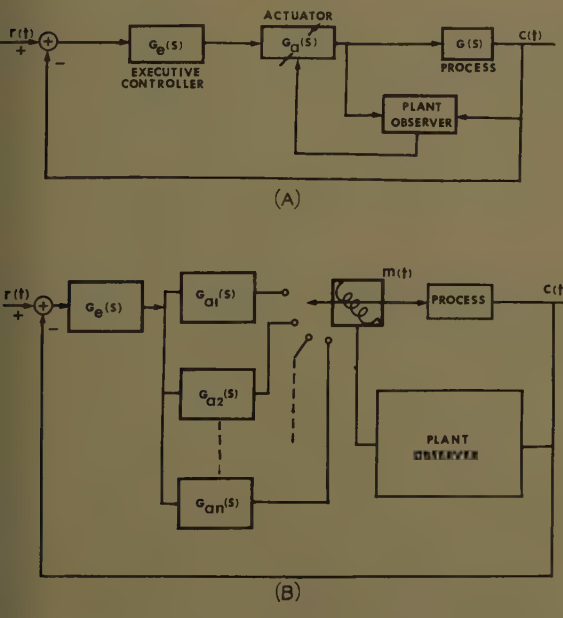


Fig. 6. Notch filter approach

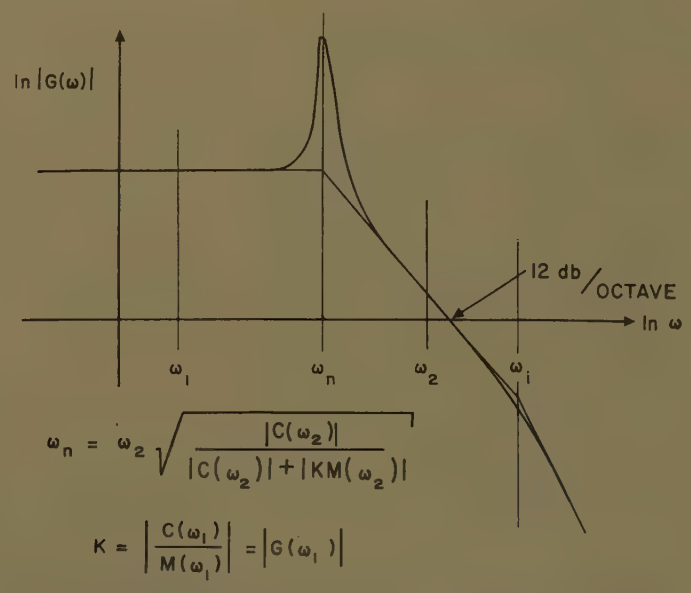


Fig. 7. Logarithmic amplitude response for system with dominant pole-pair

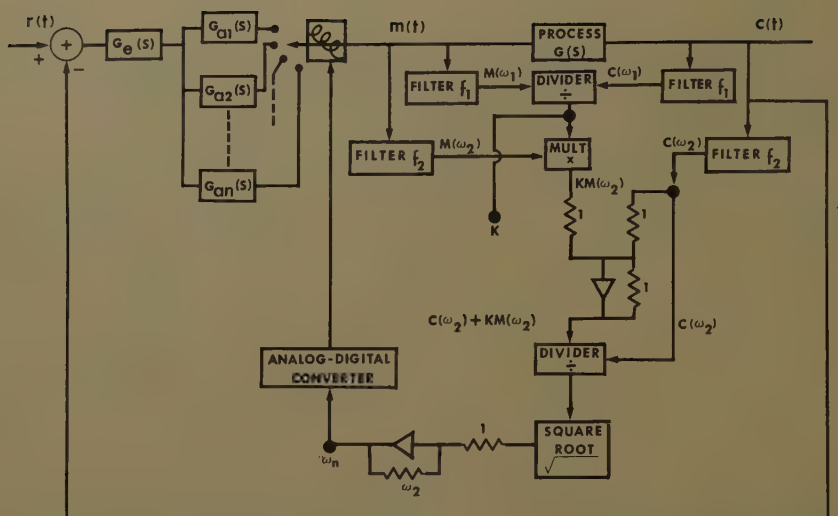


**Fig. 8. Executive-controlled system diagram for frequency-response approach**

can be used to solve equations 8 and 9. A complete executive-controlled process-adaptive system employing such a computer is illustrated in Fig. 8. It is interesting to note that in addition to the approximate pole position, the computer also supplies the value of $K=G(\omega_1)$, the low-frequency gain of the process. Thus, with slight modification, the system of Fig. 8 can be made adaptive to changes in gain as well as to changes in pole position.

If there is a pole at $s=0$, the derivative of $c(t)$ is utilized by the plant observer instead of $c(t)$. If, after accounting for the poles at the origin there are one or more poles located so that it is impossible to choose $\omega_2$ less than the smallest $\omega_i$, equation 8 can be modified so that it will still give $\omega_n$, provided the $\omega_i$ remain relatively fixed.

## Alternate Solution for Lightly Damped Varying Processes

For a lightly damped process with a dominant pole-pair, there is another interesting method of measurement based upon an impulse response characterization which is capable of supplying, $\zeta$ the relative damping ratio as well as $\omega_n$, the radial distance to the dominant pole-pair. Under the conditions imposed upon the process in the previous section ($\omega_n<\omega_i$ and $\zeta$ small), the impulse response of the process $g(t)$ is approximately that of a second-order system as drawn in Fig. 9. For this approximate second-order response it can be shown that (see Appendix II):

$$\omega_n=\frac{\pi}{T_0} \tag{10}$$

and that

$$\zeta=\frac{1}{\pi}\ln\left|\frac{g_M}{g_m}\right| \tag{11}$$

where $T_0$ is the period to the first zero of $g(t)$, and where $g_M$ and $g_m$ are the first maximum and first minimum respectively of $g(t)$ as indicated in Fig. 9.

A computer capable of determining $\omega_n$ and $\zeta$ from equations 10 and 11 is illustrated in Fig. 10. In contradistinction to the two previous methods, this approach utilizes test signals to aid in the measurement. If white noise is added to the process input, and if the process output is cross-correlated with the noise delayed by a constant $\tau$, the output from the cross-correlator is $g(\tau)$, one point on the process impulse response.[6] There is a tremendous instrumentation advantage if, instead of ordinary noise, 2-level, or so-called binary, noise is employed. For this type of signal, the noise generators can be constructed from motor-driven cams or random-toothed discs,[7] and the cross-correlators become simple relays followed by low-pass filters.[2] The delayed noise is then simply generated by synchronously driving a set of identical mechanical noise generators, each one phased slightly differently than the original, the time delay being directly proportional to the mechanical phase displacement.

For the computer of Fig. 10, four mechanical noise generators (*NG*1 to *NG*4) are driven by motor no. 1 and separated from each other by mechanical phase shifters as indicated schematically in the diagram. The noise output from *NG*1 is added to $m(t)$, the process input. *NG*2 is connected to *NG*1 through a variable phase shifter (a simple differential gearing arrangement). The output of *NG*2 is is cross-correlated with the process output $c(t)$ thereby obtaining one point on the $g(\tau)$ curve. If the phase shift is initially zero, and if the relative phase between *NG*1 and *NG*2 is continuously changed by motor no. 2, the output from the first cross-correlator will scan the $g(\tau)$ curve. A null detector at this output can be employed to stop the motor when $g(\tau)$ goes through its first zero at $\tau=T_0$. Since $\tau$ is proportional to the angle of the variable phase shifter and, since $\omega_n$ is inversely proportional to $T_0$, the value of $\omega_n$ can be obtained directly from this first phase shifter.

If *NG*3 and *NG*4 are connected to *NG*2 through fixed gear ratios of 1/2 to 1 and 3/2 to 1 respectively, when *NG*2 is delayed by $T_0$, *NG*3 will be delayed by $T_0/2$ and

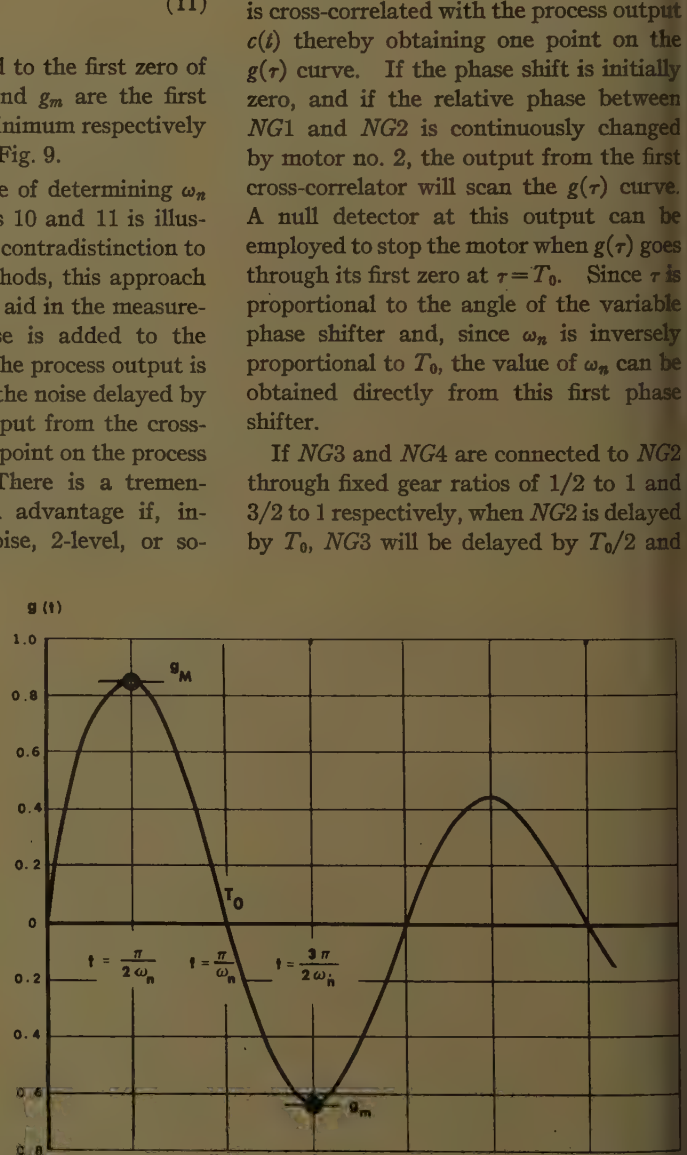


**Fig. 9. Transient response for system with dominant pole pair**

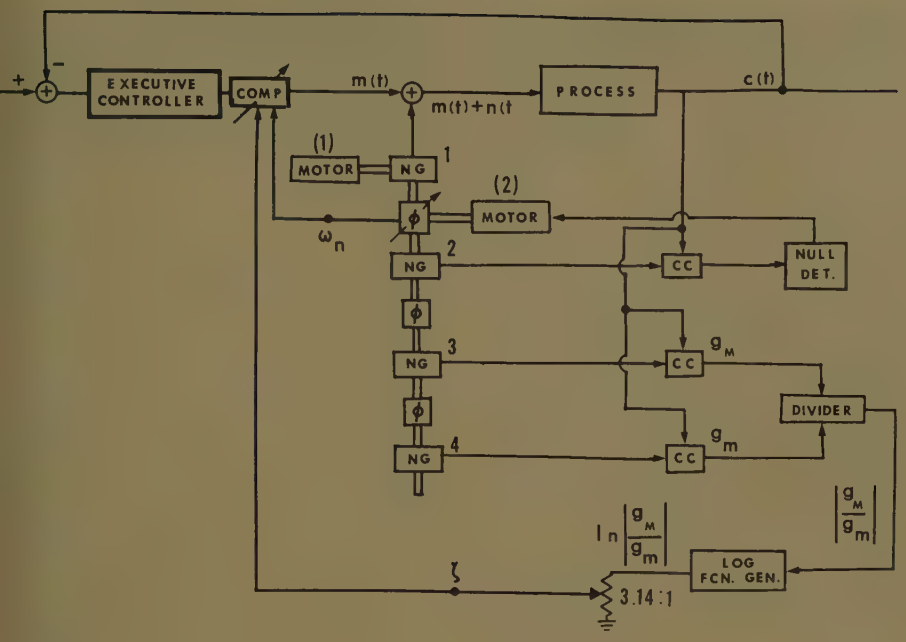


**Fig. 10. Executive-control for impulse-response approach**

*NG*4 by $3T_0/2$. But $T_0/2$ and $3T_0/2$ are approximately the values of $\tau$ at which $g(\tau)$ hits its first maximum and its first minimum. Thus, the outputs from the second and third cross-correlator are $g_M$ and $g_m$. A divider followed by a logarithmic function generator and a potentiometer divider is sufficient to obtain $\zeta$; see equation 11. The values of $\omega_n$ and $\zeta$ can then be used to adjust the compensator.

The compensator, once again, may be continuously or discretely variable. The total installation for this method is well within the limits of practical realizability. Since the emphasis in the last two sections has been on cancelling the effects of the offending process pole-pair, the resultant systems have been process-adaptive. Since in these systems, as in all executive-controlled systems, the measurement problem is divorced from the performance specification, the final installations can be made signal-adaptive by varying the transfer characteristics of the executive-controller.

One final point that should be made is that, although the performance specification can be changed instantaneously, the measurement procedures discussed herein require that the process parameters vary slowly with respect to the measurement interval. In the differential equation approach, the measurement interval is determined by the sampling intervals and by the simultaneous equation solver; for the frequency-response approach, the measurement interval is limited by the delay in the narrow-band filters; and for the transient-response method, the delay in the cross-correlators is the limiting factor.

## Conclusions

Executive-control appears to be a useful approach for the design of adaptive systems. By dividing the responsibilities of the computer into three distinct functions: process measurement, performance maintenance, and signal generation, the problems associated with process adaptability and signal adaptability can be treated separately, with the final designs fused together to form a completely adaptive system.

The major challenge, at present, is in the process-measurement stage. Attempts to solve this problem in general result in large computer requirements of questionable practicality. Fortunately, however, for specific control situations, the total installations can apprently be kept well within practical limits. Perhaps from the solution of such specialized problems, some general methods will develop which will enable the principles of adaptive control to be applied to highly complex systems.

## Appendix I

Under the conditions imposed upon the process in Figs. 5 and 7, the process-transfer function for $\omega<\omega_1$ can be considered approximately second order. Thus, for $\omega<\omega_1$:

$$G(s)=\frac{K\omega_n^2}{(s^2+2\zeta\omega_n s+\omega_n^2)} \tag{12}$$

or in terms of $\omega$,

$$G(\omega)=\frac{K\omega_n^2}{(\omega_n^2-\omega^2)+2j\zeta\omega_n\omega} \tag{13}$$

For $\omega_1\ll\omega_n$ and $\zeta$ small,

$$|G(\omega_1)|=\left|\frac{C(\omega_1)}{M(\omega_1)}\right|\cong K \tag{14}$$

For $\omega_2>\omega_n$ and $\zeta$ small,

$$|G(\omega_2)|\cong\frac{K\omega_n^2}{(\omega_2^2-\omega_n^2)} \tag{15}$$

Solving equation 15 for $\omega_n$ results in:

$$\omega_n=\omega_2\sqrt{\frac{|G(\omega_2)|}{|G(\omega_2)|+K}} \tag{16}$$

but

$$|G(\omega_2)|=\left|\frac{C(\omega_2)}{M(\omega_2)}\right| \tag{17}$$

Thus,

$$\omega_n=\omega_2\sqrt{\frac{|C(\omega_2)|}{|C(\omega_2)|+K|M(\omega_2)|}} \tag{18}$$

## Appendix II

Once again, if $G(s)$ is assumed approximately second order:

$$g(t)=\frac{K\omega_n}{\sqrt{1-\zeta^2}}\,\epsilon^{-\zeta\omega_n t}\sin(\omega_n\sqrt{1-\zeta^2}\,t) \tag{19}$$

where $g(t)$ is the process-impulse response. If the process is lightly damped, $\zeta$ is small and

$$g(t)\cong K\omega_n\epsilon^{-\zeta\omega_n t}\sin\omega_n t \tag{20}$$

The first time $g(t)$ crosses zero (excluding $t=0$) is at $t=\pi/\omega_n=T_0$. Therefore,

$$\omega_n=\frac{\pi}{T_0} \tag{21}$$

But at $t=\pi/2\omega_n=T_0/2$, $g(t)=g_M$. Hence,

$$g_m=K\omega_n\epsilon^{-\pi/2} \tag{22}$$

However, at $t=3\pi/2\omega_n=3T_0/2$, $g(t)=g_m$ where

$$g_m=-K\omega_n\epsilon^{-3\pi/2} \tag{23}$$

Therefore,

$$\left|\frac{g_M}{g_m}\right|=\epsilon^{\pi\zeta} \tag{24}$$

or

$$\zeta\cong\frac{1}{\pi}\ln\left|\frac{g_M}{g_m}\right| \tag{25}$$

## References


1. Design of a Self-Optimizing Control System, R. E. Kalman. *Transactions*, American Society of Mechanical Engineers, New York, N. Y., Feb. 1958.

2. A Self-Adjusting System for Optimum Dynamic Performance, G. W. Anderson, J. A. Aseltine. *Convention Record*, Institute of Radio Engineers, New York, N. Y., pt. 4, 1958.

3. Adaptive Servomechanisms, **R. F. Drenick, R. A. Shahbender.** *AIEE Transactions*, pt. II (*Applications and Industry*), vol. 76, Nov. 1957, pp. 286–92.

4. Executive-Controlled Adaptive Systems, **R. Staffin.** *Dissertation*, Doctorate, Electrical Engineering, Polytechnic Institute of Brooklyn, Brooklyn, N. Y., June 1959.

5. Executive-Controlled Adaptive Systems, **R. Staffin, J. G. Truxal.** *Research Report R-688-58, PIB-616*, Microwave Research Institute, Polytechnic Institute of Brooklyn, Brooklyn, N. Y., Sept. 9, 1958.

6. Automatic Feedback Control System Synthesis (book), **J. G. Truxal.** McGraw-Hill Book Company, Inc., New York, N. Y., 1955.

7. Dynamic Response Measurement in the Presence of Noise and Limiting, **E. S. Joline.** *M.S. Thesis*, Polytechnic Institute of Brooklyn, June 1955.

8. A Survey of Adaptive Control Systems, **J. A. Aseltine, A. R. Mancini, C. W. Sarture.** *Transactions*, Professional Group on Automatic Control, Institute of Radio Engineers, Dec. 1958.

# ERRATUM

**"Some Effects of Hypersonic Ionization on the Design of Electrical and Electronic Components" by W. B. Sisco and J. M. Fiskin; published in Applications and Industry, November 1959, pages 352–56.**

The authors wish to make the following corrections in their paper. On page 356, column 2, in the first paragraph the allusion to "equations 2, 3, and 4" should read "equations 1, 2, and 3." Also, items 1 and 12 of the "References" should be interchanged.

# Applications and Industry Index for 1959

## 1. Technical Subject Index


Absorber Geometry for a Solar Generator, Optimum Reflector-. Stineman....332–7
A-C Electrical System Designs, Computer Evaluation of High-Temperature Aircraft. Sollecito, Swann....434–44; disc. 444
A-C Generator for High-Temperature Electrical Systems, A Solid Rotor. Bateman..400–03; disc. 403
A-C Power Using Variable Speed Generation, Constant Frequency. Jessee, Spaven....411–16; disc. 417
A-C Servomotors Operated from Unbalanced Nonsinusoidal Voltage Sources and Nonlinear Discontinuous Source Impedances, Analysis of. Lind, Schmitz....476–9; disc. 479
Adaptive Control Systems, Use of a Mathematical Error Criterion in the Design of. Merriam...506–12
Adaptive Systems, Executive-Controlled. Staffin.....523–30
Adjustment, Control by Stochastic. Bertram...485–91
Air Filters, Electrified Fibrous. Thomas, Woodfin....276–8
(Air Transportation) A Solid Rotor A-C Generator for High-Temperature Electrical Systems. Bateman..400–03; disc. 403
(Air Transportation) An Elementary Design Discussion of Thermoelectric Generation. Bollmeier..445–50
(Air Transportation) Constant-Frequency Variable-Speed Frequency-Make-up Generators. Hoard..297–301; disc. 301
(Air Transportation) Development of Fuses and Terminals for High-Temperature Applications. Bonwitt, Buttner....267–72
(Air Transportation) Energy-Conversion Properties of Induction Machines in Variable-Speed Constant-Frequency Generating Systems. Riaz....25–30
(Air Transportation) Nuclear Radiation and Electronic Instruments. Crittenden....423–6
(Air Transportation) Optimum Reflector-Absorber Geometry for a Solar Generator. Stineman..332–7
(Air Transportation) Practical Considerations of an Ion Propulsion System. Lennert....326–31; disc. 331
(Air Transportation) Solar-Powered Thermoelectric Generator Design Considerations. Schuh, Tallent....345–52
(Air Transportation) Some Effects of Hypersonic Ionization on the Design of Electrical and Electronic Components. Sisco, Fiskin....352–6
(Air Transportation) Temperature Prediction in Thermal-Lag Equipment. Richards....462–5
(Air Transportation) Terminal Spacings for High-Altitude and Ultrahigh-Temperature Electronic Transformer Applications. Duncan, Rectanus....16–19
(Air Transportation) The Effect of Variable High-Altitude Humidity on the Wear of Nondusting Brushes. Moberly, Johnson....263–7
(Air Transportation) The Electrical Analog for Determining Temperature Distribution Electrical Components. Eckert, Hartnett, Irvine, Birkebak..5–10
(Air Transportation) Variable-Speed Constant-Frequency Devices: A Survey of the Methods in Use and Proposed. Owen....321–5; disc. 325
Aircraft A-C Electrical System Designs, Computer Evaluation of High-Temperature. Sollecito, Swann....434–44; disc. 444
Aircraft Control Equipment, Functional Cycling to Assure Reliability of. Hulsey, Kessler....356–60
Aircraft Electric Power Systems, Characteristics and Measurement of Ripple in. Markowitz....418–23; disc. 423
Aircraft, Generator Insulation Systems Development for Hypersonic. Penn, Balke, Precopio....255–9
Aircraft Generators, Reliability Analysis for. Duane, Yeager....426–34
Aircraft, New Materials for Transformer Rectifier Unit in High-Temperature. Hoop, McIlvaine..450–6
Aircraft, Variable-Speed Constant-Frequency Generator System for. Chirgwin, Stratton....304–09; disc. 309
Aluminum Bus for Shipboard Application. Thompson, Behr....239–47; disc. 247
Aluminum-Copper Joints, The Effect of Elevated Temperature on Flash-Welded. Dixon, Nelson....491–5; disc. 495
Amplifiers, Transient Response and the Stabilization of Feedback. Mulligan....495–503
Amplistat-Regulated Sectional Drive at Southland Paper Mills, Transistor. Vickery, Shaad....369–74; disc. 374
Analog Computer, Predicting the Performance of a Wind Tunnel Regulating System Using an. Herbst, Nichols, Keay, Miller....248–52
Analog for Determining Temperature Distribution in Electrical Components, The Electrical. Eckert, Hartnett, Irvine, Birkebak....5–10
Analysis for Aircraft Generators, Reliability. Duane, Yeager....426–34
Analysis of A-C Servomotors Operated from Unbalanced Nonsinusoidal Voltage Sources and Nonlinear Discontinuous Source Impedances. Lind, Schmitz....476–9; disc. 479
Analysis of Nonlinear Sampled-Data Control Systems. Kinnen, Tou:
Part I....386–90; disc. 394
Part II....390–4; disc. 394
Anode Breaker Testing with a High-Capacity Rectifier System. Harris, Scully, Stewart....43–9
Application of Continuous System Design Concepts to the Design of Sampled Data Systems. Schmidt..74–8; disc. 78
Application of Switching Transistors and Saturable Reactors in a High-Performance Servo. Cox, Johannessen....466–74
Arc Silicon-Smelting Furnace, Load Characteristics of a Submerged-. Grant....273–5; disc. 275
Automatic Gage Control, The Use of Frequency Response Tests in the Analysis of a Foil Mill. Jones, Sills....59–67
Automatic Gage Controller for a 56-Inch Reversing Steel Mill, An. Duke, Hulls....10–15; disc. 15


### B


Battery Impedance: Farads, Milliohms, Microhenrys. Willihnganz, Rohner....259–62
Bed Design for Cathodic Protection of Underground Structures, Trends in Ground. Landry, Howell..456–61; disc. 461
Beds for Cathodic Protection, Deep Ground. Trouard, Wagner....278–85
Boolean Functions, New Methods of Simplifying. Howard....134–42; disc. 142
Breaker Testing with a High-Capacity Rectifier System, Anode. Harris, Scully, Stewart....43–8
Bridged-T Complex Conjugate Compensation and 4-Terminal Network Loading, Notes on. Chandaket, Rosenstein....148–58; disc. 158
Brushes, The Effect of Variable High-Altitude Humidity on the Wear of Nondusting. Moberly, Johnson..263–7
Bus for Shipboard Application, Aluminum. Thompson, Behr....239–47; disc. 247


### C


Car History and New Developments, Detector. Keevil....233–8; disc. 238
Carrier Signal Generator for Servosystem Instrumentation, A Suppressed-. Pollard....481–5
Cathodic Protection Applications at the Hanford Works. Bucholz....394–9
Cathodic Protection, Deep Ground Beds for. Trouard, Wagner....278–85
Cathodic Protection of Underground Structures, Trends in Ground Bed Design for. Landry, Howell....456–61; disc. 461
Characteristics and Measurement of Ripple in Aircraft Electric Power Systems. Markowitz....418–23; disc. 423
Characteristics of a Submerged-Arc Silicon-Smelting Furnace, Load. Grant....273–5; disc. 275
Chart Relating Open-Loop and Closed-Loop Frequency Responses of Linear Control Systems, A New. Chen, Shen....252–5
(Chemical Industry) Battery Impedance: Farads, Milliohms, Microhenrys. Willihnganz, Rohner.259–62
(Chemical Industry) Cathodic Protection Applications at the Hanford Works. Bucholz....394–9
(Chemical Industry) Deep Ground Beds for Cathodic Protection. Trouard, Wagner....278–85
(Chemical Industry) High-Speed Restarting and Protection of Large Synchronous Motors. Phillips, Yuen....360–7; disc. 367
(Chemical Industry) Trends in Ground Bed Design for Cathodic Protection of Underground Structures. Landry, Howell....456–61; disc. 461
Chicago, Rapid Transit Is Expanding in. Forsythe....171–6
Class A Random-Wound Motor Insulation as Determined by AIEE Standard No. 510 Test Procedure, The Life Expectancy of. (Committee Report)....224–8
Closed-Loop Frequency Responses of Linear Control Systems, A New Chart Relating Open-Loop and. Chen, Shen....252–5
Closed-Loop Transfer Function Pole and Zero Locations on the Transient Response of Linear Control Systems. Elgerd, Stephens....121–7
Coefficient of Performance, Significance of Heat Pump. Bary....90–5; disc. 95
Coils, Three-Phase Induction Heating. Ross....291–4
(Committee Report) The Life Expectancy of Class A Random-Wound Motor Insulation as Determined by AIEE Standard No. 510 Test Procedure. (58-1334)....224–8
Communication Systems for Railway Traffic Control. Sibley....30–5
Compensation and 4-Terminal Network Loading, Notes on Bridged-T Complex Conjugate. Chandaket, Rosenstein....148–58; disc. 158
Complex Conjugate Compensation and 4-Terminal Network, Loading, Notes on Bridged-T. Chandaket, Rosenstein....148–58; disc. 158
Components, Some Effects of Hypersonic Ionization on the Design of Electrical and Electronic. Sisco, Fiskin....352–6
Components, The Electrical Analog for Determining Temperature Distribution in Electrical. Eckert, Hartnett, Irvine, Birkebak....5–10
Computer Evaluation of High-Temperature Aircraft A-C Electrical System Designs. Sollecito, Swann....434–44; disc. 444
Computer, Predicting the Performance of a Wind Tunnel Regulating System Using an Analog. Herbst, Nichols, Keay, Miller....248–52
Considerations of an Ion Propulsion System, Practical. Lennert....326–31; disc. 331
Considerations, Solar-Powered Thermoelectric Generator Design. Schuh, Tallent....345–62
Constant Frequency A-C Power Using Variable Speed Generation. Jessee, Spaven....411–16; disc. 417
Constant-Frequency Devices: A Survey of the Methods in Use and Proposed, Variable-Speed. Owen..321–5; disc. 325
Constant-Frequency Generating Systems, Energy-Conversion Properties of Induction Machines in Variable-Speed. Riaz....25–30
Constant-Frequency Generator System for Aircraft, Variable-Speed. Chirgwin, Stratton....304–09; disc. 309
Constant-Frequency Variable-Speed Frequency-Make-up Generators. Hoard....297–301; disc. 301
Control by Stochastic Adjustment. Bertram....485–91
Control Equipment, Functional Cycling to Assure Reliability of Aircraft. Hulsey, Kessler....356–60
Control of Infrared Radiation. Barber....54–9
Control of Multiactuator Systems, The Optimum. McCausland....67–73
Control-System Performance, Probabilistic Error as a Measure of. Zaborszky, Diesel....163–8
Control System, Signal Stabilization of a. Oldenburger, Liu....96–100; disc. 100
Control Systems, A New Chart Relating Open-Loop and Closed-Loop Frequency Responses of Linear. Chen, Shen....252–5
Control Systems, Analysis of Nonlinear Sampled-Data. Kinnen, Tou:
Part I....386–90; disc. 394
Part II....390–4; disc. 394
Control Systems, The Linear Least Squares Synthesis of Multivariable. Amara....115–19; disc. 119
Control Systems, Use of a Mathematical Error Criterion in the Design of Adaptive. Merriam....506–12
Controlled Adaptive Systems, Executive-. Staffin....523–30
Controlled Reversible Induction-Motor Drives, Elements of Reactor-. Leonhard..106–14; disc. 114
Controller, A Practical Standard Transistorized Optimum Response. Chen, Little...337–45; disc. 345

Controllers for Rubber and Plastics Industries, Proposed Recommended Practices for Medium-Voltage Motor. Watkins....504–06; disc. 506
Conversion Properties of Induction Machines in Variable-Speed Constant-Frequency Generating Systems, Energy-. Riaz....25–30
Copper Joints, The Effect of Elevated Temperature on Flash-Welded Aluminum-. Dixon, Nelson....491–5; disc. 495
Coulomb Friction and Stiction, Stability Criteria for Instrument Servomechanisms with. Pastel, Thaler....294–7
Criteria for Instrument Servomechanisms with Coulomb Friction and Stiction, Stability. Pastel, Thaler....294–7
Criterion for Nonlinear Systems, A Stability. Ku, Wolf....144–7; disc. 147
Criterion in the Design of Adaptive Control Systems, Use of a Mathematical Error. Merriam....506–12
Cycling to Assure Reliability of Aircraft Control Equipment, Functional. Hulsey, Kessler....356–60

## D

Data Systems, Application of Continuous System Design Concepts to the Design of Sampled. Schmidt....74–8; disc. 78
D-C Electric Drilling Rigs: Application and Operation. Hogwood....286–9; disc. 289
D-C High-Potential Testing of Insulation Systems in Low- and Medium-Voltage D-C Equipment, Improved. Odok, Soelaiman....186–93; disc. 193
Dead Time and Sampling, Relay-Type Feedback Control Systems with. Izawa, Weaver. 49–53; disc. 53
Deep Ground Beds for Cathodic Protection. Trouard, Wagner....278–85
Describing-Function Technique, Limit-Cycle Stability Study of a Feedback Control System by a New. Harrington....129–33; disc. 134
Design Concepts to the Design of Sampled Data Systems, Application of Continuous System. Schmidt....74–8; disc. 78
Design Considerations for Large Industrial Semiconductor Rectifiers. Bowar....1–5
Design Considerations, Solar-Powered Thermoelectric Generator. Schuh, Tallent....345–52
Design Discussion of Thermoelectric Generation, An Elementary. Bollmeier....445–50
Designs of Electric Resistance Heating, Some Unusual. Hynes....40–3
Detector Car History and New Developments. Keevil....233–8; disc. 238
Development for Hypersonic Aircraft, Generator Insulation Systems. Penn, Balke, Precopio....255–9
Development of Fuses and Terminals for High-Temperature Applications. Bonwitt, Buttner....267–72
Devices: A Survey of the Methods in Use and Proposed, Variable-Speed Constant-Frequency. Owen....321–5; disc. 325
Dielectric Materials at 915 Mc, Rapid Heating of. Feiker, Gittinger....35–9
Diesel and Electric Locomotives on the Milwaukee Road, Multiple-Unit Operation of. Wylie....316–20; disc. 320
Discussion of Thermoelectric Generation, An Elementary Design. Bollmeier....445–50
(Domestic and Commercial) Electrified Fibrous Air Filters. Thomas, Woodfin....276–8
Drilling Rigs: Application and Operation, D-C Electric. Hogwood....286–9; disc. 289
Drive at Southland Paper Mills, Transistor Amplistat-Regulated Sectional. Vickery, Shaad....369–74; disc. 374
Drives, Elements of Reactor-Controlled Reversible Induction-Motor. Leonhard....106–14; disc. 114
Dual-Mode Relay Servos. Buland, Furumoto..405–11

## E

Effect of Closed-Loop Transfer Function Pole and Zero Locations on the Transient Response of Linear Control Systems. Elgerd, Stephens....121–7
Effect of Elevated Temperature on Flash-Welded Aluminum-Copper Joints, The. Dixon, Nelson....491–5; disc. 495
Effect of Variable High-Altitude Humidity on the Wear of Nondusting Brushes, The. Moberly, Johnson....263–7
Electric and Magnetic Conditions Inside an Induction-Heated Workpiece. Tudbury....79–82; disc. 83
Electric Drilling Rigs: Application and Operation, D-C. Hogwood....286–9; disc. 289
(Electric Heating) Control of Infrared Radiation. Barber....54–9
Electric Locomotives on the Milwaukee Road, Multiple-Unit Operation of Diesel and. Wylie....316–20; disc. 320
Electric Power Systems, Characteristics and Measurement of Ripple in Aircraft. Markowitz....418–23; disc. 423
Electric Resistance Heating, Some Unusual Designs of. Hynes....40–3
Electrical Analog for Determining Temperature Distribution in Electrical Components. Eckert, Hartnett, Irvine, Birkebak....5–10
Electrical and Electronic Components, Some Effects of Hypersonic Ionization on the Design of. Sisco, Fiskin....352–6
Electrical Features of the Four Corners Pipe Line. Sonnier, Siler....209–23
Electrical System Designs, Computer Evaluation of High-Temperature Aircraft A-C. Sollecito, Swann....434–44; disc. 444
Electrical Systems, A Solid Rotor A-C Generator for High-Temperature. Bateman..400–03; disc. 403
Electrified Fibrous Air Filters. Thomas, Woodfin....276–8
Electronic Components, Some Effects of Hypersonic Ionization on the Design of Electrical and. Sisco, Fiskin....352–6
Electronic Instruments, Nuclear Radiation and. Crittenden....423–6
(Electronics) Transient Voltages in Rectifier Transformers. Biega, Lord....83–9; disc. 89
Elementary Design Discussion of Thermoelectric Generation, An. Bollmeier....445–50
Elements of Reactor-Controlled Reversible Induction-Motor Drives. Leonhard....106–14; disc. 114
Elevated Temperature on Flash-Welded Aluminum-Copper Joints, The Effect of. Dixon, Nelson....491–5; disc. 495
Energy-Conversion Properties of Induction Machines in Variable-Speed Constant-Frequency Generating Systems. Riaz....25–30
Equipment, Functional Cycling to Assure Reliability of Aircraft Control. Hulsey, Kessler....356–60
Equipment, Improved D-C High-Potential Testing of Insulation Systems in Low- and Medium-Voltage D-C. Odok, Soelaiman....186–93; disc. 193
Equipment, Temperature Prediction in Thermal-Lag. Richards....462–5
Erratum....530
Error as a Measure of Control-System Performance, Probabilistic. Zaborszky, Diesel....163–8
Error Criterion in the Design of Adaptive Control Systems, Use of a Mathematical. Merriam...506–12
Evaluation of High-Temperature Aircraft A-C Electrical System Designs, Computer. Sollecito, Swann....434–44; disc. 444
Evaluation of Transient System Response. De Mello....177–86
Executive-Controlled Adaptive Systems. Staffin....523–30

## F

Farads, Milliohms, Microhenrys, Battery Impedance: Willihnganz, Rohner....259–62
Feedback Amplifiers, Transient Response and the Stabilization of. Mulligan....495–503
(Feedback Control) A New Chart Relating Open-Loop and Closed-Loop Frequency Responses of Linear Control Systems. Chen, Shen....252–5
(Feedback Control) A Practical Standard Transistorized Optimum Response Controller. Chen, Little....337–45; disc. 345
(Feedback Control) A Stability Criterion for Nonlinear Systems. Ku, Wolf....144–7; disc. 147
(Feedback Control) A Study of Nonlinear Systems with Random Inputs. Chuang, Kazda....100–05
(Feedback Control) A Suppressed-Carrier Signal Generator for Servosystem Instrumentation. Pollard....481–5
(Feedback Control) Analysis of A-C Servomotors Operated from Unbalanced Nonsinusoidal Voltage Sources and Nonlinear Discontinuous Source Impedances. Lind, Schmitz....476–9; disc. 479
(Feedback Control) Analysis of Nonlinear Sampled-Data Control Systems. Kinnen, Tou:
Part I....386–90; disc. 394
Part II....390–4; disc. 394
(Feedback Control) Application of Continuous System Design Concepts to the Design of Sampled Data Systems. Schmidt....74–8; disc. 78
(Feedback Control) Application of Switching Transistors and Saturable Reactors in a High-Performance Servo. Cox, Johannessen....466–74
(Feedback Control) Control by Stochastic Adjustment. Bertram....485–91
(Feedback Control) Dual-Mode Relay Servos. Buland, Furumoto....405–11
(Feedback Control) Effect of Closed-Loop Transfer Function Pole and Zero Locations on the Transient Response of Linear Control Systems. Elgerd, Stephens....121–7
(Feedback Control) Evaluation of Transient System Response. De Mello....177–86
(Feedback Control) Executive-Controlled Adaptive Systems. Staffin....523–30
(Feedback Control) Input-Output Relationships for Multisampled-Loop Systems. Lendaris, Jury....375–82; disc. 382
(Feedback Control) Notes on Bridged-T Complex Conjugate Compensation and 4-Terminal Network Loading. Chandaket, Rosenstein....148–58; disc. 158
(Feedback Control) Predicting the Performance of a Wind Tunnel Regulating System Using an Analog Computer. Herbst, Nichols, Keay, Miller..248–52
(Feedback Control) Probabilistic Error as a Measure of Control-System Performance. Zaborszky, Diesel....163–8
(Feedback Control) Signal Stabilization of a Control System. Oldenburger, Liu....96–100; disc. 100
(Feedback Control) Stability Criteria for Instrument Servomechanisms with Coulomb Friction and Stiction. Pastel, Thaler....294–7
Feedback Control System by a New Describing-Function Technique, Limit-Cycle Stability Study of a. Harrington....129–33; disc. 134
Feedback Control System Design for Random Inputs, A Relay-Type. Hopkin, Wang....228–33
Feedback Control Systems with Dead Time and Sampling, Relay-Type. Izawa, Weaver....49–53; disc. 53
(Feedback Control) The Linear Least Squares Synthesis of Multivariable Control Systems. Amara....115–19; disc. 119
(Feedback Control) The Optimum Control of Multiactuator Systems. McCausland....67–73
(Feedback Control) Transfer Functions of Loaded Synchronous Machine. Hamdi-Sepen....19–24
Feedback Systems, A Method for the Symbolic Representation and Analysis of Linear Periodic. Gilbert....512–22; disc. 522
Fibrous Air Filters, Electrified. Thomas, Woodfin....276–8
56-Inch Reversing Steel Mill, An Automatic Gage Controller for a. Duke, Hulls....10–15; disc. 15
Filters, Electrified Fibrous Air. Thomas, Woodfin....276–8
Flash-Welded Aluminum-Copper Joints, The Effect of Elevated Temperature on. Dixon, Nelson....491–5; disc. 495
Foil Mill Automatic Gage Control, The Use of Frequency Response Tests in the Analysis of a. Jones, Sills....59–67
Four Corners Pipe Line, Electrical Features of the. Sonnier, Siler....209–23
4-Terminal Network Loading, Notes on Bridged-T Complex Conjugate Compensation and. Chandaket, Rosenstein....148–58; disc. 158
Frequency A-C Power Using Variable Speed Generation, Constant. Jessee, Spaven....411–16; disc. 417
Frequency Devices: A Survey of the Methods in Use and Proposed, Variable-Speed Constant-. Owen....321–5; disc. 325
Frequency Generator System for Aircraft, Variable-Speed Constant-. Chirgwin, Stratton....304–09; disc. 309
Frequency Response Tests in the Analysis of a Foil Mill Automatic Gage Control, The Use of. Jones, Sills....59–67
Frequency Responses of Linear Control Systems, A New Chart Relating Open-Loop and Closed-Loop. Chen, Shen....252–5
Frequency Variable-Speed Frequency-Make-up Generators, Constant-. Hoard....297–301; disc. 301
Friction and Stiction, Stability Criteria for Instrument Servomechanisms with Coulomb. Pastel, Thaler....294–7
Function Pole and Zero Locations on the Transient Response of Linear Control Systems, Effect of Closed-Loop Transfer. Elgerd, Stephens....121–7
Functional Cycling to Assure Reliability of Aircraft Control Equipment. Hulsey, Kessler....356–60
Functions, New Methods of Simplifying Boolean. Howard....134–42; disc. 142
Functions of Loaded Synchronous Machine, Transfer. Hamdi-Sepen....19–24
Furnace, Load Characteristics of a Submerged-Arc Silicon-Smelting. Grant....273–5; disc. 275
Fuses and Terminals for High-Temperature Applications, Development of. Bonwitt, Buttner....267–72

## G

Gage Control, The Use of Frequency Response Tests in the Analysis of a Foil Mill Automatic. Jones, Sills....59–67
Gage Controller for a 56-Inch Reversing Steel Mill, An Automatic. Duke, Hulls....10–15; disc. 15
Generating System for Motor Coaches, A High-Capacity Maintenance-Free. Larson....311–16
Generating Systems, Energy-Conversion Properties of Induction Machines in Variable-Speed Constant-Frequency. Riaz....25–30
Generation, An Elementary Design Discussion of Thermoelectric. Bollmeier....445–50
Generation, Constant Frequency A-C Power Using Variable Speed. Jessee, Spaven....411–16; disc. 417
Generator Design Considerations, Solar-Powered Thermoelectric. Schuh, Tallent....345–52

Generator for High-Temperature Electrical Systems, A Solid Rotor A-C. Bateman....400–03; disc. 403
Generator for Servosystem Instrumentation, A Suppressed-Carrier Signal. Pollard....481–5
Generator Insulation Systems Development for Hypersonic Aircraft. Penn, Balke, Precopio....255–9
Generator, Optimum Reflector-Absorber Geometry for a Solar. Sitneman....332–7
Generator System for Aircraft, Variable-Speed Constant-Frequency. Chirgwin, Stratton.304–09; disc. 309
Generators, Constant-Frequency Variable-Speed Frequency-Make-up. Hoard....297–301; disc. 301
Generators, Reliability Analysis for Aircraft. Duane, Yeager....426–34
Geometry for a Solar Generator, Optimum Reflector-Absorber. Stineman....332–7
Ground Bed Design for Cathodic Protection of Underground Structures, Trends in. Landry, Howell....456–61; disc. 461
Ground Beds for Cathodic Protection, Deep. Trouard, Wagner....278–85

## H

Hanford Works, Cathodic Protection Applications at the. Bucholz....394–9
Heat Pump Coefficient of Performance, Significance of. Bary....90–5; disc. 95
Heated Workpiece, Electric and Magnetic Conditions Inside an Induction-. Tudbury....79–82; disc. 83
Heating Coils, Three-Phase Induction. Ross...291–4
Heating of Dielectric Materials at 915 Mc, Rapid. Feiker, Gittinger....35–9
Heating, Some Unusual Designs of Electric Resistance. Hynes....40–3
High-Altitude and Ultrahigh Temperature Electronic Transformer Applications, Terminal Spacings for. Duncan, Rectanus....16–19
High-Altitude Humidity on the Wear of Nondusting Brushes, The Effect of Variable. Moberly, Johnson....263–7
High-Capacity Maintenance-Free Generating System for Motor Coaches, A. Larson....311–16
High-Capacity Rectifier System, Anode Breaker Testing with a. Harris, Scully, Stewart....43–8
High-Performance Servo, Application of Switching Transistors and Saturable Reactors in a. Cox, Johannessen....466–74
High-Potential Testing of Insulation Systems in Low- and Medium-Voltage D-C Equipment, Improved D-C. Odok, Soelaiman....186–93; disc. 193
High-Speed Restarting and Protection of Large Synchronous Motors. Phillips, Yuen..360–7; disc. 367
High-Temperature Aircraft A-C Electrical System Designs, Computer Evaluation of. Sollecito, Swann....434–44; disc. 444
High-Temperature Aircraft, New Materials for Transformer-Rectifier Unit in. Hoop, McIlvaine....450–6
High-Temperature Applications, Development of Fuses and Terminals for. Bonwitt, Buttner....267–72
High-Temperature Electrical Systems, A Solid Rotor A-C Generator for. Bateman....400–03; disc. 403
History and New Developments, Detector Car. Keevil....233–8; disc. 238
Humidity on the Wear of Nondusting Brushes, The Effect of Variable High-Altitude. Moberly, Johnson....263–7
Hypersonic Aircraft, Generator Insulation Systems Development for. Penn, Balke, Precopio....255–9
Hypersonic Ionization on the Design of Electrical and Electronic Components, Some Effects of. Sisco, Fiskin....352–6

## I

Impedance: Farads, Milliohms, Microhenrys, Battery. Willihnganz, Rohner....259–62
Impedances, Analysis of A-C Servomotors Operated from Unbalanced Nonsinusoidal Voltage Sources and Nonlinear Discontinuous Source. Lind, Schmitz....476–9; disc. 479
Improved D-C High-Potential Testing of Insulation Systems in Low- and Medium-Voltage D-C Equipment. Odok, Soelaiman....186–93; disc. 193
Induction-Heated Workpiece, Electric and Magnetic Conditions Inside an. Tudbury....79–82; disc. 83
Induction Heating Coils, Three-Phase. Ross....291–4
Induction Machines in Variable-Speed Constant-Frequency Generating Systems, Energy-Conversion Properties of. Riaz....25–30
Induction-Motor Drives, Elements of Reactor-Controlled Reversible. Leonard....106–14; disc. 114
(Industrial and Commercial) Load Characteristics of a Submerged-Arc Silicon-Smelting Furnace. Grant....273–5; disc. 275
(Industrial Control) Elements of Reactor Controlled Reversible Induction-Motor Drives. Leonhard....106–14; disc. 114
(Industrial Control) New Methods of Simplifying Boolean Functions. Howard....134–42; disc. 142
Industrial Semiconductor Rectifiers, Design Considerations for Large. Bowar....1–5
Infrared Radiation, Control of. Barber....54–9
Input-Output Relationships for Multisampled-Loop Systems. Lendaris, Jury....374–82; disc. 382
Inputs, A Relay-Type Feedback Control System Design for Random. Hopkin, Wang....228–33
Inputs, A Study of Nonlinear Systems with Random. Chuang, Kazda....100–05
Instrument Servomechanisms with Coulomb Friction and Stiction, Stability Criteria for. Pastel, Thaler....294–7
Instrumentation, A Recommended Program for Resistance-Welding. Dixon....199–209
Instrumentation, A Suppressed-Carrier Signal Generator for Servosystem. Pollard....481–5
Instruments, Nuclear Radiation and Electronic. Crittenden....423–6
Insulation as Determined by AIEE Standard No. 510 Test Procedure, The Life Expectancy of Class A Random-Wound Motor. (Committee Report)....224–8
Insulation Systems Development for Hypersonic Aircraft, Generator. Penn, Balke, Precopio....255–9
Insulation Systems in Low- and Medium-Voltage D-C Equipment, Improved D-C High-Potential Testing of. Odok, Soelaiman....186–93; disc. 193
Ion Propulsion System, Practical Considerations of an. Lennert....326–31; disc. 331
Ionization on the Design of Electrical and Electronic Components, Some Effects of Hypersonic. Sisco, Fiskin....352–6

## J

Joints, The Effect of Elevated Temperature on Flash-Welded Aluminum-Copper. Dixon, Nelson....491–5; disc. 495

## L

(Land Transportation) A High-Capacity Maintenance-Free Generating System for Motor Coaches. Larson....311–16
(Land Transporation) Communication Systems for Railway Traffic Control. Sibley....30–5
(Land Transportation) Detector Car History and New Developments. Keevil....233–8; disc. 238
(Land Transportation) Improved D-C High-Potential Testing of Insulation Systems in Low- and Medium-Voltage D-C Equipment. Odok, Soelaiman....186–93; disc. 193
(Land Transportation) Modern Systems of Traffic Control as Applied to the Seaboard Air Line Railroad Company. DePriest....168–72
(Land Transportation) Multiple-Unit Operation of Diesel and Electric Locomotives on the Milwaukee Road. Wylie....316–20; disc. 320
(Land Transportation) Rapid Transit Is Expanding in Chicago. Forsythe....474–6
(Land Transportation) Traffic Control for Railroads. Baughman....173–6
Life Expectancy of Class A Random-Wound Motor Insulation as Determined by AIEE Standard No. 510 Test Procedure, The. (Committee Report)....224–8
Limit-Cycle Stability Study of a Feedback Control System by a New Describing-Function Technique. Harrington....129–33; disc. 134
Linear Control Systems, A New Chart Relating Open-Loop and Closed-Loop Frequency Responses of. Chen, Shen....252–5
Linear Control Systems, Effect of Closed-Loop Transfer Function Pole and Zero Locations on the Transient Response of. Elgerd, Stephens....121–7
Linear Least Squares Synthesis of Multivariable Control Systems, The. Amara....115–19; disc. 119
Linear Periodic Feedback Systems, A Method for the Symbolic Representation and Analysis of. Gilbert....512–22; disc. 522
Load Characteristics of a Submerged-Arc Silicon-Smelting Furnace. Grant....273–5; disc. 275
Loaded Synchronous Machine, Transfer Functions of. Hamdi-Sepen....19–24
Loading, Notes on Bridged-T Complex Conjugate Compensation and 4-Terminal Network. Chandaket, Rosenstein....148–58; disc. 158
Locomotives on the Milwaukee Road, Multiple-Unit Operation of Diesel and Electric. Wylie....316–20; disc. 320
Loop Systems, Input-Output Relationships for Multisampled-. Lendaris, Jury....375–82; disc. 382
Loop Transfer Function Pole and Zero Locations on the Transient Response of Linear Control Systems, Effect of Closed-. Elgerd, Stephens....121–7
Low- and Medium-Voltage D-C Equipment, Improved D-C High-Potential Testing of Insulation Systems in. Odok, Soelaiman....186–93; disc. 193

## M

Machines in Variable-Speed Constant-Frequency Generating Systems, Energy-Conversion Properties of Induction. Riaz....25–30
Magnetic Conditions Inside an Induction-Heated Workpiece, Electric and. Tudbury....79–82; disc. 83
Maintenance-Free Generating System for Motor Coaches, A High-Capacity. Larson....311–16
(Marine Transportation) Aluminum Bus for Shipboard Application. Thompson, Behr...239–47; disc. 247
Materials for Transformer-Rectifier Unit in High-Temperature Aircraft, New. Hoop, McIlvaine....450–6
Mathematical Error Criterion in the Design of Adaptive Control Systems, Use of a. Merriam....506–12
Measure of Control-System Performance, Probabilistic Error as a. Zaborszky, Diesel....163–8
Measurement of Ripple in Aircraft Electric Power Systems, Characteristics and. Markowitz....418–23; disc. 423
(Metal Industry) An Automatic Gage Controller for a 56-Inch Reversing Steel Mill. Duke, Hulls....10–15; disc. 15
(Metal Industry) The Use of Frequency Response Tests in the Analysis of a Foil Mill Automatic Gage Control. Jones, Sills....59–67
Method for the Symbolic Representation and Analysis of Linear Periodic Feedback Systems, A. Gilbert....512–22; disc. 522
Methods of Simplifying Boolean Functions, New. Howard....134–42; disc. 142
Microhenrys, Battery Impedance: Farads, Milliohms, Willihnganz, Rohner....259–62
Mill, An Automatic Gage Controller for a 56-Inch Reversing Steel. Duke, Hulls....10–15; disc. 15
Mill Automatic Gage Control, The Use of Frequency Response Tests in the Analysis of a Foil. Jones, Sills....59–67
Milliohms, Microhenrys, Battery Impedance: Farads, Willihnganz, Rohner....259–62
Milwaukee Road, Multiple-Unit Operation of Diesel and Electric Locomotives on the. Wylie....316–20; disc. 320
Mode Relay Servos, Dual-. Buland, Furumoto....405–11
Modern Systems of Traffic Control as Applied to the Seaboard Air Line Railroad Company. DePriest....168–72
Motor Coaches, A High-Capacity Maintenance-Free Generating System for. Larson....311–16
Motor Controllers for Rubber and Plastics Industries, Proposed Recommended Practices for Medium-Voltage. Watkins....504–06; disc. 506
Motor Drives, Elements of Reactor-Controlled Reversible Induction-. Leonhard...106–14; disc. 114
Motor Insulation as Determined by AIEE Standard No. 510 Test Procedure, The Life Expectancy of Class A Random-Wound. (Committee Report)....224–8
Motors, High-Speed Restarting and Protection of Large Synchronous. Phillips, Yuen....360–7; disc. 367
Multiactuator Systems, The Optimum Control of. McCausland....67–73
Multisampled-Loop Systems, Input-Output Relationships for. Lendaris, Jury....375–82; disc. 382
Multivariable Control Systems, The Linear Least Squares Synthesis of. Amara....115–19; disc. 119

## N

Network Loading, Notes on Bridged-T Complex Conjugate Compensation and 4-Terminal. Chandaket, Rosenstein....148–58; disc. 158
New Methods of Simplifying Boolean Functions. Howard....134–42; disc. 142
915 Mc, Rapid Heating of Dielectric Materials at. Feiker, Gittinger....35–9
Nonlinear Discontinuous Source Impedances, Analysis of A-C Servomotors Operated from Unbalanced Nonsinusoidal Voltage Sources and. Lind, Schmitz....476–9; disc. 479
Nonlinear Sampled-Data Control Systems, Analysis of. Kinnen, Tou:
Part I....386–90; disc. 394
Part II....390–4; disc. 394
Nonlinear Systems, A Stability Criterion for. Ku, Wolf....144–7; disc. 147
Nonlinear Systems with Random Inputs, A Study of. Chuang, Kazda....100–05
Notes on Bridged-T Complex Conjugate Compensation and 4-Terminal Network Loading. Chandaket, Rosenstein....148–58; disc. 158
Nuclear Radiation and Electronic Instruments. Crittenden....423–6

## O

Open-Loop and Closed-Loop Frequency Responses of Linear Control Systems, A New Chart Relating. Chen, Shen....252–5

Optimum Control of Multiactuator Systems, The. McCausland....67–73
Optimum Reflector-Absorber Geometry for a Solar Generator. Stineman....332–7
Optimum Response Controller, A Practical Standard Transistorized. Chen, Little....337–45; disc. 345
Output Relationships for Multisampled Loop Systems, Input-. Lendaris, Jury....375–82; disc. 382

## P

Paper Mills, Transistor Amplistat-Regulated Sectional Drive at Southland. Vickery, Shaad....369–74; disc. 374
Performance, Probabilistic Error as a Measure of Control-System. Zaborszky, Diesel....163–8
Performance, Significance of Heat Pump Coefficient of. Bary....90–5; disc. 95
(Petroleum Industry) D-C Electric Drilling Rigs: Application and Operation. Hogwood....286–9; disc. 289
(Petroleum Industry) Electrical Features of the Four Corners Pipe Line. Sonnier, Siler....209–23
Pipe Line, Electrical Features of the Four Corners. Sonnier, Siler....209–23
Pole and Zero Locations on the Transient Response of Linear Control Systems, Effect of Closed-Loop Transfer Function. Elgerd, Stephens....121–7
Power Systems, Characteristics and Measurement of Ripple in Aircraft Electric. Markowitz....418–23; disc. 423
Power Using Variable Speed Generation, Constant Frequency A-C. Jessee, Spaven..411–16; disc. 417
Practical Considerations of an Ion Propulsion System. Lennert....326–31; disc. 331
Practical Standard Transistorized Optimum Response Controller, A. Chen, Little....337–45; disc. 345
Practices for Medium-Voltage Motor Controllers for Rubber and Plastics Industries, Proposed Recommended. Watkins....504–06; disc. 506
Predicting the Performance of a Wind Tunnel Regulating System Using an Analog Computer. Herbst, Nichols, Keay, Miller....248–52
Probabilistic Error as a Measure of Control-System Performance. Zaborszky, Diesel....163–8
Program for Resistance-Welding Instrumentation, A Recommended. Dixon....199–209
Properties of Induction Machines in Variable-Speed Constant-Frequency Generating Systems, Energy-Conversion. Riaz....25–30
Proposed Recommended Practices for Medium-Voltage Motor Controllers for Rubber and Plastics Industries. Watkins....504–06; disc. 506
Propulsion System, Practical Considerations of an Ion. Lennert....326–31; disc. 331
Protection of Large Synchronous Motors, High-Speed Restarting and. Phillips, Yuen...360–7; disc. 367
Pump Coefficient of Performance, Significance of Heat. Bary....90–5; disc. 95

## R

Radiation and Electronic Instruments, Nuclear. Crittenden....423–6
Radiation, Control of Infrared. Barber....54–9
Railroads, Traffic Control for. Baughman....173–6
Railway Traffic Control, Communication Systems for. Sibley....30–5
Random Inputs, A Relay-Type Feedback Control System Design for. Hopkin, Wang....228–33
Random Inputs, A Study of Nonlinear Systems with. Chuang, Kazda....100–05
Random-Wound Motor Insulation as Determined by AIEE Standard No. 510 Test Procedure, The Life Expectancy of Class A. (Committee Report)....224–8
Rapid Heating of Dielectric Materials at 915 Mc. Feiker, Gittinger....35–9
Rapid Transit is Expanding in Chicago. Forsythe....474–6
Reactor-Controlled Reversible Induction-Motor Drives, Elements of. Leonhard....106–14; disc. 114
Recommended Practices for Medium-Voltage Motor Controllers for Rubber and Plastics Industries, Proposed. Watkins....504–06; disc. 506
Recommended Program for Resistance-Welding Instrumentation, A. Dixon....199–209
Rectifier System, Anode Breaker Testing with a High-Capacity. Harris, Scully, Stewart....43–8
Rectifier Transformers, Transient Voltages in. Biega, Lord....89–9; disc. 89
Rectifier Unit in High-Temperature Aircraft, New Materials for Transformer-. Hoop, McIlvaine....450–6
Rectifiers, Design Considerations for Large Industrial Semiconductor. Bowar....1–5
Reflector-Absorber Geometry for a Solar Generator, Optimum. Stineman....332–7
Regulating System Using an Analog Computer, Predicting the Performance of a Wind Tunnel. Herbst, Nichols, Keay, Miller....248–52
Relationships for Multisampled-Loop Systems, Input-Output. Lendaris, Jury....375–82; disc. 382
Relay Servos, Dual-Mode. Buland, Furumoto..405–11
Relay-Type Feedback Control System Design for Random Inputs, A. Hopkin, Wang....228–33
Relay-Type Feedback Control Systems with Dead Time and Sampling. Izawa, Weaver....49–53; disc. 53
Reliability Analysis for Aircraft Generators. Duane, Yeager....426–34
Representation and Analysis of Linear Periodic Feedback Systems, A Method for the Symbolic. Gilbert....512–22; disc. 522
Resistance Heating, Some Unusual Designs of Electric. Hynes....40–3
Resistance-Welding Instrumentation, A Recommended Program for. Dixon....199–209
Response and the Stabilization of Feedback Amplifiers, Transient. Mulligan....495–503
Response Controller, A Practical Standard Transistorized Optimum. Chen, Little....337–45; disc. 345
Response, Evaluation of Transient System. DeMello....177–86
Restarting and Protection of Large Synchronous Motors, High-Speed. Phillips, Yuen....360–7; disc. 367
Reversible Induction-Motor Drives, Elements of Reactor-Controlled. Leonhard..106–14; disc. 114
Reversing Steel Mill, An Automatic Gage Controller for a 56-Inch. Duke, Hulls....10–15; disc. 15
Rigs: Application and Operation, D-C Electric Drilling. Hogwood....286–9; disc. 289
Ripple in Aircraft Electric Power Systems, Characteristics and Measurement of. Markowitz....418–23; disc. 423
(Rotating Machinery) Constant Frequency A-C Power Using Variable Speed Generation. Jessee, Spaven....411–16; disc. 417
Rotor A-C Generator for High-Temperature Electrical Systems, A Solid. Bateman....400–03; disc. 403
Rubber and Plastics Industries, Proposed Recommended Practices for Medium-Voltage Motor Controllers for. Watkins....504–06; disc. 506

## S

Sampled-Data Control Systems, Analysis of Nonlinear. Kinnen, Tou:
Part I....386–90; disc. 394
Part II....390–4; disc. 394
Sampled Data Systems, Application of Continuous System Design Concepts to the Design of. Schmidt....74–8; disc. 78
Sampling, Relay-Type Feedback Control Systems with Dead Time and. Izawa, Weaver...49–53; disc. 53
Saturable Reactors in a High-Performance Servo, Application of Switching Transistors and. Cox, Johannessen....466–74
Seaboard Air Line Railroad Company, Modern Systems of Traffic Control as Applied to the. DePriest....168–72
Sectional Drive at Southland Paper Mills, Transistor Amplistat-Regulated. Vickery, Shaad....369–74; disc. 374
Semiconductor Rectifiers, Design Considerations for Large Industrial. Bowar....1–5
Servo, Application of Switching Transistors and Saturable Reactors in a High-Performance. Cox, Johannessen....466–74
Servomechanisms with Coulomb Friction and Stiction, Stability Criteria for Instrument. Pastel, Thaler....294–7
Servomotors Operated from Unbalanced Nonsinusoidal Voltage Sources and Nonlinear Discontinuous Source Impedances, Analysis of A-C. Lind, Schmitz....476–9; disc. 479
Servos, Dual-Mode Relay. Buland, Furumoto..405–11
Servosystem Instrumentation, A Suppressed-Carrier Signal Generator for. Pollard....481–5
Shipboard Application, Aluminum Bus for. Thompson, Behr....239–47; disc. 247
Signal Generator for Servosystem Instrumentation, A Suppressed-Carrier. Pollard....481–5
Signal Stabilization of a Control System. Oldenburger, Liu....96–100; disc. 100
Significance of Heat Pump Coefficient of Performance. Bary....90–5; disc. 95
Silicon-Smelting Furnace, Load Characteristics of a Submerged-Arc. Grant....273–5; disc. 275
Simplifying Boolean Functions, New Methods of. Howard....134–42; disc. 142
Smelting Furnace, Load Characteristics of a Submerged-Arc Silicon-. Grant....273–5; disc. 275
Solar Generator, Optimum Reflector-Absorber Geometry for a. Stineman....332–7
Solar-Powered Thermoelectric Generator Design Considerations. Schuh, Tallent....345–52
Solid Rotor A-C Generator for High-Temperature Electrical Systems, A. Bateman....400–03; disc. 403
Some Effects of Hypersonic Ionization on the Design of Electrical and Electronic Components. Sisco, Fiskin....352–6
Some Unusual Designs of Electric Resistance Heating. Hynes....40–3
Sources and Nonlinear Discontinuous Source Impedances, Analysis of A-C Servomotors Operated from Unbalanced Nonsinusoidal Voltage. Lind, Schmitz....476–9; disc. 479
Southland Paper Mills, Transistor Amplistat-Regulated Sectional Drive at. Vickery, Shaad....369–74; disc. 374
Speed Generation, Constant Frequency A-C Power Using Variable. Jessee, Spaven..411–16; disc. 417
Squares Synthesis of Multivariable Control Systems, The Linear Least. Amara....115–19; disc. 119
Stability Criteria for Instrument Servomechanisms with Coulomb Friction and Stiction. Pastel, Thaler....294–7
Stability Criterion for Nonlinear Systems, A. Ku, Wolf....144–7; disc. 147
Stability Study of a Feedback Control System by a New Describing-Function Technique, Limit-Cycle. Harrington....129–33; disc. 134
Stabilization of a Control System, Signal. Oldenburger, Liu....96–100; disc. 100
Stabilization of Feedback Amplifiers, Transient Response and the. Mulligan....495–503
Standard No. 510 Test Procedure, The Life Expectancy of Class A Random-Wound Motor Insulation as Determined by AIEE. (Committee Report)....224–8
Standard Transistorized Optimum Response Controller, A Practical. Chen, Little....337–45; disc. 345
Steel Mill, An Automatic Gage Controller for a 56-Inch Reversing. Duke, Hulls....10–15; disc. 15
Stiction, Stability Criteria for Instrument Servomechanisms with Coulomb Friction and. Pastel, Thaler....294–7
Stochastic Adjustment, Control by. Bertram....485–9
Structures, Trends in Ground Bed Design for Cathodic Protection of Underground. Landry, Howell....456–61; disc. 461
Study of a Feedback Control System by a New Describing-Function Technique, Limit-Cycle Stability. Harrington....129–33; disc. 134
Study of Nonlinear Systems With Random Inputs, A. Chuang, Kazda....100–05
Submerged-Arc Silicon-Smelting Furnace, Load Characteristics of a. Grant....273–5; disc. 275
Suppressed-Carrier Signal Generator for Servosystem Instrumentation, A. Pollard....481–5
Survey of the Methods in Use and Proposed, Variable-Speed Constant-Frequency Devices: A. Owen....321–5; disc. 325
Switching Transistors and Saturable Reactors in a High-Performance Servo, Application of. Cox, Johannessen....466–74
Symbolic Representation and Analysis of Linear Periodic Feedback Systems, A Method for the. Gilbert....512–22; disc. 522
Synchronous Machine, Transfer Functions of Loaded. Hamdi-Sepen....19–24
Synchronous Motors, High-Speed Restarting and Protection of Large. Phillips, Yuen....360–7; disc. 367
Synthesis of Multivariable Control Systems, The Linear Least Squares. Amara....115–19; disc. 119
System Design Concepts to the Design of Sampled Data Systems, Application of Continuous. Schmidt....74–8; disc. 78
System Designs, Computer Evaluation of High-Temperature Aircraft A-C Electrical. Sollecito, Swann....434–44; disc. 444
System Response, Evaluation of Transient. De Mello....177–86
Systems, A Stability Criterion for Nonlinear. Ku, Wolf....144–7; disc. 147
Systems Development for Hypersonic Aircraft, Generator Insulation. Penn, Balke, Precopio...255–9
Systems, Executive-Controlled Adaptive. Staffin....523–30
Systems, The Optimum Control of Multiactuator Systems. McCausland....67–73
Systems with Random Inputs, A Study of Nonlinear. Chuang, Kazda....100–05

## T

Technique, Limit-Cycle Stability Study of a Feedback Control System by a New Describing-Function. Harrington....129–33; disc. 134
Temperature Aircraft A-C Electrical System Designs, Computer Evaluation of High-. Sollecito, Swann....434–44; disc. 444
Temperature Aircraft, New Materials for Transformer-Rectifier Unit in High-. Hoop, McIlvaine...450–6
Temperature Applications, Development of Fuses and Terminals for High-. Bonwitt, Buttner....267–72
Temperature Distribution in Electrical Components, The Electrical Analog for Determining. Eckert, Hartnett, Irvine, Birkebak....5–10
Temperature Electronic Transformer Applications, Terminal Spacings for High-Altitude and Ultra-high-. Duncan, Rectanus....16–19

Temperature on Flash-Welded Aluminum-Copper Joints, The Effect of Elevated. Dixon, Nelson....491–5; disc. 495
Temperature Prediction in Thermal-Lag Equipment. Richards....462–5
Terminal Spacings for High-Altitude and Ultrahigh-Temperature Electronic Transformer Applications. Duncan, Rectanus....16–19
Terminals for High-Temperature Applications, Development of Fuses and. Bonwitt, Buttner..267–72
Testing of Insulation Systems in Low- and Medium-Voltage D-C Equipment, Improved D-C High-Potential. Odok, Soelaiman....186–93; disc. 193
Testing with a High-Capacity Rectifier System, Anode Breaker. Harris, Scully, Stewart....43–8
Tests in the Analysis of a Foil Mill Automatic Gage Control, The Use of Frequency Response. Jones, Sills....59–67
Thermal-Lag Equipment, Temperature Prediction in. Richards....462–5
Thermoelectric Generation, An Elementary Design Discussion of. Bollmeier....445–50
Thermoelectric Generator Design Considerations, Solar-Powered. Schuh, Tallent....345–52
Three-Phase Induction Heating Coils. Ross....291–4
Traffic Control as Applied to the Seaboard Air Line Railroad Company, Modern Systems of. DePriest....168–72
Traffic Control, Communication Systems for Railway. Sibley....30–5
Traffic Control for Railroads. Baughman....173–6
Transfer Function Pole and Zero Locations on the Transient Response of Linear Control Systems, Effect of Closed-Loop. Elgerd, Stephens....121–7
Transfer Functions of Loaded Synchronous Machine. Hamdi-Sepen....19–24
Transformer Applications, Terminal Spacings for High-Altitude and Ultrahigh-Temperature Electronic. Duncan, Rectanus....16–19
Transformer-Rectifier Unit in High-Temperature Aircraft, New Materials for. Hoop, McIlvaine....450–6
Transformers, Transient Voltages in Rectifier. Biega, Lord....83–9; disc. 89
Transient Response and the Stabilization of Feedback Amplifiers. Mulligan....495–503
Transient Response of Linear Control Systems, Effect of Closed-Loop Transfer Function Pole and Zero Locations on the. Elgerd, Stephens....121–7
Transient System Response, Evaluation of. De Mello....177–86
Transient Voltages in Rectifier Transformers. Biega, Lord....83–9; disc. 89
Transistor Amplistat-Regulated Sectional Drive at Southland Paper Mills. Vickery, Shaad....369–74; disc. 374
Transistorized Optimum Response Controller, A Practical Standard. Chen, Little....337–45; disc. 345
Transistors and Saturable Reactors in a High-Performance Servo, Application of Switching. Cox, Johannessen....466–74
Transit Is Expanding in Chicago, Rapid. Forsythe....474–6
Transportation, Air) A Solid Rotor A-C Generator for High Temperature Electrical Systems. Bateman....400–03; disc. 403
Transportation, Air) An Elementary Design Discussion of Thermoelectric Generation. Bollmeier...445–50
Transportation, Air) Constant-Frequency Variable-Speed Frequency-Make-up Generators. Hoard....297–301; disc. 301
Transportation, Air) Development of Fuses and Terminals for High-Temperature Applications. Bonwitt, Buttner....267–72
Transportation, Air) Energy-Conversion Properties of Induction Machines in Variable-Speed Constant-Frequency Generating Systems. Riaz....25–30
Transportation, Air) Nuclear Radiation and Electronic Instruments. Crittenden....423–6
Transportation, Air) Optimum Reflector-Absorber Geometry for a Solar Generator. Stineman..332–7
Transportation, Air) Practical Considerations of an Ion Propulsion System. Lennert....326–31; disc. 331
Transportation, Air) Solar-Powered Thermoelectric Generator Design Considerations. Schuh, Tallent....345–52
Transportation, Air) Some Effects of Hypersonic Ionization on the Design of Electrical and Electronic Components. Sisco, Fiskin....352–6
Transportation, Air) Temperature Prediction in Thermal-Lag Equipment. Richards....462–5
Transportation, Air) Terminal Spacings for High-Altitude and Ultrahigh-Temperature Electronic Transformer Applications. Duncan, Rectanus....16–19
Transportation, Air) The Effect of Variable High-Altitude Humidity on the Wear of Nondusting Brushes. Moberly, Johnson....263–7
Transportation, Air) The Electrical Analog for Determining Temperature Distribution in Electrical Components. Eckert, Hartnett, Irvine, Birkebak....5–10
(Transportation, Air) Variable-Speed Constant-Frequency Devices: A Survey of the Methods in Use and Proposed. Owen....321–5; disc. 325
(Transportation, Land) A High-Capacity Maintenance-Free Generating System for Motor Coaches. Larson....311–16
(Transportation, Land) Communication Systems for Railway Traffic Control. Sibley....30–5
(Transportation, Land) Detector Car History and New Developments. Keevil....233–8; disc. 238
(Transportation, Land) Modern Systems of Traffic Control as Applied to the Seaboard Air Line Railroad Company. DePriest....168–72
(Transportation, Land) Multiple-Unit Operation of Diesel and Electric Locomotives on the Milwaukee Road. Wylie....316–20; disc. 320
(Transportation, Land) Rapid Transit Is Expanding in Chicago. Forsythe....474–6
(Transportation, Land) Traffic Control for Railroads. Baughman....173–6
(Transportation, Marine) Aluminum Bus for Shipboard Application. Thompson, Behr...239–47; disc. 247
Trends in Ground Bed Design for Cathodic Protection of Underground Structures. Landry, Howell....456–61; disc. 461

## U

Unbalanced Nonsinusoidal Voltage Sources and Nonlinear Discontinuous Source Impedances, Analysis of A-C Servomotors Operated from. Lind, Schmitz....476–9; disc. 479
Underground Structures, Trends in Ground Bed Design for Cathodic Protection of. Landry, Howell....456–61; disc. 461
Use of a Mathematical Error Criterion in the Design of Adaptive Control Systems. Merriam....506–12
Use of Frequency Response Tests in the Analysis of a Foil Mill Automatic Gage Control, The. Jones, Sills....59–67

## V

Variable High-Altitude Humidity on the Wear of Nondusting Brushes, The Effect of. Moberly, Johnson....263–7
Variable-Speed Constant-Frequency Devices: A Survey of the Methods in Use and Proposed. Owen....321–5; disc. 325
Variable-Speed Constant-Frequency Generating Systems, Energy-Conversion Properties of Induction Machines in. Riaz....25–30
Variable-Speed Constant-Frequency Generator System for Aircraft. Chirgwin, Stratton....304–09; disc. 309
Variable-Speed Frequency-Make-up Generators, Constant-Frequency. Hoard....297–301; disc. 301
Variable Speed Generation, Constant Frequency A-C Power Using. Jessee, Spaven....411–16; disc. 417
Voltage Sources and Nonlinear Discontinuous Source Impedances, Analysis of A-C Servomotors Operated from Unbalanced Nonsinusoidal. Lind, Schmitz....476–9; disc. 479
Voltages in Rectifier Transformers, Transient. Biega, Lord....83–9; disc. 89

## W

Welded Aluminum-Copper Joints, The Effect of Elevated Temperature on Flash-. Dixon, Nelson....491–5; disc. 495
Welding Instrumentation, A Recommended Program for Resistance-. Dixon....199–209
Wind Tunnel Regulating System Using an Analog Computer, Predicting the Performance of a. Herbst, Nichols, Keay, Miller....248–52
Workpiece, Electric and Magnetic Conditions Inside an Induction-Heated. Tudbury....79–82; disc. 83
Wound Motor Insulation as Determined by AIEE Standard No. 510 Test Procedure, The Life Expectancy of Class A Random-. (Committee Report)....224–8

## Z

Zero Locations on the Transient Response of Linear Control Systems, Effect of Closed-Loop Transfer Function Pole and. Elgerd, Stephens....121–7

# 2. Author Index

Amara, R. C. The Linear Least Squares Synthesis of Multivariable Control Systems. (59–214)....115–19; disc. 120
Ash, R. B.; W. H. Kim, G. M. Kranc. Disc....383

## B

Baker, R. M. Disc....83
Balke, R. L.; W. B. Penn, F. M. Precopio. Generator Insulation Systems Development for Hypersonic Aircraft. (59–864)....255–9
Barber, Ira J. Control of Infrared Radiation. (59–31)....54–9
Bary, Constantine W. Significance of Heat Pump Coefficient of Performance. (59–20)....90–5; disc. 96
Bateman, J. T. A Solid Rotor A-C Generator for High-Temperature Electrical Systems. (59–848)....400–03; disc. 405
Baughman, G. W. Traffic Control for Railroads. (59–252)....173–6
Behr, S. H.; G. J. Thompson. Aluminum Bus for Shipboard Application. (59–654)....239–47; disc. 247
Bertram, J. E. Control by Stochastic Adjustment. (59–1156)....485–91
Bhimani, B. V. Disc....194
Biega, B. C.; H. W. Lord. Transient Voltages in Rectifier Transformers. (59–149)...83–9; disc. 90
Birkebak, Richard; E. R. G. Eckert, J. P. Hartnett, T. F. Irvine. The Electrical Analog for Determining Temperature Distribution in Electrical Components. (58–920)....5–10
Bollmeier, E. W. An Elementary Design Discussion of Thermoelectric Generation. (59–867)....445–50
Bond, N. T. Disc....247
Bonwitt, W. F.; H. Buttner. Development of Fuses and Terminals for High-Temperature Applications. (59–771)....267–72
Bowar, Gerald J. Design Considerations for Large Industrial Semiconductor Rectifiers. (58–222)....1–5
Brightman, F. P. Disc....367
Bucholz, C. S. Cathodic Protection Applications at the Hanford Works. (59–821)....394–9
Buland, R. M.; N. Furumoto. Dual-Mode Relay Servos. (59–840)....405–11
Bultman, E. W.; C. W. Martin. Disc....195
Buttner, H.; W. F. Bonwitt. Development of Fuses and Terminals for High-Temperature Applications. (59–771)....267–72

## C

Cameron, A. W. W. Disc....195
Campbell, S. J.; E. C. Fox. Disc....374
Candee, A. H. Disc....290
Chandaket, Prapat; A. B. Rosenstein. Notes on Bridged-T Complex Conjugate Compensation and 4-Terminal Network Loading. (59–220)....148–58; disc. 162
Chen, C. F.; D. W. C. Shen. A New Chart Relating Open-Loop and Closed-Loop Frequency Responses of Linear Control Systems. (59–647)....252–5
Chen, Kan; D. R. Little. A Practical Standard Transistorized Optimum Response Controller. (59–838)....337–45; disc. 345
Chestnut, Harold. Disc....345
Chirgwin, K. M. Disc....403
Chirgwin, K. M.; L. J. Stratton. Variable-Speed Constant-Frequency Generator System for Aircraft. (59–872)....304–09; disc. 309
Chirgwin, K. M.; L. J. Stratton. Disc....301, 417
Chuang, Kuei; L. F. Kazda. A Study of Nonlinear Systems with Random Inputs. (59–147)...100–05
Colehower, E. W. Disc....423
Correy, Thomas B. Disc....495
Cox, Fred B.; P. R. Johannessen. Application of Switching Transistors and Saturable Reactors in a High-Performance Servo. (58–89)....466–74
Crittenden, J. R. Nuclear Radiation and Electronic Instruments. (59–873)....423–6
Curdts, E. B. Disc....195

## D

De Mello, F. P. Evaluation of Transient System Response. (59–255)....177–86
DePriest, J. R. Modern Systems of Traffic Control as Applied to the Seaboard Air Line Railroad Company. (59–251)....168–72
De Remer, J. Grant. Disc....95
Diesel, J. W.; J. Zaborszky. Probabilistic Error as a Measure of Control-System Performance. (59–199)....163–8
Dixon, A. A Recommended Program for Resistance-Welding Instrumentation. (58–210)....199–209
Dixon, C. R.; F. G. Nelson. The Effect of Elevated Temperature on Flash-Welded Aluminum-Copper Joints. (59–1162)....491–5; disc. 495
Duane, J. T. Disc....309
Duane, J. T.; L. J. Yeager. Reliability Analysis for Aircraft Generators. (59–888)....426–34

Duke, R. L.; L. R. Hulls. An Automatic Gage Controller for a 56-Inch Reversing Steel Mill. (58–903).....10–15; disc. 16
Duncan, G. I.; W. A. Rectanus. Terminal Spacings for High-Altitude and Ultrahigh-Temperature Electronic Transformer Applications. (58–118).....16–19


## E


Eckert, E. R. G.; J. P. Hartnett, T. F. Irvine, R. Birkebak. The Electrical Analog for Determining Temperature Distribution in Electrical Components. (58–920).....5–10
Eibling, J. A.; D. W. Locklin. Disc.....95
Elgerd, Olle I.; W. C. Stephens. Effect of Closed-Loop Transfer Function Pole and Zero Locations on the Transient Response of Linear Control Systems. (59–197).....121–7


## F


Feiker, G. E.; N. C. Gittinger. Rapid Heating of Dielectric Materials at 915 Mc. (59–30).....35–9
Fiskin, J. M.; W. B. Sisco. Some Effects of Hypersonic Ionization on the Design of Electrical and Electronic Components. (59–885).....352–6
Forsythe, Stanley D. Rapid Transit is Expanding in Chicago. (56–837).....474–6
Fox, E. C.; S. J. Campbell. Disc.....374
Franklin, Gene. Disc.....74
Freeman, H. Disc.....119
Furumoto, N.; R. M. Buland. Dual-Mode Relay Servos. (59–840).....405–11


## G


Gardner, W. F.; E. H. Peters. Disc.....506
Gibson, J. E. Disc.....53
Gilbert, Edward O. A Method for the Symbolic Representation and Analysis of Linear Periodic Feedback Systems. (59–1183).....512–22; disc. 523
Gittinger, N. C.; G. E. Feiker. Rapid Heating of Dielectric Materials at 915 Mc. (59–30).....35–9
Gleixner, H. Disc.....114
Grant, George, III. Load Characteristics of a Submerged-Arc Silicon-Smelting Furnace. (58–1259).....273–5; disc. 275


## H


Halacsy, Andrew A. Disc.....90
Hamdi-Sepen, D. Transfer Functions of Loaded Synchronous Machine. (58–796).....19–24
Hamilton, W. S. H. Disc.....320
Harrington, H. J. Limit-Cycle Stability Study of a Feedback Control System by a New Describing Function Technique. (59–233).....129–33; disc. 134
Harris, L. J.; T. J. Scully, V. N. Stewart. Anode Breaker Testing with a High-Capacity Rectifier System. (58–224).....43–8
Hartnett, J. P.; E. R. G. Eckert, T. F. Irvine, R. Birkebak. The Electrical Analog for Determining Temperature Distribution in Electrical Components. (58–920).....5–10
Herbst, R.; J. O. Nichols, F. W. Keay, R. W. Miller. Predicting the Performance of a Wind Tunnel Regulating System Using an Analog Computer. (59–646).....248–52
Higgins, Thomas J. Disc.....394, 444
Hoard, Bert V. Constant-Frequency Variable-Speed Frequency-Make-up Generators. (59–773).....297–301; disc. 303
Hoard, Bert V. Disc.....309, 325, 417
Hogwood, E. E., Jr. D-C Electric Drilling Rigs: Application and Operation. (59–1103).....286–9; disc. 291
Hoop, J. G.; D. K. McIlvaine. New Materials for Transformer-Rectifier Unit in High-Temperature Aircraft. (59–883).....450–6
Hopkin, A. M.; R. M. Saunders. Disc.....479
Hopkin, A. M.; P. K. C. Wang. A Relay-Type Feedback Control System Design for Random Inputs. (59–218).....228–33
Howard, R. L. New Methods of Simplifying Boolean Functions. (59–91).....134–42; disc. 143
Howell, I. N., Jr.; A. P. Landry. Trends in Ground Bed Design for Cathodic Protection of Underground Structures. (59–820).....456–61; disc. 462
Hulls, L. R.; R. L. Duke. An Automatic Gage Controller for a 56-Inch Reversing Steel Mill. (58–903).....10–15; disc. 16
Hulsey, R. E.; L. L. Kessler. Functional Cycling to Assure Reliability of Aircraft Control Equipment. (59–912).....356–60
Hynes, Lee P. Some Unusual Designs of Electric Resistance Heating. (59–77).....40–3


## I


Irvine, T. F.; E. R. G. Eckert, J. P. Hartnett, R. Birkebak. The Electrical Analog for Determining Temperature Distribution in Electrical Components. (58–920).....5–10
Izawa, Keisuke. Disc.....394
Izawa, Keisuke; L. E. Weaver. Relay-Type Feedback Control Systems with Dead Time and Sampling. (58–1026).....49–53; disc. 53


## J


Jessee, R. D.; W. J. Spaven. Constant Frequency A-C Power Using Variable Speed Generation. (59–810).....411–16; disc. 417
Johannessen, P. R.; F. B. Cox. Application of Switching Transistors and Saturable Reactors in a High-Performance Servo. (58–89).....446–74
Johnson, J. L.; L. E. Moberly. The Effect of Variable High-Altitude Humidity on the Wear of Nondusting Brushes. (59–565).....263–7
Johnson, J. S.; G. I. Moses. Disc.....198
Jones, S. J.; R. M. Sills. The Use of Frequency Response Tests in the Analysis of a Foil Mill Automatic Gage Control. (59–78).....59–67
Jury, E. I. Disc.....522
Jury, Eliahu I.; G. C. Lendaris. Input-Output Relationships for Multisampled-Loop Systems. (59–682).....375–82; disc. 382


## K


Kavanagh, R. J. Disc.....120
Kazda, Louis F.; K. Chuang. A Study of Nonlinear Systems With Random Inputs. (59–147)...100–05
Keay, F. W.; R. Herbst, J. O. Nichols, R. W. Miller. Predicting the Performance of a Wind Tunnel Regulating System Using an Analog Computer. (59–646).....248–52
Keevil, H. W. Detector Car History and New Developments. (59–267).....233–8
Kessler, L. L.; R. E. Hulsey. Functional Cycling to Assure Reliability of Aircraft Control Equipment (59–912).....356–60
Killin, A. M. Disc.....275
Kim, W. H.; R. B. Ash, G. M. Kranc. Disc.....383
Kinnen, E.; J. Tou. Analysis of Nonlinear Sampled-Data Control Systems:
Part I. (59–828).....386–90; disc. 394
Part II. (59–829).....390–4; disc. 394
Klein, N. Disc.....197
Kranc, G. M.; R. B. Ash, W. H. Kim. Disc.....383
Ku, Y. H.; A. A. Wolf. A Stability Criterion for Nonlinear Systems. (59–231)...144–7; disc. 147


## L


Landry, A. P.; I. N. Howell, Jr. Trends in Ground Bed Design for Cathodic Protection of Underground Structures. (59–820)....456–61; disc. 462
Larson, R. L. A High-Capacity Maintenance-Free Generating System for Motor Coaches. (59–779).....311–16
Lee, Reuben. Disc.....89
Lendaris, George G.; E. I. Jury. Input-Output Relationships for Multisampled-Loop Systems. (59–682).....375–82; disc. 382
Lennert, A. E. Practical Considerations of an Ion Propulsion System. (59–833)....326–31; disc. 331
Leonhard, Werner. Elements of Reactor-Controlled Reversible Induction-Motor Drives. (58–1176).....106–14; disc. 114
Lind, E. R.; N. L. Schmitz. Analysis of A-C Servomotors Operated from Unbalanced Nonsinusoidal Voltage Sources and Nonlinear Discontinuous Source Impedances. (59–1157)...476–9; disc. 480
Little, D. R.; K. Chen. A Practical Standard Transistorized Optimum Response Controller. (59–838).....337–45; disc. 345
Liu, C. C.; R. Oldenburger. Signal Stabilization of a Control System. (59–219).....96–100; disc. 100
Locklin, D. W.; J. A. Eibling. Disc.....95
Lord, H. W.; B. C. Biega. Transient Voltages in Rectifier Transformers. (59–149)...83–9; disc. 90


## M


Markowitz, Oscar. Characteristics and Measurement of Ripple in Aircraft Electric Power Systems. (59–879).....418–23; disc. 423
Martin, C. W.; E. W. Bultman. Disc.....195
McCausland, Ian. The Optimum Control of Multi-actuator Systems. (59–198).....67–73
McIlvaine, D. K.; J. G. Hoop. New Materials for Transformer-Rectifier Unit in High-Temperature Aircraft. (59–883).....450–6
Merriam, C. W., III. Use of a Mathematical Error Criterion in the Design of Adaptive Control Systems. (59–1158).....506–12
Miles, G. P. Disc.....461
Miller, R. W.; R. Herbst, J. O. Nichols, F. W. Keay. Predicting the Performance of a Wind Tunnel Regulating System Using an Analog Computer. (59–646).....248–52
Moberly, L. E.; J. L. Johnson. The Effect of Variable High-Altitude Humidity on the Wear of Nondusting Brushes. (59–565).....263–7
Moses, G. L.; J. S. Johnson. Disc.....198
Mulligan, J. H., Jr. Transient Response and the Stabilization of Feedback Amplifiers. (59–1151).....495–503


## N


Nakada, Takashi. Disc.....100
Nelson, F. G.; C. R. Dixon. The Effect of Elevated Temperature on Flash-Welded Aluminum-Copper Joints. (59–1162).....491–5; disc. 495
Nichols, J. O.; R. Herbst, F. W. Keay, R. W. Miller. Predicting the Performance of a Wind Tunnel Regulating System Using an Analog Computer (59–646).....248–52
Numakura, Toshio. Disc.....134


## O


Odok, A. M.; T. M. Soelaiman. Improved D-C High-Potential Testing of Insulation Systems in Low- and Medium-Voltage D-C Equipment. (59–247).....186–93; disc. 198
Oldenburger, R.; C. C. Liu. Signal Stabilization of a Control System. (59–219).....96–100; disc. 100
Owen, T. B. Variable-Speed Constant-Frequency Devices: A Survey of the Methods in Use and Proposed. (59–780).....321–5; disc. 325


## P


Pastel, M. P.; G. J. Thaler. Stability Criteria for Instrument Servomechanisms with Coulomb Friction and Stiction. (59–649).....294–7
Penn, W. B.; R. L. Balke, F. M. Precopio. Generator Insulation Systems Development for Hypersonic Aircraft. (59–864).....255–9
Peters, E. H.; W. F. Gardner. Disc.....506
Phillips, C. L.; M. H. Yuen. High-Speed Restarting and Protection of Large Synchronous Motors. (59–822).....360–7; disc. 367
Pollard, P. J. A Suppressed-Carrier Signal Generator for Servosystem Instrumentation. (59–1153).....481–5
Precopio, F. M.; W. B. Penn, R. L. Balke. Generator Insulation Systems Development for Hypersonic Aircraft. (59–864).....255–9


## R


Randlev, Peter L. Disc.....142
Rectanus, W. A.; G. I. Duncan. Terminal Spacings for High-Altitude and Ultrahigh-Temperature Electronic Transformer Applications. (58–118).....16–19
Riaz, M. Energy-Conversion Properties of Induction Machines in Variable-Speed Constant-Frequency Generating Systems. (58–917).....25–30
Richards, P. B. Temperature Prediction in Thermal-Lag Equipment. (59–913).....462–5
Rohner, Peter; E. Willihnganz. Battery Impedance: Farads, Milliohms, Microhenrys. (59–823)..259–62
Rosentein, Allen B.; P. Chandaket. Notes on Bridged-T Complex Conjugate Compensation and 4-Terminal Network Loading. (59–220)....148–58; disc. 162
Ross, N. V. Three-Phase Induction Heating Coils. (59–256).....291–4


## S


Salzer, John M. Disc.....382
Saunders, R. M.; A. M. Hopkin. Disc.....479
Savo, Theodore A. Disc.....158
Schmidt, Stanley F. Application of Continuous System Design Concepts to the Design of Sampled Data Systems. (58–1083).....74–8; disc. 79
Schmitz, N. L.; E. R. Lind. Analysis of A-C Servomotors Operated from Unbalanced Nonsinusoidal Voltage Sources and Nonlinear Discontinuous Source Impedances. (59–1157)...476–9; disc. 480
Schuh, N. F.; R. J. Tallent. Solar-Powered Thermoelectric Generator Design Considerations. (59–847).....345–52

Scully, T. J.; L. J. Harris, V. H. Stewart. Anode Breaker Testing with a High-Capacity Rectifier System. (58–224).....43–8
Shaad, G. E.; A. E. Vickery. Transistor Amplistat-Regulated Sectional Drive at Southland Paper Mills. (59–813).....369–74; disc. 374
Shen, D. W. C.; C. F. Chen. A New Chart Relating Open-Loop and Closed-Loop Frequency Responses of Linear Control Systems. (59–647).....252–5
Sheppard, Lyle R. Disc.....461
Shilling, W. J.; R. E. Smith. Disc.....404
Sibley, H. C. Communication Systems for Railway Traffic Control. (59–249).....30–5
Siler, H. N.; J. J. Sonnier. Electrical Features of the Four Corners Pipe Line. (58–1057).....209–23
Sills, R. M. Disc.....15
Sills, R. M.; S. J. Jones. The Use of Frequency Response Tests in the Analysis of a Foil Mill Automatic Gage Control. (59–78).....59–67
Simons, J. S. Disc.....194
Sisco, W. B.; J. M. Fiskin. Some Effects of Hypersonic Ionization on the Design of Electrical and Electronic Components. (59–885).....352–6
Smith, R. E.; W. J. Shilling. Disc.....404
Smith, Richard T. Disc.....403, 444
Soelaiman, T. M.; A. M. Odok. Improved D-C High-Potential Testing of Insulation Systems in Low- and Medium-Voltage D-C Equipment. (59–247).....186–93; disc. 198
Sollecito, W. E.; D. A. Swann. Computer Evaluation of High-Temperature Aircraft A-C Electrical System Designs. (59–907).....434–44; disc 444
Sonnier, J. J.; H. N. Siler. Electrical Features of the Four Corners Pipe Line. (58–1057).....209–23
Spaven, W. J.; R. D. Jessee. Constant Frequency A-C Power Using Variable Speed Generation. (59–810).....411–16; disc. 417
Staffin, Robert. Executive-Controlled Adaptive Systems. (59–1181).....523–30
Stephens, William C.; O. I. Elgerd. Effect of Closed-Loop Transfer Function Pole and Zero Locations on the Transient Response of Linear Control Systems. (59–197).....121–7
Stewart, V. N.; L. J. Harris, T. J. Scully. Anode Breaker Testing with a High-Capacity Rectifier System. (58–224).....43–8
Stineman, R. W. Optimum Reflector-Absorber Geometry for a Solar Generator. (59–869).....332–7
Stineman, R. W. Disc.....331
Stratton, L. J.; K. M. Chirgwin. Variable-Speed Constant-Frequency Generator System for Aircraft. (59–872).....304–09; disc. 309
Stratton, L. J.; K. M. Chirgwin. Disc.....301, 417
Stuart, J. W. Disc.....143
Swann, D. A.; W. E. Sollecito. Computer Evaluation of High-Temperature Aircraft A-C Electrical System Designs. (59–907).....434–44; disc. 444

## T

Tallent, R. J.; N. F. Schuh. Solar-Powered Thermoelectric Generator Design Considerations. (59–847).....345–52
Tauber, H. Disc.....275
Thaler, G. J.; M. P. Pastel. Stability Criteria for Instrument Servomechanisms with Coulomb Friction and Stiction. (59–649).....294–7
Thomas, J. W.; E. J. Woodfin. Electrified Fibrous Air Filters. (59–680).....276–8
Thompson, G. J.; S. H. Behr. Aluminum Bus for Shipboard Application. (59–654).....239–47; disc. 247
Tiley, G. L.; E. Zucker. Disc.....128
Toffolo, D. S. Disc.....303
Tou, J.; E. Kinnen. Analysis of Nonlinear Sampled-Data Control Systems:
Part I. (59–828).....386–90; disc. 394
Part II. (59–829).....390–4; disc. 394
Trouard, S. E.; E. A. Wagner, Jr. Deep Ground Beds for Cathodic Protection. (59–505).....278–85
Tsang, N. F. Disc.....147
Tudbury, Chester A. Electric and Magnetic Conditions Inside an Induction-Heated Workpiece (59–64).....79–82

## V

Vickery, A. E.; G. E. Shaad. Transistor Amplistat-Regulated Sectional Drive at Southland Paper Mills. (59–813).....369–74; disc. 374

## W

Wagner, E. A., Jr.; S. E. Trouard. Deep Ground Beds for Cathodic Protection. (59–505).....278–85
Wang, P. K. C.; A. M. Hopkin. A Relay-Type Feedback Control System Design for Random Inputs. (59–218).....228–33
Watkins, William S. Proposed Recommended Practices for Medium-Voltage Motor Controllers for Rubber and Plastics Industries. (59–1112).....504–06; disc. 506
Weaver, Lynn E.; Keisuke Izawa. Relay-Type Feedback Control Systems with Dead Time and Sampling. (58–1026).....49–53; disc. 53
Webb, G. W. Disc.....290
Webb, Robert H. Disc.....238
Wichmann, A. Disc.....193
Willihnganz, E.; P. Rohner. Battery Impedance: Farads, Milliohms, Microhenrys. (59–823).....259–62
Withers, W. E. Disc.....289
Wolf, A. A.; Y. H. Ku. A Stability Criterion for Nonlinear Systems. (59–231).....144–7; disc. 147
Woodfin, E. J.; J. W. Thomas. Electrified Fibrous Air Filters. (59–680).....276–8
Wylie, Laurence. Multiple-Unit Operation of Diesel and Electric Locomotives on the Milwaukee Road. (59–492).....316–20; disc. 320

## Y

Yeager, L. J.; J. T. Duane. Reliability Analysis for Aircraft Generators. (59–888).....426–34
Yuen, M. H.; C. L. Phillips. High-Speed Restarting and Protection of Large Synchronous Motors. (59–822).....360–7; disc. 367

## Z

Zaborszky, J.; J. W. Diesel. Probabilistic Error as a Measure of Control-System Performance. (59–199).....163–8
Zucker, E.; G. L. Tiley. Disc.....128

## Power Apparatus and Systems—December 1959


59-659 33-Kv Cable Terminations....Betz, Lusby, Rueckert, Foley, Gordon . . . 977
59-660 4-Kv Cable Terminations....Rueckert, Lusby, Betz . . . 983
59-663 Forced and Free Oscillations of Coils and Windings....Abetti . . . 986
59-644 Lightning Performance of Transmission Lines—II....Wagner, Hileman . . . 996
59-664 Measurement of Ambient Air Temperature....Beavers . . . 1021
59-666 Corettes: Models for Obtaining Electrical Data on Bushings....Alvord . . . 1029
59-679 Outdoor Single-Tank Oil Circuit Breakers....Balentine . . . 1032
59-643 Radio Influence Voltages Caused by Surface Imperfections....Liao . . . 1038
58-1197 Calculating Various Components of Joint Resistance....Allen . . . 1047
59-657 Torsional Vibrations in Synchronous Drives....Thames, Heard . . . 1053
59-568 Shielding 13.8-Kv Distribution Circuits....Hurstell, West . . . 1056
58-1196 Distribution Circuit Protection....Guenzel, Morris . . . 1064
59-775 Trip-and-Carrier Test for Phase-Comparison Relays....Hirtler . . . 1072
58-1322 High-Speed Air Breaker for Distribution Circuits....Sleeper, Findley . . . 1075
58-1229 Distribution Protection Used on Portland General Electric Company System.Bostwick . . . 1081
59-496 A 35-Kv Polyethylene-Insulated Cable Installation....Crowdes . . . 1086
59-683 Polyphase Induction Machine....Kesavamurthy, Rajagopalan . . . 1092
St. Lawrence H-V Submarine Cable Crossing...Farnham, Shanklin, Cunha, Short
58-78 I. Basic Data and Design . . . 1098
58-305 II. Experimental Program and Cable Manufacture . . . 1113
58-1353 III. Installation . . . 1134
58-1354 IV. Field Tests After Installation . . . 1173
59-767 Development of a Square Law Radio Noise Meter—II....Trebby . . . 1186
59-797 Special Circuits for Ground Relay Current Polarization....Oakes . . . 1191
59-783 Analysis of Transformer Application....Mitchell, Sweeny, Cantwell . . . 1196
59-281 Aging of Wire Insulation....Beavers, Brustle, Carpenter, Degnan . . . 1202
59-801 Stresses in Cables Near the Point of Support....Steidel, Jr. . . . 1207
59-781 Modular Design for Aluminum Substation Structures....Swanson, McCleer . . . 1213
59-684 Electronic Surge Testing of Universal Armatures....Weed . . . 1219
59-806 Underfrequency Protection of Power Systems....Dalziel, Steinback . . . 1227
59-814 Radio Interference on High-Voltage Transmission Lines....Stone, Gens, Gehrig . . . 1238
59-803 Amplitude Build-Up During Acceleration of Oscillatory Systems....Elgerd . . . 1248
Mathematical Models for Use in Simulation of Power Generation Outages
59-851 I. Fundamental Considerations....Baldwin, Gaver, Hoffman . . . 1251
59-849 II. Forced-Outage Distributions....Baldwin, Billings, Gaver, Hoffman . . . 1258
59-850 Economic Shutdown of Generating Units....Baldwin, Dale, Dittrich . . . 1272
59-817 Study of System Planning by Operational Gaming Models....Dillard, Sels . . . 1284
59-868 Design of Overhead Lines with 5005 Aluminum Alloy Cables....Adams . . . 1290
59-819 Large-Waterwheel-Generator Thrust Bearing Tests....Baudry, Kuhn, Cooper . . . 1300
59-807 Corona and Conductor Work Function....Dixon . . . 1316
59-818 Vaporization Cooling for Transformers....Narbut, Maslin, Wasserman . . . 1319
59-895 Lightning Protection of Equipment on Multiple Line Busses....Knable . . . 1327
59-899 Evaluation of Accessories for Aluminum in Marine Environments....Sanders . . . 1342
59-881 Automatic Controls of Hydro Stations....Hayden, Ehmayer, Baumann, Moulds . . . 1353
59-808 Electromagnetic Unbalance of Transmission Lines—III...Gross, Dinnan, Jochum . . . 1362
59-939 Response of Generating Plants to Control Tests....Klopfenstein . . . 1371
59-877 Power Plant Control Board Locations and Operation....Norell . . . 1381
59-921 Brownlee Hydro Development....Soule, Heikes, Mitchell, Schaufelberger . . . 1388
59-922 Bulk Power Stations on Southern California Edison System....Bulkley . . . 1405
59-854 Fault Pressure and Gas Detector Relays....Fohrhaltz . . . 1416
59-897 EHV Single and Twin Bundle Conductors—Characteristics and Selection....Hazan . . . 1425
59-896 EHV Single and Twin Bundle Conductors—Influence of Diameter....Stone . . . 1434
59-894 Switching Surge Voltages Due to Current Interruption....Amchin, Curto . . . 1443
58-449 High-Strength Aluminum-Alloy Conductors....Greenfield . . . 1449
Additional Discussion and Errata . . . 1456


## Conference Papers Open for Discussion

Conference papers listed below have been accepted for AIEE Transactions and are now open for written discussion until February 29. Duplicate double-spaced typewritten copies for each discussion should be sent to Edward C. Day, Assistant Secretary for Technical Papers, American Institute of Electrical Engineers, 33 West 39th Street, New York 18, N. Y., on or before February 29.

Preprints may be purchased at 40¢ each to members; 80¢ each to nonmembers if accompanied by remittance or coupons. Please order by number and send remittance to:

AIEE Order Department
33 West 39 Street
New York 18, N. Y.

59-111 Capacitance of Parallel Rectangular Cylinders....Horgan
59-837 Modified Optimum Nonlinear Control....Mitsumaki

# AIEE PUBLICATIONS

| | Member Prices | Nonmember Prices: Basic Prices*† | Nonmember Prices: Extra Postage for Foreign Subscriptions† |
|---|---|---|---|
| **Electrical Engineering** | | | |
| Official monthly publication containing articles of broad interest, technical papers, digests, and news sections: Institute Activities, Current Interest, New Products, Industrial Notes, and Trade Literature. Automatically sent to all members and enrolled students in consideration of payment of dues. (Members may not reduce the amount of their dues payment by reason of nonsubscription.) Additional subscriptions are available at the nonmember rates. | | annually $12* Single copies $1.50* | $1.00 |
| **Bimonthly Publications** | | | |
| Containing all officially approved technical papers collated with discussion (if any) in three broad fields of subject matter as follows: | | | |
| | annually | annually | |
| Communication and Electronics | $5.00 | $8.00* | $0.75 |
| Applications and Industry | $5.00 | $8.00* | $0.75 |
| Power Apparatus and Systems | $5.00 | $8.00* | $0.75 |
| Each member may subscribe to any one, two, or all three bimonthly publications at the rate of $5.00 each per year. A second subscription to any or all of the bimonthly publications may be obtained at the nonmember rate of $8.00 each per year. | | | |
| Single copies may be obtained when available. | $1.50 each | $1.50* each | |
| **AIEE Transactions** | | | |
| An annual volume in three parts containing all officially approved technical papers with discussions corresponding to six issues of the bimonthly publication of the same name bound in cloth with a stiff cover. | | | |
| | annually | annually | |
| Part I Communication and Electronics | $4.00 | $8.00* | $0.75 |
| Part II Applications and Industry | $4.00 | $8.00* | $0.75 |
| Part III Power Apparatus and Systems | $4.00 | $8.00* | $0.75 |
| Annual subscription to all three parts (beginning with vol. 77 for 1958). | $10.00 | $20.00* | $2.25 |
| Annual subscription to any two parts. | | $15.00* | $1.50 |
| **AIEE Standards** | | | |
| Listing of Standards, test codes, and reports with prices furnished on request. | | | |
| **Special Publications** | | | |
| Committee reports on special subjects, bibliographies, surveys, and papers and discussions of some specialized technical conferences, as announced in ELECTRICAL ENGINEERING. | | | |

*Discount 25% of basic nonmember prices to college and public libraries. Publishers and subscription agencies 15% of basic nonmember prices. For available discounts on Standards and special publications, obtain price lists from Order Department at Headquarters.

†Foreign prices payable in New York exchange

Send all orders to:

Order Department
American Institute of Electrical Engineers
33 West 39th Street, New York 18, N. Y.